RNA binding proteins and mRNA localisation in *Drosophila* sperm development

Dana Erin Jackson

October 2024

This thesis is submitted for the degree of Doctor of Philosophy

Funding and Technical Support

This work was supported by the Biotechnology and Biological Sciences Research Council-funded South West Biosciences Doctoral Training Partnership [Training Grant BB/T008741/1].

Microscopy and imaging training was provided by Cardiff University Bioimaging Hub Core Facility, RRID:SCR_022556.

RNA library preparations and quality control for RNA Sequencing was supported by Cardiff University Genomics Research Hub, Cardiff School of Biosciences.

Bioinformatic analysis of RNA-Sequencing data was kindly supported by Dr. Fiona Messer.

Comparative proteomics was performed by the University of Bristol Proteomics Facility.

Additional thanks to Dr. Richard Lewis for his support in the early stages of this PhD project.

Acknowledgements

To my loving family, thank you. Mutti, Dad, Nannie, Grandad and Jorge – you are my whole world, and I love and appreciate every single one of you. I really do miss you, Nannie.

As an only child, I have been spoilt in life; with the riches of always having the unfaltering love and attention I needed from both of my parents. And thanks again, Grandad, for always answering my phone calls (even when it's been a while!). I better be your favourite grandchild! Only joking… maybe.

Jorge, I love you to infinity and beyond. You are my bestest friend in the whole universe, and I do not know what I'd do without you. I am so very glad we met in GSCE German, and that you walked me home most days from the bus stop after Sixth Form. Here's to the next chapter of our lives together in Cambridge – we've got this! Ten years and counting!

Prof. Helen White-Cooper, I thank you over and over again for being an amazing primary supervisor, and for picking me up off the ground when I genuinely thought I was incapable. And to Dr. Sonia Lopez de Quinto, thank you very much for being such a supportive secondary supervisor too. I certainly got lucky in the supervisor lottery – that's for sure! Dr. Fiona Messer, you are a real whiz kid, and I cannot thank you enough for all the support you have given me over the past four years. You rock! Sabrina, I will miss our daily gossips about anything and everything. I could always rely on you to cheer me up! Finally, April, I wish I had known you for longer. I can already tell you are lovely; it's such a shame that this is goodbye!

Now to Rob: I knew you were a gem as soon as I started in the lab because, while you barely knew me, you still went on a one-man-mission to hunt down my glasses after I lost them. You are the pillar of our little Fly community and don't you forget it!

Last, but certainly not least, to my lab partner in crime: Dr. Abdulla Almoalem! Gosh, do I miss you! It wasn't the same after you left. Thank you for the best of times. I will always remember our little chats where we put the world to rights during incubation steps and washes. Thanks A, for making my PhD journey bearable.

ACKNOWLEDGEMENTS

To everyone else that I can remember – Rachel, Cris, Nehad, Jeremy, Menna, Hoi, Silvia, Sean, Jack and Nicola – thank you for making my time in the Fly Group so memorable. I cannot believe how far everyone has come since I first started my PhD in October 2020. It was a tough start, and I don't think I've cried so much in my life, but I remember Helen being there with the tissues, reassuring me that it will get better… I didn't believe her at the time, but she was right (as always!).

Cardiff will always be in my heart. It was where I met my two best friends – Elena and Rosemary – and was the first place that Jorge and I decided to call "home" together. I had never set foot in Wales before starting my undergraduate degree, and then it drew me in and kept me there for nine solid years! Who would have known!

Thanks again to Elena and Rosemary for sticking by me even when I go AWOL. I love and miss you both very much and I am so grateful that I met you when I did. I promise I will be better now (although, you have heard it all before, mind you!).

A special shoutout to Jorge's family too – thank you Jan, David, Mason and Rubble (woof!) for always making me feel like a welcome addition to your lives.

Finally, Helen, Fi, Sabrina, April and Saurabh, I will sincerely miss being part of the "Sperm Squad" (even if I never successfully made that name into a thing!) – "…Stop trying to make fetch happen! It's not going to happen!" (Mean Girls, 2004).

Hwyl fawr, Cardiff University! Hwyl fawr, Biosi! Hwyl fawr, Fly Group! I will miss you all tremendously, and I cannot thank you enough for making me the person I am today.

P.S. I love you to the moon and back, Mutti! There you go, it's in official writing now!

Summary

In *Drosophila melanogaster* sperm development, male germline cells progress through a tightly regulated program of mass displacement, growth and proliferation. Each stage is defined by cell-type-specific changes to shape, volume and gene expression profiles. After meiosis, the newly developed spermatids undergo synchronised differentiation, elongation and maturation; transforming from round cells to highly specialised and polarised, needle-like cells that extend to 1.8 mm in length. Individualisation then separates these interconnected spermatids to yield mature, coiling sperm.

While most spermatogenesis-specific transcriptional activity occurs in pre-meiotic spermatocytes, a small number of genes are also post-meiotically transcribed in the mid-to-late elongating spermatids – at a point preceding the histone-transition protein-protamine switch during chromatin reconfiguration. These genes express asymmetrically localised mRNAs that accumulate towards the tail-ends of growing spermatid cyst bundles in unusual localisation patterns of shooting speckled “comets” or U-shaped acorn “cups”.

We know that this mRNA localisation precedes the formation of distinct protein gradients but, apart from the spatiotemporal profiles of their post-meiotic expression, very little is known about the molecular and regulatory driving forces that underpin this biological phenomenon.

There are, however, several RNA binding proteins (RBPs) that are enriched in similar subcellular regions at the spermatid tail-ends. We therefore hypothesised that some of these RBPs are contributing to the post-transcriptional regulation of localised post-meiotic RNA transcripts in sperm development.

RNA-affinity pull-down assays of 11 comet and cup mRNAs revealed differential binding of 4 RBPs *in vitro*, with the amount of interacting RBP varying depending on the mRNA of interest. The highly conserved IGF-II mRNA-binding protein (Imp) was the only RBP to bind all comet and cup transcripts in our test panel.

The Imp protein family are key biological players, involved in the binding, transportation and post-transcriptional processing of various localised mRNAs,

including those that encode cell fate determinants and actin transcripts. In *Drosophila* sperm development, Imp is expressed at two spatiotemporally distinct pre-meiotic and post-meiotic phases, suggesting the possibility of pleiotropic functionality in the testis. While Imp is known to play an important role in the maintenance of male germline stem cells during early pre-meiotic sperm development, little is known about its activity throughout the latter stages (spermiogenesis) or its role within the elongating spermatids.

As Imp demonstrated consistent binding to our panel of comet and cup mRNAs, is highly expressed and localised within the spermatid tail-ends, and is implicated in numerous developmental processes, we decided to take it forward as our main candidate for further investigation.

We optimised the Cleavable-Affinity Purification (Cl-AP) to precipitate out whole, multi-protein Imp:mRNA ribonucleoprotein (RNP) complexes from pooled *Drosophila* testis homogenates. In doing so, follow-up comparative proteomics and RNA-Sequencing of the Cl-AP-purified, testis-specific Imp RNP complexes identified 29 Imp-enriched protein binding partners and 249 Imp-interacting mRNAs, respectively. Several were associated with RNA binding, actin regulation, microtubule dynamics and translational activities.

We also performed a series of phenotypic analyses via RNA interference (RNAi) screening to elucidate the functional role of *imp* in the *Drosophila* testis and late sperm development. RNAi knockdowns of *imp in vivo* resulted in a variable spectrum of abnormal testis phenotypes, including mislocalisation of mRNA transcripts, downregulation of localised RNA and fluorescent protein reporter signals, and spermatid elongation defects. Overall, this suggested a context-dependent role of Imp in the post-meiotic stages of sperm development.

Taken together, we have subsequently proposed a novel Imp-facilitated, F-actin-dependent anchoring and elongation mechanism that may regulate localised active transport and translation of post-meiotic mRNAs at the spermatid tail-ends.

Table of Contents

Table of Figures

TABLE OF FIGURES

TABLE OF FIGURES

Table of Tables

TABLE OF TABLES

List of Appendices

List of Useful Abbreviations

AA: Amino acid

BDRC: Bloomington *Drosophila* Resource Centre

BMP: Bone morphogenetic protein

BRE: Bruno Response Element

BrU: 5-Bromouridine

CDS: Coding sequence

CI-AP: Cleavable Affinity Purification

CNS: Central nervous system

DGE: Differential gene analysis

ds: Double-stranded

F1: Filial 1

FA : Fatty acid

GLM: Generalised Linear Model

GO: Gene Ontology

GSC: Germline stem cell

HCR RNA-FISH: Hybridisation Chain Reaction RNA Fluorescence *In Situ* Hybridisation

hnRNP: Heterogeneous nuclear ribonucleoprotein

HS: High sensitivity

IBE: IMP binding element

ISC: Intestinal stem cell

KH: K-homology

LB: Luria-Bertani

lncRNA: Long non-coding RNA

LSFM: Lightsheet fluorescence microscopy

MARCM: Mosaic analysis with a repressible cell marker

MCS: Multiple cloning site

miRNA: MicroRNA

MT: Microtubule

NOA: Non-Obstructive Azoospermia

PBS: Phosphate buffered saline

PBT: PBS with 0.1% Tween-20

PFA: Paraformaldehyde

PTM: Post-translational modification

QC: Quality control

RBP: RNA binding protein

RE: Restriction enzyme

RIP-Seq: RNA immunoprecipitation and sequencing

RNA-(F)ISH: RNA Fluorescence *In Situ* Hybridisation

RNAi: RNA interference

RNA-Seq: RNA-Sequencing

RNP: Ribonucleoprotein

ROI: Region of interest

RRM: RNA recognition motif

RT: Room temperature

shRNA: Short hairpin RNA

siRNA: Small interfering RNA

snRNA-Seq: Single cell RNA-Sequencing

SSC: Sodium chloride sodium citrate

SSCT: Sodium chloride sodium citrate with 0.1% Tween-20

TF: Transcription factor

TRiP: Transgenic RNA Interference Project

TMT: Tandem Mass Tagging

UAS: Upstream activation signal

UTR: Untranslated region

VALIUM: Vermilion-AttB-Loxp-Intron-UAS-MCS

VDRC: Vienna *Drosophila* Resource Center

WT: Wildtype

1. INTRODUCTION

1.1. *Drosophila melanogaster* is a powerful biological tool

Much of what we know today about genetic inheritance, evolution, development and physiology has been learnt from early studies using non-human model – or "reference" – organisms. The fruit fly, *Drosophila melanogaster*, is one such model organism.

The fruit fly is an invaluable and well-established model system in genetics and developmental biology that has been utilised for more than a century (Morgan 1910). The holometabolous metamorphosis and short generation time of *Drosophila melanogaster* have further supported its crafting into a key biological tool. The standard life cycle of a fruit fly commences with fertilisation and egg deposition and continues through a series of distinct developmental stages: embryo, first instar larva, second instar larva, third instar larva, pupa and, finally, adult fly eclosion. In total, this whole cycle is rapid and spans only ten to twelve days at 25˚C (Fernández-Moreno et al. 2007; Ong et al. 2015). In comparison to higher model organisms, the fruit fly is relatively inexpensive to maintain, requires fewer housekeeping and storage capacity demands, and does not require any form of ethical approval for experimentation. *Drosophila* also have a comparatively simplistic chromosome arrangement compared to other model organisms, comprising only four pairs of chromosomes: one pair of sex chromosomes and three pairs of autosomes.

1.2. *Drosophila* share functional and genetic homology with humans

Many of the internal organ systems possessed by fruit flies are functionally analogous to those in vertebrates, including in humans (Ugur et al. 2016). Genome-wide searches also suggest that anywhere between 50–77% of all human disease-associated genes have conserved functional homologues in *Drosophila* – however, this final percentage does depend on the database type, analysis pipeline, significance and stringency cut-off selections (Fortini et al. 2000; Rubin et al. 2000; Reiter et al. 2001; Bier 2005). Homologues for genes implicated in the development of human

cancers, neurological conditions, cardiac diseases, as well as gastrointestinal, endocrine and renal disorders have all been characterised in the *Drosophila* genome (Rubin et al. 2000; Reiter et al. 2001). Modelling in flies has proved fruitful in deciphering some of the mechanistic interplay that drives disease progression. The characterisation of many novel biological players has also been made possible; particularly in neurodegenerative disorders such as Alzheimer's Disease, Parkinson's Disease and Huntington's Disease (Bolus et al. 2020; Verheyen 2022). Various patient-specific mutations at disease-associated loci have also been generated in "fly avatar" lines for the study of relative pathogenicity and the identification of personalised, case-by-case treatments (Lin et al. 2020; Bangi et al. 2021). Therefore, *Drosophila* provide a valuable model for investigating the genetic basis and molecular mechanisms of human health and disease.

1.3. Fruit flies can be genetically manipulated with ease

Since the advent of balancer chromosomes by Muller (1918), stable fly lines containing highly complex genotypes can be sustained over time, even with a combination of different mutant chromosomes, without concern of recombination events. The fully sequenced, annotated and streamlined *Drosophila* genome has enabled the generation of a multitude of genome-wide tools and reagents (Adams et al. 2000; Misra et al. 2002; Schertel et al. 2013; Venken and Bellen 2014). P-element transposon-mediated transgenesis was developed as part of the ever-expanding *Drosophila* genetic toolkit, involving the imprecise mutation of genomic loci by insertion at random landing sites and the integration of exogenous DNA (Rubin and Spradling 1982; Spradling and Rubin 1982; Spradling et al. 1999). This was optimised with the generation of an attP site-specific ΦC31-integrase-mediated system, which overcame many of the previous issues associated with P-element mutagenesis. These included the inability to map genetic insertions or analyse transgene phenotypes due insertional position effects on expression levels (Groth et al. 2004; Bateman et al. 2006; Bischof et al. 2007; Huang et al. 2009).

More advanced gene engineering technologies have now been developed in fruit flies, and continue to be updated as new tools are invented; allowing endogenous *in vivo* genetic interaction and functional characterisation studies to be performed with ever-

improving precision and ease (St Johnston 2013; Beumer and Carroll 2014; Heigwer et al. 2018). These include RNA interference knockdown screening (Dietzl et al. 2007; Mohr 2014; Perkins et al. 2015), CRISPR/Cas9 gene editing (Bassett et al. 2013; Gratz et al. 2013; Yu et al. 2013; Port et al. 2014; Sebo et al. 2014), and gain-of-function Gal4/UAS binary expression systems (Brand and Perrimon 1993; Bischof et al. 2013), to name just a few.

1.4. Why is research into *Drosophila* sperm development important?

As a “traditional” model organism, *Drosophila* host a plethora of genetic tools that are already optimised for application and readily available for most contemporary research (Keller 2013). The study of sperm development (spermatogenesis) is one such example.

Overall, sperm is extremely important: half the population make it, there would be no us without it, and the loss of sperm development would lead to ultimate extinction. It is a fascinating biological process, and many of its complexities still need to be elucidated, even in important model organisms such as *Drosophila melanogaster*. It is vital that we understand the fundamentals of how sperm is made and what contributes to its successful final form and function. To ensure the fruit fly remains an accurate and usable model, we must continue to expand and build upon known fundamental science. Although fruit flies are one of the best understood model organisms we have, there is a great deal more we need to learn, and it is important that we systematically build upon our current knowledge.

Within the *Drosophila* testes, sperm development proceeds as a continuous process of displacement and differentiation along the entire length of the testis, and each stage can be readily observed as a spatiotemporal array. As a model system, this makes it easily accessible and amenable to experimental handling. The cell ultrastructure, phenotypic characteristics, expression profiles and key biological phases of sperm development can also be visualised clearly within whole-mount testes via microscopy (White-Cooper 2004,2009). In fact, some research suggests that the distinct stages of male germline differentiation can be studied for multiple days using *in vitro* cultures of

individual developing cysts from live *Drosophila* testes (Cross and Shellenbarge 1979; Noguchi and Miller 2003; Kawamoto et al. 2008).

Due to being a stem-cell-driven process, sperm development continues throughout the reproductive lifetime of males in many species (Fabian and Brill 2012; Matunis et al. 2012). This highly active, unipotent adult stem cell lineage provides a continuous assembly line of developing germline cells for experimentation, especially in the case of model organisms such as *Drosophila melanogaster* (Raz et al. 2023). In fact, by the early larval stage, sperm development has already begun (Sonnenblick 1941; Lindsley 1980). Moreover, sperm development in adult *Drosophila melanogaster* is a quick and efficient process, with the rate of asymmetrical germline stem cell divisions being very frequent – occurring every 10 hours in the adult testis (Lindsley 1980).

The *Drosophila* testis also offers an exceptional model system for the study of cellular morphogenesis, particularly in terms of cytoskeletal regulation. A great deal of mutants and knockdown lines are already available in stock collections, which target specific genes or aspects of sperm development in flies, and known markers for each cell type make it easy to determine their true phenotypic effects within the testis (Fuller 1993; White-Cooper 2004).

1.5. Research into *Drosophila* sperm development can be applied to other organisms and systems

Many features of *Drosophila* sperm development are conserved and shared with mammals (Raz et al. 2023). As it is a highly conserved biological process, this means what is observed in fruit flies can easily be applied to another organism, including to human sperm development. The fruit fly is therefore an effective model organism for the investigation of male fertility, reproductive health and sperm production (Hu et al. 2014; Yu et al. 2019a). As many key genes implicated in sperm development are homologous between *Drosophila* and humans, several mutants of these homologues display similar testicular and male sterile phenotypes in fly models (Hackstein et al. 2000; Yu et al. 2016). These can therefore be studied first-hand in *Drosophila* to recapitulate the aetiology and defects of human sterility, including the causes of non-obstructive azoospermia (NOA) (Yu et al. 2016).

NOA represents one of the most severe forms of male infertility, characterised in sufferers by a lack of mature and motile sperm in the seminal fluid (Yu et al. 2014). Key orthologues of human genes, which map to various NOA susceptibility risk loci related to male fertility genes, have been successfully modelled and investigated in *Drosophila* (Hu et al. 2014). This includes *CHES-1-like*, an orthologue of the human NOA-associated risk gene, *FOXN3* (Yu et al. 2016). Additionally, comparative analysis of male sterile mutations in the fruit fly can permit the identification of many more genes that contribute to different aspects of human male infertility; with anywhere up to 1500 autosomal recessive mutations suggested to be involved, and several of these are likely to have other major pleiotropic effects (Hackstein et al. 2000). Some pleiotropic disorders that are implicated in male infertility include cystic fibrosis, myotonic dystrophy and Kartagener syndrome, among many others (Hackstein et al. 2000). What we learn from *Drosophila* is therefore crucial to our understanding of human illnesses.

Ultimately, it is the successful development of healthy, viable sperm in male *Drosophila* that bestows the greatest competitive advantage in reproduction and fertility. While conventional sperm production is usually the case, sometimes things can go awry. By identifying the mechanisms underpinning normal sperm development in a healthy model system, we can then apply this knowledge to understand why and how diseases such as infertility arise aberrantly – and extrapolate, if appropriate, to human contexts of health and disease.

1.6. Sperm development in *Drosophila melanogaster*

Sperm development, also known as spermatogenesis, is a tightly regulated, testis-specific developmental program of several sequential, coordinated stages that culminates in the generation of mature, coiling spermatozoa. In *Drosophila melanogaster*, male germline cells advance through sperm development in a continuous cycle of synchronised displacement, differentiation, elongation and individualisation (Fig. 1.). Each stage of sperm development is defined by cell-type-specific changes to shape, volume and expression profiles (White-Cooper 2004,2009).

There are a number of instrumental review articles, including Fuller (1998) and Fabian and Brill (2012), and book chapters from Lindsley (1980) and Fuller (1993), which provide an extensive insight into the fascinating and complex biological process of *Drosophila* sperm development – these are summarised below.

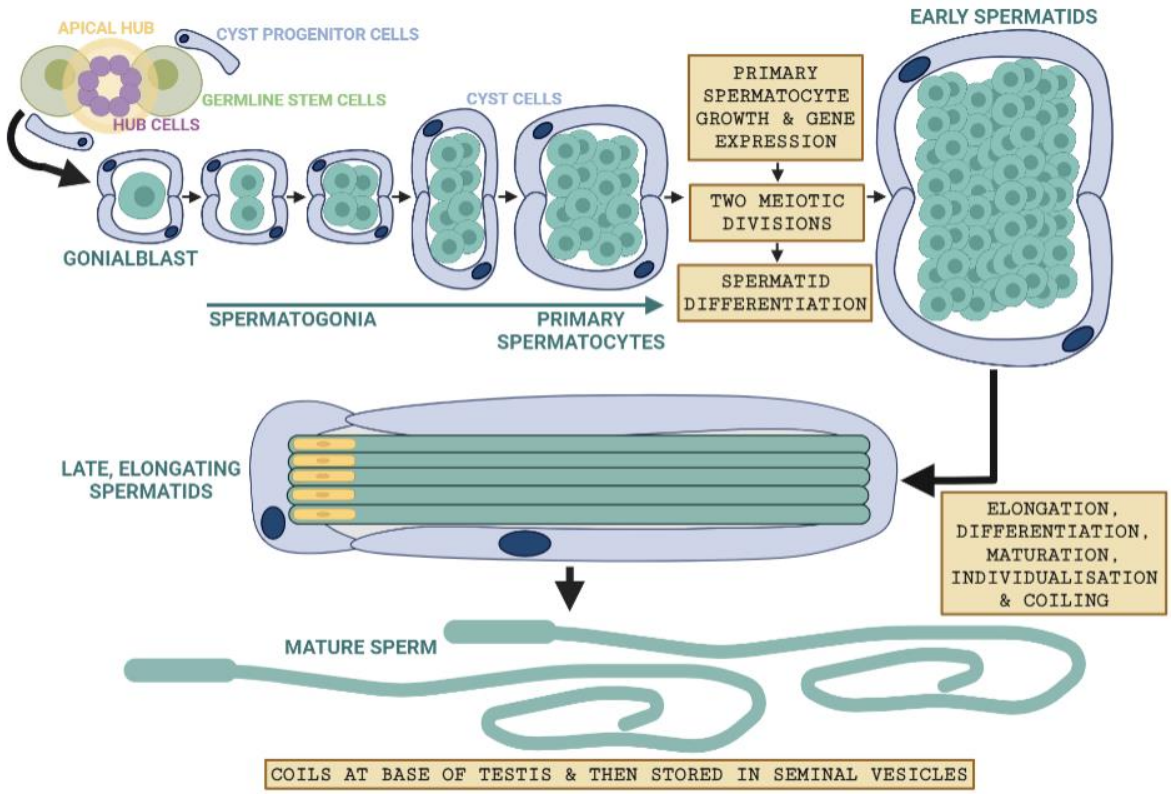

Figure 1. Schematic outlining sperm development in *Drosophila melanogaster*. Germline stem cells and cyst progenitor cells are directly docked to a cluster of post-mitotic somatic cells termed the apical hub. This provides a homeostatic, self-renewing stem cell population from which sperm production can be commenced for the entire reproductive lifetime of a male. Altogether, four rounds of mitotic spermatogonial amplification ensue, followed by spermatocyte growth and two rounds of meiosis. An immediate post-meiotic phase, spermiogenesis, demarcates the closing stages of sperm development. This produces a cyst of sixty-four round clonally related sister spermatids. Synchronised elongation and differentiation gives rise to bundles of long, interconnected spermatids which individualise to herald mature, coiling spermatozoa. **Recreated from Fuller (1998) and Kawamoto et al. (2008) using BioRender.com.**

1.6.1. Testis ultrastructure and initiation of male germline differentiation

In *Drosophila melanogaster,* the testis exists as a long, tubular “blind-ended” structure which coils to form a distinct spiral shape. It is approximately 2 mm in length and 0.1 mm in width and consists of a sheath of muscle and pigment cells, separated from the lumen by a basement membrane (Hardy et al. 1979; Lindsley 1980; White-Cooper 2004). In many wildtype (WT) *Drosophila* males, the sheath can be yellow or orange in colour. Although, this pigmentation can vary from one fly stock to another, ranging from cream to near-colourless depending on the genetic modifications made (Stern and Hadorn 1939). Displacement and differentiation occurs from the apical to basal ends of the winding tube, from start to finished product. The basal end in turn meets with the terminal epithelium, which forms the testicular duct that connects to the seminal vesicle; enabling storage of the mature, coiling sperm prior to release. Both the seminal vesicle and accessory glands are connected to the ejaculatory duct, providing a vessel through which sperm can be transferred upon mating (Lindsley 1980).

Drosophila sperm development is initiated at the stem cell niche, which is located at the apical end of the testis. Here, the basement membrane is thickened and lies adjacent to a clustered rosette of roughly twenty post-mitotic somatic cells, termed the hub (Hardy et al. 1979; White-Cooper 2004). The hub couples and secures around eight germline stem cells within the complex stem cell microenvironment – ensuring homeostatic stem cell turnover and synchronised differentiation. Each of these germline stem cells is enveloped with two cyst progenitor somatic stem cells which maintain contact with the hub cells via cytoplasmic projections (Fuller 1993).

The germline stem cells divide asymmetrically to generate one gonialblast and a second self-renewing daughter cell that remains attached to the hub. Alternatively, the gonialblast becomes displaced from the niche to commence cellular differentiation. Associated cyst progenitor somatic stem cells divide only once, generating two cyst cells per gonialblast that encapsulate and support the germline cells throughout the course of spermatogenesis (White-Cooper 2004; Lim et al. 2012; Matunis et al. 2012). The cyst cells continue to envelope the germ cells as they divide and differentiate, forming distinct cysts of cells that increase in size and number (White-Cooper and

Bausek 2010; Cheng et al. 2011; Lim et al. 2012). The second daughter cell produced by asymmetric division retains stem cell identity and remains within the hub-associated niche (Kawamoto et al. 2008).

Asymmetrical germline stem cell divisions occur relatively frequently, equating to an approximate rate of once every 10 hours in the adult testis (Lindsley 1980). Overall, sperm development in the adult *Drosophila melanogaster* male takes ~250 hours, when measuring from the first germline stem cell division to release of mature sperm (Lindsley 1980). This somewhat extensive process – and inherent delay in male maturity – is temperature-sensitive and likely relates to the time-consuming costs of producing large, complex sperm with long, elongated tails (Pitnick et al. 1995; Canal Domenech and Fricke 2023).

1.6.2. Mitotic division and pre-meiotic primary spermatocyte cyst development

Each gonialblast undergoes four rounds of mitotic spermatogonial amplification and a pre-meiotic S-phase, producing a pre-meiotic cyst of 16 primary spermatocytes (Fuller 1993; White-Cooper 2004). These cells are interconnected by cytoplasmic bridges termed “ring canals”, which are derivatives of incomplete cytokinesis (Fuller 1998; White-Cooper 2004). Throughout these ring canals, a specialised membrane-rich portion of the cytoplasm called the fusome is able to extend, thereby maintaining an intimate connection between the entire cyst of primary spermatocytes (McKearin 1997).

The primary spermatocyte stage takes place over a 90-hour period and marks a cellular switch, shifting efforts from cell division to growth and gene expression (Lindsley 1980). By doing so, this sets the foundation for the next stages of terminal differentiation (Fuller 1993). In readiness for entry into meiosis I, the primary spermatocytes undergo a 25-fold increase in volume (Lindsley 1980; Kuhn et al. 1988). Many of the gene products needed for successful late-stage sperm development, including for post-meiotic morphogenetic activities, are transcribed during this extended G2 phase and are translationally repressed until needed (Schäfer

et al. 1995). However, as detailed later on in Section 1.9, a short re-activation of transcription also arises in the spermatids after meiosis.

1.6.3. Meiosis I and II

A total of two rounds of meiosis ensues. The first meiotic division is defined by a distinct morphological transformation to the chromosomes and nuclei, which corresponds with the transition from an extended primary spermatocyte-specific G_2 phase to a meiosis-specific metaphase (Fuller 1993). Additionally, the centrally-positioned nucleus becomes more spherical with a prominent nuclear membrane (Fuller 1993; White-Cooper 2004). Meiosis I is a reductional division, resulting in the disjunction of the X and Y sex chromosomes (Fuller 1993). In both meiosis I and meiosis II, the mitochondria align in parallel along the spindle and adjacent to the nuclear membrane. This ensures that the mitochondria are evenly distributed between daughter cells upon commencement of cytokinesis (Fuller 1993). A cyst of 32 secondary spermatocyte cells, intimately linked by ring canals, is generated upon conclusion of meiosis I (White-Cooper 2004).

Interphase between the two meiotic divisions is brief, and smaller-sized cells in higher numbers distinguishes spermatocytes in meiosis II from those in meiosis I. The mitochondria gather towards one side of the secondary spermatocyte nuclei ready for a second archetypal cell division (Fuller 1993). The formation of a cyst bundle of 64 round, haploid spermatids, surrounded by two cyst cells, marks the completion of meiosis I and meiosis II.

1.6.4. Early Spermiogenesis

Spermiogenesis begins immediately after meiosis and is the final post-meiotic, haploid phase of *Drosophila* spermatogenesis that is undertaken over the course of ~135 hours (Lindsley 1980). It demarcates the conclusion of sperm development and is characterised by highly specialised cells called spermatids. Spermiogenesis commences with syncytial cysts of 64 round, clonally related sister spermatids. These cells undergo extensive differentiation, as well as distinct morphogenesis and

maturation events, to herald mature, coiling sperm (Fuller 1993; Fabian and Brill 2012).

Within the early-stage round spermatids, the mitochondria coalescence around a short axoneme encapsulated by ciliary sheath called the basal body. This occurs towards one side of the nucleus (Fuller 1993; Fabian and Brill 2012). The mitochondria aggregate and fuse together to form the Nebenkern, a round-shaped structure which consists of two distinct mitochondrial derivatives that wrap around one another (White-Cooper 2004; Fabian and Brill 2012). At the same time, the basal body migrates near the nuclear envelope, where it becomes embedded and causes envelope asymmetry. Consequently, the nuclear pores are restricted to the region of nuclear envelope corresponding to the docked basal body. This is required for proper microtubule and dynein organisation within the developing sperm cells (White-Cooper 2004; Fabian and Brill 2012).

A microtubule and actin-rich structure called the “dense body” also begins to form in this area, which will ultimately contribute to subcellular transport and nuclear morphology. Another organelle, the acroblast, develops alongside the acrosomal granule from aggregating Golgi bodies (Kondylis and Rabouille 2009; Fabian and Brill 2012). This assembly takes place on the side of the nucleus opposing the basal body and provides the source from which the acrosome is derived; forming a membrane-bound organelle specialised for fertilisation (Fuller 1993; Fabian and Brill 2012). Within the nucleus, a dark, dense structure that lacks a nucleolus is also established, the so-called “protein body” – although its composition and function are still unknown, it serves as a good developmental marker of early, pre-elongation spermatid cysts (Fuller 1993; Fabian and Brill 2012).

Each individual cell within the “onion-stage” cyst possesses its own single nucleus paired with a single spherical mitochondrial derivative (Fuller 1993). The volume and diameter of nuclei within these spermatids is proportional to the chromosome content it contains (González et al. 1989). Therefore, as long as the chromosomes have segregated correctly and undergone incomplete cytokinesis in the preceding stages of meiosis, each daughter spermatid will acquire the same amount of chromatin and mitochondria. Hence, there is a universal sizing of all nuclei and mitochondrial derivatives within round spermatids of the same cyst (Fuller 1993).

1.6.5. Elongation of spermatid cyst bundles

Spermatid elongation gives rise to interconnected bundles of 64 highly-polarised, needle-like cells that can grow to lengths of 1.8 mm and widths of ~ 1 μm – equating to a 150-fold increase in length and 5-fold increase in total surface area overall (Tokuyasu et al. 1972; Tokuyasu 1974a; Fabian and Brill 2012). This transformation from a round spermatid measuring ~15-μm in diameter into 1.8-mm-long mature motile sperm requires extensive cellular remodelling (White-Cooper 2004).

Elongation of the syncytial cyst is driven by the assembly of sperm flagellar axonemes within the spermatids, which develops as an extension of the basal body (Noguchi and Miller 2003). The axoneme comprises nine outer-doublet microtubules which encase a central pair of singlet microtubules, all of which are covered by a double membrane derivative of the endoplasmic reticulum termed the axonemal sheath (Tokuyasu 1974a; Lindsley 1980; Fuller 1993). The mitochondrial derivatives unfold and elongate in synchrony with the growing axoneme, extending the entire length of the spermatid tail (Fuller 1993). Flagellar cytoplasmic microtubules also develop in a uniform and evenly spaced pattern. These run parallel to the long axis of the mitochondrial derivatives and are thought to support their elongation throughout the spermatid tails (Tokuyasu 1974a).

As the mitochondrial derivatives continue to elongate alongside the axoneme, they start to resemble leaf blades. At an intermediatory point of elongation (“the comet stage”), the nuclear-located protein body disappears and the mitochondrial derivatives separate to form the major and minor mitochondrial derivatives (Fuller 1993). Both share an angular relationship with the plane of the central microtubule pair in the axoneme, which varies somewhat as spermatid elongation progresses. However, generally speaking, the major mitochondrial derivative lies at an angle of between 60˚ and 90˚ from the plane, whereas the minor mitochondrial derivative subtends at an a ~30˚ angle relative to the plane (Tokuyasu 1974a). Apart from in the very early phase of spermatid elongation, these mitochondrial derivatives are radially arranged in relation to the axoneme centre (Tokuyasu 1974a). As elongation and axoneme development concludes, dense central fibres are deposited in the accessory microtubules of the axoneme. At the same time, the rounded spermatid nuclei also elongate to form long, thin hook-shaped needles (Tokuyasu 1974b; Fuller 1993).

Indeed, spermatid elongation is accompanied by extraordinary changes in nuclear shape. The nuclei become flattened on one side, driving a morphological transformation into a concave shape; the cavity of which is filled with the deposition of perinuclear microtubules in parallel to the long axis of the nucleus. These, along with an array of microtubules which develop on the convex side of the nucleus, support nuclear elongation and remain until the concave cleft is lost (Tokuyasu 1974b; Fuller 1993). Nuclear shaping concludes as the chromatin undergoes hypercondensation via a distinct histone-to-protamine reconfiguration that is driven by a specific set of transition proteins (Jayaramaiah Raja and Renkawitz-Pohl 2005; Rathke et al. 2007). Nuclear volume is also reduced via the caudal budding off of the envelope and nucleoplasm. Paracrystalline material saturates the major mitochondrial derivative as it gradually swings round, making contact to reduce the size of the minor mitochondrial derivative. The accompanying flagellar cytoplasmic microtubules disappear just before the start of individualisation (Tokuyasu 1974a; Fuller 1993). Together, this remarkable combination of morphogenetic events generates a cyst bundle of 64 elongated spermatids that extends the length of the testis.

1.6.6. Head-tail alignment, spermatid individualisation and spermatozoa generation

Further development and polarisation occurs in synchrony within the elongated spermatid cyst bundles. Enveloping cyst cells arrange themselves asymmetrically to orient the spermatids appropriately within the testis, ready for individualisation and coiling. The asymmetric cyst cells organise intentionally so that the elongating tails extend apically while the heads lie basally within the testis (White-Cooper 2004,2010). These spermatid heads equate to around 10 μm of the total elongated length of the cells (Tokuyasu 1974a). The “head” cyst cell is associated with this region containing the nuclei, whereas the “tail” cyst cell remains in intimate contact with the tail-end portion of the polarised spermatid bundle (Lindsley 1980).

Spermatid individualisation begins at the head region of the cells as actin-based investment cones start to assemble as a complex around the condensed nuclei (Tokuyasu et al. 1972; Fabrizio et al. 1998; White-Cooper 2004). This individualisation

complex is then displaced from the nuclei, and it goes on to drive coordinated individualisation throughout the full length of the spermatid cyst bundle (White-Cooper 2004). As individualisation proceeds, it eliminates the syncytial cytoplasmic connections which bridge the spermatids, while also ridding the cells of unwanted organelles and excess nuclear membrane, nucleoplasm and cytoplasm. The remaining volume of the minor mitochondrial derivative is also reduced further (Tokuyasu et al. 1972). As a consequence, each individual spermatozoa becomes highly invested in its own plasma membrane. Individualisation propagates as an enlarged cystic bulge that traverses along the spermatids, increasing in size as it accumulates waste. As the cystic bulge is detached in waste bags from the caudal tail-ends of the spermatid cyst bundles, it's degraded contents of redundant and leftover components are collected and discarded from the testis (Tokuyasu et al. 1972; Fuller 1993).

Upon completion of individualisation, the resultant sperm bundles coil down to the base of the testis. This is due to the head cyst cell becoming entrapped within the terminal epithelium, which provides a basal anchoring site from which coiling is initiated (Tokuyasu et al. 1972; Lindsley 1980). The tail cyst cell breaks down around the sperm tails as they coil (Fuller 1993). The cyst cells and waste bag are disposed of via phagocytosis by the terminal epithelial cells. Once coiled, these mature, individualised spermatozoa pass into the testis lumen and then on into the seminal vesicles, ready for copulation (Tokuyasu et al. 1972).

1.7. The *Drosophila* testis is an archetypal model organ

As germline cells are the only cell type that transmit genomic information generationally, the production of healthy gametes – including sperm cells – preserves the continuity of evolutionary lineages across evolutionary time (Kitaoka and Yamashita 2024). Moreover, an ever-increasing body of research argues that male-biased genes associated with spermatogenesis and reproduction show the highest rates of divergence and evolution overall (Civetta and Singh 1995; Meiklejohn et al. 2003; Torgerson and Singh 2004; Zhang et al. 2004; Richards et al. 2005).

An analysis of single nucleus RNA-seq (scRNA-seq) data from adult *Drosophila* tissues suggests that the high number of tissue-specific genes expressed in the testis are subject to some of the strongest selection pressures of all fly tissue types (Li et al. 2022). Due to these strong selection pressures, the testis is deemed to be the most rapidly-evolving organ of any organism at both the genomic and molecular level (Kaessmann 2010). Previous reports reinforce this evidence of a strong evolutionary drive within the testis, which favours the development and expression of novel genes, and suggests that many of these young *de novo* genes tend to be testis-biased (male-biased) (Levine et al. 2006; Witt et al. 2019). The *Drosophila* testis itself therefore provides an excellent archetypal model organ for the investigation of gene evolution, divergence and diversification *in vivo*. We can also use it as a canonical system to study the fast-paced evolution of reproductive traits, including how tissues such as the testes adapt to specialise for function (Torgerson and Singh 2004).

Moreover, the “rules” of differentiation, from gonial precursor cells to motile spermatozoa, are not limited to sperm development alone and can be applied to the study and genetic analysis of other biological processes in other systems (Noguchi and Miller 2003). The well-defined niche of the testis apical hub, from which spermatogenesis is commenced, also provides a good model for the study of stem cell identity and the mechanistic interplay of the niche microenvironment which supports cell “stemness” (Kawamoto et al. 2008). However, sperm development in *Drosophila* does bear one substantial difference to its mammalian counterpart; it relies on two distinct adult stem cell lineages. Together, within a well-defined niche, these lineages co-differentiate into intimately associated subpopulations of germ cells and somatic support cells, respectively (Fuller 1998).

1.8. There are striking differences in *Drosophila* sperm characteristics

There is an incredible and dramatic variation in sperm characteristics that is exhibited throughout the *Drosophila* species. On first consideration, the 1.8 mm lengths of *Drosophila melanogaster* sperm appear to be giant when equated to the size of human

sperm (Fig. 2.). Such a length makes it approximately three-hundred times longer than mature human sperm, when normalised to host organism size (Pitnick et al. 1995).

Sperm gigantism is common in *Drosophilidae family*, with *D. pachea* and *D. hydei* producing sperm that grow up to roughly 16 mm and 23 mm long, respectively (Pitnick 1993; Pitnick and Markow 1994). However, the truly giant sperm of *D. bifurca* is the longest known sperm in the animal kingdom – it measures an average of 58 mm in length and is twenty times larger than the actual fly itself (Joly et al. 1995; Pitnick et al. 1995).

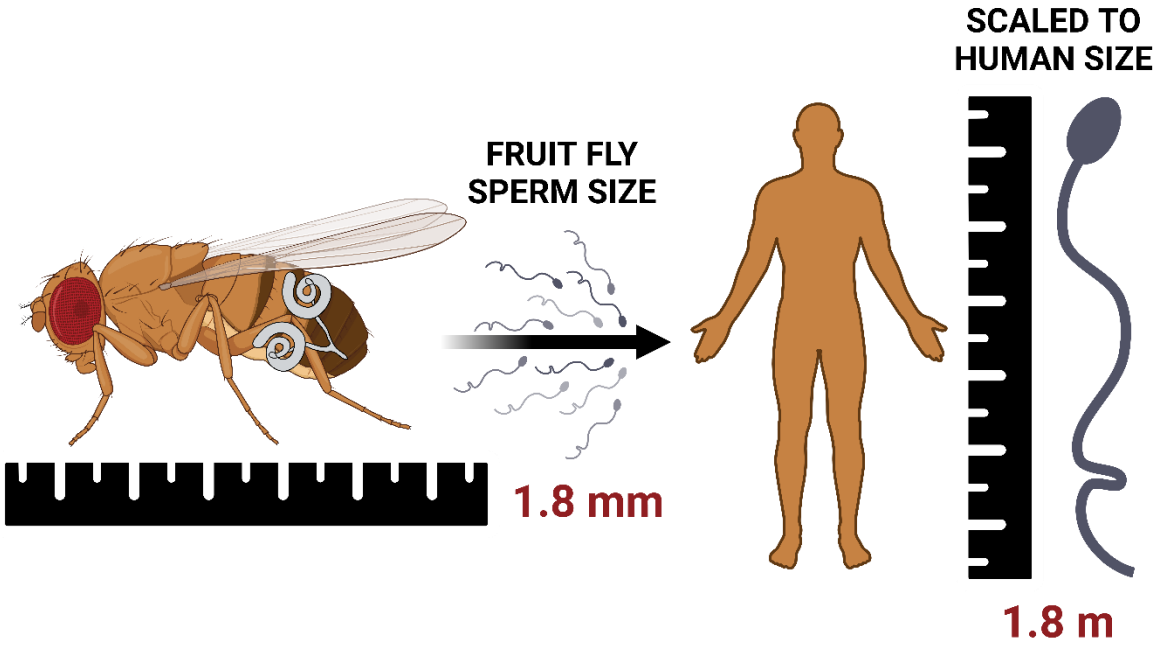

Figure 2. Direct comparison of spermatozoa produced by *Drosophila melanogaster* when scaled up in size to the equivalent of a human sperm cell. Mature fruit fly sperm can reach lengths of up to 1.8 mm when fully elongated (Tokuyasu et al. 1972; Tokuyasu 1974a; Fabian and Brill 2012). It therefore requires a testis that can accommodate the development of such long specialised cells. In fact, the full size and length of *Drosophila melanogaster* testes equates to ~5% of a male's total dry body mass (Pitnick et al. 1995). **Created using BioRender.com.**

This makes mature *D. bifurca* sperm at least two-and-a-half times longer than that of its *D. hydei* counterpart (Pitnick et al. 1995). The male reproductive tract of *D. bifurca* is equally as long and large to accommodate the developing sperm; measuring up to 69 mm in sexually mature adults and occupying over half of their abdominal cavities (Joly et al. 1995).

Moreover, males of some *Drosophila* species can generate multiple types of sperm in two or more distinct size classes, termed “sperm heteromorphism” – not all forms of which are fertilising (Joly et al. 1989; Joly and Lachaise 1994; Snook 1997; Alpern et al. 2019).

1.9. Post-meiotic transcription and localisation of comet and cup mRNA transcripts in *Drosophila* spermatids

As mentioned previously in Section 1.6.2., the main bulk of spermatogenesis-specific transcription occurs pre-meiotically and, until the mid-90s, there was limited evidence of transcription after meiosis in *Drosophila* spermatids (Olivieri and Olivieri 1965; Gould-Somero and Holland 1974; Schäfer et al. 1995).

Based on this original hypothesis, the entire developmental programme of spermiogenesis – including the dramatic structural and morphological changes that drive maturation of post-meiotic spermatids – relies heavily on the mass transcription that occurs early in primary spermatocytes alone. For a delayed execution of this scale, all mRNAs encoding proteins required in in late sperm development must be stored in a uniform, repressed state within cytoplasmic ribonucleoprotein (RNP) complexes to prevent premature and ectopic translation at the wrong cell stages (Schäfer et al. 1990; Schäfer et al. 1995). This period of silencing, occurring between pre-meiotic transcription in the primary spermatocytes and post-meiotic translation in late sperm development, is gene dependent (Kuhn et al. 1988).

1.9.1. Early studies of transcription in the developing *Drosophila* sperm cells

1.9.1.1. Characterisation of testis-specific *Mst(3)CGP* gene expression

For genes such as *Mst87F/mst(3)gl-9*), this translational delay can take place for at least three days (Kuhn et al. 1988). *Mst87F* is member of the *Mst(3)CGP* gene family, which is made up of seven *Mst(3)CGP* genes in total. These genes encode a set of important male-specific mRNAs that accumulate exclusively within the male germline of the testis and are subsequently translated into structural proteins of the sperm tail (Schäfer 1986; Kuhn et al. 1988). In fact, RNA samples extracted from male flies without germ cells are completely devoid of *Mst(3)CGP*-specific mRNA transcripts altogether (Kuhn et al. 1991). All gene members are located on the third chromosome in *Drosophila* and were identified by successive cloning, screening and mutagenesis experiments – including P element-mediated transformation (Schäfer 1986; Kuhn et al. 1988; Schäfer 1990; Kuhn et al. 1991; Schäfer 1993).

Through extensive characterisation of the *Mst(3)CGP* gene family, it was evidenced that their expression is tightly regulated at a post-transcriptional level to coordinate the spatiotemporal delay between their transcription and translation during sperm development. While their gene products accumulate via spermatocyte-specific transcription, they remain silenced until spermiogenesis, when they undergo spermatid-specific translation (Kuhn et al. 1988; Schäfer et al. 1990). Mutagenesis of their *cis*-acting sequences was therefore associated with ectopic, pre-meiotic translation, while male sterility experiments – that halted spermiogenesis prior to individualisation – resulted in a complete loss of normal post-meiotic translation (Kuhn et al. 1988; Schäfer et al. 1993). Moreover, homozygous deletion of the *Mst84Da*, *Mst84Db*, *Mst84Dc* and *Mst84Dd* gene cluster was found to correspond to the production of fewer motile sperm overall, likely driven by a combination of early axoneme malformations at an ultrastructural level (Kuhn et al. 1991).

In the case of *Mst87F*, mRNA transcripts accumulate pre-meiotically and are stabilised via *cis*-acting signals located in their 5’ UTR until the completion of spermatid elongation. Translation into the sperm flagellum structural protein of Mst87F is

therefore repressed until the spermatids are fully elongated (Kuhn et al. 1988). This mechanism of translational regulation was also investigated in two other members of the *Mst(3)CGP* gene family, *Mst98Ca* and *Mst98Cb* (Schäfer et al. 1993). In male sterile mutants with impaired individualisation, expression of the *Mst98Ca* and *Mst98Cb* proteins was also impaired at the translational level – thus suggesting translational repression of both Mst98C transcripts until the end of sperm development. *Mst98Ca* and *Mst98Cb* transcripts were found to have particularly long half-lives as the synthesis of their proteins did not occur in the early diploid stages, but was instead detected throughout the tails of elongating spermatids (Schäfer et al. 1993).

Members of the sperm flagellum-specific *Mst(3)CGP* gene family were subsequently found to contain a conserved twelve nucleotide (ACATCNAAATTT) translational control element within their 5' UTRs. This *cis*-acting sequence performs a dual function in the negative translational control and secondary polyadenylation of *Mst(3)CGP* mRNA transcripts (Schäfer et al. 1990). Upon deletion or modification of this region via *in vitro* mutagenesis, the translational control mechanism for *Mst87F* mRNA was lost. Moreover, the length of its poly(A) tail was found to increase and become more heterogeneous when *Mst87F* mRNA was recruited for translation in the cytoplasm. Upon translational recruitment, the length of its poly(A) tail rose from 140 nucleotides to 380 nucleotides. However, in mutant conditions where ectopic premeiotic transcription had occurred, the length of poly(A) tail remained unaltered. Hence, the concomitant rise in cytoplasmic polyadenylation functionally correlated with translational control, suggesting that poly(A) lengthening was also a direct result of the conserved regulatory element in its 5' UTR (Schäfer et al. 1990). Taken together, this supported a stable period of transcriptional dormancy instigated prior to meiosis I and meiosis II.

1.9.1.2. Historical autoradiography and transcriptional inhibition experiments

Olivieri and Olivieri (1965) were first to argue that transcription was restricted to the diploid stages of *Drosophila* sperm development. By utilising the radioactive precursor

of ^{3}H-uridine, they proposed that the latest mature stage at which uridine incorporation, and hence transcription, occurs is in the primary spermatocytes. Using this method of detection, Olivieri and Olivieri (1965) showed that transcription took place continuously within the spermatogonia and young spermatocytes, mainly in the nuclei. No radioisotope labelling was observed indicative of transcriptional activity within the post-meiotic cell types. ^{3}H-uridine incorporation was, however, visualised in some of the non-germline components of the testis, including the sheath cells, cyst cells, terminal epithelium cells and cells of the seminal vesicle wall. Altogether, they concluded that transcription ceases before the germline cells enter into their meiotic divisions, and that this loss of transcriptional activity is not essential for successful spermiogenesis – likely due to pre-meiotically transcribed RNAs persisting in the cytoplasm of spermatids and sperm.

Other early autoradiographic and inhibition studies by Gould-Somero and Holland (1974) strengthened this notion. After culturing *D. melanogaster* testes *in vitro*, ^{3}H-uridine and ^{3}H-leucine were added to monitor transcription and translation, respectively. Under the same premise as Olivieri and Olivieri (1965), autoradiograms of fixed testes showed ^{3}H-uridine incorporation only in regions containing the spermatogonia, primary spermatocytes, terminal epithelium and sheath cells. Post-meiotic cells, including the round and elongating spermatids, remained unlabelled. Thus, these results once again confirmed that transcription dominates within the early, pre-meiotic male germline cells, but not within the late stages of sperm development.

Additionally, transcriptional inhibition was performed alongside radioactive labelling to determine what effects, if any, there would be on spermiogenesis and the post-meiotic differentiation of spermatids (Gould-Somero and Holland 1974). When treated with Cordycepin (3'-deoxyadenosine), primary spermatocytes were still able to differentiate into elongating spermatids, but some adverse effects were observed in highly transcriptionally active cells like the early spermatocytes. ^{3}H-leucine incorporation indicated sustained translational activity in both late primary spermatocytes and spermatids, despite the elimination of transcription. They therefore concluded that most, if not all, of the RNA necessary for the sperm differentiation and elongation is transcribed within primary spermatocytes, before it is actually required. Then, translation proceeds, as and when it is needed (Gould-Somero and Holland 1974).

However, due to the limits of resolution and assay sensitivity, any small-scale spikes in transcription were unlikely to be detected via the autoradiographic methods used by Olivieri and Olivieri (1965) and Gould-Somero and Holland (1974). This is especially the case when RNAs are only synthesised for a relatively short-lived phase of spermiogenesis – which is something I will cover later in this section. Moreover, the culturing procedure employed by Gould-Somero and Holland (1974) did not allow for visualisation of spermatid individualisation and the maturation of motile, coiling sperm. Therefore, they were unable to make any well-defined conclusions about the extended effects of transcriptional interference on final-stage sperm production.

1.9.2. Recent research developments substantiate post-meiotic gene expression in the male germline

Together, this led to a switch in the narrative in 1991. Despite the literature at this time suggesting transcriptional inactivity after meiosis, Bendena et al. (1991) showed that *hsr-omega* RNA transcripts were transcribed later in sperm development. When using a radioactive RNA *in situ* hybridisation assay (RNA-ISH), *hsr-omega* RNAs were specifically detected within the differentiating spermatid stages. Unsurprisingly, the *hsr-omega* locus was also heat-shock inducible within these developing spermatids. Yet, constitutive transcription of the *hsr-omega* heat-shock gene did not occur within the primary spermatocytes, suggesting that expression of *hsr-omega* was specific to the post-meiotic stages. However, issues with reproducibility have since called these findings into question, and further research into the incidence of post-meiotic transcription during *Drosophila* spermiogenesis was lacking until 2008 (Barreau et al. 2008a).

While follow-up work failed to reproduce the findings of Bendena et al. (1991), it still provided fresh evidence supporting post-meiotic gene expression in the late developing sperm cell population of the *Drosophila* testis. Colorimetric RNA-ISH assays were followed-up by highly sensitive single cyst quantitative RT-PCR screening (qRT-PCR), which in turn demonstrated definitive evidence of post-meiotic expression for twenty-four key protein coding genes (Table 1.) (Barreau et al. 2008a; Barreau et al. 2008b).

Table 1. List of twenty-four comet and cup genes that are post-meiotically expressed and asymmetrically localised in *Drosophila* sperm development, as characterised by qRT-PCR and RNA-ISH experiments. Includes gene names, symbols and associated CG identifiers. **Recreated from Barreau et al. (2008a).**

POST-MEIOTIC GENE	SYMBOL (ABBREVIATION)	CG NUMBER	CLASSIFICATION BASED ON LOCALISATION PATTERN
schumacher-levy	*schuy*	CG17736	**COMET**
hale-bopp	*hale*	CG7570	
sungrazer	*sunz*	CG15179	
solwind	*sowi*	CG15178	
borrelly	*boly*	CG30362	
comas sola	*cola*	CG30363	
hug-bell	*hubl*	CG30364	
spacewatch	*spaw*	CG30365	
whipple	*whip*	CG34218	
swift-tuttle	*swif*	CG30366	
scotti	*soti*	CG8489	
phosphoglyceromutase 87 / phosphoglycerate mutase 2	*pglym87 / pgam2*	CG17645	
calcutta-cup	*c-cup*	CG15623	**CUP**
walker-cup	*wa-cup*	CG10113	
ryder-cup	*r-cup*	CG10998	
davis-cup	*d-cup*	CG14387	
presidents-cup	*p-cup*	CG12993	
world-cup	*w-cup*	CG7363	
stanley-cup	*s-cup*	CG30044	
tetleys-cup	*t-cup*	CG31858	
flyers-cup	*f-cup*	CG9611	
heineken-cup	*h-cup*	CG6130	
mann-cup	*m-cup*	CG11896	
oo18 RNA-binding protein	*orb*	CG10868	

In the *Drosophila* genome, the loci of these twenty-four genes was varied, with some located in two specific gene duplication clusters, while others were scattered throughout the genome as either single copy genes or un-clustered duplicated genes. Low-level transcription of an exclusive subset of mRNA products, encoded by this small number of genes, was detected initially in primary spermatocytes before a sudden disappearance and spiked re-activation in elongating spermatids at a point preceding the histone–transition protein–protamine switch (Barreau et al. 2008a; Barreau et al. 2008b).The initiation of post-meiotic transcription was pinpointed to just before the deposition of transition protein, when the chromatin was still nucleosomal (Barreau et al. 2008a; Barreau et al. 2008b).

Most intriguingly, Barreau and colleagues found that these post-meiotic mRNAs all undergo asymmetric subcellular localisation to the extreme distal tail-ends of the growing spermatid cyst bundles. Here, they accumulate in one of two localisation patterns; with twelve mRNA transcripts arranging as speckled, shooting “comets” while the remaining twelve arrange in U-shaped, acorn “cups” (Fig. 3.) (Barreau et al. 2008a; Barreau et al. 2008b). Characterisation of these localisation patterns hence gave rise to their respective gene designations, with them in turn being classified as post-meiotic comet and cup genes. These localisation patterns were, however, only identifiable during the discrete, mid-to-latter stages of spermatid elongation. No robust signals for comet and cup transcripts were detected in early elongation. The expression of some comet and cup mRNAs did persist after histone-to-protamine remodelling, but signals somewhat declined upon protamine deposition (Barreau et al. 2008a; Barreau et al. 2008b). This was because, upon initiation of the histone-to-protamine transition, the elimination of histones results in a return to complete transcriptional inactivation. Post-meiotic elongating spermatids lose their canonical chromatin-based transcriptional responses once again, uncoupling transcription and translation for a second time during sperm development (Kitaoka and Yamashita 2024).

Additional independent research has provided direct support of these ground-breaking findings, including further evidence of post-meiotic RNA-polymerase II activity (Vibranovski et al. 2010). A global gene expression analysis of region-specific testis content also corroborated the enhanced expression profiles of *schuy* comet and *tetley-cup* genes in post-meiotic cell samples (Vibranovski et al. 2009).

Vibranovski et al. (2010) demonstrated *de novo* post-meiotic transcription of nascent RNAs by utilisation of 5-bromouridine (BrU) incorporation, labelling and signal visualisation. Strong levels of BrU incorporation were observed in isolated bundles of elongating spermatids, which could be eliminated upon the RNase-induced degradation of RNA and inhibition of RNA synthesis. Three-dimensional reconstructions of isolated BrU-expressing elongating spermatid bundles also validated the occurrence of periodic "waves" of post-meiotic transcriptional activity – with high-intensity BrU signals arising on either side of intervening signal-less areas. It was argued that this dynamic activity was a result of gene expression within the caudal spermatid nuclei before subsequent active transport of RNAs down the spermatid bundle towards the distal tail-ends (Vibranovski et al. 2010).

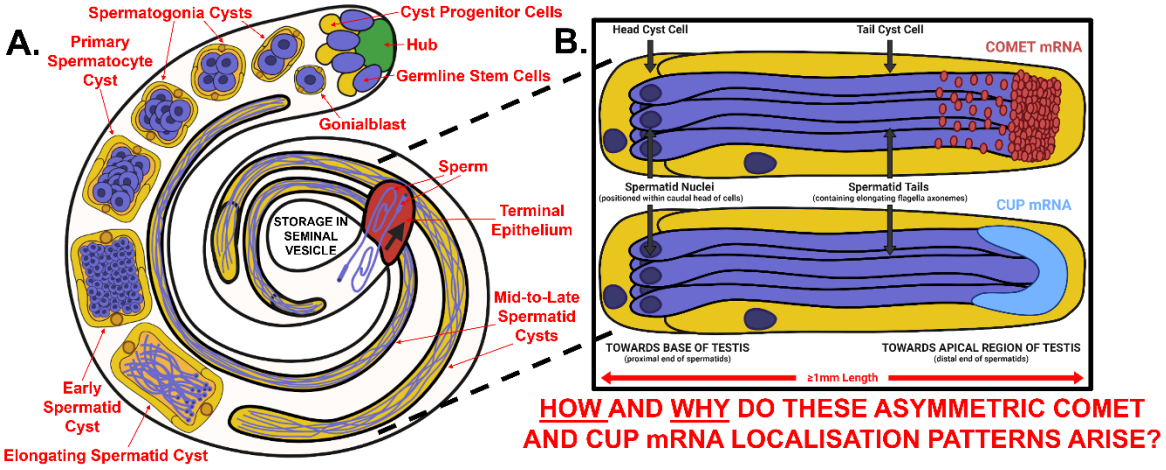

Figure 3. Annotated illustration of sperm development and post-meiotic mRNA localisation in *Drosophila melanogaster* testes. (A) Model of the testis structure, demonstrating the spatiotemporal assay of developing sperm cells. As the cells differentiate, displacement occurs away from the testis stem cell niche at the apex of the testis and continues down the full length of the testis until the release of mature, coiling spermatozoa. (B) Growing spermatid cyst bundles, exhibiting the asymmetrical, subcellular localisation patterns of comet and cup mRNA transcripts**.** These distinctive non-uniform comet mRNA (red speckles) and cup mRNA (blue U-shape) distributions localise specifically to the extreme apical ends of mid-to-late elongating spermatid tails. **Re-created from Barreau et al. (2008a), Raz et al. (2023) and Messer (2022) using BioRender.com.**

More recent support for post-meiotic transcription within mid-to-late elongation stage spermatids was published in the 2022 Fly Cell Atlas (FCA) study, after trajectory analysis was performed on the individual testis cell lineages (Li et al. 2022; Raz et al. 2023). Trajectory inferences on the separate testis subsets of spermatocytes and spermatids showed distinct differences in their transcriptomic profiles when analysed over pseudotime. In line with previous expectations, the spermatocyte pool showed a continuous rise in the number of genes undergoing transcription, including several differentially expressed genes that were strongly upregulated yet not identified in any other cell type. Late primary spermatocytes did, however, show low level expression of non-germline-specific marker genes. A very low number of nuclear transcripts were detected in early spermatids, as represented via a lack of unique molecular identifiers (UMIs), which confirmed transcriptional quiescence at this stage. However, as predicted, this was swiftly followed by a spike in new transcriptional activity in elongating spermatids, including the annotation of numerous cup genes. Single cell RNA-Sequencing (ScRNA-Seq) of the mid-to-late elongating spermatid subsets also revealed the expression of at least 152 differential post-meiotically transcribed genes – hence indicating the existence of many more potential comet and cup mRNA transcripts requiring additional characterisation (Li et al. 2022; Raz et al. 2023).

However, with the exception of large-scale transcriptomic analyses, very little follow-up research has been attempted to explain this unusual biological phenomenon that was discovered more than a decade ago. While the spatiotemporal profiles of comet and cup mRNA localisation are now known, the same question remains unanswered: what is the mechanistic driving force of this remarkable localisation event and why is it required?

1.10. What is asymmetrical, subcellular RNA localisation?

Post-transcriptional localisation of RNAs is an important biological mechanism that provides an essential regulatory checkpoint in cells, systems and whole living organisms. RNA localisation enables cells to control and compartmentalise protein function in space and time by predefining their sites of synthesis (Du et al. 2007). In

Drosophila, RNA localisation is a very frequent phenomenon. In fact, 71% of 2314 mRNA transcripts expressed during the early developmental stages of *Drosophila* embryogenesis have been shown to undergo some degree of subcellular localisation (Lécuyer et al. 2007).

The establishment of cell-specific polarisation, differentiation and architectural events all rely upon the spatiotemporal pinpoint accuracy of RNA transport and distribution (Lécuyer et al. 2007). Numerous functional studies have validated the mechanism of localised translation of asymmetrically enriched mRNAs in differentiated cells, which facilitates the assembly of functionally distinct compartments. This is also employed at the higher level of developing organisms to ensure the strict partition of cell fate determinants, and hence the correct establishment of body axis patterning (Reviewed in St Johnston 2005 and Du et al. 2007).

RNA localisation has been extensively investigated in many different cell types, such as oocytes, fibroblasts, epithelial cells, neurons, and glial cells like oligodendrocytes (Lipshitz and Smibert 2000). It is an evolutionarily-ancient process, which has not only been documented in higher eukaryotes but also in yeast (Long et al. 1997; Gonsalvez et al. 2005), bacteria (Keiler 2011), molluscs (Lambert and Nagy 2002; Kingsley et al. 2007) and plants (Crofts et al. 2005), to name just a few. Growing evidence suggests that RNA localisation is an evolutionarily conserved mechanism, acquired to de-centralise genomic information and distribute regulatory control “remotely” to the wider subcellular compartments (Holt and Schuman 2013; Jung et al. 2014).

1.10.1. RNA localisation regulates downstream protein expression and function

Multiple cycles of protein synthesis can be initiated from each localised mRNA at an exact location, which prevents ectopic expression and toxicity while reducing the metabolic energy consumption associated with post-translational transport (Jansen 2001). The localisation of mRNAs is therefore much more energetically favourable and cost-efficient compared to the localisation of proteins, since many proteins can be transcribed from one single mRNA transcript, cutting transportation costs to the cell (Du et al. 2007). Additionally, many localised mRNAs encode protein products that do

not have their own sorting signal. The subcellular distribution of these proteins is therefore completely dependent on the localisation of their transcripts prior to translation (St Johnston 2005).

RNA localisation guarantees that newly-synthesised proteins are directed immediately to their site of action, which helps to regulate protein concentrations more quickly and efficiently in response to a signal or stimulus (Gallagher and Ramos 2018). Local protein synthesis by these means ensures a rapid and dynamic turnover of the proteome, as and when it is needed. Moreover, research suggests that proteins synthesised after the post-transcriptional localisation of their mRNAs are structurally and functionally dissimilar to their post-translationally transported protein counterparts (Weatheritt et al. 2014). Locally translated proteins are instead subject to more post-translational modifications overall and show a higher tendency to contain domains that drive protein-protein interactions. Together, these features instil an additional layer of regulatory control, and onsite translation counteracts potential off-target promiscuity by spatiotemporally restricting protein interaction fidelity (Weatheritt et al. 2014).

1.11. RNA binding proteins (RBPs) and ribonucleoprotein (RNP) complexes modulate active transport of localising RNAs

Whether an mRNA is destined to undergo localisation or not is mainly defined by the 3’ untranslated region (UTR), which dictates nuclear export, as well as many other aspects of mRNA metabolism (Andreassi and Riccio 2009). Asymmetrical mRNA localisation by RNA binding proteins (RBPs) is, for the most part, determined by specific, evolutionarily-conserved *cis*-acting regulatory elements located within the 3’ UTR – however, there are incidences of these “localisation elements” arising elsewhere, including in the 5’ UTR or coding sequence of transcripts (Kislauskis and Singer 1992; Martin and Ephrussi 2009). Although, the nuclear history of a localising mRNA is also said to play a crucial role in the determination of its cytoplasmic fate, and the dynamics of nuclear export can be a limiting factor for mRNA metabolism and lifespan once in the cytoplasm (Hachet and Ephrussi 2004; Giorgi and Moore 2007; Müller et al. 2024).

The identification of consensus sequences and secondary structures that make-up RNA localisation elements in putative targets of ZBP1 and Staufen have demonstrated that RBPs can bind and regulate hundreds of potential mRNA transcripts with high specificity (Patel et al. 2012; Laver et al. 2013). The recognition and binding of these target RNA sequences and/or secondary structures by RBPs is fundamental for many aspects of RNA function. For example, at the level of gene expression, RBP:mRNA binding in the nucleus can mediate transcript processing, splicing and nucleocytoplasmic export. Cytoplasmic RBP activity, in contrast, is needed for translational regulation. RBPs in the cytoplasm are involved in many post-transcriptional control events, including subcellular localisation, translational silencing and activation, and at various checkpoints of mRNA stabilisation, protection and decay (Reveal et al. 2011). RBPs are therefore master regulators of the mRNA life cycle.

After nuclear export into the cytoplasm, regulated RNA transcripts can associate with many different protein factors and be subjected to a variety of transport mechanisms. One main mode of interest is active transport, which involves the interaction of *trans*-acting RBPs and introduction into nonmembrane-bound RNP complexes (Weber and Brangwynne 2012). RBPs can recognise specific sequences and/or structural features within target RNAs to form direct binding interactions, or indirect associations via linker and adaptor proteins (Medioni et al. 2012; Chin and Lécuyer 2017). RBPs often bind to multiple short stretches within the target mRNA transcript with relatively weak binding affinities; together, these weak interactions work in combination to increase overall RBP:mRNA binding affinities and specificities (Lunde et al. 2007).

RBPs also engage with other components such as translation machinery, cytoskeletal tracks and molecular motor proteins to direct passage throughout the cell via the cytoskeleton. RNAs can then be retained by anchoring at their final destination (Fig. 4.) (Wilkie and Davis 2001; Weil et al. 2006). Together, this generates a complex that can translationally repress transcripts and protect them from decay – enabling undisturbed localised protein production (Besse and Ephrussi 2008; Medioni et al. 2012; Gallagher and Ramos 2018).

RNP complexes can vary in size and configuration. Remodelling of RNP complexes is performed continuously as they undergo long-range transit throughout the cell (Mhlanga et al. 2009). The composition of localising RNP complexes is therefore

extremely complex and dynamic; containing a heterogeneous co-assembly of multiple mRNA molecules and different mRNA species, alongside a manifold of RBPs and other co-factors that are constantly subject to exchange depending on regulatory demands and complex type/function (Elvira et al. 2006; Lange et al. 2008; Fritzsche et al. 2013). Because of this, mRNA:mRNA interactions can be just as important as RBP:mRNA interactions, with oligomerisation between co-localising mRNA molecules contributing to the formation, stability and maintenance of large RNP structures (Ferrandon et al. 1997).

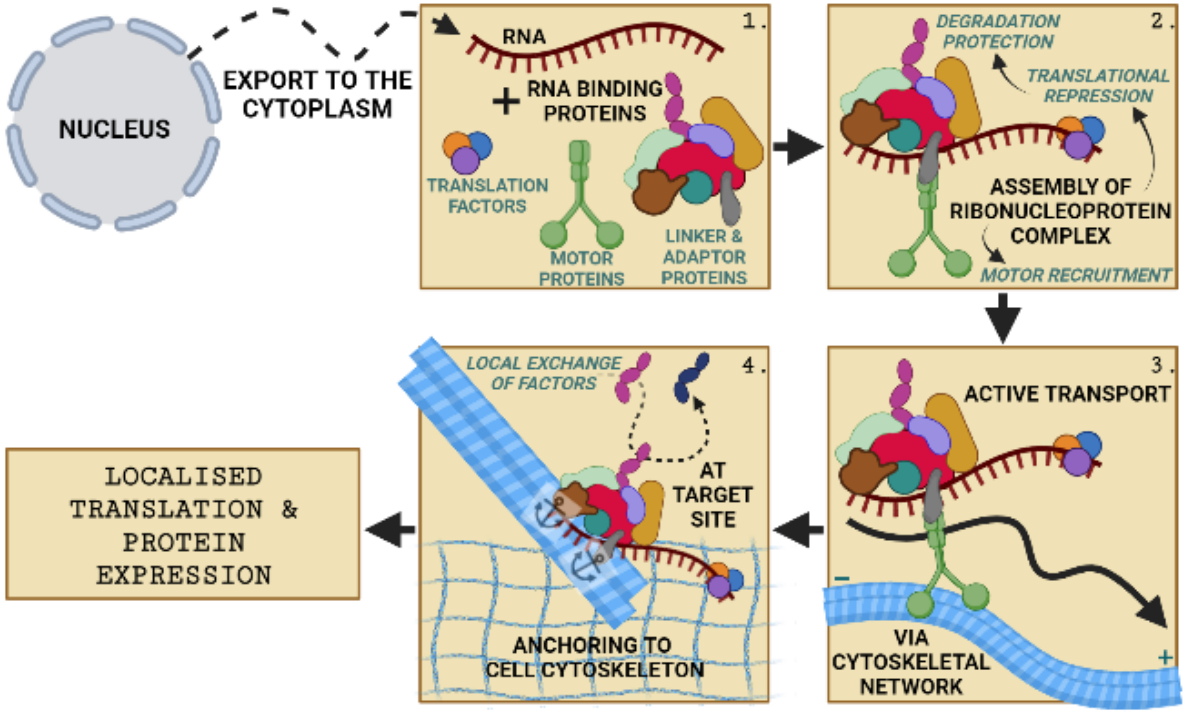

Figure 4. Diagram summarising the RBP-regulated active transport of RNAs after nucleocytoplasmic export. Localised transport of target RNAs require the contribution of multiple proteins and co-factors to enable passage throughout the cell via the cytoskeletal network. RBP-mediated segregation of RNAs can take place in many different cell types, including oocytes, fibroblasts, epithelial cells, neurons, and glial cells such as oligodendrocytes (Lipshitz and Smibert 2000). **Adapted from Parton et al. (2014b) using BioRender.com.**

Active transport-dependent mRNA localisation within RNP complexes therefore relies on the precise interaction of mRNAs with an ever-changing combination of RBPs, RNA species, motors and adaptors (Buxbaum et al. 2015). RBPs coordinate various aspects of this mRNA-specific binding during the localisation process, and reports suggest that increased RBP and motor protein binding correlates with an increase in processivity, run lengths and net travel distance along the cell cytoskeleton (Amrute-Nayak and Bullock 2012; Alami et al. 2014). The number of localisation elements within a single transcript can also relate to the number of motors that can be recruited for transit, and the interplay of adaptor proteins can have a substantial influence on transport properties, including motor processivity during the localisation of mRNAs (Amrute-Nayak and Bullock 2012; McKenney et al. 2014; Schlager et al. 2014).

1.11.1. Active transport facilitates the localisation of maternally derived mRNA determinants

The body morphogens, *bicoid (bcd)* and *gurken* (*grk*), undergo multi-step active transport in the *Drosophila* oocyte. The proper localisation of their mRNAs requires dual, interdependent cooperation of both dynein- and kinesin-mediated motor mechanisms of action (Brendza et al. 2002; Duncan and Warrior 2002; Januschke et al. 2002; MacDougall et al. 2003). In the latter stages of localisation, *bcd* mRNA is localised to the anterior pole of the oocyte along the microtubules, predominantly by action of the minus end-directed motor protein, dynein (Pokrywka and Stephenson 1991; Cha et al. 2001; Januschke et al. 2002). The interplay of other *trans*-acting factors, including the Exuperantia and Staufen proteins, also contribute to various stages of *bcd* localisation at the anterior cortex (Berleth et al. 1988; Johnston et al. 1989; Schnorrer et al. 2000).

Grk mRNA is localised to the anterodorsal corner of the oocyte via microtubule-directed transport, driven again by dynein motor activity (MacDougall et al. 2003; Cáceres and Nilson 2005; Clark et al. 2007; Delanoue et al. 2007). A whole multitude of interacting factors have been characterised in *grk* localisation complexes, including the Syncrip, Imp, Hrb27C and Squid proteins (Norvell et al. 1999; Goodrich et al. 2004; Geng and Macdonald 2006; McDermott et al. 2012). Multi-subunit cytoplasmic motors,

including dynein and kinesin, therefore operate in concert to establish intracellular polarity and biomolecular gradients; driving active transport of localising RBP:mRNA complexes via the cell cytoskeleton to opposing microtubule ends (Januschke et al. 2002).

All cellular functions of the molecular motor, dynein, rely on its interaction with the multiprotein dynactin complex (King and Schroer 2000; King et al. 2003). This dynein-dynactin complex can selectively modulate apical transport of localising mRNAs, including the *wg* mRNAs, pair-rule transcripts encoded by the *hairy* gene, and the axis determinants stated above, via its association with core components, Bicaudal D (BicD) and Eqalitarian (Egl) (Bullock and Ish-Horowicz 2001; Wilkie and Davis 2001; Bullock et al. 2003; Clark et al. 2007).

In *Drosophila* embryos, localising mRNAs have been shown to undertake bidirectional transport on microtubules, but it is the differential recruitment of the BicD-EgI-Dynein complex to target transcripts that mediates their minus-end-directed motility (Bullock et al. 2006). This preferential binding depends on the presence and dosage of the "right" *cis*-acting elements, which in turn regulate the frequency, velocity and duration of motor-modulated minus-end active transport. The relative cytoplasmic concentration of each individual transport protein can also selectively influence active transport properties, with BicD-EgI-Dynein-driven localisation of mRNAs being concentration dependent at the level of transport complex assembly (Bullock et al. 2006). Dynein also acts as an anchor protein in *Drosophila* embryogenesis by maintaining the apical localisation of target mRNAs at their final destination after microtubule-dependent, minus end-directed active transport (Delanoue and Davis 2005; Delanoue et al. 2007).

1.11.2. The assembly and dynamic composition of higher order RNP complexes improves localisation and translation efficiency

RNP complexes can co-assemble into larger, highly diverse conformations called RNP particles, RNP granules and RNP bodies – these terms can be used interchangeably, but usage typically depends on constituents and overall function (Weber and

Brangwynne 2012; Hubstenberger et al. 2013). The assembly of these large transport units is another method that improves the cost-effectiveness of subcellular mRNA localisation because the co-transportation and/or co-localisation of several mRNAs at once is more cost-efficient than transporting individual localising transcripts on their own (Lange et al. 2008). This transportation mechanism also facilitates the simultaneous and large-scale storage, repression and protection of mRNA transcripts; with some neuronal RNP granules even containing essential components for protein production that readies them for the instantaneous, stimuli-induced changeover from translational silencers to actively translating pools of localised biomolecules (Krichevsky and Kosik 2001; Kanai et al. 2004) The co-transportation of translational apparatus therefore facilitates an efficient switch to protein synthesis and assembly, which can be commenced immediately upon reaching the target site of localisation (Lange et al. 2008).

The uncoupling of transcription and translation is just vital as its coupling, and RNP structures also contribute to these mechanisms. Guo et al. (2022) has shown that dynamic changes in the 3’ poly(A) tail length of mRNAs contributes to this uncoupling action in developing male murine germline cells. Through microRNA-mediated deadenylation, the poly(A) tails of target mRNA transcripts can be shorted and, as a consequence, physically sequestered into RNP granules for translational repression and stabilisation. Upon re-polyadenylation, on the other hand, there may be a switch that favours the translocation of previously repressed mRNAs, transporting them out of the silencing RNP granules and to polysomes that drive simultaneous synthesis of multiple proteins (Guo et al. 2022). This is particularly important in elongating spermatids when nuclear condensation occurs and post-transcriptional uncoupling acts as an underlying regulatory mechanism to delay mass translation until it is needed in late spermiogenesis.

In some RNP assemblies, this switch in function is accompanied with a complementary change in state, termed liquid-liquid phase separation (LLPS) condensation. Under the collaborative control of repressors, kinases and helicases, among other factors, RNP structures can undergo a regulated phase transition between diffuse and condensed states, as well as highly orchestrated RNP exchanges (Li et al. 2012; Hubstenberger et al. 2013; Elbaum-Garfinkle et al. 2015). For example, cytoplasmic phase condensates such as processing bodies (P-bodies) have a dual,

context-dependent role in the sequestration and translational repression of mRNA reservoirs for protection and decay pathways. Stress granules, on the other hand, regulate the triaging, remodelling and translational reinitiation of mRNA transcripts after stress-induced translational arrest (Kedersha et al. 1999; Kedersha et al. 2000; Brangwynne et al. 2009; Aizer et al. 2014; Hubstenberger et al. 2017; Wang et al. 2018).

Modulation of reversible multivalent interaction kinetics between complexed biomolecules, including multimerization of RNAs, drives LLPS condensation in RNP particles (Li et al. 2012; Bevilacqua et al. 2022). The mRNAs themselves can also govern the biophysical properties and behaviours of these phase condensates, and local mRNA concentrations can act to buffer/inhibit LLPS condensation, when necessary (Zhang et al. 2015; Langdon Erin et al. 2018; Maharana et al. 2018; Garcia-Jove Navarro et al. 2019). LLPS condensation hence introduces an additional layer of post-transcriptional spatiotemporal mRNA control through expanded compartmentalisation and segregation.

1.12. Other mechanisms of subcellular RNA transport and localisation

RNA localisation can also be mediated by two less common and energy inefficient mechanisms: (i) by local stabilisation and regulated degradation or, (ii) via passive diffusion and local trapping (Martin and Ephrussi 2009). Typically, these mechanisms of RNA localisation are performed in parallel to achieve a shared goal in their target system, including in the successful establishment of the anteroposterior and dorsoventral body axes via localisation of cytoplasmic cell determinants during *Drosophila* oogenesis (Moore 2005). *Oskar* (*osk*) mRNA is localised to the posterior pole, in association with RBPs such as Staufen and Polypyrimidine tract-binding protein (dmPTB), via active transport along the microtubules by the plus end-directed motor protein, kinesin (Clark et al. 1994; Brendza et al. 2000; Palacios and Johnston 2002; Zimyanin et al. 2008; Besse et al. 2009). *Osk* is then anchored at its target site by its own gene product in cooperation with actin-binding proteins such as

Tropomyosin, Moesin and Bifocal (Erdélyi et al. 1995; Jankovics et al. 2002; Babu et al. 2004; Moore 2005).

Nanos mRNAs, despite also being posterior pole mRNAs, are instead localised in a translationally repressed state by a combination of diffusion, actin-dependent anchoring and regional stabilisation (Gavis and Lehmann 1992,1994; Gavis et al. 1996; Forrest and Gavis 2003). While rapid microtubule-dependent movements occur in the cytoplasm to aid translocation, site-specific actin-based entrapment captures target *nanos* mRNAs and maintains their asymmetrical subcellular localisation at the posterior pole (Forrest and Gavis 2003). However, facilitated diffusion and entrapment is not particularly efficient on its own, and so it is merged with a regulated protection/degradation mechanism to guarantee proper posterior-restricted activity of *nanos* (Bergsten and Gavis 1999; Martin and Ephrussi 2009). Only ~4% of total *nanos* mRNA is actually localised at the posterior pole; this pool of developmental transcripts is locally protected as they accumulate, while the remaining population of dispersed *nanos* is targeted for translational repression and degradation by the RBP, Smaug (Bergsten and Gavis 1999; Dahanukar et al. 1999; Smibert et al. 1999; Zaessinger et al. 2006). Upon association with the 3' UTR of unlocalised *nanos* mRNAs, Smaug directs their de-adenylation, destabilisation and decay to ensure that the concentration of posterior-localised *nanos* is over one hundred times greater than anywhere else in the oocyte (Zaessinger et al. 2006; Martin and Ephrussi 2009).

1.13. What functions does RNA localisation fulfil?

1.13.1. RNA localisation is important for the establishment of cell polarity and body patterning axes

RNA localisation underpins numerous developmental pathways in many different organisms and cell types (Lipshitz and Smibert 2000). This includes successful cell division, cell fate specification, directional cell movement, and even synaptic plasticity and memory (Lipshitz and Smibert 2000; Sardet et al. 2003; Condeelis and Singer 2005; Takatori et al. 2010). It can also dictate the architectural and morphological properties of a cell. An interesting example of this is the coordinated spatial

segregation of different Brain-Derived Neurotrophic Factor (BDNF) transcripts. The subcellular localisation and compartmentalisation of different BDNF splice variants, to either the cell body or the proximal and distal compartments of dendrites, results in differential shaping of these compartments to control the overall architecture of the cells (Baj et al. 2011).

Localisation of RNAs is instrumental for morphogen gradient formation in cells and tissues. By establishing an intracellular concentration gradient of morphogens, this can drive functions such as body plan patterning during embryogenesis (Christian 2012). One important instance of this is the *bcd* and *nanos* morphogens. In late *Drosophila* oogenesis, *bcd* and *nanos* mRNAs localize to opposite poles of the oocyte; *bcd* accumulates at the anterior pole via active transport while *nanos* amasses posteriorly via diffusion and entrapment (Fig. 5A.) (Forrest and Gavis 2003; Weil et al. 2006). In early embryogenesis – once egg activation and fertilisation has taken place – this asymmetric distribution of translated mRNAs enables opposing Bcd and Nanos protein gradients to be formed. At a protein level, this together facilitates stringent patterning of the anterior-posterior body axis in developing embryos (Driever and Nüsslein-Volhard 1988a,b; Gavis and Lehmann 1992).

A different germ cell determinant called *germ cell-less* (*gcl*) is responsible for primordial germ cell (PGC) formation and cell fate specification in the *Drosophila* embryo. However, to perform this function correctly, the *gcl* transcripts must be localised to the posterior pole of the egg cell during oogenesis. Loss of posterior-localised *gcl* mRNAs results in a “grandchildless” mutant phenotype, comprising sterile adult progeny which lack germ cells due to failed production of PGC precursors (Jongens et al. 1992). While the resultant progeny are infertile, adult flies appear viable and morphologically normal, with no developmental defects. This confirmed that *gcl* activity is only required for the early stages of germ cell lineage development, including for the initial formation of pole buds (Jongens et al. 1992; Robertson et al. 1999). The gcl protein product is concentrated within similar subcellular regions to *gcl* mRNAs, evidencing local translation following non-uniform mRNA accumulation. It then undergoes protein localisation to pores of the PGC nuclear envelope, which acts to promote the generation of PGCs after pole bud establishment by coordinating the spatial segregation of centrosomes (Jongens et al. 1992; Jongens et al. 1994; Robertson et al. 1999; Lerit et al. 2017). *Gcl* is therefore another prime example of a localised

developmental morphogen, but it is instead required to regulate a different aspect of development – to initiate the germ cell specification pathway and ensure proper germline cell formation.

1.13.2. RNA localisation is important for the determination of cell fates

The precise subcellular accumulation of localised mRNAs, and even whole organelles, can in turn modulate cell fates and lineages. One key example of this is in early neurogenesis, with the cell cycle-dependent localisation of *inscuteable* (*insc*) and *prospero* (*pros*) mRNAs that mediates asymmetric division of *Drosophila* neuroblasts. Both *insc* and *pros* localise to the apical and basal regions of the neuroblast cell cortex at specific stages of the cell cycle and encode proteins that are important determinants of cell fate in the developing central nervous system (CNS) (Doe et al. 1991; Hirata et al. 1995; Kraut and Campos-Ortega 1996; Kraut et al. 1996; Li et al. 1997). In addition to the strict control of protein localisation and apicobasal mitotic spindle orientation, *insc* drives the mitotic partition of *pros* mRNAs and Pros protein into one daughter cell of the neural progenitor's progeny (Kraut et al. 1996; Li et al. 1997).

In late interphase neuroblasts, the *pros* RNA and Pros protein co-localise in a crescent at the apical cortex but, upon transition from prophase to telophase, Insc drives the switch to a non-uniform accumulation at the basal cortex. In doing so, the *pros* RNA and Pros protein undergo preferential segregation into the more basally-positioned daughter cell, which is turn specified as a ganglion mother cell (Spana and Doe 1995; Li et al. 1997; Broadus et al. 1998). In contrast, *insc* mRNA and Insc protein only co-localise to the apical cortex during interphase. After this stage, the *insc* transcripts accumulate in the cell cytoplasm, due to being independent of Insc protein localisation (Li et al. 1997; Knoblich et al. 1999). The efficient targeting and functional activity of Insc protein does, however, depend on the correct localisation of *insc* mRNAs in the neuroblast (Hughes et al. 2004). Altogether, the combined interplay of these localised developmental determinants provides the positional information and apicobasal cell polarity needed to prime neuroblasts for asymmetric division and cell fate determination (Knoblich et al. 1995; Kraut et al. 1996; Broadus et al. 1998).

1.13.3. RNA localisation facilitates precise extracellular signalling

RNA localisation within cells can also help with the establishment of signal gradients outside of cells to mediate more widespread effects throughout the surrounding tissue. For example, in the Wnt signalling pathway during *Drosophila* embryogenesis. The mRNAs that encode the secreted glycoprotein, Wnt/Wingless (Wg), are asymmetrically localised in a stable gradient to the anterior surface of the cell apical membrane (Baker 1987; Simmonds et al. 2001). This apical localisation of the *wg* transcripts occurs within cells of the embryonic ectoderm and requires active transport via the cytoskeleton (Simmonds et al. 2001; Wilkie and Davis 2001).

Once localised, *wg* is precisely translated, enabling the Wnt signalling pathway to function correctly for the determination of cell fates during segmentation of the ventral epidermis (Simmonds et al. 2001). However, redistribution of localised *wg* mRNAs, via mutation of discrete regulatory elements within the 3' UTR, leads to mis-localised Wg protein expression and a loss of Wnt signalling activity. Mis-localisation of *wg* mRNAs also corresponds with the development of a segment polarity phenotype, in which embryos lose a naked cuticle in each segment (Simmonds et al. 2001). Therefore, the native intracellular localisation of endogenous *wg* mRNAs ensures Wg protein synthesis near to its target site of extracellular secretion, priming it for activation of the Wnt signalling pathway.

1.13.4. Directional cell movement is evidenced in polarised cells exhibiting localisation of actin mRNAs

Induction of cell polarisation by localised RNAs occurs in several motile cell types and is in turn linked to the regulation of their mobility. Subcellular localisation of target mRNAs, including those that encode cytoskeletal regulators and components, couples with an upregulation in the local expression of the proteins. This feeds down into an increased deposition of cytoskeletal elements and binding interactors at the leading

edge – driving forward directional movement of the cell in question (Lawrence and Singer 1986).

A well-known example of this is *beta-actin* (*β-actin*) mRNA localisation in the polarisation of different motile cell types (Fig. 5B.) (Kislauskis et al. 1994; Kislauskis et al. 1997; Hüttelmaier et al. 2005). Actin mRNAs have long been understood to accumulate at the extremities of cells, including in chicken embryo myoblasts and fibroblasts (Lawrence and Singer 1986). The highest concentration of actin transcripts can be detected at the cell periphery within dynamic protrusions/projections called lamellipodia that define the leading edge of migratory cells (Lawrence and Singer 1986). Follow-up work quickly confirmed that *β-actin* mRNA is indeed localised to the actin-rich leading edge of cultured cells via action of the highly-conserved oncofoetal RBP termed Zipcode binding protein 1 (ZBP1) – an orthologue of *Drosophila* Insulin-like growth factor II mRNA binding protein (Imp) (Kislauskis et al. 1997; Ross et al. 1997; Oleynikov and Singer 2003).

In cultured cell lines, zipcode-dependent binding of ZBP1 regulates both the transport and translational repression of *β-actin* mRNAs, preventing premature protein synthesis in the cytoplasm by inhibition of translation initiation (Hüttelmaier et al. 2005; Rodriguez et al. 2006). In association with ZBP1, *β-actin* mRNAs remain translationally silenced until the bound complex reaches its target destination at the cell periphery. At this point, the protein kinase, Src, promotes dissociation and de-repression of *β-actin* via phosphorylation of a specific tyrosine residue in ZBP1 that is required for its RNA binding activity. ZBP1 tyrosine-396 phosphorylation reduces its binding affinity for *β-actin*, leading to release of localised *β-actin* mRNAs that are primed for translation at the leading edge of the cells (Hüttelmaier et al. 2005). This RBP:mRNA interaction therefore establishes cell polarity by shuttling regulated mRNAs to the leading edge, providing them with the directed movement needed at the “front” to influence whole cell phenotypes and behaviours.

Time-lapse experiments have shown that polarised cells with localised *β-actin* transcripts migrate significantly further over a specified duration when compared to cells with non-localised mRNAs (Kislauskis et al. 1997; Shestakova et al. 2001). Furthermore, the distribution of localised *β-actin* mRNAs not only correlates with the magnitude of cell movement, but also with its directionality (Kislauskis et al. 1997).

Inhibition of *β-actin* mRNA localisation significantly reduced migratory distance and resulted in mutant cell phenotypes with abnormal morphologies, lamellipodia structuring and actin fibre organisation (Kislauskis et al. 1994; Kislauskis et al. 1997; Shestakova et al. 2001). It was concluded that polymerisation of these locally-synthesised actin monomers drives assembly of actin filaments in lamellipodia at the leading edge, which in turn contributes to the mechanical force needed for cell locomotion (Lawrence and Singer 1986; Kislauskis et al. 1997). Enrichment of localised cytoskeletal mRNA transcripts, including β-actin, at the leading edge of polarised motile cells is therefore an extremely important driving factor for the regulation of directed cell movement.

1.13.5. Transcripts for actin regulators are also localised to the leading edge of polarised motile cells

Localisation of mRNAs that encode all seven subunits of the Actin-related protein 2/3 (Arp2/3) complex has also been detected at the leading edge of polarised motile fibroblasts, in addition to the fully translated and assembled Arp2/3 complex itself (Mingle et al. 2005; Johnston et al. 2008). In cultured migratory cells, each of the *Arp2/3 complex* mRNA transcripts accumulates within the lamellipodia at the leading edge of the cells, which in turn corresponds to the site of Arp2/3 complex function (Mingle et al. 2005). This precise subcellular targeting of localised *Arp2/3* mRNAs is dependent on ZBP1/Imp-regulated transport via actin microfilament bundles and microtubules, likely under the control of a myosin motor dependent mechanism (Mingle et al. 2005; Gu et al. 2012).

Post-transcriptional regulation at the level of *Arp2/3* mRNA localisation therefore confers downstream spatiotemporal restriction of protein subunit production and assembly. This overcomes the diffusion constraint that would otherwise be associated with transporting a multiprotein complex of such a large size. The local, highly concentrated translation of all seven components in close proximity also improves the efficiency of assembly, rate of response for complex activity, and prevents other promiscuous, off-target protein interactions from being established (Mingle et al. 2005).

The multiprotein Arp2/3 complex has long been known to have an evolutionarily conserved role in the nucleation and pointed-end capping of actin polymerisation in lamellipodia, promoting the assembly of branched actin networks that participate in lamellipodial protrusion, cell spreading and directed cell movement (Machesky et al. 1997; Welch et al. 1997; Mullins et al. 1998; Johnston et al. 2008; Wu et al. 2012). Hence, the strict regulation of mRNAs that encode its protein subunits not only ensure the proper structure and function of the Arp2/3 complex, but also the proper structure and function of the mobile cell types within which it is expressed (Liao et al. 2011; Willett et al. 2013).

1.13.6. Localisation of noncoding RNA species controls their own RNA activities

However, not all RNA localisation occurs with the principal function of regulating spatiotemporal expression of proteins. For example, the subcellular localisation of long noncoding RNAs (lncRNAs) is a primary determinant of their molecular functions at the level of RNA, not protein (Fig. 5C.) (Chen 2016; Carlevaro-Fita and Johnson 2019). As lncRNAs do not contain an explicit open reading frame and express very little protein, their ultimate product is RNA (Derrien et al. 2012). Their overall functionality therefore depends on the physical interactions they form with different RNA counterparts (Carlevaro-Fita and Johnson 2019).

lncRNAs have long been recognised as nuclear-enriched and chromatin-restricted, but a new population of cytoplasmic lncRNAs has since been identified – with other roles outside epigenetic regulation. Localised cytoplasmic lncRNAs are now implicated in signalling, scaffolding and translational control (in association with ribosomes), and may even contribute to biological processes such as mitochondrial respiration (Carlevaro-Fita and Johnson 2019).

Indeed, a great deal of research supports a defined set of lncRNAs enriched in the nucleus, alongside an extensive localisation of lncRNAs in the cytoplasm (Chen 2016). Comparative fractionation of subcellular lncRNA pools in human cell lines evidences widespread expression of lncRNAs that can be classified into a specific nuclear-enriched subset and a substantially larger enrichment in the cytosol and in association

with ribosomes (van Heesch et al. 2014). RNA-FISH surveys of 61 different lncRNAs does, however, suggest some non-specific overlap in addition to these distinct subcellular localisation profiles (Cabili et al. 2015).

Other RNA-FISH experiments on *Drosophila* embryos has revealed that 90% of lncRNAs undergo subcellular localisation, with cytoplasmic enrichment of lncRNAs being more prevalent than in the nucleus (40% vs. 4%) (Wilk et al. 2016). Global profiling of lncRNA content in whole-cell human and *Drosophila* fractions has since validated this, after finding that ~90% of lncRNAs were asymmetrically localised across all subcellular fractions. Although, they did detect a higher percentage of lncRNAs (~75%) enriched within cytoplasmic compartments (Benoit Bouvrette et al. 2018). Taken together, this suggests that many localised lncRNAs have a clear link to cytoplasmic processes, some of which may pertain to functions in ribosomal complexes. Although, ribosomal associations may also relate to a mechanism of lncRNA-targeted degradation to maintain cellular turnover of the lncRNA population (Carlevaro-Fita et al. 2016).

Investigation of ribosome-associated lncRNAs and ribosome-free lncRNAs in mammalian cell culture demonstrates that, while both share a higher tendency to localise to the nucleus, ribosome-associated lncRNAs are more likely to be present in the cell cytoplasm (Carlevaro-Fita et al. 2016; Zeng et al. 2018). The association of lncRNAs with ribosomes and endoplasmic reticulum typically corresponds with roles in translational regulation. This includes the lncRNA, *ZFAS1*, which has been described in human breast cancer lines as a regulator of mRNAs that encode key ribosomal proteins involved in ribosome biosynthesis (Hansji et al. 2016).

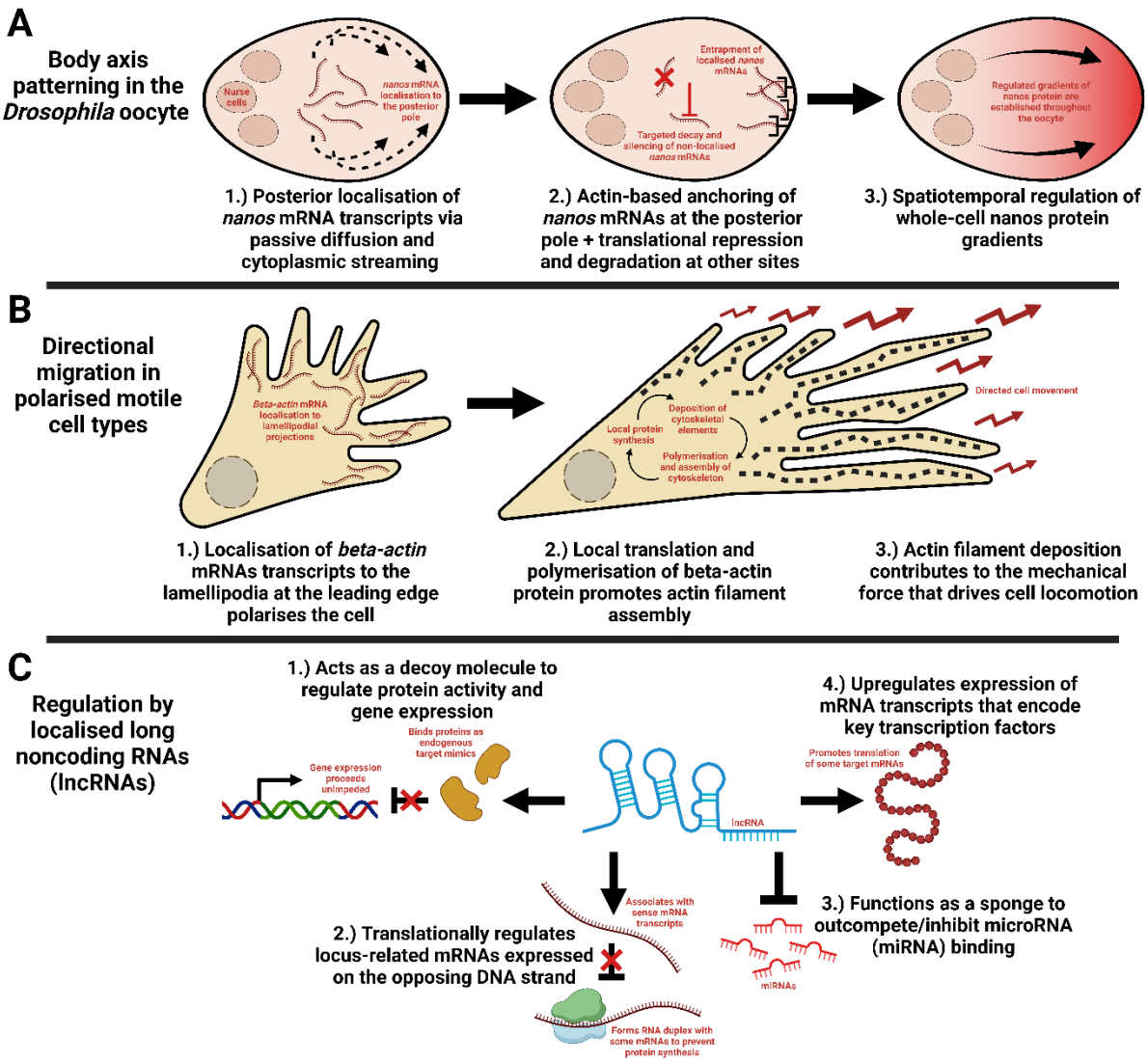

Figure 5. The different functions and mechanisms of asymmetrical RNA localisation. The localisation of RNAs is versatile and diverse. While it is an evolutionarily conserved and universal process of spatiotemporal RNA regulation, it is clear that RNA localisation has been adapted by different cells, organisms and systems to orchestrate fundamental roles that ensure their development and survival. (A) Specification of the anterior-posterior body axis in *Drosophila* by localisation of *nanos* mRNA transcripts to the posterior pole of the oocyte, using a combined mechanism of passive diffusion, trapping and local protection/degradation. (B) Directional cell movement as a result of the tightly regulated localisation of *β-actin* mRNA transcripts to the lamellipodia at the leading edge of fibroblasts. (C) Examples of the RNA-based regulatory activities performed by localised long noncoding RNAs (lncRNAs). **Adapted from Buxbaum et al. (2015) using BioRender.com.**

Another lncRNA called *linc-MD1* is also localised to the cell cytoplasm, but in a ribosome-free form. It has been found to indirectly regulate other RNAs in human and murine myoblasts by competing for access to shared cytoplasmic microRNAs (miRNAs). By binding to *miR-133* and *miR-135*, which otherwise translationally repress the mRNAs of muscle-regulatory transcription factors (TFs), *MAML1* and *MEF2C*, respectively, *linc-MD1* can post-transcriptionally regulate the timing of muscle differentiation. *Linc-MD1* acts as an endogenous decoy for the miRNAs, which permits the MAML1- and MEF2C-induced activation of muscle-specific gene expression and progression of the myogenic programme (Cesana et al. 2011).

Up to 5000 different loci have been identified with the potential to encode lncRNAs in *Drosophila melanogaster* genome (Li et al. 2009b). Several lncRNAs in *Drosophila* embryos exhibit tissue-specific expression and localisation profiles, but many of these show high intra-species variation. This suggests that, while lncRNAs may have functions in embryogenesis, they are not fixed within the fly population (Schor et al. 2018). Upregulation of lncRNA expression is also stage-specific, with the highest abundances of lncRNAs detected in key transitional phases of *Drosophila* development and metamorphosis (Li et al. 2009b; Chen et al. 2016).

An ever-growing list of testis-enriched lncRNAs has also been identified, which are expressed during sperm development and undergo distinct subcellular localisations (Young et al. 2012; Brown et al. 2014; Lee et al. 2019; Shao et al. 2024). Systematic screening of testis-specific lncRNAs has revealed that at least some of these are essential for fertility and late-stage sperm development in male flies (Wen et al. 2016). CRISPR-induced knockouts of these lncRNAs corresponded with a spectrum of mutant phenotypes, including morphological abnormalities in the testis and sperm cells, defective nuclear condensation and synchronisation of cell cysts, impaired spermatid individualisation, and fewer numbers of mature motile sperm in the seminal vesicles. Taken together, this evidences the widespread functions of lncRNAs in male gametogenesis, predominately in the morphogenesis and differentiation of late-stage germline cells (Wen et al. 2016). This high prevalence of cytoplasmic lncRNA expression, localisation and function in many developmentally-relevant biological contexts suggests that lncRNA-specific activity is extremely important for whole fly development – and may even be involved in the regulation of developmental timing.

Overall, this wealth of evidence confirms that lncRNAs, alike their protein-coding mRNA counterparts, accumulate in specific subcellular localisation patterns which likely relate to their wide-ranging functions (Chen 2016; Carlevaro-Fita and Johnson 2019). Subcellular localisation of lncRNAs remains poorly characterised, particularly in the context of fruit flies. Although, studies into lncRNAs known to be involved in human health and disease so far indicate functional conservation in *Drosophila* development (Rogoyski et al. 2017). At the level of DNA, lncRNA sequence conservation between species is poor – making identification of orthologues a near-impossible task to undertake. However, the functions of lncRNAs appear to be somewhat conserved between different *Drosophila* species, and when compared to mammals, indicating that conservation hinges on more than just genomic sequence (Lee et al. 2019; Camilleri-Robles et al. 2022).

1.14. RNA localisation is commonplace in the male germline

In *Drosophila* germline cells, the main bulk of mRNA localisation feeds directly into downstream protein production and function – with localisation of transcripts regulating spatiotemporally-restricted protein expression (Weil 2014). There are numerous examples of this reviewed in *Drosophila* developmental biology (Johnstone and Lasko 2001; Palacios and Johnston 2001; Weil 2014).

Recent scRNA-seq data from the FCA study suggests that the adult *Drosophila* testis possesses the highest complexity of mRNAs when compared with the transcriptomic datasets of other fly-specific tissues. Overall, the testis was shown to have the highest number of specifically expressed genes, followed in turn by the Malpighian tubule and male reproductive glands (Li et al. 2022). This is supported by microarray analyses from both Chintapalli et al. (2007) and Andrews et al. (2000), with the latter using high quality expressed sequence tags (ESTs) to explore the repertoire of testis-specific genes in *Drosophila*. Computational analysis of EST frequency and microarray expression profiles demonstrated that the testis mRNA population is highly complex and shows an extended range of transcript abundance (Andrews et al. 2000). This vast transcriptomic profile is representative of the sheer number of important

differentiation and remodelling events that take place during sperm development in the testis (Raz et al. 2023). With such a large number of testis-specific mRNAs being expressed, it is likely that at least some of these undergo RNA localisation events.

One key example comes from the RBP activity of cytoplasmic polyadenylation element binding (CPEB) protein, Orb2. It is widely expressed in the adult male germline and is implicated in some vital sex-specific functions that ensure progression of sperm development by modulation of meiosis and spermatid differentiation (Xu et al. 2012; Gilmutdinov et al. 2021). Work by Xu et al. (2014) has revealed that Orb2 also mediates the asymmetric, comet-like localisation of *protein kinase C* (*aPKC*) mRNA in the extreme distal tips of elongating *Drosophila* spermatid bundles. FISH experiments confirmed the non-uniform, comet-like distribution of *aPKC* mRNAs at the elongating spermatid tail-ends, and antibody probing of whole-mount testes detected localised aPKC protein signals as stripes parallel to the long axis of the spermatids. The highest concentration of aPKC mRNA and protein also co-localised with Orb2 protein, in turn matching-up with the heightened accumulation typical of the leading comet-like “head” arrangement. Orb2 was most concentrated as a clumped band towards the distal tips of the growing axonemes, resembling that of the comet localisation pattern at the spermatid tail-ends. Orb2 was also found to persist in spermatids until elongation and nuclear condensation had ended (Xu et al. 2012; Xu et al. 2014).

By spatially restricting the accumulation of *aPKC* mRNA and localising protein activity to the tail-ends of the spermatid cysts during differentiation, this correctly orientated the direction of spermatid cyst polarisation relative to the apical-basal testis axis. Orb2-*aPKC* cross-regulation could also be responsible for establishing a self-sustaining Orb2 cycle: (i) Orb2 likely binds, localises and activates translation of *aPKC* mRNAs, (ii) aPKC protein activity then drives Orb2 self-interactions and translational activation of its own *orb2* mRNAs, (iii) and this in turn sets up an autoregulatory loop to orientate and polarise differentiating spermatids (Xu et al. 2014; Gilmutdinov et al. 2021).

A second example is the precise spatiotemporal localisation of mRNAs that encode Y-linked testis-specific axonemal dynein motor proteins (Fingerhut et al. 2019; Fingerhut and Yamashita 2020). The transcripts of these Y-chromosome fertility factors, including *kl-3* and *kl-5*, co-localise with the AAA+ ATPases, Reptin (Rept) and Pontin (Pont), at the distal ends of cytoplasmic cilia in the *Drosophila* male germline.

Together, these are transported within highly polarised cytoplasmic RNP granules in late spermatocytes and elongating spermatids, the proper formation of which is mediated by Rep and Pont activity (Fingerhut et al. 2019; Fingerhut and Yamashita 2020). Two RBPs, Blanks and dmPTB, also specifically localise to Y-loops at the transcriptional loci of *kl-3* and *kl-5*, and further analyses have shown that these are fundamental *trans*-acting factors with roles in various aspects of Y-loop gene expression, RNP granule formation and in the post-transcriptional regulation of these localising transcripts (Fingerhut et al. 2019). During the two successive meiotic divisions of sperm development, the RNP granules undergo equal cellular segregation and accumulate at the distal cilial ends as the axoneme elongates in growing spermatid tail-ends. Concentrated local translation of the axonemal dynein motors then promotes their efficient uptake and incorporation into the axoneme, directly from the exposed cytoplasm, to drive the assembly and maturation of cytoplasmic cilia during sperm-specific ciliogenesis (Fingerhut and Yamashita 2020).

The above studies reiterate the importance of asymmetric subcellular mRNA localisation in sperm development. However, investigations into how localised mRNAs are coupled to localised protein expression in *Drosophila* spermatogenesis are lacking, and a large proportion of the comet and cup gene candidates remain functionally uncharacterised. As only a small proportion of the post-meiotic comet and cup genes have been found to encode sperm proteins, it is unlikely that they provide any significant structural role or physical components central to sperm development (Barreau et al. 2008a; Barreau et al. 2008b; Garlovsky et al. 2022; Raz et al. 2023). Although, knockouts of the *scotti (soti)* comet gene do result in male sterility due to the catastrophic malfunction of spermatid individualisation (Barreau et al. 2008a; Barreau et al. 2008b).

Further work has confirmed that, through the establishment of precise and opposing localised protein gradients, *soti* regulates the inhibition of caspase activation during spermatid individualisation; ensuring a level of caspase activity that is just enough to promote whole spermatid differentiation, without inducing apoptosis due to prolonged exposure (Kaplan et al. 2010). Therefore, the comet and cup proteins may together possess some unknown, functional importance that primes the spermatid tail-ends for maturation into individualised, coiling sperm. It is possible that the proteins encoded

by these two gene subsets perform a variety of different regulatory activities – for example, in the modulation of sperm differentiation.

RNA localisation is not a random phenomenon – it is highly organised. Regardless of the organism, tissue or cell type, the localisation of RNAs orchestrates an array of instrumental and diverse functions. Considering this, it may be hypothesised that the comet and cup mRNA transcripts have evolved a role that is akin to at least one of the examples outlined above.

1.15. Project aims and objectives

RBPs are widely expressed throughout sperm development, and their roles in post-transcriptional control are instrumental in all stages of germ cell development (Sutherland et al. 2015). They are needed in germ cell nuclei to mediate alternative splicing of specific mRNA isoforms and are equally as vital in the cytoplasm; where the translation of proteins involved in chromatin condensation and cell morphology dynamics must be tightly regulated long after transcription has concluded (Venables and Eperon 1999).

In this research, we are focusing on the latter stages of *Drosophila* sperm development, where there is a subcellular accumulation of an exclusive set of post-meiotically transcribed mRNAs in non-uniform localisation patterns. We know that this localisation phenomenon occurs at the extreme tail-ends of spermatids in the mid-to-late elongation stages, with transcripts resembling either shooting speckled “comets” or U-shaped acorn “cups” – however, we still do not know how or why this happens (Barreau et al. 2008a; Barreau et al. 2008b).

Analysis of *Drosophila* YFP exon-trapped lines have revealed the high-level, localised expression of at least five different RBPs also at the spermatid tail-ends, in similar subcellular regions to the comet and cup mRNAs introduced in Section 1.9. (Lowe et al. 2014). These include: dmPTB, Imp, Lost, Pascilla and Orb (Lowe et al. 2014). In addition, previous unpublished screening of transgenic fluorescently tagged reporter constructs indicate that the localisation of comet and cup mRNAs prefigures the formation of distinct protein gradients within the spermatids. We know that the testis is a highly transcriptionally active organ with a large and diverse population of mRNAs, and that it may require an equally varied catalogue of regulatory activity mechanisms. So, are some of these RBPs responsible for the fundamental molecular driving forces that underpin comet and cup localisation?

In light of these developments, we have been investigating the hypothesis that a small number of RBPs, including the highly conserved Insulin-like growth factor II mRNA binding protein (Imp), are contributing to the post-transcriptional regulation of comet and cup mRNAs in the *Drosophila* testis.

As such, we aimed to determine an opening list of prospective RBP candidates that bound to a panel of these post-meiotic mRNAs. An in-house RNA-affinity pull-down approach and Western Blotting Analysis was therefore employed to elucidate an initial repertoire of direct and indirect binding interactions. We then exploited this data output to select an RBP contender for further testing. Indications of comet and cup binding preferences and relative abundances guided us in our selection, which resulted in a single lead RBP candidate being taken forward for additional characterisation.

In the next phase of testing, we implemented a modified cleavable affinity purification (Cl-AP) assay to revalidate our findings in a more testis-authentic context. We explored the RBP interactome and its regulatory roles in the broader context of its RNP complexes, including the identification of protein and RNA interactors that likely influenced these activities.

Finally, we brought these investigations full circle, by delving into the primary functions of RBPs within the spermatids, and as part of the broader sperm development programme of the *Drosophila* testis. This involved the use of RNA interference (RNAi) screening to study the effects of RBP knockdown deficiencies on the localisation and translation of comet and cup mRNA transcripts in RNAi-expressing lines. Analyses of RBP-RNAi phenotypes also provided a good starting point for determining the involvement of RBPs in the regulation of these localised mRNAs – whether this be through post-transcriptional mRNA processing, stabilisation, transportation, translational activation and/or repression, for example.

To achieve these aims, we divided the project into four central areas of interest, each defined by a specific question outlined below.

Key questions:

1. **Which RNA binding proteins (RBP) contribute to the post-transcriptional comet and cup mRNA localisation in the spermatid cyst bundles and by what regulatory mechanism are they likely involved?**

2. **Which RBPs interact with post-meiotically transcribed mRNA transcripts such as the comet and cup mRNAs?**

3. **What other protein components are associated with these RBPs to facilitate their binding and RNA processing activities?**

4. **What functional role do specific RBPs (e.g., Imp) play in the *Drosophila* testis?**

Using the above strategy, we were aiming to address the overarching question: **how** and **why** does asymmetrical, post-meiotic comet and cup mRNA localisation take place in *Drosophila* spermatid cyst bundles?

2. MATERIALS AND METHODS

2.1. Fly stock husbandry and gonad dissections

Drosophila melanogaster were bred and raised in vials on standard culture medium, containing dextrose, maize, yeast and agar. Nipagen (10% dilution in ethanol) and propionic acid were also added as anti-fungal and anti-microbial agents, respectively. All fly stocks were maintained at temperatures between 18 °C to 30 °C, with regular turnover, depending on intended use. For temperatures above 25 °C, flies were kept in an incubator on 12:12 hour light:dark cycle. A summary of the main fly lines used in this work can be found in Table 2.

For gonad dissections, *Drosophila melanogaster* were anaesthetised on a gas pad of humidified carbon dioxide. Using an Olympus SZ51 Binocular Stereo Microscope with KL 200 LED Fibre Optic Light Source (Olympus Life Science), gonads were precisely dissected into droplets of 1X Testis Buffer (183mM KCl, 47mM NaCl, 10mM Tris-HCl, pH 6.8) or 1X Phosphate-buffered saline (PBS; 137mM NaCl, 2.7mM KCl, 11.9mM Phosphates, pH 7.4) on a modified petri dish lid. In brief, flies were placed with their abdomens positioned at the edge of the buffer drop, and their head and thorax secured with a pair of dissection forceps. A second pair of forceps was then used to draw out the abdomen base towards the buffer. Gonads were separated away from the gastrointestinal tract, detached from the rest of the abdomen and extracted into the buffer via surface tension manipulation. In-tact gonads were transferred into a fresh drop of buffer for cleanup using a tungsten needle.

Table 2. List of key *Drosophila melanogaster* lines used in this work. This includes our main fly stocks, protein-trap insertion lines, and Imp-UAS-RNAi lines. Other relevant details such as source notes, stock number and reference citations are included where possible.

NAME	GENOTYPE	STOCK NUMBER	RELEVANT REFERENCES	EXTRA NOTES
BASE FLY STOCKS				
Imp-GFP (G80)	– Protein-trap / exon-trap fly line, G00080 insertion	–	Quiñones-Coello et al. (2007)	From: Cooley Lab, Yale, USA
Squid-YFP	w; If/CyO; CPTI 239/TM6B	115104 (Original stock, Kyoto DSC)	Lowe et al. (2014)	From: Cambridge Protein Trap Consortium; CPTI-000239 protein trap fly line
Squid-YFP	w; BI/CyO; CPTI 239/TM6B	115104 (Original stock, Kyoto DSC)	Lowe et al. (2014)	From: Cambridge Protein Trap Consortium; CPTI-000239 protein trap fly line
Bam-Gal4:VP16	w; Tft/CyO; P{w+ BamGal4:VP16}	–	Chen and McKearin (2003a), Chen and McKearin (2003b)	Expresses a transgenic germline Gal4 driver
schuy-TagGFP; Bam-Gal4:VP16	w; schuy-TagGFP/(CyO); Bam-Gal4:VP16/(TM3,Sb)	–	Barreau et al. (2008a), Barreau et al. (2008b)	Generated for this PhD project
c-cup-TagGFP; Bam-Gal4:VP16	w; c-cup-TagGFP/(CyO); Bam-Gal4:VP16/(TM3,Sb)	–	Barreau et al. (2008a), Barreau et al. (2008b)	Generated for this PhD project

10XUAS-CD8-GFP	w; P{y[+t7.7] w[+mC]=10XUAS-IVS-mCD8::GFP}attP40	BL32186	Pfeiffer et al. (2010)	From: Bloomington DSC
Tropomyosin-1-GFP (Tm1-GFP)	w; P{y[+t7.7] w[+mC]=VT042001-p65.AD}attP40	BL51537	Tirian and Dickson (2017)	From: Bloomington DSC
SINGLE UAS-RNAi LINES				
Val20-Imp-attP2 RNAi	w; +/+; Val20-Imp-attP2 RNAi/Val20-Imp-attP2 RNAi	BL34977	Ni et al. (2011), Perkins et al. (2015)	From: Transgenic RNAi Project (TRiP), Bloomington DSC; From VALIUM20 vector, expresses UAS-inducible 21 nt dsRNAi hairpin for *imp* gene knockdowns
Imp-GD RNAi	w; +/+; Imp-GD RNAi/Imp-GD RNAi	20321	Dietzl et al. (2007)	From GD RNAi library, Vienna DRC; From P-element insertion on Chr. 3, expresses UAS-inducible 316 nt long RNAi hairpin against the *imp* gene
UAS-Dicer2;Imp-GD RNAi	UAS-Dicer2/FM6/7; +/CyO; Imp-GD RNAi/TM6	20321 (Imp-GD stock, Vienna DRC)	Dietzl et al. (2007)	Generated by S. Lopez de Quinto from the Imp-GD 20321 stock; Expresses UAS-inducible Dicer2 that aids Imp-GD RNAi hairpin processing in the nucleus

DOUBLE UAS-RNAi LINES				
Double Val20-Imp-attP2 RNAi	w; Val20-Imp-attP2 RNAi/CyO; Val20-Imp-attP2 RNAi/TM3,Sb	Double Imp-UAS-RNAi line generated in this project	Ni et al. (2011), Perkins et al. (2015)	Generated by S. Lopez de Quinto from original TRiP stock
Double Val20-Imp-attP2 RNAi; Imp-GD RNAi	w^{-}; Val20-Imp-attP2 RNAi/CyO; Imp-GD RNAi/TM3,Sb	Double Imp-UAS-RNAi line generated in this project	Dietzl et al. (2007), Ni et al. (2011), Perkins et al. (2015)	Generated by S. Lopez de Quinto from original TRiP and GD stocks
Double homozygous Val22-Imp RNAi	w; Val22-Imp RNAi/Val22-Imp RNAi; Val22-Imp RNAi/Val22-Imp RNAi	Double Imp-UAS-RNAi line generated in this project	Ni et al. (2011), Perkins et al. (2015)	Generated by S. Lopez de Quinto from original TRiP stock; From VALIUM22 vector, expresses UAS-inducible 21 nt dsRNAi hairpin for *imp* gene knockdowns

2.2. Standard molecular cloning of vectors

For *in vitro* transcription of our comet and cup mRNAs, all gene regions were cloned individually into the multiple cloning site (MCS) of the pBlueScript (pBS) II SK+ vector (Stratagene) to generate template constructs. The pBS II SK+ vector was chosen as it's MCS is flanked on either side with T7 and T3 RNA polymerase promoters, respectively. pBS II SK+ also contains an Ampicillin resistance gene region, which enabled correct selection of transformed bacterial colonies.

2.2.1. Genomic DNA and total RNA extractions

In accordance with the GenElute™ Mammalian Genomic DNA Miniprep Kit Protocol (Sigma), genomic DNA (gDNA) was extracted from a total of sixty pairs of WT w^{1118} ovaries. However, four of the eleven comet and cup genes contained at least one intron so molecular cloning could not be performed directly from gDNA sources. To account for these, total RNA was extracted from twenty WT w^{1118} testes using the RNAqueous™-Micro Total RNA Isolation Kits (Invitrogen, Cat. No. AM1931). All experimental DNA and RNA concentrations were estimated using the NanoDrop™ ND1000 Spectrophotometer (Thermo Scientific).

2.2.2. Reverse transcription and PCR amplifications

Resultant total RNA was implemented as a template for the reverse transcription reaction, and a non-specific library of all single-stranded cDNAs was synthesised using the GoScript™ Reverse Transcription System (Promega). This cDNA library was then diluted 10-fold in the RNAqueous™-Micro Total RNA Isolation Kits (Invitrogen, Cat. No. AM1931).

Using either the PCRBIO HiFi Polymerase (PCR Biosystems) or 2X DreamTaq Green PCR Master Mix (Thermo Scientific), diluted cDNA was PCR-amplified to generate intronless, double-stranded DNA corresponding to three comet and cup sequences of interest (*calcutta-cup, sungrazer* and *walker-cup*). Due to issues with reaction efficiency, *schumacher-levy* was ultimately PCR-amplified with the 2X PCRBIO

VeriFi™ Polymerase Ready Mix. Regions of interest (ROI) corresponding to the other seven intronless comet and cup genes (*borrelly*, *comas sola*, *heineken-cup, phosphoglyceromutase 87, scotti*, *tetleys-cup* and *whipple*) were also PCR-amplified, from genomic sources, using the PCRBIO HiFi Polymerase (PCR Biosystems).

In brief, either 1 µL of diluted cDNA or ~50 ng of gDNA was used as a template in each standard 25 µL reaction mixture, alongside 0.4 µM of custom-designed sense and antisense primers (Integrated DNA Technologies and Sigma). A varied programme of annealing temperatures, ranging from 52.0°C–64.0°C, was tested to simultaneously screen for the optimal annealing temperature conditions of our primers. Extension times and cycle numbers were adjusted accordingly, depending on ROI length and complexity and the amplification rate of the polymerase enzyme (seconds per kilobase). Sense and antisense primer sequences were designed to flank our gene regions, guide amplification of this DNA stretch in both directions/orientations, and introduce specific, flanking restriction enzyme (RE) sites (Table 3.). This permitted compatible insertion into the pBS II SK+ MCS. Primer pairs were designed manually, with assistance of the online OligoAnalyzer™ (Integrated DNA Technologies) and OligoEvaluator™ (Sigma) tools. This enabled evaluation of respective melting temperatures (T_m), and the propensity to form secondary hairpin structures and hetero/homodimers.

Table 3. List of gene-specific sense and antisense primers used for cloning, with oligo sequences given in the 5' to 3' orientation. The 3 starting adenines correspond to the restriction enzyme requirement for complete digestion. Sequences highlighted in red and green correspond to specific restriction enzyme recognition sites. The corresponding pair of restriction enzymes needed for each double restriction digestion is also provided alongside this in the final column, with a matching colour-code. Shorthand designations for each comet or cup gene/mRNA/protein name are given in brackets.

COMET OR CUP GENE	PRIMER NAME	OLIGO SEQUENCE (5' – 3')	RESTRICTION ENZYME
borrelly (boly)	**SENSE:** boly_forward	**AAA**CTCGAGTGCTGTTATCGTTATTAGTTC	XhoI
	ANTISENSE: boly_reverse	**AAA**TCTAGAGTTGTAACATGAGAAGAGATTAG	XbaI
calcutta-cup (c-cup)	**SENSE:** ccup_forward	**AAA**AAGCTTCTGATTTTGCACTCGAATATATTTC	HindIII
	ANTISENSE: ccup_reverse	**AAA**CGGCCGGATATCTTCAATAATTTTGTTTATTCTAC	Eco52I
comas sola (cola)	**SENSE:** cola_forward	**AAA**CTCGAGCTTCACCCTTTCGGC	XhoI
	ANTISENSE: cola_reverse	**AAA**TCTAGAGGGTGACTCCGAAATAATC	XbaI
heineken-cup (h-cup)	**SENSE:** hcup_forward	**AAA**CTCGAGTGCCCTGAGAAGTCC	XhoI
	ANTISENSE: hcup_reverse	**AAA**TCTAGACGGAGATCGAGCGG	XbaI
phospho-glyceromutase 87 (pglym 87)	**SENSE:** pglym_forward	**AAA**CTCGAGAAATGAACACGATATAGACTGC	XhoI
	ANTISENSE: pglym_reverse	**AAA**TCTAGATGGGACCCAGAACCG	XbaI

schumacher-levy (schuy)	**SENSE:** schuy_forward	**AAA**GTCGACGATATACTTTTTGATATGCGTTAGG	SalI
	ANTISENSE: schuy_reverse	**AAA**CGGCCGGAGTTATAGAAATAGATATGCTATTCATC	Eco52I
scotti (soti)	**SENSE:** soti_forward	**AAA**CTCGAGTAAATTCAGTTCTAAATCAAACTCAG	XhoI
	ANTISENSE: soti_reverse	**AAA**TCTAGAGGTGCTGCAAGAGGG	XbaI
sungrazer (sunz)	**SENSE:** sunz_forward	**AAA**GTCGACCACACACCCGAAACAC	SalI
	ANTISENSE: sunz_reverse	**AAA**CGGCCGGTGTGTACTTAATGGAAAATGAC	Eco52I
tetleys-cup (t-cup)	**SENSE:** tcup_forward	**AAA**CTCGAGATTAAAACTTTGGCTAAACACAG	XhoI
	ANTISENSE: tcup_reverse	**AAA**TCTAGAGCACCAACCGTGTGG	XbaI
Walker-cup (wa-cup)	**SENSE:** wacup_forward	**AAA**GTCGACATAAAGCACACCTCTTTTTTATACTTG	SalI
	ANTISENSE: wacup_reverse	**AAA**CGGCCGATTAATATACCTTTAAAATAGTTGTATTTTTTC	Eco52I
whipple (whip)	**SENSE:** whip_forward	**AAA**CTCGAGCATTGCAGTCATCTATAAAATGAATC	XhoI
	ANTISENSE: whip_reverse	**AAA**TCTAGACTATGTGTGCTTCTTATTCGG	XbaI

2.2.3. Agarose gel electrophoresis and purification of PCR Products

Aliquots of the PCR products were size separated using agarose gel electrophoresis to check for primer specificity, amplification/reaction efficiency and optimal annealing temperatures. Briefly, 1% (w/v) agarose gels comprising TBE buffer (Tris base, Boric acid, 0.5 M EDTA, pH 8.0), with either SYBR® Safe DNA Gel Stain (Life Technologies) or SafeView Nucleic Acid Stain (NBS Biologicals), were used to visualise bands corresponding to our expected DNA fragments. The GeneRuler™ 1kb Plus DNA Ladder (Thermo Scientific) or Quick-Load® 1kb DNA Ladder (New England BioLabs) was run alongside the samples for estimation of DNA fragment sizes. Subsequent gels were then analysed via UV light exposure, using the UVP GelDoc-It® 310 Imaging System (Ultra Violet Product).

To increase DNA concentrations sufficiently, products from the PCR reactions that were run at annealing temperatures of 59.3°C and 64.0°C were pooled together for *boly, cola, h-cup, pgylm 87* and *t-cup*, respectively. PCR products from three other reaction variations were pooled together for *whip* (53.2°C, 59.3°C and 64.0°C) and *schuy* (52.0°C, 54.0°C and 58.0°C). Only the PCR products from the 55.0°C reaction were taken forward for *c-cup, schuy, sunz* and *wa-cup*, and from the 64.0°C annealing temperature for *soti*. Amplified DNA fragments were then purified from these pooled PCR reaction volumes using the GeneJET PCR Purification Kit (Thermo Scientific), according to the manufacturer's instructions.

2.2.4. Restriction enzyme digestion and purification

Simultaneous RE double digestions were undertaken using the FastDigest™ XhoI, XbaI, HindII, SalI and Eco52I REs in 10X FastDigest™ Universal Buffer (Thermo Scientific). Each double digestion reaction was undertaken at 37°C for one to two hours to eliminate additional adenines from the prospective gene inserts, and excise either the XhoI-XbaI fragment (for *boly*, *cola*, *h-cup, pglym 87, soti*, *t-cup* and *whip*), SalI-Eco52I fragment (for *schuy, sunz* and *wa-cup*) or HindIII-Eco25I fragment (for *c-cup*) from the pBS II SK+ vector MCS. Approximately 1.5 µg of pBS II SK+ vector was digested in a 40 µL reaction volume, while 0.6 – 1.5 µg of gene insert was digested in

a 100 µL reaction volume. To reduce the likelihood of plasmid self-re-ligation, the pBS II SK+ vector was de-phosphorylated at 37°C for a further fifteen minutes using FastAP Alkaline Phosphatase (Thermo Scientific). All digestion mixtures were placed on ice and DNA-purified using the GeneJET PCR Purification Kit (Thermo Scientific).

2.2.5. Ligation reactions and bacterial transformation

Using the Rapid DNA Ligation Kit (Thermo Scientific) as standard, we ligated our purified gene inserts individually into the purified pBS II SK+ vector – downstream of the T7 promoter and in place of the fragment site. All ligation reactions were carried out in a 5 µL volume at room temperature (RT) for thirty minutes.

After thawing on ice, constructs were subsequently transformed into competent DH5α bacterial cells using the Mix & Go *E. coli* Fast Transformation Kit (Zymo Research). For each clone, 25 µL – 50 µL of competent DH5α *E. coli* cells were gently mixed with 1 µL – 2 µL of ligation mixture and incubated together for five minutes on ice. Using aseptic technique, resultant mixtures were then divided into 10% and 90% aliquots and each spread with 200 µL of plain, Luria-Bertani (LB) broth onto two separate, selective 100 µg/mL Ampicillin LB agar plates (pre-warmed to RT).

2.2.6. Screening for insert-positive *E. coli* colonies via colony PCR

After overnight incubation at 37°C, a selection of Ampicillin-resistant colonies were screened for successful construct uptake/transformation. Using a diagnostic, in-house colony PCR approach with 2X PCRBIO Taq Mix Red (PCR Biosystems), individual colonies were randomly selected for each clone and PCR-tested for the presence of a ligated, insert-positive pBS II SK+ plasmid. In short, a single colony was introduced into a standard 20 µL PCR mixture, alongside 0.5 µM of commercial T7 (sense) and 0.5 µM of commercial T3 (antisense) promoter primers (Invitrogen). A negative control reaction of unmodified, empty pBS II SK+ plasmid (10 ng; Stratagene) was also included.

Using the MJ Mini™ Personal Thermal Cycler (Bio-Rad Laboratories), PCR amplifications were performed with an extended preliminary denaturation step of five minutes and an annealing temperature of 55°C to match the primers' optimal T_m. Extension times were once again amended depending on gene insert properties and PCRBIO Taq Polymerase amplification rate. As before (Section 2.2.3.), aliquots of all PCR-amplified mixtures were size-separated via 1% (w/v) agarose gel electrophoresis, and experimental DNA bands were size-estimated. Sizes were then compared to the empty, negative control to determine which bacterial colonies contained amplified DNA fragments at estimated sizes indicative of our ligated gene inserts (plus neighbouring endogenous nucleotides from the encompassing MCS).

2.2.7. Plasmid DNA extraction and sequence verification

For each clone, multiple random insert-positive colonies were taken forward and inoculated into 3 mL of sterile Ampicillin-selective LB broth (100 µg/mL). Bacterial cultures were then grown-up overnight in a rocking incubator set at 37 °C with 220 rpm shaking. The next day, these cultures were transferred to sterile Eppendorf tubes and pelleted by microcentrifugation for two minutes at 12,000 rpm. After supernatant disposal, plasmid DNA was isolated and purified from the pellets using the EZ-10 Spin Column Plasmid DNA Minipreps Kit (Bio Basic). Plasmid DNA aliquots (100 ng/µL) were sent off for third-party sequencing analysis using the T7 and T3 promoter primers (Eurofins Scientific).

2.3. Preparations for *in vitro* transcription

To prepare sequence-verified constructs for *in vitro* transcription, larger starting volumes and higher concentrations of plasmid DNA per clone were required. Original *E. coli* colonies were inoculated into 20 mL of sterile Ampicillin-selective LB broth (100 µg/mL), grown overnight as above and pelleted by centrifugation at 3000 rpm at 21 °C for fifteen minutes. The supernatant was discarded, and plasmid DNA was extracted, again using the EZ-10 Spin Column Plasmid DNA Minipreps Kit and accompanying kit protocol (Bio Basic). An equivalent of four miniprep extractions were performed per clone to account for the increased starting culture volume.

2.3.1. Plasmid linearisation and purification

Between 6.0 µg – 7.5 µg of plasmid DNA was linearised in a 120 µL – 150 µL digestion reaction volume using either the FastDigest™ XbaI RE (for *boly*, *cola*, *h-cup, pglym 87, soti*, *t-cup* and *whip*) or FastDigest™ Eco52I RE (for *c-cup, schuy, sunz* and *wa-cup*) in 10X FastDigest™ Universal Buffer (Thermo Scientific). Single digestions were undertaken at 37°C for one hour, with extra RE added after thirty minutes. This cut the pBS II SK+ construct at the end of each insert on the T3 promoter side – ensuring correct transcription initiation at the T7 promoter in the sense direction. Linearised plasmid DNA was purified using the GeneJET PCR Purification Kit (Thermo Scientific) and 1 µL of the linearised products were run on a 1% (w/v) agarose gel alongside an undigested pBS II SK+ plasmid reference to confirm complete digestion.

A standard DNA Precipitation procedure was also carried out for *cola, pglym 87, whip* and *t-cup* to pool together concentrated aliquots of linearised DNA from 2 separate digestion reactions.

2.3.2. *In vitro* transcription of biotinylated mRNA probes

Using an in-house, standardised three-day protocol, biotinylated-labelled RNA probes were *in vitro* transcribed for subsequent RNA-affinity pull-down assays. The TranscriptAid T7 High Yield Transcription Kit (Thermo Scientific) was employed as standard, with a minimum of 0.5 µg linearised DNA template used per 10 µL reaction volume alongside Biotinylated-UTP (1:7 unmodified-UTP:modified-UTP ratio; Roche). After overnight incubation at 37°C, DNase I was added and incubated for a further thirty minutes at 37°C to digest the plasmid DNA. To begin RNA precipitation, RNase-free water and Lithium Chloride was added and the reaction mixtures chilled overnight at –20°C. On the final day, the precipitated RNA was pelleted by microcentrifugation at 13,000 rpm for fifteen minutes at 4°C. The pellet was then washed with cold 75% ethanol and re-centrifuged as before, followed by air-drying at RT and resuspension in 50 µL 1X Tris-EDTA Buffer (pH 8.0). A ~1 µg aliquot was then heated to 70°C and loaded onto a 1% (w/v) agarose gel, alongside the RiboRuler High Range RNA Ladder (Thermo Scientific), to verify mRNA probe size and integrity.

2.4. RNA-affinity pull-down assays

To characterise Bruno (Bru1), Polypyrimidine-Tract-Binding Protein (dmPTB), Alan Shepard (Shep) and IGF-II mRNA-binding protein (Imp) binding interactions with our biotinylated comet and cup mRNA probes, we used an in-house pull-down assay protocol to acquire bound fractions of our probes against a pool of soluble, cytoplasmic proteins from *Drosophila* ovaries. A positive RNA-control of the *osk* 3' UTR and an unrelated negative RNA control of the y14 coding sequence (CDS) were also included (Besse et al. 2009).

2.4.1. Preparation of S10 cytoplasmic ovarian extract

Twenty to thirty pairs of ovaries were dissected per mRNA probe, depending on ovary size and condition. After pooling together, ovaries were washed twice in cold 1X PBS, followed by washing in cold Hypotonic Buffer (10 mM HEPES-KOH, pH 7.4, 10 mM K-Acetate, 1.5 mM Mg-Acetate, 2.5 mM DTT), with and without protease inhibitors (PI; Roche). The ovaries were then homogenised in a 1:1 volume of the Hypotonic Buffer/PI mixture using ~30 strokes of a sterile plastic Eppendorf pestle, and the homogenate centrifuged at 10,000 rpm for ten minutes at 4°C. The resultant supernatant was recovered, and 100% RNase-free glycerol added to a final concentration of 5%. This soluble protein extract was then maintained on ice until required.

2.4.2. Binding biotinylated-mRNA probes to Streptavidin magnetic beads

Roughly 30 µL – 40 µL of Streptavidin-conjugated magnetic beads (New England Biolabs and Roche) were used per mRNA probe. Placement onto a DynaMag™-2 Magnet (Thermo Fisher) retained beads throughout all subsequent washes and solution removals. Buffer transfer was commenced by washing three times in MB-TEN^{100} (10 mM Tris-HCl, pH 8.0, 1 mM EDTA, pH 8.0, 100 mM NaCl), before a final MB-TEN^{100} resuspension in a volume equivalent to 250 µL per mRNA point. Equimolecular amounts of each biotinylated mRNA (~2 µg), relative to the positive

RNA control, were added directly to the corresponding suspension. To promote Streptavidin-biotin binding, the mixture was then incubated on a rotating wheel for thirty minutes at RT and any unbound RNAs eliminated by washing twice in NEB Buffer (for NEB magnetic beads) or MB-TEN[100] (for Roche magnetic beads; 10 mM Tris-HCl, pH 8.0, 1 mM EDTA, pH 8.0, 100 mM NaCl). Two further washes were then conducted in 2X Binding Buffer (10 mM HEPES, pH 7.9, 3 mM $MgCl_2$, 5 mM EDTA, pH 8.0, 5% glycerol, 2 mM DTT, 0.5% IGEPAL, 40 mM KCl).

2.4.3. Binding of S10 protein extract to Streptavidin-biotin beads

A common mix of the S10 ovarian extract, 2X Binding Buffer, 3 µg/µL Heparin and 0.5 µg/µL yeast tRNA was made up to a final volume of between 135 µL – 145 µL per mRNA point. This was then added to the Streptavidin-biotin beads and incubated on a rotating wheel for one hour at 4°C to promote Streptavidin-biotin-protein binding.

2.4.4. Elution of bound protein fraction

After incubation, the unbound protein fraction was recovered and the Streptavidin-biotin-protein-complexed beads were washed four times with 2X Binding Buffer, including five minute incubations on a rocking platform, to maintain low-salt conditions for weaker RBP:mRNA interactions. Bound protein fractions were then eluted by the addition of 30 µL 2X SDS Protein Loading Buffer (National Diagnostics) and an incubation at 90°C – 95°C for three minutes, followed by collection of the final eluate.

2.5. SDS-PAGE and Western Blot Analysis

Bound fractions were loaded alongside the Precision Plus Protein™ Dual Colour Standard Protein Ladder (Bio-Rad) and run on hand-cast polyacrylamide mini-gels comprising an 8% – 10% separating gel and 5% stacking gel. Separated RBP:mRNA complexes were then transferred onto Trans-Blot Turbo Mini Nitrocellulose Membranes (Bio-Rad) using the Trans-Blot® Turbo™ Transfer System (Bio-Rad).

Immunoblotting was then undertaken to detect any binding of Bru1, dmPTB, Shep and Imp to our biotinylated comet and cup mRNA probes (Table 4.). Membranes were dried-down, rehydrated in 1X PBS and blocked in either PBT + 5% milk (1X PBS, 0.1% Tween-20) or Intercept® PBS Blocking Buffer (Li-Cor) for one hour at RT. Incubation with primary antibodies, diluted in either PBT + 5% milk or Intercept® T20 PBS Antibody Diluent (Li-Cor), was performed overnight at 4°C on a rocking platform. Membranes were washed for ten minutes in 1X PBT three times and then incubated with secondary antibodies in PBT + 5% milk, before subsequent washing as before. Following a final wash in 1X PBS, RBP:mRNA interactions were detected using the Odyssey® CLx Imaging System (Li-Cor). Membrane images were visualised and adjusted for clarity using Image Studio Lite (v5.2.5; Li-Cor). To re-use the membranes, stripping was performed using 0.2N Sodium Hydroxide for ten minutes at RT with gentle shaking.

Quantification of Western Blot protein signal intensities was performed using ImageJ v1.52d (Schneider et al. 2012). Regions of interest (ROIs) were manually selected; serving as a selection frame that was used as a standardised ROI for all signals corresponding to the dominant isoform of the interacting RBP in that blot. The pixel intensity of each resolved band (or a region corresponding to the molecular weight (MW) of the RBP candidate where a protein band would otherwise be expected) was in turn measured. This same ROI was also used for measurement of background signals in a region directly above or below each protein band undergoing quantification. The pixel intensity data recorded by ImageJ for the samples, controls and background signals were all inverted by taking each value away from 255 (the maximum pixel value for an 8-bit image). The net protein signal was determined by deducting the inverted background value for each lane from the inverted protein value for that RBP:mRNA combination. The net protein signal corresponding to the binding interaction between each test mRNA and each RBP candidate was then divided by the net protein signal for *osk* 3' UTR with that same RBP, and multiplied by 100 to give a percentage of RBP:mRNA binding relative to this positive control. Resultant data was subsequently plotted as bar graphs using Microsoft Excel.

Table 4. Important details about all antibodies used for immunostaining in our Western Blot Analyses.

PRIMARY ANTIBODIES				
ANTIBODY	**HOST**	**DILUTIONS**	**REFERENCE**	**ACKNOWLEDGEMENT**
α-Bruno	Rabbit	1:1000 to 1:3000	–	Gift from A. Ephrussi (EMBL, Heidelberg, Germany)
α-dmPTB	Rat	1:3000 to 1:5000	Besse *et al*., Genes & Dev 2009 (DOI: 10.1101/gad.505709)	Gift from A. Ephrussi (EMBL, Heidelberg, Germany)
α-dmPTB	Rabbit	1:1000	Besse *et al*., Genes & Dev 2009 (DOI: 10.1101/gad.505709)	Gift from A. Ephrussi (EMBL, Heidelberg, Germany)
α-GFP	Rat	1:1000	Commercially available monoclonal antibody (1 mg/mL)	ChromoTek (Cat. No. 3H9)
α-Imp	Rat	1:2500	Medioni *et al*., Current Biology 2014 (DOI: 10.1016/j.cub.2014.02.038)	Gift from F. Besse (Nice, France)

α-Shep	Rabbit	1:1000 to 1:2000	Chen *et al*., Genetics 2014 (DOI: 10.1534/genetics.114.166181)	Gift from K. Beckingham (Houston, USA)
α-Shep	Rabbit	1:1000 to 1:2000	Matzat *et al*., PLoS Genetics 2012 (DOI: 10.1371/journal.pgen.1003069)	Gift from E. Lei (NIH, Maryland, USA)

SECONDARY ANTIBODIES

ANTIBODY	HOST	DILUTIONS	NAME	COMPANY AND PRODUCT NUMBER
α-Rabbit	Goat	1:15000	IRDye680RD Goat anti-Rabbit	Li-Cor; 926-68071
α-Rabbit	Goat	1:10000 or 1:15000	IRDye800CW Goat anti-Rabbit	Li-Cor; 926-32211
α-Rat	Goat	1:15000	IRDye800CW Goat anti-Rat	Li-Cor; 926-32219

2.6. Optimisation of RNA-affinity pull-down assay for switch to testis-specific protein extracts

2.6.1. Measurement of total protein concentrations in testes vs. ovaries

A new stage of optimisation was then commenced to coordinate the swap to an alternative testis-specific source of endogenous, cytoplasmic RBPs. Using the Imp-GFP G80 protein-trap fly line (G00080 exon-trap line; Quiñones-Coello et al. 2007), two starting crude protein stocks were prepared to compare and calibrate protein levels between *Drosophila* ovaries and testes, respectively. Varying quantities of whole, in-tact gonads were mixed and lysed in a 1:1 volume of 2X Laemmli Sample Buffer (Sigma) and denatured at 90˚C – 95˚C for three to five minutes. An ovary-specific stock was prepared with twenty ovaries to an overall concentration of 1 ovary/µL, while a testis-specific stock was prepared with fifty testes to an overall concentration of 1 testis/µL. For this, and all further testis-specific protein extracts, testes were dissected from young males aged 0 – 1 day old.

From these starting stocks, individual volumes for crude protein extracts equating to 2, 6, 12 and 24 *Drosophila* testes and 1, 2 and 4 *Drosophila* ovaries were taken and successively loaded onto a 9% separating / 5% stacking polyacrylamide mini-gel. Protein samples were then analysed alongside the Precision Plus Protein™ Dual Colour Standard Protein Ladder (Bio-Rad) via SDS-PAGE and Western Blotting, as above (Section 2.5.). After rehydration in 1X PBS, the resultant membrane was stained for total protein using the Revert™ 700 Total Protein Stain Kit Components (Li-Cor) to enable a direct, qualitative comparison between the total protein concentrations of each sample. While the Two-Colour Western Blot Method (Li-Cor) was followed as standard, a 1:1 dilution of Revert™ 700 Total Protein Stain Solution was instead implemented to prevent overstaining. Total protein concentrations were imaged on the red 700 nm channel using the Odyssey® CLx Imaging System (Li-Cor) and processed via Image Studio Lite (v5.2.5; Li-Cor).

2.6.2. Immunoblotting for RBP expression in testes vs. ovaries

After imaging, the membrane was destained using the Revert™ Destaining Solution (Li-Cor) for ten minutes at RT with gentle agitation. The membrane was rinsed in 1X PBS and blocked in Intercept® PBS Blocking Buffer (Li-Cor) before immunodetection of the sex-specific differences in the expression levels of Bru1, dmPTB and Imp-GFP. To re-use the membrane and immunoblot for different proteins, stripping was performed with 0.2N Sodium Hydroxide. All membrane images were visualised and adjusted for clarity using Image Studio Lite (v5.2.5; Li-Cor).

2.6.3. Comparison of testis-specific protein extract preparation conditions

A failed RNA-affinity pull-down attempt, using a *Drosophila* testis-sourced RBP extract based on the above analyses, extended this process of optimisation further. Despite the testis-specific pull-down extract being prepared with >200 testes, equating to ~70 testes per RNA point, no binding interactions were immunodetected. Follow-up total protein staining revealed a complete loss of protein in all sample lanes.

To determine the exact cause of this total protein loss, four testis-specific extract conditions were prepared and comparatively tested, with roughly twenty *Drosophila* testes used per sample condition type. Pairs of testes were dissected into individual droplets of 1X Testis Buffer and pooled together for rinsing and counting within fresh 1X Testis Buffer. In sequential rounds, twenty individual testes were transferred into the lids of clean Eppendorf tubes, each containing a 1X Testis Buffer droplet. To test the effects of freezing, some of these testis samples were then flash-frozen in liquid nitrogen and stored at –80˚C for a minimum of 24 hours.

A simple crude protein extract was prepared by mixing and lysing whole, freshly dissected testes in a 1:1 volume of 2X Laemmli Sample Buffer (Sigma). This was used as a reference for the maximum concentration of total protein that could be achieved from twenty fresh *Drosophila* testes, consisting of both soluble and insoluble protein. The other three samples comprised testis-specific pull-down extracts, made-up in the

same manner by which they would be in preparation for a standard RNA-affinity pull-down assay (See Section 2.4.). All three testis-specific pull-down extracts were prepared by combining *Drosophila* testes, contained within a small volume of residual 1X Testis Buffer (~10 µL), with a 1:1 volume of Hypotonic Buffer/PI mix. These were then manually homogenised with a sterile plastic Eppendorf pestle for 60 seconds and centrifuged at 10,000 rpm for 10 minutes at 4˚C to remove insoluble proteins and other tissue debris. After recovery, the cytoplasmic supernatant was mixed with 1 µL of 100% RNase-free glycerol and combined with a 1:1 volume of 2X Laemmli Sample Buffer (Sigma). All extracts were kept on ice throughout this process.

The first and second pull-down extracts were prepared with same-day-dissected testes, with the former being left out on ice for at least two hours prior to 2X Laemmli Sample Buffer addition. The third and final pull-down extract was prepared after thawing the flash-frozen testes on ice. Samples were denatured at 90˚C – 95˚C for three to five minutes and loaded onto a 10% separating / 5% stacking polyacrylamide mini-gel beside the Precision Plus Protein™ Dual Colour Standard Protein Ladder (Bio-Rad). After SDS-PAGE and membrane transfer, the membrane was stained and imaged for total protein concentrations, as described previously.

2.6.4. Evaluation of sonication and homogenisation effectiveness

To investigate whether a combination of sonication and manual homogenisation could successfully improve cell lysis and protein release during extract preparation, optimisation trials with the Diagenode Bioruptor® Sonication System were performed. A simple crude protein extract and three testis-specific pull-down extracts were prepared individually using twenty flash-frozen *Drosophila* testes thawed on ice. Once the testes were introduced into the Hypotonic Buffer/PI mix, this methodology was modified to incorporate sonication prior to manual homogenisation.

The Bioruptor® sonication intensity (Diagenode) was set to the highest power setting and a standard cycle of 30 seconds on / 30 seconds off was chosen to preserve the samples from rapid heating due to the ultrasound energy. This equated to a 30 second sonication pulse followed by a 30 second rest interval, with continuous rotation of the

carousel sample holder throughout. The sonicator water bath was filled with ice, and regularly replenished to minimise sample heating. The number of successive sonication cycles was incrementally increased to test the effectiveness of different cycle number variations.

A total of three different sonication pulse cycle rounds – 4, 6 and 8 successive cycles – were tested. After sonication cycle completion, samples were manually homogenised for sixty seconds with a plastic Eppendorf pestle and processed in the same way as before. After SDS-PAGE, the resultant protein gel was stained for total protein using the ReadyBlue™ Protein Gel Stain, as instructed in its standard protocol (Sigma). Gel analysis and image processing were carried out using the Odyssey® CLx Imaging System (Li-Cor) and accompanying Image Studio Lite software (v5.2.5; Li-Cor).

Follow-up tests were then conducted to assess whether the precise order of sonication and homogenisation had any overall effect on the final protein concentration. To test this hypothesis, the assay was repeated with the same experimental set-up as above, with the order of sonication and manual homogenisation reversed – homogenising first and sonicating second.

2.6.5. Optimising homogenisation conditions to improve total protein extraction yield from testes

In a final attempt to increase the total concentration of protein recovered in our starting testis input homogenate, the type of tissue homogeniser, homogenisation buffer and sonication pulse duration were all modified in tandem.

A simple crude protein extract and two testis-specific pull-down extracts were prepared individually using thirty flash-frozen *Drosophila* testes. For the testis-specific pull-down extracts, flash-frozen discs of dissected testes were pooled together and homgenised in a 1:1 ratio of 2X Binding Buffer with protease inhibitors (10 mM HEPES, pH 7.9, 3 mM $MgCl_2$, 5 mM EDTA, pH 8.0, 5% glycerol, 2 mM DTT, 0.5% IGEPAL, 40 mM KCl) in place of the usual Hypotonic/PI Buffer (10 mM HEPES-KOH, pH 7.4, 10 mM K-Acetate, 1.5 mM Mg-Acetate, 2.5 mM DTT). Manual homogenisation was performed for sixty seconds, this time using a small capacity borosilicate glass micro-tissue

grinder and pestle set-up with a 0.1 mm to 0.15 mm clearance to improve testis sheath breakdown (VWR, Cat. No. 432-1280).

Siliconised sterile glass Pasteur pipettes were used to transfer the two resultant homogenates into separate Eppendorf tubes. One homogenate was retained on ice for further analysis, while the other was subjected to a single sonication pulse, equivalent in time to one full rotation of the Diagenode Bioruptor® Sonication System carousel tube holder unit. A single 360˚ sonicator rotation equated to 17 seconds of constant high-power sonication. As before, an SDS-PAGE was performed on the samples, and the total protein content stained for using the ReadyBlue™ Protein Gel Stain, as instructed in the manufacturer's protocol (Sigma). The Odyssey® CLx Imaging System (Li-Cor) and Image Studio Lite software (v5.2.5; Li-Cor) were used for imaging and analysis.

Sonication was subsequently removed from the homogenate preparation methodology. Adaptions to the homogenate buffer composition and glass pestle/vessel micro-tissue grinder were, however, incorporated into a small-scale pilot of the RNA-affinity pull-down assay. Using these modified conditions, the assay was undertaken as in Section 2.4. using a starting input equating to ~100 *Drosophila* Imp-GFP G80 testes per RNA point (G00080 exon-trap line; Quiñones-Coello et al. 2007). This amended set-up was used to pull-down endogenous cytoplasmic testis-specific proteins against two experimental biotin-labelled mRNA probes for *soti* and *h-cup*, as well as the *osk* 3' UTR positive control and the y14 CDS negative control. SDS-PAGE and Western Blotting of bound and unbound extracts was again performed to probe for RBP:mRNA binding interactions.

2.7. Finalised Cleavable Affinity Purification (Cl-AP) experimental protocol

A muti-step Cleavable Affinity Purification (Cl-AP) assay was performed to obtain the repertoire of Imp's binding partners, including identification of protein interactors and associated RNAs in purified Imp RNP complexes. Sqd-YFP was implemented as an internal RBP control to compare the Imp-GFP proteomics and RNA sequencing (RNA-

Seq) datasets against. The final, optimised CI-AP protocol is described herein (Fig. 6.).

2.7.1. Preparation of GFP-TRAP-Sulfo beads

2.7.1.1. Desalting of the ChromoTek GFP V_HH recombinant binding protein nanobody

The unconjugated 13.9 kDa nanobody, ChromoTek anti-GFP V_HH, purified alpaca recombinant binding protein (Proteintech UK, Prod. Code: gt-250), required complete desalting before first use. The initial storage buffer was in turn exchanged for 1X PBS prior to modification with Sulfo-NHS-SS-Biotin. This was performed using the Zeba™ Spin Desalting Columns (7K MWCO, 2 mL capacity) in accordance with the manufacturer's instructions (ThermoFisher Scientific UK). Columns were provided as part of the EZ-Link™ Micro Sulfo-NHS-SS-Biotinylation Kit (Cat. No. 21945), which was developed for labelling of 50 µg – 200 µg protein in a 200 µl – 700 µl total reaction volume.

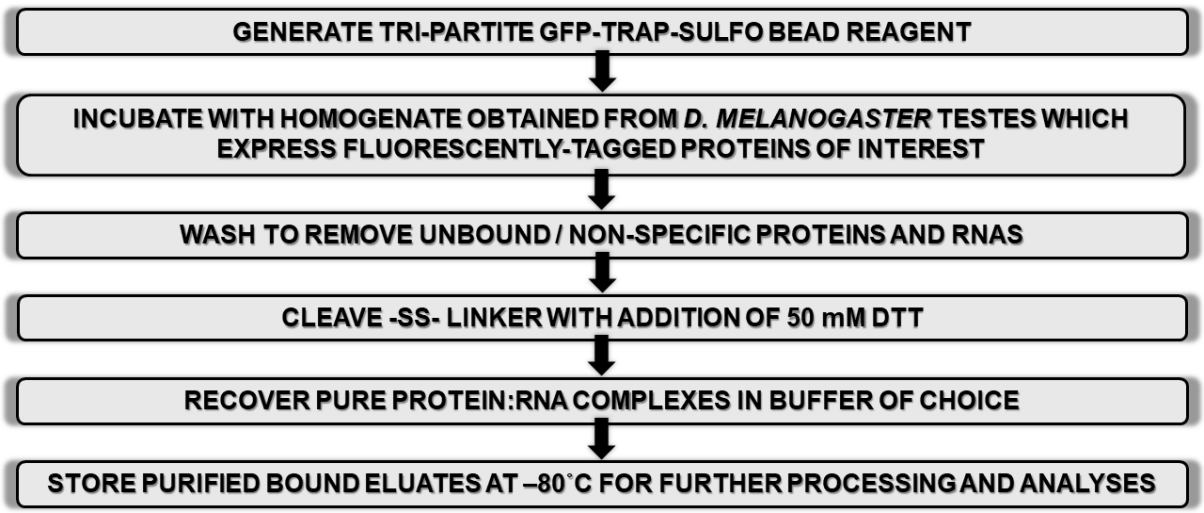

Figure 6. Sequential flow diagram outlining fundamental steps in the Cleavable Affinity Purification (CI-AP) protocol.

The EZ-Link™ Sulfo NHS-SS Biotinylation Kit (Thermo Scientific UK, Cat. #21445) generates a biotinylated amine-reactive thiol-cleavable linker that permits the easy cleavage of the disulphide bond within the extended spacer arm of the GFP-TRAP-Sulfo bead reagent The presence of an amine-reactive region (with N-Hydroxysuccinimide [NHS] esters) in the resultant GFP-TRAP-Sulfo beads means that it reacts with primary amino groups (–NH2) to form stable amide bonds. This includes primary amines in lysine side-chains and in the amino N-terminus of polypeptides. Overall, the spacer arm is of medium length, with a total length of 24.3 angstroms added to the target. It consists of a native biotin valeric acid group extended by a 7-atom chain. This extended spacer arm reduces the risk of any steric hindrance that may be implicated in avidin binding.

In brief, the “starting” column was centrifuged at 1000 *x g* for two minutes using a benchtop microfuge and the resultant flow-through discarded to remove the initial storage buffer. The column was then equilibrated with 1 mL 1X PBS, followed by centrifugation at 1000 *x g* for two minutes. The flow-through was disposed of and this process was repeated two more times for full equilibration. 200 µL of the 1 mg/mL buffered aqueous nanobody solution was applied directly onto the column filter, followed by a further round of centrifugation at 1000 *x g* for two minutes. The newly desalted nanobody was then collected and retained on ice, ready for biotinylation.

2.7.1.2. Sulfo-NHS-SS-Biotin labelling of GFP V_HH nanobody

The vial of EZ-Link Sulfo-NHS-SS-Biotin from the EZ-Link™ Micro Sulfo-NHS-SS-Biotinylation Kit (ThermoFisher Scientific UK, Cat. No. 21945) was acclimatised to ambient temperature before opening. Immediately before use, the 1 mg Sulfo-NHS-SS-Biotin powder was dissolved in the universal solvent of N,N-Dimethylformamide (anhydrous 99.8% DMF, Sigma-Aldrich UK, Prod. No. 227056) to give an 8mM solution. 86.1 µL of the Sulfo-NHS-SS-Biotin solution was added to the desalted nanobody and mixed instantly by inversion. The reaction mixture was incubated on ice at 4˚C for two hours. The reaction was ceased by desalting using a fresh Zeba™ Spin Desalting Column (7K MWCO, 2 mL capacity, ThermoFisher Scientific UK), pre-

equilibrated as above. Desalting eliminated any excess biotin reagent and unreacted linker.

2.7.1.3. Linking the biotinylated nanobody to streptavidin agarose beads

The Pierce™ High Capacity Streptavidin Agarose (ThermoFisher Scientific UK, Cat. No. 20357) beaded resin was mixed to ensure an even, homogenised suspension. 40 µL of agarose bead slurry (20 µL packed beads) was taken and washed by resuspension in 1 mL of 1X PBS. After inverting ten times, the beads were pelleted by centrifugation at 2500 *x g* for 3 minutes and the supernatant discarded. Washing with 1X PBS was repeated for a further three times. The biotinylated nanobody solution was then combined with the washed beads and the mixture incubated on a rotating disc mixer for one hour at 4˚C to promote antibody-bead binding.

Any unbound nanobody was removed by washing three times with 1 mL Precipitation Buffer (10 mM Tris-HCl, pH 7.5 , 150 mM NaCl, 0.5 mM EDTA, pH 8.0, 1 mM PMSF, 0.1% IGEPAL, Roche cOmplete Mini protease inhibitors, Roche PhosSTOP phosphatase inhibitors). After the final wash, the resultant GFP-TRAP-Sulfo beads were resuspended in Precipitation Buffer to maintain a 50% (40 µL) bead slurry. Beads were then stored 4˚C until required.

2.7.2. Tissue homogenisation and supernatant preparation

Testes from young Imp-GFP G80 males (G00080 exon-trap line; Quiñones-Coello et al. 2007), and young Sqd-YFP males (Sqd CPTI 239 lines; Lowe et al. 2014) were dissected in batches as standard (in 1X Testis Buffer), flash frozen in liquid nitrogen and stored at –80˚C until needed.

After dissection and storage, all subsequent steps were performed on ice or in a 4˚C cold room with pre-chilled buffers and pipette tips. Each of the “frozen testis discs” were transferred individually and accumulated together in separate glass

homogenisers on ice – one glass homogeniser per sample type (one homogenate for Imp-GFP and one homogenate for Sqd-YFP). Glass homogenisers were cleaned thoroughly before and after use to minimise contamination and RNase activity.

All testis samples were retained on liquid nitrogen prior to and throughout the transfer process. The testes were then homogenised in 100 µL of Lysis Buffer (10 mM Tris-HCl, pH 7.5, 150 mM NaCl, 0.5 mM EDTA, pH 8.0, 1 mM PMSF, 0.5% IGEPAL, Roche cOmplete Mini protease inhibitors, Roche PhosSTOP phosphatase inhibitors) supplemented with 1 µL RiboShield™ RNase Inhibitor (PCR Biosystems, Cat. No. PB30.23-02). Both homogenates were checked regularly under a simple stereoscope to confirm that appropriate tissue grinding was taking place. The resulting homogenates were centrifuged at 14,000 *x g* for ten minutes at 4˚C. The clear supernatants were then taken forward into fresh tubes and kept on ice for further use, with care taken to avoid the residual debris and sedimented pellets.

2.7.3. Incubation of diluted input homogenates with CI-AP GFP-TRAP-Sulfo Beads

To dilute the IGEPAL detergent, Dilution Buffer (10 mM Tris-HCl, pH 7.5, 150 mM NaCl, 0.5 mM EDTA, pH 8.0, 1 mM PMSF, Roche cOmplete Mini protease inhibitors, Roche PhosSTOP phosphatase inhibitors) was added to the supernatants to a final volume of 500 µL. RiboShield™ RNase Inhibitor (PCR Biosystems, Cat. No. PB30.23-02) was added to 0.25 µL for every 20 µL of sample volume. Of this diluted homogenate, 20% was retained as aliquot of input material and stored at –80˚C for Western Blot, proteomics and RNA analysis. The remaining volume of each input homogenate was then incubated with 20 µL (1:1 slurry) of the GFP-TRAP-Sulfo beads in parallel for one hour on a rotating wheel at 4˚C.

2.7.4. Cleavage of disulphide bond and collection of trapped extract

After the hour-long incubation period, the mixture was centrifuged at 3000 *x g* for three minutes. The supernatant was then collected and stored separately at –80˚C to constitute the unbound extract. This was kept for RNA checks and immunoblotting.

The GFP-TRAP-Sulfo Beads were washed with 1 mL of Wash Buffer (10 mM Tris-HCl, pH 7.5, 150 mM NaCl, 0.5 mM EDTA, pH 8.0, 1 mM PMSF, 0.05% IGEPAL, Roche cOmplete Mini protease inhibitors, Roche PhosSTOP phosphatase inhibitors) for a total of three times to remove any unbound and non-specifically bound proteins. Washing involved resuspending in buffer, inverting 10 times and then pelleting via centrifugation at 3000 *x g* for 3 minutes before discarding the waste supernatant.

After the final wash and supernatant removal, the beads were resuspended in 100 µL of Wash Buffer. Upon mixing, 50 µL of the homogeneous solution (containing beads) was collected for each sample type and stored at –80˚C. This provided an independent bound fraction from which purified RNAs could be extracted for downstream RNA analyses, without the need for DTT cleavage at RT. To cleave the disulfide bond in the spacer arm, and obtain the second bound fraction for proteomics analysis, DTT was added to the remaining 50 µL volume to a final concentration of 50 mM. This was then incubated on a rocking platform for two hours at RT.

Upon completion of the incubation period, the fractions were inverted 10 times and the beads pelleted by centrifugation at 3000 *x g* for 3 minutes. This second bound extract was also kept at –80˚C to prior to preparations for proteomics analysis. For Western Blotting, proteins were detected using a 1:1000 dilution of the rat anti-GFP monoclonal antibody (ChromoTek, Cat. No. 3H9).

2.8. Extraction and analysis of CI-AP-purified interacting RNAs

2.8.1. Kit-based extraction and purification of RNAs

Purified RNAs were isolated from 25 µL of the resultant input, unbound and bound samples for Imp-GFP and Sqd-YFP, respectively, using the RNAqueous™-Micro Total RNA Isolation Kit from Invitrogen™ (Thermo Fisher Scientific, Cat. No. AM1931). RNA extractions were undertaken in accordance with the manufacturer's guidance.

Some small modifications were, however, incorporated to minimise the potential of RNA degradation and RNase contamination. All benchtop centrifugations were performed at maximum speed for one minute, while the final elution collection was increased to a two-minute centrifugation. To commence the kit-based RNA purification protocol, 100 µL of the proprietary Lysis Buffer was combined with 25 µL of each individual sample, mixed well via vortexing and then left to incubate at RT for ten minutes. After this, one half-volume of RNase-free 100% Ethanol (i.e., 62.5 µL) was added to each sample and vortexed briefly. Due to the volume restrictions associated with the micro filter cartridge assemblies, the sample mixtures were loaded onto the filter resin as sequential aliquots in two successive passes to bind all RNAs in the full total volume. The remaining centrifugation and washing steps were conducted as standard (with proprietary Wash Solution 1 and Wash Solution 2/3), but with one key exception: the flowthrough was not discarded after every step but was instead disposed of only once – at the point preceding filter drying and elimination of residual fluid from the column.

For each sample, the RNA elutions were performed twice in the same 22 µL volume of 75°C-preheated Elution Solution (i.e., in two sequential passes through the column). A two-minute incubation of the eluate on the cartridge resin was conducted at RT both times prior to a two-minute centrifugation at maximum speed. A 2 µL volume of the eluted RNAs were retained on ice for an immediate rudimentary measurement of RNA concentration using NanoDrop™ ND1000 Spectrophotometry (Thermo Scientific). RiboShield™ RNase Inhibitor was added to the main aliquot of RNA at 1 µL per 20 µL sample volume (PCR Biosystems, Cat. No. PB30.23-02). After mixing, the RNA

samples were stored at –80˚C for a more accurate analysis of RNA concentrations and integrity.

2.8.2. Analysis of RNA concentrations using Qubit™ 4 Fluorometry

The benchtop Qubit™ 4 Fluorometer (Invitrogen, Cat. No. Q33226) was used to output an accurate quantitation of our CI-AP RNA samples using highly sensitive fluorescence-based Qubit™ assays. The instrument was set-up in accordance with the Qubit™ 4 Fluorometer User Guide (Invitrogen, Pub. No. MAN0017209). Both the samples and standards were prepared according to the Quick Reference instructions provided with the Qubit™ RNA High Sensitivity (HS) Assay Kit (Invitrogen).

In brief, Qubit™ RNA HS Standard #1 and Standard #2 were equilibrated to RT prior to assay commencement. RNA samples were thawed on ice and all reagents were mixed thoroughly before use. A 1:10 dilution of the Imp-GFP and Sqd-YFP input and bound RNA samples was undertaken using RNase-free water so that the concentration of all six RNA samples fell within an approximate 4 ng to 200 ng range. A master mix of the Qubit™ working solution was prepared by diluting the Qubit™ reagent 1:200 in the Qubit™ buffer for all samples and standards, equating to a final assay volume of 200 µL for each. Reaction components were combined in assay-specific thin-walled, clear 0.5 mL PCR tubes (Axygen). For each standard assay, 10 µL of the Qubit™ RNA HS Standard (#1 or #2) was combined with 190 µL of the Qubit™ working solution. For the RNA sample assays, 2 µL of RNA was combined with 198 µL of the Qubit™ working solution. After mixing and a brief centrifugation, the reactions were incubated at RT for two minutes to allow the assay to reach maximum fluorescence. Care was taken to avoid the introduction of bubbles into the solutions as this could cause errors in readings. The assays were performed at RT, and all reaction mixtures were retained at RT at the time the readings were taken.

The instrument was calibrated using the appropriate standard assay mixtures for Qubit™ RNA HS Standard #1 and Standard #2, respectively. This outputted the raw fluorescence values for both standard solutions and displayed an RFU range in the form of a Fluorescence vs. Concentration graph. Measurement of CI-AP sample RNA

concentrations were in turn made by direct comparison to these calibration parameters. Sample measurements were made immediately after standard calibration. Data was outputted in sample units of ng/mL and exported in both a CSV (comma separated value) and PDF file format.

2.8.3. Analysis of RNA quality and integrity using the Agilent 4200 TapeStation

The 4200 TapeStation System and RNA ScreenTape technology (Agilent Technologies, Part. No. G2991BA) was used for high-throughput automated electrophoresis to separate, analyse and output quality control (QC) measurements for our Cl-AP RNA samples.

Due to the range of concentrations preliminarily indicated by the Qubit™ 4 measurements, both types of RNA ScreenTape analyses were employed. The standard Agilent RNA ScreenTape device was used to measure the quality and integrity of RNA in the input homogenates and unbound extracts of Imp-GFP and Sqd-YFP, respectively. This was because it had a quantitative range and RIN^e functional range of 25 ng/µL – 500 ng/µL. The Agilent HS RNA ScreenTape assay, on the other hand, provided efficient and reliable separation of RNA samples of limited abundance down to 100 pg/µL, with a quantitative range of 500 pg/µL – 10,000 pg/µL and a RIN^e functional range of 1,000–25,000 pg/µL. HS RNA ScreenTape analysis was therefore used for the QC measurement of RNAs in both the Imp-GFP and Sqd-YFP bound Cl-AP fractions.

The RNA ScreenTape Assays were performed as stated in their respective System Quick Guides (Agilent Technologies). To summarise these protocols, the individual RNA ScreenTape Devices and sample buffers for each assay (HS and standard) were acclimatised to RT. Both corresponding RNA ScreenTape ladders (HS and standard) were placed on ice alongside the RNA samples. All reagents were thoroughly mixed before use. Assay reactions were assembled in specialist optical tube strips (Agilent, 8x Strip, Part. No. 401428 / 401425). For the Agilent RNA ScreenTape assays, 5 µL RNA sample buffer and 1 µL RNA sample were combined per tube for the Imp-GFP input RNA, Imp-GFP unbound RNA, Sqd-YFP input RNA, and Sqd-YFP unbound

RNA, respectively. For the Agilent HS RNA ScreenTape Assays, 1 µL of HS RNA sample buffer and 2 µL RNA were combined per tube for the Imp-GFP and Sqd-YFP bound RNA samples.

After a quick centrifugation, the assay mixtures were vortexed at 2000 rpm for one minute using the IKA MS3 Vortexer (Agilent). Assay mixtures were centrifuged again to ensure any interfering air bubbles were removed, then denatured by heating at 72°C for three minutes before transferring onto ice for two minutes. After a final spin down, all assay mixtures were loaded into the 4200 TapeStation System (Agilent Technologies, Part No. G2991BA) alongside the appropriate RNA ScreenTape ladder and device. Electrophoretic separation was run immediately via the Agilent TapeStation Controller software. A single report was automatically generated that integrated multiple analyses of the size, quantity, quality and integrity of the CI-AP sample RNAs. Results were presented in the form of an electropherogram, a gel image and a data table that was then exported as a PDF file.

2.9. RNA-Sequencing (RNA-Seq) of the CI-AP RNA samples

Four RNA library preparations were generated by the Cardiff University Genomics Research Hub (Cardiff School of Biosciences) using the NEBNext® Single Cell/Low Input RNA Library Prep Kit for Illumina® (New England Biolabs, Cat. No. E6420S/L). These corresponded to the CI-AP-purified RNAs that were isolated from the Imp-GFP input homogenate, Imp-GFP bound extract, Sqd-YFP input homogenate and Sqd-YFP bound extract, respectively. RNA library quality and fragment size were also assessed by the Cardiff University Genomics Research Hub (Cardiff School of Biosciences) using the 4200 TapeStation System and RNA ScreenTape technology as described above (Agilent Technologies). Resultant CI-AP RNA libraries were stored at –20˚C prior to sequencing.

QC and sequencing of all four CI-AP RNA libraries was undertaken by Novogene UK using the Illumina NovaSeq X Plus Sequencing System (PE150). Partial lane sequencing was performed to a sequencing depth of approximately 20 million 150

base pair (bp) paired-end reads per sample library, with at least 6Gb of RNA-Seq data generated for each.

2.9.1. RNA-Seq bioinformatics analysis pipeline

All initial stages of the RNA-Seq bioinformatics pipeline, including trimming, quality control, reference genome annotation and alignment, sorting and genomic feature counting were kindly supported by Dr. Fiona Messer in the White-Cooper Lab (Post Doctoral Research Associate, Cardiff University School of Biosciences).

RNA-Seq data was uploaded and stored in the FASTQ file format on the Cardiff University School of Biosciences high-performance computing (HPC) service cluster, *iago*. Initial processing of this RNA-Seq data was performed via the MobaXterm server and SSH client.

Sequence quality assessments were carried out at various points along the pipeline using the FastQC tool (Andrews 2010). Sequences were trimmed and filtered using Trim Galore (version 0.6.10) and Cutadapt (version 4.1) in paired-end trimming mode (Krueger 2012). All adaptor sequences, overrepresented sequences, low-quality sequences (Phred < 20) and any sequences less than 50 bp in length were subsequently removed from the read data. Sequences were also trimmed by 10 bp at their 5' and 3’ ends to avoid poor qualities and biases in reads (Krueger 2012).

Sequence reads were aligned to the *Drosophila melanogaster* reference genome, release version 6.57 (Dmel6.57), using the STAR (Spliced Transcripts Alignment to a Reference) aligner tool, v2.7.6a (Dobin et al. 2013; Öztürk-Çolak et al. 2024). This involved a two-step alignment strategy in which a genome index file was generated first, combining the Dmel6.57 reference genome assembly with its annotations, followed by mapping of the RNA-Seq reads to this newly annotated reference genome index. The *Drosophila melanogaster* reference genome and genome annotation data files for r6.57 were retrieved from the FlyBase Genomes FTP repository (release version: FB2024_03).

After genome alignment, unmapped and duplicate reads were filtered from the RNA-Seq datasets, and aligned BAM files were sorted based on chromosomal coordinates using the SAMtools package (v1.17) (Li et al. 2009a). The read summarisation

programme, FeatureCounts (v2.0.2), was then used to quantify all RNA-Seq reads that had been mapped to annotated genomic features and output these as a count matrix (Liao et al. 2014). The same *Drosophila melanogaster* genome annotation data file for r6.57 was used for this, as in the STAR mapping stage (FlyBase Genomes FTP repository, release version: FB2024_03).

2.9.2. Statistical analysis and normalisation of RNA-Seq count data

Concluding stages of the RNA-Seq R-based bioinformatics pipeline, including gene identification, statistical analysis and differential gene analysis (DGE) were kindly conceptualised and conducted by Dr. Fiona Messer (Post Doctoral Research Associate, Cardiff University School of Biosciences). The edgeR package was used for DGE analysis with a Generalised Linear Model (GLM) in RStudio (Robinson et al. 2010; McCarthy et al. 2012; R Core Team 2024). The R script code for this R-based bioinformatics pipeline can be found in Appendix B, Supplementary Code File 1 and the raw data outputted from this analysis is available in Appendix B, Supplementary Data File 2.

Many challenges came to fruition regarding the application of an appropriate statistical model that could be run without experimental replicates or a defined negative control. Therefore, the normalised RNA-Seq count data was instead manually interrogated to identify transcripts enriched in the Imp-GFP bound CI-AP sample. Normalised count data was calculated using the normalisation factors outputted from the edgeR DGE analysis, which was run according to the R script code in Appendix B, Supplementary Code File 1 (Robinson et al. 2010; McCarthy et al. 2012; R Core Team 2024).

2.9.3. Identification of enriched Imp-interacting transcripts

Imp-enriched transcripts were identified by comparing fold changes between the normalised RNA-Seq counts of the Imp-GFP-bound transcripts vs the combined input of transcripts. Filtering and ordering of these normalised fold changes (values >1.5)

yielded 249 enriched Imp-associated transcripts. The top 20 gene hits were investigated in more detail and gene functions for each of these gene/transcript entries were retrieved and summarised from manual literature searches via FlyBase (release version: FB2024_04). Characterised gene IDs (non-CG numbers) for all outputs were retrieved from FlyBase using the ‘ID Validator’ function (release version: FB2024_04).

2.10. Comparative proteomics analysis of CI-AP protein samples

SDS-PAGE and Western Blot Analysis was performed as described in Section 2.5. to confirm efficient and effective protein trapping and release using the CI-AP GFP-TRAP-Sulfo beads.

Comparative proteomics of the CI-AP-purified Imp-GFP and Sqd-YFP bound protein samples was conducted by the University of Bristol Proteomics Facility. Protein samples were labelled using Tandem Mass Tagging (TMT), in accordance with the manufacturer’s instructions (Thermo Scientific). The TMT-labelled proteins were then pooled and subject to clean-up via off-line High pH Reversed-Phase (RP) Chromatography Fractionation using the Ultimate 3000 Bio-RS HPLC system (Thermo Scientific). This improved proteome coverage and quantitative accuracy. Analysis of the resultant High pH RP fractions was then performed by Nano-LC MS/MS using the Orbitrap Fusion Tribrid Mass Spectrometer (Thermo Scientific). Altogether, this combined approach eliminated run-to-run variability and any 'missing values' that would otherwise be an issue with some label-free approaches. The Proteome Discoverer software (Thermo Scientific) was used to process and quantify the raw datafile outputs. This generated a Microsoft Excel report listing all proteins identified and how the levels of those proteins changed between the two sample conditions under comparison (Imp-GFP and Sqd-YFP).

2.10.1. Identification of enriched Imp-interacting protein binding partners

The proteomics dataset was filtered down to remove any common and non-*Drosophila* contaminants, as well as protein entries with missing quantitation values. The abundance ratio (Sqd-YFP / Imp-GFP) outputted for GFP was set as the threshold to distinguish between putative Imp-enriched protein interactors (<1.245) and putative Sqd-enriched protein interactors (>1.245). Functional enrichment analysis of the Imp-enriched and Sqd-enriched protein lists was performed using the web-based G:Profiler tool (Kolberg et al. 2023). The top highly enriched protein hits in each dataset were explored further, and potential protein functions were determined via manual literature searches using FlyBase (release versions: FB2024_03 and FB2024_04).

2.11. Live cell F-actin staining of *Drosophila* testes

To investigate the co-localisation and spatial overlap of F-actin expression with Imp, Schuy and Tropomyosin-1 (Tm1), respectively, live cell staining of F-actin in the spermatid cyst bundles was performed using SPY555-FastAct™ (SC205, Spirochrome). We stained for F-actin in whole *Drosophila* testes from males of the following fly lines: Imp-GFP G80 protein-trap (BDSC, G00080 exon-trap line; Quiñones-Coello et al. 2007), Tropomyosin-1-GFP (Tm1-GFP, BL51537) and Schuy-TagGFP;Bam-Gal4:VP16 (generated in this project).

In brief, the 1000X DMSO stock solution of SPY555-FastAct™ (SC205, Spirochrome) was diluted to 1:1000 in Schneider's *Drosophila* Medium (Gibco™, cat. no. 21720024). Whole testes were dissected in this modified insect medium, transferred into a fresh droplet on a clean glass slide and the testis contents emptied to isolate individual spermatid cyst bundles. After incubation in the dark for fifteen minutes at RT, testis preparations were squashed with a coverslip. Phase contrast and fluorescence microscopy was performed using the Olympus BX50 fluorescence upright microscope (Olympus Life Science). Single channel greyscale fluorescence images were processed by background subtraction with a rolling ball radius of 100 pixels. Separate channels were assigned/overlayed with pseudo-colouring and then merged into a single image via ImageJ v1.52d (Schneider et al. 2012). Quantification of mean pixel

intensity and production of corresponding signal profile plots was performed in ImageJ v1.52d via its segmentation line measurement tool (Schneider et al. 2012). Composite figures were created in Adobe Photoshop 2024.

2.12. *Drosophila* genetics and phenotypic analysis of *imp* gene knockdowns

2.12.1. Crossing to yield a bipartite Bam-Gal4/Imp-UAS-RNAi expression system

Virgin females were selected from a stable stock expressing the genotype of either w; *schuy*-TagGFP/(CyO); Bam-Gal4:VP16/(TM3,Sb) or w; *c-cup*-TagGFP/(CyO); Bam-Gal4:VP16/(TM3,Sb). These flies express at least one copy of a TagGFP-fused comet or cup transgene on the second chromosome. This arrangement comprises the gene's 5' UTR and its coding sequence, followed by the TagGFP sequence which is in turn flanked by the gene-specific 3' UTR. Altogether, it encodes a fluorescent variant of the TagGFP-tagged schuy or c-cup protein, which is expressed alongside the native, endogenous comet and cup protein in the *Drosophila* testis. This stock also expresses a near-homozygous viable Bam-driven Gal4 gene arrangement inserted on the third chromosome, which drives Gal4 protein expression in the late spermatogonia and early-to-mid spermatocytes of *Drosophila melanogaster* (Chen and McKearin 2003a; Chen and McKearin 2003b). The Bam-Gal4:VP16 driver comprises a germ cell associated ~900bp genomic promoter and a 5' UTR, both from the *bag-of-marbles* (*bam*) transcriptional unit, as well as a 3' UTR from *Hsp70* (White-Cooper 2012). The DNA-binding domain of Gal4 is fused to a transcriptional activation domain from the Herpes simplex virus Type 1 VP16 gene to generate Gal4::VP16, an artificial transcriptional driver with enhanced activity and efficiency (Sadowski et al. 1988).

Virgin females were crossed with various transgenic Imp-UAS-RNA inference (RNAi) males at 25˚C (See Table 2. in Section 2.1.). A parallel cross to WT w^{1118} males provided a negative control of the WT genetic background. Without the Bam driver or Gal4 sequence present, there would be no Gal4-mediated activation of transcription, no expression of the UAS-hairpin upon crossing and hence no RNAi knockdown phenotype to report in this condition. As the level of RNAi hairpin expression and gene

knockdown activity can be manipulated by rearing flies at different temperatures, a strict temperature scheme was selected to maximise hairpin expression. Immediately after crossing, parental flies were placed at 25˚C for 2 – 3 days, before subsequent transfer into fresh food vials. Resultant Filial 1 (F1) cultures were then transferred to 29˚C, where they were maintained throughout their life cycle until eclosion and male collection.

2.12.2. Preliminary screening of RNAi-mediated phenotypes using phase contrast and fluorescence microscopy

Our RNAi screening process can be divided into two distinct parts. In the preliminary screen, we were looking to determine whether the translation and protein expression patterns of localised mRNAs, *schuy* and *c-cup*, were modified in any observable way when crossed with a selection of Imp-RNAi lines (Table 2. in Section 2.1.). The testis phenotype of F1 RNAi adult males aged 0 – 2 days post-eclosion were analysed using the Olympus BX50 fluorescence upright microscope (Olympus Life Science) for both phase contrast and fluorescence microscopy (Fig. 6.).

Phase contrast microscopy was performed to observe any RNAi-induced phenotypic variations in testis ultrastructure and morphology, along with any changes to cell cycle progression and the program of differentiation. Fluorescence microscopy enabled visualisation of alterations to schuy-TagGFP and c-cup-TagGFP protein expression and distribution, including modifications to the characteristic speckling (schuy) and gradient (c-cup) localisation patterns and their distribution of local translation throughout the spermatid tail-ends. Composite figures were created in Adobe Photoshop 2024.

Quantification of mean signal intensities was performed using both the segmentation line tool and standardised ROI measurement features in ImageJ v1.52d (Schneider et al. 2012). Analysis of descriptive statistics was performed using the jamovi Cloud Online Statistical Software (version 2.6.44), which was accessed here: https://www.jamovi.org/.

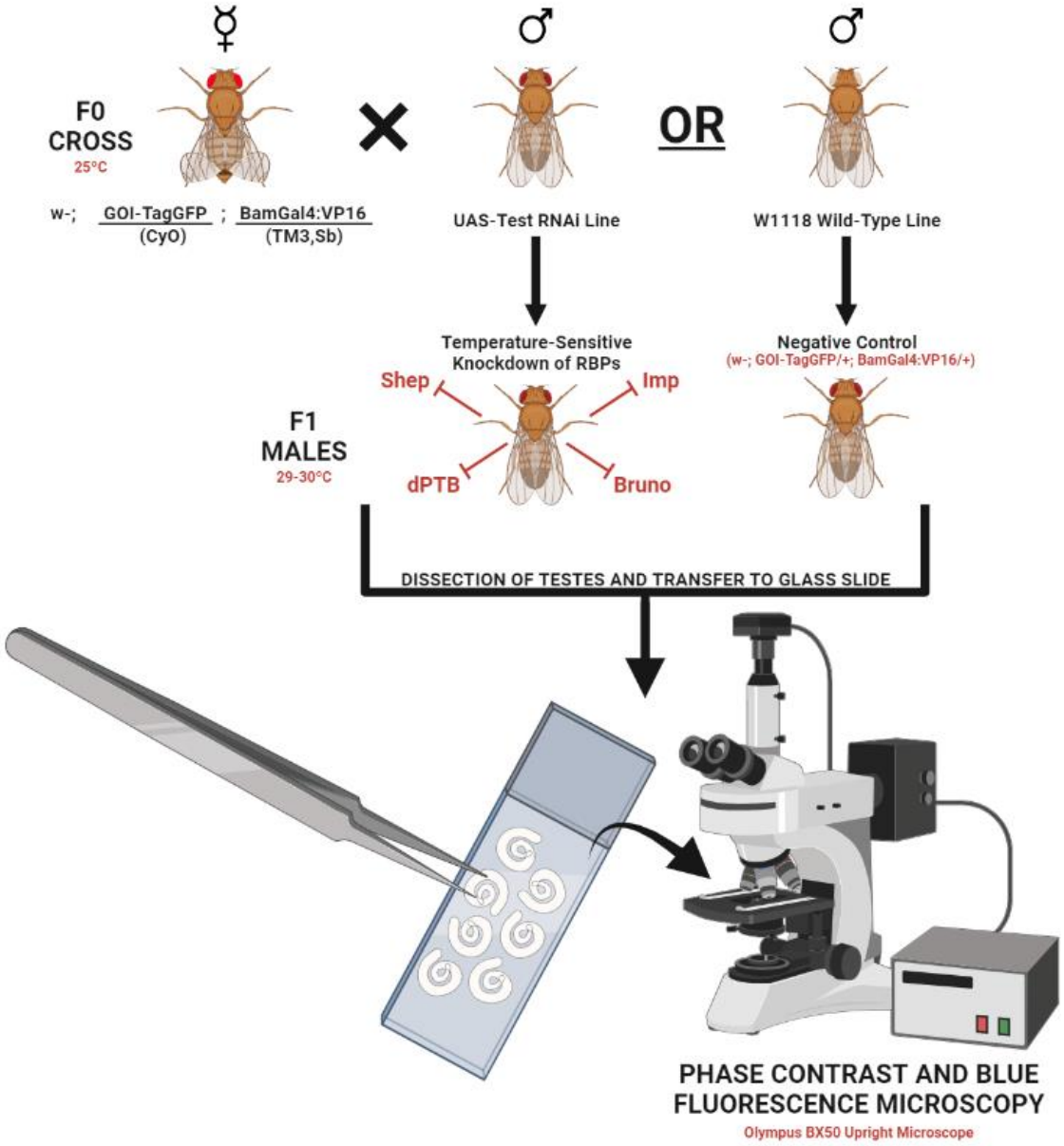

Figure 7. General overview of the *Drosophila* genetic mating scheme and Imp-UAS-RNAi screening strategy. Phenotypic analysis was performed to characterise testis-specific *imp* gene functions. Testes from resultant genotyped Imp-RNAi F1 males were screened to determine what impacts, if any, the *imp* gene knockdowns had on sperm development. The effects of *imp* depletion on post-meiotic comet and cup protein expression in the spermatid cyst bundles was also explored. **Created using BioRender.com.**

The Shapiro-Wilk test for normality was performed prior to statistical analysis using the web-based calculator provided by "Statistics Kingdom". This online tool was accessed via the following weblink: https://www.statskingdom.com/shapiro-wilk-test-calculator.html. None of our mean pixel signal intensity datasets showed a significant statistical deviation away from the normal distribution. Using the jamovi Cloud Online Statistical Software (version 2.6.44), we thus conducted a series of paired samples t-tests to directly compare the significance of the mean pixel intensity signals quantified between the testes of our WT control crosses and the different Imp-UAS-RNAi knockdown genotypes.

2.12.3. Hybridisation chain reaction RNA fluorescence *in situ* hybridisation (HCR RNA-FISH) to visualise localised mRNAs in whole-mount *Drosophila melanogaster* testes

In part two of the screen, hybridisation chain reaction RNA fluorescence *in situ* hybridisation (HCR RNA-FISH) and Lightsheet Fluorescence Microscopy (LSFM) was performed to ascertain whether the RNAi-induced defects seen in preliminary screening were attributed to translational disruption alone, or whether this dysregulation was detectable at an earlier point of mRNA production, stability and/or localisation (Fig. 7.). The expression profiles and localisation patterns of RNA transcripts for two genes previously characterised as comet and cup genes, *schuy* and *c-cup*, were therefore investigated further.

HCR RNA-FISH is a two-stage procedure including the first point of sample dissection and storage, followed by three subsequent phases of hybridisation, amplification and washing. The method described here follows an updated protocol based on publications from Choi et al. (2016) and Choi et al. (2018). Previous iterations are also described by Choi et al. (2010) and Choi et al. (2014).

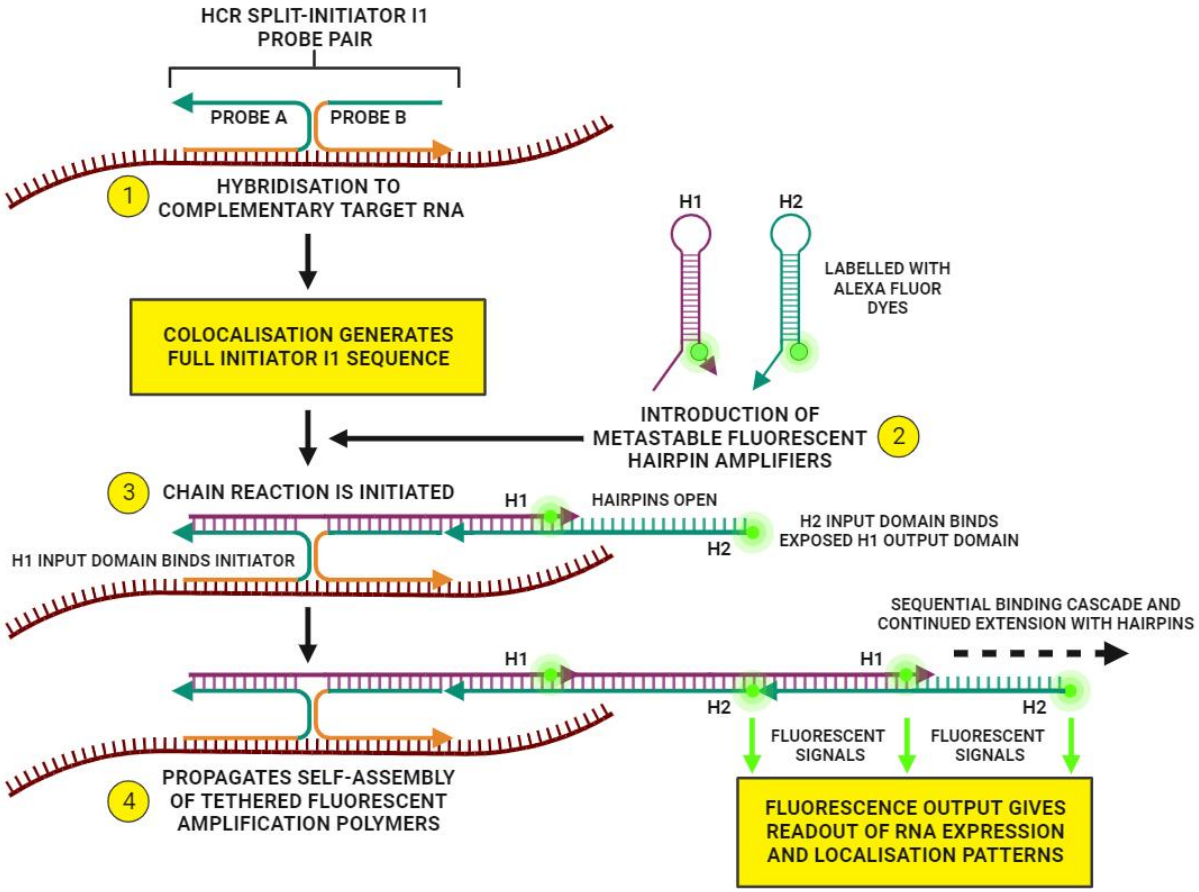

Figure 8. The HCR RNA-FISH approach performed on *Drosophila melanogaster* testes. The metastable HCR hairpin amplifiers comprise pairs of two kinetically trapped DNA hairpin species, H1 and H2. Both are structured hairpins with a duplex stem, and are fluorophore-labelled with specific, spectrally distinct Alexa dyes (Choi et al. 2016; Choi et al. 2018). Energy stored within these hairpins drives a conditional chain reaction – a self-assembly cascade – when triggered by exposure to a full, co-localised initiator I1 sequence. This is only possible upon completion of the complementary initiator, which is brought together upon binding of cooperative split-initiator probes to adjacent sites in the target transcript of interest (Dirks and Pierce 2004; Choi et al. 2014). Initiator I1 hybridises to the input domain of hairpin H1, unfolding the hairpin to expose its output domain. The exposed H1 output domain in turn hybridises to the input domain of hairpin H2, which triggers the sequential opening of hairpin H2 and exposure of an output domain that is identical in sequence to initiator I1. Together, this provides the basis for a chain reaction of alternating H1 and H2 polymerisation phases, culminating in the self-assembly of a tethered fluorescent amplification polymer. Strong fluorescent signals can then be detected as a readout of *in vivo* mRNA transcript expression patterns (Choi et al. 2010; Choi et al. 2018). **Recreated from Choi et al. (2016) and Choi et al. (2018) using BioRender.com.**

2.12.3.1. Designing RNA-specific split-initiator probe pairs for HCR RNA-FISH

Probes were designed using an HCR RNA-FISH-specific “Probe Picker” Python script, kindly provided by Matthew Jachimowicz (University of Toronto). All scripts were run via the interface PyCharm 2022.2.2 (Community Edition) to automatically generate a breadth of split-initiator probe pairs.

All split-initiator probe pairs were designed to be complementary to specific sub-sequences within a mRNA target of interest or to an associated tagged label sequence (e.g., TagGFP). Each probe comprised a DNA oligonucleotide sequence, which included a ~25 nt stretch to match the target, a HCR amplifier-specific initiator sequence and a short spacer. The generation and selection of these probes was performed to account for strict criteria. All sub-sequences were designed so that they: (i) fell within accessible regions, with as few known difficult structures or folds as possible (i.e., not the absolute 5’ UTR or extreme 3’ UTR end), (ii) had no off-target hits/homologies elsewhere that could interfere and cause non-specific, off-target binding interactions, and (iii) were chosen to reflect regions with a high stringency for GC percentage (%GC) content.

In short, the 717 bp coding sequence for TagGFP was downloaded and copied over into a .txt file format from the pTagGFP2-N vector (Evrogen, cat. no. FP192) and implemented as the input sequence for the probe design process (Xia et al. 2002; Subach et al. 2008). To change the initiator sequence that was added into the final probe design, the script was modified to incorporate 1 of 6 fluorescent HCR hairpin amplifiers of choice (i.e. B1, B2, B3, B4, B5 or B6). These fluorescent HCR hairpin amplifiers were ~100 nt long with a 32 nt initiator-specific domain and a 70 nt stem-loop, and each one was labelled with a specific Alexa fluor dye. If multiplexing, this choice was adjusted to remove non-overlapping initiator sequences and to account for a suitable combination of labelled Alexa fluor dyes that would minimise emission spectrum intersection and channel bleed-through. For high GC-rich sequences like TagGFP, a stringent %GC range of 40% – 60% was used to select specific sub-sequences for probe generation.

Once these amendments were incorporated, all potential probes were outputted in a multi-FASTA format that gave the two half probes in each pair, and all possible pairs for the transcript of interest. A second separate “Specificity Check” multi-FASTA file was also simultaneously created that only contained the mRNA-specific sub-sequences each probe will bind to, not including the initiator sequence and spacer nucleotides.

All split-initiator probe pairs were individually checked to prevent off-target complementarity and binding specificity using NCBI's Web Nucleotide Basic Local Alignment Search Tool (BLASTN) (Altschul et al. 1990). The mRNA-specific subregions of each individual probe from the Specificity Check file were submitted as query sequences for comparison and alignment against the *Drosophila melanogaster* reference RNA sequences (refseq_rna) database. The search was also amended to highly similar sequences (megablast) to ensure that all probe sub-sequences were unique to the target transcript. Final selections were based on BLASTN results that showed no significant off-site hits and a low percentage identity that only matched to short stretches of the probe sequence.

From these, a final set of four split-initiator probe pairs were picked for the TagGFP coding sequence, so that they bound at regular intervals along the sequence, with coverage along the entire length of the TagGFP transcript (Table 5.). The split-initiator probe sets were then synthesised as purified 25 nmole DNA oligonucleotides with standard desalting (Integrated DNA Technologies). Individual probes were reconstituted to a working stock concentration of 100 μM by resuspending in distilled water.

Table 5. Final selection of four HCR RNA-FISH split-initiator probe pairs designed to target the TagGFP mRNA transcript. Probes were generated for specific complementarity to the TagGFP coding sequence. Summary includes the TagGFP-complementary sequence, as well as the full probe sequence combined with both the spacer nucleotides and the B2 initiator sequence. Probe regions highlighted in yellow correspond to the B2-specific hairpin amplifier sequences, which together make-up the full-length initiator I1 sequence when co-localised. These four split-initiator probe pairs, comprising eight individual probes in total, were ultimately taken forward because they were complementary to evenly spaced sequence regions along the transcript length and had a low number of continuous base pairs that matched to other off-target sequences.

HCR PROBE	TagGFP SPECIFIC REGION	FULL PROBE SEQUENCE
TagGFP_B2_1A	CTCTGCTACGGCATCCAGTGCTTCG	CCTCgTAAATCCTCATCAAACGAAGCACTGGATGCCGTAGCAGAG
TagGFP_B2_1B	CCCGCTACCCCGAGCACATGAAGAT	ATCTTCATGTGCTCGGGGTAGCGGGAAATCATCCAgTAAACCgCC
TagGFP_B2_2A	AAGTACAAGACCCGCGGCGAGGTGA	CCTCgTAAATCCTCATCAAATCACCTCGCCGCGGGTCTTGTACTT
TagGFP_B2_2B	AGTTCGAGGGCGACACCCTGGTGAA	TTCACCAGGGTGTCGCCCTCGAACTAAATCATCCAgTAAACCgCC
TagGFP_B2_3A	CAAGCTGGAGTACAGCTTCAACAGC	CCTCgTAAATCCTCATCAAAGCTGTTGAAGCTGTACTCCAGCTTG
TagGFP_B2_3B	CACAACGTGTACATCCGCCCCGACA	TGTCGGGGCGGATGTACACGTTGTGAAATCATCCAgTAAACCgCC
TagGFP_B2_4A	CCCGTGCTGATCCCCATCAACCACT	CCTCgTAAATCCTCATCAAAAGTGGTTGATGGGGATCAGCACGGG
TagGFP_B2_4B	ACCTGAGCACTCAGACCAAGATCAG	CTGATCTTGGTCTGAGTGCTCAGGTAAATCATCCAgTAAACCgCC

2.12.3.2. Sample dissection, fixation and storage for HCR RNA-FISH

An initial 40% paraformaldehyde (PFA) stock solution, supplemented with 2N potassium hydroxide, was prepared and heated over boiling water until the PFA was fully dissolved. The 40% PFA fixative solution was cooled on ice for five minutes, then filtered into 1X PBS with 0.1% Tween-20 (1X PBT) via a 0.22 µM filter unit (Millex GP) and 1 mL syringe (BD Plastipak) to generate a diluted 4% PFA fixative solution. A further 1:10 dilution was also performed to create an accompanying 0.4% PFA Dissection Buffer.

All F1 RNAi adult males aged 0 – 2 days post-eclosion were collected and genotype-selected for dissection. *Drosophila melanogaster* males expressing the required genetic markers, and hence indicating a correct genotype, were rendered unconscious and their testes dissected into 0.4% PFA Dissection Buffer. A total of twenty to forty testes were accumulated per RNAi cross, followed by fixing in 600 µL 4% PFA fixative solution on a rocking platform for thirty minutes at RT. After fixing, samples were washed twice for five minutes in 1X PBT, followed by washing for five minutes in 100% methanol. A final aliquot of fresh 100% methanol was then added to 1 mL and samples stored at –20˚C until required.

2.12.3.3. Hybridisation of split-initiator probe pairs to target mRNA transcripts

Testis samples were transferred over from –20˚C storage to RT and the 100% methanol aspirated, before rinsing with 1X PBT. After washing for ten minutes at RT, the 1X PBT was removed and pre-hybridisation commenced with the addition of 100 µL 37˚C-preheated 30% probe hybridisation buffer (30% formamide, 30% 5X sodium chloride sodium citrate (SSC), 9 mM citric acid, pH 6.0, 0.1% Tween-20, 50 µg/mL heparin, 5X Denhardt's solution, 10% dextran sulphate). The pre-hybridisation step was performed for thirty minutes at 37˚C.

While incubating, a probe + 30% hybridisation mix was prepared by adding 0.4 µL of each individual 100 µM split-initiator probe (for all probe pairs) into 100 µL 37˚C-

preheated 30% Probe Hybridisation Buffer. Once the pre-hybridisation period had ended, both the testis samples and the probe + 30% hybridisation mix were heated at 80˚C for five minutes using a PCR thermocycler machine. The 30% probe hybridisation buffer was carefully removed from the testis samples and the 100 µL of 80˚C-heated probe + 30% hybridisation mix was added to each individual sample tube. Finally, split-initiator probe hybridisation was initiated by incubating for five minutes at 80˚C and then incubating overnight at 37˚C.

2.12.3.4. Fluorescent HCR hairpin amplification

Following the overnight hybridisation step, the samples were washed four times for twenty minutes with 37˚C-preheated 30% probe wash buffer (30% formamide, 5X SSC, 9 mM citric acid, pH 6.0, 0.1% Tween-20, 50 µg/mL heparin) to remove any unused, un-hybridised DNA probes.

During this ongoing wash step, the HCR hairpin amplification solution was also prepared. In their proprietary hairpin storage buffer, 2 µL of each individual 3 µM fluorescent HCR hairpin amplifier (H1 and H2; Molecular Instruments, Inc.) was heated separately to 95˚C for 90 seconds and then snap-cooled to 18˚C for at least thirty minutes in a PCR thermocycler machine. The HCR amplifier mix was then prepared by adding 2 µL of each snap-cooled hairpin (4 µL total for H1 + H2) into 50 µL of amplification buffer (5X SSC, 0.1% Tween-20, 10% dextran sulphate) at RT. The final volume of each HCR hairpin amplifier in the pair was modified depending on the number of different samples being probed for the same TagGFP transcript. When a master mix was prepared for this, the volumes of the H1 hairpins, H2 hairpins and amplification buffer were all multiplied by the total number of reactions. Fluorescent HCR hairpin amplifiers were kept in the dark on ice between uses to minimise light exposure and thermal degradation.

After removing the final wash of 37˚C-preheated 30% probe wash buffer, 100 µL of plain hairpin amplification buffer (without HCR hairpin amplifiers) was added to commence the pre-amplification reaction. The samples were then incubated at RT for thirty minutes. Upon completion of the pre-amplification step, the final HCR amplifier

mix was added to ~54 µL per sample. Amplification was then performed by incubating overnight on a nutator at RT, rocking gently in the dark to prevent photobleaching.

2.12.3.5. Washing and preparing samples for imaging

Testis samples were washed four times for five minutes in 5X sodium chloride sodium citrate with 0.1% Tween-20 (5X SSCT) to remove unused, un-polymerised HCR amplifier hairpins. After removal of the final 5X SSCT wash, samples were washed three times for five minutes in 1X PBS to remove any remnants of detergent. Samples were maintained in the dark throughout washing. The concluding 1X PBS wash was then replaced with 1 mL fresh 1X PBS, and the samples kept in the dark at 4˚C until mounting. If counterstaining for DNA, a 1:1000 dilution of Hoechst 33258 was added to this final 1X PBS storage volume for at least one hour prior to mounting for microscopy.

2.12.3.6. Sample preparation and embedding in agarose for Lightsheet Fluorescence Microscopy (LSFM)

A solution of 1% (w/v) low gelling temperature agarose (Sigma-Aldrich, A9414) was made up in 1X PBS, requiring regular vortexing and heating to ≥60˚C for at least thirty minutes until fully dissolved. After melting, the agarose was maintained at this temperature throughout the mounting process and returned back to the heat block between uses.

Testis samples were transferred over to a pre-warmed glass concave staining dish in ~50 µL of the 1X PBS storage volume. The majority of 1X PBS was then aspirated and carefully replaced with 1 mL of molten 1% (w/v) agarose, ensuring that all testes were well-covered. Unless stated otherwise, the green-collared, size 3 glass capillary tube (1.5/2.0 mm diameter) and plunger combination was used for all cases of sample mounting.

Prior to sample uptake, plain melted agarose was brought up into the capillary-plunger set-up to a midway point (~1.25 cm) between the capillary end and the green collar band. Testis samples were then taken up into the capillary, at evenly spaced intervals along its length, to a final preparation of four to six testes of the same genotype per agarose cylinder. Care was taken to minimise air bubble uptake. A small final volume of plain melted agarose was brought up to seal off the matrix and provide a short distance between the final sample and capillary end. Using manual dexterity, the capillaries were then gently rotated in a horizontal orientation for twenty minutes to position the testes towards the centre of the agarose cylinder as it solidified. The capillaries were then transferred into a falcon tube containing 5 – 8 mL of 1X PBS to prevent the agarose from drying out. Mounted samples were stored upright in the dark at 4˚C until imaging.

2.12.3.7. LSFM imaging to generate three-dimensional, multicolour datasets

A fully integrated turn-key Zeiss Lightsheet Z.1 single plane illumination microscope (SPIM) system equipped with 10x/0.2 Illumination Optics, 20x/1.0 Pan Neofluar Corr (WD = 5.6 mm) Detection Optics and two high resolution sCMOS PCO.Edge cameras was used to image the whole-mount *Drosophila melanogaster* testes. Once solidified, the testis samples were embedded in a free-hanging agarose cylinder within the capillary, which could then be inserted into a mount and held in place within the Zeiss Lightsheet Z.1 System. The sample-embedded agarose cylinder was then pushed out of the capillary for imaging in the aqueous environment of a closed, internally confined 1X PBS filled chamber. This enabled three-dimensional, multi-colour imaging of thick fluorescent samples with high spatiotemporal resolution and optical sectioning (Huisken et al. 2004).

Image acquisition, processing and rendering of images was achieved using the Zeiss Zen software and Arivis Vision4D software. Acquisition parameters were set at a 16-bit depth with dual side fusion and pivot scan. The 405nm laser line was used to visualise nuclear DNA staining with Hoechst 33258 and the 488nm laser line was used to visualise the B2-Alexa488 hairpin amplifiers corresponding to TagGFP. Each laser

line was calibrated with the auto-adjust feature prior to imaging. Using the range indicator function as guidance, laser power and exposure time were adjusted accordingly for each sample to prevent oversaturation. In general, laser power was set to 9.0% – 11.0%, while exposure time ranged from 90ms – 130ms. The first and last slices were designated to obtain a Z-stack of approximately 300 – 500 slices per dataset, and the optimal interval option was selected to automatically define the micron slice depth. Composite figures were created in Adobe Photoshop 2024. Training and microscope access was provided by the Cardiff University Bioimaging Hub Core Facility, RRID:SCR_022556.

3. RESULTS CHAPTER 1: Characterisation of binding interactions with comet and cup mRNAs using RNA-affinity pull-down assays

3.1. Elucidating putative RNA binding protein interactions with comet and cup mRNAs

As mentioned in the Introduction (Section 1.15.), a number of different RBPs localise to the distal tail-ends of growing spermatids, in regions similar to the comet and cup mRNAs. One hypothesis is that some of these RBPs are responsible for regulating the localisation and/or anchoring of comet and cup mRNA transcripts to their target sites. If so, it is also possible that this regulation could extend to the modulation of mRNA behaviour, once localised. These RBPs could also be key players in the regulation of post-transcriptional processing, mRNA stability and degradation, translational repression and/or activation. By investigating a small selection of these RBPs, this PhD project looks to address this hypothesis. We chose Bruno (Bru1), Polypyrimidine-Tract-Binding Protein (dmPTB), Alan Shepard (Shep) and IGF-II mRNA-binding protein (Imp) as our primary candidates of interest because they are all known to be key players in the post-transcriptional regulation of a variety of developmentally-relevant mRNAs. Our research group has also had previous experience working with these particular RBPs and, fundamentally, we already had optimised assay reagents available for their targeted investigation.

I will now introduce each of these RBPs individually, before then delving into our experimental outcomes and interpretations.

3.2. Bruno (Bru1)

Drosophila Bruno (Bru1) is an evolutionarily conserved RBP encoded by the *arrest (aret)* gene locus (Kim et al. 2015). It is an integral member of the CELF/Bruno-like

(BRUNOL) family and is a relative of the Elav family of proteins (Good et al. 2000; Barreau et al. 2006). Bru1 can physically interact with multiple mRNAs to drive their translational repression and/or activation, and even alternative splicing (Webster et al. 1997a; Reveal et al. 2010; Spletter et al. 2015). Bru1 is also a known regulator of several female germline mRNAs, and its high degree of evolutionary conservation indicates that it is of great importance in many different organisms (Webster et al. 1997a; Moore et al. 2009).

Mutant analyses have together confirmed that *bru1* is a pleiotropic gene, with a vast and ever-evolving repertoire of genetic and physical interactions (Yan and Macdonald 2004). Observations within *Drosophila* oocytes and flight muscles suggest that Bru1 can shuttle freely between the cytoplasm and nucleus to mediate such wide-ranging roles (Snee et al. 2008; Spletter et al. 2015).

It is a phosphoprotein that contains three conserved RNA recognition motif (RRM) domains and is post-translationally phosphorylated at its amino terminal domain (Snee et al. 2008; Kim et al. 2015). Two of its RRMs are positioned towards the amino terminus and an extended RRM is located at its C terminus. It has been proposed that these three different RNA binding domains in Bru1 are responsible for its combinatorial binding capabilities (Reveal et al. 2011). Bru1 recognises and interacts with targets via these RRMs, binding specific repeated sequences called Bruno Response Elements (BREs) (Kim-Ha et al. 1995). Together, these RRM domains enable Bru1 to achieve high levels of target specificity and affinity (Reveal et al. 2011). Bru1 also possesses an N-terminal prion-like domain, comprising an unstructured region enriched for serine and asparagine, which likely contributes to a role in scaffolding and the formation of higher-order particle complexes (Chekulaeva et al. 2006; Bose et al. 2022).

3.2.1. Bru1 may be implicated in male fertility and post-meiotic differentiation

Bru1 is enriched within the *Drosophila* ovaries and has hence been described extensively in this context. However, considerably less information has been published about *bru1* expression within the *Drosophila* testis and its function within late spermatogenesis. The most in-depth work published thus far employed a combined

approach of Northern Analysis, Western Blotting and UV-Crosslinking experiments to analyse testis extracts (Webster et al. 1997a). In doing so, they were able to characterise the expression of two large sex-specific isoforms of Bru1, enriched exclusively within the *Drosophila* testis (Webster et al. 1997a; Venables and Eperon 1999).

Early studies also described the testis-specific mutant phenotypes of the *aret* locus, but these were very brief. Mutagenesis of the *aret* locus was linked to male-sterility and post-meiotic differentiation defects, including a deficiency in motile sperm and a reduced number of sperm bundles within the testis (Schüpbach and Wieschaus 1991; Castrillon et al. 1993).

Bru1 regulates a whole host of mRNAs involved in female and male gametogenesis, as well as in early embryogenesis (Webster et al. 1997a). Bru1 therefore makes for an interesting and novel RBP candidate to include in our investigations because it is necessary for fertility in both sexes, yet little is known about Bru1's function in the testes.

3.2.2. Bru1 is a known regulator of translational activity in *Drosophila* oogenesis

Bru1 is a known interactor and regulator of many known determinants responsible for the establishment of body patterning in *Drosophila*, which makes it an extremely important developmental RBP (Schüpbach and Wieschaus 1991; Webster et al. 1997a). For example, interactions of Bru1 with the *osk* 3' UTR have been characterised in oogenesis, prior to the localisation of *osk* mRNAs to the posterior pole of the oocyte (Kim-Ha et al. 1995). Bru1 has subsequently been found to repress *osk* translation, acting to control *osk* localisation at the protein level (Kim-Ha et al. 1995; Gunkel et al. 1998; Castagnetti et al. 2000). A multitude of *trans*-acting factors, including Apontic, Bicaudal-C, Me31B and p50, have all been linked to the Bru1-dependent translational repression of *osk* in egg development (Wharton and Struhl 1991; Lie and Macdonald 1999; Johnstone and Lasko 2001; Wilkie et al. 2003). This suggests that Bru1 possesses an extensive interacting network and operates in

conjunction with different protein binding partners to mediate the translational co-repression of mRNA targets such as *osk*.

There are at least three more key targets of Bru1-mediated translational repression that have been published in the literature: *Sex-lethal* (*Sxl*), *gurken* (*grk*) and *Cyclin A* (*CycA*) (Filardo and Ephrussi 2003; Sugimura and Lilly 2006; Wang and Lin 2007; Moore et al. 2009). With regards to the interplay of Bru1 with *grk*, Bru1 can interact with the *Drosophila* heterogenous nuclear RBP (hnRNP), Squid (Sqd), to couple *grk* mRNA localisation and translation in egg development (Norvell et al. 1999). Results from *in vitro* association and *in vivo* co-immunoprecipitation assays suggest that, as Sqd directs nuclear export of *grk* mRNAs for localisation within the oocyte cytoplasm, it physically interacts with Bru1 and recruits it for the translational regulation of *grk* transcripts (Norvell et al. 1999). This once again supports the ability of Bru1 to bind and cooperate with a network of several different interactors to facilitate the post-transcriptional regulation/translational control of localised developmental mRNAs.

3.2.3. Bru1 is heavily implicated in large repressive RNP assemblies

More recent findings have proposed that Bru1's translational repression activity is attributed to its amino-terminal domain (Kim et al. 2015). Bru1 has even been shown to act as a "dual repressor" in *in vitro* cell-free translation systems derived from *Drosophila* ovaries and embryos (Chekulaeva et al. 2006). By interacting with Cup and eIF4E, this can drive Bru1-dependent oligomerisation of target *osk*,mRNAs and promote their sequestration into large RNP silencing particles (Nakamura et al. 2004; Chekulaeva et al. 2006). By doing so, this simultaneously restricts accessibility of translation machinery and protects suppressed mRNAs against degradation machinery, providing an additional layer of translational regulation. Together, this suggests that Bru1 is a translational regulator in the pre-translational transition of target mRNAs; coupling to post-transcriptional mRNA transport and localisation, rather than regulating them both directly (Chekulaeva et al. 2006). It also indicates that Bru1 can establish high order, multi-functional RNP complexes.

3.3. Polypyrimidine-Tract-Binding Protein (dmPTB)

Drosophila Polypyrimidine-Tract-Binding Protein (dmPTB) is a RBP homologue of mammalian PTB, encoded by the *hephaestus (heph)* gene. PTB was first identified in vertebrates via UV crosslinking experiments of HeLa cell nuclear extracts, and was found to bind intronic polypyrimidine tracts upstream of multiple 3' pre-mRNA splice sites (García-Blanco et al. 1989). dmPTB is a multi-functional hnRNP, which contains four distinct RRMs and a putative N-terminal nuclear localisation signal (Davis et al. 2002; Oberstrass et al. 2005; Besse et al. 2009). Unlike other functionally-similar RBPs, dmPTB lacks any substantial disorder, with no obvious unstructured regions in its protein structure (Bose et al. 2022).

dmPTB is a nucleo-cytoplasmic shuttling protein, with known roles in translational regulation and as a structural component of key developmentally-related RNP complexes (Besse et al. 2009). It recognises and binds polypyrimidine-rich tracts, which generally comprise motifs such as UCUU, UUCU, UCUUC and UUCUCU embedded in wider, extended pyrimidine-rich sequences (Singh et al. 1995; Pérez et al. 1997). dmPTB has been implicated in several key regulatory events, including the activation and repression of alternative splicing, formation of RNP-complexes, post-transcriptional regulation of mRNA stability and 3' processing, and modulation of translation (Knoch et al. 2004; Sawicka et al. 2008; Besse et al. 2009; Kafasla et al. 2012). As with its mammalian homologues, dmPTB expression and activity is enriched throughout the testis and male germline (Lilleväli et al. 2001; Davis et al. 2002).

3.3.1. Early characterisation of dmPTB in male sterility screening assays

dmPTB was first identified by Castrillon et al. (1993) from a genetic screen for male sterility in *Drosophila melanogaster*. Of 83 recessive autosomal male-sterile mutations generated by single P-element transposon mutagenesis, the loss-of-function $heph^{1}$ and $heph^{2}$ mutants were subsequently described. Both mutants were found to be male-sterile, female-fertile and showed good viability overall. The main mutation phenotype observed was a dilation of the mutant testis tip, up to roughly two times that of the WT circumference, suggesting early evidence of a sex-specific role in male

fertility (Castrillon et al. 1993). Subsequent *in situ* hybridisations and antibody staining supported this; with high-level dmPTB expression reported in regions slightly posterior to the extreme distal tip of the testis, corresponding to the nuclei of primary spermatocytes. This gave an early indication of dmPTB's role within the post-meiotic stage of male gamete development (Davis et al. 2002; Robida et al. 2010).

More specifically, dmPTB has been linked to the expression of large *Y*-chromosome-associated genes kl-5, kl-3 and ks-1 in primary spermatocytes (Fingerhut et al. 2019). These *Y*-linked genes contain gigantic megabase-sized introns, encoding a selection of "fertility factors" and go on to form lampbrush-like nucleoplasmic structures termed Y-loops. Analysis of GFP-protein traps, *heph* mutant lines and RNA-FISH has shown that at least one isoform of dmPTB specifically localises to the kl-5 and ks-1 Y-loops. It is hypothesised that dTPB can act to structurally organise and regulate the processing and stability of Y-loop transcripts (Fingerhut et al. 2019). While dmPTB is broadly expressed throughout the testis, its interactions with these abundant nuclear *Y*-chromosome fertility transcripts allow dmPTB to be utilised as a spermatocyte-enriched marker of spermatogenesis (Anderson et al. 2023).

3.3.2. dmPTB plays a role in spermatid individualisation

The unusual mutant tip enlargement associated with $heph^2$ was later verified in follow-up research (Robida and Singh 2003). Northern analysis revealed that expression of the abundant male-specific isoform of dmPTB is abolished in homozygous $heph^2$ mutants. While cysts containing elongated spermatids continued to accumulate within mutant testes, there was no culmination in the normal, WT production of separated motile sperm. Abnormal bulging along the length of the spermatid tails was indicative of an individualisation defect, suggesting that a loss of dmPTB leads to aberrant spermatid differentiation (Robida and Singh 2003). Northern Analysis preliminarily suggested that expression of the most abundant dmPTB isoform predominates exclusively within the male germline of adult *Drosophila melanogaster*. However, upon prolonged exposure, expression of minor dmPTB transcripts were also revealed in female RNA extracts (Robida and Singh 2003).

In-depth molecular genetic analysis of the loss-of-function *heph*^{2} mutant confirmed that male sterility occurs due to interference with the actin cones of the spermatid individualisation complex (Robida et al. 2010). Comparative staining of WT and *heph*^{2} mutant testes, with fluorescently labelled actin-binding phalloidin and DNA-binding DAPI, confirmed that loss of dmPTB correlates with the disorganisation and uncoordinated, defective movement of actin cones. This showed that WT dmPTB expression is indeed necessary for proper spermatid individualisation, which in turn feeds into the production of normal, motile sperm.

The sex-specific molecular defects of *heph*^{2} mutants in *Drosophila* spermatogenesis have recently been investigated using unbiased high-throughput RNA-seq and independent verification via RT-PCR analysis (Sridharan et al. 2016). According to transcriptome profiling, approximately 96% of *dmPTB* transcripts in the homozygous *heph*^{2} mutant were truncated. Comparative analysis of differentially expressed genes in the WT control vs. this *heph*^{2} mutant showed that levels of Nedd2-like caspase, which was previously characterised in a caspase activation pathway essential for spermatid individualisation, declined by half (Huh et al. 2003; Sridharan et al. 2016). In contrast, levels of oxen, originally identified in the same pioneering genetic screen of male-sterile mutants as *heph*^{2}, rose by ~2.5 times (Castrillon et al. 1993; Sridharan et al. 2016).

A multitude of transcripts were also found to be abnormally expressed in the *heph*^{2} mutant, showing mis-regulation of exon skipping and splicing of alternative 5’ ends. Most interestingly, the splicing patterns of transcripts related to actomyosin cytoskeletal components were significantly affected, including *Myosin light chain 1* (*Mlc1*), which was aberrantly spliced with increased exon skipping. Phylogenetic analysis of twelve *Drosophila* species revealed a conserved extended C/U-rich sequence within the skipped *Mlc1* exon, which in turn resembled a high-affinity dmPTB consensus binding site. These findings together reinforce the importance of dmPTB in the male germline-specific regulation of transcript processing, particularly for those transcripts implicated in the actomyosin cytoskeletal-related process of spermatid individualisation. This regulation cytoskeletal machinery may, speculatively, be extended to possible anchoring and localisation of other targets, including mRNAs. Altogether, these findings unveil dmPTB as a key biological player in male fertility and a rational RBP candidate to investigate further.

Previous screening of the YFP exon-trapped insertion line for dmPTB has also shown that the RBP is expressed and localised to a single large particle at the elongating tail-ends of each spermatid throughout spermiogenesis, being lost only at individualisation stages (H. White-Cooper, Personal Communication; Lowe et al. (2014)). As this is similar to what we see in post-meiotic comet and cup localisation, this adds further to our rationale for investigation.

3.4. Alan Shepard (Shep)

Shep is an architectural RBP that is highly expressed within the *Drosophila* CNS (Olesnicky et al. 2014; Chen et al. 2018; Chen et al. 2021). All isoforms of Shep contain two RRMs and bind nuclear RNA. These RRMs are highly conserved, and conservation of *shep* is shown in both flies and vertebrates (Matzat et al. 2012; Chen et al. 2018).

Overall, *shep* has been described in the neurons of the peripheral nervous system and wider CNS, as well as in the mouthparts, second and third antennal segments, distal leg regions/joints, and wing margins/joints (Tunstall et al. 2012). As a neurodevelopmental gene, loss of functional *shep* has been linked to developmental lethality and diminished adult viability (Chen et al. 2014b).

Shep was originally characterised in *Drosophila melanogaster*, as part of a forward genetic screen to test various gravitaxis-deficient mutants and identify key genes involved in the gravitaxic fly response (Armstrong et al. 2006). A further genetic screen of over 500 gene trap insertion lines subsequently revealed the expression of *shep* within adult fly olfactory organs, with high levels of Shep protein localised to the olfactory receptor neurons (Tunstall et al. 2012). However, their homozygous olfactory-positive line for *shep* displayed high levels of mortality, preventing further interrogation of any olfactory-driven behaviours associated with its hypomorphic mutation. This suggested that *shep* is an essential gene required for proper adult fly viability and function, and supports the hypothesis that *shep* is an important player in other adult tissues outside of the fly nervous system (Tunstall et al. 2012).

Since then, Shep has been extensively implicated in the positive regulation of dendritogenesis and neurogenesis in *Drosophila* (Olesnicky et al. 2014; Chen et al.

2018). In fact, *shep* is required for the development of a diverse range of complex cell types within the nematode and fly nervous systems (Schachtner et al. 2015).

3.4.1. Shep is a tissue-specific regulator of insulator activity

Shep is incorporated into *gypsy* insulator protein complexes by direct, physical binding to the core *gypsy* insulator protein components of Su(Hw), Mod(mdg4)2.2, and CP190 (Matzat et al. 2012). Mutations in *shep* improve *gypsy*-dependent enhancer blocking and alter the nuclear localisation of insulator complexes in the brain, but this activity was not observed in any other tissue types tested – suggesting that Shep functions in a CNS-specific manner. Based on these conclusions, it is likely that Shep plays different roles depending on the tissue in question and, in the case of the CNS, can act as a negative regulator of insulator activity to modulate chromatin states and gene expression (Matzat et al. 2012).

Later work by Chen et al. (2019) revealed that mutations in Shep's RRM domains corresponded with loss of RNA binding ability and the diminished capacity to antagonise insulator-induced barrier activities and enhancer blocking. This validated the role of Shep as a regulator of insulator functionality in the CNS, and revealed the importance of its RNA binding activity to achieve this role – thereby supporting neuronal maturation processes within the *Drosophila* CNS (Chen et al. 2019).

Shep can also associate with chromatin during transcription (Dale et al. 2014). At least some of this co-transcriptional recruitment of Shep was found to be mediated through interactions with *gypsy* insulator-associated nuclear mRNAs; suggesting that Shep serves an CNS-specific RBP adapter for the *gypsy* insulator complexes and likely requires the contribution of other additional protein factors (Dale et al. 2014). By interacting directly with its chromatin targets, including inhibitors of BMP signalling, Shep has been found to negatively regulate their transcriptional programs to promote neuronal remodelling and neuropeptidergic signalling during metamorphosis (Chen et al. 2014b; Chen et al. 2017; Chen et al. 2018). Hence, Shep is able to undertake tissue-specific co-transcriptional regulation of gene expression in the *Drosophila* nervous system.

3.4.2. Shep mediates targeted RNA binding and processing activities

While it is Shep's RNA binding ability which likely facilitates and guides insulator regulation, Shep-mediated regulation can vary considerably, depending on the interactor of interest (Dale et al. 2014; Olesnicky et al. 2018; Chen et al. 2019). RNA immunoprecipitation and sequencing (RIP-Seq) of embryonic lysates has elucidated 77 significantly enriched Shep-specific target RNAs with high confidence (Olesnicky et al. 2018). Of these, very few were noncoding RNAs, and *shep* RNA itself was annotated, indicating that Shep regulates its own mRNA during embryonic development. Gene Ontology (GO) enrichment analysis of this dataset revealed that many of these RNAs encode downstream protein products associated with modulation of dendrite development, synaptic transmission, gene expression, translation, and even an RNA-binding activity of their own. Shep can therefore be concluded as an important post-transcriptional regulator of many diverse RNAs, especially during dendrite morphogenesis (Olesnicky et al. 2018). The potential interactome of *shep* also appears to be extremely wide-ranging, with an extensive network of important interactors that likely support an equally important range of biological roles depending on the tissue in question.

3.4.3. Non-neuronal roles of Shep in *Drosophila*

Shep is described as a key "insulator protein", but roles outside of the nervous system, and within the testes, remain largely unexplored. The non-neuronal expression and functional activity of Shep in *Drosophila* oogenesis has, however, been recently investigated in our wider research group (Almoalem 2023). As such, this made it another good RBP candidate to include in our screening since we already had easy access to readily available reagents in the lab.

In the same study outlined above by Olesnicky et al. (2018), a conserved interaction between Shep and *orb* mRNA was identified via RIP-Seq analysis. As mentioned in Table 1. (Section 1.9.2.), *orb* was one of the first "cup" genes to be described as post-meiotically transcribed and asymmetrically localised during *Drosophila* sperm development. As *orb* mRNA has been characterised as a putative target of Shep

during *Drosophila* sensory neuron dendrite morphogenesis, it could be hypothesised that a similar interaction / biological interplay may also be taking place in the post-meiotic elongating spermatids of the testis.

Shep has also recently emerged as a protein of interest following the collaborative, cross-laboratory development of an annotated snRNA-seq atlas of the entire adult fly (Li et al. 2022). Transcripts encoded by *shep* were detected in the male germline, in the expression profiles of male GSCs through to spermatocyte stages (Li et al. 2022). Initial analyses suggested that there may be some post-meiotic transcription of *shep*, although this was not robustly supported by follow-up work (Raz et al. 2023). Despite this, there is still a gap in our understanding. What function does *shep* play in the testis and in sperm development, if any?

3.5. IGF-II mRNA-binding protein (Imp)

IGF-II mRNA-binding protein (Imp) is a *Drosophila* homologue of the highly conserved family of RBPs called VICKZ, named via the first letter of its founding members (Yaniv and Yisraeli 2002). Family members are all involved in post-transcriptional RNA regulation, including control of RNA stability, translation and localisation (Yisraeli 2005).

In mammals, there is a subfamily of three Imp members – IMP1, IMP2 and IMP3. These proteins share a highly similar structure in terms of domain order and spatial arrangement, and each encodes a cytoplasmic protein containing two canonical RNA-recognition motifs (RRMs) and four hnRNP K-homology (KH) domains (Degrauwe et al. 2016). In general terms, mammalian IMPs are regarded as oncofoetal and commonly localise to the lamellipodia of motile cells (Nielsen et al. 1999; Nielsen et al. 2002; Fabrizio et al. 2008). In contrast, the *Drosophila* Imp protein comprises four KH domains but does not have any N-terminal RRMs. dImp does, however, share between 69-95% amino acid (AA) identity with other closely-related vertebrate homologues, including that of the Human, *Xenopus* and Chicken Imp proteins (Nielsen et al. 2000).

A conserved Imp recognition motif comprising UUUAY has been described in *Drosophila*, termed the “IMP-binding element (IBE)”. This UUUAY motif was found to

be the optimal binding sequence for both of Imp's KH3 and KH4 domains (Munro et al. 2006). When UUUAY was mutated to GGGCG, KH3 domain RNA-binding affinity decreased by one order of magnitude, while a single nucleotide change from UUUAY to UUgAY also caused a significant reduction in affinity. Follow-up electrophoretic mobility shift assays (EMSAs) corroborated this by showing distinct Imp-mediated shifts in the mobility of those RNAs containing UUUAY, but not in those containing nucleotide changes (Munro et al. 2006).

3.5.1. Expression of Imp in the *Drosophila* testis

In the testis, Imp is strongly expressed in two distinct stages of *Drosophila* spermatogenesis (Fabrizio et al. 2008). A total of four GFP-tagged Imp protein trap lines have been studied in the testis by epifluorescence microscopy, including one third-chromosome insertion and three X-chromosome insertions. All revealed expression toward the tail-ends of spermatid cysts and within the apical tip of the testis. Follow-up immunofluorescence analysis of testes from an Imp enhancer trap line revealed that Imp expression predominated within mitotically active pre-meiotic cells of the apical tip. It must be noted, however, that direct detection of individual alternate Imp transcripts was not possible by this means (Fabrizio et al. 2008). Nevertheless, Nerusheva et al. (2009) has since supported this biphasic expression of Imp in the testis.

An in-house analysis of YFP-FLAG exon trapped lines in the adult male genital tract has also revealed the precise expression of several RBPs throughout the distal tails of elongating spermatid cysts, including that of this highly-conserved Imp protein (Lowe et al. 2014) Imp is present throughout the spermatid cytoplasm, but is considerably more abundant at the elongating tail-ends of spermatids – where it accumulates en masse at high concentrations (H. White-Cooper, Personal Communication). As Imp's protein distribution is similar to what we see in post-meiotic comet and cup localisation, this supports our rationale for further investigation.

3.5.2. Imp regulates germline stem cell maintenance in early spermatogenesis

In the *Drosophila* testis, a significant decline in the self-renewal factor, Unpaired (Upd), presents as a hallmark of ageing alongside concomitant loss of GSCs (Boyle et al. 2007; Toledano et al. 2012). From a screen of putative GFP-tagged protein regulators of Upd in the hub cells, Imp was identified as a possible candidate. Antibody staining showed that the levels of Imp expression were reduced by ~50% in hub cells of older male testes, and further analysis revealed this to be an outcome, at least in-part, of targeted regulation by the heterochronic microRNA (miRNA), let-7. Investigation of hub-cell-specific Imp-RNAi knockdowns and Imp mutants using FISH and immunofluorescence revealed that Imp-RNAi corresponded with a decline in Upd mRNA levels (and hence JAK-STAT signalling) in hub cells. Although, overexpression of Upd in this Imp-RNAi background did successfully rescue these defects. Mutant analyses showed that null mutations in Imp led to lethality at the pharate adult stage, but other Imp mutants were found to have a significant reduction in Upd expression, as well as in the average number of GSCs and hub cells. Imp rescue experiments sufficiently reversed these deficits, which together suggests that Imp functions upstream to positively regulate Upd mRNAs, niche integrity and GSC maintenance in the testis (Toledano et al. 2012).

Toledano et al. (2012) confirmed that Imp binds to the Upd mRNA, likely via the first 250 bp of the 3’ UTR, with the first 33 bp constituting a possible target sequence. A heterologous system of an Upd 3’UTR-tagged GFP reporter mRNA in *Drosophila* S2 cells also showed that: (i) reporter transcriptional levels were upregulated when co-expressed with Imp and, (ii) Imp protects against various endogenous small interfering RNAs (siRNAs) to stabilise Upd mRNA. Without the protection of Imp, Upd mRNA becomes susceptible to degradation by the siRNA pathway.

3.5.3. Functions of Imp in embryogenesis and the developing CNS

The biological role of Imp in different *Drosophila* cell and tissue types has been widely published. For example, maternal Imp has an essential role in embryogenesis (Munro et al. 2006). Null mutations for *imp* do not affect oogenesis but are zygotic lethal. A loss of Imp was found to be fatal to the zygote upon fertilisation, which prevented prenatal development from taking place. All resultant embryos from *imp* germline clones failed in late embryogenesis and could not be rescued by a WT paternal gene copy (Munro et al. 2006).

Boylan et al. (2008) reinforced this finding, with loss-of-function Imp mutants dying late as pharate adults, prior to eclosion. Germline clones homozygous for lethal *imp* mutations showed decreased hatching rates of embryos. Any successfully surviving progeny were female, indicative of zygotic rescue by a paternal WT X chromosome. Both abnormal extremes of Imp loss-of-function and overexpression were found to modify synaptic terminal growth, induce locomotion deficits and reduce adult survival rates. Hence, Imp is likely transported pre-synaptically to the neuromuscular junction; there, it can act as a translational regulator of specific mRNA targets involved in proper neuromuscular junction growth and neuromuscular activity (Boylan et al. 2008). Taken together, this indicates that Imp plays a fundamental embryonic role that ensures proper development, adult viability and survival.

3.5.4. The Imp protein family can bind and process RNAs in different cell contexts

RNA-binding has been evidenced for many homologues of the Imp protein family (Degrauwe et al. 2016). Multiple nuclear export signals have also been characterised in mammalian IMPs; it has hence been proposed that the “loading” of IMP proteins onto their target mRNAs in the nucleus is what determines the cytoplasmic fate of these transcripts (Nielsen et al. 2003; Oleynikov and Singer 2003). IMPs may associate with mRNAs co-transcriptionally, driving cytoplasmic RNA localisation via interactions with actomyosin and the actin cytoskeleton (Oleynikov and Singer 2003).

In vitro studies suggest that it is the KH domains that bestow this RNA binding capacity, while RRMs likely contribute to the stability of Imp:RNA complexes (Nielsen et al. 2004; Wächter et al. 2013). This explains why *Drosophila* Imp has retained all four of these domains in its structure; to support high affinity binding interactions.

In murine embryonic fibroblast cells, IMP homologues have been implicated in the localisation of mRNAs to discrete, subcellular regions such as the leading edge of lamellipodia (Runge et al. 2000). Immunocytochemical analysis of IMP proteins has also shown that they localise to specific sub-cytoplasmic regions in a growth-dependent and cell-specific manner. At target sites, IMPs can act as translation regulators and mediate the dose-dependent translational repression of mRNA transcripts, including the chimeric IGF-II leader 3-luciferase mRNA (Nielsen et al. 1999).

Moreover, antibody and immunogold staining against the chicken homologue of Imp, ZBP1, has revealed a distinct co-localisation of the RBP with both actin bundle filaments and microtubules. This association suggests a role in the localisation and anchoring of its binding partners (Oleynikov and Singer 2003). Such freedom of unrestricted movement throughout the cells makes Imp, and its related homologues, an interesting RBP candidate for the regulation of many different RNAs in a whole host of different cell types, including in the male germline cells. While Imp may not be expressed exclusively within the testis, its functional importance in all of these other tissue- and process-specific contexts further adds to the argument that it likely plays a similarly important function within the *Drosophila* testis and in sperm development.

3.6. Experimental approaches and aims of chapter

The first way we set out to elucidate direct and indirect binding interactions for this set of RBPs was by using a combination of standard molecular cloning methods and *in vitro* biochemical techniques.

We cloned and *in vitro* transcribed a set of seven biotin-labelled comet mRNAs and four biotin-labelled cup mRNA transcripts, then used these in multiple rounds of RNA-affinity pull-down assays (Fig. 9.). In doing so, we could extract out bound, interacting fractions of comet and cup mRNAs with a pool of endogenous RBP interactors

prepared from *Drosophila* ovary extracts. Western Blot Analysis was then used to detect and characterise this small number of potential pair-wise binding interactions with the four candidate RBPs outlined above: Bru1, dmPTB, Shep and Imp.

This was performed to answer two key objectives:

1. When using a pool of endogenous, cytoplasmic *Drosophila* proteins, do any of these RBPs bind, either directly or indirectly, with our selection of comet and cup mRNA transcripts *in vitro*?

2. If so, what is the relative abundance of these binding interactions and how do these interactions compare across the panel of comet and cup mRNAs tested here?

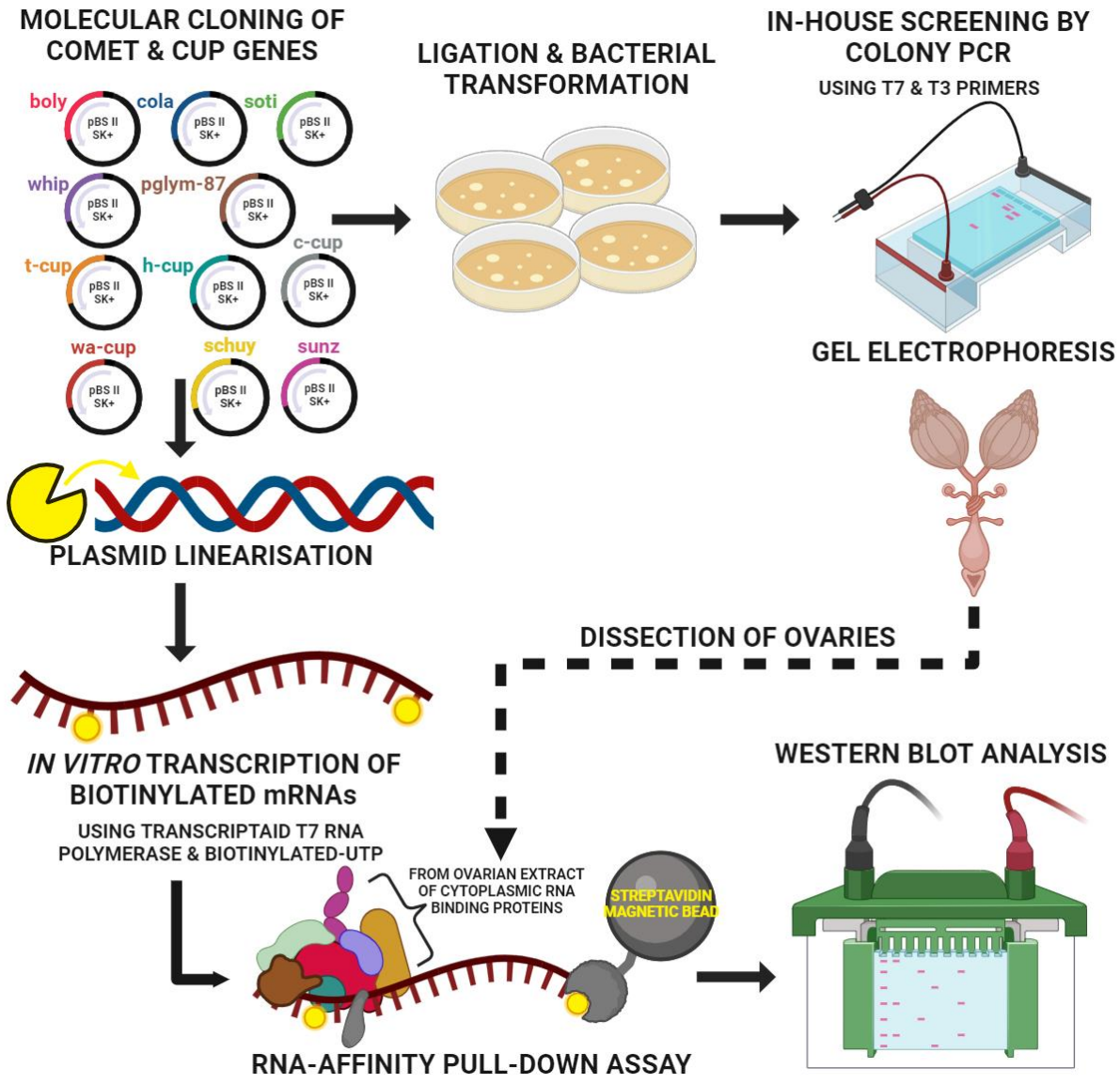

Figure 9. RNA-affinity pull-down approach taken to isolate purified RBP:mRNA complexes *in vitro*. Following cloning and *in vitro* transcription of comet and cup mRNA probes, an RNA-affinity pull-down assay was conducted using full-length biotin-labelled mRNAs, immobilised on Streptavidin-conjugated beads, and pulled-down against cytoplasmic S10 ovarian extracts from w^{1118} and the Imp-GFP G80 protein-trap fly line (G00080 exon-trap line; Quiñones-Coello et al. 2007). **Created using BioRender.com.**

3.7. Robust characterisation of *in vitro* RBP:mRNA interactions

The elongating tail-ends of *Drosophila* spermatids contain a set of localised RNAs and several known RBPs – some of which I have reviewed above. To investigate the hypothesis that these RBPs are implicated in the regulation of non-uniform, subcellular comet and cup mRNA localisation, we set out to determine whether the Bru1, dmPTB, Shep and Imp proteins interacted with seven comet transcripts (*borrelly, comas sola, phosphoglyceromutase 87, schumacher-levy, scotti, sungrazer* and *whipple*) and four cup transcripts (*calcutta-cup, heineken-cup, tetleys-cup* and *walker-cup*).

The 3' UTR of *osk* mRNA was implemented as a positive control because it is known to bind all four of our RBP candidates *in vivo*. A negative unrelated RNA control of the y14 CDS was chosen because it is not known to form a significant interaction with RBPs, based on previous findings (Besse et al. 2009).

As expected, all candidate RBPs consistently bound our positive control, the *osk* 3' UTR, but did not interact with our unrelated negative RNA control of the *y14* coding sequence (*y14* CDS) (Fig. 10.1.).

The Precision Plus Protein™ Dual Colour Standard (Bio-Rad Laboratories) was utilised as the MW marker of choice for all Western Blotting applications in this PhD research. This MW marker remained visible on all membrane blot images due to comprising ten recombinant, pre-stained standard proteins – eight blue-stained protein bands and two pink reference protein bands at 25kDa and 75kDa, respectively – which were commercially supplied in a two-colour form with fluorescent properties that were compatible with fluorescent blotting. Therefore, this MW marker could be used in conjunction with the multiplex fluorescent detection capabilities of the 700 Channel (685nm laser) and 800 Channel (785nm laser) employed by the Odyssey® CLx Imaging System (Li-Cor). It also permitted SDS-PAGE progress to be monitored in real-time, provided an immediate indication of gel orientation and a direct confirmation of membrane transfer quality and efficiency.

Quantification of relative protein signal intensities was performed on the Western Blot outputs from the second experimental round – since this comprised the full panel of binding interactions between the 11 test mRNAs and 4 RBP candidates (Fig. 10.1D.

and 10.1E.). Relative protein signal intensities were determined for each membrane blot by direct comparison to the protein binding signals between the *osk* 3' UTR positive control and the RBP in question. These quantifications have therefore been presented as two separate bar graphs (Fig. 10.2A. and 10.2B.).

For each test mRNA, relative quantification of protein signals confirmed what we could qualitatively observe by eye. Interestingly, *pglym 87* was the only test mRNA that showed consistently low amounts of bound protein for three out of the four candidate RBPs.

The results for each individual RBP candidate are analysed below.

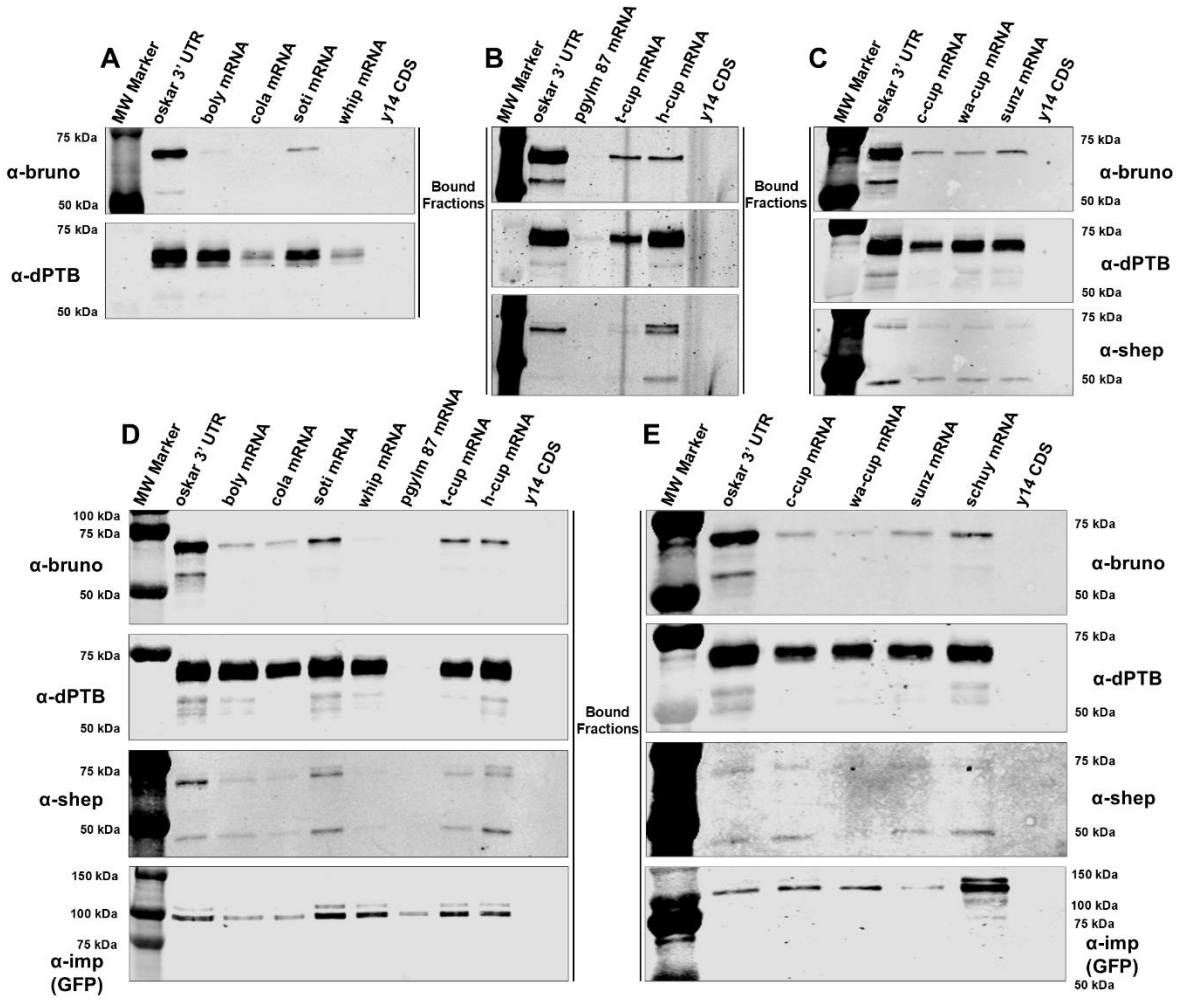

Figure 10.1. Characterisation of direct and indirect binding of Bru1, dmPTB, Shep and Imp to 11 biotinylated comet and cup mRNAs. Results represent multiple Western Blots of bound pull-down fractions using extracts of soluble, cytoplasmic RBPs from *Drosophila* ovaries (n=2). The *oskar* 3' UTR was implemented as a verified positive control, while the coding sequence (CDS) of *y14* was implemented as an unrelated negative RNA control. Images A through to C correspond to the first round of pull-down assays, conducted in three batches. Images D and E correspond to a second "full" repeat, including detection of binding interactions against all 4 RBPs. Due to delays in generating the biotinylated *schuy* mRNA probe and optimising the anti-GFP antibody dilution, full analysis was only performed once in the second round, with no subsequent repeat.

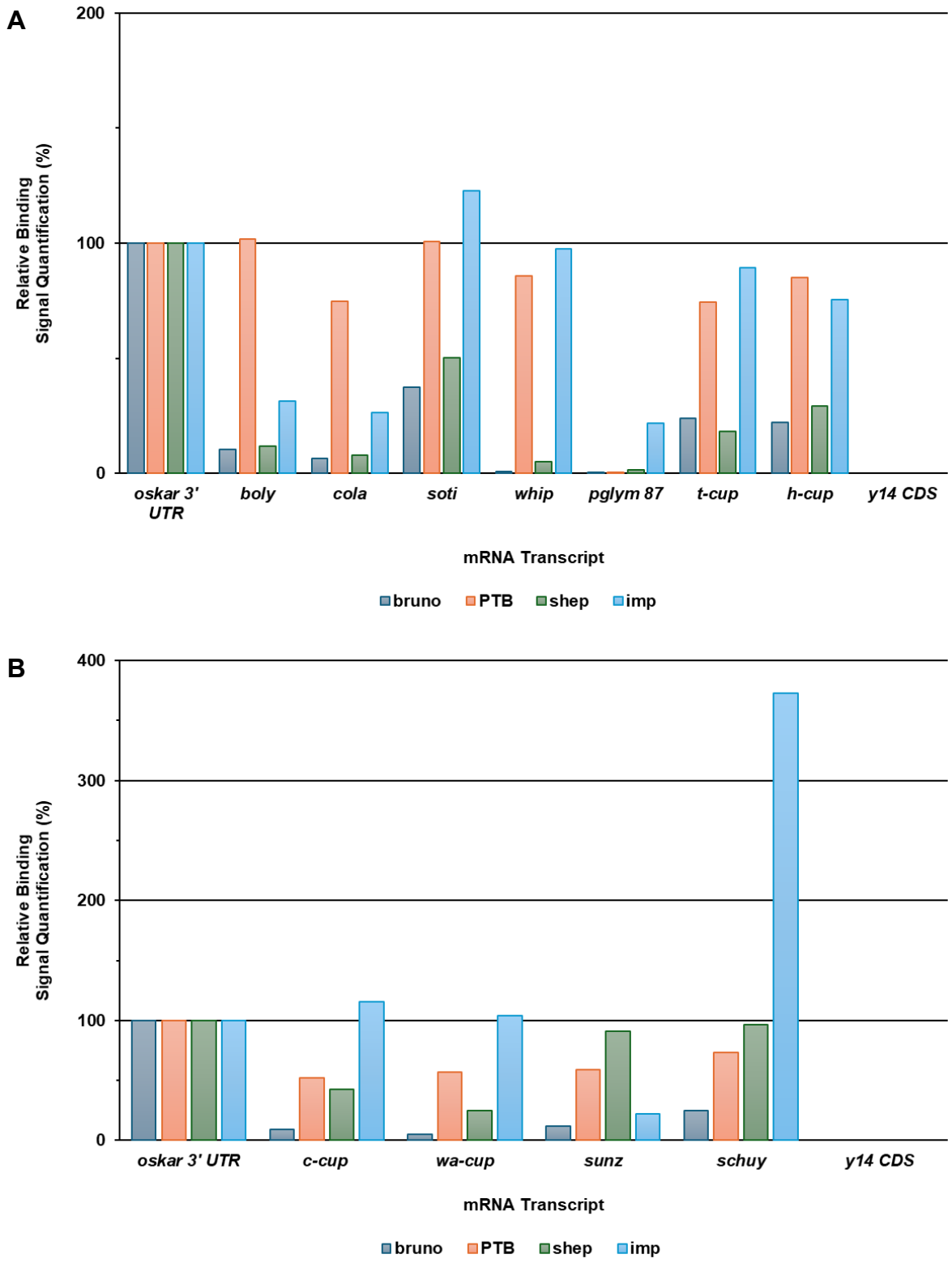

Figure 10.2. Quantification of the relative binding signal intensities of Bru1, dmPTB, Shep and Imp when pulled down against 11 biotinylated comet and cup mRNAs. As there was no loading control to compare against, net protein signals were quantified relative to the net binding signal between each RBP and the positive control of the *osk* 3' UTR. As such, binding to the *osk* 3' UTR was set as 100% and all other mRNA-bound RBP signals

were determined as a relative percentage to this. Graph (A) represents the relative intensities of the mRNA-bound RBPs in Fig. 10.1D. Graph (B) represents the relative intensities of the mRNA-bound RBPs in Fig. 10.1E. For simplicity, only the relative signal intensity of the most dominant RBP isoform (i.e., based on the strongest intensity by eye relative to the positive control) was quantified in each case. With regards to Shep, only protein signals corresponding to the second highest MW isoform were quantified for consistency in both Western Blot rounds.

3.7.1. Bru1 binds nine biotinylated comet and cup mRNAs

We found that Bru1 binds nine of the eleven comet and cup mRNAs robustly and comparatively across two experimental rounds (Fig. 10.1.). Binding of Bru1 to two comet mRNAs – *soti* and *schuy* – and two cup mRNAs – *t-cup* and *h-cup* – resulted in the highest amount of bound Bru1 protein overall. Quantification of protein signal intensities relative to the *osk* 3' UTR revealed that the relative abundance of interacting Bru1 was approximately 37% and 25% for the *soti* and *schuy* mRNAs, respectively. The relative amount of Bru1 bound to *t-cup* was roughly 24% while ~22% of Bru1 bound to the *h-cup* transcripts (Fig. 10.2.).

In the first experimental round, binding of Bru1 to *pglym 87* was extremely low and no binding interactions were detected with the *whip* mRNA. These observations were somewhat swapped in the repeat, with some low-level binding evidenced for *whip* (~0.7% bound Bru1) but not for *pgylm 87* (~0.04% bound Bru1). This may require further validation.

3.7.2. dmPTB binds ten biotinylated comet and cup mRNAs

We were able to conclude robust binding of dmPTB to ten of the eleven experimental mRNAs (Fig. 10.1.). These were all represented by a large amount of bound dmPTB and the majority showed protein signals that were similar to the positive control interaction.

Measurement of protein signal intensities confirmed that the relative abundance of interacting dmPTB was greater for the *boly* and *soti* mRNA transcripts compared to the positive control of *osk* 3' UTR – equating to 102% dmPTB binding for *boly* and 101% dmPTB binding for *soti* overall (Fig. 10.2A.). The amount of dmPTB protein bound to two comet mRNAs – *schuy* and *sunz* – and two cup mRNAs – *wa-cup* and *c-cup*– was slightly lower and more variable; roughly corresponding to 73%, 59%, 57% and 52%, respectively, relative to the *osk* 3' UTR (Fig. 10.2B.). Binding of dmPTB to the comet mRNA, *pglym 87*, was barely detectable (~0.09% bound dmPTB).

3.7.3. Shep binds ten biotinylated comet and cup mRNAs

Shep was shown to bind ten of the eleven test mRNAs, with *soti* and *h-cup* showing the highest abundance of bound Shep of them all (Fig. 10.1.). However, when compared to dmPTB, the amount of Shep protein interacting with the comet and cup mRNAs was consistently lower.

Due to difficulties with protocol troubleshooting, including optimisation of antibodies and immunoblot components, Shep binding was not tested against the *boly*, *cola*, *soti* and *whip* mRNAs in the first experimental round (Fig. 10.1A.).

Visualisation of Shep in Fig. 10.1B. was slightly different to the others; this owing to the use of a different anti-Shep primary antibody, which preferentially detected against the larger Shep protein isoforms.

When Shep protein signal intensities were quantified, the abundance of interacting Shep relative to the *osk* 3' UTR positive control was 50% for *soti*, 29% for *h-cup* and 18% for the *t-cup* mRNAs (Fig. 10.2A.). The background noise in Fig. 10.1E. did, however, make it difficult to reliably quantify the relative Shep protein signal intensities and bound Shep abundances. Nevertheless, background signals were, of course, accounted for as much as possible in all measurements and calculations. As such, the relative amount of Shep bound to the *sunz* and *schuy* transcripts was around 91% and 96%, respectively (Fig. 10.2B.). Relative binding of Shep to the *whip* mRNA was once again low (~5% bound Shep) and minimal binding to *pglym 87* was also detected (~2% bound Shep).

3.7.4. Imp is the only RBP candidate that binds all eleven biotinylated comet and cup mRNAs

In contrast to the other the RBPs tested here, Imp did indeed interact with *pglym 87* (~28% bound Imp), and it was therefore the only RBP to bind – whether directly or indirectly – to all eleven comet and cup transcripts (Fig. 10.1. and Fig. 10.2.). However, in accordance with our other pull-down results, there was, once again, no distinct divide in the amount of interacting Imp protein based on comet and cup classification alone. Instead, a large amount of Imp consistently bound to all four of the cup mRNA transcripts in the panel, as well as to the comet mRNAs of *soti*, *whip* and, most notably, *schuy*.

Quantification of Imp protein signal intensities relative to the *osk* 3' UTR suggested that the relative abundance of Imp was approximately 116% and 104% for the *c-cup* and *wa-cup* mRNAs, respectively; thereby binding to both of these transcripts more than the positive control itself. In addition, compared to the positive control of *osk* 3' UTR, the relative abundance of bound Imp was also greater for the *schuy* and *soti* mRNA transcripts – equating to 373% Imp binding for *schuy* and 123% Imp binding for *soti* overall (Fig. 10.2.). Relative binding of Imp to the *whip* mRNA was just below that of the positive control (~98% bound Imp).

While two distinct isoforms of Imp appear to only bind a select number of mRNAs in our panel, such as *soti*, *whip*, *t-cup*, *h-cup*, c-*cup* and, most evidently, *schuy*, overexposure of the membrane confirms that both Imp isoforms do indeed interact with all of the biotinylated transcripts tested here (including the *boly*, *cola*, *pglym 87*, *wa-cup* and *sunz* mRNAs).

3.8. Imp is enriched at the tail-ends of *Drosophila* spermatid cyst bundles

Since Imp binds to all eleven test comet and cup mRNAs, we briefly looked at the expression of Imp-GFP in the testes of Imp-GFP G80 protein trap males (G00080 exon-trap line; Quiñones-Coello et al. 2007).

In line with Fabrizio et al. (2008) and Nerusheva et al. (2009), we confirmed that Imp is highly expressed at the tail-ends of each individual spermatid that makes up the elongating spermatid cyst bundles of the *Drosophila* testis (Fig. 11.).

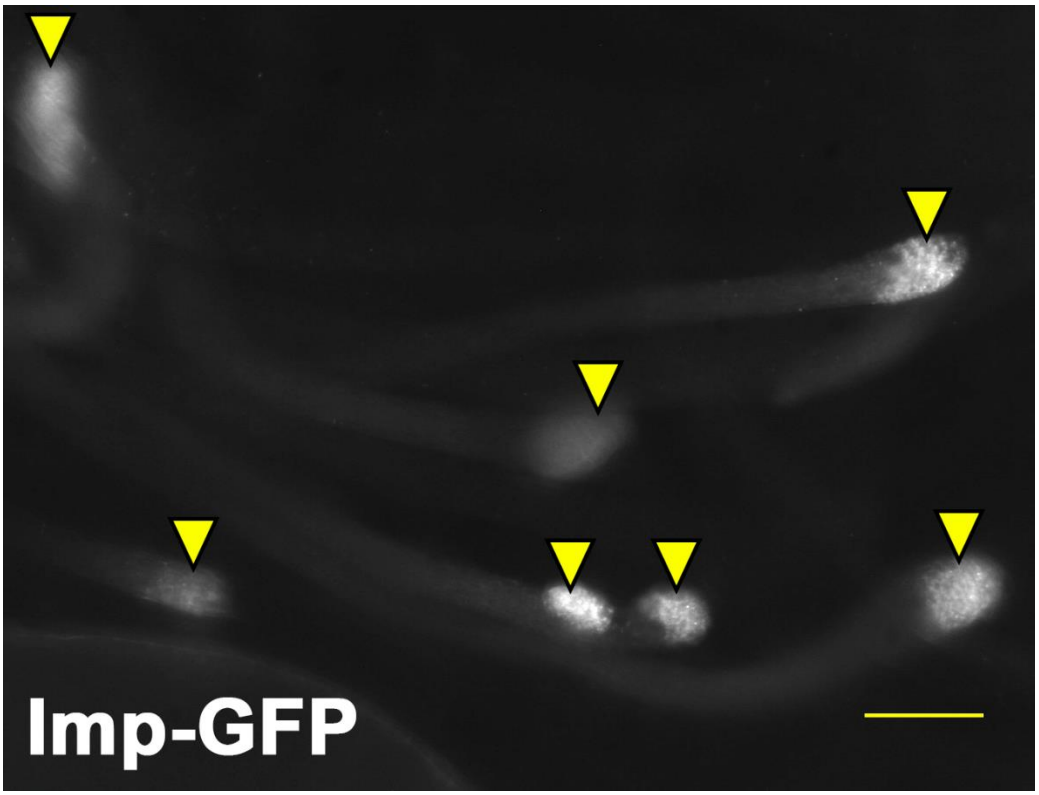

Figure 11. Localised Imp-GFP protein expression at the extreme tail-ends of mid-to-late elongating spermatid cyst bundles. Testes were dissected from males of the Imp-GFP G80 protein-trap *Drosophila melanogaster* line (Quiñones-Coello et al. 2007) and were imaged as live whole-mount samples in Schneider's *Drosophila* Medium using single channel GFP fluorescence microscopy. Yellow arrow heads denote the high intensity fluorescent signals of Imp-GFP, which hence corresponds to the high level of protein localised to these distinct regions of the spermatid tail-ends. Gain: 1.0. Exposure: 1.0. Scale bar: 25 μm.

3.9. Optimisation of testis-specific protein extracts for repetition of RNA-affinity pull-down assays

After establishing binding interactions *in vitro* using ovarian homogenates, the next appropriate step was to optimise the RNA pull-down set-up further. Specifically, by shifting away from the use of an S10 ovarian extract as the primary source of cytoplasmic RBPs. By switching to an alternative, endogenous testis protein extract, we hoped to validate all of the binding interactions we had found thus far in a more applicable, testes-specific context.

3.9.1. The amount of total protein in *Drosophila* ovaries is greater than in testes

To begin the initial stages of optimisation, for the coordinated switch from an ovarian S10 cytoplasmic extract to a testis-sourced protein extract, we evaluated the total amount of protein expressed in the *Drosophila melanogaster* testes and ovaries.

Individual simple crude protein extracts were prepared with varying quantities of testes and ovaries, respectively. The level of protein expression within these samples was then measured by total protein staining to enable a direct, qualitative comparison between the total amount of protein yielded from each homogenate preparation (Fig. 12.).

Total protein expression within the ovaries was found to be greater than in that of the testes (Fig. 12.). In fact, the amount of protein extracted from just four ovaries was so great that it was enough to distort the running of the lanes.

Qualitative comparisons indicated that the total protein content of one ovary was most similar to twelve testes, and the content of two ovaries most closely resembled twenty-four testes. Overall, this suggests that the amount of total protein in the *Drosophila* ovary preparations was approximately twelve times greater than in that of the *Drosophila* testis preparations. This correlates well with the sexually dimorphic size difference between the gonads, as the ovaries are larger reproductive organs in *Drosophila melanogaster.*

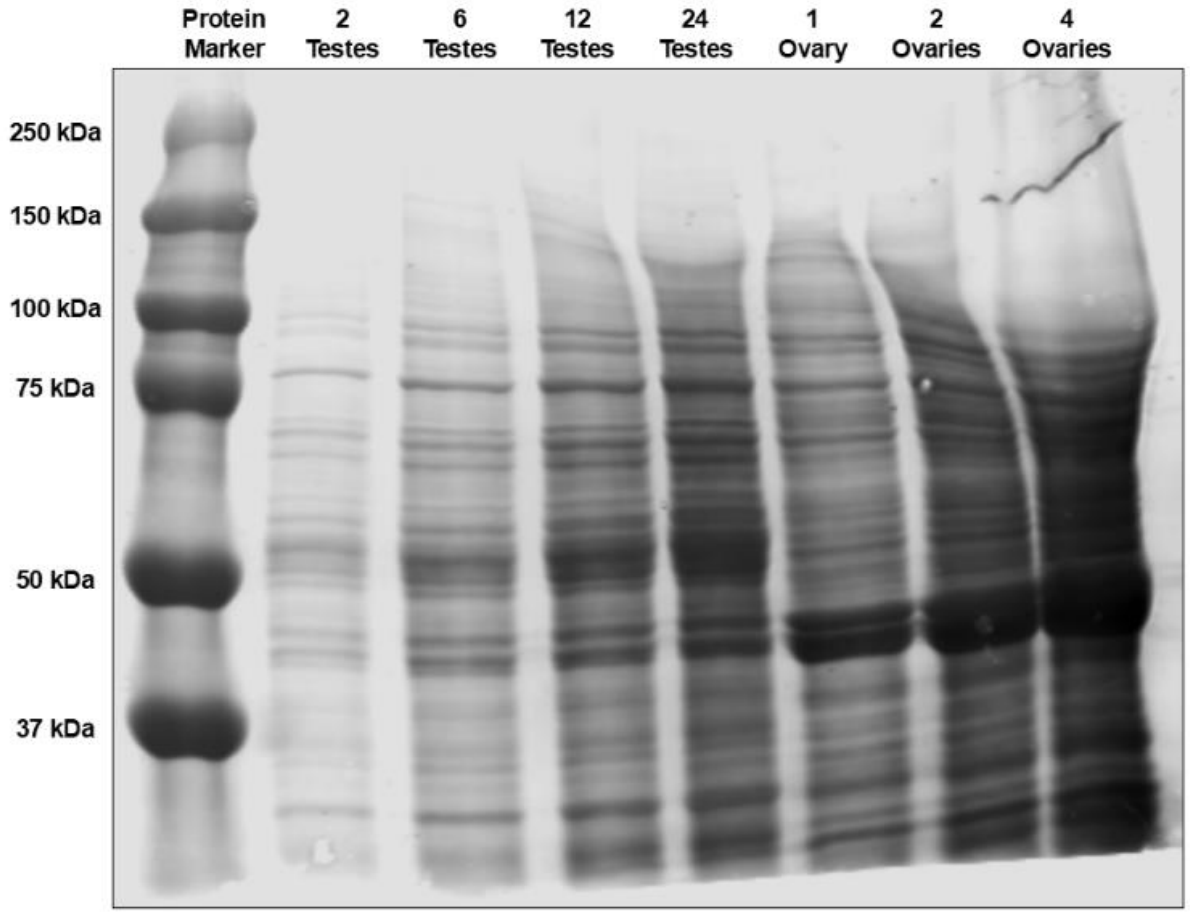

Figure 12. Comparison of total protein in *Drosophila melanogaster* testes and ovaries. Total protein staining of the membrane was performed using the Revert™ 700 Total Protein Stain Kit (Li-Cor). Measurement of total protein content for 1, 3, 6 and 12 pairs of testes is shown here, alongside the protein levels for 1 single ovary, as well as 1 single pair and 2 pairs of ovaries, respectively (n=1). Qualitative estimations and comparisons could be made between the protein levels of this varying quantity of testes and ovaries. Overall, the total amount of protein was greater within the *Drosophila* ovaries than in the testes. A higher number of testes would therefore be needed to match the equivalent level of ovarian protein content.

Hence, our results support there being more total protein in homogenates prepared from *Drosophila* ovaries compared to testes, likely owing to the relative size difference between the two organs – with the ovary being visibly larger than its testis counterpart.

Total protein membrane staining was performed instead of a Bradford protein assay because it could be combined with Western Blotting to give a readout of potential sex-specific differences contributing to differential total protein expression. A direct comparison between expression levels of specific protein isoforms could also be made.

3.9.2. Candidate RBP expression varies between *Drosophila* testes and ovaries

Immunoblotting was then carried out on the same membrane after total protein staining, allowing for the relative sex-specific expression of candidate RBPs to be qualitatively measured (Fig. 13.).

dmPTB expression was generally higher in the testes compared to the ovaries, with three larger, predominating testis-specific isoforms overall. This agrees with previous hypothesises of dmPTB sexual dimorphism (Robida et al. 2010).

The expression of Imp, on the other hand, was much greater in the ovaries than in the testes. No sex-specific isoform differences were detected for Imp.

Finally, Bru1 expression was highest in the ovaries but predominated as an ovary-specific isoform which was comparatively smaller than in that of the testes. This sex-specific variation in Bru1 isoforms is supported by the literature (Webster et al. 1997b).

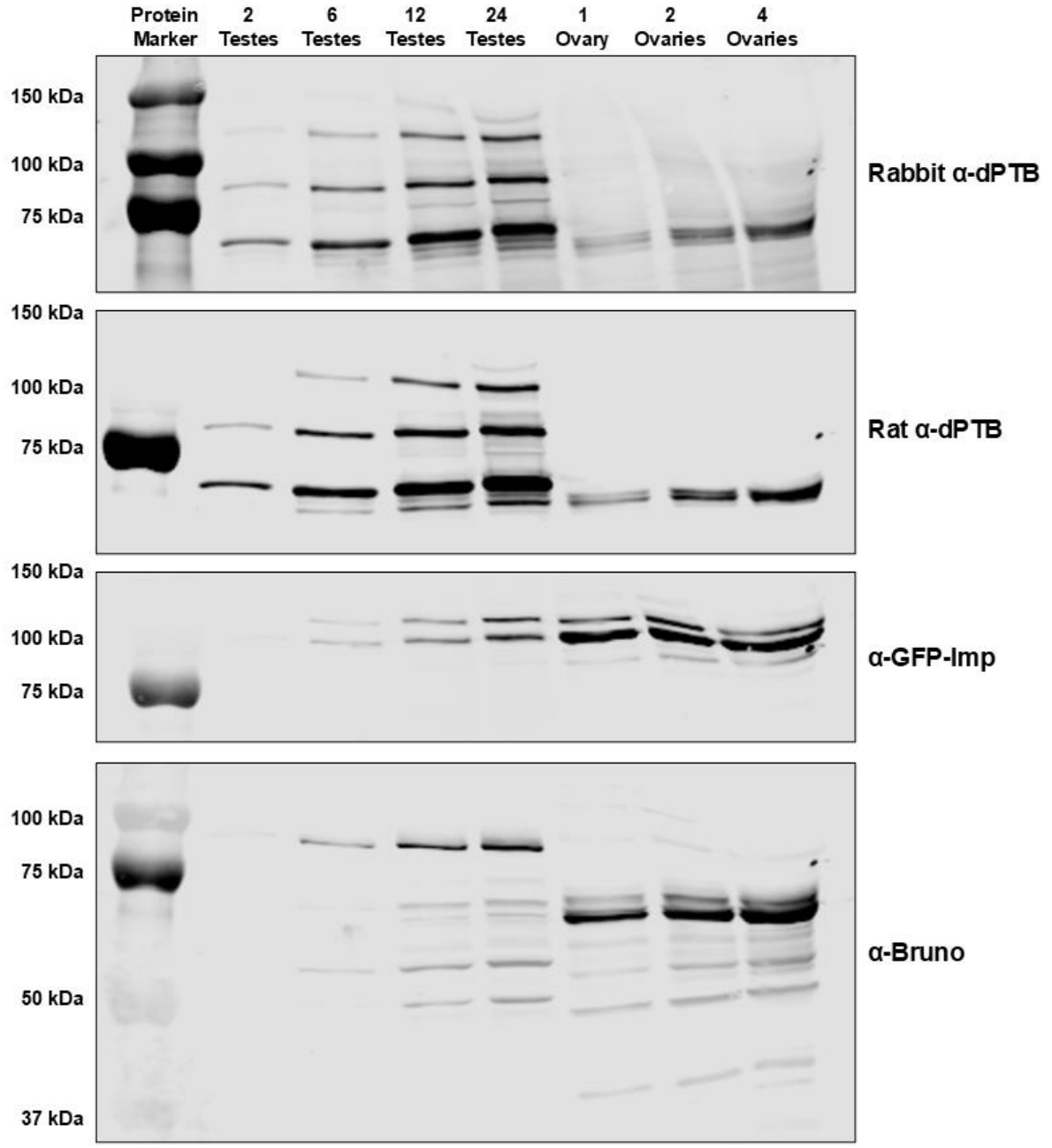

Figure 13. Relative sex-specific expression of candidate RBPs in *Drosophila melanogaster* testes and ovaries. Immunoblotting for specific RBPs was performed on the membrane after total protein staining (n=1). This enabled the RBP expression levels in 1, 3, 6 and 12 pairs of testes to be detected and compared to those in 1 single ovary, as well as in 1 single pair and 2 pairs of ovaries, respectively. As testes and ovaries were dissected from a GFP-tagged-Imp-expressing *Drosophila* line **(**Quiñones-Coello et al. 2007), this permitted the detection of Imp protein levels by use of the rat anti-GFP primary antibody. Visualisation of dmPTB was performed using two different antibodies to compare the quality of detection and levels of background after initial protein staining. Detection of Shep was not undertaken in this optimisation step due to issues with antibody availability.

3.9.3. Protein is lost during preparation of the testis-specific pull-down extract

Unfortunately, the first attempt of an RNA-affinity pull-down assay using *Drosophila* testes for the pool of cytoplasmic RBPs did not work (not shown here). No binding interactions for any of the candidate RBPs were detected after running Western Blot analysis with both the mRNA-RBP bound and unbound fractions.

Follow-up total protein staining of both membranes showed no protein of any kind in the sample lanes. To ascertain the root cause of this complete protein loss, direct comparisons were made between the total protein concentrations of a crude testis protein extract and three variable sample preparation conditions (Fig. 14.). The crude extract was used as a point of reference for the maximum level of total protein that could be obtained from twenty fresh *Drosophila* testes. By comparing to this reference, and between different preparation approaches, any evidence of protein degradation during the process of endogenous testis-specific protein extract preparation could be determined.

Total protein staining showed that, when compared to the crude extract, at least 80% of the total protein content was being lost when using the in-house pull-down method of RBP homogenate preparation (Fig. 14.). While the total protein concentration in the extract prepared with fresh testes appeared to be greater than the other two conditions, this was likely attributed to a slight discrepancy in preparation volume; upon loading, this sample’s volume was considerably more concentrated than its counterparts. Therefore, it may be argued that neither the pre-freezing of testes, nor a prolonged wait prior to extract loading and analysis, had any major impact on total protein content. This suggests that protein degradation may not have been responsible for protein loss in this case. Could it be that these lower protein concentrations were instead a consequence of insufficient cell lysis?

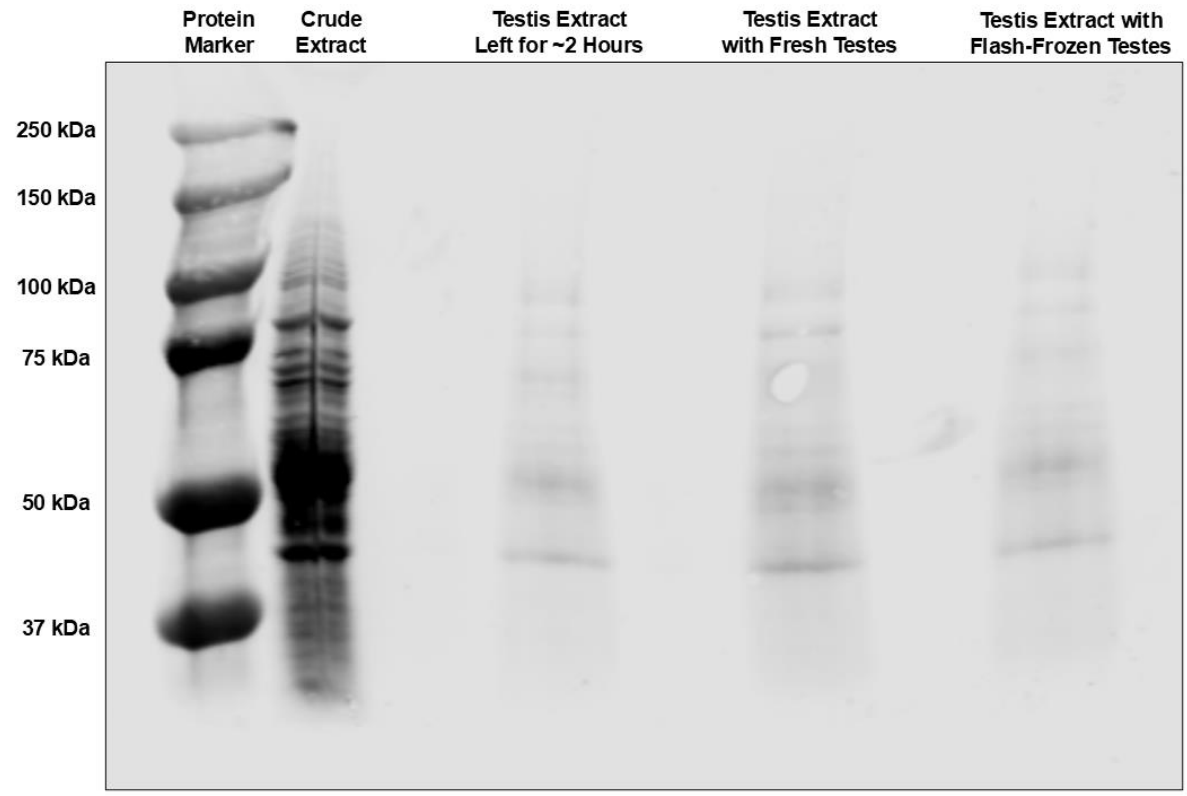

Figure 14. Comparison of total protein concentrations in *Drosophila melanogaster* testis-specific crude protein and RNA-affinity pull-down extract preparation conditions. Total protein staining of the SDS-PAGE gel was performed using the ReadyBlue™ Protein Gel Stain (Sigma). Four testis-specific extract conditions were tested: (i) a simple crude protein extract prepared with frozen testes, (ii) a pull-down extract prepared with same-day dissected testes, left out on ice for a minimum of two hours before loading, (iii) a pull-down extract prepared and loaded immediately after dissection of fresh testes, and (iv) a pull-down extract prepared from testes that had been dissected, flash-frozen in liquid nitrogen and stored at –80˚C for at least 24 hours. Approximately twenty testes were dissected for each sample condition type (n=1). As freezing and time delays did not appear to result in any marked increase in protein loss, it is unlikely that protein degradation was at play.

3.9.4. Combined sonication and homogenisation improves cell lysis and protein release

It was possible that the method of extract preparation was at fault, thus resulting in reduced protein yields. Although manual homogenisation with autoclavable plastic microtube pestles was working at an ultrastructural level, cells within the testes might not be fully lysed using this method alone – leading to insufficient protein release. One feasible solution to this was the sonication of testis samples in place of, or alongside of, manual homogenisation. To investigate this hypothesis, sonication was introduced as a potential amendment to our RNA-affinity pull-down methodology.

Regardless of the number of sonication cycles performed, sonicated testis-specific pull-down extracts showed considerably higher total protein concentrations when compared to the previous results of manual homogenisation alone (Fig. 15A. vs. Fig. 14.). However, the level of total protein was still not as high as the simple crude extract – meaning some protein was still being lost during the preparation process. There was also a slight but evident increase in total protein content as the number of sonication cycles were increased (Fig. 15A.).

Our original aim was to test the effectiveness of sonication as a direct alternative to manual homogenisation; however, after high-intensity sonication, the ultrastructure of the testes had remained in-tact due to the testis muscle sheath maintaining organ integrity. Hence, follow-up homogenisation of the samples was required to ensure successful release of the lysed cellular content.

However, could the precise order of sonication and homogenisation make any difference to total protein concentrations? To test this, the assay was repeated with the same experimental set-up as before, but the order of processing was interchanged – manual homogenisation with autoclavable plastic microtube pestles was performed first, followed by sonication. The concentration of total protein in the testis-specific pull-down extracts showed no notable change or improvement when this order was switched, and protein levels were still not as high as the crude extract (Fig. 15B.).

Nevertheless, total protein content was greater when the testis sample was sonicated over eight on/off cycles; suggesting that longer sonication pulses and/or more sonication cycles may be required for improved protein release.

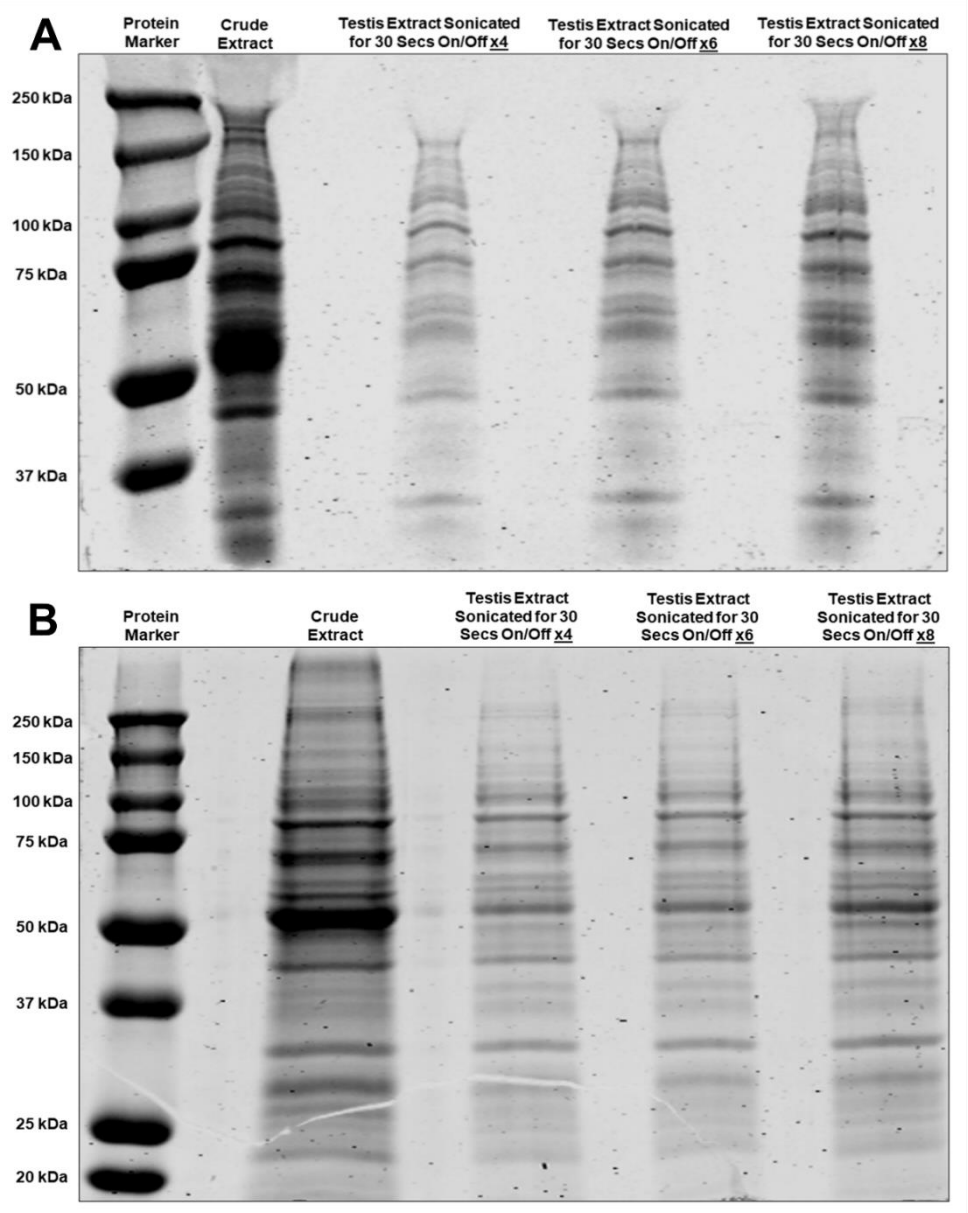

Figure 15. Total protein concentrations of a *Drosophila melanogaster* crude testis protein extract vs. sonicated testis-specific RNA-affinity pull-down extracts. Total protein staining of the SDS-PAGE gel was performed using the ReadyBlue™ Protein Gel Stain (Sigma). Each sample extract was prepared with approx. twenty *Drosophila* testes (n=1). Testis-specific pull-down extracts were prepared by: (A) high-power sonication of testes in an in-house Hypotonic Buffer/Protease Inhibitor mix, followed by manual homogenisation for 60 seconds or, (B) manual homogenisation of testes for 60 seconds in a Hypotonic Buffer/Protease Inhibitor mix prior to high-power sonication. Successive sonication cycles of 30 seconds on/off were tested, equating to 4, 6 and 8 cycles, respectively. Results showed that, regardless of processing order, a combined sonication and homogenisation with autoclavable plastic microtube pestles approach was effective at improving cell lysis and ultimate protein release.

3.9.5. Adjusting the composition of homogenisation buffer increases total protein extraction yield and eliminates the need for sonication

As sample preparation is a fundamental step in guaranteeing the reliability and robustness of downstream protein analyses, this was our last point of call to close out the final stages of optimisation.

Interestingly, a systematic study of sonication parameters has been published, which used the Diagenode Bioruptor® XL Water Bath Sonicator to improve the strategy of Chromatin Fragmentation and Protein Immunoprecipitation (Pchelintsev et al. 2016). For optimal high-power sonication cycles, they recommend that on/off interval times should be amended to correspond to the time it takes for one full rotation of the carousel tube holder unit. This guarantees that each sample tube is exposed to all possible intensity zones as it continues throughout each sonication cycle, regardless of its position within the carousel (Pchelintsev et al. 2016). The water bath sonicator set-up they used for this study was similar to our Diagenode Bioruptor® Sonication System operated here but comprised two integrated rotator units instead of one. This recommendation was therefore highly relevant to our work and was something that we decided to investigate further.

Another important factor to consider was the choice of homogenisation tool, as this could vary depending on the physical characteristics of the sample. Clearance size must also be modified as appropriate to ensure effective lysis. However, unnecessary excessive force can cause extreme shearing and heat production, denaturing endogenous proteins. The overall type of homogeniser chosen could therefore have a considerable impact on the accuracy of protein coverage and the biological interpretations of the data (Ye et al. 2013).

Going forward, we hence decided to switch to a glass pestle/vessel micro-tissue grinder in place of the plastic micropestle set-up we had used previously. This was because the improved mechanical shear force generated by a glass pestle could help to rapidly and efficiently release RBPs from intracellular and extracellular compartments (Ye et al. 2013). We also knew that, regardless of the tissue type in question, the composition of homogenisation buffer could have considerable effects

on the efficiency of protein extraction yield, particularly when required for proteomics analysis (Karpiński et al. 2022).

Hence, the aims of our last attempt at optimisation were two-fold: (i) to determine whether a change in homogenisation buffer composition would recover higher concentrations of total protein and, (ii) to test whether a single sonication pulse equivalent to the time taken for one full rotation of the tube holder carousel was sufficient enough to improve total protein recovery.

We replaced our usual Hypotonic Buffer/PI mix with a 2X Binding Buffer/PI alternative, again adding it at a 1:1 ratio to our final volume of accumulated testes. As the 2X Binding Buffer was also implemented in the latter stages of our protocol, for the purposes of streptavidin bead-binding and washing of unbound protein prior to elution, we knew that this would have minimal effect on the stability or integrity of endogenous proteins. Moreover, the introduction of a non-ionic, non-denaturing detergent alongside a defined concentration of salts acts to enhance solubilisation and cell lysis, while also mimicking physiological conditions to sustain non-aggregating native proteins. We found that a full 360˚ sonicator rotation corresponded to 17 seconds of constant maximum-level sonication. We therefore tested manual homogenisation in the 2X Binding Buffer/PI mix, using a new glass micro-tissue grinder, with and without a high-power 17 second sonication pulse (Fig. 16.).

After applying these adjustments, we found that homogenisation in the 2X Binding Buffer/PI mix with a glass pestle/vessel micro-tissue grinder achieved the highest total protein extraction yield thus far (Fig. 16.). However, when compared to the crude testis extract, the concentration of total protein was still nowhere near the maximum that could possibly be isolated from thirty whole testes. Overall, there was a loss of proteins at either end of the molecular weight spectrum; some higher molecular weight proteins, which were possibly muscle components of the sheath, as well as lower molecular weight proteins were still being eliminated.

Nevertheless, our results evidenced a sufficient improvement in the acquisition of soluble protein in both testis-specific pull-down homogenates. Remarkably, the combined sonication and homogenisation condition appeared to contradict our results in Section 3.9.4. (Fig. 15.), with sonication in this scenario making little improvement to the total protein concentration yield (Fig. 16.). In view of this, we made the decision

to exclude sonication from the homogenate preparation stages of our modified RNA-affinity pull-down methodology.

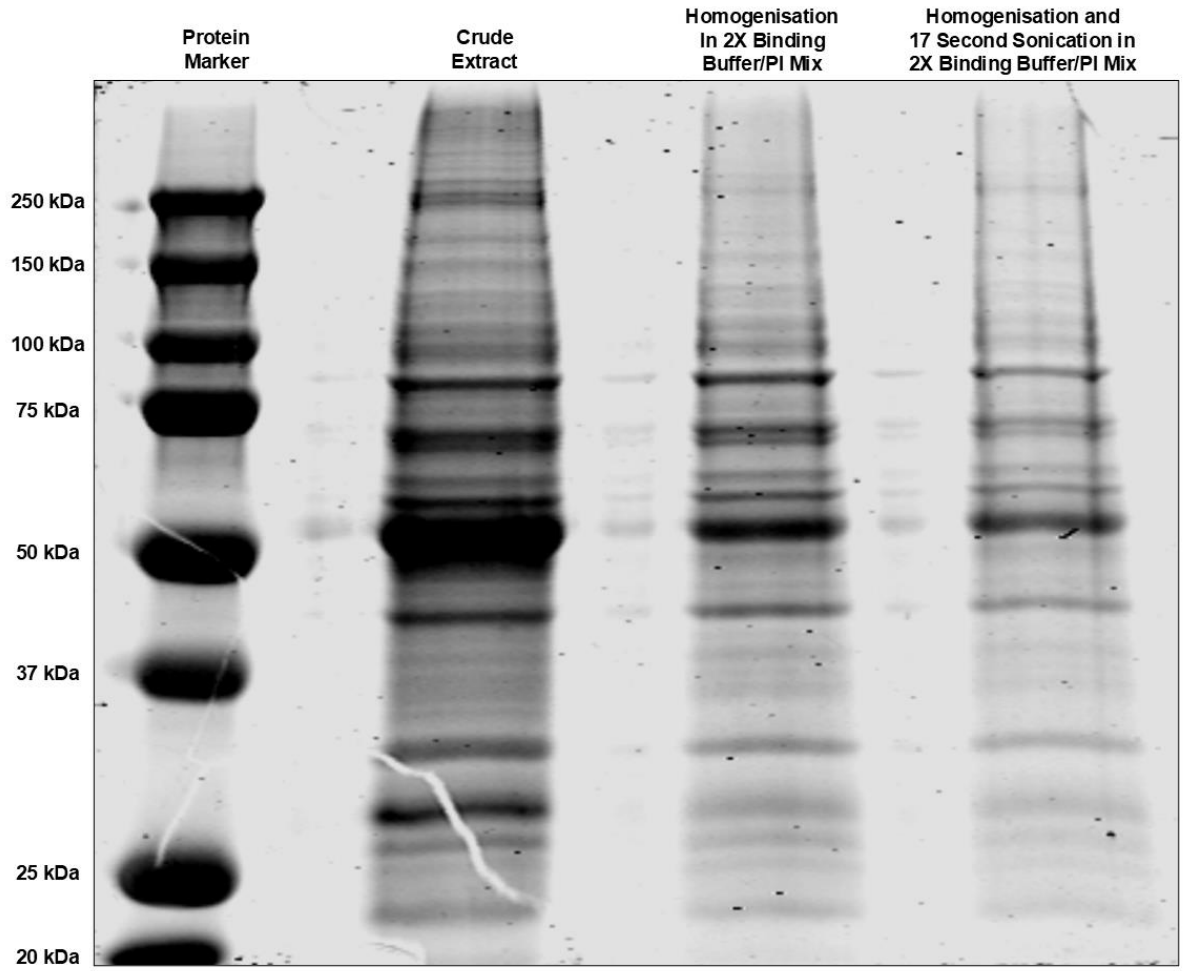

Figure 16. Total protein recovery yields of a *Drosophila melanogaster* crude testis protein extract and testis-specific RNA-affinity pull-down extracts after additional homogenisation optimisation. Total protein staining of the SDS-PAGE gel was performed using the ReadyBlue™ Protein Gel Stain (Sigma). Each sample extract was prepared with roughly thirty flash-frozen *Drosophila* testes (n=1). A panel of three testis-specific homogenate conditions were tested: (i) a simple crude protein extract, (ii) a pull-down extract prepared by manual homogenisation of testes for 60 seconds in a 2X Binding Buffer/Protease Inhibitor mix, and (iii) a pull-down extract prepared by manual homogenisation of testes for 60 seconds in a 2X Binding Buffer/Protease Inhibitor mix followed by a high-power sonication pulse for 17 seconds. By exploiting a different homogenisation buffer composition and glass pestle/vessel micro-tissue grinder for manual homogenisation, this appeared to improve the total protein levels extracted at the homogenate preparation step. Optimised sonication time, however, did not have any meaningful effect on total protein extraction yield.

3.10. Implementation of RNA-affinity pull-down modifications still results in inconsistent Western Blot signals

After many rounds of optimisation, we conducted a small-scale RNA-affinity pull-down assay that combined all the revisions we had established. At least 400 testes were dissected and amassed in the preparation of our starting input homogenate. We tested this modified set-up against two experimental biotin-labelled mRNA probes for *soti* and *h-cup*, respectively, to ensure that the test run was representative of at least one comet and one cup mRNA. Both *soti* and *h-cup* had also exhibited the most consistent binding to all our RBP candidates when the S10 cytoplasmic ovarian extract had been previously used (Section 3.7., Fig. 10.1. and Fig. 10.2.).

Good signals were demonstrated for the binding of dmPTB to the *soti* and *h-cup* transcripts, with the amount of dmPTB interacting with *h-cup* mRNA comparable to the positive control of *osk* 3' UTR (Fig. 17.). However, unlike before, less dmPTB protein bound to *soti* than to *h-cup* and the positive control.

As in Section 3.7., multiple isoforms of dmPTB bound to the comet and cup mRNAs, with the highest molecular weight isoform predominating in this testis-specific binding context. Overall, dmPTB binding was generally lower in this trial pull-down assay, and Bru1-binding was non-existent in the bound conditions. It may be argued that, compared to dmPTB and Imp, Bru1 already showed a comparably low level of binding when interacting with our panel of biotinylated comet and cup mRNAs in Section 3.7 (Fig. 10.1. and Fig. 10.2.). However, in this trial, Bru1 did not bind *soti* or *h-cup* at all. Even for our positive control of *osk* 3' UTR, only a relatively small amount of bound Bru1 protein was shown (Fig. 17.).

Binding of Imp to *h-cup* was evidenced, with signals indicating that a greater amount of Imp may be interacting with *h-cup* than with our positive control of *osk* 3' UTR (Fig. 17.).

For *soti* mRNA, on the other hand, it was difficult to determine whether there was a true binding interaction with Imp. Overexposure of the membrane suggested that there may be a small amount of bound Imp protein, but this interaction was at the extreme lower end of detection capabilities.

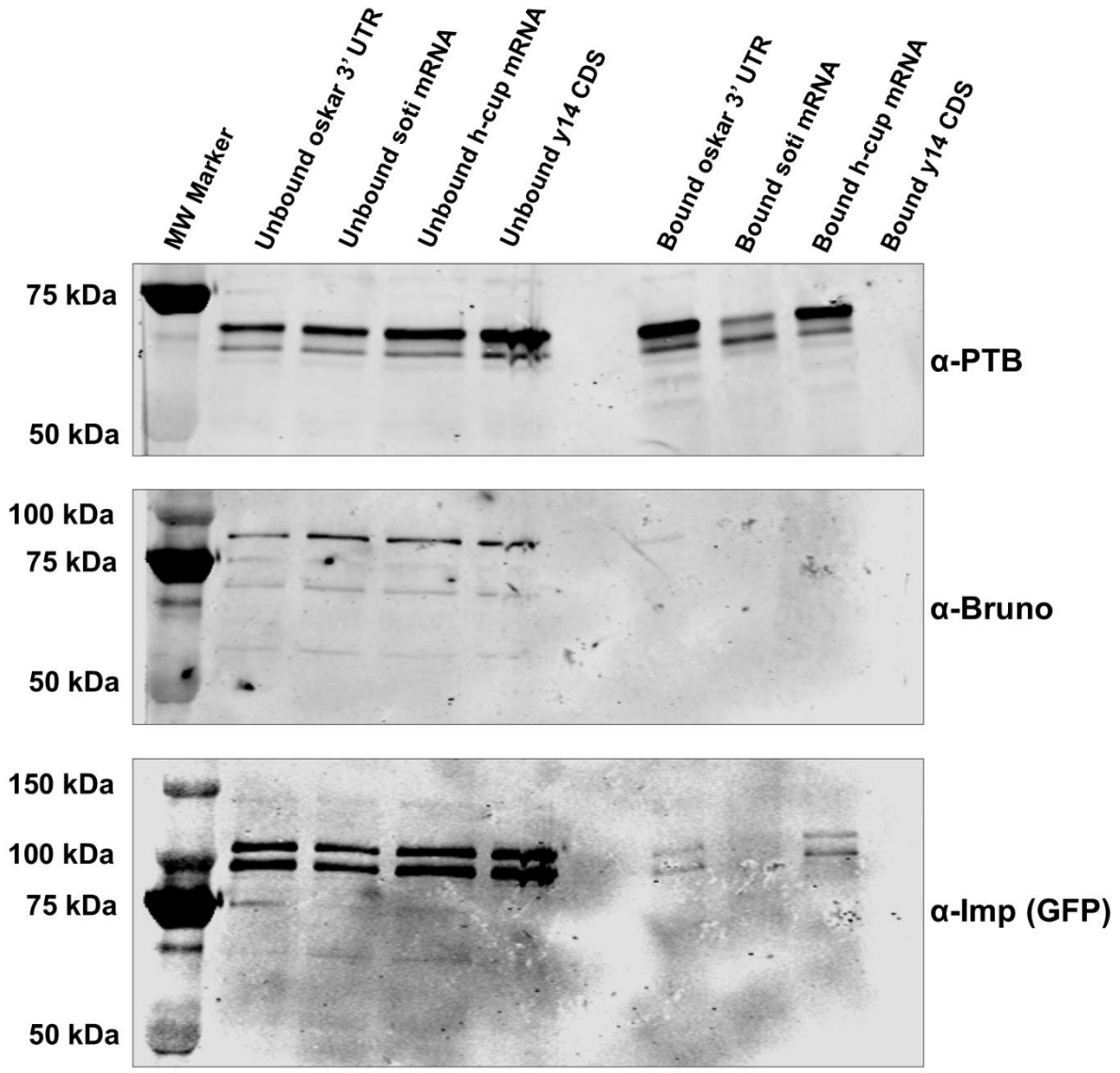

Figure 17. Characterisation of binding interactions between the *soti* and *h-cup* mRNAs and testis-specific Bru1, dmPTB and Imp proteins. Results shown here are from a Western Blot Analysis of bound and unbound pull-down fractions after bead incubation (n=1). For the sake of consistency, immunoblotting was performed sequentially on the same membrane for all RBPs, after adequate destaining and re-probing procedures. The *oskar* 3' UTR was implemented as a verified positive control, while the coding sequence of *y14* (y14 CDS) was implemented as an unrelated negative RNA control. The input protein extract equated to ~100 testes per RNA point. Due to limited antibody availability, detection of Shep was not conducted in this trial experiment. Despite the optimisation of numerous experimental modifications, blotchy background noise and inconsistencies with bound protein signals were still apparent.

This contradicts our *in vitro* binding data in Section 3.7. (Fig. 10.1. and Fig. 10.2.), as we found a high relative abundance of Imp interacting with *soti* – which was somewhat greater than the binding of Imp with *h-cup*. The presence and interaction of two Imp isoforms was much more apparent in this Western Blotting compared to our earlier RNA-affinity pull-down assay (Fig. 17. vs. Fig. 10.1.).

When probed for dmPTB and Imp, there were clear protein signals in all unbound extract conditions, indicating a sufficient starting source of protein and a high concentration of both RBPs not binding during bead incubation (Fig. 17.). However, the immunostaining of unbound extracts for Bru1 suggested a very low initial concentration of the RBP since there was an equally low level of Bru1-binding in the bound extracts, even in the positive control.

3.11. Chapter-specific discussion

3.11.1. Summary

We have successfully begun to study the biological significance of asymmetrical *Drosophila* comet and cup mRNA localisation in this chapter. By implementing and optimising *in vitro* molecular biology and biochemical techniques, we have been able to positively identify *in vitro* binding interactions between the 4 candidate RBPs of Bru1, dmPTB, Shep and Imp and a selection of 11 biotinylated comet and cup mRNA probes.

The RBP candidates we have investigated are all expressed by vital developmental regulation genes. They have several properties in common that make them a good start for our characterisation study, and there is a wealth of published evidence to support their combined importance in many different cell and tissue types. For example, the mRNAs expressed by *dmPTB, shep* and *imp* are all unusual because they make up only a small number of mRNAs, but show a wide range of distinct alternative transcripts depending on the tissue and developmental stage within which they are transcribed (Hilgers et al. 2011).

Our findings provide preliminary evidence of differential binding, with the amount of interacting RBP varying depending on the mRNA of interest. While these *in vitro* pull-down findings cannot discriminate between direct and indirect binding contexts, the

relative abundance of bound RBP was found to be highly variable, which suggests that the machinery involved in comet and cup post-transcriptional regulation is much more diverse within their respective classifications than between them. Our results may also indicate that this regulatory overlap feeds into overlapping gene functions for these comets and cups that do not necessarily match their transcript localisation characteristics.

For now, little is known about the regulatory driving forces that underpin post-meiotic comet and cup mRNA localisation in the mid-to-late elongating spermatids. Our data provides a stepping stone towards the elucidation of multiple RBPs that may contribute, directly or indirectly, to a wider interacting network that post-transcriptionally regulates comet and cup mRNAs in dynamic, localising RNP complexes.

3.11.2. Dynamic and differential binding interactions may indicate functional redundancy and cooperation of multiple *trans*-acting factors

It is highly likely that the comet and cup mRNAs interact with a whole host of different regulatory machineries as they are transported throughout the spermatids *in vivo* – including various RBPs and *trans*-acting co-factors. This leads to differences in the composition of their encompassing RNP complexes, shown here through varying levels of *in vitro* binding interactions. It is likely that there is a redundancy and flexibility conferred by these different combinations of RBPs and co-factors, which feeds into the specificity and spatiotemporal control of comet and cup fates – including their targeted localisation and translation. This may even occur as a dynamic remodelling of the RNP complexes as they travel throughout the spermatids (Otero et al. 2001; Parton et al. 2014a).

This hypothesis of a precise and unique combination of many different binding factors, which is modified during the life cycle of mRNA transcripts, is supported by the literature (Parton et al. 2014a). For example, the isolation of yeast RNP complexes, affinity-purified with tagged proteins, has indicated clear compositional overlaps and the association of different pools of RNPs as the mRNA maturation pathway

progresses (Oeffinger et al. 2007). However, the details as to how these types of exchanges actually occur remains elusive, and the massive, yet overlapping, diversity in *trans*-acting protein factors only adds to this complexity (Castello et al. 2012; Castello et al. 2013).

3.11.3. Imp is an interesting RBP candidate that requires further investigation and characterisation

As Imp is indeed enriched at the growing ends of spermatid tails, this suggests a possible overlap between the expression profile of Imp protein and the previously characterised comet and cup mRNA transcripts (Barreau et al. 2008a; Barreau et al. 2008b; Fabrizio et al. 2008).

Spatially, Imp and this set of localised mRNA transcripts can be detected in very similar subcellular regions at the extreme tail-ends of elongating spermatid cysts and, temporally, both can be detected in mid-to-late spermatid elongation. This information, combined with a “full house” of binding interactions in our RNA-affinity pull-down results, makes Imp a standout candidate to pursue further. Although, alike Bru1, dmPTB and Shep, there did not appear to be a division in comet and cup binding preferences when we investigated pairwise binding interactions with Imp here.

According to FlyBase, the *imp* gene encodes a set of twelve RNA isoforms designated A through to M (Öztürk-Çolak et al. 2024). The CDS of the *imp* isoforms denoted A, B, and C are identical, Imp-L and Imp-M are identical, and the sequences shared by isoforms D, E, F, G and H are also identical. Together, this results in the translation of only five unique protein products in flies, with predicted MWs ranging from 62.1 kDa to 69.9 kDa. In RNA-Seq data generated from the transcriptome of the adult fly testis by the FlyAtlas 2 Consortium, they found that, at a minimum, only the B, E, H and L isoforms of Imp were consistently expressed within the male gonads (Leader et al. 2018; Krause et al. 2022). As the Imp G00080 exon-trap line was developed by inserting a promoter trap element into the intron upstream of the furthest 5' exon shared by all spliced isoforms of Imp, this will therefore continue to be an excellent choice of fly line for the ongoing analysis of Imp in the *Drosophila* testes (Quiñones-Coello et al. 2007).

From the literature, we know that there are many biological implications of IMP homologues in mammalian fertility and testicular disease. After PCR and Northern analyses substantiated the expression of mammalian IMP1 and IMP3 mRNAs in the mature murine testis (Morin et al. 2001; Wang et al. 2003b), Hammer et al. (2005) studied the specific expression patterns of IMP1, IMP2 and IMP3 during the development and maturation of testes in mice and human models. Investigations were also conducted which explored the expression and implications of IMPs throughout a range of human-based testicular cancers – with a specific focus placed on those derived from human germ cells. Immunostaining of the embryonic testis indicated the presence of all three IMPs in the gonocytes, while IMP2 was also detected in the interstitial tissue. In the adult testis, IMP1 and IMP3 predominated in the spermatogonia, whereas IMP2 was expressed in the immature Leydig cells. Interestingly, all full-length IMPs were described in human semen samples using Western Blotting. This suggested that IMPs show differential expression throughout gonadal development and are also subject to defined sex-specific gender differences (Hammer et al. 2005).

The developmental expression patterning of IMP1 and IMP3 in the human testis sparked further investigations into their potential roles in testicular neoplasia (Hammer et al. 2005). IMP expression was detected via immunohistochemistry in an array of germ-cell neoplasm types, including pre-invasive testicular carcinomas *in situ*. High levels of expression were, most notably, recorded in undifferentiated embryonal carcinomas. The relative expression of these IMP1, IMP2 and IMP3 proteins varied among the different tumour types, and IMP1 was the only member to be found in all carcinoma *in situ* cells. Together, these findings suggest that the IMP family (primarily IMP1) could offer effective auxiliary markers for the diagnosis of testicular neoplasia (Hammer et al. 2005). As the IMPs appear to be linked to mammalian cancers, metastasis and malignancy, the wider Imp protein family may also provide interesting key players in the development of biological dysfunction and disorder.

Several studies have also been published in the wider literature that indicate the involvement of Imp homologues in the oncogenesis and tumorigenesis of different tissue types (Reviewed in Yaniv and Yisraeli 2002). Overexpression of IMP1 and IMP3 in adult transgenic mouse models has also been shown to induce tumour malignancy in the mammary duct epithelium and acinar-ductal metaplasia in the pancreas,

respectively (Wagner et al. 2003; Tessier et al. 2004). Together this suggests that the Imp protein family members play a substantial role in health and disease at a whole-tissue level and in many different organisms – making *Drosophila* Imp at even more intriguing protein to study.

With this ever-growing wealth of evidence of Imp's involvement in normal and dysfunctional testes, Imp quickly became our lead RBP candidate to investigate going forward. We decided to conduct a series of follow-up experiments to characterise Imp in the testis of *Drosophila melanogaster*, both *in vitro* and *in vivo*. We next sought to determine the functional role of Imp within the testis and sperm development; firstly, by validating what we had observed here in a more exhaustive, testis-exclusive context (See Results Chapter 2). This was followed by a specific focus on Imp's contributions to the post-transcriptional regulation of comet and cup mRNA localisation in the spermatids (See Results Chapter 3).

3.11.4. Long-term considerations regarding the RNA-affinity pull-down methodology

We have demonstrated that proper optimisation of homogenisation tools and buffer compositions is necessary to improve cell lysis and protein release within testis-specific pull-down extracts. However, we were unable to recapitulate the RNA-affinity pull-down set-up using a testis-derived homogenate as the input of endogenous, cytoplasmic RBPs.

In our small-scale pull-down with testis homogenates, RBP-binding to our positive control was consistently weaker than we would otherwise expect. We know from the wider literature and from our findings in Section 3.7 (Fig. 10.1. and Fig. 10.2.) that Bru1, dmPTB and Imp all bind the *osk* mRNA at its 3' UTR (Kim-Ha et al. 1995; Munro et al. 2006; Besse et al. 2009). We chose the *osk* 3' UTR as a positive control for this very reason. So, why is it that the levels of our RBPs in the unbound positive control conditions were comparable to the unbound negative control conditions of *y14*-CDS? The concentration of RBPs after bead incubation should, in theory, be lower in the unbound positive control extract – because the RBPs should be interacting with the *osk* 3' UTR and remaining associated to the immobilised bead complex until elution.

This suggested that a high concentration of our RBP candidates were remaining unbound and were not binding to the *osk* 3' UTR as anticipated. When taking this into account, it was difficult to ascertain whether the input protein concentrations were high enough to fully "saturate" the beads and bind the immobilised RNAs effectively. Unfortunately, additional troubleshooting was again required, but we decided to explore other experimental avenues instead, having already validated at least some these binding interactions.

If we were to repeat this again, our central focus would be to maximise the homogenate preparation stages to improve starting concentrations as much as possible. Ultimately, more testes are required per sample. However, even with the batch-flash-freezing process we had developed for our Cleavable Affinity Purification (Cl-AP) assay in Results Chapter 2, this was a difficult thing to achieve for multiple RNA points. The fresh sample strategy we were attempting to implement initially is not a feasible solution; the difference between hundreds and thousands of testis dissections is considerable and is something that cannot be completed on the same day of experimentation without an entire team of dissectors. Even with flash-freezing, the requirement of at least two hundred testes per RNA point equates to well over two thousand testes for all eleven of our test mRNAs – and this would not even cover any experimental repeats.

Overall, buffer composition is a key component of *in vitro* assays, and it can be one of many rate-limiting steps that must be overcome when troubleshooting complications with protocols. When optimising compositions of homogenisation buffers for immunoprecipitation experiments, for example, the buffer pH at the stage of lysis should always match, as closely as possible, to that of the wash buffer (DeCaprio and Kohl 2017). As a consequence, this can make buffer modifications extremely complicated, particularly if this means having to adjust multiple in tandem. Using hypotonic buffers, in combination with glass homogenisers, is typically the go-to approach. This is because, in theory, the cell cytoplasm should swell, causing cell membranes to rupture by mechanical force and making them much more susceptible to lysis by manual homogenisation (DeCaprio and Kohl 2019).

In terms of other sample types, such as rodent brain tissue, it is suggested that homogenisation buffer comprising a pre-determined percentage of detergent generally

gives the highest yield of protein extraction overall (Shevchenko et al. 2012; Karpiński et al. 2022). In fact, buffers containing detergent exhibit higher efficiencies of protein extraction, and correspond to protein concentrations that are roughly three times higher than that of detergent-free buffer conditions (Shevchenko et al. 2012; Karpiński et al. 2022). Although, this of course fluctuates depending on the tissue in question. Different research groups use their own in-house-developed analytical protocols for protein extraction, as is the case here. These can vary substantially in detail, and are contingent on the sample type, target subcellular compartment and/or set of proteins of interest. At present, there is no universal laboratory procedure that can analyse complete proteomes for every possible biological target (Karpiński et al. 2022).

Nevertheless, our biotinylated RNA-affinity pull-down method is an important starting point because it is free from the complexity and restraints of a cell-based system. By starting with an *in vitro* cell-free approach like this, it can be applied, theoretically, to analyse any and all endogenous RBPs of interest (Panda et al. 2016; Gemmill et al. 2019). Although, the experimental methodology must be worked around the tissue sample type in question. The in-house-developed RNA-affinity pull-down assay we performed here has been purposely optimised for use on S10 cytoplasmic ovarian homogenates and, unsurprisingly, this is what it works best for – not for testis samples.

Another plan of action would be an attempt to increase sonication efficiency by altering the sonication pulse time further. A methodical assessment of this would be most appropriate; including a progressive increase in pulse length with fewer on/off rounds to determine whether levels of total protein are gradually improved to a point of plateau. However, due to time-constraints, we were unable to properly test this approach.

Unfortunately, we could not generate a testis homogenate with starting protein concentrations great enough to be captured within the bound output, or with an abundance that could consistently meet the lower thresholds of Western Blot detection. We instead pursued other avenues for the detection of testis-specific RBP:mRNA interactions, and moved forward with the design and conception of a second method of validation. This was where the novel Cleavable Affinity Purification (Cl-AP) experimentation came into play.

4. RESULTS CHAPTER 2: Using Cleavable Affinity Purification (Cl-AP) to trap and purify multi-protein Imp:mRNA complexes

In this chapter, we were looking to substantiate what we found in our *in vitro* RNA-affinity pull-down assays in Results Chapter 1, but in an unbiased, testis-exclusive context. To achieve this, we have optimised a modified Cleavable Affinity Purification (Cl-AP) assay that has allowed us to extract out whole Imp:mRNA RNP complexes for the identification of protein and mRNA interactors *in vivo*. Our protocol is based upon a proof-of-principle paper from Tariq et al. (2020a) and a follow-up protocol published online by Tariq et al. (2020b).

4.1. What is Cleavable Affinity Purification (Cl-AP)?

Cleavable Affinity Purification, otherwise termed “Cl-AP”, is a recent development which moves away from the traditional co-immunoprecipitation bead set-up. It is a one-step affinity purification of lysates from tissues expressing tagged proteins, in our case – GFP and YFP. In short, Cl-AP involves sequential stepwise incubations that enables fluorescent variants of protein complexes to be isolated in their soluble form from intact cells.

It is based on a tripartite system of Protein-A-Streptavidin beads and a target-specific nanobody, coupled together via a biotinylated amine-reactive thiol-cleavable linker (Tariq et al. 2020a; Tariq et al. 2020b). Therefore, it is this GFP-TRAP-Sulfo bead tripartite composition which traps and immobilises the GFP-tagged protein complexes via the covalent linkage of the biotinylated fluorescently labelled protein of interest to the immobilised nanobody. Protein:RNA complexes remain attached to the Streptavidin agarose matrix prior to precipitation to yield an eluate/extract of any bound protein:RNA complexes. These can be readily released from the overall protein-GFP-biotinylated-nanobody-bead complex via cleavage with 50mM DTT (Tariq et al. 2020a; Tariq et al. 2020b).

Resultant samples should, theoretically, be ready for near-instantaneous analysis and detection. In fact, quantification from Western Blotting has confirmed that >90% of GFP is effectively and reproducibly released from the GFP-TRAP-Sulfo beads upon incubation with DTT (n ≥10). Subsequent to this, Cl-AP was successfully used to isolate purified GFP-tagged Augmin and gamma-TuRC from *Drosophila* embryo homogenates to study and reconstitute branching microtubule (MT) nucleation and polymerisation dynamics *in vitro* (Tariq et al. 2020a). Hence, the binding and release capacity of these GFP-TRAP-Sulfo reagent is highly efficient, and the overall effectiveness of the Cl-AP assay is supported by published evidence.

4.2. Advantages of protein and RNA precipitation using the Cl-AP protocol

There are many benefits to implementing Cl-AP for the precipitation of purified protein:RNA complexes. For example, employing this modified Cl-AP protocol actively circumvents non-specific protein binding because an extra layer of “protection” is implemented at the bead level. The GFP-TRAP-Sulfo beads are only able to recognise and trap specific fluorescently labelled proteins – which can be controlled for, quite simply, by using cells and/or tissues from lines of specific genotypes that only express target proteins of interest with fluorescent tags.

Additionally, the cleavable nature of the disulphide bond in the GFP-TRAP-Sulfo bead reagent allows the biotin label to be removed using a range of reducing agents such as DTT, leaving behind only a small sulfhydryl group attached to the target protein molecules. Protein complexes can therefore be obtained without any disruption to the intra-subunit and inter-subunit interactions of trapped constituents.

The Sulfo-NHS-SS-Biotinylation reagent is also water-soluble, meaning that the nanobody-biotinylation reaction can be performed in the absence of organic solvents. This is particularly important for downstream processing as the presence of solvents may preclude or interfere with some applications.

Using biotin for this conjugation process is advantageous because of its small size (244 Da) and high binding affinity for avidin and avidin-like proteins. It can therefore target and trap a number of proteins and immobilise them quite strongly to the

Streptavidin agarose with minimised risk of disruption to their biological functions (Della-Penna et al. 1986; Hermanson 2013). Avidin, and other avidin-like matrices, are also beneficial because their structures are highly stable and resistant to denaturation. This stability is increased further upon binding to biotin molecules, meaning we can have confidence that our immobilised protein:RNA RNP complexes will remain securely trapped until DTT-induced release (Cuatrecasas and Wilchek 1968; Bodanszky and Bodanszky 1970; Hermanson 2013). The ionic interactions formed between Streptavidin beads and other molecules can also help to reduce the amount of nonspecific binding events (Hermanson 2013).

4.3. Using fluorescent tags to isolate purified endogenous RNP complexes

Multiple key experimental steps must be performed to attain the precipitated protein:RNA RNP complexes with Cl-AP (Fig. 18.). However, it is targeted activity of the tripartite bead reagent which provides the specificity needed to trap and isolate a subset of tagged proteins and their interacting RNAs.

We have implemented both GFP and YFP as our affinity tags for this specific piece of work. As such, we have used the ChromoTek GFP V_HH recombinant binding protein (Proteintech UK, Product Code: gt-250) as the specific detecting nanobody of choice because of its specificity. The Alpaca anti-GFP V_HH purified recombinant binding protein used here can target a variety of fluorescent tags, including CFP, pHluorin, Venus, Citrine, eGFP, eYFP – and, of course, GFP and YFP. The V_HH corresponds to a recombinant autonomous single variable domain that is derived from the antigen-binding fragment of camelid heavy-chain-only antibodies (De Meyer et al. 2014). This fragment has in turn been engineered into a nanobody form by fusion of the V_HH to GFP-binding proteins. As the V_HH is very stable, it can fold into functional antigen-binding entities, even when expressed in a reducing physiological environment of the cell cytoplasm (De Meyer et al. 2014).

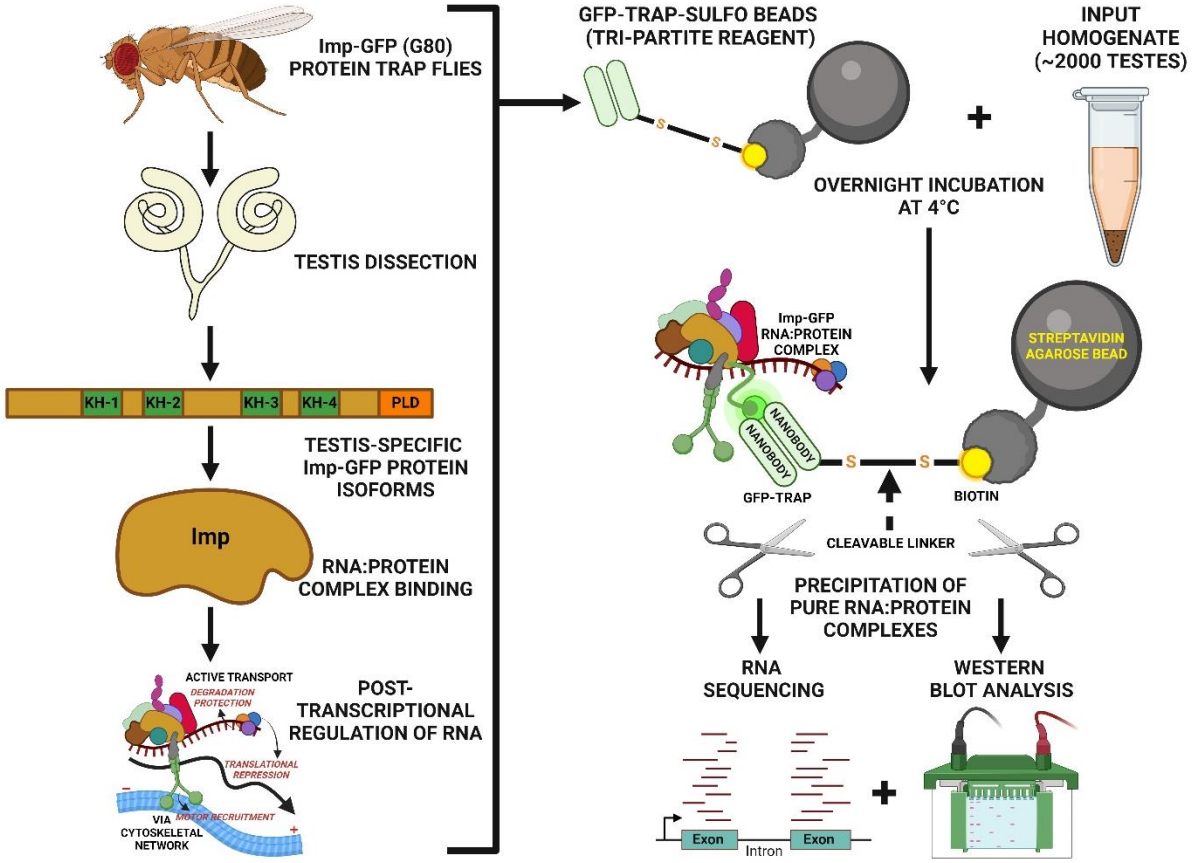

Figure 18. Schematic outlining the major stages of Cleavable Affinity Purification (Cl-AP) for the isolation of multi-protein Imp:RNA complexes. The GFP-TRAP-Sulfo beads were first prepared in a stepwise fashion: the antibody of choice was desalted, followed by an incubation to covalently link it to the biotinylated, amine-reactive thiol-cleavable linker of Sulfo-NHS-SS-Biotin. A subsequent incubation with high-capacity Streptavidin agarose resin resulted in the formation of a complete tripartite reagent. Input homogenates were prepared by homogenisation of flash-frozen testes, followed by centrifugation to remove debris. The resultant homogenate was then incubated with the GFP-TRAP-Sulfo beads to trap target proteins. After bead incubation and washing to remove any unbound and non-specific components, washed beads were incubated for two hours at RT with buffer containing a final concentration of 50 mM DTT. This cleaved the disulphide bond in the thiol-cleavable linker, releasing the immobilised, purified protein complexes and their respective RNA interactors for downstream analyses, including Western Blotting and RNA checks. **Created using BioRender.com.**

4.4. Cl-AP captures Imp binding activity *in vivo* during *Drosophila* sperm development

We have chosen Cl-AP to answer two key questions:

1. What proteins are interacting with Imp-GFP in the *Drosophila* testis?

2. Which RNAs are interacting with Imp-GFP in the *Drosophila* testis?

However, the original Cl-AP protocol was only applied to *Drosophila* embryos. It was also developed with the primary intention of trapping and isolating purified, active and molecularly-defined proteins, as well as protein complexes, with their *in vivo* post-translational modifications in-tact (Tariq et al. 2020a). Cl-AP was indeed established with the goal of purifying from any biological system of interest, but this did not encompass other non-protein interactors, including associated RNAs (Tariq et al. 2020a).

Thus, in order to achieve our aims, and enhance our current understanding of Imp's interaction and regulatory network in *Drosophila* sperm development, we first had to optimise the Cl-AP set-up. The main troubleshooting aspect of this, unsurprisingly, was the modification of buffer compositions. However, we also had to adjust our input homogenate preparations and incubation times accordingly to suit our sample type of *Drosophila* testes and our desired purification output of multi-protein, mRNA-containing RNP complexes. Compensating for both at the same time, without running the risk of increased degradation and sample loss, was therefore the first challenge.

4.5. The *Drosophila* hnRNP homologue, Squid (Sqd), acts as an internal control to compare Imp's protein and RNA interactome against

We have performed our Cl-AP experimentation in parallel on two samples in total, including one experimental RBP sample (Imp-GFP) and one control RBP sample (Squid-YFP). Each input sample homogenate equated to a combined pool of interactions from at least two thousand *Drosophila melanogaster* testes. The main

experimental RBP sample was prepared from testes dissected from Imp-GFP G80 protein trap males (G00080 exon-trap line; Quiñones-Coello et al. 2007) and the control RBP sample was generated from testes obtained from the CPTI 239 protein trap fly line, which expresses a fluorescently tagged transgenic variant of Squid-YFP (Sqd-YFP; Lowe et al. 2014). Sqd was therefore exploited as an internal control dataset, which we used to cross-compare against to elucidate the genuine, putative protein and RNA binding partners of Imp.

Sqd-YFP was implemented as an internal control as opposed to Sqd-GFP because there were only two verified *Drosophila melanogaster* lines available that could stably express a fluorescent Sqd fusion protein and were readily accessible in our lab. In both cases, these flies expressed Sqd-YFP instead of Sqd-GFP and were from protein trap lines that had been previously validated in our research group as part of the Cambridge Protein Trap Consortium (Lowe et al. 2014). As such, we could have confidence in the fly genotypes, the confirmed status of the YFP fusion, and the expected spatiotemporal expression profile of the Sqd-YFP protein.

4.5.1. What makes Sqd-YFP a good internal control sample?

4.5.1.1. Imp and Sqd expression is spatiotemporally distinct

Sqd is a well-conserved *Drosophila* homologue of human hnRNP D (Matunis et al. 1992a; Matunis et al. 1992b). *Sqd* encodes one of the most abundant *Drosophila* hnRNPs and is sometimes referred to as *hrp40*. Since its discovery, characterisation of *sqd* has been predominantly focused upon in *Drosophila* oogenesis (Matunis et al. 1992a; Matunis et al. 1992b; Kelley 1993; Matunis et al. 1994).

hnRNPs have long been implicated in the nucleocytoplasmic export of mRNA targets, and Sqd is no exception (Norvell et al. 1999). Genome-wide analyses of target RNAs and alternative splicing patterns regulated by Sqd, among other *Drosophila* hnRNP homologues, have confirmed their conserved RNA binding, processing and splicing capacities (Blanchette et al. 2009).

Alike Imp, Squid (Sqd) is another RBP that is expressed within the *Drosophila* testis. However, it is predominantly expressed in primary spermatocytes and is present in a spatially and functionally different subcellular location to Imp (Fig. 19.).

We know from previous *in vivo* analyses that Imp is expressed very early on in the male germline; it is uniformly distributed in the cytoplasm of spermatogonia within the apical hub region, before a steep decrease in signal. Some negligible, uniform Imp protein may persist in the cytoplasm of late spermatogonia and spermatocytes. However, high level local translation of Imp is detected again in the cytoplasm of post-meiotic elongating spermatids, with there being very strong, localised protein expression that is concentrated to the growing ends of the developing spermatid tails (Fabrizio et al. 2008; Nerusheva et al. 2009). In contrast, protein trap screening of testes expressing chimeric Sqd – generated by a Venus-YFP insertion and affinity protein exon-tagged hybrid of the *piggyBac* vector – have demonstrated that Sqd protein expression is opposite to that of Imp in *Drosophila* sperm development. Sqd is instead enriched at intranuclear structures of Y-loop DNA sites within the nuclei of primary spermatocytes (Lowe et al. 2014). Therefore, Imp and Sqd protein are subcellularly compartmentalised away from one another in time and space.

Y-loops correspond to regions in the heterochromatic Y chromosome, which comprise less than twenty genes – many of which encode gene products that are termed “fertility factors”. The expression of at least six of these are expressed exclusively in spermatogenesis and are required for sperm maturation (Hardy et al. 1981; Carvalho et al. 2015; Fingerhut et al. 2019). Three of these Y-chromosome-associated genes, which in turn contain gigantic megabase-sized introns, are called kl-5, kl-3 and ks-1. They are known to form Y-loops; lampbrush-like nucleoplasmic structures in spermatocytes that reflect the robust transcription of underlying genes and large stretches of repetitive DNA (Bonaccorsi et al. 1988; Piergentili 2007).

Fingerhut et al. (2019) have since confirmed this localisation pattern of Sqd and found that it labels Y loops at sites where fertility factors are being actively transcribed. While RNAi knockdowns of *sqd* did not show any obvious phenotypic changes to normal Y-loop gene transcription, there was evidence of sperm head scattering and male sterility – suggesting that any regulatory role performed by localised Sqd in the primary spermatocytes does not occur at the gene level and is most likely post-transcriptional.

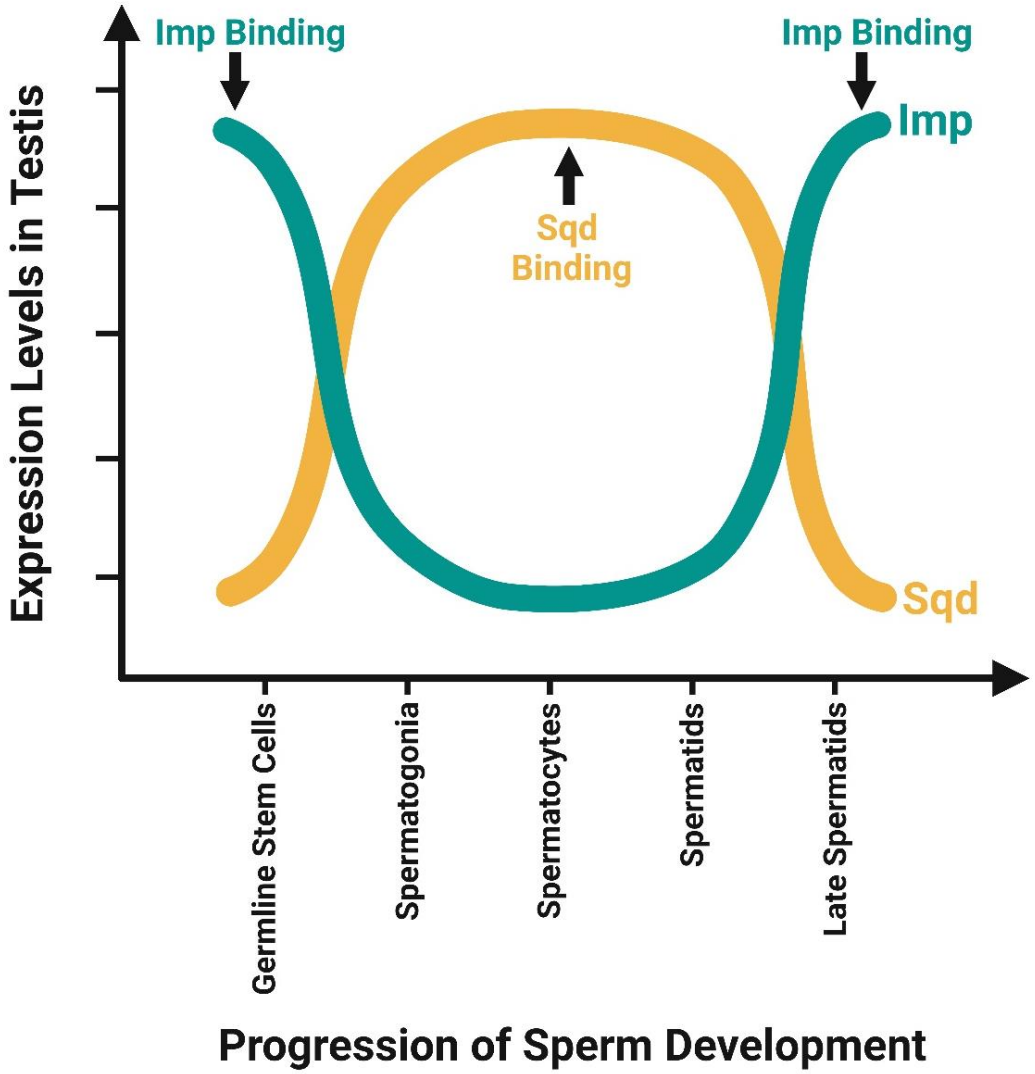

Figure 19. Imp and Sqd are expressed in spatiotemporally and functionally distinct stages of *Drosophila* sperm development. The expression profiles of Imp and Sqd are in opposing patterns to one another, with their levels of expression corresponding to an inversely proportional relationship overall. Moreover, Imp and Sqd exhibit subcellular compartmentalisation, with Sqd predominating in the nucleus whereas Imp is primarily located within cytoplasmic regions of the developing sperm cells (Fabrizio et al. 2008; Nerusheva et al. 2009; Lowe et al. 2014; Fingerhut et al. 2019). The greatest number of direct, high affinity Imp-specific and Sqd-specific binding interactions should be formed when each protein is expressed at its highest concentration in the system. For Imp, this will be in two stages: within the early pre-meiotic male germline cells and then later in the elongating spermatid cyst bundles (Fabrizio et al. 2008; Nerusheva et al. 2009). For Sqd, on the other hand, this will be in the primary spermatocytes (Nerusheva et al. 2009; Lowe et al. 2014; Fingerhut et al. 2019). Thus, Sqd is a good RBP control that will provide a contrasting dataset of interactors to which we can directly compare and validate Imp's interactome against. **Created in BioRender.com.**

Further support for these differences in the spatiotemporal expression profiles of Imp and Sqd comes from Nerusheva et al. (2009). The localisation of Sqd protein was found to change as sperm development progressed; with Sqd first expressed in the nuclei of primary spermatocytes during their growth stage. The concentration of Sqd within the spermatocyte nucleoplasm increased over time until entry into meiosis, when Sqd became expressed in the cytoplasm and was no longer detectable in the nuclei. Then, in the onion stage spermatids, this cytoplasmic expression transitioned into a uniform distribution, prior to a complete disappearance in the elongation-stage and individualising spermatids (Nerusheva et al. 2009). As primary spermatocytes are developing germline cells that are confined to the late pre-meiotic stages of sperm development, this makes Sqd's optimal expression profile temporally distinct to Imp. Hence, due to their differential expression profiles, Sqd-YFP-expressing testes were chosen as a valid internal control sample because Sqd should, in theory, possess different, non-overlapping binding partners when compared to the Imp interactome.

4.5.1.2. Sqd may play sex-specific roles in gametogenesis and act antagonistically against Imp

Imp is known to physically interact with Sqd protein in the *Drosophila* ovary and with *sqd* mRNAs in embryo-derived *Drosophila* S2 cell line cultures (Geng and Macdonald 2006; McDermott et al. 2012; Hansen et al. 2015). During oogenesis, Imp forms an RNA-dependent RNP complex with Sqd and another protein called Hrp48, and these together regulate the localised expression of *grk* and *osk* mRNA transcripts in the oocyte. However, it is hypothesised that Sqd and Imp may act in a competitive manner, with Imp performing a largely redundant role which only really comes into play after localisation defects arise. Excess *imp* activity also corresponds to a concurrent decline in *sqd* activity, supporting the hypothesis of competition between the two (Geng and Macdonald 2006). Therefore, the Sqd-Imp protein interaction is somewhat antagonistic, likely exhibiting opposing effects that, for now, have only been described in the ovary.

Moreover, sex-specific differences in the transcriptional regulation and alternative splicing of *sqd* has also been detected between male and female fly transcriptomes (Hartmann et al. 2011). Differences in the alternatively spliced isoforms of *sqd* corresponded to differences in expression levels of the Sqd protein between the two sexes – resulting in a higher concentration of Sqd protein in females. Not only that, but Sqd itself was found to play a role in tissue-specific sex determination events, including in the establishment of sex-specific splicing patterns (Hartmann et al. 2011). As Sqd is known to be subject to sex-specific differences in expression, this likely feeds down into differences at a functional level between the female and male reproductive systems. Hence, we still feel that Sqd is a good contrasting control that will permit us to characterise the Imp interactome in the *Drosophila* testis.

According to FlyBase, the *sqd* gene encodes a set of five RNA isoforms designated A through to E (Öztürk-Çolak et al. 2024). The CDS of the Sqd isoforms denoted C and E are identical, resulting in the translation of an indistinguishable 308 AA polypeptide with a predicted MW of ~33.1 kDa. As such, the overall expression of *sqd* corresponds to the production of only four unique protein products - ranging from 18.3 kDa to 36.2 kDa in MW. In RNA-Seq data obtained from the transcriptome of the adult fly testis by the FlyAtlas 2 Consortium, they found that all isoforms of Sqd were reasonably expressed within the male gonads, except for the largest isoform, Sqd-B (MW: ~36.2 kDa, 344 AA) (Leader et al. 2018; Krause et al. 2022). Since our Sqd CPTI 239 protein trap line was developed via an in-frame YFP insertion that corresponded to a site within the 3’ UTR of Sqd-A and an intron shared by Sqd isoforms B, C, D and E, this therefore provided a good fly line for the analysis of Sqd interactors in the *Drosophila* testes.

4.6. Optimisation of the CI-AP protocol required several rounds of experimental troubleshooting

4.6.1. Initial CI-AP optimisation using testis homogenates and RIPA buffer suggests complete loss of interacting RNAs

In my first attempt of this assay, preliminary testing with CI-AP confirmed the successful generation and functioning of our GFP-TRAP-Sulfo reagent. Western Blot analysis validated the presence of high concentrations of our fluorescently tagged protein variants in the bound eluates, supporting the effective trapping and purification of Imp-GFP and Sqd-YFP at good levels (Fig. 20.).

A higher concentration of Imp-GFP and Sqd-YFP protein in the bound samples post-cleavage with 50 mM DTT confirmed that the two-step process of trapping and DTT-induced release had indeed taken place (Fig. 20.). The evident loss of Imp-GFP and Sqd-YFP proteins in the unbound extracts and a concurrent increase in the levels of both tagged proteins in the DTT-cleaved eluates revealed efficient depletion upon incubation with the GFP-TRAP-Sulfo beads.

However, any bound RNAs were unfortunately washed away due to use of a more “stringent” buffer (1X RIPA) than necessary. This could be primarily attributed to the incorporation of more detergent than required. RIPA buffer was consistently used throughout the experiment, which itself contained 1% NP-40 and 0.25% deoxycholic acid, and was in turn supplemented with even more detergent (0.1% IGEPAL) at every stage of the CI-AP assay (e.g., bead generation, washing, high-speed supernatant preparation, etc.). Such an incredibly high concentration of detergent in this buffer composition was almost certainly responsible for eliminating any accompanying RNA constituents.

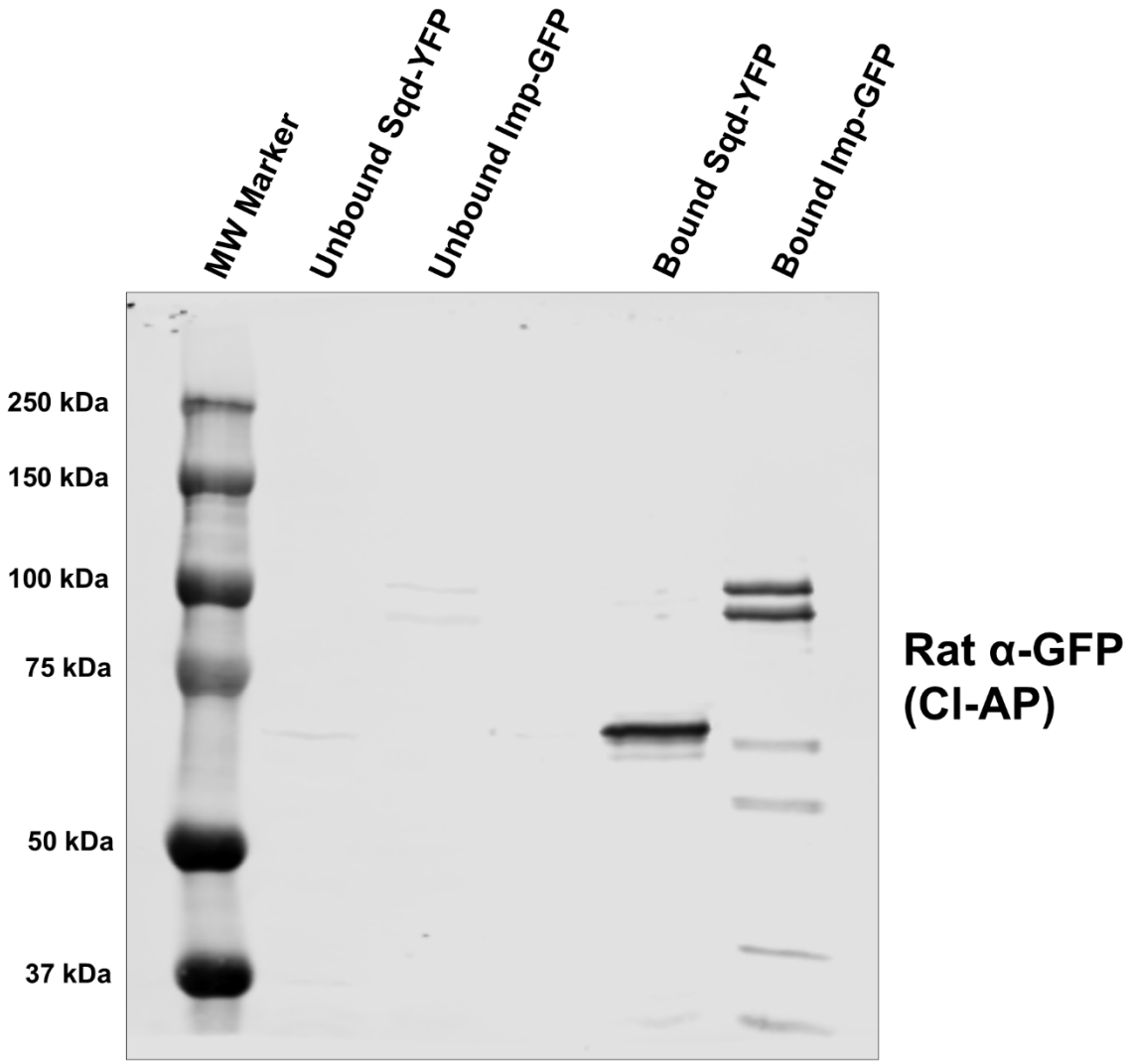

Figure 20. Western Blotting confirms the effective trapping and purification of Imp-GFP and Sqd-YFP proteins using the Cl-AP methodology. The high concentrations of Imp-GFP and Sqd-YFP signals in the bound eluates relative to the unbound fractions showed that these fluorescently tagged proteins had been trapped effectively and efficiently from the input pool of endogenous proteins. This evidenced the targeted functioning of the tripartite GFP-TRAP-Sulfo bead reagent, which was generated in accordance with the published Cl-AP protocol (Tariq et al. 2020a; Tariq et al. 2020b). Unbound samples correspond to the unbound remnants and non-specific proteins that were left over after incubation of the input homogenate with the GFP-TRAP-Sulfo beads. The initial input homogenate comprised an ultracentrifuged high-speed supernatant prepped from the homogenisation of more than 2000 testes, dissected from the Imp-GFP G80 protein trap (Quiñones-Coello et al. 2007) and Sqd CPTI 239 fly lines (Lowe et al. 2014), respectively (n=1). MW Marker: Precision Plus Protein™ Dual Colour Standard (Bio-Rad Laboratories). Probed with rat anti-GFP monoclonal antibody (1:1000; ChromoTek, Cat. No. 3H9).

Our aim was to use this method to obtain whole testis-specific multi-protein complexes with bound, in-tact RNAs. We ultimately wanted to sequence the RNAs that were interacting with our proteins of interest to determine whether comet and cup mRNAs were a substantial component of Imp's transcript interactome. However, this would not be possible if interacting RNAs were being omitted throughout the CI-AP experiment.

Further modifications were therefore required to overcome these issues and retain complete RNP complexes for analysis.

4.6.2. Longer DTT-induced cleavage times correlate with a higher efficiency of protein trapping and release

To address these concerns, we sought resolution from an in-house co-immunoprecipitation approach, developed and optimised for use with *Drosophila* ovaries. We decided to repeat this process again, in the hopes of troubleshooting our initial struggles by switching to the optimised buffer conditions developed in the Lopez de Quinto lab (Almoalem 2023).

We trialled a combination of four different buffers – Precipitation Buffer, Lysis Buffer, Dilution Buffer and Washing Buffer – the compositions for which had all been determined as part of similar assays in the Lopez de Quinto lab (Almoalem 2023). All buffers had distinct percentages of detergent, that were varied depending on the requirements of that experimental stage. So, for example, the final concentration of detergent was higher in the early lysis and homogenisation stage compared to that of the final wash and elution stage (0.5% vs. 0.05%).

Additionally, we remained concerned about the potential RNA degradation that could result from a two-hour DTT-cleavage incubation at RT – even after RNase inhibitor treatment. So, we also wanted to utilise this optimisation run to compare between shorter duration and lower temperatures for the concluding DTT cleavage step. This included three timepoints covering two temperatures in total: incubation for 5 minutes, 20 minutes and 2 hours at both RT and 4˚C, respectively.

While depletion of Imp-GFP protein in the unbound extract versus the starting input did not appear to be as effective as seen previously, our findings still showed the successful isolation of purified Imp-GFP protein in clean eluates (Fig. 21.). A 5-minute incubation at RT and at 4˚C with DTT was not sufficient to induce cleavage while 20 minutes at RT and 2 hours at 4˚C seemed to result in comparable levels of Imp-GFP release. There also appeared to be a small amount of Imp-GFP protein isolated upon a 20-minute DTT incubation at 4˚C. However, our findings are in accordance with Tariq et al. (2020a) – the most efficient trapping and release of Imp-GFP protein corresponded to a 2-hour incubation with 50mM DTT at RT (Fig. 21.).

Yet, despite these modifications, and the clear presence of Imp-GFP in almost all samples, Qubit™ 4 Fluorometry (Invitrogen, Cat. No. Q33226) confirmed that there was no RNA in any of our bound eluate variants after column-based extraction, despite being equivalent to twenty whole ovaries.

But what was most concerning, was the fact that there was very little RNA in our input homogenate and unbound extract – bearing in mind the high amount of protein shown in just 10 µL of each. While we conducted the RNA extraction on a volume of input homogenate that equated to 15 ovaries in total, only 5.7 ng/µL of RNA was detected. In the unbound fraction, this was even less, measuring an RNA concentration of just 4.0 ng/µL.

So, while follow-up troubleshooting using ovary homogenates had facilitated optimisation of buffer compositions, issues with RNA outputs persisted throughout. The same question remained: how and where was RNA being lost in this process?

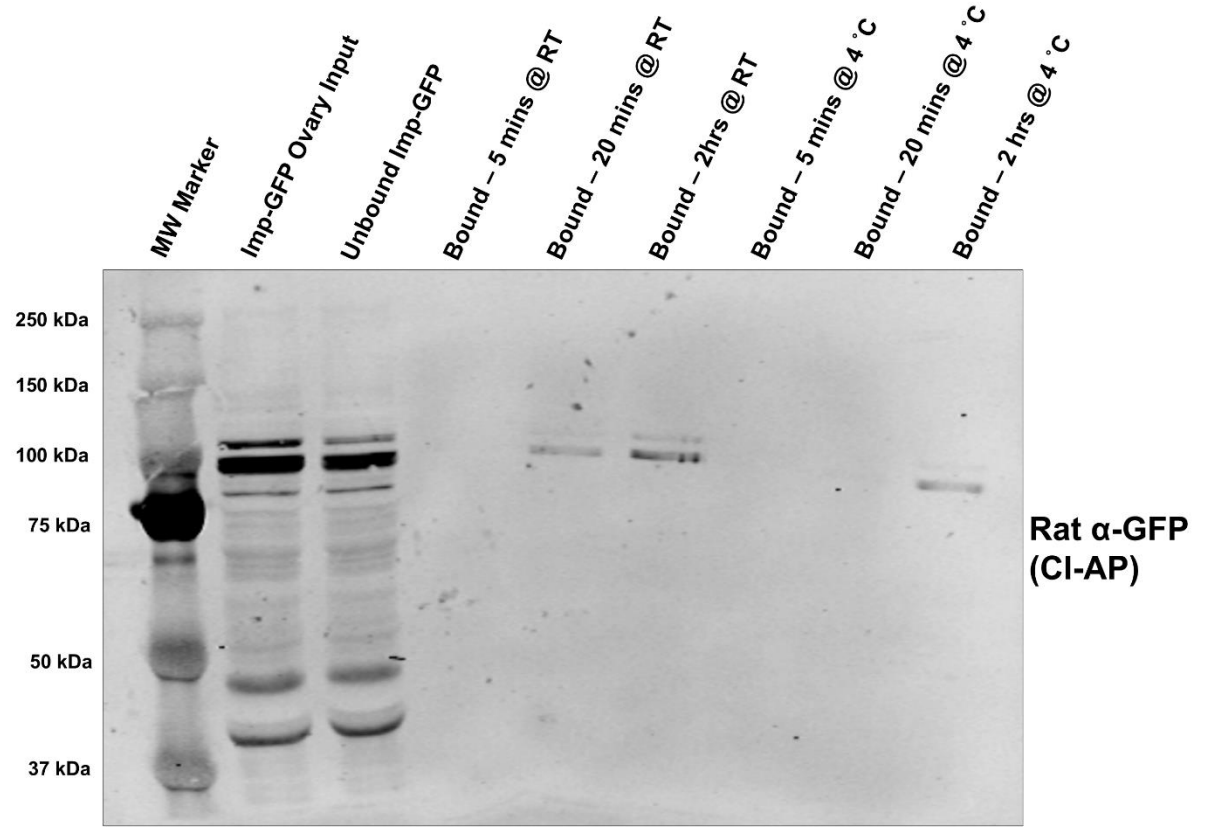

Figure 21. Adapted buffer compositions work well in the CI-AP assay and longer DTT incubations at higher temperatures improve the subsequent release of purified Imp-GFP protein. Imp-GFP has been trapped and released in four of the six cleavage conditions tested, to varying degrees of success. Incubation with 50 mM of DTT for 2 hours at RT appeared to be the most optimal of these, leading to the highest concentration of purified Imp-GFP protein overall (n=1). The input homogenate consisted of an ultracentrifuged high-speed supernatant prepped from the homogenisation of ~150 pairs of ovaries, dissected from Imp-GFP G80 protein trap females (Quiñones-Coello et al. 2007). The unbound sample corresponded to the unbound remnants and non-specific proteins that were left over after incubation of the input homogenate with the GFP-TRAP-Sulfo beads. MW Marker: Precision Plus Protein™ Dual Colour Standard (Bio-Rad Laboratories). Probed with rat anti-GFP monoclonal antibody (1:1000; ChromoTek, Cat. No. 3H9).

4.6.3. Comparison of RNAqueous™-Micro Kit purification outputs confirms kit fault

To determine the true explanation and answer the above question, we wondered whether there could be an inherent issue with the initial homogenate preparation or the way in which the final phase of RNA extraction was being performed. A test was thus conducted using two RNAqueous™-Micro Total RNA Isolation Kits (Invitrogen, Cat. No. AM1931) – including the kit that was used in previous attempts and a newly-opened equivalent.

Tissue homogenisation and homogenate preparation was performed as before to generate two individual and independent homogenates, using thirty Imp-GFP-expressing ovaries for each (G00080 exon-trap line; Quiñones-Coello et al. 2007).

After two rounds of high-speed ultracentrifugation, rather than incubating with the GFP-TRAP-Sulfo beads, the RNA extraction step was immediately undertaken using the old and new kits. Purified RNAs were collected in 20 µL of proprietary elution solution for each.

The aims of this test were to determine one of two possibilities:

1. If the concentration of purified RNA is the same in both conditions (i.e., both low and around the same values) then RNA loss and/or degradation is occurring early on during the sample preparation phase.
2. If the concentration of purified RNA is at a higher concentration (and at a reasonable value) in the previously unused kit vs. the old one, then this suggests that there was an error at the point of RNA extraction and there is something at fault with the kit in question.

Measurement and comparison of the resultant RNA concentrations shed some light on the situation (Table 6.). The concentration of total purified RNA isolated using the new kit was almost seven times greater than that of the old kit elution; a spectacular change, the effects of which were magnified considerably in the CI-AP technique.

As the amount of RNA being trapped was already relatively low – due to the GFP-TRAP-Sulfo beads only capturing a specific subset of RNAs that were interacting with and/or were associated with Imp-GFP and Sqd-YFP complexes, respectively – this additional point of elimination appeared, initially, to be the root cause of our RNA depletion.

Table 6. Comparison of two RNAqueous®-Micro-purified RNA concentrations confirms kit failure. Two RNAqueous™-Micro Total RNA Isolation Kits (Invitrogen, Cat. No. AM1931) were tested and compared against to determine whether there was an impairment to the old, communal kit-based extraction of purified RNAs. RNA concentrations were quantified using the NanoDrop™ ND1000 Spectrophotometer (Thermo Scientific).

KIT TYPE	RNA CONCENTRATION (ng / µL)	TOTAL ELUTED RNA CONCENTRATION (ng)
OLD RNAqueous™-Micro Kit	22.6	454.0
NEW RNAqueous™-Micro Kit	156.6	3132.0

4.6.4. Errors attributed to kit-based RNA extractions do not fully explain depleted levels of purified RNA

With the above information known, a switch in RNAqueous™-Micro Total RNA Isolation Kits (Invitrogen, Cat. No. AM1931) was made and a repeat test of 50 mM DTT cleavage conditions was performed using our now-optimised buffers.

To once again investigate the effects of DTT-initiated cleavage duration and temperature on isolated protein and RNA concentrations, 150 pairs of Imp-GFP-expressing ovaries (G00080 exon-trap line; Quiñones-Coello et al. 2007) were used for the Cl-AP homogenate. However, in this round, we instead included two timepoints with two temperatures in total: 30 minutes at RT, 2 hours at RT, 30 minutes at 4˚C and 2 hours at 4˚C.

Western Blot analysis was undertaken upon a 10 µL volume of the input homogenate, the unbound extract and all four bound extracts (30 minutes and 2 hours at RT and 4˚C, respectively). Yet again, it revealed consistent trapping and release of Imp-GFP protein (Fig. 22.).

As before, modification of DTT-cleavage conditions corresponded with differences in the efficiency of Imp-GFP protein purification; although, the levels of purified protein appeared to be much more similar between 30 minutes at RT, 2 hours at RT and 2 hours at 4˚C in this test (Fig. 22.). Qualitatively, the concentration of purified Imp-GFP trapped and released in the 2-hour DTT incubation at RT was still slightly higher (Tariq et al. 2020a). Incubation with 50 mM DTT for 30 minutes at 4˚C was not, however, enough to induce effective cleavage and Imp-GFP release.

Purified RNAs were then extracted from 25 µL, which was taken from the remaining volume of all samples and eluted in 20 µL. Once more, the NanoDrop™ (ND1000 Spectrometer, Thermo Scientific) readings were suggestive of minimal purified RNA content (Table 7.). As the concentration of RNAs in both the input homogenate and unbound extract were well below a 10 ng / µL threshold, it was apparent that a change in RNA extraction kit had not successfully resolved our RNA depletion problem.

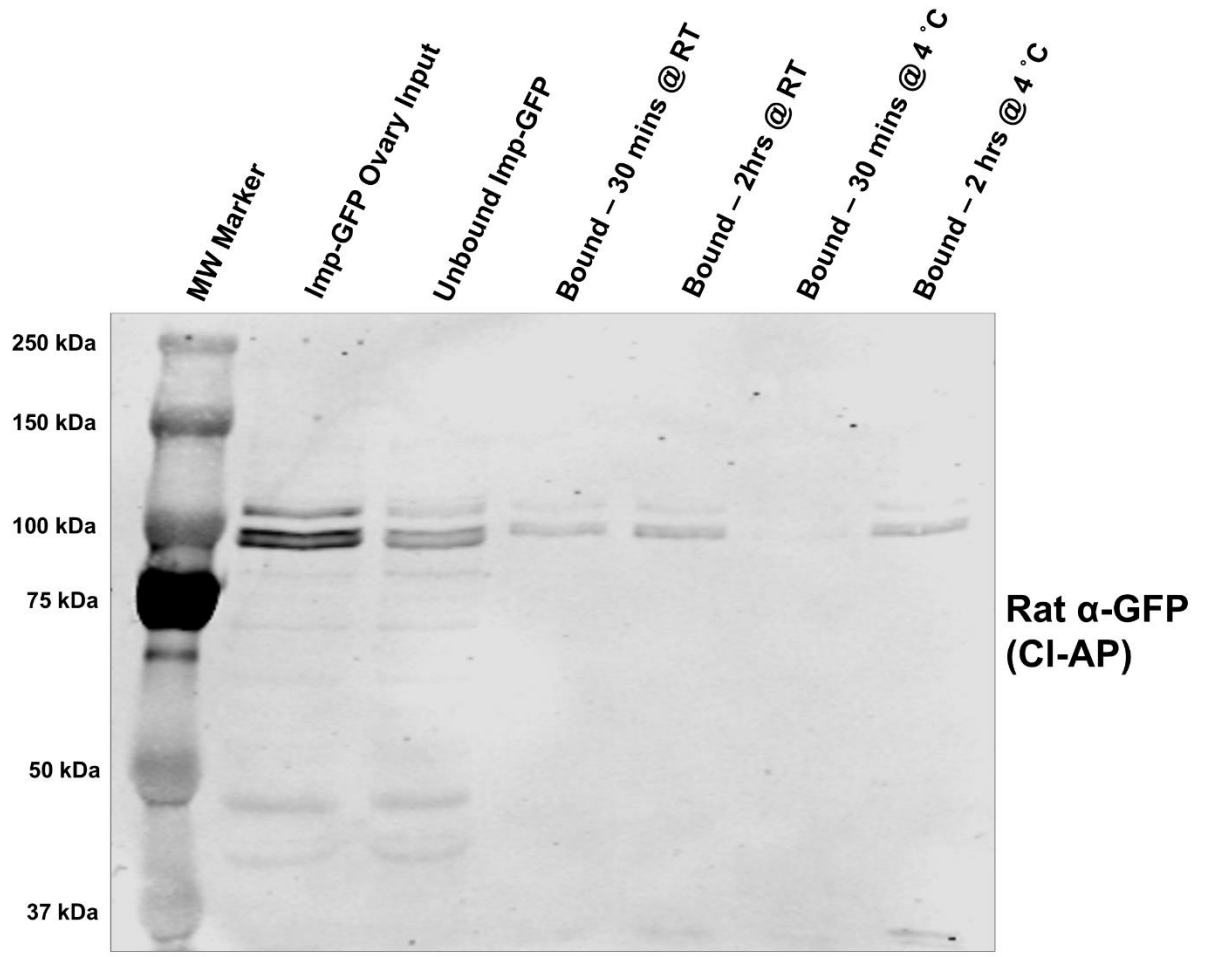

Figure 22. Western Blotting demonstrates cleaner CI-AP-derived Imp-GFP purifications and increased efficiency of protein release upon exposure to longer DTT incubations. Imp-GFP has been trapped and released in all four cleavage conditions tested, but concentrations of release vary depending on the condition parameters (n=1). Incubation with 50 mM of DTT for 2 hours at RT was the most efficient for protein isolation, resulting in the highest concentration of purified Imp-GFP protein overall. The input homogenate was an ultracentrifuged high-speed supernatant prepped from the homogenisation of ~150 pairs of ovaries, dissected from Imp-GFP G80 protein trap line (Quiñones-Coello et al. 2007). The unbound extract represented unbound remnants and non-specific proteins that remained behind after incubation of the input homogenate with the GFP-TRAP-Sulfo beads. MW Marker: Precision Plus Protein™ Dual Colour Standard (Bio-Rad Laboratories). Probed with rat anti-GFP monoclonal antibody (1:1000; ChromoTek, Cat. No. 3H9).

Table 7. Abnormally low concentrations of RNA are still outputted after the CI-AP assay, despite purification from a starting input of 150 pairs of *Drosophila* ovaries and replacement of the RNAqueous™-Micro Kit. While such low measurements were not particularly reliable quantification-wise, these confirmed that RNA was still being lost at various stages of the CI-AP experiment in spite of these changes. RNA concentrations were determined using the NanoDrop™ ND1000 Spectrophotometer (Thermo Scientific).

RNA SAMPLE TYPE	DESCRIPTION	RNA CONCENTRATION (ng / µL)
INPUT	High-speed supernatant generated from ~300 homogenised Imp-GFP ovaries	5.6
UNBOUND	Unbound proteins remaining in extract after incubation with GFP-TRAP-Sulfo beads	5.5
30 MINS @ RT	Bound Imp-GFP sample cleaved via incubation with 50 mM DTT for 30 minutes at RT	2.6
2 HRS @ RT	Bound Imp-GFP sample cleaved via incubation with 50 mM DTT for 2 hours at RT	9.9
30 MINS @ 4˚C	Bound Imp-GFP sample cleaved via incubation with 50 mM DTT for 30 minutes at 4˚C	2.9
2 HRS @ 4˚C	Bound Imp-GFP sample cleaved via incubation with 50 mM DTT for 2 hours at 4˚C	11.0

4.6.5. Ultracentrifugation is responsible for the sedimentation of endogenous RNAs

When optimising a novel experiment for the first time, it is unwise to stray away from the source material. Amending too much of the set-up at once can also lead to multiple confounding factors arising, some of which may or may not contribute to the success or failure of the experimental outcome. With this in mind, we had kept to what was known already – using two rounds of ultracentrifugation to generate a high-speed supernatant for incubation with the GFP-TRAP-Sulfo bead reagent.

In the twinned publications by Tariq et al. (2020a) and Tariq et al. (2020b), this ultracentrifugation step was performed twice in the CI-AP protocol; at 100,000 *xg* for 10 minutes and 30 minutes at 4˚C, successively. To align with this as much as possible, the Tabletop Beckman Coulter Optima™ TLX Preparative Ultracentrifuge was used with the TLS-55 Swinging Bucket Rotor. A rotor speed of 40,000 RPM was chosen as this equated to an approximate Relative Centrifugal Field at r_{av} (59.4 mm) of 106,000 *x g*.

The Wakefield group had originally developed this methodology with the primary aim of purifying out and analysing protein components, including individual subunits of larger protein complexes. As no RNA sequencing or analyses were included as part of this, no consideration to how ultracentrifugation would affect associated RNA interactors was needed. Additionally, the only explanation given for these two rounds of ultracentrifugation was for the clarification of the extract (Tariq et al. 2020a; Tariq et al. 2020b). So, could ultracentrifugation therefore be acting as another contributing factor to the loss of RNA in our experiments?

To test this hypothesis, we decided to conduct a multi-sampling experiment in which we collected and analysed the levels of RNA at every stage of homogenate preparation. After dissecting ~150 pairs of ovaries from Imp-GFP G80 females (G00080 exon-trap line; Quiñones-Coello et al. 2007) in batches and pooling together on ice, the standard homogenisation procedure was followed as described previously (Materials and Methods, Section 2.7.2.). From this point onwards, an aliquot equating to 12.5 pairs worth of RNA was attained at each key transitionary step.

The starting homogenate was centrifuged at 14,000 *x g* for 10 minutes at 4˚C using a standard benchtop centrifuge to eliminate debris and clarify the sample. A resultant 120 µL volume of supernatant was acquired, equating to 1.25 pairs worth of Imp-GFP ovaries for every 1 µL of starting input. At this point, a 10 µL aliquot corresponding to 12.5 pairs of ovaries was taken and stored temporarily at –20 ˚C (Aliquot 1).

The remaining supernatant was subsequently transferred into an open-top thickwall polycarbonate Beckman tube and ultracentrifuged at 106,000 *x g* for 12 minutes at 4˚C using the Beckman Coulter Optima™ TLX Preparative Ultracentrifuge and its TLS-55 Swinging Bucket Rotor. The next aliquot was taken at this point and stored temporarily at –20 ˚C (Aliquot 2).

For the second high-speed spin, the supernatant was carefully transferred into a fresh Beckman tube and ultracentrifuged again at 106,000 *x g* for 33 minutes at 4˚C. A third aliquot was then extracted and stored temporarily at –20 ˚C (Aliquot 3).

The remaining volume was combined with Dilution Buffer to dilute the detergent composition accordingly, and RiboShield™ RNase Inhibitor (PCR Biosystems, Cat. No. PB30.23-02) was added at 0.25 µL for every 20 µL of homogenate. A fourth and final aliquot was obtained at this stage, then stored temporarily at –20 ˚C (Aliquot 4).

For each of these four distinct aliquots, a further fraction was taken forward that equated to 5 pairs of Imp-GFP ovaries. These subaliquots were combined with RNase-free water to a final volume of 25 µL and each was mixed with 150 µL of the proprietary Lysis Solution component of the RNAqueous™-Micro Total RNA Isolation Kit (Invitrogen, Cat. No. AM1931). After incubation at RT for ten minutes, the standardised kit-based extraction of purified RNAs was then performed for each of these stage-specific subaliquots. The concentration of purified RNAs extracted from these four subaliquots was measured via the NanoDrop™ Spectrophotometry (Thermo Scientific).

Overall, the differences in RNA content after each key preparative step were striking (Table 8.). NanoDrop™ spectrophotometer readings revealed that there was a >5-fold decline in the concentration of RNA isolated in subaliquot 1 compared to subaliquot 2, indicating a loss of approximately 80% upon conducting the first round of high-speed ultracentrifugation.

Table 8. The sizable reduction in RNA concentrations upon high-speed ultracentrifugation evidences a gradual sedimentation of RNAs in the original CI-AP protocol. More than 99.9% of the total input RNA that was quantified in subaliquot 1 was lost by the time the final measurement of RNA in subaliquot 4 was made. Subaliquot readings are listed in their chronological order of acquisition during the CI-AP procedure. RNA concentrations were assessed using the NanoDrop™ ND1000 Spectrophotometer (Thermo Scientific).

ALIQUOT DESIGNATION	DESCRIPTION	RNA CONCENTRATION (ng / µL)
SUBALIQUOT 1	Aliquot extracted from starting input after first round of normal centrifugation at speeds of 14,000 *x g*	**1073.8**
SUBALIQUOT 2	Aliquot extracted from high-speed supernatant after first round of ultracentrifugation at 106,000 *x g* for 12 minutes	**198.0**
SUBALIQUOT 3	Aliquot extracted from high-speed supernatant after second round of ultracentrifugation at 106,000 *x g* for 33 minutes	**5.0**
SUBALIQUOT 4	Aliquot extracted from final input homogenate after addition of Dilution Buffer and RNase inhibitors	**1.0**

Between subaliquot 2 and subaliquot 3, the concentration of RNA dropped nearly 40-fold following the second round of high-speed ultracentrifugation, equating to a loss of 99.5% of RNA compared to the initial reading.

Finally, there was another 5-fold decrease in purified RNA between subaliquot 3 and subaliquot 4, meaning that by the time the final diluted homogenate was fully prepared for bead incubation, there was less than 0.1% total RNA remaining compared to the starting input.

High-speed ultracentrifugation was clearly causing the progressive sedimentation of our endogenous RNAs, and was resulting in the elimination of our entire starting pool of input RNA once the second round of ultracentrifugation had been completed. Ultimately, this data suggests that a large proportion of the RNAs expressed within the *Drosophila* testis are associated with the insoluble and membranous components of the tissue – including those of the developing sperm cells and encapsulating cyst cells. Many of these RNAs are likely bound to insoluble constituents such as membrane proteins, which explains why such a large amount of endogenous RNAs were being sedimented out during the ultracentrifugation steps of high-speed supernatant preparation.

As there was practically no input RNA going into our CI-AP trapping set-up in the first place, this also explains why we were not outputting any Imp-GFP-bound RNAs by the end of the experiment. Considering this, the two-stage ultracentrifugation and generation a high-speed supernatant was subsequently excluded from our modified CI-AP protocol.

4.6.6. DTT-cleavage conditions affect the quality and integrity of purified Imp-GFP-complexed RNAs

The use of thiol-cleavable tags for purification purposes was first developed by Fridy et al. (2015) and has been an invaluable addition to this modified affinity purification set-up. It enables native tagged protein complexes to be purified in non-denaturing elution conditions using a combination of thiol-cleavable linkers and mild reducing agents, with minimal contamination and non-specific binding (Fridy et al. 2015). However, RNA is a very unstable biomolecule outside of its native physiological

environment. The temperature-dependent component of this cleavage step could therefore pose a major risk for degradation and be a contributing factor to the detrimental loss of interacting RNAs.

We know already that ultracentrifugation has been a leading cause of RNA elimination, and so has our use of an old, communal RNAqueous™-Micro Total RNA Isolation Kit (Invitrogen, Cat. No. AM1931). We were therefore keen to avoid any further sources of potential RNA loss in later Cl-AP stages. To counteract this, we wanted to re-test the DTT cleavage conditions more thoroughly, especially since we had excluded some key sources of RNA loss already.

We repeated the full Cl-AP assay again, but without the high-speed ultracentrifugation. To investigate the impact that cleavage duration and temperature has on isolated protein and RNA concentrations, we once again tested the following conditions: 30 minutes at RT, 2 hours at RT, 30 minutes at 4˚C and 2 hours at 4˚C. Western Blotting was performed as before, using 10 µL of input homogenate and unbound extract alongside all four Imp-GFP bound extracts (30 minutes and 2 hours at RT and 4˚C, respectively).

There was efficient trapping and release of the Imp-GFP protein, regardless of the sample type (Fig. 23.). In general, protein signals were better resolved with higher clarity and exhibited greater concentrations of Imp-GFP protein, suggesting an improvement in protein trapping and release when compared to the previous attempt (Fig. 23. vs Fig. 22.). Although, variations in the DTT-cleavage condition did correspond to slight differences in the efficiency of Imp-GFP protein purification.

The levels of purified Imp-GFP protein were most similar when cleaving for 2 hours at RT and 2 hours at 4 ˚C. Incubation with DTT for 30 minutes at RT also yielded an acceptable level of purified Imp-GFP, but this overall concentration of protein was still lower than that released after 2 hours at RT and 2 hours at 4 ˚C, respectively. Incubation with 50 mM DTT for 30 minutes at 4 ˚C remained the least efficient at inducing cleavage and Imp-GFP release (Fig. 23.).

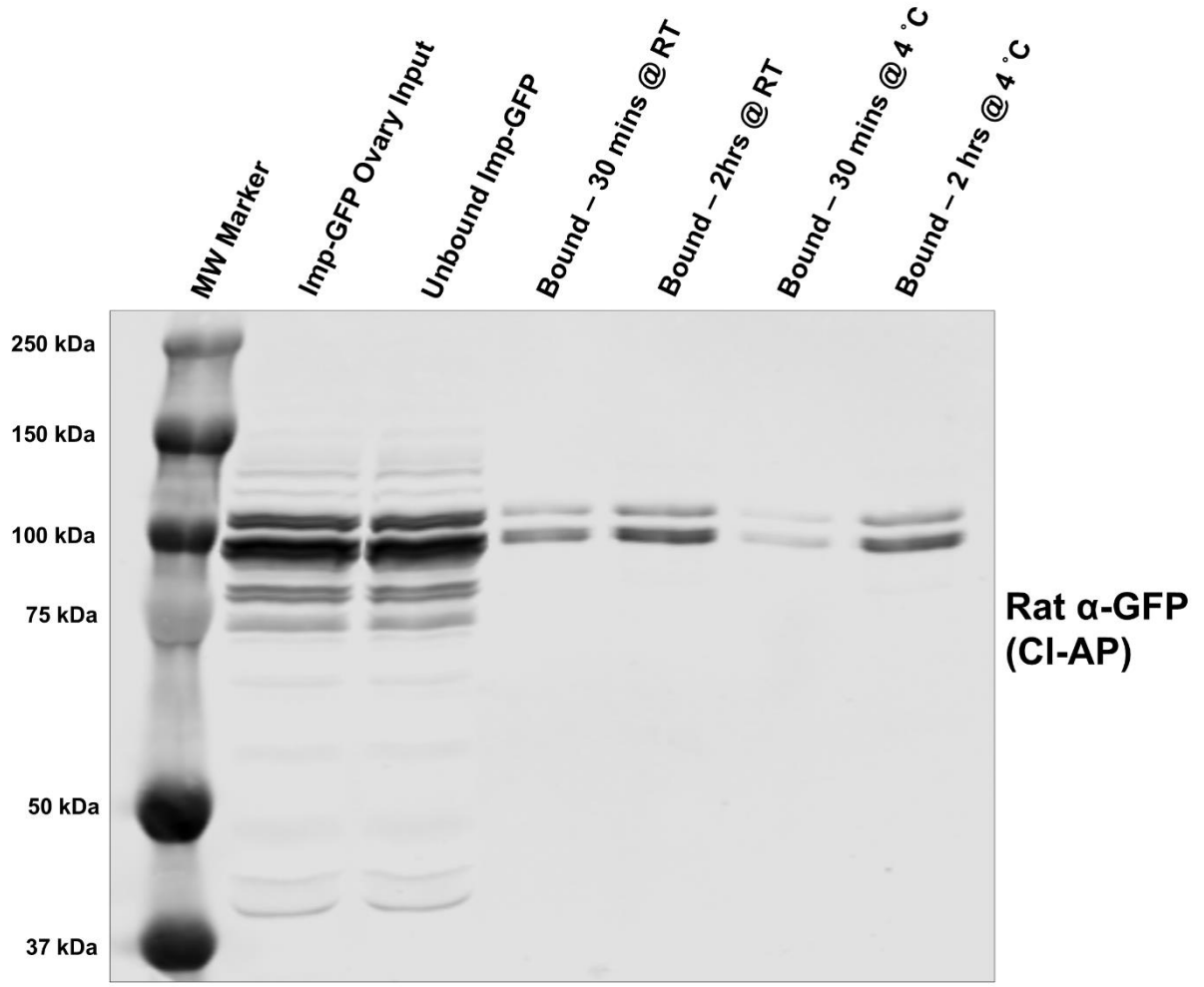

Figure 23. CI-AP-purified Imp-GFP proteins are trapped and released with variable efficiencies depending on the DTT cleavage parameters tested, but no conditions induce degradation or denaturation. Imp-GFP has been trapped and released in all four incubation types tested, but concentrations of release did fluctuate between these conditions (n=1). Once again, incubation with 50 mM of DTT for 2 hours at RT was most sufficient for thiol-linker cleavage, bringing about the highest concentration of purified Imp-GFP protein overall. The input homogenate was an ultracentrifuged high-speed supernatant prepared from the homogenisation of 150 Imp-GFP ovary pairs, dissected and pooled from the G80 protein trap fly line (Quiñones-Coello et al. 2007). The unbound extract represented unbound remnants and non-specific proteins that persisted in the supernatant after incubation of the input homogenate with the GFP-TRAP-Sulfo beads. MW Marker: Precision Plus Protein™ Dual Colour Standard (Bio-Rad Laboratories). Probed with rat anti-GFP monoclonal antibody (1:1000; ChromoTek, Cat. No. 3H9).

Nevertheless, the highest concentration of purified Imp-GFP was isolated after cleavage with 50 mM DTT for 2 hours at RT, in line with what was found previously by us and by Tariq et al. (2020a). Once again, this confirmed that cleavage with 50 mM DTT for 2 hours at RT was the most efficient and effective condition for the trapping and release of purified Imp-GFP protein complexes.

The remaining sample volumes that were not used for immunoblotting were subject to RNA extraction. A more extensive set of RNA checks and quality control measures were taken at this stage to determine whether these mass changes in methodology had indeed been effective. RNA concentrations were measured using high sensitivity Qubit™ 4 fluorometry (ThermoFisher Scientific) and the quality and integrity of RNA was determined using the High Sensitivity RNA ScreenTape System (Agilent).

Aside from the ovarian Imp-GFP input homogenate (~1560 ng/μL) and unbound fraction (~1580 ng/μL), RNA concentrations were all out of the range of our Qubit™ standards. However, investigation of the underlying data, given in raw fluorescence units (RFU), confirmed that the RFU readings for all Imp-GFP bound extracts fell within the RFU range of the Qubit™ standards – hence indicating that RNA was indeed present in all our samples, albeit at very low concentrations.

RNA quality assessments from the Agilent 4200 TapeStation technology reported high quality RNA for both the ovarian Imp-GFP input homogenate and unbound fraction (RIN^e 9.7), whereas degradation was evident in all Imp-GFP bound extracts that had been subject to DTT cleavage (Fig. 24.).

Unsurprisingly, the greatest amount of RNA degradation was evidenced after incubation with 50 mM DTT for 2 hours at RT (RIN^e 3.3), followed by cleavage for 30 minutes at RT (RIN^e 3.4) and for 2 hours at 4˚C (RIN^e 5.0). The least degraded RNA of all Imp-GFP bound samples was from that isolated with DTT after an incubation for 30 minutes at 4˚C, which exhibited an average level of RNA integrity (RIN^e 7.0).

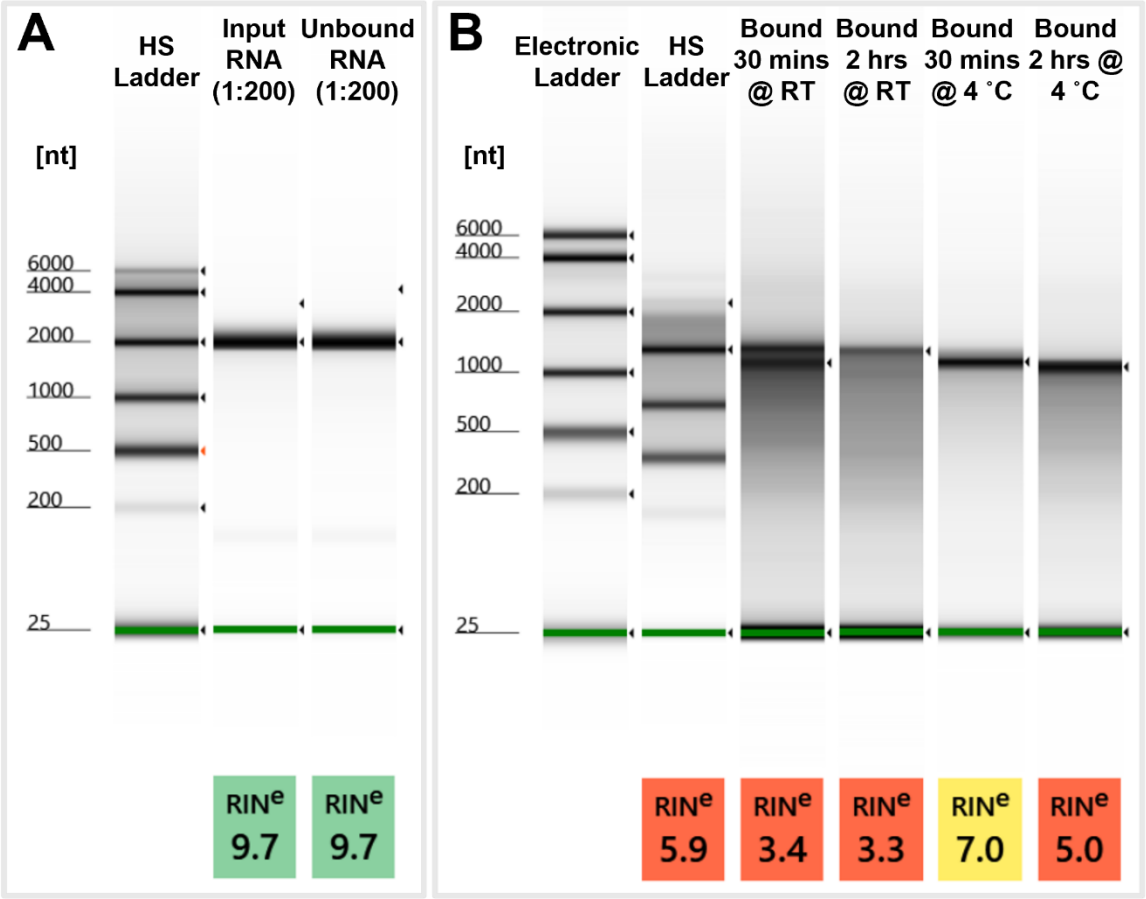

Figure 24. Modification of DTT-cleavage conditions affects the overall quality and integrity of purified Imp-GFP-interacting RNAs isolated via CI-AP. (A) Gel image presenting the electrophoretic separation profiles of purified RNA from a 1:200 dilution of the ovarian Imp-GFP input homogenate from the start of the CI-AP experiment and a 1:200 dilution of the ovarian Imp-GFP unbound fraction extracted at the end of the experiment. (B) Gel image displaying the electrophoretic separation profiles of purified RNA from the ovarian Imp-GFP bound extracts isolated after incubations with 50 mM DTT for 30 minutes at RT, 2 hours at RT, 30 minutes at 4˚C and 2 hours at 4˚C. Analysis was performed using the High Sensitivity RNA ScreenTape® and 4200 TapeStation System (Agilent) (n=1). Objective evaluation of RNA degradation was delivered with an RNA Integrity Number Equivalent (RIN^e). RIN^e calculates at a scale from 1 to 10, where 10 was the highest quality RNA and 1 was completely degraded RNA. A high RIN^e in green therefore indicated highly intact RNA, a mid-range RIN^e in yellow indicated an average level of RNA integrity, and a low RIN^e in orange indicated a degraded RNA sample. HS: high sensitivity. RT: room temperature. nt: nucleotides.

While the Aligent ScreenTape® technology was a useful addition to our analyses, it must be noted that this system had been developed and optimised for the analysis of total Eukaryotic RNA samples that include ribosomal RNAs (rRNAs). Such RNA quality assessments were therefore based on electrophoretic separation in accordance with peaks for the 28S and 18S rRNAs. Our bound samples were not total RNAs, they were precipitates containing a specific subset of mRNAs with little to no rRNA. Moreover, *Drosophila* rRNA sizes differ somewhat because their 28S rRNA is processed into two fragments that migrate in a similar manner to the 18S rRNA. Therefore, these factors may have in turn affected the integrity scores reported for our bound extracts.

Nevertheless, the pattern of increasing RNA degradation which correlated with increasing DTT incubation time and temperature must not be overlooked. After ensuring that the GFP-TRAP-Sulfo beads did not obstruct the RNA extraction columns or perturb the kit-based extraction process in any way, we therefore decided that all aliquots designated for RNA-Seq would be taken and stored separately, prior to the DTT cleavage step. By doing so, this would avoid the potential impact of temperature-driven RNA degradation and denaturation but would still allow us to conduct DTT-induced cleavage – via a 2-hour incubation at RT – on our remaining sample volume for the purification and identification of all protein interactors in this CI-AP fraction.

4.7. The final, optimised CI-AP assay yielded a small but clean amount of Imp-GFP and Sqd-YFP interacting RNAs

By this point of finalised optimisation, we had accounted for several factors that were thwarting our ability to trap, isolate and purify multi-protein RNA-associated Imp and Sqd RNP complexes with high efficiency and effectiveness.

To summarise, our changes to the original CI-AP protocol were four-fold:

1. Buffer compositions were modified in accordance with in-house protocols;
2. A new, unused RNAqueous™-Micro kit was implemented for extraction of purified RNAs;

3. High-speed ultracentrifugation was removed from the assay in its entirety;
4. DTT-mediated cleavage was only performed on samples destined for proteomics analysis.

After conducting our newly modified Cl-AP assay in full, with a minimum of two thousand testes worth of native RNA and protein from the Imp-GFP G80 protein trap (G00080 exon-trap line; Quiñones-Coello et al. 2007) and Sqd-YFP CPTI 239 fly lines (Lowe et al. 2014), respectively, we were finally able to yield a valuable output.

Prior to the generation of RNA libraries, RNA checks and QC assessments were performed to ensure that these four key changes in methodology had indeed been effective in maintaining the pool of endogenous RNA throughout the Cl-AP procedure. The concentration, quality and integrity of RNA were analysed using the RNA ScreenTape® System (Agilent). The presence of a low concentration of RNA was detected in all Cl-AP samples. Approximate RNA concentrations of 91.1 ng/μL, 112.0 ng/μL and 0.628 ng/μL were measured in the Imp-GFP input, Imp-GFP unbound fraction and Imp-GFP bound eluate, respectively. For the Sqd-YFP input, Sqd-YFP unbound fraction and Sqd-YFP bound eluate, RNA concentrations of 139.0 ng/μL, 147.0 ng/μL and 0.576 ng/μL were quantified, respectively.

RNA quality assessments from the Agilent 4200 TapeStation technology were very reassuring (Fig. 25.). High quality RNA was reported for the Imp-GFP input (RIN^e 9.4) and Imp-GFP unbound fraction (RIN^e 8.7), while Imp-GFP-bound RNA was evaluated as being of average integrity (RIN^e 6.6). For the Sqd-YFP control, high quality RNA was only detected in the input homogenate (RIN^e 8.2). Average RNA integrity was reported in the Sqd-YFP unbound fraction (RIN^e 7.1), and some RNA degradation was detected in the Sqd-YFP bound control (RIN^e 6.5).

As mentioned in Section 4.6.6., inherent optimisation of the Aligent ScreenTape® technology may in turn lead to variations in integrity scores and, as such, should always be considered when analysing nucleic acid samples derived from *Drosophila* species. An RNA Integrity Number Equivalent (RIN^e) value greater than 6 was therefore deemed to be acceptable for our downstream library preparations and RNA-Seq requirements.

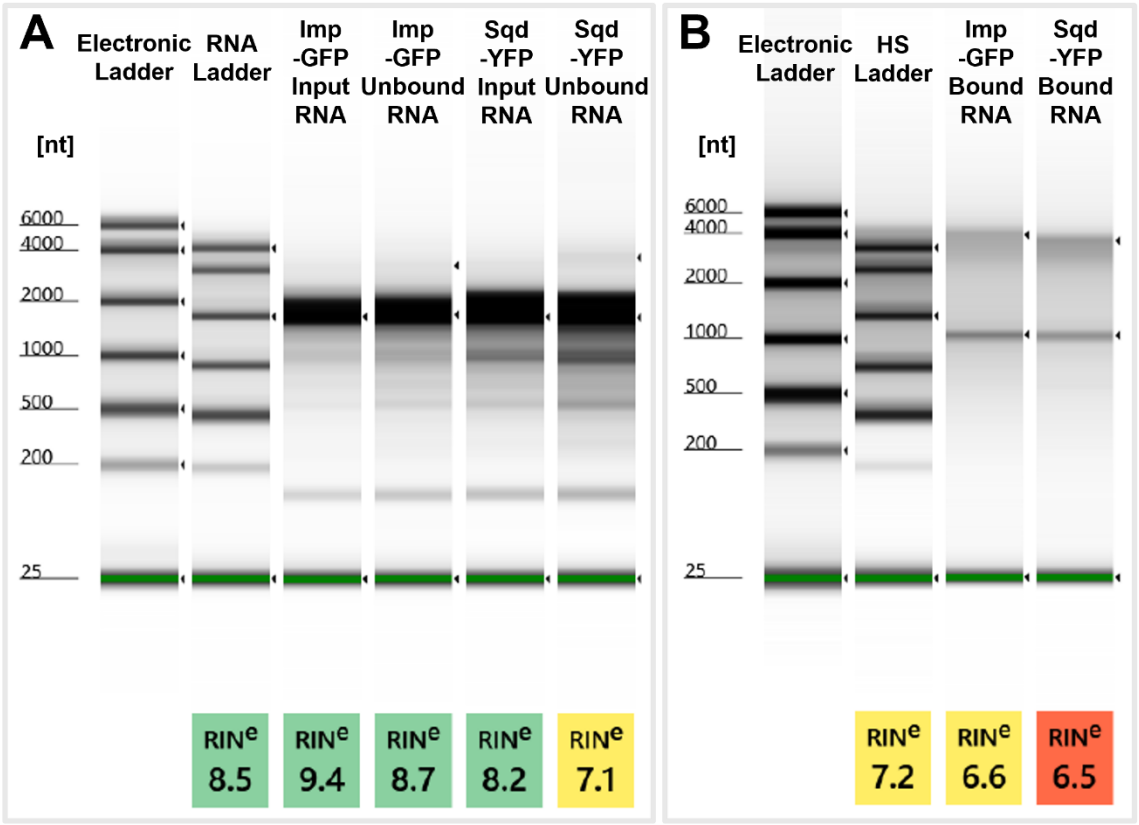

Figure 25. Good quality RNAs have been successfully purified via CI-AP, including those associated with Imp-GFP and Sqd-YFP. (A) Gel image presenting the electrophoretic separation profiles of purified RNAs extracted from the ovarian Imp-GFP and Sqd-YFP input homogenates at the start of the CI-AP assay and from the ovarian Imp-GFP and Sqd-YFP unbound fractions at the end of the assay. (B) Gel image displaying the electrophoretic separation profiles of purified RNAs isolated from the ovarian Imp-GFP bound and Sqd-YFP bound eluates, without any prior DTT-induced cleavage. Analysis was performed via the Agilent 4200 TapeStation System using the standard RNA ScreenTape® for the input and unbound samples and High Sensitivity RNA ScreenTape® for the bound CI-AP extracts (n=1). Objective evaluation of RNA degradation was delivered with an RNA Integrity Number Equivalent (RIN^e). RIN^e calculates at a scale from 1 to 10, where 10 was the highest quality RNA and 1 was completely degraded RNA. A high RIN^e in green therefore indicated highly intact RNA, a mid-range RIN^e in yellow indicated an average level of RNA integrity, and a low RIN^e in orange indicated a degraded RNA sample. HS: high sensitivity. nt: nucleotides.

In line with this, the RNA content of all CI-AP samples was judged to be of sufficient quality and integrity. Purified input and bound RNA samples for both Imp-GFP and Sqd-YFP were taken forward for our RNA-Seq analyses. RNA-Seq results will be described later in Section 4.9., after the description of our comparative proteomics findings.

4.8. Comparative proteomics suggests the presence of hundreds of purified protein interactors

Having successfully conducted the testis-specific purification of two spatiotemporally distinct RBPs, Imp and Sqd, along their respective multi-protein mRNA:RNP complexes, the CI-AP-purified samples were sent off for comparative proteomics analysis at the University of Bristol Proteomics Facility. Off-line High pH RP Chromatography Fractionation allowed us to detect more proteins in total and match more spectra to each protein. In doing so, this improved our overall accuracy of quantitation. The off-line fractionation also acted as a very effective clean-up step. We could therefore have more confidence that many contaminants, which would otherwise affect how the TMT pool runs on the Nano-LC Mass Spectrometry system (Thermo Scientific), were effectively withdrawn early on from our analyses.

As the samples for both RBPs had the same cell type complexity, we hypothesised that all non-specific interactors would be present in both samples in equal abundance. Under this assumption, any non-specific interactions at an equal level in both the Imp-GFP and Sqd-YFP samples would effectively become controls for one another – allowing us to discount them from further investigation. Under this premise, any notable protein interactors would effectively “stand out” in their prevalence by being highly enriched in one purification output compared to the other. These binding partners would hence be considered specific interactors of one bait protein but not the other.

Ultimately, we wanted to focus first on any substantial differences in the two protein lists and use literature searches to support the functions of these putative interactors in the context of the wider multi-protein RNP complex. Differences between the main experimental Imp-GFP sample and Sqd-YFP control allowed us to work out which

proteins were being purified out with Imp-GFP, but not with Sqd-YFP, in the testis. Any similarities were considered spurious overlapping protein interactors, artefacts and/or contaminants.

We started with the identification of 427 proteins in total, which was then filtered down to 400 proteins (or 403 when protein entries for GFP, Sqd and Imp isoforms D and K were included) by removal of any common and non-*Drosophila* contaminants. Any protein entries with missing quantitation values, including abundance values and counts for example, were also excluded – yielding 131 proteins at this stage.

The GFP entry was set as the threshold to define Imp-enriched protein interactors vs. Sqd-enriched protein interactors. GFP was used as the cut-off because it should, theoretically, be similar in abundance levels between the samples. This includes YFP because it is a genetic derivative of GFP. Both GFP and YFP are very similar in sequence and only differ by a small number of amino acids, so have been detected in bulk as GFP only.

The abundance ratio (Sqd-YFP / Imp-GFP) of GFP was 1.245. This threshold offered a good cut-off value because it was fairly close to 1, with 1 theoretically being equal abundances in the Sqd-YFP control vs. the Imp-GFP sample. However, this would only be the case if we were to assume a degree of normalisation, e.g. that both samples started with relatively the same amount of protein in each – although we have no evidence to make this assumption so did not normalise according to this.

Therefore, once the abundance ratios were arranged from low to high, with GFP being the cut off, all proteins with abundance ratios below 1.245 were expected to be candidates enriched in the Imp-GFP sample. Alternatively, any abundance ratios above 1.245 were assumed to be enriched in the Sqd-YFP controls.

Overall, this gave a final output of 29 protein interactors in the Imp-GFP sample, once Imp-GFP itself had been accounted for. A total of 102 enriched proteins/genes were detected in the Sqd-YFP control, after Sqd-YFP had been discounted. The full filtered list of these protein interactors is available in Appendix A, Supplementary Data File 1.

4.8.1. All 29 Imp-specific protein interactors are associated with RNA processing and gametogenesis-related GO terms

Comparative proteomics identified 29 putative protein binding partners enriched in the purified Imp-GFP CI-AP sample. A simple functional enrichment analysis of this group of 29 Imp-enriched proteins was performed using the web-based G:Profiler tool (Kolberg et al. 2023). This searches for over-represented GO terms, biological pathways, regulatory elements, disease annotations and protein:protein interaction networks using a combination of data types that are available from several different databases. Outputs are based on statistical enrichment analysis using Fisher's one-tailed test (cumulative hypergeometric probability) (Kolberg et al. 2023). The GO analysis revealed a small range of overlapping molecular functions, biological processes and cellular component categories overall. This suggested that protein interactors of Imp are predominantly involved in RNA binding, actin and cytoskeletal interactions, splicing, ribosomal functioning, and translation, among other roles (Fig. 26.).

A more in-depth analysis of these proteins was in turn pursued to gain an understanding of how they may interact with Imp to regulate testis-specific activities and contribute to Imp RNP complexes in *Drosophila* sperm development (Table 9.).

4.8.2. Several protein components linked to translation initiation and ribosome synthesis have been purified

At least 11 of the 29 Imp-associated protein binding partners were strongly implicated in translational regulation and ribosome biogenesis (Table 9.). These protein interactors may therefore represent a specific subset of multi-protein Imp:mRNA RNP complexes that have been captured by CI-AP as they undergo translational activation – following localisation of their protected, bound mRNAs to target sites at the extreme tail-ends of spermatid cyst bundles.

It is interesting that Clouse et al. (2008) has previously identified Polyadenylate-binding protein (PABP) as a component of Sqd-associated RNP complexes in

Drosophila oogenesis, yet here we shown that there is a greater enrichment of PABP in the Imp-GFP-bound Cl-AP sample compared to the Sqd-YFP-bound Cl-AP sample. The Sqd-YFP/Imp-GFP abundance ratio for PABP was, however, 0.726 – which may be interpreted as being very similar in abundances between the two samples since this value was relatively close to 1.245, the pre-defined threshold of equal abundance ratio of for GFP/YFP (Table 9.). The raw abundance counts for PABP in the Imp-GFP and Sqd-YFP samples were 1623.2 and 1179.1, respectively (Appendix A, Supplementary Data File 1.). Nevertheless, while the abundance of PABP was not substantially different between the Imp-GFP sample and Sqd-YFP control, PABP was indeed more abundant in the Imp-GFP condition overall.

Moreover, Clouse et al. (2008) not only detected direct interactions between Sqd and PABP in the immunoprecipitated Sqd protein complexes, but also positively identified Imp by mass spectrometry in these same samples obtained from ovarian lysates. This validates what we have found here and confirms that PABP is a key member of the Imp interactome.

It is known already that the eukaryotic cap-dependent translation of target mRNAs requires input from multiple protein components, some of which have been found here in Imp-GFP-enriched precipitates. Cap-dependent translation involves the association of PABP to their 3' polyA tails, which controls cytoplasmic polyadenylation and triggers recruitment of translation initiation machinery components (Benoit et al. 2005). This includes the molecular scaffolding protein, eIF4G, which is the backbone of the eIF4F translation initiation complex and is a docking site for initiation factors such as eIF4E and eIF4A (Hernández et al. 1998; Prévôt et al. 2003; Richter and Sonenberg 2005). Interestingly, one *Drosophila* homologue of eIF4G, an isoform termed eIF4G2, has been identified here as a direct protein interactor of Imp.

The PAPB-eIF4G interaction is said to enhance the overall binding affinity for eIF4E, which is bound to the 5' 7-methyl guanosine cap of target mRNAs, to effectively and successfully outcompete other interfering, repressive proteins such as Cup (Nelson et al. 2004; Zappavigna et al. 2004). eIF4G is also associated with specific ribosomal subunits, including the 40S ribosomal subunit (Richter and Sonenberg 2005). Interestingly, we also isolated a key 40S-associated subunit, RpS15, in our Imp-bound precipitates.

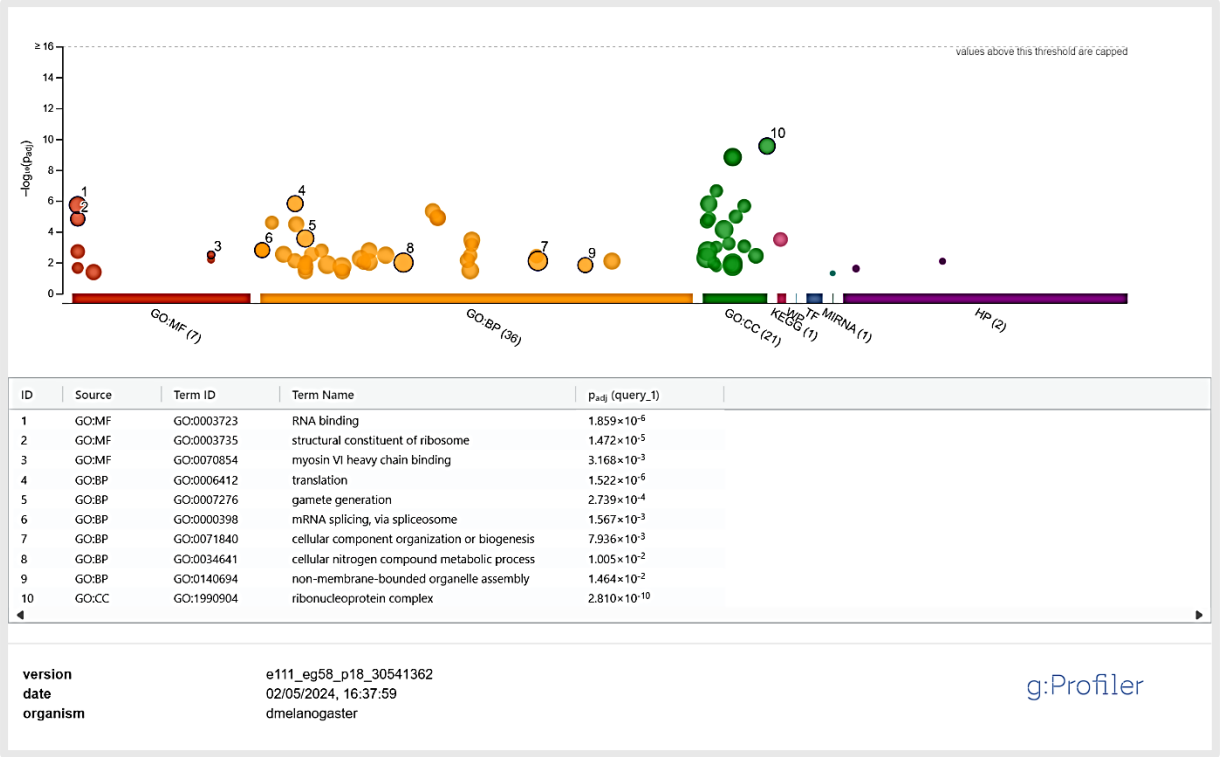

ID	Source	Term ID	Term Name	p_{adj} (query_1)
1	GO:MF	GO:0003723	RNA binding	1.859×10^{-6}
2	GO:MF	GO:0003735	structural constituent of ribosome	1.472×10^{-5}
3	GO:MF	GO:0070854	myosin VI heavy chain binding	3.168×10^{-3}
4	GO:BP	GO:0006412	translation	1.522×10^{-6}
5	GO:BP	GO:0007276	gamete generation	2.739×10^{-4}
6	GO:BP	GO:0000398	mRNA splicing, via spliceosome	1.567×10^{-3}
7	GO:BP	GO:0071840	cellular component organization or biogenesis	7.936×10^{-3}
8	GO:BP	GO:0034641	cellular nitrogen compound metabolic process	1.005×10^{-2}
9	GO:BP	GO:0140694	non-membrane-bounded organelle assembly	1.464×10^{-2}
10	GO:CC	GO:1990904	ribonucleoprotein complex	2.810×10^{-10}

Figure 26. Capped Manhattan-like-plot generated by G:Profiler after direct functional profiling analysis of the 29 Imp-enriched proteins interactors. Circle sizes relate to the corresponding term size, with larger terms exhibiting larger circles. Circle numbers correspond to the top 10 enriched term IDs. The x-axis represents functional terms that are grouped and colour-coded by data sources, and the value in brackets alongside the x-axis labels relates to the total number of significantly enriched terms from this source. The y-axis represents the adjusted enrichment p-values in negative $\log_{10}$ scale. Term circles with p-values less than 10^{-16} were grouped due to capping, as this fixed the y-axis scale to maintain comparability between different queries. P-values smaller than 10^{-16} could all be summarised as highly statistically significant (Kolberg et al. 2023). Red: Molecular Function (MF). Orange: Biological Process (BP). Green: Cell Component (CC). Pink: KEGG Pathways. Blue: microRNA targets from miRTarBase (MIRNA). Purple: Human Phenotype Ontology (HP). Other sources not included: WikiPathways (WP) and TRANSFAC (TF). **Generated and taken from G:Profiler (https://biit.cs.ut.ee/gprofiler/gost).**

Table 9. Summary of twenty-nine testis-specific Imp-enriched protein interactors that were isolated from *Drosophila melanogaster* testes using multi-step CI-AP experimentation. Bracketed gene/protein names correspond to the abbreviations, symbols and/or synonyms commonly used as alternatives to the full given names. Abundance ratios correspond to a single, comparative value that represents the abundance of a protein of interest in the Sqd-YFP-bound control sample vs. its protein abundance in the Imp-GFP-bound experimental sample[a,b]. Key functions and associated reference citations are provided for each gene/protein entry, based on manual literature searches performed via FlyBase (release versions: FB2024_03 and FB2024_04). All filtered comparative proteomics data can be found in Appendix A, Supplementary Data File 1. MT: microtubule. TF: Transcription Factor.

GENE / PROTEIN	ABUNDANCE RATIO[a,b]: (SQD-YFP) / (IMP-GFP)	SUMMARY OF KNOWN FUNCTIONS	KEY REFERENCES
Coronin (Coro)	0.306	F-actin binding; Actin cap formation; Membrane trafficking; Anti-fungal immune defence response; Directed cell movement; Adult somatic muscle development; Interacts with Histone 1; Expressed in peripodial membrane of wing disc	Pallavi and Shashidhara (2003), Bharathi et al. (2004), Rybakin and Clemen (2005) (Review), Jin et al. (2008), Schnorrer et al. (2010), Kavi et al. (2015), Xie et al. (2021), Ikawa et al. (2023)
Dihydrolipoyllysine-residue succinyltransferase component (CG5214, alpha-KGDHC, Dlst)	0.570	Mitochondrial enzyme in cellular respiration; Structural subunit of 2-oxoglutarate dehydrogenase enzyme	González Morales et al. (2023), François et al. (2023)

		complex (tricarboxylic acid cycle, TCA cycle); Muscle organisation; Core component of myofibrils; Localises to Z-disc; Non-essential metabolic enzyme in sperm production	
Meiotic P26, isoform F (Mei-P26)	0.582	RING-containing ubiquitin-ligase; Tumour suppressor homologue; Germline differentiation, Meiotic entry and gametogenesis in both sexes; Regulation of proliferation and miRNA activity in female germline; Regulated by Tut, Bam and Bgcn	Page et al. (2000), Neumüller et al. (2008), Ying et al. (2011), Insco et al. (2012), Chen et al. (2014c), Wu et al. (2016)
Actin-57B (Act57B)	0.638	Major embryonic and larval gene; Encodes myofibrillar actin; Transcriptional target of Mef2 and Cf2; Synapse organisation; Cytokinesis	Kelly et al. (2002), Eggert et al. (2004), Elgar et al. (2008), Shah et al. (2011), Blunk et al. (2014)
Tropomyosin 2, isoform E (Tm2)	0.665	Myogenesis; Component of contractile apparatus in muscle; Translationally regulated by Hoip in developing myotubules; Flight muscle protein; Cardiac development;	Tansey et al. (1991), Lin et al. (1996), Wolf et al. (2006), Texada et al. (2011), Williams et al. (2015)

		Ensures physical integrity and performance of heart; Regulates Actin-57B expression; Transcriptional target of Mef2; Minor component of Yuri-65 protein complex	
Tropomyosin-1, isoforms 9A/A/B (Tm1)	0.689	F-actin stabilisation; Spermatid individualisation; Cell migration; MT-dependent transport; RNA localisation; Major component of Yuri-65 protein complex	Zimyanin et al. (2008), Texada et al. (2011), Cho et al. (2016), Veeranan-Karmegam et al. (2016), Gáspár et al. (2017), Dimitrova-Paternoga et al. (2021)
Polyadenylate-binding protein (PABP)	0.726	PolyA tail binding; Recruitment of translation initiation machinery; Circadian rhythm involvement; RNA synthesis and metabolism; Regulates maternal mRNA expression	Lefrère et al. (1990), Benoit et al. (2005), Sonenberg and Hinnebusch (2009), Satterfield and Pallanck (2006), Lee et al. (2017), Wang et al. (2017)

Cytoplasmic linker protein 190, isoform M (CLIP-190)	0.744	Actin binding; Regulation of MT dynamics; Kinetochore binding; Linking of the Golgi and endocytic vesicles to MTs; Endocytosis	Lantz and Miller (1998), Sisson et al. (2000), Dzhindzhev et al. (2005), Sanghavi et al. (2012), Beaven et al. (2015)
Combover, isoform A (Cmb)	0.801	Rho kinase substrate; Spermatid individualisation; Binds axonemal component Rsp3; Actin wing hair formation; Component of Planar Cell Polarity pathway; Interacts with Idgf3; Dorsal appendage tube formation	Fagan et al. (2014), Steinhauer et al. (2019), Espinoza and Berg (2020)
Wurstfest (Fest, CG9975)	0.836	Translational repression; Regulates Cyclin B1 activity in spermatocytes; Male meiosis; Interacts with Rbp4, Lut and Syp in male germline	Baker et al. (2015), Baker et al. (2023)
Syncrip, isoform D (Syp)	0.874	Interacts with Imp; Cell fate specification; Male meiosis; Regulates Cyclin B1 expression in spermatocytes; Interacts with Fest, Lut and Rbp4 in male germline; RNA localisation and translation; Synapse formation and	McDermott et al. (2012), McDermott et al. (2014), Liu et al. (2015), Ren et al. (2017), Yang et al. (2017), Titlow et al. (2020), Baker et al. (2023)

		plasticity; Neuroblast decommissioning	
Zinc finger protein on ecdysone puffs (Pep)	0.930	DNA and RNA binding; Interacts with hnRNP complexes; Associates with active ecdysone-inducible puff loci on polytene chromosomes; Involved in transcription and processing of RNAs from ecdysone-regulated genes	Amero et al. (1991), Amero et al. (1993), Hamann and Strätling (1998)
CG8136	0.940	Uncharacterised gene with limited published evidence, although expression is highly testis-enriched – may be implicated in intestinal stem maintenance and Notch signalling	Mummery-Widmer et al. (2009), Zeng et al. (2015)
Maternal protein exuperantia (Exu)	0.972	Protein binding and homodimerisation; Maternal RNA localisation; Establishment of cell polarity; Determination of body axis patterning; Associates with large cytoplasmic RNP complexes and sponge bodies; Male fertility	Schupbach and Wieschaus (1986), Hazelrigg et al. (1990), Macdonald et al. (1991), Wilsch-Bräuninger et al. (1997), Wilhelm et al. (2000), Nakamura et al. (2001), Lazzaretti et al. (2016)

Ypsilon schachtel (Yps)	1.025	Dendrite morphogenesis; RNA localisation and translation; Binds and co-localises with Exu and Orb; Regulates maternal RNA expression; Promotes female GSC maintenance, proliferation and differentiation; Post-meiotically expressed in the testis	Wilhelm et al. (2000), Mansfield et al. (2002), Martin et al. (2003), Wilhelm et al. (2005), Olesnicky et al. (2018), Zou et al. (2020)
CG10317	1.030	Uncharacterised gene with limited published evidence, although expression is highly testis-enriched	– N/A –
Small ribosomal subunit protein eS6 (Rps6)	1.076	Major phosphoprotein component of 40S ribosomal subunit; Tumour suppressor protein; Ribosome biogenesis and translation; Linked to proliferation of haemopoietic cell and tissue types; Regulates efferocytosis; Modulates F-actin remodelling; Male fertility	Watson et al. (1992), Stewart and Denell (1993), Marygold et al. (2007), Lin et al. (2011), Xiao et al. (2015), Fasulo et al. (2020)

Large ribosomal subunit protein eL24 (RpL24)	1.094	Cytoplasmic translation; Ribosome biogenesis; Structural component of ribosomes; Associates with the whole 80S ribosome, particularly in the ovary	Marygold et al. (2007), Hopes et al. (2022)
Lost (Lost Boys, CG14648, Growl, Neverland)	1.103	RNA localisation and metabolism; Germ pole plasm formation; Determination of body axis patterning; Interacts and functions with Rump; Regulates maternal RNA expression; Associates with large cytoplasmic RNP complexes and sponge bodies; Ecdysteroid biosynthesis; Female GSC proliferation and maintenance; Female fecundity	Yoshiyama et al. (2006), Snee and Macdonald (2009), Sinsimer et al. (2011), Yoshiyama-Yanagawa et al. (2011), Schoborg et al. (2015), Ameku and Niwa (2016), Ameku et al. (2017)
Calmodulin, isoform C (Cam)	1.144	Calcium binding; Calcium signalling; Myogenesis; Muscle organisation and maintenance; Regulation of actin dynamics; Growth cone motility and axon guidance; MT spindle and centrosome assembly; Phototransduction and	VanBerkum and Goodman (1995), Scott et al. (1997), Xu et al. (1998), Wang et al. (2003a), Marrone et al. (2011), Galletta et al. (2014), Nelson et al. (2014)

		photoreception; Synaptic transmission; Autophagy	
Short spindle 3, isoform B (CG18397, Ssp3)	1.166	SCAPER orthologue; Regulates MT dynamics and spindle assembly; Chromosome segregation and cytokinesis; Male meiosis; Male fertility	Goshima et al. (2007), Wormser et al. (2021)
Eukaryotic translation initiation factor 4G2, isoform A (eIF4G2)	1.174	RNA binding and processing; Translation initiation machinery; eIF4G homologue; Interacts with eIF4E-1/3 in testis-specific eIF4F complexes; Testis-specific translation; Male meiosis; Spermatid differentiation and elongation	Baker and Fuller (2007), Franklin-Dumont et al. (2007), Hernández et al. (2012), Ghosh and Lasko (2015)
Large ribosomal subunit protein L23A (RpL23A)	1.189	Cytoplasmic translation; Ribosome biogenesis; Structural component of ribosomes; Interacts with PARP1; Histone and DNA binding	Koyama et al. (1999), Marygold et al. (2007), Pinnola et al. (2007), Ross et al. (2007)

Large ribosomal subunit protein eL6 (RpL6)	1.189	Cytoplasmic translation; Ribosome biogenesis; Structural component of ribosomes; Interacts with Srlp; Regulates spliceosome and ribosome function in testes; Regulates differentiation and self-renewal properties of male GSCs	Marygold et al. (2007), Yu et al. (2019b)
CG5787	1.196	Uncharacterised gene with limited published evidence	– N/A –
Small ribosomal subunit protein uS12 (RpS23)	1.206	Cytoplasmic translation; Ribosome biogenesis; Structural component of ribosomes; Constituent of 40S ribosomal subunit; Interacts with Gustatory Receptors 64 (Gr64)	Marygold et al. (2007), Recasens-Alvarez et al. (2021), Baumgartner et al. (2022)

Large ribosomal subunit protein eL22 (RpL22)	1.207	Cytoplasmic translation; Ribosome biogenesis; Structural component of ribosomes; Associates with whole 80S ribosome; Embryonic development; Interacts with PARP1; Histone and DNA binding; Regulates male germline development and differentiation; Autoregulates self-repression via own *circular RpL22* RNAs; Mediates genetic compensation with *RpL22-like* paralogue	Koyama et al. (1999), Marygold et al. (2007), Kearse et al. (2011), Mageeney et al. (2018), Mageeney and Ware (2019), Gershman et al. (2020), Minervini et al. (2022), Ng et al. (2024)
14-3-3 protein epsilon (14-3-3ε)	1.212	Component of Hippo and Ras/MAPK signalling pathways; Regulates Yorkie activity and localisation; Modulates histone phosphorylation and acetylation for transcription elongation; Promotes spindle assembly and organisation; Regulates TF, Zfh-1; Germ cell migration; Axon guidance; Cell growth; Eye development;	Chang and Rubin (1997), Acevedo et al. (2007), Karam et al. (2010), Ren et al. (2010), Tsigkari et al. (2012), Yang and Terman (2012), Beaven et al. (2017), Nam et al. (2022)

		Embryonic hatching; Female fecundity	
40S ribosomal protein S15 (Small ribosomal subunit protein uS19, RpS15)	1.213	Ribosome biogenesis and translation; Structural component of ribosomes; Localises to sites of active transcription in nucleus and to the nucleolus; Substrate of LRRK2 kinase activity; Associates with embryonic lipid droplets	Brogna et al. (2002), Cermelli et al. (2006), Marygold et al. (2007), Rugjee et al. (2013), Martin et al. (2014)

Footnotes: *[a]An abundance ratio of 1.245 has been set as a defined threshold to distinguish between Imp-enriched and Sqd-enriched protein interactors because this corresponds to the amount of GFP/YFP, which should be equal in both sample types; [b]An abundance ratio of <1.245 therefore indicates high level protein enrichment in the Imp-GFP sample, with the highest enrichment scores corresponding to the lowest abundance ratios.*

eIF4G bridges eIF4E, and other protein factors located at the 5' end, with the 40S ribosomal subunit – thereby circularising the mRNA (Mendez and Richter 2001; Sonenberg and Hinnebusch 2009). This drives the recruitment of a whole host of ribosomal-associated subunits and related co-factors to the mRNA, some of which have been purified here, in association with Imp. Together, this promotes assembly of the ribosome and initiates translational activities. As multiple translation-related proteins had been identified in this proteomics dataset after purification with CI-AP, this appeared to be a genuine subset of interactions established by Imp-GFP in the testis and likely corresponded to a post-localised version of the dynamic Imp RNP complex.

4.8.3. A selection of muscle and non-muscle actin types and actin binding proteins are highly enriched

At least 10 out of the 29 Imp-enriched protein binding partners are associated with actin binding and the regulation of cytoskeletal components (Table 9.).

There are four major structures that extend throughout the longitudinal axis of elongating spermatids: the axoneme, cytoplasmic MTs, mitochondria and F-actin cables (Noguchi et al. 2011). It is therefore logical that many of Imp's protein binding partners would regulate or be association with at least some of these, whether this be directly as part of the Imp RNP complex or indirectly via other supporting scaffolding and adaptor *trans*-acting factors.

Interestingly, the two *Drosophila* Tropomyosin proteins, Tm1 and Tm2, were detected with near-identical protein abundance ratios of 0.689 and 0.665, respectively, suggesting an equal degree of enrichment for both proteins in the Imp-GFP experimental sample vs. the Sqd-YFP control (Table 9.). However, Tm2 was present at a higher abundance, with a raw abundance value of 307.5 in the Imp-GFP sample and 204.4 in the Sqd-YFP control, whereas Tm1 had a raw abundance of 87.2 in the Imp-GFP sample vs. 60.1 in the Sqd-YFP control (Appendix A, Supplementary Data File 1.).

4.8.4. Detection of other known testis-involved RBPs validates the RNA binding and processing activity of Imp and its wider interacting RNP complex

Of the 29 putative protein binding interactors of Imp purified and isolated here, at least four of them were already protein candidates of interest with evident RNA binding and regulatory activities in the testis (Table 9.).

Screening of YFP exon-trapped lines previously revealed that the RBP termed Lost (otherwise known as Growl) is one of a very small number of proteins that localise subcellularly to the extreme tail-ends of elongating spermatid cyst bundles – accumulating at sites which may overlap with localised comet and cup mRNAs (H. White-Cooper, Personal Communication; Lowe et al. 2014). Interestingly, Lost has been detected here as enriched within the Imp-GFP precipitate, with an abundance ratio (Sqd-YFP/Imp-GFP) of 1.103 (Table 9.). Overall, Lost was detected at quite high protein abundance levels within both the Imp-GFP CI-AP sample and Sqd-YFP CI-AP control (Appendix A, Supplementary Data File 1.). However, our reviews of the current literature have shown that the role of Lost in late sperm development has yet to be explored.

4.8.5. All 102 Sqd-specific protein interactors are associated with a diverse array of molecular functions, biological processes and cellular components

Comparative proteomics revealed that 102 putative protein interactors were enriched in the purified Sqd-YFP CI-AP control sample. A simple functional enrichment analysis of this list of 102 Sqd-enriched proteins was performed using the G:Profiler online tool (Kolberg et al. 2023). The GO analysis returned a series of varied GO terms that were associated with such processes as molecular chaperoning, RNA binding, gametogenesis, metabolism, chemosensory perception and an assortment of enzymatic activities, among others (Fig. 27.).

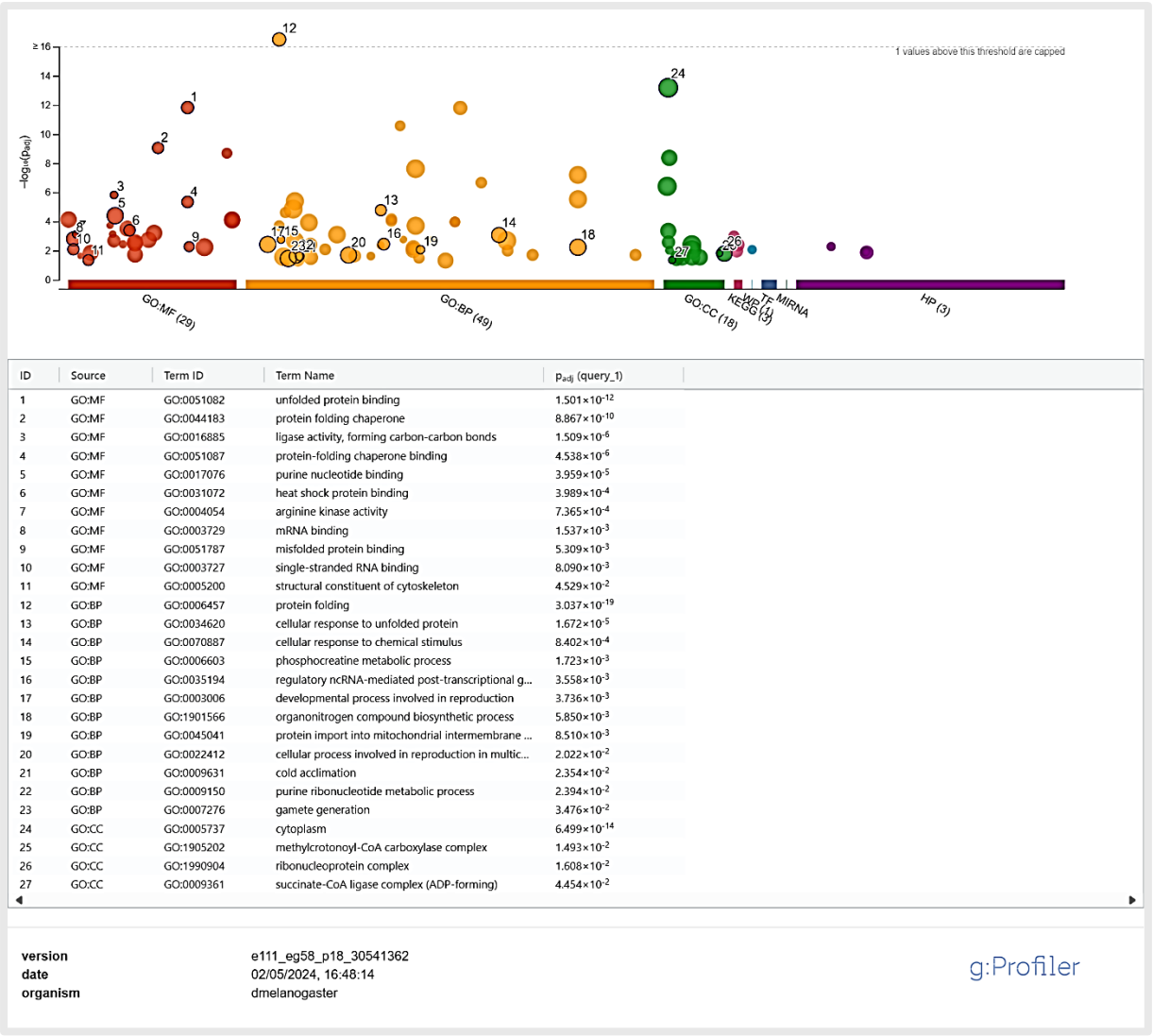

ID	Source	Term ID	Term Name	p_{adj} (query_1)
1	GO:MF	GO:0051082	unfolded protein binding	1.501×10^{-12}
2	GO:MF	GO:0044183	protein folding chaperone	8.867×10^{-10}
3	GO:MF	GO:0016885	ligase activity, forming carbon-carbon bonds	1.509×10^{-6}
4	GO:MF	GO:0051087	protein-folding chaperone binding	4.538×10^{-6}
5	GO:MF	GO:0017076	purine nucleotide binding	3.959×10^{-5}
6	GO:MF	GO:0031072	heat shock protein binding	3.989×10^{-4}
7	GO:MF	GO:0004054	arginine kinase activity	7.365×10^{-4}
8	GO:MF	GO:0003729	mRNA binding	1.537×10^{-3}
9	GO:MF	GO:0051787	misfolded protein binding	5.309×10^{-3}
10	GO:MF	GO:0003727	single-stranded RNA binding	8.090×10^{-3}
11	GO:MF	GO:0005200	structural constituent of cytoskeleton	4.529×10^{-2}
12	GO:BP	GO:0006457	protein folding	3.037×10^{-19}
13	GO:BP	GO:0034620	cellular response to unfolded protein	1.672×10^{-5}
14	GO:BP	GO:0070887	cellular response to chemical stimulus	8.402×10^{-4}
15	GO:BP	GO:0006603	phosphocreatine metabolic process	1.723×10^{-3}
16	GO:BP	GO:0035194	regulatory ncRNA-mediated post-transcriptional g...	3.558×10^{-3}
17	GO:BP	GO:0003006	developmental process involved in reproduction	3.736×10^{-3}
18	GO:BP	GO:1901566	organonitrogen compound biosynthetic process	5.850×10^{-3}
19	GO:BP	GO:0045041	protein import into mitochondrial intermembrane ...	8.510×10^{-3}
20	GO:BP	GO:0022412	cellular process involved in reproduction in multic...	2.022×10^{-2}
21	GO:BP	GO:0009631	cold acclimation	2.354×10^{-2}
22	GO:BP	GO:0009150	purine ribonucleotide metabolic process	2.394×10^{-2}
23	GO:BP	GO:0007276	gamete generation	3.476×10^{-2}
24	GO:CC	GO:0005737	cytoplasm	6.499×10^{-14}
25	GO:CC	GO:1905202	methylcrotonoyl-CoA carboxylase complex	1.493×10^{-2}
26	GO:CC	GO:1990904	ribonucleoprotein complex	1.608×10^{-2}
27	GO:CC	GO:0009361	succinate-CoA ligase complex (ADP-forming)	4.454×10^{-2}

version	e111_eg58_p18_30541362
date	02/05/2024, 16:48:14
organism	dmelanogaster

g:Profiler

Figure 27. Capped Manhattan-like-plot generated by G:Profiler after direct functional profiling analysis of the 102 Sqd-enriched protein interactors. Circle sizes relate to the corresponding term size, with larger terms exhibiting larger circles. Circle numbers correspond to the top 27 enriched term IDs. The x-axis represents functional terms that are grouped and colour-coded by data sources, and the value in brackets alongside the x-axis labels relates to the total number of significantly enriched terms from this source. The y-axis represents the adjusted enrichment p-values in negative $\log_{10}$ scale. Term circles with p-values less than 10^{-16} were grouped due to capping, as this fixed the y-axis scale to maintain comparability between different queries. P-values smaller than 10^{-16} could all be summarised as highly statistically significant (Kolberg et al. 2023). Red: Molecular Function (MF). Orange: Biological Process (BP). Green: Cell Component (CC). Pink: KEGG Pathways. Blue: WikiPathways (WP). Purple: Human Phenotype Ontology (HP). Other sources not included: TRANSFAC (TF) and microRNA targets from miRTarBase (MIRNA). **Generated and taken from G:Profiler (https://biit.cs.ut.ee/gprofiler/gost).**

The top 14 most enriched proteins in the Sqd-bound control Cl-AP sample are listed and summarised in Table 10. All of these protein binding partners displayed enrichment in the Sqd-YFP control sample that was greater than the amount of detectable Sqd protein. In the comparative proteomics dataset, Sqd itself was therefore the 15th protein hit identified as enriched in the Sqd-YFP-bound Cl-AP control. Sqd (Isoform E) had an abundance ratio (Sqd-YFP/Imp-GFP) of 6.981, with a raw protein abundance value of 1281.6 in the Sqd-YFP control compared to 183.6 in the Imp-GFP sample (Appendix A, Supplementary Data File 1.).

Sqd-enriched protein interactors accounted for roughly 78% of the final number of proteins captured in our comparative proteomics dataset. However, many of these may also be relatively abundant in the Imp-GFP sample but, because there was more of this protein in the Sqd-YFP control, these were allocated as Sqd-enriched. A large proportion of these could likely be discounted as spurious overlapping and non-specific protein interactors, artefacts and contaminants due to being too similar in abundance between the two samples.

But there were grey areas that were difficult to control for or designate with confidence. For example, the protein for Schumacher-levy (Schuy), a product expressed by a known post-meiotic comet gene, was not particularly abundant in the Imp-GFP sample (9.2) or in the Sqd-YFP control (31.7) but gave an abundance ratio (Sqd-YFP/Imp-GFP) of 3.449 (Appendix A, Supplementary Data File 1.). Yet, we know that *schuy* undergoes asymmetrical subcellular localisation and local translation in cytoplasmic regions at the tail-ends of growing spermatids, which neither supports it a true interactor of Sqd nor as a spurious result (Barreau et al. 2008a; Barreau et al. 2008b).

Furthermore, those with abundance ratios (Sqd-YFP/Imp-GFP) just above the threshold of 1.245 could be argued as being potential Imp interactors. It was therefore not easy to separate out the two datasets based on differences alone, and this may have led to a more stringent designation of Imp-enriched protein binding partners than necessary. However, we proceeded with this analysis in the way originally intended because we could have a high degree of confidence that the 29 putative Imp protein interactors we have elucidated here are indeed genuine members of the Imp interactome.

Table 10. Summary of the top 14 most Sqd-enriched protein hits, identified from a total of 102 testis-specific Sqd-enriched protein interactors. All proteins were isolated from *Drosophila melanogaster* Sqd-YFP-expressing testes (Lowe et al. 2014) using multi-step CI-AP experimentation. Bracketed gene/protein names correspond to the abbreviations, symbols and/or synonyms commonly used as alternatives to the full given names. Abundance ratios correspond to a single, comparative value that represents the abundance of a protein of interest in the Sqd-YFP-bound control sample vs. its protein abundance in the Imp-GFP-bound experimental sample[a,b]. Key functions and associated reference citations are provided for each gene/protein entry, based on manual literature searches performed via FlyBase (release versions: FB2024_03 and FB2024_04). All filtered comparative proteomics data can be found in Appendix A, Supplementary Data File 1. FA: Fatty acid. MT: Microtubule. TF: Transcription factor.

GENE / PROTEIN	ABUNDANCE RATIO[a,b]: (SQD-YFP) / (IMP-GFP)	SUMMARY OF KNOWN FUNCTIONS	KEY REFERENCES
Vasa intronic gene (Vig)	1000	RNA binding; Component of the RISC enzyme complex; RNA interference and degradation activity; Heterochromatin organisation and stabilisation; Localises to polytene chromosomes; Putative kinase substrate	Caudy et al. (2002), Caudy et al. (2003), Ivanov et al. (2005), Gracheva et al. (2009)
CG1324	16.3	Uncharacterised gene with limited published evidence, although expression is high testis-enriched	– N/A –

Clot ***(Cl, Thioredoxin domain-containing protein 17)***	10.1	Protein-disulfide reductase; Thioredoxin reductase and glutathione peroxidase enzymatic activity; Component of glutathione redox system; Biosynthesis of drosopterins; Red eye pigment formation	Wiederrecht and Brown (1984), Giordano et al. (2003), Kim (2018)
Prefoldin 1 ***(Pfdn1, CG13993)***	10.0	Subunit component of Prefoldin molecular chaperone complex; Regulates asymmetric division; Suppresses dedifferentiation; May interact with the DNA-binding insulator protein, BEAF	Palumbo et al. (2015), Zhang et al. (2016), Dong et al. (2020)
Pyruvate carboxylase ***(Pcb, PC)***	9.7	Biotin-dependent carboxylase; Glial metabolic enzyme; Anaplerotic component of TCA cycle; TORC activation; Regulates D-serine production; Dendrite pruning	Yamazaki et al. (2014), Marzano et al. (2021), Jouandin et al. (2022), Neophytou and Pitsouli (2022)
CG7768 ***(Peptidyl-prolyl cis-trans isomerase)***	8.8	Limited published evidence – Peptidylprolyl isomerase activity; May be an X-linked retroposed gene of *Cyp1* parent gene; Expressed in adult testis	Betrán et al. (2002), Langille and Clark (2007)

Arginine kinase 2 (Argk2, AK2, CG5144)	8.3	Limited published evidence – Creatine kinase; Gene duplication; May be implicated in cold hardiness/survival	Uda et al. (2006), Teets and Hahn (2018)
Prolyl endopeptidase (CG5355)	8.2	Limited published evidence – Carboxylesterase; Encodes predicted prolyl oligopeptidase domain; Predicted esterase/lipase superfamily member; May be involved in fat body metabolism; Potential target of Dicer-1 in oocytes	Nakahara et al. (2005), Birner-Gruenberger et al. (2012)
CG5217	8.0	Uncharacterised gene with limited published evidence, although expression is testis-enriched	– N/A –
Ciboulot, isoform A (Cib)	7.6	Actin binding and assembly; Actin-based motility; Axonal growth; Central brain metamorphosis; Development of immature adult neurons in larval CNS; Interacts with profilin protein, Chickadee; Muscle modelling; Prevents muscle degeneration/atrophy	Boquet et al. (2000a), Boquet et al. (2000b), Clyne et al. (2003), Jodoin et al. (2015), Brooks et al. (2021), Corrales et al. (2022)

Hsc/Hsp70-interacting protein 1 (HIP)	7.4	Hsp70 protein co-factor; Co-chaperone activity; Stabilises Hsp70 ADP state; Enhances Hsp70:substrate binding; Drives Hsp70 refolding cycle; Promotes ubiquitination and polyQ AR proteasomal degradation; Gene duplicate of *HIP-R*	Hogan and Bettencourt (2009), Wang et al. (2013)
Acetyl-CoA carboxylase (ACC)	7.3	Biotin-dependent carboxylase; Rate-limiting enzyme for FA synthesis; Conserved lipogenic enzyme activity; Lipid metabolism, storage and transport; Myogenesis; Larval development; Regulates feeding behaviour; Regulates developmental signalling pathways; Maintains watertightness and integrity of the tracheal respiratory system; Activated by the TF, SREBP; MT dynamics and spindle assembly	Pan and Hardie (2002), Katewa et al. (2012), Parvy et al. (2012), Sasamura et al. (2013), Garrido et al. (2015), Cinnamon et al. (2016), Westfall et al. (2018), Lee et al. (2018), Zhang et al. (2021), Fang et al. (2023)

Odorant-binding protein 44a, isoform A (Obp44a)	7.1	Member of major odour-sensing gene family; Odorant binding activity; FA binding activity; Olfactory perception; Lipid metabolism, storage and transport; Redox homeostasis; Abundantly expressed in glial cells that ensheathe and support sensory and motor axons; Locomotive and sleep behaviours; Spermatid nuclear bundle organisation	Vieira and Rozas (2011), Bouska and Bai (2021), He et al. (2023), Cotten et al. (2024), Park et al. (2024), Yin et al. (2024)
SCP-containing protein C (Scpr-C, CG5106)	7.0	Limited published evidence – Testis-biased gene; Highly enriched and preferentially expressed in testes; May be involved in male reproduction; May interact with Boule	Xu et al. (2003), Kovalick and Griffin (2005), Begun et al. (2007), Yu et al. (2023)

Footnotes: *[a]An abundance ratio of 1.245 has been set as the lower cut-off value to determine Sqd-enriched protein binding partners by because this corresponds to the amount of detectable GFP/YFP and should be equal in both the Sqd-YFP control and in the Imp-GFP sample; [b]An abundance ratio of >1.245 therefore corresponds to protein enrichment in the Sqd-YFP control sample, with greatest enrichment corresponding to the highest abundance ratios.*

4.9. RNA-Seq data has been aligned to annotated genomic loci and can be interrogated to uncover enriched bound mRNAs

4.9.1. Paired-end reads exhibit good quality raw sequences for all CI-AP RNA libraries

Preparation of four RNA libraries – for the Imp-GFP input homogenate, Imp-GFP bound extract, Sqd-YFP input homogenate and Sqd-YFP bound extract, respectively – was performed by the Cardiff University Genomics Research Hub (Cardiff School of Biosciences) using the NEBNext® Single Cell/Low Input RNA Library Prep Kit for Illumina® (New England Biolabs, Cat. # E6420S/L).

QC and sequencing of these pre-made libraries was carried out by Novogene UK using partial lane sequencing to a sequencing depth of at least 6Gb per sample library (20M paired-end reads each, Illumina NovaSeq X Plus Series PE150). All four CI-AP RNA libraries were successfully sequenced to generate 150 base pair (bp) paired-end reads. Quality control data from Novogene confirmed that the sequence quality of the raw paired-end reads was high, with more than 90% of read sequences having a Phred score > 20 (Table 11.).

All initial stages of RNA-Seq data processing, including the analyses to yield annotated genomic feature counts, were kindly supported by Dr. Fiona Messer (Post Doctoral Research Associate, Cardiff University School of Biosciences).

Preliminary sequence quality checks were performed with the FastQC tool, which confirmed that the sequence length distribution of all raw paired-ends was indeed 150 bp (Andrews 2010). Sequences were trimmed and filtered using Trim Galore (version 0.6.10) and Cutadapt (version 4.1) to remove adaptor sequences, overrepresented sequences, and sequences that had been assigned low quality scores (Phred < 20) (Krueger 2012). Any low-quality sequences shorter than 50 bp in length were also eliminated. Post-trimming and filtering FastQC reports showed that paired-end reads for all RNA libraries were of high base sequence quality and content, and were of satisfactory lengths – with all lying within a 50 to 130 bp range (Andrews 2010). Paired-end read counts before and after trimming are summarised below, in Table 12.

Table 11. Post-RNA-Seq quality control information provided by Novogene UK upon completion Illumina NovaSeq X Plus paired-end sequencing. Pre-made RNA libraries corresponding to the Imp-GFP input homogenate, Imp-GFP bound extract, Sqd-YFP input homogenate and Sqd-YFP bound extract were all subject to sequencing. For each RNA library sample, the table includes the raw data depth generated in Gb, base quality value (Q_{phred}) as a percentage, and the percentage of total guanine and cytosine content (%GC). $Q_{phred}20$ corresponds to a Phred score of 20, which relates to a sequencing error rate of 1 in 100 bases. $Q_{phred}30$ corresponds to a Phred score of 30, which relates to a sequencing error rate of 1 in 1000 bases.

RNA LIBRARY SAMPLE	RAW DATA (Gb)	$Q_{phred}20$ SCORE (%)	$Q_{phred}30$ SCORE (%)	%GC
Imp-GFP INPUT	8.0	93.48	87.36	48.70
Imp-GFP BOUND	7.5	92.38	85.60	48.39
Sqd-YFP INPUT	7.7	93.44	87.51	48.88
Sqd-YFP BOUND	7.8	91.76	84.25	49.50

Table 12. Paired-end read counts of the sequencing data for the Imp-GFP input, Imp-GFP bound, Sqd-YFP input and Sqd-YFP bound RNA libraries. The number of reads before and after the process of trimming and filtering are presented, in addition to a quantification of the total number of sequences removed as a percentage of the raw paired-end data.

RNA LIBRARY SAMPLE	RAW PAIRED-END READ COUNTS	TRIMMED AND FILTERED PAIRED-END READ COUNTS	SEQUENCES REMOVED (%)
Imp-GFP INPUT	26588443	22429386	15.6
Imp-GFP BOUND	25082594	20547196	18.1
Sqd-YFP INPUT	25766496	22238989	13.7
Sqd-YFP BOUND	26112174	19965124	23.5

4.9.2. Alignment to the annotated *Drosophila melanogaster* genome yields a high number of mapped reads to identifiable genomic loci

Sequence reads were aligned to the *Drosophila melanogaster* reference genome version r6.57 (Dmel6.57) using the STAR RNA-Seq aligner tool, v2.7.6a (Dobin et al. 2013; Öztürk-Çolak et al. 2024). Counts were collated for all reads that were successfully mapped to the annotated genomic loci and for any unmapped reads that failed to undergo alignment (Table 13.).

None of the RNA-Seq datasets had unmapped reads due to excessive mismatches, and all demonstrated genomic mapping for at least 85% of their total sequence reads. This indicated good quality sequencing data that could be assigned to specific genomic loci with high confidence.

After alignment to the annotated reference genome, unmapped and duplicated reads were filtered from the RNA-Seq datasets, and mapped read alignments were sorted based on chromosomal coordinates using the SAMtools package (v1.17) (Li et al. 2009a). FeatureCounts (v2.0.2) was then used to count the RNA sequence reads that had been successfully mapped to annotated genomic features (Liao et al. 2014).

A total of 17,561 annotated features of the *Drosophila melanogaster* genome were included and represented at this point of the analysis pipeline. Raw, gene-annotated count data from the FeatureCounts programme (v2.0.2) is available in Appendix B, Supplementary Data File 1 for all four RNA-Seq datasets.

Further processing with the edgeR package resulted in a list of 13,760 differentially expressed genes (Robinson et al. 2010; McCarthy et al. 2012).

Table 13. Mapped and unmapped read counts from sequencing data of the Imp-GFP input, Imp-GFP bound, Sqd-YFP input and Sqd-YFP bound RNA libraries. The number of uniquely mapped reads, multi-mapped reads and unmapped reads have been determined following STAR alignment to the *Drosophila melanogaster* reference genome (Dmel 6.57 release) (Dobin et al. 2013; Öztürk-Çolak et al. 2024). Unmapped read counts were broken down into two categories: (i) unmapped reads that were too short for alignment and, (ii) unmapped reads that were discounted due to other factors. For the respective RNA-Seq datasets, bracketed quantifications represent the read counts for each category type as a percentage of the total number of input reads.

RNA LIBRARY SAMPLE	UNIQUELY MAPPED READ COUNTS	MULTI-MAPPED READ COUNTS	UNMAPPED READ COUNTS (TOO SHORT)	UNMAPPED READ COUNTS (OTHER)
Imp-GFP INPUT	19422819 (86.6%)	573600 (2.6%)	2388538 (10.6%)	44429 (0.2%)
Imp-GFP BOUND	17720628 (86.2%)	571,267 (2.8%)	2166570 (10.5%)	88731 (0.4%)
Sqd-YFP INPUT	19370239 (87.1%)	540,442 (2.4%)	2290946 (10.3%)	37362 (0.2%)
Sqd-YFP BOUND	17165371 (86.0%)	608886 (3.0%)	2118640 (10.6%)	72227 (0.4%)

4.9.3. Differential analysis of interacting mRNAs proves difficult without experimental replicates and a true negative control

Multiple approaches have been attempted to determine an identifiable list of sample-specific mRNA transcripts in our RNA-Seq data. This includes the development of a Differential Gene Expression (DGE) pipeline with a Generalised Linear Model (GLM), which was conceptualised by Dr. Fiona Messer (Post Doctoral Research Associate, Cardiff University School of Biosciences) using the edgeR package in RStudio (Robinson et al. 2010; McCarthy et al. 2012; R Core Team 2024).

Among other endeavours, RNA-Seq feature count data from the Imp-GFP input and Sqd-YFP input RNA libraries was merged as a single reference group. Count data from the Imp-GFP bound RNA library was then compared to this to gauge a list of differentially expressed genes/transcripts that were enriched in the Imp-GFP bound vs. that of the combined input reference group. The R script code for this R-based bioinformatics pipeline can be found in Appendix B, Supplementary Code File 1 and the raw data outputted from this edgeR DGE analysis with GLM is provided in Appendix B, Supplementary Data File 2. A list of 639 top gene hits were yielded from this analysis, not all of which were statistically significant (Appendix B, Supplementary Data File 3.).

However, the lack of experimental replicates and a defined negative control had complicated matters extensively, making analysis of these outputs extremely convoluted and confusing. Because of this, we therefore decided to investigate the normalised feature count data for the bound vs input RNA libraries manually instead, with RNA-Seq feature counts for the Imp-GFP input and Sqd-YFP input RNA libraries once again combined as a pooled reference group for these comparisons.

A matrix of raw and normalised RNA-Seq counts was created in R Studio using the normalisation factors generated from the edgeR DGE analysis above, facilitating manual exploration of these datasets (Robinson et al. 2010; McCarthy et al. 2012; R Core Team 2024).

Normalisation factors were based on the computed RNA library size, allowing the number of RNA-Seq feature counts for each sample to be adjusted/scaled accordingly

to account for inherent composition biases and technical variations, including differences in sequencing depth (Table 14.) (Bolstad et al. 2003; Robinson and Oshlack 2010). Normalisation by scaling to library size was logical, given that sequencing of an RNA sample to half the depth should theoretically, result in half the number of reads, on average, mapping to each gene (Robinson and Oshlack 2010).

All raw and normalised RNA-Seq feature counts from the edgeR analysis are available in Appendix B, Supplementary Data File 4.

Table 14. RNA library sizes and normalisation factors as determined by edgeR for scaled adjustment of the RNA-Seq data counts. Group assignment information is also given for the Imp-GFP input, Imp-GFP bound, Sqd-YFP input and Sqd-YFP bound RNA samples, with Group 1 corresponding to a combined reference group comprising both the Imp-GFP input and Sqd-YFP input RNA-Seq normalised feature counts.

RNA LIBRARY SAMPLE	COMPUTED LIBRARY SIZE	NORMALISATION FACTOR	GROUP ASSIGNMENT
Imp-GFP INPUT	35855020	1.023507602	GROUP 1
Imp-GFP BOUND	32572522	0.87377612	GROUP 2
Sqd-YFP INPUT	35559978	1.047620729	GROUP 1
Sqd-YFP BOUND	30791646	1.067344639	GROUP 3

4.9.4. Several uncharacterised transcripts, mitochondrial RNAs and post-meiotically expressed comet and cups are enriched in the Imp-GFP dataset

A list of 249 gene hits were yielded from this analysis, representing a putative subpopulation of Imp-GFP-enriched mRNA transcripts associated with endogenous Imp RNP complexes *in vivo* (Appendix B, Supplementary Data File 5.).

The top 20 of these genes/transcripts are summarised in Table 15., from most to least enriched. Half of these corresponded to uncharacterised genes while two mitochondrial genes were also outputted in the top 20.

Genes with other characterised functions were also present, such as *Jupiter*, which is known to be involved in microtubule binding and regulation (Karpova et al. 2006; Martinez et al. 2021).

Additionally, genes with published functions in enzymatic pathways and signalling cascades were represented in the top 20 gene hits, and two distinct lncRNAs, *lncRNA:CR34335 (MRE16)* and *lncRNA:CR9284* were also detected (Table 15.).

Interestingly, two post-meiotic comet and cup genes were identified as having gene products interacting with Imp. Both *world-cup (w-cup)* and *scotti (soti)* make up the 5th and 19th most enriched mRNAs, respectively, that were in association with the Imp-GFP bound sample (Table 15.). Two other comet and cup genes were also found within the wider RNA-Seq dataset, with *borrelly (boly)* and *solwind (sowi)* both enriched in the set of 249 Imp-interacting post-meiotic transcripts (Appendix B, Supplementary Data File 5.).

Another uncharacterised gene, *CG2127*, was also found in the top 20 Imp-enriched hits. Although not a post-meiotically transcribed gene, it is expressed from a genomic locus that neighbours a comet gene cluster. It is actually a paralogue of the post-meiotic genes that make-up that nearby comet cluster, which include *boly, cola, swif, whip, hubl* and *spaw* (Barreau et al. 2008a).

Table 15. Summary of the top 20 most Imp-enriched gene/transcript hits, obtained from 249 putative testis-specific Imp-enriched mRNA interactors. Hits were determined using normalised RNA-Seq feature counts that were assigned and annotated using a standard bioinformatics processing pipeline. RNA-Seq data corresponded to RNA libraries that were generated from an eluate of endogenous Imp-interacting RNAs. These were in turn purified from *Drosophila melanogaster* Imp-GFP-expressing testes using a multi-step CI-AP methodology. Characterised gene IDs (non-CG numbers) were retrieved from FlyBase using the 'ID Validator' function (release version: FB2024_04). Bracketed gene/protein names correspond to the abbreviations, symbols and/or synonyms commonly used as alternatives to the full given names. Key functions and references are provided for each gene/transcript entry, based on manual literature searches performed via FlyBase (release version: FB2024_04). Raw and normalised feature count data is available in Appendix B, Supplementary Data File 5. MT: Microtubule. TF: Transcription factor.

GENE / TRANSCRIPT	SUMMARY OF KNOWN FUNCTIONS	KEY REFERENCES
CG4218	Uncharacterised gene with limited published evidence; Highly testis-enriched	– NA –
CG18628	Sexual reproduction; Seminal fluid protein-encoding gene; Testis-enriched; Highly expressed in seminal receptacle; Female courtship	Lawniczak and Begun (2004), Findlay et al. (2008), Prokupek et al. (2009), Sirot et al. (2014)
CG2127	Sperm development; Extracellular matrix patterning; Highly testis-enriched; Paralogue of some comet genes	Barreau et al. (2008a), Khokhar et al. (2008)

CG9016	Uncharacterised male-biased gene with limited published evidence; Highly testis-enriched	Huylmans and Parsch (2014)
World-cup (w-cup)	Post-meiotically transcribed comet gene in sperm development; uncharacterised function	Barreau et al. (2008a), Barreau et al. (2008b)
Mitochondrial Cytochrome b (mt:Cyt-b)	Mitochondrial respiration; Ubiquinol-cytochrome c reductase complex component; Core component of testis-specific mitochondria complex III; Sperm development; Male fertility	Clancy et al. (2011), Seddigh and Darabi (2018), Salminen et al. (2019)
CG12861	Uncharacterised male-biased gene with limited published evidence	Huylmans and Parsch (2014)
CG4983	Uncharacterised gene with limited published evidence	– NA –

Effete (eff)	E2 ubiquitin-conjugating enzyme; Protein ubiquitination and degradation; Regulates Hedgehog signalling and Gli/Ci TF processing; Regulates proper telomere behaviour; Eye development; Apoptosis and dendrite pruning; Female GSC maintenance	Treier et al. (1992), Cenci et al. (1997), Neufeld et al. (1998), Ryoo et al. (2002), Kuo et al. (2006), Herman-Bachinsky et al. (2007), Chen et al. (2009), Pan et al. (2017)
Glutathione S transferase S1 (GstS1)	Multi-enzyme activity; Glutathione-conjugating activity; Detoxification of electrophiles and reactive oxygen species; Antioxidant; Protects against oxidative stress; Regulates mitochondrial numbers, length and fusion in axons	Beall et al. (1992), Singh et al. (2001), Agianian et al. (2003), Whitworth et al. (2005), Saisawang et al. (2012), Smith et al. (2019), Chen et al. (2020)
Jupiter	Regulates MT dynamics; Promotes MT stabilisation; MT marker	Karpova et al. (2006), Martinez et al. (2021)
CG9920	Male fertility; Proper morphogenesis of mitochondria during sperm tail elongation; Spermatid individualisation; *Drosophila* ortholog of Hsp10	Owusu-Ansah et al. (2013), Li et al. (2024)

CG2291	Uncharacterised gene with limited published evidence	– NA –
lncRNA:CR34335 (MRE16)	mRNA-like long non-coding RNA; Ubiquitously expressed; Implicated in testicular terminal epithelium ageing; Highly expressed in glia; Expressed during embryogenesis	Inagaki et al. (2005), Davie et al. (2018), Talross and Carlson (2023), Chen et al. (2024)
Mitochondrial Cytochrome c oxidase subunit II (mt:CoII)	Subunit of cytochrome-c oxidase; Last component of mitochondrial transport chain; Modulates rate of proton translocation; Part of testis-specific mitochondrial complex IV; Sperm development; Spermatid individualisation; Male fertility	Sohal et al. (2008), Patel et al. (2016)
CG2955	Uncharacterised gene with limited published evidence – may be involved in oviposition behaviour	Fanara et al. (2023)
lncRNA:CR9284	Long non-coding RNA – Uncharacterised gene with limited published evidence	– NA –

14-3-3 protein epsilon (14-3-3ε)	Hippo and Ras/MAPK signalling; Regulates Yorkie activity and localisation; Modulates histone phosphorylation and acetylation for transcription elongation; Promotes spindle assembly and organisation; Regulates TF, Zfh-1; Germ cell migration; Axon guidance; Cell growth; Eye development; Embryonic hatching; Female fecundity	Chang and Rubin (1997), Acevedo et al. (2007), Karam et al. (2010), Ren et al. (2010), Tsigkari et al. (2012), Yang and Terman (2012), Beaven et al. (2017), Nam et al. (2022)
Scotti (soti)	Post-meiotically transcribed comet gene in sperm development; Male fertility; Spermatid individualisation; Inhibitor of Cullin-3-based E3 ubiquitin ligase complex; Non-apoptotic caspase activation; Regulated by eIF4E-5 in elongating spermatids; Interacts with Orb2; Downregulated during male reproductive dormancy	Barreau et al. (2008a), Barreau et al. (2008b), Kaplan et al. (2010), Xu et al. (2012), Aram et al. (2016), Kubrak et al. (2016), Shao et al. (2023)
CG6527	Uncharacterised gene with limited published evidence	– NA –

14-3-3 protein epsilon (14-3-3ε) was found to be Imp-enriched in both our comparative proteomics and RNA-Seq datasets. Two lower-enriched mRNA transcripts for *tropomyosin-1 (tm1)* and *calmodulin (cam)*, both of which are associated with actin and microtubule dynamics, were also identified in the wider Imp-enriched RNA-Seq dataset and in turn corresponded to proteins detected in our comparative proteomics analysis (VanBerkum and Goodman 1995; Texada et al. 2011). Transcripts encoding *imp* and *sqd* were also detected (Appendix B, Supplementary Data File 5.). Altogether, this suggested that Imp RNP complexes can bind these interactors at both a protein and RNA level.

4.10. Several of Imp's protein binding partners correspond to regulatory functions in actin binding and cytoskeletal dynamics

We have found that a large proportion of Imp's interactome is implicated in actin binding and the regulation of cytoskeletal dynamics, suggesting roles in active transport and/or anchoring of localised mRNAs to their target subcellular locations. The fact that transcripts for *Actin87E* and *Actin42A* were also detected in the wider Imp-enriched RNA-Seq dataset further supports this hypothesis (Appendix B, Supplementary Data File 5.). It may also indicate an involvement in the localisation of *actin* mRNAs for the local translation, deposition and polymerisation of actin proteins that provide the driving force for cell growth and motility (Ghosh-Roy et al. 2004; Hüttelmaier et al. 2005).

Proper regulation of actin and MT organisation is needed at every stage of *Drosophila* sperm development, to drive successive rounds of growth, differentiation, morphogenesis and individualisation (Frappaolo et al. 2022). The most dramatic of these remodelling events, spermatid elongation, yields a 150-fold increase in length and 5-fold increase in total surface area, which would not be possible without the combined activities of the F-actin and MT networks (Tokuyasu et al. 1972; Tokuyasu 1974a; Noguchi et al. 2011). Impediment of F-actin based processes in developing sperm cells therefore leads to spermatid bundle disassembly and ectopic release of premature sperm inside the testis (Desai et al. 2009). Taken together, this binding

between Imp and several F-actin-allied proteins may be representing a series of genuine interactions that correspond with the latter stages of sperm development, such as in spermatid growth and differentiation.

We therefore propose that the presence of multiple actin regulators in association with Imp represent a genuine set of interactions which are together indicative of contributions to a wider multi-protein cytoskeleton-associated Imp RNP complex. In this hypothesis, we theorise that this large Imp-containing structure “caps” the tail-ends, in a region overlapping with localised Imp at the extreme tail-ends of the spermatid cyst bundles and may or may not provide an anchor point for localising post-meiotic mRNA transcripts at the spermatid tail-ends. While time constrains prevented us from testing this hypothesis in any real depth, we did attempt to substantiate some of these interpretations rudimentarily by conducting a fluorescence imaging of testes from transgenic fly lines already in the lab.

To test this hypothesis of an F-actin anchoring Imp RNP complex in spermatid cyst bundles, we investigated whether there was any co-localisation of Imp protein and F-actin at the apical tail-end regions of the spermatid cyst bundles (Fig. 28.1. and Fig. 28.2.). We also wanted to explore whether F-actin expression showed any spatial overlap with the distribution of Tm1 and schuy protein at the spermatid tail-ends. To do so, we conducted live cell labelling of F-actin in spermatid cyst bundles using SPY555-FastAct™ (SC205, Spirochrome) – a fluorescent live cell actin probe that labels actin filaments, permitting regions of filamentous assemblies to be visualised *in vivo* in living spermatids (Fig. 28.). We stained for F-actin in *Drosophila* testes from males of the following fly lines: Imp-GFP G80 protein-trap (G00080 exon-trap line; Quiñones-Coello et al. 2007), Tropomyosin-1-GFP (Tm1-GFP, BL51537; Tirian and Dickson 2017) and schuy-TagGFP;Bam-Gal4:VP16 (generated in this project).

In all co-localisation conditions, we found that F-actin was expressed in a consistent gradient throughout the entire length of the spermatid cyst bundles (Fig. 28.1A’’, Fig. 28.1B’’ and Fig. 28.1C’’, Fig. 28.2.). There was a striping pattern of F-actin localisation down the length of the bundles, which distinguished each of the individual sister spermatid cells within the syncytial cyst.

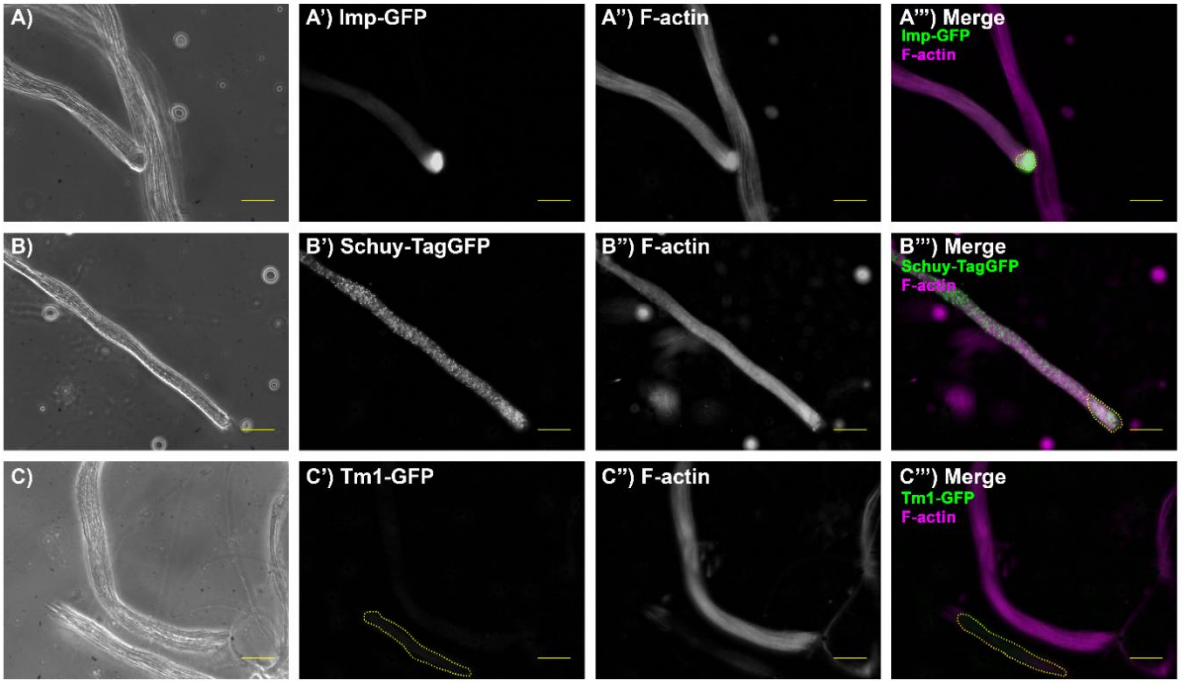

Figure 28.1. Co-localisation screening of F-actin in *Drosophila* spermatids expressing Imp-GFP, schuy-TagGFP and Tropomyosin-1-GFP (Tm1-GFP). (A – C) Phase contrast images of individual spermatid cyst bundles isolated from squashed whole testis preparations. (A' – C') Single channel GFP fluorescence images of the same spermatid cysts. (A'' to C'') Corresponding single CY3 filter channel fluorescence images of F-actin deposition in spermatids. (A''' – C'''). Two-channel RGB colour overlay of fluorescence signals from the GFP-tagged proteins of interest (488 nm) (green) and SPY555-FastAct™ stained F-actin (magenta). Yellow dotted lines indicate regions of co-localised spatial overlap between (A''') F-actin and Imp-GFP and (B''') F-actin and schuy-TagGFP, while yellow dotted zones in (C' and C''') outline low intensity Tm1-GFP fluorescence signals in a single spermatid cyst bundle. Imaging was performed using the upright Olympus BX50 Microscope. All images were taken at 40X magnification and are representative of the dual co-localisation conditions tested in three spermatid cyst bundles from the testes of three different, independent males (n=3). All fluorescence images were subject to background subtraction with a rolling ball radius of 100 pixels using ImageJ v1.52d (Schneider et al. 2012). Gain: 1.0. Exposure: 1.0. Scale bars: 25 µm.

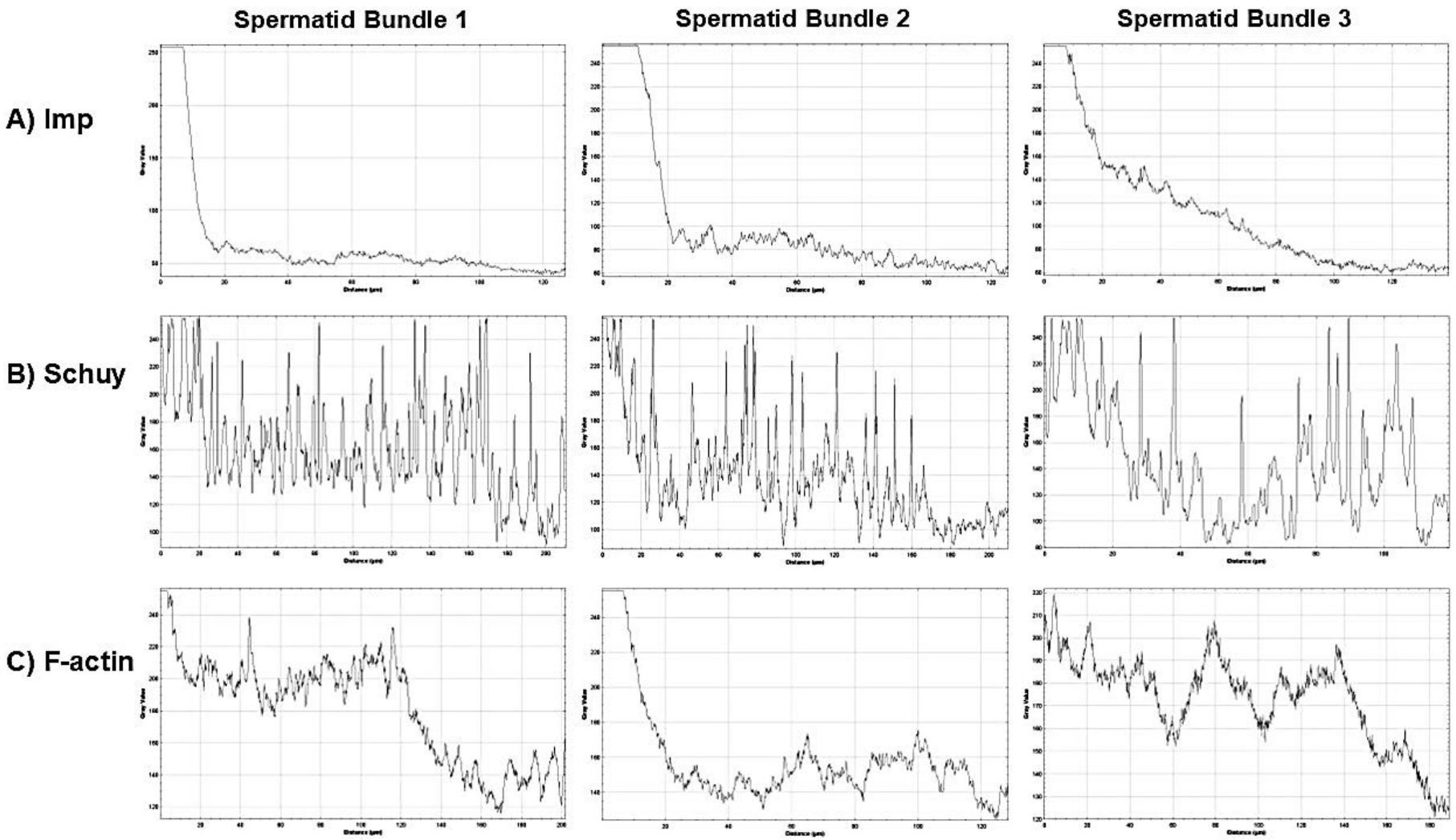

Figure 28.2. Plot profiles representing the mean pixel intensities of fluorescent signals expressed by Imp-GFP, schuy-TagGFP and F-actin along the length of three independent *Drosophila* spermatid cyst bundles. All signal quantifications correspond to the co-localisation

experiment performed in Fig. 28.1. These plot profiles display the mean pixel intensities expressed across the length of three individual spermatid cyst bundles for: (A) Imp-GFP, (B) schuy-TagGFP, and (C) SPY555-FastAct™ stained F-actin. X-axes represent “gray values”: the mean pixel intensity of signals ranging from 0-255 for each 8-bit 40X fluorescence image analysed. Y-axes: correspond to the distance over which the signal intensities were measured, in µm, from the extreme tail-end of each spermatid cyst bundle to a defined cut-off point at the end of the visible bundle in the respective image. Tm1-GFP expression was not subject to quantification due to the fluorescence signals being too weak to measure with confidence. Plot profiles represent average signal gradients along the tail length of three spermatid cyst bundles obtained from three different, independent males of each genotype (n=3). All images were taken at the same intensity settings using the upright Olympus BX50 Microscope. Quantification and profile plot generation was performed in ImageJ v1.52d via its segmentation line measurement tool (Schneider et al. 2012).

F-actin was present in some spermatids at a higher concentration than others, which may be due to variable penetration into the tissue or could instead correspond to actin composition differences in the elongation stages. A large proportion of the spermatids did, however, contain tail-end localised F-actin, which was apparent at high concentrations in some spermatid cyst bundles, but not in others (Fig. 28.1. and Fig 28.2.). At its brightest point, localised F-actin corresponded to an average mean signal intensity of 225 (n=3, SE=16.80). This may imply that the putative F-actin rich structure dissociates once spermatids have reached their desired length. Quantification generally supported a progressive but defined drop in F-actin signals, with expression gradually declining as the distance away from the extreme spermatid tail-ends increased (Fig. 28.2.). Although not shown here, we were also able to visualise F-actin in the investment cones of the individualisation complexes as they passed along the fully elongated spermatids of the testis.

Imp protein was expressed in a highly concentrated “ball” that accumulated at the tail-ends of spermatids (Fabrizio et al. 2008; Fig. 28.1A’ and Fig. 28.2.). At its brightest point, localised Imp-GFP corresponded to an average mean signal intensity of 249 (n=3, SE=5.38). We found spatial overlap in the expression of Imp-GFP and F-actin, with this co-localisation providing an initial indication of a possible interaction between the two at the spermatid tail-ends (Fig. 28.1A”’).

There may also be some co-localisation between the tagged comet protein, schuy-TagGFP, and F-actin at the extreme distal region of the spermatid tail-ends (Fig. 28.1B”’). However, the punctate speckling of schuy-TagGFP protein expression made it difficult to determine the true extent of this spatial overlap and may in turn reflect the efficient turnaround and transient nature of *schuy* localisation (Fig. 28.2.); as these transcripts are being rapidly and dynamically transported, anchored and locally translated along the F-actin network. The particulate nature of localised schuy-TagGFP expression may also be suggestive of the protein accumulating within discrete, compartmentalised condensates throughout each individual spermatid. At its brightest point, schuy-TagGFP measured an average mean signal intensity of 212 (n=3, SE=7.31).

Tm1-GFP was expressed at very low levels in a uniform distribution throughout most spermatid cyst bundles. Unfortunately, these fluorescence signals barely rose above

the background autofluorescence, which made it difficult to distinguish any key features of the Tm1 expression profile. Once background subtraction was performed to merge the channels in a composite figure, Tm1 expression was hardly visible (Fig. 28.1C'). This suggested that Tm1, and likely Tm2, are not major components of the Imp-facilitated F-actin structure at the tail-ends of the spermatids. They may have instead been captured in our proteomics dataset as part of an earlier set of interactions with Imp, including those identified with Mei-P26. We therefore excluded Tm1 and Tm2 from any further model hypotheses to reflect our preliminary findings.

Unfortunately, we were unable to optimise our immunolabelling protocol to enable multiplexing of antibody stains for visualisation of multiple protein targets. If we had more time, this would be something we would investigate further; with the aim of screening for other potentially co-localising actin-related proteins in the spermatid tail-ends, focusing on those that we have identified in our comparative proteomics analysis.

4.11. Chapter-specific discussion

4.11.1. CI-AP experiments confirm testis-specific protein and RNA interactions

We have successfully purified endogenous protein and RNA extracts that were in association with Imp-GFP and Sqd-YFP, respectively, in the *Drosophila* testis. By cross-comparing relative enrichment in the outputs of each CI-AP purified sample, we have been able to determine a list of these putative interacting proteins and RNAs for the Imp protein. We have been able to stringently identify which binding partners were specific to each of our bait proteins and use their known functions and wider interaction network to build-up a bigger picture of Imp's role within sperm development.

Interestingly, multiple mRNA transcripts that were Imp-enriched within the wider RNA-Seq dataset (Appendix B, Supplementary Data File 5.) were also found to encode one of the 29 proteins in association with Imp, including transcripts for *imp* itself. This suggests a highly intricate network of interactions within the multi-protein mRNA:Imp RNP complexes that may indicate evidence of autoregulatory feedback mechanisms. The physical interaction of a protein with its own mRNA typically indicates

autoregulation, with this activity controlling the stead-state production, concentration and subcellular distribution of that protein (Müller-McNicoll et al. 2019).

4.11.2. A small number of post-meiotic comet and cup transcripts are enriched in the Imp RNA-Seq dataset

Of the 249 putative Imp-interacting gene hits manually interrogated using normalised RNA-Seq feature count data, four represent post-meiotically transcribed comet and cup genes (Barreau et al. 2008a; Barreau et al. 2008b).

From most to least Imp-enriched, mRNAs corresponding to *w-cup*, *soti*, *boly* and *sowi* were all detected as being in association with purified Imp:mRNA RNP complexes. We tested for *in vitro* binding interactions between Imp and the *soti* and *boly* mRNAs in Results Chapter 1. We found that testis Imp isoforms bound both mRNA transcripts in our assay, although the interaction with *soti* was much stronger in binding affinity than was shown with *boly*. This coincides with what we have found here, with *soti* being enriched within the top 20 Imp-interacting gene hits while *boly* is detected further down in the wider RNA-Seq dataset.

Speculatively, Imp may form a direct interaction with a subset of these comet and cup mRNA transcripts but may not bind directly to all of them. Although, we do not have strong evidence of this either way. It could, however, explain the fluctuations we see in bound protein in the RNA-affinity pull-down assay, since it does not differentiate between direct and indirect interactions.

Indirect binding of Imp may be mediated via scaffolding and adaptor proteins in the broader Imp RNP complex. As these are constantly subject to remodelling in living cells, indirect – and potentially weaker – RNA interactions may be transient and dynamic depending on the sperm development stage, and we may not have captured all of these in the higher-order Imp RNP complexes we purified in our CI-AP experimentation (Doetsch et al. 2011).

4.11.3. Presence of Meiotic-P26 suggests that early, pre-meiotic Imp RNP complexes may have been captured in our proteomics dataset

With regards to our proteomics data, we were looking to delve deeper into the protein interactome of Imp in spermiogenesis, with a specific focus on its putative functions in the post-meiotic elongating spermatids. However, due to the biphasic nature of Imp protein expression within the *Drosophila* testis, we may have also captured some interactions that correspond to Imp RNP complexes assembled prior to meiosis. Meiotic P26 (Mei-P26) may represent an example of this.

Isoform F of the Mei-P26 protein has been identified here as an enriched interactor of the Imp-GFP CI-AP sample. Originally characterised by Page et al. (2000), loss-of-function phenotypic analysis of Mei-P26 mutants revealed roles in gamete generation, germline differentiation and meiosis in both male and female flies. In normal testes, Mei-P26 is highly expressed in the GSCs, gonialblasts, early spermatogonial cells and in the spermatocytes, and is suggested to be essential for GSC differentiation and entry into meiosis (Chen et al. 2014c).

Mei-P26 also facilitates the transition from transit-amplification to spermatogonial differentiation via the establishment of a negative feedback loop between Mei-P26 and Bam; which together ensures the proper accumulation of Bam and regulates accurate transit-amplifying divisions in sperm development (Insco et al. 2012; Wu et al. 2016). This tight regulatory network is further reinforced by the control of Mei-P26 expression through distinct splicing events, with the *mei-p26* pre-mRNA being a downstream target of the major spliceosome component, U2A, during spermatogonial differentiation (Wu et al. 2016).

Most importantly, however, is the fact that the expression profile of Mei-P26 predominates up until the spermatocyte stages, before the meiotic divisions have commenced. Moreover, endogenous Mei-P26 interacts with, and is translationally repressed by, the miRNA of *let-7* in early male germ cells *in vivo*. Adjustments to *let-7* expression correlate with inversely proportional changes in the expression levels of Mei-P26 (Insco et al. 2012). Imp, and its non-*Drosophila* homologues, are also known to form direct interactions with heterochronic *let-7* miRNAs in a number of tissue types,

including in the *Drosophila* testis. These are in turn referred to as "*let-7*–regulated oncofetal genes", or LOGs, and interactions tend to correspond with *let-7*-induced repression (Boyerinas et al. 2008; Toledano et al. 2012).

In the testis stem cell niche, Imp undergoes an age-related decline in expression levels as a consequence of its targeted regulation by *let-7* miRNAs in the hub cells (Toledano et al. 2012). This overlap in a mutual *let-7* miRNA regulator cannot be down to coincidence alone. Altogether, this confirms that Mei-P26 may indeed be a true binding partner of Imp, but the Imp:Mei-P26 protein interaction was most likely isolated from an earlier timepoint of sperm development within the apical hub region of the testis, rather than being a constituent of Imp RNP complexes in the tail-ends of spermatids during the elongation phase.

4.11.4. Syncrip is a known interactor of Imp in the fly nervous system

Syncrip (Syp) has long been implicated in the regulation of RNA stability, localisation and translation, particularly in *Drosophila* oogenesis and in the developing nervous system (McDermott et al. 2012; McDermott et al. 2014; Titlow et al. 2020). However, expression of Syp has also been recently characterised in the *Drosophila* testis, where it is said to form RNA-dependent interactions with proteins such as the C2H2 zinc-finger protein, Doublefault (Dbf). In doing so, Syp may support the translation of specific mRNA transcripts in the spermatocytes, ensuring proper meiotic division and normal progression of sperm development (Sechi et al. 2019).

Moreover, spermatocyte-specific isoforms of Syp have also been found to localise to the cytoplasm, where they are required for the timely expression of cell cycle regulatory protein, Cyclin B (CycB), in mature spermatocytes prior to meiosis. Syp binds the 5' and 3' UTRs of *CycB* transcripts with high affinity and, in cooperation with a complex of other protein factors, regulates the timepoint-specific stabilisation and translation of *CycB* mRNAs; permitting normal entry into the meiotic divisions and progression into post-meiotic differentiation stages of sperm production (Baker et al. 2023).

Of most interest, however, is the intimate link that Syp has with Imp in the nervous system, as published in the wider literature. Through the establishment of descending Imp and ascending Syp expression gradients, Imp and Syp coregulate temporally defined cell fate specifications. In the *Drosophila* mushroom body and antennal lobe lineages, Syp establishes opposing temporal gradients with Imp to regulate multiple time-dependent cell fate decisions (Liu et al. 2015). This is achieved by Syp repressing translation of the TF, Chinmo, whereas Imp drives its translational activation – yet neither ever affect *chinmo* transcript levels. Through this inversely proportional, antagonistic relationship, they govern the age-dependent developmental potential of neural stem cell progenitors, driving neuronal temporal fate specification so that different neurone types are produced at different developmental timepoints. In doing so, Syp promotes late neuronal fates while Imp promotes early neuronal fates (Zhu et al. 2006; Liu et al. 2015).

This same type of opposing gradient formation has been corroborated by numerous studies; including in the regulation of E93 protein expression for the developmentally-timed termination of neurogenesis via autophagy, and in the Castor/Seven-up induction of Imp/Syp temporal gradients within type II neuroblasts, which serves as a mechanism to diversify the cell fates of transiently amplifying intermediate neural progenitors (Ren et al. 2017; Pahl et al. 2019).

Temporal protein gradients of Syp and Imp also result in a novel role within the two-step decommissioning process of neuroblasts to drive terminal neuronal differentiation in a lineage-specific manner (Yang et al. 2017). By working in collaboration with one another, Imp regulates the first phase of time-specific neuroblast shrinkage during metamorphosis, followed then by the second stage of Sqd-dependent accumulation of Prospero in the nucleus. This in turn promotes exiting from the cell cycle and differentiation into neurones. However, Imp is dominant to Sqd; with Sqd only able to drive cell cycle exit in Imp-negative decommissioned neuroblasts, once Imp expression levels have declined enough to induce cell shrinkage (Yang et al. 2017).

Taken together, this offers some evidence in support of a possible connection and genuine interaction between Imp and Syp in the testis, as we have subsequently found in our proteomics data. Since Imp and Syp may be protein binding partners during

Drosophila sperm development, it would be intriguing to find out whether the antagonistic relationship they share neuronally is recapitulated in the male germline.

4.11.5. Several of Imp's protein binding partners correspond to regulatory functions in translational activation

Translational control is a critical regulatory mechanism in *Drosophila* sperm development. This is because of the defined periods of long-term silencing that must be appropriately maintained and coordinated, both after mass transcription in growth-stage-specific primary spermatocytes and then again after post-meiotic transcriptional reactivation in mid-to-late elongating spermatids. Ensuring that these two sets of mRNAs are only translated as and when needed, despite such variable and differential spatiotemporal profiles of expression, is no mean feat.

As 11 of the 29 Imp-enriched protein interactors were associated with translational regulation and ribosome biogenesis, this suggests that these interactions with Imp correspond to the post-transport stages of mRNA localisation. Seven of these proteins (PABP, small ribosomal subunit protein eS6, eIF4G2, large ribosomal subunit protein eL6, small ribosomal subunit protein uS12, large ribosomal subunit protein eL22 and 40S ribosomal protein S15) may define the transition from translational repression and degradation protection to active local translation of localised mRNAs within Imp RNP complexes at their target subcellular destinations in spermatids.

There is, of course, the possibility that these components were themselves undergoing transport as part of the Imp RNP complex when they were captured by CI-AP. However, we also know that there are several heterogeneous populations of ribosomes in the testis and developing sperm cells, including ribosomes throughout the spermatid tail-ends (Tokuyasu 1975; Mageeney and Ware 2019). One set of specialist ribosomes can even be found in subcellular region towards the tip of the elongating axonemes in spermatids – with these specific ribosomes only present during, but not after, elongation (Tokuyasu 1975). Taken together, this suggests a defined requirement for protein synthesis at the tail-ends of the spermatids, which may perhaps coincide with the final anchoring site of localising Imp RNP complexes.

4.11.5.1. PABP is a highly conserved core constituent of localising RNP complexes

Drosophila PABP has been strongly implicated in modulating the switch of translationally repressed RNP-complexed mRNAs into a translationally active state, so it makes sense that it has been isolated from the purified multi-protein Imp RNP complexes. It has long been characterised as a common and conserved core component of many RNP complexes, and has been thoroughly investigated in terms of the organisation and localised transport of maternally-derived developmental mRNAs (Clouse et al. 2008; Vazquez-Pianzola et al. 2011). Therefore, it is not unreasonable to assume that PABP may be performing similar regulatory mechanisms in the male spermatid cyst bundles, by interacting and functioning alongside Imp to drive the localisation and local translation of post-meiotic mRNAs at the spermatid tail-ends.

However, screening of a chimeric PABP-GFP protein trap line suggests that PABP is localised as a single ring-like granule in the nuclei of elongating spermatids – which gradually increases in signal and is spatially separated from the chromatin. This is notably different to the concentrated pool of localised Imp protein that is expressed at the spermatid tail-ends, and instead suggests an earlier, contrasting role in the post-meiotic transcription of comet and cup mRNAs, rather than in their post-transcriptional regulation or localisation (Nerusheva et al. 2009).

PABP is not a testis-specific protein. Nevertheless, there is clear evidence that PABP has roles in the male germline. For example, hypomorphic *PABP* mutants show several meiotic defects in the primary spermatocytes, including abnormalities in the centrosomes, spindles and centrioles, which together result in male sterility (Blagden et al. 2009). *PABP* deficient testes also had “onion stage” spermatid cysts that only contained a syncytium of thirty-two interconnected cells instead of the normal sixty-four – suggesting that only one round of meiosis had been completed in place of the usual two meiotic divisions. On top of this, the mutant onion stage nuclei and Nebenkern were unusually large, and, in some cases, there was only a single enlarged Nebenkern associated with multiple nuclei in the spermatids, indicating cytokinesis failure (Blagden et al. 2009).

Pertceva et al. (2010) reinforced these findings by confirming that mutations in *PABP* do indeed cause severe impairments to *Drosophila* sperm development, including defects in meiotic cytokinesis and in spermatid elongation. In the onion and post-elongation stages of *PABP* mutant spermatids, there were irregularities in the size and shaping of nuclei and Nebenkern at the final stages of spermatid differentiation. Mutant nuclei failed to elongate into their characteristic needle-like morphology, and did not polarise to the “head” end of the spermatids; they were instead scattered in disarray throughout the elongating spermatid cyst bundles. The mitochondrial derivatives were also found to disintegrate and fragment in the absence of PABP and were unable to form an effective attachment to the axonemes in elongating spermatids. This suggests important roles for PABP in multiple stages of male gametogenesis, with functions in meiosis, cytokinesis and spermatid elongation that are all essential for proper *Drosophila* sperm development.

Altogether, PABP is an interesting protein binding partner of Imp. Outside of the testis, it is known to be involved in promoting cell growth and proliferation in wing tissues (Roy et al. 2004), as well as dendrite morphogenesis and branch development in sensory neurons (Olesnicky et al. 2018). Activities such as these could be possibly adapted by PABP when it operates in the testis, facilitating similar regulatory functions in the production of properly developed, mature sperm.

4.11.5.2. The testis-specific eukaryotic initiation factor, eIF4G2, is crucial for male fertility

There are multiple isoforms of eIF4G in *Drosophila*, some of which are testis-enriched (Ghosh and Lasko 2015). While there is a canonical eIF4G protein, the eIF4G2 isoform we have detected here is testis-specific. Both do, however, interact with PABP and share strong conservation in their middle domains and C-termini (Baker and Fuller 2007; Franklin-Dumont et al. 2007; Ghosh and Lasko 2015). eIF4G2 mutant flies remain viable and female fertile, but males are sterile – thus confirming the fundamental effects of eIF4G2 activity in the testis (Baker and Fuller 2007; Ghosh and Lasko 2015). It is extremely reassuring that it is this eIF4G2 isoform which has been

specifically flagged up in our Imp-GFP enriched samples; indicating that Imp:eIF4G2 binding is indeed a testis-exclusive interaction.

Unlike canonical *eIF4G*, transcripts for the *eIF4G2* isoform persist throughout the spermatocytes and in post-meiosis – and so too does expression of the eIF4G2 protein – suggesting that eIF4G2 may serve as the main eIF4G factor for translational control in the late stages of *Drosophila* sperm development (Baker and Fuller 2007; Franklin-Dumont et al. 2007; Ghosh and Lasko 2015). In fact, the expression pattern of eIF4G2 in the growing spermatids seems to include a localised accumulation of eIF4G2 protein to the extreme tail-ends of the cells, which overlaps spatially with Imp protein expression (Fabrizio et al. 2008; Nerusheva et al. 2009; Ghosh and Lasko 2015). This indicates that the Imp:eIF4G2 we have captured in our CI-AP proteomics data is from the latter cell stages, predominantly from the elongating spermatid cyst bundles, which we have a particular interest in.

Early characterisation of eIF4G2 mutant testes revealed stalling at the spermatocyte stage, with these spermatocytes failing to execute the meiotic G_2-M transition or proceed into spermatid differentiation and elongation. Knockdowns in eIF4G2 can correspond to the development of a severe meiotic arrest phenotype or, if meiosis does proceed, an omission of several key events of the meiotic divisions (e.g., aberrant chromosome condensation) (Wakimoto et al. 2004; Baker and Fuller 2007; Franklin-Dumont et al. 2007). Should early eIF4G2 mutant spermatids develop, they are morphologically abnormal, with large nuclei, aberrant mitochondrial and MT organisation, and stunted elongation (Baker and Fuller 2007). Altogether, this confirms the widespread effects of eIF4G2 in proper meiotic cell cycle progression and in post-meiotic spermatid differentiation.

A more recent systematic, stage-specific UAS-RNAi knockdown of *eIF4G2* in the male germline and somatic cells has revealed that eIF4G2 is needed at multiple points throughout sperm development (Ghosh and Lasko 2015). In early germ cells, eIF4G2 ensures proper meiotic entry and division, whereas in spermatids it regulates elongation. Knockdown of *eIF4G2* in the spermatocytes results in meiotic arrest at the G_2-M transition. In developing spermatids, a loss of eIF4G2 corresponds with aberrant nuclear changes, as well as a loss of elongating flagellar axonemes and a loss of

elongated, differentiated tails – with some cells arresting in early elongation and degenerating soon after (Ghosh and Lasko 2015).

In contrast, *eIF4G2* knockdowns did not reveal any phenotypic effect on somatic cyst cells. While loss of eIF4G on its own did not display a phenotype or any consequences on male fertility, a combined knockdown of both eIF4G and eIF4G2 amplified phenotypic severity above that observed in the single *eIF4G2* deficient testes. Double knockdowns led to more severe defects in early sperm development, including arrest at the spermatogonial phase; hence indicating functional redundancy and cross-talk between the two factors (Franklin-Dumont et al. 2007; Ghosh and Lasko 2015).

eIF4G2 is thus required for the production of viable sperm cells, and is likely part of an alternative, specialised eIF4F complex in the *Drosophila* testis. However, eIF4G2 is not required for the translation of all mRNAs in mature spermatocytes and post-meiotic germ cells (Baker and Fuller 2007). Therefore, eIF4G2 must function specifically for the translation of a subset of testis-specific transcripts in late-stage sperm development.

Considering this, eIF4G2 may even be employed for the targeted translational regulation of post-meiotic gene products, including the comet and cup mRNAs. At least some of eIF4G2's activity may be attributed to its distinct interactions with Imp in post-localised RNP complexes.

4.11.5.3. Enrichment of the large ribosomal subunit protein eL22 (RpL22) supports a role in the post-transcriptional regulation

The large ribosomal subunit protein eL22 (RpL22) is associated with a whole host of functions in *Drosophila* (Table 9.), but its role in eukaryotic ribosome heterogeneity is of significant relevance here. RpL22 is essential in fly development and is necessary for proper sperm maturation and male fertility (Mageeney et al. 2018). It is assembled into ribosomes and polysomes in a stage-specific manner during the course of sperm development (Kearse et al. 2013; Mageeney and Ware 2019).

RNA-Seq analysis of RpL22 ribosomes and polysomes, along with those of its RpL22-like paralogue, has revealed a differential association of certain subsets of mRNAs, including, most importantly, those that are encoded by the comet and cup genes. In fact, twenty of the original twenty-four comet and cups were identified in the RNA-Seq dataset, sixteen of which (~67%) were found to be in association with both RpL22 paralogue-specific ribosome types. mRNA transcripts for *davis-cup*, *stanley-cup* and *flyers-cup* were all enriched on the RpL22 polysomes, while *ryder-cup* mRNAs were associated with RpL22-like polysomes. This was the only subset of late-stage testis-specific transcripts that were found to be preferentially associated with RpL22, suggesting that a subpopulation of RpL22 ribosomes and polysomes function specifically in the post-meiotic elongating spermatids for the translation of these comet and cup mRNA transcripts (Mageeney and Ware 2019). These preferential interactions may in turn correspond to a distinct change in the subcellular localisation of the majority of RpL22, which is characterised by a cytonuclear shift in its distribution as the germ cells progress into the meiotic spermatocyte stage (Kearse et al. 2013; Mageeney and Ware 2019).

Together, this presents additional evidence in support of specialised roles in translation that are specific to the latter stages of male germline differentiation; the regulation of which may involve Imp in some way, as indicated by the Imp:RpL22 interaction we have elucidated here. Quite remarkably, RpL22 may be a key interactor of Imp-GFP that not only sheds light on Imp's regulatory function in the post-meiotic stages of *Drosophila* sperm development, but on the mRNA constituents of its wider RNP complexes. Most crucially, however, this reinforces our RNA-affinity pull-down findings in Results Chapter 1 and provides an unquestionable link between Imp and the post-transcriptional regulation of comet and cup mRNAs in growing post-meiotic spermatid cyst bundles – whether this be through a direct interaction, or indirectly via other scaffolding and adaptor protein factors in the wider Imp RNP complex.

4.11.6. Using endogenous tissues for protein:RNA complex characterisation in CI-AP outperforms the alternative of heterologous systems

Although many *in vitro* biochemical immunoprecipitation approaches rely on heterologous expression – including bacterial expression systems – we have instead used *Drosophila* testes as a direct source of native, endogenous RNAs and proteins here. While we have indeed extracted these biomolecules out of their *in vivo* cell-based physiological environment to probe for interactions, the CI-AP assay has been optimised to be as least denaturing and harmful as possible.

Our CI-AP procedure does rely on fluorescent transgenic lines for specific tagging of Imp and Sqd proteins, but this is where genetic engineering ends. Heterologous expression of target proteins and respective mRNA complexes, on the other hand, is driven by entirely genetic manipulation – via the introduction of one species-specific gene into another "host" species system. This can have various advantages depending on the recipient expression system in question but can also result in inefficient expression and low protein yields (Watts *et al.,* 2021).

It is known that factors such as mRNA processing, splicing activities and post-translational modifications (PTMs) are all crucial for downstream protein structure and function (Watts *et al.,* 2021). Reports from work in plants suggest that, even in the case of heterologous systems where "strong" promoters have been implemented, the expression of proteins can be inefficient or hindered entirely when these features have not been properly considered (Haseloff *et al*., 1997; Diehn *et al*., 1998). However, when it comes to methods such as CI-AP, no extra concerns about endogenous PTMs and native structural folding is necessary. A good compromise is made between utilising endogenous target proteins and their interacting RNAs expressed from *in vivo* sources and precipitating them out in a purified form *in vitro* via the tripartite GFP-TRAP-Sulfo bead reagent.

In either case, affinity tags can be utilised for the precipitation of both endogenously expressed proteins and heterologous-expressed recombinant proteins. For the purification of protein complexes, including via the GFP-TRAP-Sulfo beads employed here, affinity tagging offers one common, high-throughput method for the effective

trapping of nearly all target proteins – whether characterised or otherwise. Moreover, utilising GFP and YFP as our affinity tag of choice has the added advantage of permitting the dynamic *in vivo* localisation and functionality of the Imp and Sqd fusion proteins within the testis, prior to isolation (Tariq et al. 2020b). We could therefore exploit this to explore localised RNP complexes in the tail-ends of spermatid cyst bundles. As a combinatorial approach, it also had the additional benefit of not being reliant on any pre-existing knowledge of a protein's biochemical properties or biological functions (Arnau *et al*., 2006).

Overall, we have demonstrated the ability to trap and purify interacting factors via a ChromoTek GFP-binding nanobody (Product Code: gt-250), but, in theory, any type of antibody or nanobody could be coupled to the beads and used as a CI-AP reagent.

4.11.7. The choice of control requires further consideration for all future experimental repeats

Since performing this study, an experimental replicate has been undertaken with ease, following the exact set-up as presented here. While the follow-up comparative proteomics and RNA-Seq analysis of this repeat has yet to be completed for us to compare these results against, we can have confidence in the modified protocol we have developed here.

Both Imp and Sqd are known RBPs but are active and upregulated at different points during *Drosophila* sperm development – therefore, we assumed that they would have distinct sets of protein and RNA binding partners. Under this premise, proteins present with the greatest difference in abundances between the Sqd-YFP-bound control and Imp-GFP-bound sample were deemed to be genuine interactions. Any other overlapping proteins were attributed to biomolecular artefacts that may have been captured inadvertently due to the wide-ranging binding capacities of both RBPs. Similarly, RNAs upregulated in both the Sqd-YFP-bound control and Imp-GFP-bound sample, when compared to the input, were also assumed to be non-specific or background. This choice of internal control made the most sense when we were first determining how to tackle the characterisation of the Imp interactome.

Prior to this experimentation, we had some initial expectations as to the suspected pool of RNAs and proteins that would present uniquely. We were also aware that there would likely be some crossover, with some proteins and RNAs likely to be co-purified in both conditions – but we did not think there would be many. However, unfortunately, this idea of a mainly “all or nothing” overlap between the interactome of Imp and Sqd was not as unequivocal or straightforward as we had anticipated. The fact that *sqd* transcripts were also detected in the wider Imp-enriched RNA-Seq dataset reinforces these complications (Appendix B, Supplementary Data File 5.). Perhaps we should have had a greater consideration of the putative overlap between Imp and Sqd that has been indicated outside of the testis before settling on Sqd-YFP as an internal control (Geng and Macdonald 2006; Clouse et al. 2008; Hansen et al. 2015).

A third Cl-AP experiment has subsequently been conducted by other colleagues in the lab, with a slight deviation to our initial method of control sample employed here. Instead of an internal control, they chose to implement a non-fluorescently labelled WT control, comprising testes that should not express any tagged-protein component. Based on this assumption, any protein or RNA detected in the resultant control samples were deemed to be contaminants or non-specific background that could then be discounted from the main experimental dataset. In retrospect, we would revert to this choice if we were to repeat this experiment for a final time.

4.11.8. Conclusions

Many of Imp’s protein binding partners we have identified and focused on here exhibit quite varied overarching functions in translation regulation and F-actin binding/organisation. Yet, they appear to be either directly linked to spermatid elongation and individualisation or have morphological and growth-related roles in other systems that could indicate similar activities in spermiogenesis if they were to be investigated further within the male fly reproductive system. We therefore thought it would be interesting to see whether Imp itself is directly involved in the morphological remodelling and elongation of spermatids, and hence whether an RNAi-induced knockdown of the *imp* gene resulted in any observable phenotypic defects in spermatid differentiation in affected testes.

We also wanted to see whether an absence of functional Imp had any consequences on the post-meiotic expression and localisation of comet and cup mRNAs because of their identification in our RNA-Seq data. Since there appears to be a tight association between Imp and translational activators, there may also be effects on the translation and protein distribution of comet and cups in *Drosophila* spermatid cyst bundles. A loss of functional *imp* may therefore lead to a loss of the foundation of the RNP complex, which is in turn responsible for the recruitment of various translational activators for the local translation of these post-meiotic mRNA transcripts.

Unfortunately, we were unable to incorporate entirely what we had found here, including knowledge of new potential Imp interactors, into our follow-up phenotypic analysis of *imp* gene knockdowns (Results Chapter 3). This was because we only succeeded in performing the full, optimised CI-AP experiment, with all corresponding proteomics and RNA-Seq data returned and ready for analysis, once the main bulk of Imp-UAS-RNAi screening had already been completed. As such, we had no time to integrate in the characterisation of these putative multi-functional, multi-protein Imp RNA complexes *in vivo*. We did, however, investigate the impact that loss of *imp* has on post-meiotic comet and cup regulation in the spermatids.

5. RESULTS CHAPTER 3: Using phenotypic analyses of Imp-RNAi knockdown lines to determine the functional role of Imp in *Drosophila* sperm development

In this chapter, we will wrap up our investigation of Imp in the *Drosophila* testis and in the context of comet and cup mRNA localisation within the spermatid cyst bundles.

To achieve this, we have conducted RNAi screening to investigate the functional roles of Imp in sperm development, with a specific focus on the differentiation and elongation of highly specialised and polarised spermatids.

5.1. RNAi screening was performed using the robust Gal4/UAS binary expression system and validated UAS-RNAi lines

The main premise of RNAi is that the phenotypic effects detected in knockdown mutants can be confidently attributed to the targeted action of RNAi hairpins alone. In *Drosophila*, RNAi knockdown experiments therefore rely on the precise, tissue-specific expression of disruptive RNAi-hairpins to prevent non-specificity and off-target target activities. This is achieved via the use of the spatiotemporally regulated Gal4/Upstream Activating Sequence (UAS) bipartite expression system.

Fischer et al. (1988) and Brand and Perrimon (1993) pioneered the successful adaption of the yeast binary Gal4/UAS expression in *Drosophila* (Fig. 29.). This involves the promoter for a specific gene of interest being cloned and integrated upstream of the yeast-derived transcription factor gene, *Gal4*. The presence of this tissue-specific promotor ensures that the precise expression of the transgenic construct, and hence the Gal4 protein, is under the experimenter's control. As the Gal4 protein has no endogenous targets within *Drosophila*, this provides an extra level of control in time and space. Gal4 will only be functional when introduced into a system

that also contains a corresponding transgene arrangement containing the complementary yeast promoter element of the UAS. In such scenarios, Gal4 recognises and binds to the transgenic UAS target, activating the precise expression of a downstream gene that may encode a short UAS-RNAi hairpin or a fluorescently tagged reporter protein, for example (Brand and Perrimon 1993; Jones 2009).

The two-component Gal4/UAS expression system has been fundamental for forward genetics screening, including the identification of gene functions via phenotypic analyses of overexpression, knockdown and ectopic expression experiments, as well as in mutagenesis-based enhancer and gene trapping. It has also been exploited for gain-of-function and loss-of-function studies, and for the purposes of annotation and fluorescent labelling to track biological processes, changes in expression profiles, and architectural/morphological modifications over time and space (Duffy 2002; del Valle Rodríguez et al. 2012). While the Gal4/UAS expression system is not reversible, it can be modified by changes to temperature. Therefore, the temperature of rearing can be adjusted to modulate Gal4 expression, enabling investigations to be pinpointed to specific stages of the fly lifecycle (McGuire et al. 2003; McGuire et al. 2004).

Various large-scale projects have been undertaken with the sole objective of generating collections of tissue-specific Gal4 promoters and/or libraries of UAS-driven genetic tools of interest, including transgenic RNAi hairpin constructs against specific genes. These are widely available to researchers around the world and may be shared between collaborators or purchased in the form of fly-expressing lines from key stock centre distributors. Tissue-restricted Gal4 lines have been developed for the study of *Drosophila* en masse (Hayashi et al. 2002), including in neurobiology (Pfeiffer et al. 2008; Jenett et al. 2012; Li et al. 2014a), embryogenesis (Kvon et al. 2014), and the gastrointestinal tract (Lim et al. 2021), to name just a few. Some genome-wide UAS-RNAi libraries include the Transgenic RNAi Project (TRiP) provided by the Bloomington *Drosophila* Resource Centre (BDSC) (Zirin et al. 2020; Hu et al. 2021), as well as the GD Transgenic RNAi Library (Dietzl et al. 2007), KK RNAi Library and shRNA Transgenic RNAi Library (Ni et al. 2011), all supplied by the Vienna *Drosophila* Resource Center (VCRC).

Overall, the tissue-specific Gal4/UAS binary expression system has become a core component of a Drosophilist’s ever-growing arsenal of genetic tools, and is central to

our understanding and characterisation of the endogenous genetic and functional interplay of novel genes *in vivo*. We will therefore be utilising it here for the investigation of Imp's activity in late *Drosophila* sperm development.

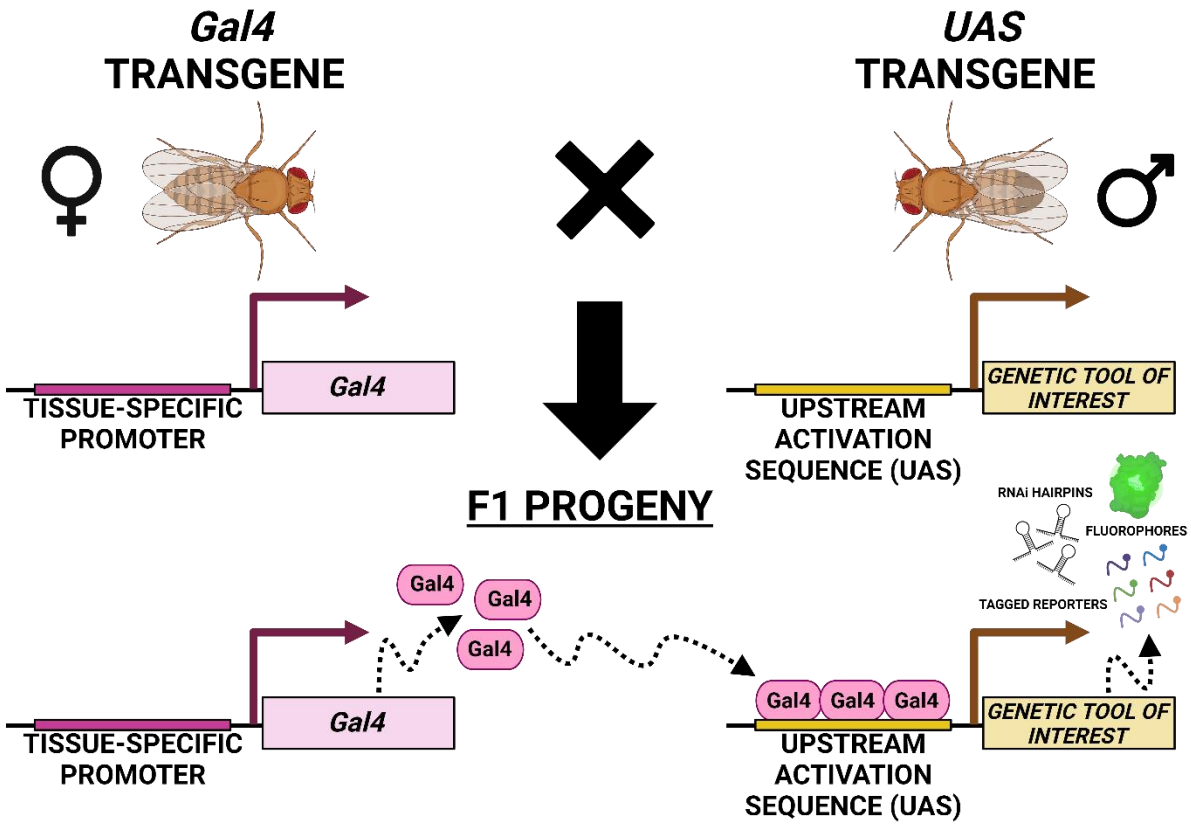

Figure 29. Schematic of the Gal4/Upstream Activating Sequence (UAS) binary expression system in *Drosophila*. Genetic crosses result in the Gal4-driven expression of transgenic UAS genetic tools of choice in fly progeny, all with an extremely high level of spatiotemporal control. Fly driver lines expressing the transgenic arrangement of the tissue-specific Gal4 promoter can be crossed with a separate fly line that carries the UAS effector transgene. This drives expression of the yeast transcription factor, Gal4, in a particular organ of choice or subset of cells within the resultant progeny, which now also possess the transgenic UAS configuration. The Gal4 protein recognises and binds to this UAS target, activating transcription of an associated gene of interest in tissue-specific expression patterns (Brand and Perrimon 1993; Jones 2009). **Re-created with modifications from Brand and Perrimon (1993) and Jones (2009) using BioRender.com.**

5.1.1. Development of the Bam-Gal4:VP16/UAS system in *Drosophila*

There are three main Gal4 drivers that permit the study of gene function within the male germline in *Drosophila*: Nanos-Gal4, Vasa-Gal4 and Bam-Gal4:VP16 (Doren et al. 1998; Tracey et al. 2000; Chen and McKearin 2003b; Zhao et al. 2013). Each have slightly different, but overlapping, spatiotemporal profiles of expression.

All transgenic Nanos-Gal4 configurations are expressed within the GSC and early germline cysts, but activity beyond the spermatogonial stages is little, if any. The Vasa-Gal4 driver line, on the other hand, is expressed up to late spermatogonia and early spermatocytes, but the expressed gene product can persist throughout the male germline – even into round spermatids (Demarco et al. 2014; Butsch et al. 2023). Finally, the Bam-Gal4:VP16 arrangement is active throughout the mitotic germline cysts and in the spermatogonia, but the expressed gene product can persist well into the spermatocytes and post-meiotic round spermatids (Chen and McKearin 2003a; Chen and McKearin 2003b; White-Cooper 2012). The Bam-Gal4/UAS expression system is typically employed in our research group because it has the most useful pattern of expression. In the wildtype *Drosophila* testis, *bam* gene expression is first detected in two to sixteen cell transit-amplifying spermatogonial cysts and is not observable within the preceding germline stem cells or gonialblasts (Kiger et al. 2000; Tran et al. 2000; Singh et al. 2006; Demarco et al. 2014).

The transgenic Bam-Gal4:VP16 driver construct we have used here is a homozygous viable insertion on the third chromosome, originally cloned into pCaSpeR, which consists of a ~900bp testis-specific, germ cell-associated genomic *bam* promoter, 5’ UTR of the *bam* transcriptional unit, *Gal4::VP16* open reading frame and 3’ UTR of the *Hsp70* gene (Chen and McKearin 2003b; White-Cooper 2012). The Gal4::VP16 is part of this artificial transcriptional driver, which has been developed via fusion of the transcriptional activation domain from the Herpes simplex virus Type 1 *VP16* gene to the DNA-binding domain of Gal4 to enhance activity and efficiency of UAS transcriptional activation (Sadowski et al. 1988).

The activity of Bam-Gal4:VP16 has been successfully validated for the activation of expression of tagged fusion proteins and UAS-RNAi hairpin constructs in the testes

(Jiang et al. 2007; Doggett et al. 2011). For example, when recombined with a third-chromosome UAS-EGFP-Tombola (Tomb) insertion, fluorescence microscopy has demonstrated that the Bam-Gal4-VP16 transgene can drive strong expression of the EGFP-Tomb fusion protein – a tesmin/TSO1 CXC-domain member – in *Drosophila* primary spermatocytes. In doing so, this resulted in a rescue of the meiotic-arrest testis phenotype in homozygous *tomb* mutant males (Jiang et al. 2007). This same Bam-Gal4:VP16 driver was also used for the UAS-RNAi knockdown of the *Drosophila lin-52* homologue, *wake-up-call* (*wuc*), in the testis. A highly efficient knockdown effect on *wuc* transcript levels was subsequently determined via qRT-PCR and Western Blotting revealed a considerable depletion in WUC protein when compared to WT controls (Doggett et al. 2011). The Bam-Gal4/UAS system has even been effectively used for the ectopic expression of the apoptotic transgene, *hid*, in early differentiating male germ cells (Roach and Lenhart 2024).

Products from Bam-Gal4:VP16-driven UAS transgene expression are first detected in eight cell spermatogonial cysts; levels of UAS transgene products continue to rise, reaching a climax in early-mid primary spermatocytes before a subsequent decline as the spermatocytes mature (White-Cooper 2012). However, the longevity of this Bam-Gal4/UAS transgene expression profile does depend on the stability of its transgenic UAS-activated product, which may even persist into late-elongation stage spermatids in some cases (White-Cooper 2012). Overall, this Bam-Gal4:VP16 driver line enables the sustained effects of UAS effector transgene expression to be observed in spermatocytes and through into meiotic divisions to some extent (Demarco et al. 2014).

In our case, Bam-Gal4:VP16 was the best Gal4 driver option because GSC divisions could take place as normal within the testis stem cell niche, and early stages of sperm development could proceed unimpeded to establish a differentiated pool of early mitotic germline cysts in the *Drosophila* testis. Transcriptional activation of the Imp-UAS-RNAi effector transgene at this timepoint would therefore facilitate an in-depth phenotypic analysis that focused on the latter stages of sperm development. To truly determine the effects of our Imp-UAS-RNAi hairpin constructs, and hence the functionally of Imp, we needed this type of Gal4 driver expression pattern. This would establish modest knockdown phenotypes for our analysis by pinpointing the Imp-UAS-

RNAi hairpin expression to cover the pre-meiotic to post-meiotic transition (Demarco et al. 2014).

5.1.2. Experimentally validated UAS-RNAi hairpins from the Transgenic RNA Interference Project (TRiP) and Vienna GD Transgenic RNAi Library

For RNAi gene silencing to work efficiently and effectively, UAS-RNAi hairpin transgenes must be designed and constructed with precision. There are many factors to consider during this design process, which is why we instead relied on pre-made *Drosophila* RNAi lines that had already been subject to experimental validation. For example, RNAi-mediated degradation of gene-specific target mRNAs using long double-stranded hairpins requires perfect complementarity of at least nineteen nucleotides in length. When creating double-stranded UAS-RNAi hairpins, this is therefore an important parameter that must always be considered to avoid false positive error rates arising from off-target RNAi effects (Kulkarni et al. 2006).

Some of the Imp-UAS-RNAi lines used in this project are derived from those generated by the Transgenic RNA Interference Project (TRiP) and are commercially available from the BDSC (Perkins et al. 2015). These have been developed from the second-generation series of VALIUM (Vermilion-AttB-Loxp-Intron-UAS-MCS) knockdown vector constructs, pVALIUM20 and pVALIUM22, using modified microRNA scaffolding technology with a miR-1 cassette (Ni et al. 2008; Ni et al. 2009; Ni et al. 2011; Perkins et al. 2015).

pVALIUM20 and pVALIUM22 contain different backbones, with different promoter types and polyadenylation signals. This leads to differences in the attB/P site-specific integration of the RNAi hairpin structures into the *Drosophila* genome, as well as variations in expression levels depending on cell context (Table 16.). Among other features, both vectors contain: a *vermilion* selectable marker gene, an Ampicillin resistance gene (AmpR), a multiple cloning site and two groups of 5X UAS sites flanked by distinct loxp sites. The presence of distinct polyadenylation sequences facilitates expression, processing and nuclear export of the full-length UAS-RNAi hairpin structure (Ni et al. 2011; Perkins et al. 2015). Both VALIUM RNAi vector types

were used in this project to ensure that the full phenotypic effects of Imp-UAS-RNAi knockdowns were observed in the testis, regardless of cell context.

Table 16. Key properties of the *Drosophila* VALIUM knockdown constructs, as generated by the TRiP library. This includes the original vector plasmids, integration landing sites, optimal expression profiles, promoter types, polyadenylation (polyA) signal source and RNAi hairpin structures. Design strategies centred on combining features that permit the highest levels of gene-specific inducible expression (Ni et al. 2011; Perkins et al. 2015). Selection of attP2 and attP40 as optimal landing sites for ΦC31 integration of the transgenic TRiP UAS-RNAi hairpin constructs was based on analyses of basal and Gal4-inducible expression profiles using integrated UAS:luciferase reporter assays (Markstein et al. 2008). The attP40 landing site was located on the second chromosome whereas attP2 was located on the third chromosome. Both insertions were homozygous viable (Markstein et al. 2008; Perkins et al. 2015). pVALIUM22 also showed some weaker knockdown effects in the male germline.

Knockdown vector	Genomic landing sites	Strongest cell type knockdown	Promoter type	Source of polyA signal sequence	Structure of RNAi hairpin
pVALIUM20	attP2 and attP40	Soma and male germline	Hsp70 TATA basal promoter	SV40 3' UTR	Short, double-stranded 21 nt RNA
pVALIUM22		Female germline	P-transposase core promoter	K10 PolyA	

These hairpin-containing UAS transgenes are incorporated into specific regions of the *Drosophila* genome using an optimised, site-specific recombination method that utilises ΦC31 integrase activity. Targeted introduction into the genome via the optimal landing sites of attP2 and attP40 enhances TRiP line production and potency, and reduces the incidence of false negatives – this improves upon random integration methods, which have the potential to incorporate into poorly expressed genomic loci (Groth et al. 2004; Ni et al. 2008). Design of the gene-specific short RNA (shRNA) hairpin sequence itself was automated via a proprietary TRiP Perl program (Perrimon and Mathey-Prevot 2007; Ni et al. 2008). Overall, the TRiP Imp-UAS-RNAi hairpin constructs express short, double-stranded hairpin RNAs with a perfect duplex structure that consist of a 21-bp targeting sequence embedded into a micro-RNA (miR-1) scaffold. This offers effective gene knockdowns in both the germline and somatic cells, with ~65% of the TRiP RNAi lines, on average, exhibiting knockdown efficiencies that are greater than 50% (Ni et al. 2011; Perkins et al. 2015).

The final Imp-GD UAS-RNAi construct used here is part of the GD Transgenic RNAi Library and is commercially available from the Vienna *Drosophila* Resource Center (VDRC). The GD Transgenic RNAi Library currently comprises more than 16,000 molecularly validated transgenic fly lines (Dietzl et al. 2007). All GD UAS-RNAi transgenes within the collection were originally constructed by cloning short, inverted repeats into a modified pUAST vector called pMF3. These repeats were amplified from gene-specific regions – many of which corresponded to exons common to all predicted transcripts for that gene, or included regulatory regions such as the 5’ and 3’ UTRs (Brand and Perrimon 1993; Dietzl et al. 2007). Together, the GD UAS-RNAi transgenes, including the Imp-GD UAS-RNAi construct, contain gene-specific inverted repeats of between 300 to 400 bp, which are downstream of a UAS promoter that consists of 10 copies of the UAS signal to enhance expression levels (Dietzl et al. 2007).

All GD UAS-RNAi lines were generated by integration into the *Drosophila* genome via P-element-mediated transposition. This random integration into the genome can potentially result in positional effects, wherein expression levels of the GD UAS-RNAi hairpins can vary depending on the integration site (Dietzl et al. 2007). However, it is estimated that at least 80% of the GD RNAi lines drive sufficient levels of UAS-RNAi transgene expression to mediate targeted gene silencing (Dietzl et al. 2007).

Successful conditional inactivation of single protein-coding genes, including *imp*, also depends on the GD UAS-RNAi hairpin structure itself. When expressed in *Drosophila*, these GD UAS-RNAi constructs encode double-stranded long hairpin RNAs. For the Imp-GD UAS-RNAi line specifically, the transgene construct is a P-element insertion on Chromosome 3, which expresses a UAS-inducible 316 nucleotide long double-stranded RNAi hairpin against the *imp* gene with zero official off-targets. The Imp-GD-UAS-RNAi transgene can also be combined with UAS-Dicer2 to increase RNAi potency, as is the case here (Dietzl et al. 2007).

All RNAi lines used here, regardless of the source collection, expressed inducible UAS-RNAi hairpin constructs, with targeted tissue-specific gene expression mediated under the control of the temperature-sensitive UAS promoter (Brand and Perrimon 1993; Ni et al. 2011).

Each *Drosophila* line expressed a Gal4-dependent, RNAi-specific UAS-hairpin transgene comprising Gal4 binding sites within its preceding UAS enhancer. Crossing of our parental Bam-Gal4:VP16-containing flies with these Imp-UAS-RNAi flies therefore introduced the yeast transcription factor, Gal4, into the two-part system of the resultant F1 progeny. Gal4-UAS binding activated transcription, inducing expression of the UAS-RNAi hairpins. These recognised and targeted the *imp* gene, knocking down expression of Imp in the eight cell spermatogonial cysts and beyond (Fischer et al. 1988; Brand and Perrimon 1993; White-Cooper 2012).

From our understanding of the wider literature, the Bam-Gal4:VP16 driver has not been described as a "leaky" Gal4 transgene in the *Drosophila* testis. Hence, our parallel cross to w^{1118} provided a negative control of the WT genetic background. Without the Bam-Gal4:VP16 driver present, there would be no expression of the Gal4 protein and no downstream Gal4-mediated transcriptional activation of the transgenic Imp-UAS-RNAi construct. In the absence of Imp-UAS-RNAi hairpin expression, there should be no Imp-RNAi knockdown phenotype to report.

5.2. Preliminary characterisation of transgenic fluorescently tagged comet and cup protein reporter constructs

Before performing our Bam-Gal4:VP16/Imp-UAS-RNAi screening, we first conducted a validation screen of four transgenic TagGFP-labelled comet and cup protein reporter constructs (*c-cup*-TagGFP, *schuy*-TagGFP, *sunz*-TagGFP and *wa-cup*-TagGFP fusions). We did so with the aim of validating the identity and sustained expression of each fluorescently tagged transgenic variant. We also set out to sort the lines for further analysis and determine which constructs would provide the best candidates for phenotyping *imp* gene function in the context of its knockdown effects.

As part of our current stock collection, we already had access to seven fluorescently tagged reporter constructs for four cup genes (*c-cup*, *wa-cup*, *d-cup* and *p-cup*) and three comet genes (*schuy*, *sunz* and *soti*) in total. Of these, the transgenes for *d-cup*, *p-cup* and *soti* were all tagged with TagRFP while the rest were tagged with TagGFP. These TagRFP and TagGFP reporter constructs were all generated as part of a previous project, but their corresponding fly lines had yet to be properly analysed or published in full. However, we did know from preliminary in-house investigations that, whilst the TagGFP signals for *c-cup*, *wa-cup*, *schuy* and *sunz* were all generally quite strong overall, expression of the TagRFP fused to *d-cup*, *p-cup* and *soti* was relatively weak. We now believe that the TagRFP reporter signals may have been weaker due to the extended maturation half-time and lower photostability of the fluorophore compared to TagGFP (Subach et al. 2008). Nevertheless, for experimental ease, we chose to exclude these TagRFP fly lines from further investigation. As such, only the four TagGFP-tagged reporter constructs for *c-cup*, *wa-cup*, *schuy* and *sunz* were considered in our initial round of selection.

These lines have been genetically engineered for the post-meiotic synthesis of comet and cup TagGFP fusion proteins alongside the native, endogenous non-tagged comet and cup proteins to replicate their asymmetrical, subcellular localisation patterns. The level and distribution of comet and cup fusion protein expression was qualitatively examined and compared in each fly line by visualising the fluorescence signals under the microscope. Fluorescence signal strength corresponded to the expression levels

of these transgenic TagGFP-labelled comet and cup proteins in developing spermatid cyst bundles of the *Drosophila* testis (Fig. 30.).

Here, we present developing cyst bundles of 64 interconnected spermatids, in whole *Drosophila* testes, which were representative of the average signal intensity and asymmetric expression patterns exhibited by our comet and cup TagGFP reporter lines (Fig. 30.). As predicted, the fluorescent protein reporters were all subject to local translation and protein gradient formation due to their preceding non-uniform mRNA localisation patterns. This was an extremely novel result when considering that these transgenes had yet to be published or properly described elsewhere.

In chronological order, there was a relatively uniform but striped expression pattern of the c-cup-TagGFP fusion protein, which extended throughout the entire length of the spermatid cyst bundles. This corresponded to expression throughout the mitochondrial derivatives. Fluorescence signals indicated the establishment of a gradient of c-cup-TagGFP protein upon local translation, which was highest at the spermatid tail-ends and declined in concentration towards the nuclear head-end (Fig. 30A – 30A”). Although not shown here, localised c-cup-TagGFP was also expressed in the mitochondria of spermatocytes.

In the *schuy*-TagGFP line, on the other hand, there was a distinctive speckling of schuy-TagGFP fusion protein in discrete puncta that corresponded to each individual spermatid cell, with expression predominantly localised to the tail-ends of growing spermatid cyst bundles. A gradient of decreasing protein concentration extended throughout the spermatid lengths towards the nuclear head-end, with the highest amount of schuy-TagGFP protein accumulating in a site at the extreme tail-ends subsequent to local synthesis (Fig. 30B – 30B”).

When compared to the other three transgenic fluorescent reporter lines, the *sunz*-TagGFP fusion was by far the most uniformly and weakly expressed throughout the spermatid cyst bundles, with the lowest intensity of fluorescence signals overall. After local translation, the sunz-TagGFP protein did not remain restricted to regions similar to its localised mRNA transcripts and was instead much more diffuse along the length of the spermatids towards the nuclear head-ends (Fig. 30C – 30C”).

Finally, the *wa-cup*-TagGFP reporter line exhibited a striped appearance of wa-cup-TagGFP protein expression in the spermatids. Following local protein production, the

wa-cup-TagGFP fusion protein accumulated at high concentrations and was primarily localised to discrete regions at the extreme tail-ends of the spermatids, similar to its localised mRNA transcripts. Minimal fluorescence signals were detected elsewhere in the spermatid cyst bundles (Fig. 30D – 30D'').

In general, the expression profiles for all our transgenic comet and cup fluorescent reporter lines meet our expectations of local protein production and protein gradient formation. We can conclude that all fly lines continue to express their respective comet and cup TagGFP fusion proteins stably, in the spatiotemporal patterns predicted from earlier work. When comparing overall fluorescence signal intensities, the *sunz*-TagGFP and *wa-cup*-TagGFP lines were certainly weaker in expression than *schuy*-TagGFP and *c-cup*-TagGFP (Fig. 30.). However, this was partially anticipated due to previous experiences using these lines (H. White-Cooper, Personal Communication).

Overall, we have validated the identity of all relevant comet and cup fluorescent reporter fly lines we have available in the lab. We can confirm the continued and stable local synthesis of all fluorescently tagged comet and cup protein reporters, and the continued generation of their dynamic yet characteristic localised protein gradients throughout the spermatid cyst bundle tails.

The schuy-GFP and c-cup-GFP fusions generally offered better prospects for microscopy-based phenotypic analysis because they consistently produced robust fluorescence signals that were superior to sunz-TagGFP and wa-cup-TagGFP – hence indicating greater levels of local protein expression overall. On the basis of this preliminary screen, we decided to take forward the schuy-TagGFP and c-cup-TagGFP lines for our phenotypic RNAi analysis; so that we could determine the function of Imp in the post-transcriptional regulation of at least one comet and one cup gene candidate. Our RNA-affinity pull-down findings in Results Chapter 1 also support the *in vitro* binding of Imp to *schuy* and *c-cup* mRNA transcripts – which is a good starting point for both.

While we still suspect that the regulatory mechanisms which govern comet and cup mRNA localisation are more diverse within the gene classifications than between them, we aimed to examine the effect of *imp* deficiencies *in vivo*, in the context of both post-meiotic gene classes. Investigating Imp-UAS-RNAi gene silencing in these *schuy*-TagGFP and *c-cup*-TagGFP lines should achieve this aim.

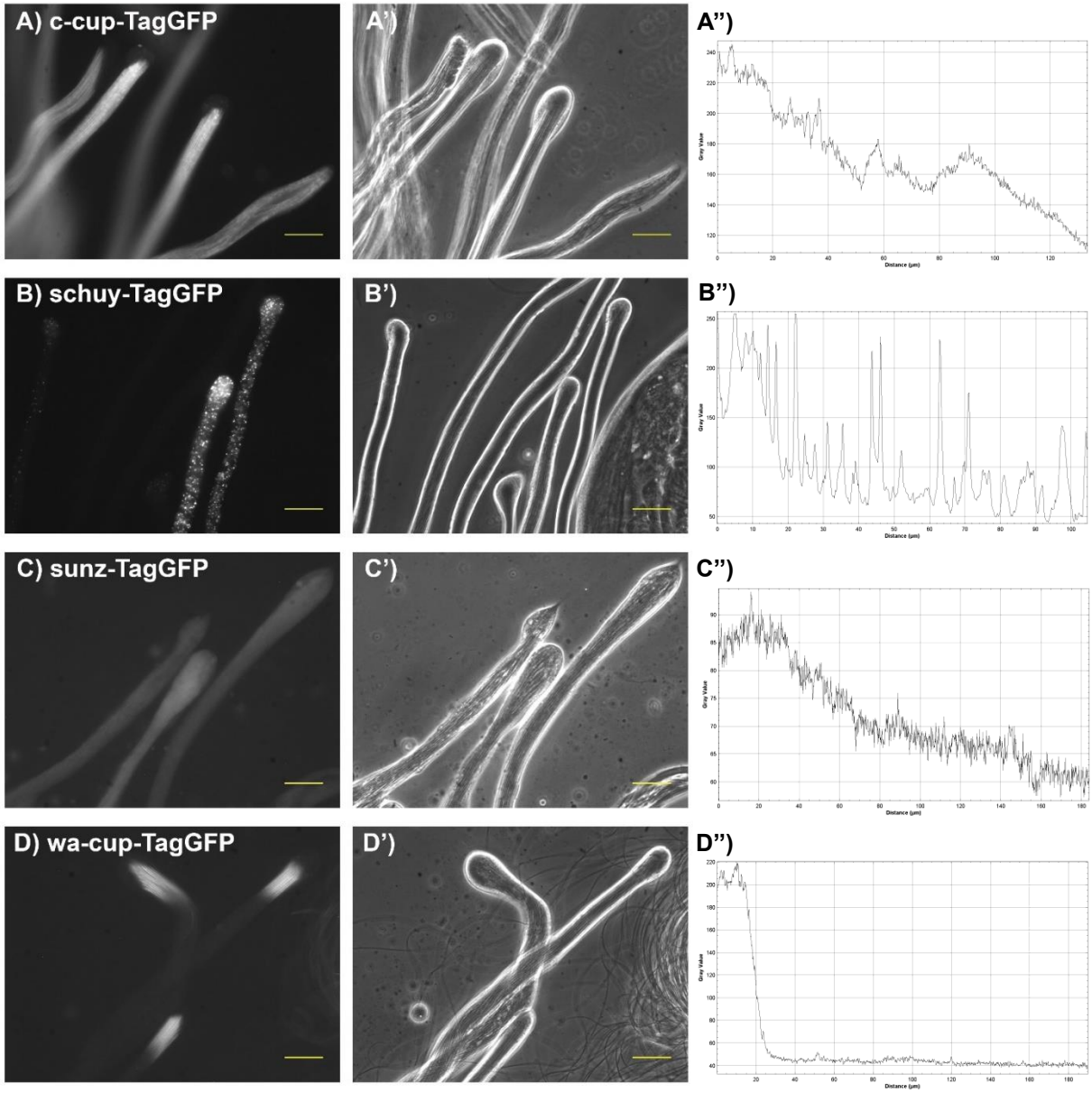

Figure 30. Elongating tail-ends of spermatid cyst bundles, imaged in squashed whole-mount preparations of *Drosophila melanogaster* testes from four different comet and cup fluorescent protein reporter lines. For each TagGFP-labelled transgenic fly line, a pair of images is presented which corresponds to the structural and morphological cell features and protein expression levels of the same set of 64-cell spermatid cyst bundles. Images (A – D) are outputs from single-channel GFP fluorescence microscopy, while (A' – D') are images from phase contrast microscopy of the same region. Graphs (A'' – D'') are the corresponding plot profiles, which represent the quantification of mean pixel signal intensities over distance (µm). These plots reinforce the distinct protein gradients established by each comet and cup reporter, which leads down the length of the spermatid bundles from the extreme tail-ends. All images and pixel intensity plots are representative of at least two spermatid cyst bundles from the testes of three independent males. Gain: 1.0. Exposure: 1.0. Scale bars: 25 µm.

5.3. The actin-associated interactome and spermatid-specific expression of Imp may indicate a regulatory function in spermiogenesis and mRNA localisation

We anticipated that the RNAi-mediated knockdown of *imp* would lead to defects in the *Drosophila* testis that could in turn be used to infer the biological role of Imp's RNA binding and processing activities. We know that Imp is expressed at high levels at the tail-ends of growing spermatids, mirroring that of the non-uniform distributions established by localised comet and cup mRNA transcripts (Fabrizio et al. 1998; Barreau et al. 2008a; Barreau et al. 2008b). Hence, we aimed to determine what contributions, if any, Imp has on the localisation of these mRNAs.

Moreover, we extended our analyses to encompass fluorescent protein reporter constructs corresponding to expression of transgenic TagGFP-tagged fusions of the comet and cup protein products. Investigating comet and cup protein gradients was mutually informative for our wider interest in the localised post-meiotic mRNAs because both are intrinsically linked. Bcd again provides another prime example of this; the establishment of a preceding *bcd* mRNA gradient is what supports Bcd protein gradient formation throughout the *Drosophila* oocyte for body axis patterning – with both gradient profiles appearing near-identical in all observations (Spirov et al. 2009). Therefore, a loss of Imp may result in dysregulation that is not only detectable at an earlier point of mRNA production, stability and/or localisation, but is substantial enough to feed down into translational impediments.

In the literature, there is also a clear implication of the IMP RBP family being actively involved in growth, metastasis and motility, with actin-binding properties contributing extensively to this role (Kislauskis et al. 1997; Havin et al. 1998; Shestakova et al. 1999; Ioannidis et al. 2001; Oleynikov and Singer 2003). This reinforces what we found with regards to the Imp interactome in our comparative proteomics and RNA-seq data in Results Chapter 2. We therefore hypothesised that, in addition to defective comet and cup expression profiles, these *imp* deficient RNAi phenotypes would correspond to abnormalities in the latter stages of spermiogenesis, wherein spermatid elongation and morphological remodelling is key to the motile properties of the developing spermatozoa.

Using the *schuy*-TagGFP and *c-cup*-TagGFP reporter lines stated above as our starting fly stocks, we performed a series of crosses to generate two final *Drosophila melanogaster* lines that express at least one copy of the *schuy*-TagGFP fusion or one copy of *c-cup*-TagGFP fusion on the second chromosome, as well as the homozygous viable Bam-Gal4:VP16 driver on the third chromosome. The CyO balancer and TM3,Sb balancer were introduced into the line to stabilise the second and third chromosomes, respectively:

1. w; *schuy*-TagGFP/(CyO); Bam-Gal4:VP16/(TM3,Sb)
2. w; *c-cup*-TagGFP/(CyO); Bam-Gal4:VP16/(TM3,Sb)

After establishing stable fly lines, virgin females carrying these genotypes were crossed with transgenic Imp-UAS-RNAi males at 25˚C. As the level of hairpin expression and RNAi gene knockdown activity could be manipulated by rearing flies at different temperatures, a strict temperature scheme was selected to maximise Imp-UAS-RNAi hairpin expression. We also included several different transgenic Imp-UAS-RNAi fly lines here, with each Imp-UAS-RNAi construct representing a slightly different genetic background and generating RNAi hairpins with varying constituencies and lengths. We had done this to confirm that any Imp-RNAi phenotypes identified were representative of a genuine *imp* knockdown, rather than being a consequence of off-target effects or attributed to the genetic context of the RNAi line.

Immediately after crossing, parental flies were placed at 25˚C for two to three days of mating, before subsequent transfer into fresh food vials supplemented with additional yeast powder extract. Resultant F1 cultures were transferred to 30˚C, where they were maintained throughout their life cycle until eclosion and F1 male collection. Regular turnover was continued by these means until progeny yield showed a sizeable decline.

In the presence of the Bam-Gal4:VP16 driver transgene, Gal4-mediated activation of the UAS promoter should promote the directed production of shRNA structures in F1 males, driving targeted silencing of *imp* throughout mid-to-late sperm development by the Imp-UAS-RNAi hairpins. The testis phenotype of F1 Imp-RNAi adult males was therefore analysed using the Olympus BX50 fluorescence upright microscope (Olympus Life Science) for both phase contrast and fluorescence microscopy. RNAi-induced changes to testis ultrastructure and morphology, as well as impediments to the differentiation programme or cell cycle progression, were visualised by phase

contrast microscopy. Any alterations to the expression and distribution of TagGFP-labelled comet and cup fusion proteins were detected by single-channel fluorescence microscopy of the spermatid cyst bundles. By using a standardised ROI measurement in ImageJ v1.52d (Schneider et al. 2012), the average mean pixel intensities of the brightest and weakest points of expression were quantified in three spermatid cyst bundles per image, representing two independent testes/males per genotype. Mean pixel signal intensities for the brightest regions were then compared between datasets, using paired samples t-tests to identify statistical differences in fluorescence outputs of the WT control testes and each Imp-UAS-RNAi knockdown group (significance level, $p > 0.05$). Only fluorescence images acquired at the same intensity settings were subject to this analysis.

5.4. Knockdown of *imp* leads to loss of schuy-TagGFP protein signal and defects in spermatid elongation

To investigate the hypothesis that RBPs such as Imp are implicated in the regulation of non-uniform, subcellular mRNA localisation, we employed a series of RNAi screens to investigate the specific functional role of Imp in the *Drosophila* testis. By looking thoroughly into the targeted, RNAi-induced knockdown of the *imp* gene, we hoped to determine whether a decline in the levels of this functional protein *in vivo* resulted in an obvious RNAi phenotype that could be traced back to disruption at the level of transcription and mRNA localisation.

In short, we were studying whether a loss of Imp gives rise to any observable changes to the overall testis structure and/or perturbation of normal sperm development, with a particular interest on the post-meiotic spermatid cyst bundles in spermiogenesis. With this in mind, we first investigated the translation of our localised mRNAs, *schuy*-TagGFP and *c-cup*-TagGFP, in two standalone Imp-UAS-RNAi lines.

In the WT testis, there was expression of the characteristic speckled schuy-TagGFP protein gradient, with strong expression at the spermatid tail-ends that trails-off down the length of the cyst bundles (Fig. 31.1A – 31.1A''). At its brightest point, WT spermatid cyst bundles measured an average mean pixel intensity signal of 136 (n=6, SE=7.76), while regions of weaker signal expression measured an average mean pixel intensity

of 65 (n=6, SE=1.87). A direct comparison of the average mean pixel intensities measured for all single Imp-UAS RNAi genotypes vs. this WT data is presented in Fig 31.2A.

When comparing to this WT control of F1 male progeny from the parental w-; *schuy*-TagGFP; BamGal4:VP16 x w^{1118} cross, resultant testis phenotypes varied both within and between the Imp-UAS-RNAi crosses. The Val20-Imp and UAS-Dicer2;Imp-GD RNAi knockdown phenotypes shown here revealed a great deal of variable severity, including inconsistent effects on spermatid elongation and schuy-TagGFP protein expression.

For both the Val20-Imp-attP2 RNAi and UAS-Dicer2;Imp-GD RNAi testes, schuy-TagGFP-expressing testes were either completely “wildtype-looking” with elongated spermatid cyst bundles and similar levels of localised fluorescent reporter signal intensities (Fig. 31.1B – 31.1B’’ and Fig. 31.1D – 31.1D’’) or exhibited a somewhat variable dysregulated phenotype (Fig. 31.1C – 31.1C’’ and Fig. 31.1E – 31.1E’’). With regards to the latter, there appeared to be considerable phenotypic disruption at multiple levels of sperm development. There were disruptions to spermatid elongation and a concurrent loss of fluorescent protein reporter signal due to there being few, if any, elongating spermatids within which the particulate-like schuy protein localisation could arise. The mean pixel intensities measured for both dysregulated testis phenotypes showed a significant difference to the WT control, indicating a clear loss of fluorescent reporter protein signal upon Imp-UAS-RNAi knockdown (Fig. 31.2B; Paired samples t-tests, $P<0.001$).

For the w-/y; schuy-TagGFP/+; BamGal4:VP16/Val20-Imp-attP2 RNAi flies, this rare RNAi phenotype presented with disrupted spermatid elongation (Fig. 31.1C – 31.1C”). While there was some early elongation, the majority remained stunted and many of the round clonally related sister spermatids did not progress into the phase of synchronised elongation.

The UAS-Dicer2/y; schuy-TagGFP/+; BamGal4:VP16/Imp-GD flies, on the other hand, showed a dysregulated phenotype in which spermatid elongation proceeded as normal, but the overall signal for schuy-TagGFP protein expression was substantially reduced at the extreme distal tail-ends compared to the WT control. There was also a

loss of the characteristic speckling gradient typically established after local translation of the schuy-TagGFP protein (Fig. 31.1E – 31.1E'').

The resultant "wildtype" Imp-UAS-RNAi testis phenotypes exhibited a near-normal protein expression pattern for both the Val20-Imp and UAS-Dicer2;Imp-GD RNAi lines – there was a speckled schuy-TagGFP protein gradient, with strong expression at the spermatid tail-ends that tapered in concentration towards the nuclear head-end of the spermatid cyst bundles (Fig. 31.1B – 31.1B'' and Fig. 31.1D – 31.1D'', Fig. 31.2.). Although, the mean pixel intensity signals for the Val20 Imp-RNAi WT-like testis sample did show a statistically significant difference when compared to the WT control via a paired samples t-test ($P<0.05$). Interestingly, the computed *t* statistic suggested a small decrease in schuy-TagGFP fluorescence upon the RNA-mediated knockdown of *imp* (Fig 31.2B.; $t=3.39$, $P=0.019$).

Surprisingly, rudimentary counts in two independent crossing rounds suggested that the dysregulated phenotype only occurred at an approximate frequency of 1 in every 10 males, regardless of the Imp-UAS-RNAi construct used. Both testes in the pair were always equally affected.

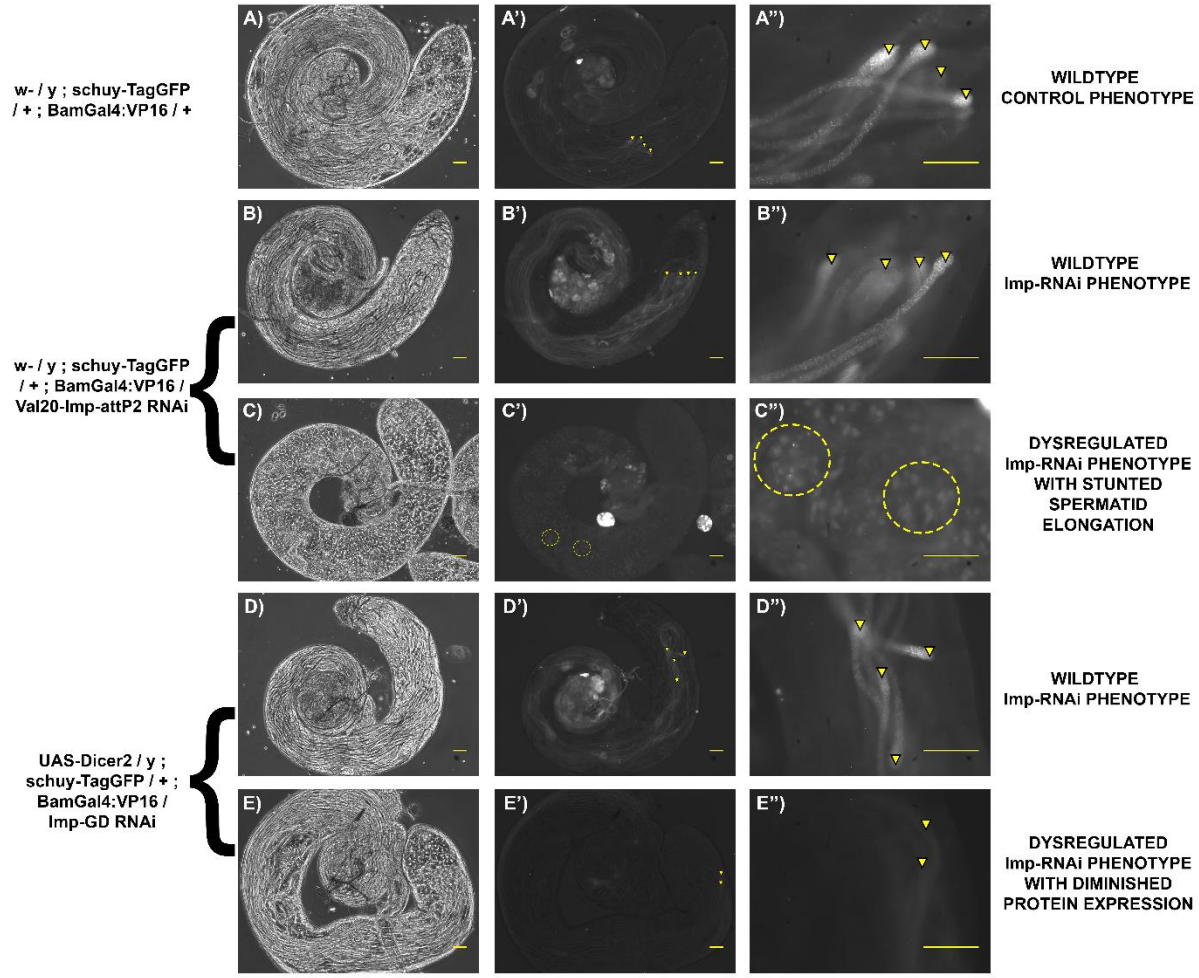

Figure 31.1. Phenotypic effects of Imp-RNAi knockdowns on the translation and expression patterns of localised schuy-TagGFP protein gradients in *Drosophila melanogaster* testes. Whole testes and encompassing elongating spermatid cyst bundles were first imaged by phase contrast microscopy to visualise testis ultrastructure, cell morphology and sperm development progression. Fluorescence microscopy was then performed to visualise TagGFP fluorescence signals from the transgenic fluorescently tagged schuy protein. (A – E) Whole testis phase contrast images, taken at 10X magnification. (A' – E') Whole testis schuy-TagGFP fluorescence images, taken at 10X magnification. (A'' – E'') Single channel schuy-TagGFP fluorescence images, captured at 40X magnification. Yellow arrowheads flag spermatid cyst bundles of particular interest. Yellow dashed lines indicate regions of mislocalised schuy-TagGFP protein in early round spermatids. All images are representative of testes from at least two independent males per genotype. Gain: 1.0. Exposure: 1.0. Scale bars: 25 μm.

A

TYPE OF CROSS	AVERAGE MEAN PIXEL INTENSITIES	
	BRIGHTEST REGION	WEAKEST REGION
schuy-TagGFP x WT control	136 (SE=7.76)	65 (SE=1.87)
schuy-TagGFP x Val20-Imp RNAi (WT-like phenotype)	122 (SE=9.96)	75 (SE=5.71)
schuy-TagGFP x Val20-Imp RNAi (Dysregulated phenotype)	71 (SE=8.42)	57 (SE=5.45)
schuy-TagGFP x UAS-Dicer2; Imp-GD RNAi (WT-like phenotype)	121 (SE=6.01)	63 (SE=2.59)
schuy-TagGFP x UAS-Dicer2; Imp-GD RNAi (Dysregulated phenotype)	45 (SE=2.18)	40 (SE=0.98)

B

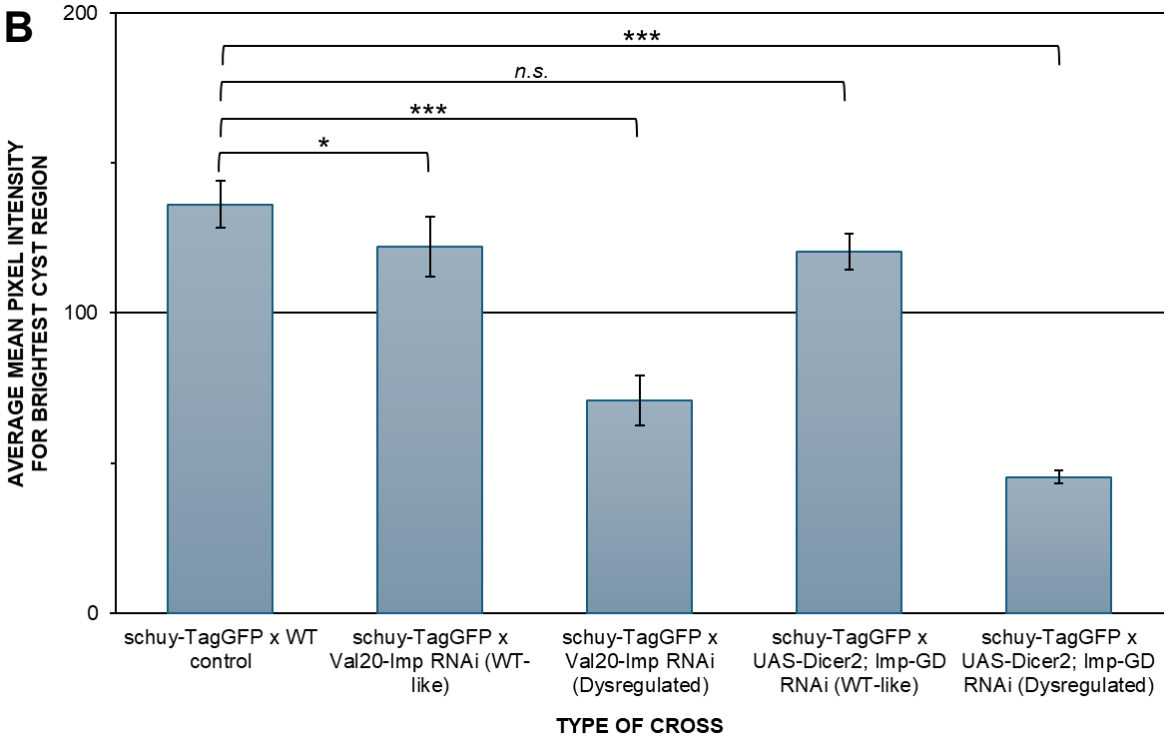

Figure 31.2. Quantification of average mean pixel intensities outputted from the single Imp-UAS-RNAi phenotypic screen of fluorescent schuy-TagGFP protein signals. (A) Average mean pixel intensity signals recorded for the brightest and weakest fluorescence regions of the sampled spermatid bundles for each crossed progeny. (B) Graphical plotting of values for the brightest signals for each F1 genotype/cross. Paired t-tests were performed using the jamovi Cloud Online Statistical Software (v2.6.44) to identify significance between the mean pixel signal intensities of the WT control spermatid cysts compared to the different Imp-UAS-RNAi knockdown genotypes. Significant differences in average mean pixel intensity values indicated a clear division in schuy-TagGFP expression between the WT-like testis

phenotypes and dysregulated testis phenotypes vs. the WT control cross. Error bars represent the standard error (SE) for each dataset. All quantification data are representative of fluorescence signals from three spermatid cyst bundles taken from the testes of two independent males per genotype (n=6). Asterisks indicate significance: *, P<0.05; ***, P<0.001. *n.s.*, non-significant difference between the groups at p>0.05.

5.5. Double Imp-UAS-RNAi knockdowns in schuy-TagGFP-expressing fly lines improve penetration efficiency

The phenotypic abnormalities we detected in the testes of our single Imp-RNAi knockdown F1 male progeny were inconsistent, and the incidence of these dysregulated phenotypes was not as common as their “wild-type” looking counterparts – regardless of the RNAi hairpin construct used. We therefore decided to repeat this RNAi screening approach using newly double Imp-UAS-RNAi transgene configurations to enhance the phenotypic effects of our *imp*-targeted RNAi knockdowns. By doubling-up on the number of UAS-RNAi constructs, and providing two sources of RNAi hairpin expression rather than one, it was hypothesised that two copies of the Imp-UAS-RNAi effector transgenes would improve the efficiency and penetrance of RNAi hairpin expression against the *imp* gene (Dietzl et al. 2007).

Double Imp-UAS-RNAi *Drosophila* lines with insertions on both the second and third chromosome were kindly generated by Dr. Sonia Lopez de Quinto. These included three Imp-UAS-RNAi combinations:

1. A double w; Val20-Imp-attP2/CyO; Val20-Imp-attP2/TM3,Sb UAS RNAi line ;
2. A w; Val20-Imp-attP2/CyO; Imp-GD/TM3,Sb UAS RNAi line ;
3. A double homozygous w; Val22-Imp/Val22-Imp; Val22-Imp/Val22-Imp UAS RNAi line.

In the second combination, the long Imp-GD UAS-RNAi hairpin was no longer being co-expressed with UAS-Dicer2, as was the case in the single Imp-RNAi screen.

As expected, the WT control testis exhibited a protein gradient of schuy-TagGFP puncta, with concentrated expression at the tail-ends of the spermatid cyst bundles that progressively decreased down the length of the cells towards the nuclear head-end (Fig. 32.1A – 32.1A''). At its brightest point, WT spermatid cyst bundles measured an average mean pixel intensity signal of 156 (n=6, SE=12.12), while regions of weaker signal expression measured an average mean pixel intensity of 103 (n=6, SE=5.92). A direct comparison of the average mean pixel intensities measured for all double Imp-UAS-RNAi genotypes vs. this WT data is presented in Fig 32.2A.

However, when two Imp-UAS-RNAi constructs were combined and flies were mated with the *schuy*-TagGFP fusion line, direct comparisons to this WT testis phenotype did not yield any clear-cut answers regarding *imp* gene functionality from the spermatogonial stages of sperm development and beyond.

Crosses to the double Val20-Imp-attP2 and Val20-Imp-attP2;Imp-GD RNAi lines revealed a great deal of phenotypic variability, but did somewhat validate the disruption to spermatid elongation and schuy-TagGFP protein expression we saw previously (Fig. 32.1B – 32.1E'' and Fig. 32.2.).

Yet again, the Val20-Imp-attP2;Imp-GD and double Val20-Imp-attP2 RNAi knockdowns in schuy-TagGFP-expressing testes resulted in either completely wildtype-looking phenotypes with elongated spermatids, punctate schuy-TagGFP protein expression and comparable fluorescent signal intensities (Fig. 32.1B – 32.1B'' and Fig. 32.1D – 32.1D'') or showed signs of spermatogenesis defects that varied in severity (Fig. 32.1C – 32.1C'' and Fig. 32.1E – 32.1E'').

In dysregulated double Imp-RNAi phenotypes, there was substantial phenotypic disruption at multiple levels of sperm development. The expression of two Imp-UAS-RNAi hairpin constructs in the same schuy-TagGFP line reinforced the abnormalities we found in the single Imp-RNAi screen. In fact, defects in spermatid elongation and schuy-TagGFP protein signal loss were more pronounced when Val20-Imp-attP2;Imp-GD and double Val20-Imp-attP2 RNAi knockdowns were used (Fig. 32.1C – 32.1C'' and Fig. 32.1E – 32.1E''). Although, this result was not deemed statistically significant when mean pixel intensities were compared to the WT control via a paired samples t-test (Fig. 32.2B; t=-2.057, P=0.095). The mean pixel intensities measured for dysregulated Val20-Imp-attP2;Imp-GD testis phenotypes, on the other hand, showed

a significant difference to the WT control, indicating a depletion in fluorescent reporter protein signal (Fig. 32.2B; Paired samples t-test, $P<0.05$).

Both double Imp-RNAi knockdown conditions corresponded to the most severe levels of disruption to spermatid elongation and a simultaneous loss of localised fluorescent protein reporter signal. As there were next to no elongating spermatid cyst bundles in these double Imp-RNAi testes, there were no spermatid tail-ends within which schuy protein could accumulate after asymmetrical mRNA localisation and local translation.

In spite of these dramatic double Imp-RNAi effects, WT testis phenotypes still persisted in the Val20-Imp-attP2;Imp-GD and double Val20-Imp-attP2 RNAi knockdown conditions. These resultant “wildtype” testis phenotypes showed a speckled localisation pattern of schuy-TagGFP protein, expressed in a tapering gradient down towards the nuclear head-end of the spermatid cyst bundles, which was comparable in signal intensity to the WT control (Fig. 32.1B – 32.1B’’ and Fig. 32.1D – 32.1D’’, Fig. 32.2.).

Interestingly, *imp*-directed RNAi knockdowns with the new double homozygous Val22-Imp-attP40 RNAi construct did not produce any obvious defects in spermatid elongation or changes to localised schuy-TagGFP protein signals (Fig. 32.1F – 32.1F’’). Instead, mean pixel intensities were found to be statistically significant when compared to the WT control, suggesting a slight overall increase in fluorescent reporter signal (Fig. 32.2B; Paired samples t-test, $t=-4.571$, $P=0.006$).

Therefore, the level of *imp* deficiency-induced dysfunction depended upon the precise combination of UAS-RNAi effector transgenes used for the knockdown. As the Val22-attP40 construct was originally optimised for RNAi hairpin expression during *Drosophila* oogenesis in the female germline, this was somewhat expected (Ni et al. 2011).

With the exception of our double homozygous Val22-Imp RNAi construct, expression of RNAi hairpins from two copies of the Imp-UAS-Imp RNAi transgenes improved RNAi penetration efficiency. Rudimentary counts of the double Imp-RNAi flies (across two independent rounds of crossing) also suggested that the incidence of our dysregulated testis phenotype could affect up to 7 out of 10 males, which is certainly an improvement on our single Imp-RNAi knockdowns. As in the single Imp-RNAi screen, both testes in the pair were equally as affected.

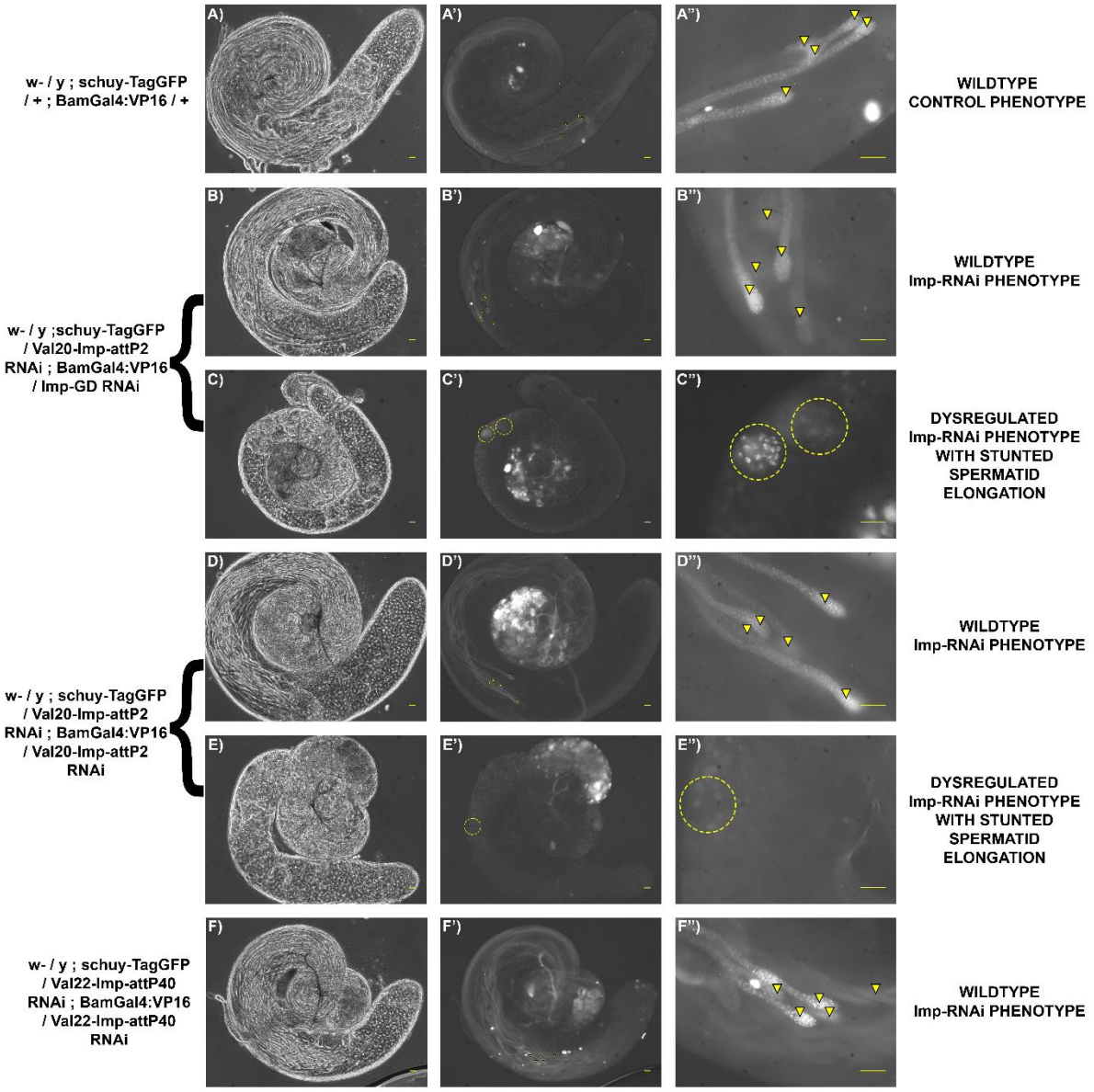

Figure 32.1. Phenotypic effects of double Imp-RNAi knockdowns on the translation and expression patterns of localised schuy-TagGFP protein gradients in *Drosophila melanogaster* testes. Whole schuy-TagGFP-expressing testes from crosses to double Imp-UAS-RNAi lines were imaged by phase contrast microscopy and fluorescence microscopy to screen for enhanced imp-deficient testis phenotypes. (A – F) Whole testis phase contrast squashes, taken at 10X magnification to capture the entire testis structure and its internal anatomy. (A' – F') Equivalent whole testis schuy-TagGFP fluorescence squashes, also taken at 10X magnification. (A'' – F'') Single channel schuy-TagGFP fluorescence images, captured at 40X magnification. Yellow arrowheads pinpoint some spermatid cyst bundles of note. Yellow dashed lines indicate regions of mislocalised schuy-TagGFP protein in early round spermatids. All images are representative of at least two testes from two independent males per genotype. Gain: 1.0. Exposure: 1.0. Scale bars: 25 μm.

A

TYPE OF CROSS	AVERAGE MEAN PIXEL INTENSITIES	
	BRIGHTEST REGION	WEAKEST REGION
schuy-TagGFP x WT control	156 (SE=12.12)	103 (SE=5.92)
schuy-TagGFP x Val20;Val20-Imp RNAi (WT-like)	186 (SE=8.83)	111 (SE=2.95)
schuy-TagGFP x Val20;Val20-Imp RNAi (Dysregulated)	115 (SE=7.03)	93 (SE=1.68)
schuy-TagGFP x Val20;Imp-GD RNAi (WT-like phenotype)	144 (SE=13.97)	100 (SE=0.89)
schuy-TagGFP x Val20;Imp-GD RNAi (Dysregulated phenotype)	125 (SE=18.50)	67 (SE=4.95)
schuy-TagGFP x Val22;Val22-Imp RNAi	203 (SE=16.34)	108 (SE=5.54)

B

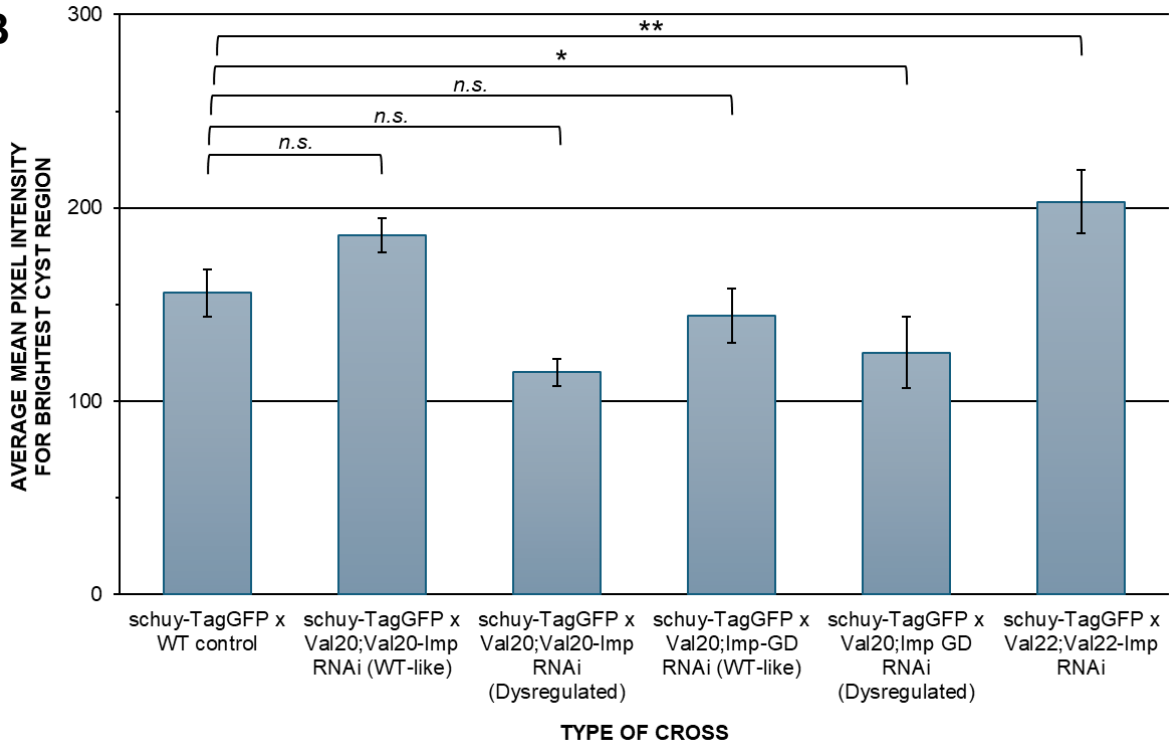

Figure 32.2. Quantification of average mean pixel intensities outputted from the double Imp-UAS-RNAi phenotypic screen of fluorescent schuy-TagGFP protein signals. (A) Average mean pixel intensity signals recorded for the brightest and weakest fluorescence regions of the sampled spermatid bundles for each crossed progeny. (B) Graphical plotting of values for the brightest signals from each F1 genotype/cross. Paired t-tests were performed using the jamovi Cloud Online Statistical Software (v2.6.44) to identify significance between the mean pixel signal intensities of the WT control spermatid cysts compared to the different doubled-up Imp-UAS-RNAi knockdowns. Significant differences in average mean pixel

intensity values did not indicate such an evident division in schuy-TagGFP expression between the WT-like testis phenotypes and dysregulated testis phenotypes vs. the WT control cross. However, this was likely due to the high schuy-TagGFP protein signals that mislocalised within the early round spermatids – as opposed to the usual expression of schuy in elongating spermatids. All quantification data are representative of fluorescence signals from three spermatid cyst bundles taken from the testes of two independent males per genotype (n=6). Error bars represent the standard error (SE) for each dataset. Asterisks indicate significance: *, P<0.05; **, P<0.01. *n.s.*, non-significance between the groups at p>0.05.

5.6. Single and double UAS-RNAi knockdowns of *imp* in c-cup-TagGFP-expressing fly lines have no apparent testis effects

Conversely, we saw no apparent effect on c-cup-TagGFP at a protein level in either of our single or double Imp-UAS-RNAi screens – irrespective of whether we crossed to single Val20-Imp-attP2 RNAi and UAS-Dicer2;Imp-GD RNAi lines (Fig. 33.1. and Fig 33.2.) or Val20-Imp-attP2;Imp-GD RNAi, double Val20-Imp-attP2 RNAi and double homozygous Val22-Imp RNAi lines (Fig. 34.1. and Fig 34.2.).

When compared to the WT control of F1 male progeny from the parental w-; c-cup-TagGFP; BamGal4:VP16 x w^{1118} cross (Fig. 33.1A – 33.1A" and Fig. 34.1A – 34.1A"), resultant Imp-RNAi testis phenotypes remained fundamentally wildtype-looking – with elongated bundles of spermatids and similar fluorescence reporter signals – regardless of the single or double Imp-UAS-RNAi line used. In fact, when compared to the WT control, the mean pixel intensities quantified for c-cup-TagGFP reporter expression were consistent in all Imp-UAS-RNAi testes (Fig. 33.2. and Fig. 34.2.).

Sperm development remained unchanged, and the testis ultrastructure and morphology resembled that of its WT counterpart. Moreover, there appeared to be no difference in c-cup-TagGFP protein signal levels. Although, when analysed via a paired samples t-test, the mean pixel intensity values for the Val20;Imp-GD RNAi spermatid cyst bundles were significantly different to the WT control; with the *t* statistic suggesting a small increase in c-cup-TagGFP reporter expression upon knockdown of *imp* (Fig

34.2B.; *t*=-3.189, P=0.024). Some background fluorescence may have contributed to this difference.

Nevertheless, the overall expression profile of the c-cup-TagGFP fusion protein remained uniform in all Imp-UAS-RNAi knockdown conditions, with a striped pattern down the length of the spermatid cyst bundles corresponding to mitochondrial localisation. There was a small gradient of the c-cup-TagGFP protein throughout the cells; with the highest concentration of protein established at the spermatid tail-ends, after translation of its localised mRNA transcripts. Some weaker expression was also detected in early sperm development, within the spermatocytes, as expected.

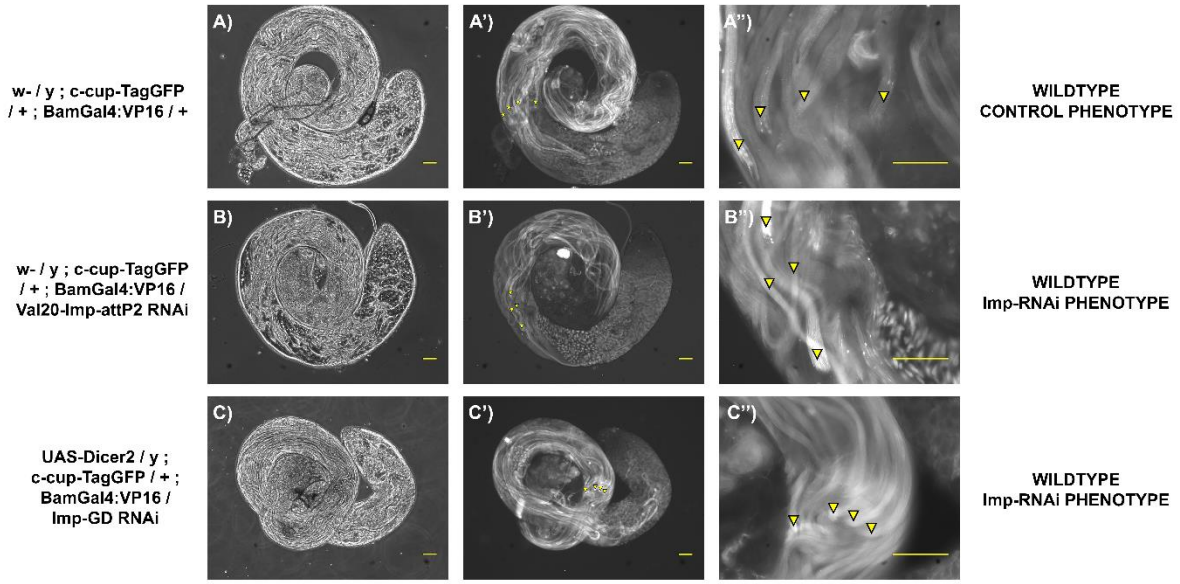

Figure 33.1. Phenotypic effects of Imp-RNAi knockdowns on the translation and expression patterns of localised c-cup-TagGFP protein gradients in *Drosophila melanogaster testes*. Whole testes and encompassing elongating spermatid cyst bundles were first imaged by phase contrast microscopy to visualise testis ultrastructure, cell morphology and sperm development progression. Blue light fluorescence microscopy was then performed to visualise TagGFP fluorescence signals from the transgenic fluorescently tagged c-cup protein. (A – C) Whole testis phase contrast images, taken at 10X magnification. (A' – C') Whole testis c-cup-TagGFP fluorescence images, taken at 10X magnification. (A'' – C'') Single channel c-cup-TagGFP fluorescence images, captured at 40X magnification. Yellow arrowheads emphasise spermatid cyst bundles of particular interest. All images are representative of testes from a minimum of two independent males per genotype. Gain: 1.0. Exposure: 1.0. Scale bars: 25 μm.

A

TYPE OF CROSS	AVERAGE MEAN PIXEL INTENSITIES	
	BRIGHTEST REGION	WEAKEST REGION
c-cup-TagGFP x WT control	228 (SE=8.56)	99 (SE=3.20)
c-cup-TagGFP x Val20-Imp RNAi	234 (SE=6.03)	92 (SE=7.78)
c-cup-TagGFP x UAS-Dicer2;Imp-GD RNAi	209 (SE=1.72)	83 (SE=3.46)

B

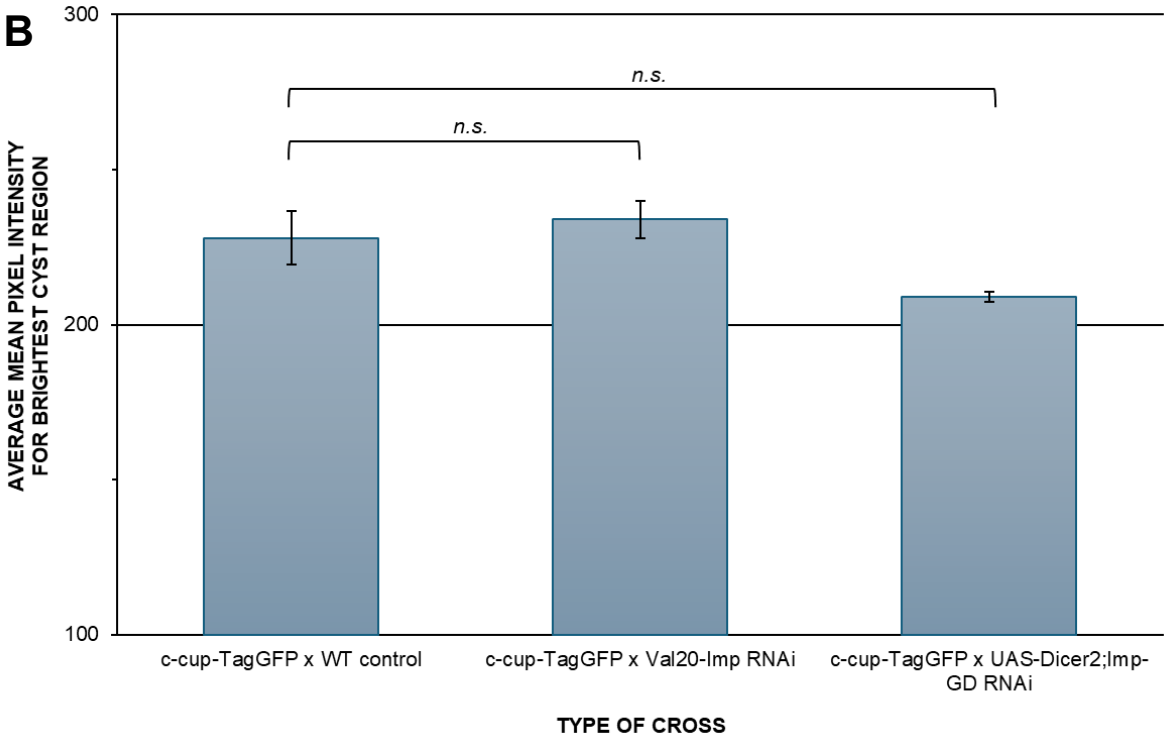

Figure 33.2. Quantification of average mean pixel intensities outputted from the single Imp-UAS-RNAi phenotypic screen of fluorescent c-cup-TagGFP protein signals. (A) Average mean pixel intensity signals recorded for the brightest and weakest fluorescence regions of the sampled spermatid bundles for each crossed progeny. (B) Graphical plotting of values for the brightest signals for each cross of interest. Paired t-tests were performed using the jamovi Cloud Online Statistical Software (v2.6.44) to identify significance between the mean pixel signal intensities of the WT control spermatid cysts compared to those in the Imp-UAS-RNAi knockdown testes. No significant differences in the average mean pixel intensity values were recorded for either knockdown condition when compared to the WT control. This indicated that the RNAi-mediated knockdown of *imp* had no significant effect on c-cup-TagGFP fluorescent reporter expression. Error bars represent the standard error (SE) for each dataset. All quantification data are representative of fluorescence signals from three spermatid cyst bundles taken from the testes of two independent males per genotype (n=6). *n.s.*: non-significance between group comparisons at $p>0.05$.

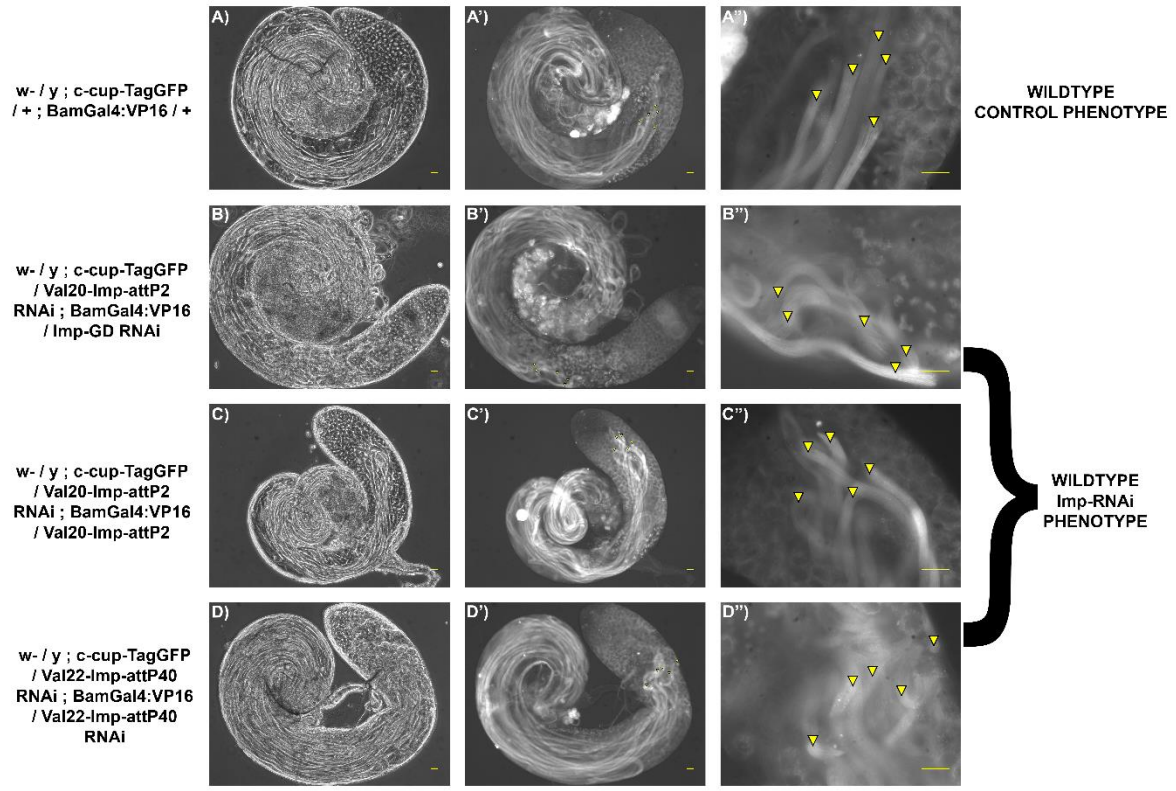

Figure 34.1. Phenotypic effects of double Imp-RNAi knockdowns on the translation and expression patterns of localised c-cup-TagGFP protein gradients in *Drosophila melanogaster* testes. Whole c-cup-TagGFP-expressing testes from crosses to double Imp-UAS-RNAi lines were imaged by phase contrast microscopy and fluorescence microscopy to screen for any heightened defects that may arise due to loss of imp activity. (A – D) Whole testis phase contrast squashes, taken at 10X magnification to include the entire assembly line and spatiotemporal array of sperm development. (A' – D') Same whole testis c-cup-TagGFP squashes taken at 10X magnification in single channel GFP fluorescence. (A'' – D'') Single channel c-cup-TagGFP fluorescence images, captured at 40X magnification. Yellow arrowheads highlight specific spermatid cyst bundles of interest. All images are representative of testes from a minimum of two independent males per genotype. Gain: 1.0. Exposure: 1.0. Scale bars: 25 μm.

A

TYPE OF CROSS	AVERAGE MEAN PIXEL INTENSITIES	
	BRIGHTEST REGION	WEAKEST REGION
c-cup-TagGFP x WT control	169 (SE=10.68)	85 (SE=5.47)
c-cup-TagGFP x Val20;Val20-Imp RNAi	176 (SE=16.68)	77 (SE=3.41)
c-cup-TagGFP x Val20;Imp-GD RNAi	220 (SE=9.02)	92 (SE=2.38)
c-cup-TagGFP x Val22;Val22-Imp RNAi	180 (SE=5.76)	102 (SE=2.55)

B

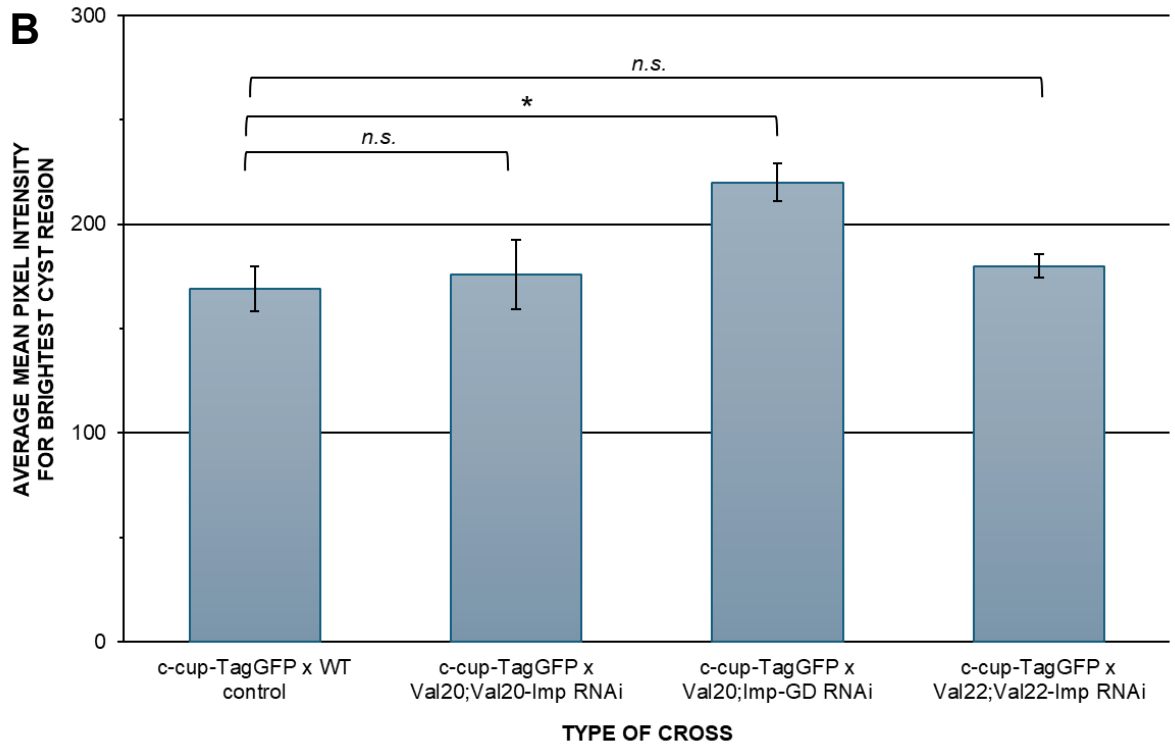

Figure 34.2. Quantification of average mean pixel intensities outputted from the double Imp-UAS-RNAi phenotypic screen of fluorescent c-cup-TagGFP protein signals. (A) Average mean pixel intensity signals recorded for the brightest and weakest fluorescence regions of the sampled spermatid bundles for each crossed progeny. (B) Graphical plotting of values for the brightest signals for each cross of interest. Paired t-tests were performed using the jamovi Cloud Online Statistical Software (v2.6.44) to identify significance between the mean pixel signal intensities of the WT control spermatid cysts compared to those in the double Imp-UAS-RNAi knockdown males. Average mean pixel intensity measurements generally remain consistent throughout all genotypes, regardless of the Imp-UAS-RNAi construct used. Error bars represent the standard error (SE) for each dataset. All quantification data are representative of fluorescence signals from three spermatid cyst bundles taken from the testes of two independent males per genotype (n=6). * corresponds to significance at $P<0.05$ and *n.s.* corresponds to non-significance between groups at $p>0.05$.

5.7. The Bam-Gal4:VP16 driver is indeed present in our c-cup-TagGFP-expressing reporter lines, despite there being no impact from Imp-RNAi knockdowns

While we had anticipated that there would be a few marked differences in the regulatory role that Imp plays for some comet and cup genes versus others, we did not hypothesise that this contribution would be so drastic between schuy and c-cup or that it would result in such massive phenotypic extremes upon knockdown of *imp*. We were therefore concerned that the original w; *c-cup*-TagGFP/(CyO); Bam-Gal4:VP16/(TM3,Sb) line was missing the Bam-Gal4:VP16 driver, and hence unable to express the Gal4 protein for induction of transcriptional activation upon crossing to our Imp-UAS-RNAi lines.

To check if this were indeed the case, we crossed our *c-cup*-TagGFP; Bam-Gal4:VP16 line with 10XUAS-CD8-GFP-expressing flies (10XUAS-IVS-mCD8::GFP-attP40, BDRC #32186). The 10XUAS-CD8-GFP line is a P-element attP40 insertion on the second chromosome; which expresses an mCD8-tagged GFP under the control of 10 UAS signals, with an intron (IVS) interposed between the UAS and coding region (Pfeiffer et al. 2010).

mCD8-tagged GFP is a fluorescently labelled membrane marker that integrates and expresses in certain membranous regions, as specified by tissue-specific Gal4-UAS activity. We knew that a positive result, indicating the presence of the Bam-Gal4:VP16 driver, would be the expression of mCD8-GFP fluorescence signals towards the apex of the testis, which would predominate as a strong membranous band corresponding to the spermatogonial and early spermatocyte region (Yuan et al. 2019).

Upon conducting fluorescence microscopy of testes dissected from F1 male progeny, we found this characteristic profile of mCD8-GFP expression; thus confirming that our c-cup-TagGFP-expressing line did indeed contain the Bam-Gal4:VP16 driver transgene (Fig. 35.).

We were also able to validate this finding by cross-checking to images of Bam-Gal4-driven UAS-CD8-GFP patterns published by Yuan et al. (2019), following their screening of spermatogonial divisions in wildtype control and *Pif1A* mutant testes.

We could therefore have confidence that what we were seeing in these c-cup-TagGFP; Bam-Gal4:VP16 x Imp-UAS-RNAi fly crosses was not a consequence of an incomplete BamGal4/UAS system that lacked its Gal4 transgene component. This may indeed represent a genuine outcome of the *imp*-targeted RNAi knockdowns – i.e., that Imp is not consistently involved in *Drosophila* spermatid elongation or a direct regulator of local c-cup translation in the spermatid cyst bundles. However, further evidence from follow-up validation experiments is required to fully support this speculation, as I will discuss later in this chapter.

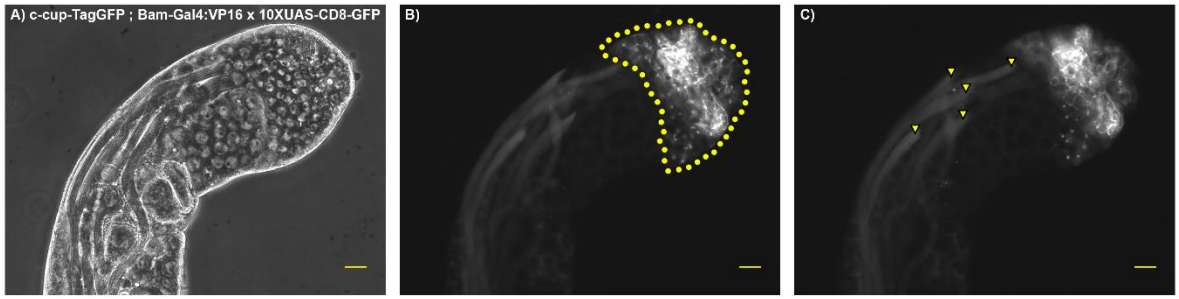

Figure 35. Positive result validating the presence of Bam-Gal4:VP16 and *c-cup*-TagGFP in the w; *c-cup*-TagGFP/(CyO); Bam-Gal4:VP16/(TM3,Sb) line by crossing to 10XUAS-CD8-GFP flies. (A) Phase contrast image of the apical region of an F1 testis, taken at 20X magnification. (B) Corresponding single channel GFP fluorescence image, also taken at 20X magnification and focused in on mCD8-GFP fluorescence. The yellow dotted zone outlines a band of high intensity mCD8-GFP fluorescence signal, which represents Bam-Gal4-driven expression of UAS-CD8-GFP in membranes of spermatogonial and early spermatocyte cysts. (C) A second single channel GFP fluorescence image of the same apical region, taken at 20X magnification but focused in on the elongating spermatids. Yellow arrowheads select out the tail-ends of these spermatid cyst bundles, confirming local c-cup-TagGFP protein expression. All images are representative of both testes dissected in pairs from three males, equating to six testes in total. Gain: 1.0. Exposure: 1.0. Scale bars: 25 μm.

5.8. HCR RNA-FISH confirms variable mislocalisation and loss of *schuy*-TagGFP mRNA transcripts upon knockdown of *imp*

We decided to follow-up on these RNAi testis phenotypes to ascertain whether the Imp-UAS-RNAi-induced defects we were observing at the level of schuy protein expression and spermatid elongation were attributed to translational disruption alone, or whether this dysregulation was detectable at an earlier point of mRNA production, stability and/or localisation.

To trace this highly variable translational disruption back to the stage of comet and cup transcription and mRNA localisation, we used HCR RNA-FISH and LSFM to study the transcript profiles of *schuy*-TagGFP and *c-cup*-TagGFP mRNAs upon expression of the Imp-RNAi hairpins in these lines. Once again, this phenotypic analysis was performed in two separate screening rounds; one screen tested single Imp-UAS-RNAi knockdowns while a second screen tested double Imp-UAS-RNAi knockdowns.

Overall, we found that both single and double *imp*-specific knockdowns in testes from F1 Imp-RNAi males were actually associated with a greater degree of variation at a transcriptional level than was the case when analysing the phenotypic effects on schuy-TagGFP protein expression (Fig. 36. and Fig. 37.).

When compared to the WT control of w; schuy-TagGFP; BamGal4:VP16 x w^{1118} testes, resultant testis phenotypes differed in their *schuy*-TagGFP transcript profiles depending on the different type of Imp-RNAi hairpin transgene used. In the WT control, we could see the distinctive comet-like localisation of *schuy*-TagGFP mRNA transcripts as they accumulated asymmetrically in subcellular regions at the extreme tail-ends of growing spermatid cyst bundles. These localised *schuy*-TagGFP mRNA signals could be detected in mid-to-late elongating spermatid cyst bundles of varying lengths throughout the control testis but were mainly concentrated to spermatid tail-ends in the mid-to-apical region of the organ (Fig. 36A – 36A'' and Fig. 37A – 37A'').

As before, *schuy*-TagGFP-expressing testes were either: (i) "wildtype-looking", with *schuy*-TagGFP transcript expression accumulating in near-native, non-uniform comet-like *schuy* mRNA localisation patterns (Fig. 36B – 36B'', Fig. 37B – 37B'' and Fig. 37D and 37D'') or (ii) abnormal, with highly mislocalised *schuy*-TagGFP mRNAs that

predominated towards the basal region of the testis, likely due to a lack of elongating spermatid cyst bundles (Fig. 36C – 36C'' and Fig. 37C – 37C'').

In the case of the dysregulated phenotype, there was a clear mislocalisation and loss of *schuy*-TagGFP mRNA transcripts. This dysregulation was in line with our above analyses as a mislocalisation of the underlying *schuy*-TagGFP mRNA transcripts likely correlated with a downstream loss of protein expression.

Once again, we found that dysfunction could be detected at multiple levels in *schuy*-TagGFP-expressing testes, as indicated by the mislocalisation of *schuy*-TagGFP mRNA transcripts in the single Val20-Imp-attP2 RNAi testes (Fig. 36C – 36C'') and a loss of *schuy*-TagGFP mRNA in the double Val20-Imp-attP2 RNAi testes (Fig. 37C – 37C'').

As in Section 5.5., doubling to two copies of the Val20-Imp-attP2 RNAi transgene resulted in a loss of localised *schuy*-TagGFP mRNA transcripts. There may also be some low-level fluorescence signals that suggest transcript mislocalisation in spermatids of the double Val20-Imp-attP2 RNAi cross, but the lack of signal overall made it difficult to determine whether this was truly mislocalised *schuy*-TagGFP mRNA or simply background signal (Fig. 37.).

However, there were still some inconsistencies, particularly with regards to the development and persistence of this wildtype-like testis phenotype. Surprisingly, *imp*-specific knockdowns with the Val20-Imp-attP2;Imp-GD RNAi hairpins did not have any dysregulatory effect on the presence or localisation of *schuy*-TagGFP mRNAs, despite evidence of a clear Imp-RNAi-mediated translational defect that altered the schuy-TagGFP protein expression profile (Fig. 37D – 37D'').

As anticipated, the double homozygous Val22-Imp-attP40 RNAi knockdown did not lead to any evident mislocalisation or loss of *schuy*-TagGFP mRNA transcripts (Fig. 37F – 37F'').

HCR RNA-FISH and LSFM has hence confirmed a variable, but evident mislocalisation and loss of *schuy*-TagGFP mRNA transcripts in *Drosophila* spermatid cyst bundles when *imp* is knocked down via both single and double Imp-UAS-RNAi hairpin expression.

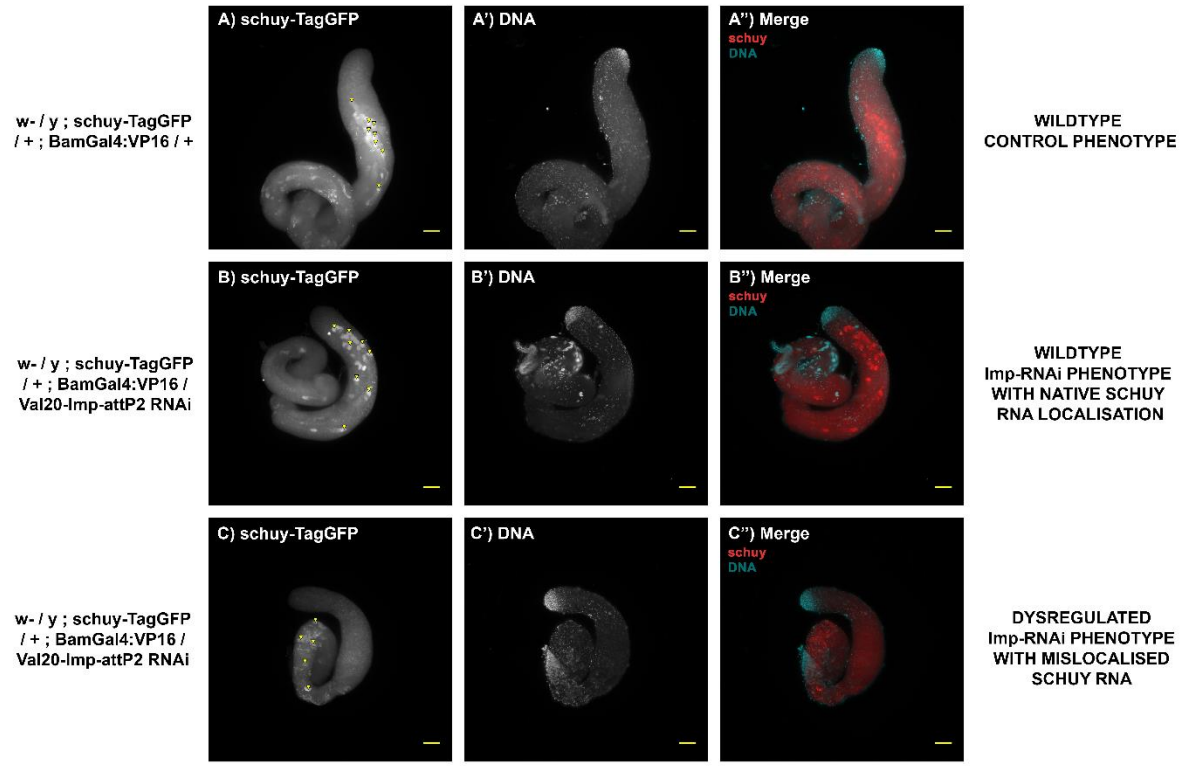

Figure 36. Phenotypic effects of single Imp-RNAi knockdowns on the transcription and localisation of *schuy*-TagGFP mRNA transcripts in *Drosophila melanogaster* testes. Whole mount testes were imaged via LSFM to visualise the distinct expression and localisation patterns of transgenic *schuy* mRNAs. (A – C) Greyscale *schuy*-TagGFP mRNA fluorescence signals, imaged on the 488nm GFP channel. (A' – C') Greyscale Hoechst 33258 DNA counterstaining, imaged on the 405nm DAPI channel. (A'' – C'') Two-channel RGB colour overlay of *schuy*-TagGFP mRNA (red) and DNA (cyan). Yellow arrowheads mark specific *schuy*-TagGFP mRNA fluorescence signals, including evidence of mislocalisation in (C). Only the Val20-Imp-attP2 RNAi line was investigated at this level due to issues with F1 male progeny collections. All images are maximum intensity projections and are representative of single testes dissected from at least one independent male. Scale bars: 25 μm.

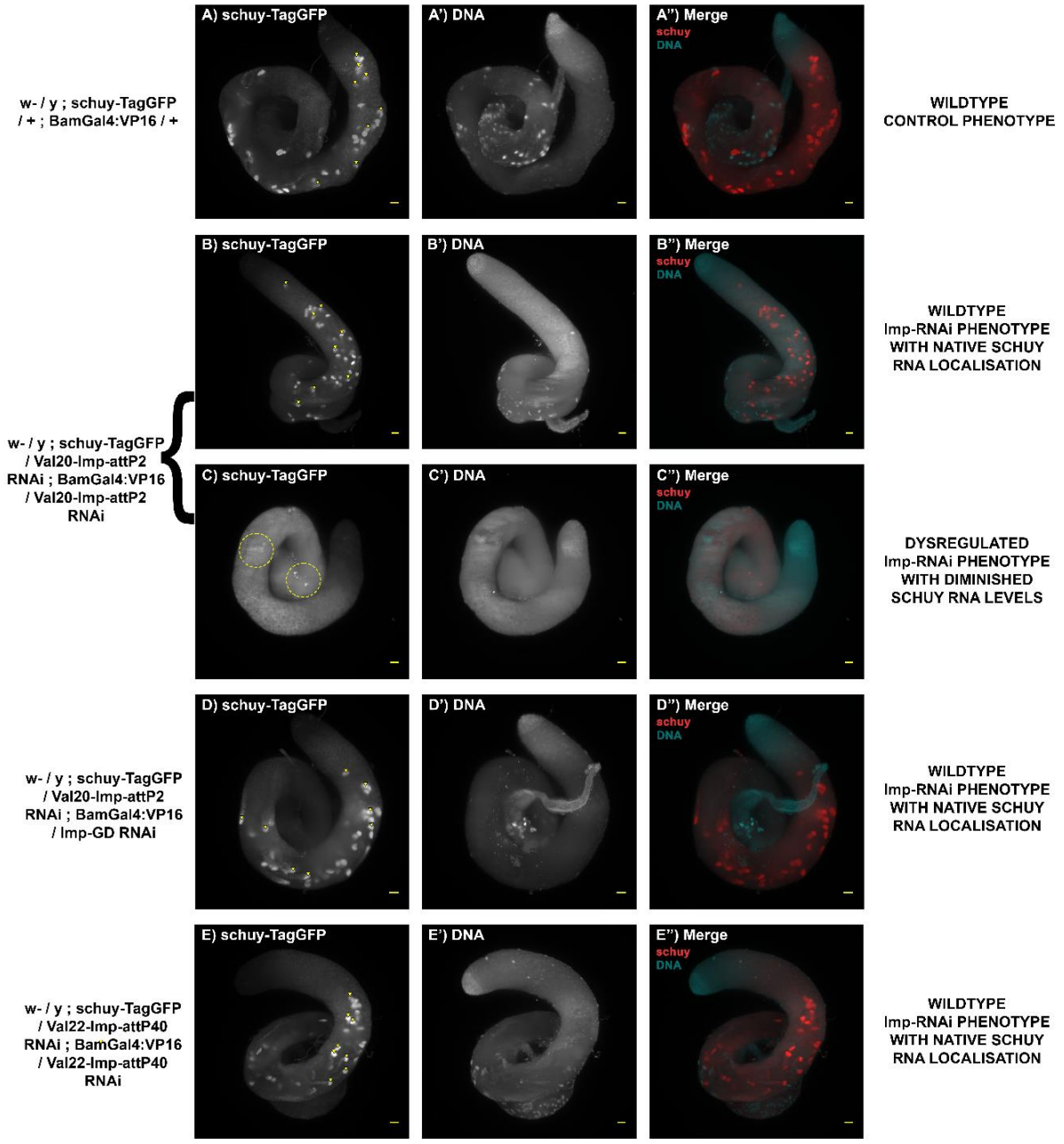

Figure 37. Phenotypic effects of double Imp-RNAi knockdowns on the transcription and localisation patterns of *schuy*-TagGFP mRNA transcripts in *Drosophila melanogaster* testes. Whole mount testes were imaged via LSFM to determine whether the translational defects associated with *imp*-directed RNAi knockdowns could be traced back to issues in transgenic *schuy* mRNA transcript production and localisation. (A – E) Greyscale *schuy*-TagGFP mRNA fluorescence signals, imaged on the 488nm GFP channel. (A' – E') Greyscale Hoechst 33258 DNA counterstaining, imaged on the 405nm DAPI channel. (A'' – E'') Two-channel RGB colour overlay of *schuy*-TagGFP mRNA (red) and DNA (cyan). Yellow arrowheads correspond to some sites of localised *schuy*-TagGFP mRNA transcripts. Yellow dashed lines in (C) indicate regions of mislocalised *schuy*-TagGFP fluorescence signals. All

images are maximum intensity projections and are representative of single testes dissected from at least one independent male. Scale bars: 25 μm.

5.9. HCR RNA-FISH reiterates normal transcription and localisation of *c-cup*-TagGFP mRNA transcripts upon knockdown of *imp*

When compared to the WT control, single and double Imp-UAS-RNAi knockdown crosses again yielded no post-transcriptional consequences on *c-cup*-TagGFP regulation at the level of mRNA.

WT control testes from the w; c-cup-TagGFP; BamGal4:VP16 x w^{1118} fly crosses exhibited the characteristic U-shaped, cup-like localisation patterns that were representative of a non-uniform build-up of *c-cup*-TagGFP mRNA transcripts in the tail-ends of mid-to-late elongating spermatid cyst bundles. These subcellularly-localised *c-cup*-TagGFP mRNA signals could be detected at a number of discrete sites throughout the control testis, which in turn corresponded to the tail-ends of spermatids of varying lengths that predominated in the mid-to-apical region of the organ (Fig. 38A – 38A'' and Fig. 39A – 39A'').

Resultant *c-cup*-TagGFP-expressing testes from F1 Imp-RNAi males displayed *c-cup*-TagGFP transcript expression and mRNA localisation patterns that were all comparable to the WT control – regardless of whether these were progeny from the single Val20-Imp-attP2 RNAi cross (Fig. 38B – 38B'') or from crosses to the Val20-Imp-attP2;Imp-GD RNAi, double Val20-Imp-attP2 RNAi or double homozygous Val22-Imp-attP40 RNAi lines (Fig. 39B – 39B'', Fig. 39C – 39C'' and Fig. 39D – 39D'').

There did not appear to be any alteration in *c-cup*-TagGFP mRNA production, and the acorn-cup localisation of *c-cup*-TagGFP transcripts remained unchanged. This supported the results we found in our above analyses, confirming that expression of the single and double Imp-RNAi hairpins does not affect the transcription or localisation of the underlying *c-cup*-TagGFP mRNAs in any way, nor does it alter the downstream expression of c-cup protein gradients within the developing spermatids.

Hence, it did not matter whether one or two copies of the Imp-UAS-RNAi transgene were expressed; Imp-RNAi testes continued to be fundamentally wildtype in terms of the post-meiotic regulation of localised *c-cup*-TagGFP mRNA transcripts, irrespective of the single or double knockdown condition tested.

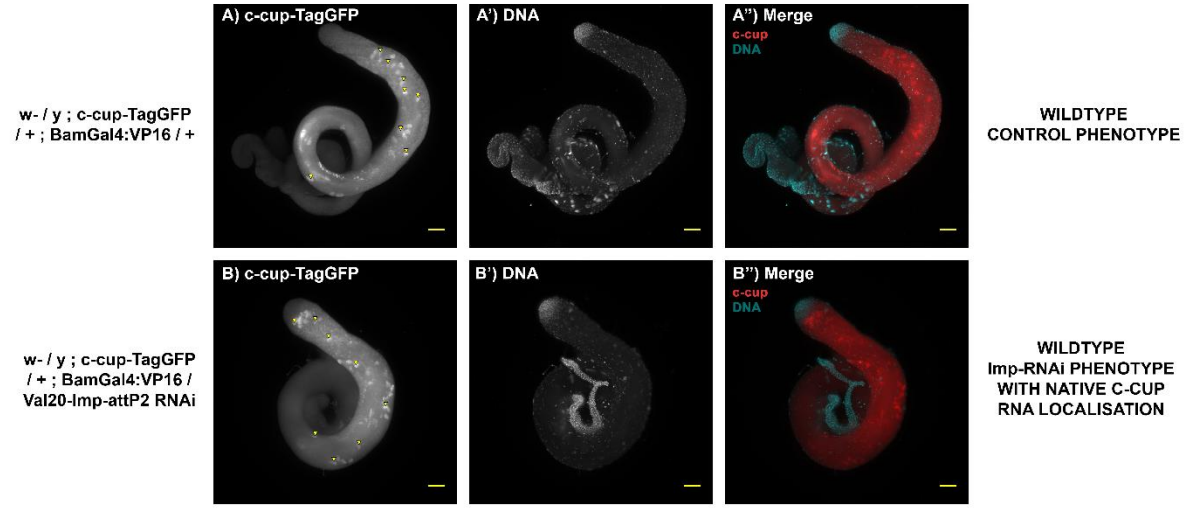

Figure 38. Phenotypic effects of single Imp-RNAi knockdowns on the transcription and localisation of *c-cup*-TagGFP mRNA transcripts in *Drosophila melanogaster* testes. Whole mount testes were imaged via LSFM to visualise the distinct expression and localisation patterns of transgenic *c-cup* mRNAs. (A and B) Greyscale *c-cup*-TagGFP mRNA fluorescence signals, imaged on the 488nm GFP channel. (A' and B') Greyscale Hoechst 33258 DNA counterstaining, imaged on the 405nm DAPI channel. (A'' and B'') Two-channel RGB colour overlay of *c-cup*-TagGFP mRNA (red) and DNA (cyan). Yellow arrowheads identify specific *c-cup*-TagGFP mRNA fluorescence signals. Only the Val20-Imp-attP2 RNAi line was investigated at this level due to issues with F1 male progeny collections. All images are maximum intensity projections and are representative of single testes dissected from at least one independent male. Scale bars: 25 μm.

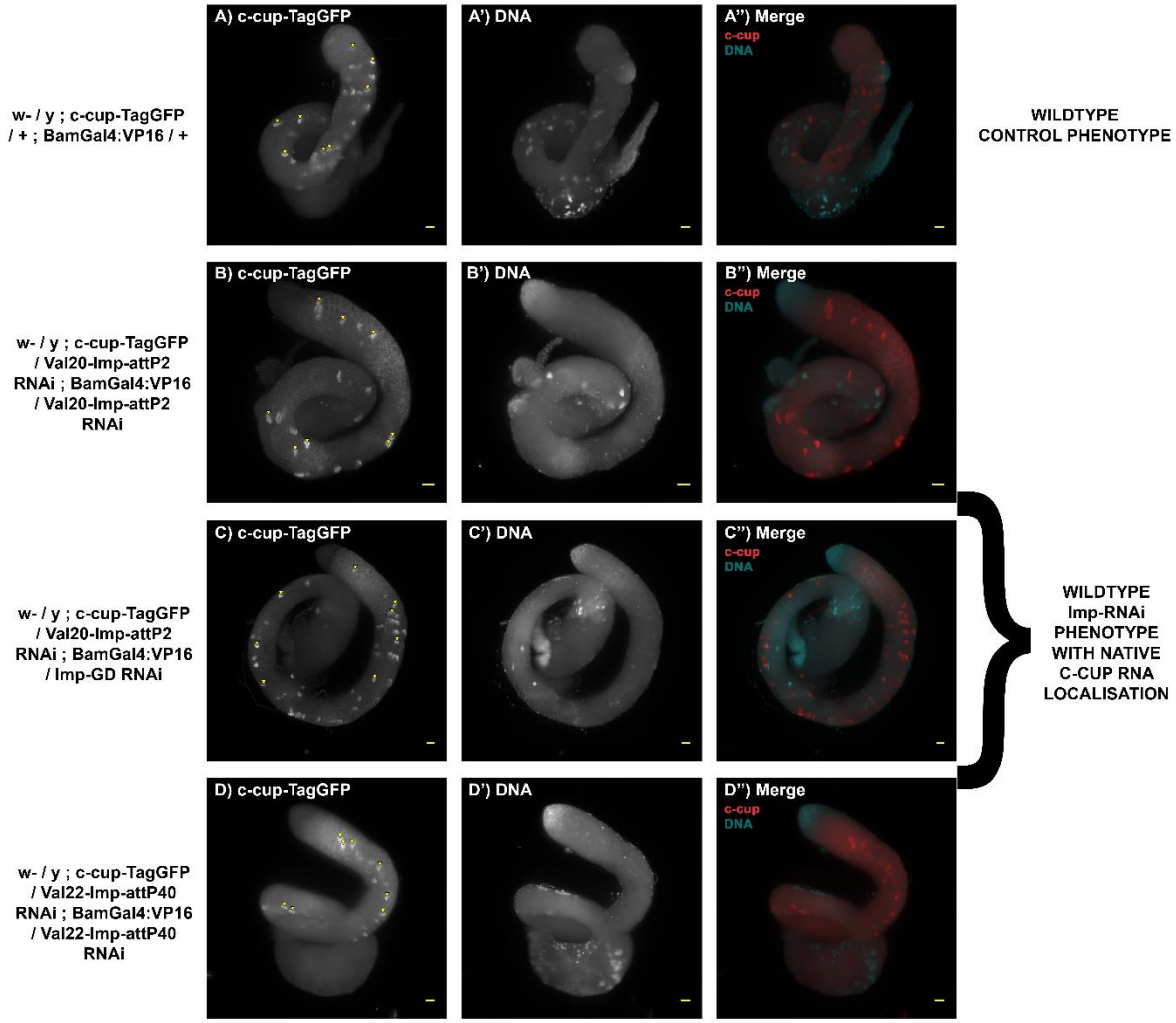

Figure 39. Phenotypic effects of double Imp-RNAi knockdowns on the transcription and localisation patterns of *c-cup*-TagGFP mRNA transcripts in *Drosophila melanogaster* testes. Whole mount testes were imaged via LSFM to determine whether there were any pronounced defects in transgenic *c-cup* mRNA transcript production and localisation that could be attributed to the expression of two copies of the Imp-RNAi hairpin transgenes. (A – D) Greyscale *c-cup*-TagGFP mRNA fluorescence signals, imaged on the 488nm GFP channel. (A' – D') Greyscale Hoechst 33258 DNA counterstaining, imaged on the 405nm DAPI channel. (A'' – D'') Two-channel RGB colour overlay of *c-cup*-TagGFP mRNA (red) and DNA (cyan). Yellow arrowheads correspond to localised *c-cup*-TagGFP mRNA transcripts. All images are maximum intensity projections and are representative of single testes dissected from at least one independent male. Scale bars: 25 μm.

5.10. Chapter-specific discussion

5.10.1. Imp contributes to the regulation of spermatid elongation and localised post-meiotic gene products in a context-dependent manner

Here, we have used the testis-specific BamGal4:VP16/Imp-UAS-RNAi set-up for the expression of our *imp*-targeted short TRiP and long GD RNAi hairpins. By regionally restricting Imp-RNAi effects to the mitotic germline cysts and spermatogonia by such means, GSCs, early germline cysts and other unaffected regions of the wider testis served as an internal control (Heigwer et al. 2018). Through this approach, we have found that a knockdown of *imp* leads to a range of dysregulated testis phenotypes, which show variability between one comet gene (*schuy*) and one cup gene (*c-cup*) at both a transcript and translational level. Results shown here therefore suggest that the BamGal4-UAS-mediated RNAi knockdown of Imp results in high phenotypic variation between: (i) the comet and cups at both a protein and RNA level, and (ii) the different experimental rounds of single and double Imp-UAS-RNAi screening.

For *schuy*, it appeared that these RNAi-induced defects were not attributed to translational disruption alone, but that this dysregulation was detectable at an earlier point of mRNA production, stability and/or localisation. The expression of Imp-RNAi therefore correlated with considerable phenotypic disruption at multiple levels in *schuy*-TagGFP-expressing fly lines – including a mislocalisation of transcripts, loss of localised mRNAs, depletion of fluorescent protein reporter signals, and stunting of spermatid elongation.

In contrast, Imp-RNAi hairpin expression showed no obvious phenotypic impact on *c-cup*-TagGFP testes, even when investigated at the level of both tagged protein and mRNA production. The overall transcriptional profile and localisation of the *c-cup*-TagGFP mRNA transcripts in the spermatid cyst bundles resembled that of the WT in all Imp-UAS-RNAi knockdown conditions, indicating that a loss of *imp* has no phenotypic effect on *c-cup*-TagGFP mRNAs. Moreover, there seemed to be an unusual context-dependent activity of Imp which was specific to the process of spermatid elongation; with Imp sometimes contributing to elongation and sometimes not.

Taken together, these findings tentatively suggest that Imp is involved in spermatid elongation and in the post-transcriptional regulation of localised post-meiotic mRNAs – however, the extent of this interplay may vary depending on the comet and cup in question and could be indicative of functional redundancy and/or binding partner cooperation, as I will discuss below.

5.10.2. Why is there variation in the severity of our Imp-RNAi phenotypes?

5.10.2.1. Is the variability associated with functional redundancy and binding partner cooperation?

Unlike *schuy*, Imp does not appear to directly regulate *c-cup* post-transcriptionally in the *Drosophila* spermatids, whether this be terms of mRNA localisation or local translation of c-cup protein. This does somewhat match with our RNA-affinity pull-down findings in Results Chapter 1, since the relative amount of Imp interacting with *c-cup* mRNA transcripts was lower than was the case with Imp and *schuy* mRNA binding. Although, these results were only representative of an *in vitro* binding environment, and do not differentiate between direct and indirect binding interactions.

Hence, it could be that, while Imp binds and regulates *schuy* mRNA transcripts directly, the interaction between Imp and c-cup mRNA is indirect – with Imp not being a fundamental contributor to proper *c-cup* regulation. If this were indeed true, it may explain why the loss of functional Imp does not have any post-transcriptional effect on *c-cup in vivo*; simply because there was another intermediary *trans*-acting factor that was compensating for this loss – perhaps through recruiting an alternative RBP or group of co-factors to offset this absence and compensate for any regulatory deficits.

Functional redundancy is commonplace in the Imp protein family. Breeding data from IMP1-deficient mice carrying an *Imp1* gene-specific trap insertion suggests that males and females remain fertile upon downregulation of the IMP1 isoform, and that there is some degree of compensation in the absence of one IMP isoform (Hansen et al. 2004). As the mammalian IMP proteins form homodimers and heterodimers, and share considerable overlap in their target RNA interactions and specificities, it is also

possible that the IMP family members are functionally redundant (Hansen et al. 2004; Nielsen et al. 2004). If this is the case for mammalian IMP isoforms, then it could also be a feasible possibility for *Drosophila* Imp.

In a recent study of endogenous human IMP protein activity, Conway et al. (2016) supported this argument of functional redundancy, but with one exception. By using an integrated combination of enhanced UV crosslinking, immunoprecipitation and high-throughput sequencing (enhanced iCLIP), the endogenous *in vivo* RNA targets of IMP1, IMP2, and IMP3 were determined in human pluripotent stem cells (hPSCs), and RNA Bind-n-seq (RBNS) was then used to elucidate *in vitro* binding preferences of full-length IMP1 and IMP2 proteins. Despite the hIMP proteins sharing a conserved domain architecture and targeted cytoplasmic localisation, it was concluded that IMP1 and IMP2 possessed highly overlapping binding preferences, but these were distinct from IMP3. The IMP1 and IMP2 isoforms showed highly similar binding preferences to the 3' UTRs of mature mRNAs, while IMP3 binding was predominately enriched for coding exons (Conway et al. 2016).

Interestingly, Conway et al. (2016) also found widespread enrichment of IMP1 and IMP2 binding to certain regions of genes – mainly that of the 3' UTR – rather than a preference for interacting with a specific subset of RNA substrates. Thus, even within the mammalian IMP subfamily, members play both a redundant and distinct regulatory function, and these roles can be traced back to the level of binding target preference. With some modifications, this set of experiments could theoretically be applied to the wider analysis of specific target binding sites for Imp in the *Drosophila* testis – thereby providing a future direction to follow-up on what we have found here.

Similarly, Nielsen et al. (2004) has proposed that mammalian IMP complexes bind sequentially and cooperatively to RNAs. Through a binding mechanism comprising an initial fast step and slow second step, IMP1 interacts with the murine *Igf-II* mRNA 3' UTR and human *H19* RNA in this way. Upon binding, IMP isoforms were also found to undergo dimerization; to support the formation of a stable complex with target RNAs. They showed that the first stage of RNA binding generates a transient, low stability intermediate while the second stage converts the putative RNA target into a 'locked', highly stable RNP particle bound to at least one IMP dimer.

Early titration experiments also confirmed that two whole molecules of IMP1 bind the mouse *Igf-II* 3' UTR, and results from EMSAs revealed the formation of a pure IMP1 homodimer species, as well as the formation of heterodimers between all three mammalian IMP Isoforms and a IMP2 splice variant (Nielsen et al. 2004). This ability to dimerise upon interacting with RNAs, to form and stabilise RNP complexes with protein-protein interactions, is in turn driven via the activity of IMP's hnRNP KH domains (Nielsen et al. 2002; Nielsen et al. 2004). Hence, as Imp homologues can interact within and between their isoforms, it may be possible that this overlap extends to other functions and binding partners – including RNA interaction profiles.

One final supporting example of functional redundancy is the overlapping pathophysiological functions shared between Imp homologues and the small RBP, LIN28 – a known regulator of development. Despite being involved in entirely separate molecular mechanisms that involve different effector complexes, they both have been described as key regulators of *let-7* miRNA biogenesis and protectors of let-7 target genes; which feeds directly into the successful establishment and maintenance of stem cell populations (Thornton and Gregory 2012; Degrauwe et al. 2016). Both are targets of *let-7* themselves so form part of a double-negative feedback loop, are functionally analogous and have a number of common mRNA targets between them (Thornton and Gregory 2012; Degrauwe et al. 2016). Similar temporal and spatial expression patterns have also been observed during normal embryonic and neural development using whole-mount RNA-ISH for murine LIN28 and IMP mRNA isoforms (Christiansen et al. 2009; Balzer et al. 2010).

We know that *Drosophila* Imp protects against *let-7* miRNAs and contributes to GSC maintenance in the testis (Boyle et al. 2007; Toledano et al. 2012). Moreover, new research has shown that Lin28 itself is also expressed within the hub cells of the *Drosophila* testis, where it acts to bind, stabilise and protect *upd* transcripts from *let-7* activity in a mechanism similar to but independent of Imp (Sreejith et al. 2019). In doing so, this prolongs the architecture, functionality and integrity of both the testis hub and stem cell niche. Both Lin28 and Imp bind independently to different sites in the 3' UTR of *upd* mRNAs, but this could potentially indicate a cooperative interaction – via the induction of positive conformational changes in the *upd* structure or through synergistic functions in parallel pathways that together stabilise the *upd* mRNA (Sreejith et al. 2019).

Recently, Imp has even been found to physically interact and cooperate with Lin28 for the synergistic regulation of intestinal stem cell (ISC) proliferation in the midgut of *Drosophila* adults (Sreejith et al. 2022). Therefore, it is highly likely that at least one other RBP, such as Lin28, could be performing in a compensatory manner to reinforce Imp-like functionality in the apical hub and/or spermatids – hence counteracting the absence of functional Imp in knockdown conditions. To test this hypothesis, a series of competitive binding assays could be performed in the future; using EMSA to ascertain whether an increase in the concentration of Imp and other protein factors such as Lin28 – both together and separately – corresponds to changes in binding affinities, as well as the amount of protein bound to specific post-meiotic comet and cup mRNAs (O'Day et al. 2015). In addition, potential binding sites in comet and cup transcripts could even be mutated, and the binding ability of each mutant then analysed by EMSA assays to determine if and how these interactions are affected upon comet and cup mutagenesis. The overexpression of Imp and other proteins of interest, both individually and combined, would also provide a good readout for future experiments (Sreejith et al. 2022). Phenotypic screening of overexpression in the testis could help to identify whether the post-transcriptional regulation and localisation of comet and cups is synergistically improved upon increased expression of RBP levels.

5.10.2.2. Is the variability attributed to the RNAi knockdown mechanism?

As mentioned previously, RNAi is an effective technique for gene knockdowns, rather than gene knockouts. When gene expression is knocked down via RNAi, resultant phenotypes can help to identify the functions of a target gene of interest – as we have attempted here with the characterisation of *imp* activity in *Drosophila* sperm development.

However, even with experimental methods that are deemed to be “best practice” like Gal4/UAS-driven RNAi, variances can still arise. Statistical comparisons of microwell plate cell-based RNAi screening and small-molecule screening suggest that RNAi screens can be less robust and more variable; leading to a broader range of biological hits overall (Birmingham et al. 2009). One possible explanation for this is that there is

a “window” of optimal RNAi effects which can vary depending upon the gene in question. Assaying or analysing too soon can therefore generate false negative results if not enough time has been given to generate a measurable phenotype. Assaying too late, on the other hand, can drive the interpretation of false positives because confounding secondary feedback and downstream effects can influence a host of weaker RNAi phenotypes (Perrimon and Mathey-Prevot 2007; Birmingham et al. 2009). However, when RNAi screening is applied *in vivo* within living model organisms such as *Drosophila*, this definition of a strict, gene-specific assay endpoint is difficult to determine.

Incidences of off-target effects can also occur when there is complementary sequence identity between the interfering RNA and random mRNA transcripts. This can weaken RNAi specificity, leading to inadvertent RNAi-mediated knockdown expression of other non-targeted genes. In *Drosophila* RNAi screens such as those conducted here, off-target effects are often a significant source of error. Due to this, it is important to conduct follow-up experiments to experimentally and systematically validate that the RNAi phenotype is indeed a direct result of targeted gene deficiency (Qiu et al. 2005).

There are many different factors that can promote the incidence of off-target RNAi effects, including dsRNA length. Computational studies suggest that the probability of off-target RNAi reactivity increases as the length of the initial dsRNA sequence increases – although, this effect is more extreme in organisms with larger genomes. A compromise to balance between high sequence specificity and low off-target reactivity was found upon optimisation of *in vivo* RNA to 21 nt in length (Qiu et al. 2005). Presence of the enzyme, Dicer, supports this optimal 21 nt length *in vivo*. Dicer exhibits RNase activity and can cut dsRNA into shorter fragments of approximately 21 nt. Subsequent siRNAs can then associate with the multi-protein RNAi silencing complex (RISC), and their minus-strand sequence can be directed to any target RNA transcripts with complementary sequence identity. By doing so, these molecules undergo RISC-mediated cleavage to yield post-transcriptional RNAi knockdown of gene expression (Qiu et al. 2005). This is why we introduced the cross with a UAS-Dicer2 expressing Imp-GD RNAi line into our analyses; to validate our rare RNAi phenotype showing comet mislocalisation and aberrant spermatid elongation.

By adding Dicer into our *in vivo* genetic mix, we knew it would drive the optimal balance of 21 nt siRNAs and hopefully enhance the efficiency of our Imp-GD RNAi knockdown. We could also have a high degree of confidence in the specificity of our TRiP RNAi constructs because their shorter hairpin length made them less susceptible to off-target effects, when compared to earlier iterations in the design process that contained longer inverted repeats (Ni et al. 2011).

Furthermore, RNAi analysis may not be a good option for the characterisation of genes whose functions must undergo a complete loss for the development of an observable phenotype (Qiu et al. 2005; Perrimon and Mathey-Prevot 2007). This may somewhat explain the spectrum of phenotypes that we detect when *imp* is knocked down in schuy-TagGFP expressing males. Moreover, if *imp* is a pleiotropic spermatogenesis gene, as is the case for the AAA+ ATPase, Valosin-containing protein (VCP), the Imp protein may serve multiple functions that regulate different stages of *Drosophila* sperm development in different ways depending on the timepoint (Butsch et al. 2023). To truly silence all of these biological activities, at all timepoints, may be difficult to achieve with enough selectivity in a single Gal4/UAS RNAi system, unless multiple specific Gal4 driver types are combined in one line to counteract potentially lethal and off-target effects.

One final possibility is that the pre-defined timepoint at which we knocked down *imp* with RNAi may not have been the most appropriate to determine its true function within the testis. Fabrizio et al. (2008) has shown that Imp is expressed in the pre-meiotic, mitotically active cells at the apical hub area of testis, as well as at the extreme tail-ends of the post-meiotic, elongating spermatid cyst bundles. So, the activity of expressed Imp-UAS-RNAi hairpins within the eight-cell transit amplifying spermatogonia onwards may only be enough to silence *imp* expression later on in sperm development, while a small proportion of the *imp* gene products from this earlier pre-meiotic site of expression may be persisting in the late developing germline cells.

If this was indeed the case, then perhaps there was a degree of compensatory activity taking place, whether this be in the post-transcriptional regulation of comet and cup mRNA localisation and/or in the spermatid elongation stages of spermiogenesis. Indeed, this differing expression of Imp in time and space may again indicate a potential pleiotropic effect of Imp, with its function depending on the spatiotemporal

profile of its expression. However, because our focus was on the mid-to-late elongating spermatids in the latter stages of post-meiotic sperm development, a knockdown of *imp* that was driven even earlier than this with extended effects – such as is the case with the Vasa-Gal4 driver line – could have meant that we never saw what delayed effects *imp* deficiency causes because sperm development may have become disrupted well before this point, as is the case in meiotic arrest, for example. With this in mind, it is difficult to truly strike a balance between the ever-expanding possibilities of gene functionality in an already complicated and elaborate biological process like sperm development.

5.10.3. There are advantages and drawbacks of using the *Drosophila* Gal4/UAS binary expression system

The Gal/UAS system is a gold-standard for studying forward genetics in *Drosophila*. However, the temperature sensitivity of Gal4 activity in *Drosophila* can be both a blessing and a curse.

In fly models, the temperature-dependent nature of this tool bestows greater spatiotemporal control over UAS-transgene expression. A rearing temperature of ~29°C (± 1°C) provides a fine balance between providing a permissive temperature for optimal Gal4 activity and minimising the adverse effects that high temperatures can have on fertility, fecundity and viability due to inadequate mating, growth and/or survival rates. On the contrary, rearing at 16°C falls at the other end of the spectrum, wherein minimal Gal4 activity takes place. Hence, a simple modification to the incubation temperature can accomplish a wide range of tissue-specific expression levels – thereby expanding the flexibility of the system (Duffy 2002). However, this flexibility can also make a consistent “all-or-nothing” phenotypic response difficult to obtain with confidence.

For the Bam-Gal4:VP16 driver transgene, the severity of RNAi testis phenotypes is highly dependent on variations in rearing temperatures (Doggett et al. 2011). At 30°C, the Bam-Gal4:VP16-driven UAS-RNAi knockdown of the testis-enriched *lin-52* paralogue, *wuc*, was characterised by male sterility and a severe meiotic arrest phenotype in primary spermatocytes. Yet, at 29°C, there was some evidence of, albeit

abnormal, meiosis and early spermatid differentiation in the F1 RNAi testes, along with some spermatid elongation when rearing temperatures were reduced to 25°C. The production of a small number of motile sperm was noted when F1 RNAi progeny were incubated at 18°C, although males still remained sterile (Doggett et al. 2011). Therefore, a change of only a few degrees can have massive impact on the strength of RNAi phenotype in *Drosophila* sperm development. With this in mind, we made the utmost of efforts to control for rearing temperatures as much as possible. We placed all F1 Imp-RNAi cultures in the same 30°C incubator, with restricted access, as to avoid any unnecessary temperature fluctuations that could affect our Imp-RNAi testis phenotypes. We had previously tested a rearing temperature of 29°C (not shown here), but this corresponded to an even greater variability in RNAi testis phenotypes overall. Perhaps increasing the incubation temperature to 31°C would be an option to investigate going forward, but we have so far avoided this due to concerns regarding the potential negative effects that higher rearing temperatures can have on *Drosophila* ageing, life span and viability (Miquel et al. 1976; Mołoń et al. 2020).

5.10.3.1. Bam-Gal4/Imp-UAS-RNAi knockdowns may vary in penetrance and efficiency

While sufficient Bam-Gal4:VP16-induced UAS-RNAi knockdowns have been verified in the literature, penetrance and efficiency is not always 100%, and there has been inconsistent outcomes when using Bam-Gal4:VP16 and other germline-specific transgenic drivers of RNAi hairpin production in the *Drosophila* testis (White-Cooper 2012). Unfortunately, regardless of Gal4 driver choice, partial gene silencing can only ever be achieved with RNAi knockdown approaches, unlike in complete knockouts. However, we know that complete homozygous *imp* knockout mutations in germline clones leads to embryonic lethality, so testis-specific RNAi knockdowns are our best option when it comes to analysing the effects of *imp* depletion on male gametogenesis alone – without risking any detrimental off-target effects to whole-fly viability (Munro et al. 2006; Boylan et al. 2008).

Although Imp mutants are homozygous lethal, Sreejith et al. (2022) has recently employed Mosaic analysis with a repressible cell marker (MARCM) for the successful

heat shock-induced generation of *imp* mutant clones in adult *Drosophila* ISC populations. This clonal analysis enabled the effective induction and tracing of labelled *imp* homozygous mutant ISC lineages in otherwise heterozygous flies. Considering this novel possibility, MARCM could provide a robust tool for the follow-up analysis of *imp* knockdown phenotypes in the testis; thereby circumventing the variability we have so far experienced with our current Bam-Gal4/Imp-UAS-RNAi screening set-up (Wu and Luo 2006).

Expression of Mst36F-UAS-RNAi transgenes using a single copy of several different Gal4 driver lines has demonstrated that, despite *mst36F* gene silencing inducing an obvious reduction in male fertility and compromising fecundity, all Gal4 drivers exhibited effects far from a superior complete knockdown of *mst36F* expression – irrespective of the type of line tested. RT-PCR assays revealed that Bam-Gal4:VP16 could only drive an RNAi-induced decline in fertility to ~80% of control fertility levels while the nanos-Gal4 driver exhibited the best silencing effect overall, dropping fertility down to 70% (Di Cara et al. 2010). However, the strength of RNAi phenotypes may be improved by adjusting the combination of Gal4 drivers and UAS-RNAi transgenes used, including switching to a homozygous Gal4 transgene arrangement (Di Cara et al. 2010). In fact, flies expressing one copy of the Bam-Gal4:VP16 driver were found to downregulate target wildtype *wuc* mRNA levels to roughly 9% when expressed in the presence of the corresponding Wuc-UAS-RNAi transgene at 29°C. Flies with two copies of the Bam-Gal4:VP16 driver showed an even greater reduction, down to around 3% of target wildtype mRNA levels (Doggett et al. 2011). Thus, Gal4 dosage is the most important factor for strengthening the phenotypic effects of RNAi silencing.

This may give some explanation as to why we see so much variation in the severity of our Imp-RNAi phenotypes – simply because, while our starting Bam-Gal4:VP16 driver fly line is a homozygous configuration on the third chromosome, only one copy is transmitted to the F1 RNAi males upon crossing.

5.10.3.2. Phenotypic differences are unlikely to be a consequence of the Imp-UAS-RNAi genetic backgrounds

The Val22-Imp-attP40 UAS-RNAi constructs have been optimised for transgene expression in the female germline whereas the Val20-Imp-attP2 UAS-RNAi constructs are effective in both the soma and germlines of both sexes (Ni et al. 2011). There is an intimate, complex interplay between the developing male germline cells and their enveloping somatic cyst cells, which we know provides a regulated microenvironment that is essential for the proper maintenance and differentiation of the germline cell population during sperm development (Gönczy and DiNardo 1996; Kiger et al. 2000; Tran et al. 2000; Lim and Fuller 2012; Fairchild et al. 2017; Bazylev et al. 2021). As the Val20-Imp UAS-RNAi construct expresses Imp-RNAi hairpins efficiently in both the germline and somatic cells, it was therefore expected to generate the strongest effects of the two in *Drosophila* testes. We have indeed confirmed this finding here and can have confidence that the Imp-UAS-RNAi hairpins have been working as expected. Although, we have not had time to quantify the level of *imp* gene knockdowns in any of our F1 Imp-RNAi males by RT-PCR.

We used Imp-UAS-RNAi hairpin constructs from both the TRiP and GD libraries in this project (Ni et al. 2011; Perkins et al. 2015). The *imp* gene knockdowns were therefore driven by, and compared between, different Imp-UAS-RNAi lines from different collections, which in turn encoded Imp-specific RNAi hairpins of different lengths. While the short TRiP RNAi constructs expressed a 21 nt hairpin sequence and the long GD RNAi constructs expressed a 316 nt hairpin sequence, both still targeted the same common exon encoded in the coding sequence of *imp*. Therefore, we can conclude that this diversity of Imp-RNAi phenotypes was not an outcome of different RNAi gene silencing mechanisms.

What's more, we can assume that the phenotypic fluctuations we have observed upon knocking down *imp* were not due to any of the Imp-UAS-RNAi transgenes we have used here. This is because, the variation we have observed is not restricted to one RNAi construct and not the other – we see wildtype-like and dysregulated testis phenotypes regardless of whether the short TRiP Val20-attP2 RNAi hairpins or long

GD RNAi hairpins have been expressed. Therefore, we can conclude that these variable phenotypic effects were not due to the genetic background of the Imp-UAS-RNAi constructs.

Nevertheless, if future experimental repeats of this screening were to be conducted again, we would include qRT-PCR to accurately and sensitively analyse the knockdowns at the *imp* mRNA level – both with and without UAS-RNAi hairpin induction. In doing so, we would be able to measure the expression levels of endogenous *imp* mRNA in the testes of: (i) uncrossed males, (ii) the F1 progeny from all our Bam-Gal4 x Imp-UAS-RNAi conditions, and (iii) the F1 progeny of the negative control cross with w^{1118}. We could also investigate this at the level of Imp protein expression by conducting quantitative Western Blotting on samples prepared from these same fly conditions. In both cases, this would enable a direct comparison to be made between the expression level of *imp* transcripts and Imp protein in all scenarios, allowing us to determine to what extent Imp is truly being knocked down.

Many recent studies in the wider literature have validated the performance of Bam-Gal4 in the *Drosophila* testis and have used qRT-PCR to quantify the extent of their Bam-Gal4/UAS RNAi knockdowns with high degrees of success (Fang et al. 2024; Petit et al. 2024; Xu et al. 2024). For example, Petit et al. (2024) demonstrated that, when the *Drosophila* Phosducin-like protein 3 (PhLP3) was knocked down in the male germline via a Bam-Gal4 driven UAS-*PhLP3*-RNAi, this corresponded with a 77% decline in the relative expression of *PhLP3* (23% of the *PhLP3* levels measured in the Bam-Gal4 control testes). In light of this, the phenotypic variations we have found here are more likely to be attributed to our various Imp-UAS-RNAi hairpin constructs, as opposed to issues with the Bam-Gal4:VP16 driver efficiency. Although, the fact that this variability arose regardless of the Imp-UAS-RNAi line used does make this difficult to conclude either way without follow-up testing. qRT-PCR may therefore help to clarify such uncertainties.

We could also generate a stock that stably expresses both the Imp-GFP and Bam-Gal4:VP16 driver transgene, then screen the testes of F1 progeny after crossing to our various Imp-UAS-RNAi fly lines. By performing fluorescence microscopy on these, alongside an appropriate set of positive and negative control crosses, this would allow us to quantify and compare the relative fluorescence signal intensities of Imp-GFP in

each testis. A quantifiable reduction in Imp-GFP fluorescence signals would be indicative of a genuine knockdown of endogenous *imp* expression.

5.10.4. Evaluation of experimental techniques used for RNAi screening

5.10.4.1. LSFM offers high resolution, three-dimensional imaging of intact, whole-mount *Drosophila* testes

Here, we have successfully used LSFM to observe the continuous, unimpeded dynamics of asymmetrical, subcellular localisation of comet and cup mRNA transcripts. We chose LSFM because it is a straightforward fluorescence microscopy technique that brings together intrinsic optical sectioning and multiple-angled-view imaging. By mounting the specimen onto a motorised translation and rotation stage, then changing the orientation and direction, a stack of sectional images can be acquired plane-by-plane along all three dimensions. These optical sections are layered to generate three-dimensional reconstructions, thus enabling spatiotemporal, volumetric imaging (Huisken et al. 2004; Reynaud et al. 2008).

The testis sample is illuminated via a single, side-on sheet of light whose centre aligns with the focal plane of the detection objective lens system. In doing so, excitation is limited to the fluorophore population inhabiting the volume nearest the focal plane (Greger et al. 2007; Reynaud et al. 2008). This offers a low phototoxicity and photobleaching set-up, which makes LSFM amenable to the *in toto* imaging of entire organisms in size ranges up to a few millimetres (Krzic et al. 2012). When compared directly to standard confocal fluorescence microscopy, LSFM can cut-down phototoxicity and photobleaching up to three orders of magnitude (Reynaud et al. 2008).

LSFM has quickly become a leading choice for the visualisation of developmental dynamics. This is attributed to its high performance and superior spatiotemporal resolution – making it possible for *in toto*, whole-mount imaging of specific tissues, organs and whole living systems (Schmied and Tomancak 2016). The advent of LSFM

has also led to more efficient acquisition speeds and a higher signal-to-noise ratio (Khairy and Keller 2011).

Developmental and molecular biology has seen LSFM be utilised with great effect; with it widely exploited for the whole-mount imaging of *Drosophila*. It has been used for the visualisation of *Drosophila* embryogenesis (Tomer et al. 2012; Schmied and Tomancak 2016), whole larval CNS (Lemon et al. 2015), eye-antenna disc primordium formation (Huang et al. 2017) and early gastrulation (Rauzi et al. 2015). LSFM has also permitted the comprehensive, volumetric analysis of three-dimensional tissue topography based on laser excitation, which has even been successfully applied to the visualisation of whole murine testes (Pinkert-Leetsch et al. 2022). With careful sample manipulation and mounting, specimens can remain completely intact throughout the process and can be imaged at regular intervals for up to three days without any harm to embryogenesis and development (Huisken et al. 2004).

One point to raise regarding this technique, however, is the difficulty that can arise from mounting and imaging samples with unusual morphologies and internal heterogeneities. The main challenge we found was that the spiralled structure of *Drosophila melanogaster* testes made it difficult to achieve exact positioning and precise alignment within the agarose gel matrix, and these placement effects were not truly known until imaging was commenced. As LSFM relies on a single plane of laser excitation, this could sometimes result in a “blurring” effect and loss of signal resolution. The overall clarity of fluorescence signals could therefore be obscured when regions of the testis were out of the focal plane. Because the “tube” of the testis was somewhat flexible and could uncoil at will after dissection out of the *in vivo* physiological environment, a range of movement could occur during mounting, before the agarose had enough time to set. As a consequence, the quality of signals within the three-dimensional dataset were not always consistent throughout the whole organ. We also found that the outer muscle sheath of the testis could produce autofluorescence and high levels of background, especially when pigmented, which led to further obscurities.

However, all types of optical-based microscopy, including LSFM, show a gradual decline in performance as the depth of imaging into the sample is increased. In general, imaging beyond the 20 μm – 100 μm threshold tends to require a modified

microscopy approach that includes adaptive, compensatory optics in both excitation and detection pathways – although, the extent of these adaptations does depend on the overall volume and optical heterogeneity of the sample (Chen et al. 2014a; Wang et al. 2014). Hence, *in vivo* imaging, particularly in a three-dimensional context, will always entail inevitable compromises between resolution, speed and phototoxicity; including trade-offs between laser power and exposure levels which can vary depending on the specimen in question and fluorophore of choice (Chen et al. 2014a).

Nevertheless, LSFM is advantageous in the case of *Drosophila melanogaster* testes because they are relatively thick samples that are complex in morphology due to their large encompassing cell population. The intricate anatomy of a testis, regardless of the organism, reflects its factory-like function of providing a constant and continuous pipeline of sperm cell production for maturation and storage. We therefore required an imaging modality that would facilitate an unimpeded, holistic view of this whole assembly line – something two-dimensional microscopy is unable to sufficiently achieve (Pinkert-Leetsch et al. 2022).

LSFM allowed us to visualise post-meiotic comet and cup mRNA localisation throughout the testis, without the usual requirement of specimen squashing, which could somewhat distort visualisation. It gave us the opportunity to observe the phenotypic effects of RNAi gene silencing in three-dimensional, rotational space, without the risk of missing out on any abnormalities in RNA localisation that would only have been apparent in the wider context of the testis.

5.10.4.2. HCR RNA-FISH vs. RNA-ISH staining: how does automatic background suppression and simultaneous multiplexing compare?

RNA-ISH staining is dependent on standard anti-sense RNA probes. These can bind non-specifically within specimen samples, leading to an amplified background that can diminish resolution and mask specific localisation sites/patterns of target RNAs. In HCR RNA-FISH, on the other hand, the specially designed split-initiator probes are paired so that each one carries half of the HCR initiator sequence. Thus, a chain reaction of sequential hairpin recognition, binding and amplification can only be

triggered once both probes bind their exclusive target transcript and co-localise the full initiator I1 sequence. This automatic background suppression is maintained throughout signal amplification because the DNA amplifier hairpins are kinetically trapped and their polymerisation is conditional on the presence of I1. The non-specific association of probes and/or hairpins will therefore fail to diminish performance or robustness, and no false chain reactions will be initiated as a result (Choi et al. 2018).

Another point to note is that the HCR amplifier sequences are independent of the target mRNA sequences. Instead, they rely on the presence of I1 initiator sequences that have been integrated into the split-initiator probe design. Because of this, validated amplifiers can be reused without continual modification, and a new repertoire of mRNAs can be investigated simply by re-performing the design process to generate new sets of DNA probe pairs (Choi et al. 2016).

Since the HCR-FISH split-initiator probe sets can be designed to complement up to five independent, coloured amplifiers carrying spectrally-distinct fluorophores (e.g., B1 H1/H2, B2 H1/H2, B3 H1/H2, B4 H1/H2 and B5 H1/H2 hairpin pairs), this means that several different RNAs can be hybridised, imaged and analysed at once without risk of sample degradation (Choi et al. 2010; Choi et al. 2014; Choi et al. 2016). As the corresponding hairpin amplifiers are themselves associated with different fluorescent Alexa dyes, this process of mix-and-matching enables multiplexing of multiple independent HCRs within the same sample at the same time, independent of the number of target mRNAs in question (Choi et al. 2016; Shah et al. 2016). HCR RNA-FISH is therefore a one-step multiplexing methodology, with quantitative signal amplification that targets all RNAs simultaneously.

5.10.4.3. HCR RNA-FISH vs. RNA-ISH staining: how does high level subcellular and single-transcript resolution compare?

A combination of fluorescent tagging (e.g. GFP), protein labelling, protein trapping and antibody staining can also be implemented into a modified HCR RNA-FISH protocol to investigate high-resolution co-localisation of specific proteins alongside hybridised RNAs. This can be exploited to support the investigation into compartmentalisation

and molecular localisation relative to specific subcellular structures and organelles within cells, such as the fusome. HCR RNA-FISH hence facilitates relative quantification of mRNAs with a subcellular and single-molecule resolution that can be studied holistically in the context of whole-mount tissues, including *Drosophila* testes (Choi et al. 2014; Choi et al. 2018).

The short, double-stranded nature of the amplification hairpin oligos also acts to ensure that there is deep penetration into thick samples. Successful and efficient mapping to a single-molecule resolution is therefore possible; allowing single transcript signals to be elucidated in whole tissue specimens and in the context of preserved spatial and anatomical architecture (Shah et al. 2016). The main commercial supplier, Molecular Instruments Inc., even postulates a 5 mm penetrant potential.

This resolution is somewhat lacking in the RNA-ISH staining technique. Diffusion of the “reporter” reaction products away from the hybridisation site can occur in enzyme-based, colour assays such as RNA-ISH staining. In such circumstances, this can lead to the development of diffusion artifacts, which diminishes overall resolution and the ability to pinpoint subcellular transcript localisation with confidence (Speel 1999). In contrast, the HCR amplification polymers remain tethered to their initiating DNA probes to counteract any possibility of signal diffusion away from target mRNAs (Choi et al. 2014; Choi et al. 2016). In doing so, HCR-FISH improves single transcript resolution, and enables quantification and informatics analysis. Because the HCR signal and voxel intensity scales linearly with mRNA abundance, mRNA expression can be analysed semi-quantitatively (Trivedi et al. 2018).

RNA-ISH staining has a very time-dependent nature to it; the time needed for the colour staining reaction and signal development can vary anywhere from ten minutes to one hour. Some transcripts may even require an incubation lasting for several hours, or potentially overnight (Morris et al. 2009). However, the longer this incubation period, the greater the risk of overstaining and background staining – both of which can mask genuine and specific mRNA expression patterns. Real signals present as a purple/blue colour initially, but development of a pinkness may indicate background staining. Subsequent ethanol dehydration washes and clearing with compounds such as methyl salicylate can help to dissipate some of this background, but at a sacrifice of dissolving a proportion of real colour product (Morris et al. 2009). RNA-ISH staining can therefore

be quite subjective, and experienced judgement and transcript-dependent optimisation are key factors in its proper implementation. It relies heavily on compromise and consistency to achieve a compelling result.

Overall, when all of these considerations are taken into account, HCR RNA-FISH supersedes RNA-ISH for the efficient and effective attainment of experimental needs. HCR RNA-FISH has now cemented its place in our research group's arsenal of in-house protocols and will continue to be employed in place of traditional RNA-ISH staining.

5.10.5. The unrestricted and rapid subcellular movement of Imp supports its regulatory role in comet and cup mRNA localisation

As we have shown here, a knockdown of functional Imp protein can cause a severe impairment to normal spermatid elongation.

One possible explanation for this is that the downregulation of Imp hampers localisation of important target RNAs, including comet and cup mRNA transcripts; this then impedes directed elongation and growth in a mechanism similar to the directed movement observed in metastatic cancers. The ability of Imp homologues to establish polarisation has already been tentatively linked to metastatic cancers, with IMP3 being the mammalian isoform most commonly implicated in human cancer development (Reviewed in Lederer et al. 2014; Degrauwe et al. 2016).

IMP1 has also been heavily implicated in oncogenesis and increased metastatic potential (Dimitriadis et al. 2007; Mongroo et al. 2011). Analysis of colorectal cancer xenografts by Hamilton et al. (2013) provided further support of this association, with overexpression of IMP1 driving xenograft tumour growth and metastatic entrance into the bloodstream. IMP1 overexpression was also associated with a range of metastasis-like phenotypes, suggesting that IMP1 is a key player in the initiation of tumour growth and the modulation of early metastatic events. If homologues of *Drosophila* Imp are able to drive directional cell movement and establish phenotypes reminiscent of metastasis via polarisation, then perhaps Imp itself may also be an

important regulator of normal, wildtype biological processes in polarised cells, including in the spermatid cysts during sperm development.

Growing spermatids can elongate to a length of 1.8 mm (Fabian and Brill 2012). As the nuclei are at one extreme end and the tail-ends are at the other distal pole, Imp would need to make this long-distance transit quickly and efficiently for sufficient comet and cup mRNA localisation. Oleynikov and Singer (2003) provides potential support of this. Using high-speed imaging, they found that the chicken Imp homologue, ZPB1, once exported from the nucleus into the cytoplasm of fibroblasts, underwent actin filament- and microtubule-dependent localisation at velocities of 0.6 μm/s. ZPB1-GFP was found to shuttle bidirectionally between the nucleus and lamellipodia in an active motor-driven process, with the ability to redistribute and accumulate at regions of nascent protrusion formation. This dynamic movement of ZBP1 supports the rapid rate at which sites of both targeted mRNA accumulation and localised protein synthesis can be relocated as a direct response to cell morphology transformations (Oleynikov and Singer 2003).

We know that distinct morphological changes occur throughout the process of *Drosophila* sperm development so it is likely that Imp:RNA interactions and subsequent localisation may play an important role in response to these changes in spermatogenic cell shape and volume. If we assume that Imp can localise at the same rate of velocity as ZPB1, we can use this value to determine how long it would take for Imp to transport associated mRNAs from the proximal nucleus to the extreme apical ends of the spermatid cyst bundles. Using a velocity of 0.6 μm/s and a maximum spermatid length of 1.8 mm, we can infer that it would take ~50 minutes for Imp to localise to the tail-ends of spermatids (Oleynikov and Singer 2003).

We could, of course, test this theory ourselves by designing a time course experiment that would enable the cytoplasmic localisation of the Imp fluorescent reporter (e.g., Imp-GFP) to be observed throughout living, and actively elongating, spermatid cyst bundles *in vivo*. By tracking Imp transport throughout living spermatids as single fluorescent particles to a final stable, stationary point of accumulation at the tail-ends, this would provide us with an initial understanding of the migration dynamics and velocity of Imp transport within the *Drosophila* testis (Nielsen et al. 2002; Oleynikov and Singer 2003). LSFM using the same Zeiss Lightsheet Z.1 System would still be a

feasible option for this fluorescence imaging approach, since the whole living testis could be mounted – without fixing – in agarose prepared with insect culturing medium, and the sample chamber filled with the same culture media. By utilising the temperature and CO_2 environmental control settings, physiologically relevant incubation conditions could also be precisely defined within the closed sample chamber to support testis viability and longevity.

This highlights the dynamic nature of Imp-mediated transport in different systems and cell types, and thus supports the likelihood that Imp has some contribution to the localisation of mRNAs in *Drosophila* sperm development. Moreover, at steady state, Imp homologues are primarily cytoplasmic and, in fibroblasts, ZBP1 is at a nuclear concentration that is ~2.5 times less than in the cytoplasm. Overall, this equates to a steady state distribution of 92% of cellular ZBP1 in the cytoplasm versus 8% in the nucleus (Nielsen et al. 1999; Oleynikov and Singer 2003). Taken altogether, this evidences the unrestricted freedom of Imp; it can pass throughout the distinct subcellular regions of cells with ease. This means that, in theory, the elongating length of spermatids would be of no challenge to Imp – which relates well to its characterised localisation at the extreme spermatid tail-ends, well away from the nucleus.

5.10.6. Conclusions

To conclude, we have used RNAi screens to investigate the functional role of Imp in the *Drosophila* spermatids. We have studied the effects of Imp-RNAi expression on the localisation and translation of *schuy*-TagGFP and *c-cup*-TagGFP mRNA transcripts in Imp-RNAi lines. We found that a knockdown of functional Imp leads to a spectrum of abnormal testis phenotypes with varying severity, and, in some cases, this includes mislocalisation of mRNA transcripts, loss of localised RNA and fluorescent protein reporter signals, and considerable disruption to spermatid elongation.

There could be many reasons for this variation, including inconsistencies associated with RNAi efficiency and/or the interplay of other binding factors in the testes. Nevertheless, our findings still suggest that *imp* plays a context-dependent regulatory role in spermatid elongation and in the post-meiotic expression of localised *schuy*.

6. DISCUSSION

We started this project with the aim of determining why and how the subcellular, asymmetric localisation of post-meiotic comet and cup mRNA transcripts occurs within elongating *Drosophila melanogaster* spermatids. This offered quite a broad scope of research direction, so we focused this down to address four primary research questions:

1. Which RBPs contribute to the post-transcriptional comet and cup mRNA localisation in the spermatid cyst bundles and by what regulatory mechanism are they likely involved?

2. Which RBPs interact with post-meiotically transcribed mRNA transcripts such as the comet and cup mRNAs?

3. What other protein components are associated with these RBPs to facilitate their binding and RNA processing activities?

4. What functional role do specific RBPs (e.g., Imp) play in the *Drosophila* testis?

In turn, we have performed an extensive functional analysis of the *Drosophila* IGF-II mRNA-binding protein (Imp) and have implicated it as an RBP that contributes to the post-transcriptional regulation of some comet and cup mRNAs, among other putative roles in the elongating spermatid cyst bundles. We have conducted various rounds of optimisation and troubleshooting for all of our *in vivo* and *in vitro* approaches, paving the way for the next round of functional gene analysis.

6.1. Summary of key findings

1. RNA-pull down-assays of comet and cup mRNAs provide definitive evidence of differential RBP binding *in vitro*, with the relative abundance of interacting RBP varying depending on the mRNA of interest. As there was no clear division in comet and cup binding preference, this indicates that the regulatory machinery involved

in post-transcriptional comet and cup localisation and processing is much more diverse within their respective gene classifications than between them.

2. While the relative amount of bound RBP can be quite variable depending on the mRNA in question, Imp bound to all eleven of our comet and cup transcripts *in vitro* – making it an exciting candidate to take forward for further analysis.

3. When following this up with a modified CI-AP assay, we found that only a small number of post-meiotic comet and cup transcripts were enriched in the Imp-bound RNA-Seq dataset, which may indicate dynamic and indirect binding interactions that may not have been captured in our bound purification.

4. We have shown that Imp itself has a rich and vibrant interactome of binding partners, and these may in turn help to set-up a complex multifunctional, muti-protein network that together influence different phases of mRNA metabolism. This includes the localisation, anchoring and local translation of target mRNAs, such as post-meiotic and actin transcripts.

5. We also speculate that the wider Imp RNP complex has roles in the assembly, function and/or maintenance of an actin-containing structure at the spermatid tail-ends, which may contribute to the trapping of localised mRNAs and/or elongation of the spermatid cyst bundles.

6. Preliminary analysis confirmed a small amount of co-localisation between Imp and F-actin at the extreme tail-ends of the spermatids.

7. Interrogation of *imp* gene function in the *Drosophila* male germline by targeted Imp-UAS-RNAi knockdowns revealed a range of phenotypic effects in sperm development, all with varying degrees of severity.

8. Loss of *imp* led to mislocalisation of mRNA transcripts, loss of localised reporter signals, and considerable disruption to spermatid elongation in *schuy*-TagGFP testes.

9. Loss of *imp* had no effect on *c-cup*-TagGFP regulation, with *c-cup*-TagGFP-expressing males exhibiting no visible RNAi phenotype.

10. Findings tentatively indicate a context-dependent involvement of Imp in the regulation of spermatid elongation and localisation of post-meiotic gene products.

6.2. Does the comet and cup gene terminology require reclassification?

In theory, the RNA binding activity of RBPs should correspond to confined motifs or specific structural elements within a select number of target mRNAs. However, in practice, many RBPs possess broad range specificity and, as such, can effectively interact with a large proportion of the cellular mRNA population (Reveal et al. 2011). With this in mind, we initially expected that all comet and cup mRNAs would bind with an overlapping profile of RBPs – although, due to their differing localisation patterns, we hypothesised that binding specificities and affinities would vary between the comet and cup classifications. However, so far, there is very little evidence to suggest that the comet and cup gene classifications extend any further than the characterisation of their respective transcript localisation patterns. Therefore, perhaps the use of this terminology is not as clear-cut as first thought. In the original publications upon which this research is founded, Barreau et al. (2008a) and Barreau et al. (2008b) provide evidence of these separate gene/mRNA classes, with comet and cup mRNA localisation characterised via traditional RNA-ISH staining. However, only the expression and localisation of 24 post-meiotically transcribed genes were initially described by these means. Moreover, the genomic context of these genes showed no remarkable features that could distinguish them from one another or from other non-post-meiotic genes. All comet and cup genes are located within regions of euchromatin, including on the X chromosome, without any defining genomic features at a genomic level (Barreau et al. 2008b).

Since the pioneering characterisation of comet and cup genes, huge leaps have been made in the development of modified, higher resolution ISH experimentation. Many methods have now stepped away from the traditional colour-based ISH assay set-up

utilised by Barreau et al. (2008a) and Barreau et al. (2008b). There are many explanations for this change in preference, as I will discuss in Results Chapter 3, but the main reason is that the qualitative analysis associated with this old method can be highly subjective. Hybridisation conditions and colour development time tends to require a huge amount of optimisation, and non-specific probe binding and background signal intensities can lead to misinterpretations of results. Hence, the choice of *in situ* protocol, along with sample preparation type (e.g., whole mount tissue, squashes, sections, etc.) can lead to a subjective interpretation of tissue-specific RNA expression profiles and localisation patterns.

Recent single molecule FISH (smFISH) and RNA-FISH experiments have, however, revealed distinct differences in the localisation of *f-cup* and *wa-cup* mRNAs that may again correspond with intra-class variation (Raz et al. 2023). Imaging of whole testes showed different patterns of mRNA localisation for these post-meiotically transcribed genes, with *wa-cup* transcripts localising to the tail-ends of fewer spermatid cyst bundles compared to *f-cup*. Moreover, *wa-cup* shows greater consistency in its U-shaped localisation pattern at the spermatid ends, whereas *f-cup* mRNAs accumulate with a somewhat trailing tail, resembling that of its “comet” counterparts (Raz et al. 2023). A possible spatial and temporal overlap between *f-cup*, *wa-cup* and *soti* has also been suggested that is indicative of shared comet and cup localisation properties. One unpublished theory suggests that the “shooting comet” mRNAs are a physical, overlapping extension of the “acorn cup” mRNAs. However, many more multiplexed co-localisation ISH assays of the comet and cup gene combinations are needed to fully validate this conclusion.

As the expression profiles of newly identified post-meiotically transcribed genes are explored further, we will likely find that a proportion of these also produce asymmetrically localised mRNAs in the mid-to-late elongating spermatids (Li et al. 2022; Raz et al. 2023). But are these definitive “comets” and “cups”, or is there be some shared localisation characteristics? We can preliminarily speculate it to be the latter from what we have found here.

6.3. Protein redundancy and cooperative, combinatorial binding offers a partial explanation for the differences in Imp-RNAi knockdown testis phenotypes

Although RBPs may be able to bind tens to hundreds of mRNAs, this does not necessarily mean that they have a core nonredundant or fundamental role that is truly instrumental to the post-transcriptional regulation of all of them. Instead, these RBPs may only regulate certain events in the life cycle of an RNA or none at all (Moore 2005; Shahbabian and Chartrand 2012). This may in turn be the case for Imp and the comet and cup mRNA transcripts and could go some way to explain why knockdown of *imp* resulted in the dysregulation of *schuy* but yet showed no apparent effect on *c-cup*.

This does not, however, explain the differences we saw at the ultrastructural level when *imp* was knocked down in the schuy-TagGFP-expressing line vs. the c-cup-TagGFP-expressing line – since defects in spermatid elongation were only observed in the schuy-TagGFP-expressing testes. Instead, this may be attributed to the fact that mRNAs are bound by a whole host of different RBPs in the context of the broader Imp RNP complex, not just Imp alone. As such, multiple RBPs may function in a cooperative and collaborative manner in the Imp RNP complex and are then able to act redundantly when needed; thus ensuring that the regulation of localising mRNA transcripts still occurs, even if an RBP counterpart is lost for whatever reason (Dreyfuss et al. 2002).

Functional redundancy and cooperation is universal in eukaryotic RBP populations. A systematic analysis identified over 12,000 mRNA:RBP interactions in yeast with high confidence (Hogan et al. 2008). While a diverse range of RBPs were represented in their data, many were found to associate with functionally related, overlapping sets of mRNAs. Despite only investigating a subsample of forty candidates out of a possible six hundred known yeast RBPs, thirty-one of the RBPs were found to reproducibly bind at least ten mRNAs, and each mRNA in the dataset could interact with three RBPs, on average. Interestingly, this is suggested to be a conservative underestimation of target binding (Hogan et al. 2008).

Similar findings have also been demonstrated on a smaller scale in human mRNA:RNP complexes. Mass spectrometry of all native proteins that co-purified with

a single species of spliced mRNA yielded approximately forty-five distinct protein interactors. The composition of these individual RNP complexes encompassed a rich and diverse set of proteins. Some of these proteins were novel, with no direct role in splicing, suggesting that they work together in concert to regulate the life of an mRNA accordingly (Merz et al. 2007).

The broad specificity of RBPs evidenced in these studies supports the idea that functional redundancy and combinatorial binding between proteins is commonplace within many biological systems. Redundancy has been developed as a highly conserved, endogenous mechanism, put in place to ensure that the absence of one RBP does not impact the regulatory process being governed by the overall RNP complex – whether this be localisation, translation or decay.

We have found multiple protein candidates in the Imp interactome that are known to possess RNA binding, processing and localisation activities. These RBPs include Lost, Exu and YPS, to name just a few. Any one of these, or more, could be undertaking a redundant, combinatorial role in the absence of Imp. Moreover, recent work suggests that Imp preferentially binds to transcripts with long 3' UTRs in *Drosophila* S2 cells, which is typically a hallmark of RBP:mRNA interactions that involve cooperative multimerisation (Hansen et al. 2015). However, the localised post-meiotic mRNAs expressed in spermatids do not have long 3' UTRs, suggesting that this finding may not apply to all tissues.

6.4. Are biomolecular phase-separated condensates at play?

At a higher regulatory level, Imp RNP complexes containing post-meiotic comet and cup mRNAs may be coalescing within larger, phase-separated condensates. Phase separated condensation may therefore be responsible dynamic localisation of comet and cup mRNA transcripts in the spermatid tail-ends, and they may also account for the variability we have seen throughout all stages of our analysis, including the variations of *in vitro* binding abundances.

Biomolecular condensates assemble as spatiotemporally controlled, membraneless compartments within cells. They behave as phase-separated liquids comprising

various biomolecules – including many different proteins and nucleic acids – that can in turn establish multiple, transient interactions (Fig 40.). By localising these components together, and forming a high local concentration of biomolecules, condensates can actively increase reaction kinetics, promote intermolecular interactions, and speed up the rate of transportation (Flory 1942; Cohen and Benedek 1982; Banani et al. 2017).

RNA:protein condensates such as the nucleolus, RNA processing bodies (P-bodies), and transport and stress granules are mRNA-enriched, and are implicated in numerous biological processes and cellular reactions. These include: RNA transcription and transport, post-transcriptional processing, translational regulation and RNA metabolism, as well as signal transduction and even the DNA damage response (Banani et al. 2017; Currie and Rosen 2022). Considering these activities, we may somewhat speculate that our comet and cup mRNAs are part of similar RNP-containing particles *in vivo*.

Additionally, proteomic and transcriptional analyses of biochemical reconstitutions and purifications of P-bodies and stress granules have shown that hundreds of proteins and thousands of mRNA species can constitute individual condensates (Jain et al. 2016; Khong et al. 2017; Currie and Rosen 2022). RBP recruitment, phase-separation and condensate formation can also be mRNA-dependent. These mRNAs can in turn use specific sequence and structural motifs to bind different combinations of RBPs, permitting their localisation to, and/or promotion of, different cytoplasmic condensates (Zhang et al. 2015; Langdon Erin et al. 2018; Chen and Mayr 2022). Condensates such as P-bodies and stress granules can dock dynamically to one another, remaining as distinct structures while enabling RNAs to transfer vectorially. This depends on whether the mRNA is destined for degradation or requires storage and sorting prior to translation (Kedersha et al. 2005; Buchan et al. 2008; Sanders et al. 2020).

These properties may together explain the variation we see in binding interactions within each comet and cup classification. It is possible that our comet and cup mRNAs can transfer between complexes within these condensates, therefore interacting with different compositions of RBPs and other co-factors in the process. This hypothesis also fits well with our thoughts that the comet and cup mRNAs are capable of

interacting with multiple different RBPs *in vivo*, depending on their ultimate target site and function.

Imp has also been implicated in phase condensate formation in the *Drosophila* nervous system, where it has been found to coalesce at high concentrations with profilin transcripts and the conserved DEAD-box helicase, Me31B. Together, these form large, translationally repressive cytoplasmic granules within ageing brains. Interestingly, this was found to be a systematic process, whereby multiphase heterogenous RNP condensates were formed with distinct compositions that never mixed and instead corresponded to specific age-dependent changes in the differential recruitment of RNP constituents (Pushpalatha et al. 2022). Evidence of these dynamic neuronal Imp-containing condensates, with components that can shuttle between the granular and soluble pools in a regulated manner, is strongly supported in the wider literature (Vijayakumar et al. 2019; Formicola et al. 2021). However, further work is needed to substantiate this concept in the context of the *Drosophila* testis.

1,6-hexanediol (1,6-HD) is commonly utilised for the analysis of phase-separated biomolecular condensates in the wider literature. It is a small-molecular, aliphatic alcohol that globally interferes with weak hydrophobic protein-protein and/or RNA-protein interactions within condensates, allowing for their characterisation *in vitro* and *in vivo* (Kroschwald et al. 2017; Cermakova and Hodges 2018). 1,6-HD can dissolve dynamic, liquid-like biomolecular condensates in living cells, including P-bodies (Updike et al. 2011), transcription factories (Sabari Benjamin et al. 2018) and RNA-protein granules (Kroschwald et al. 2015). However, the conditions under which 1,6-HD is used can vary massively from one study to the next, and the parameters of 1,6-HD treatment have yet to be fully standardised – with higher concentrations associated with cell death and membrane rupturing (Kroschwald et al. 2017; Ming et al. 2019; Liu et al. 2021).

Nevertheless, 1,6-HD is a powerful, universal tool that is non-cell-type-specific, does not require genomic manipulation, and demonstrates rapid reversible recovery after treatment removal (Kroschwald et al. 2017; Cermakova and Hodges 2018; Liu et al. 2021). Hence, we propose its optimisation for applications in the *Drosophila* testis, alongside adequate non-treatment negative controls, to determine whether the post-meiotic comet and cups are localised within biomolecular condensates. In such

experiments, we could investigate the effects of 2.5% and 5% 1,6-HD treatment over time on the localisation of our TagGFP-tagged reporter proteins using time-lapse fluorescence microscopy (Updike et al. 2011; Uebel and Phillips 2019). A classic hallmark of phase-separated biomolecular condensates is their reversible sensitivity to disruption via 1,6-HD treatment. Therefore, if there were visible changes to the characteristic expression profiles of our localised comet and cup proteins upon 1,6-HD exposure, this could indicate that their localisations are governed at a higher regulatory level of LLPS biomolecular condensates.

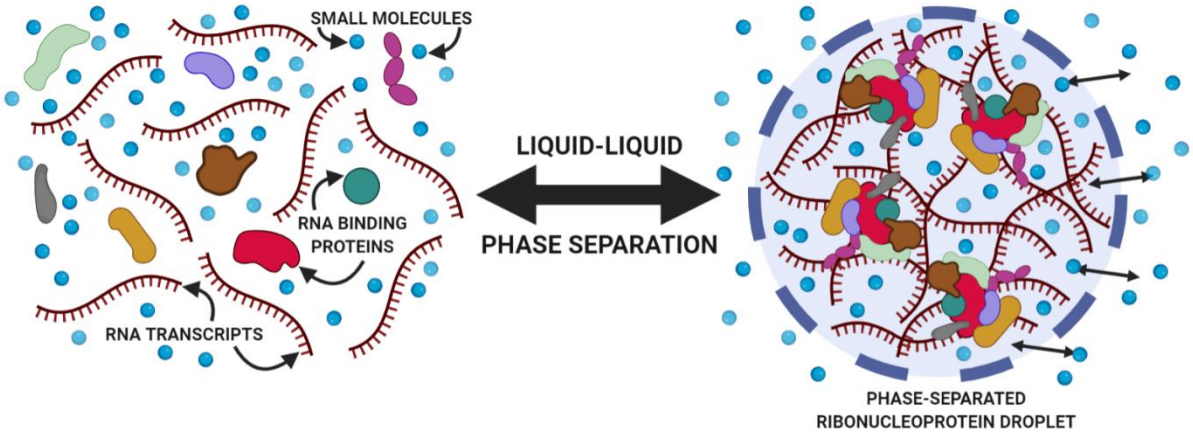

Figure 40. Graphical representation demonstrating the basic concept of phase-separated formation of RNA-protein condensates. The molecular mixture separates into two distinct phases: a large, low-concentration dilute phase, and a small, high-concentration condensed phase. This phase-separated state has minimum free energy and is at equilibrium. While there is no net diffusive flux between the phases, small individual biomolecules can still move rapidly between them, maintaining localisation within the concentrated compartment and allowing for dynamic exchanges. The greater the number of high affinity interactions, such as protein binding, and/or the stronger their affinities, the greater the interacting biomolecules' propensity to oligomerise. These in turn assemble into large complexes that enable phase separation at lower concentrations. As the entropic cost of restricting these complexes to the condensed phase is lower than confining their individual components, the solubility of complexes decreases as their size increases. This concentrates proteins and RNAs further, perpetuating the establishment of more binding interactions and weak inter-molecular interactions, which favours continued oligomerisation and complex formation (Flory 1942; Cohen and Benedek 1982; Banani et al. 2017). **Recreated from Kohata and Miyoshi (2020) using BioRender.com.**

6.5. Actin and MT regulators in the Imp interactome may together indicate the assembly of a multi-protein, cytoskeletal-associated Imp RNP structure at the spermatid tail-ends

In a recent single-shot proteomics analysis of the *Drosophila* testis, Gärtner et al. (2019) identified a proteome amassing more than 5000 proteins – many of which were linked to RNA binding functionality. Some stage-specific differences in enrichment were noted for a small subset of proteins between the larval, pupal and adult testis proteomes, but the overall majority of proteins were present in all three developmental stages. We have likely been very conservative with our approach to identifying Imp protein binding partners and, in light of this expansive testis proteome, there may have been many that were discounted here due to overlap with Sqd RNP complexes.

Nevertheless, we have shown that the enriched binding network of Imp contains numerous actin-associated and actin-binding proteins, in addition to the *actin* mRNAs itself. Based on our comparative proteomics analyses, our overarching theory is that, while Imp may be a pleiotropic gene due to its differential, biphasic expression, it is also interacting within an actin-cytoskeletal multi-protein complex at the *Drosophila* spermatid tail-ends – whether this be directly or indirectly via specific adaptor proteins. Further support for *Drosophila* Imp's role in actin- and microtubule-based regulation comes from the *Xenopus* homologue of Imp, termed Vg1 RBP. It has a direct role in the vegetal localisation of maternal RNA determinants, which in turn sets up the vegetal pole of oocytes. Vg1 RBP is itself also known to be a microtubule and microfilament-associated protein, so it is plausible that this property may be conserved (Schwartz et al. 1992; Elisha et al. 1995; Havin et al. 1998).

In addition, fluorescent immunolabelling of individual wildtype elongating spermatid cysts has shown that F-actin is present at cortical regions towards the distal area of the spermatid tails (Ghosh-Roy et al. 2004). F-actin assembly also overlaps with a zone of spectrin enrichment (cytoskeletal scaffolding), localising to a cortical boundary just beneath the extreme tail-ends of each individual growing spermatid. This enveloping F-actin-rich band is detected consistently throughout the developing spermatid cyst bundles (Ghosh-Roy et al. 2004). Recent work has since confirmed

that this patch of co-localised spectrin and F-actin expression does indeed correspond to decoration of the axoneme elongation complexes at the tail-ends of the elongating spermatid cyst bundles (Steinhauer et al. 2019).

Overall, Ghosh-Roy et al. (2004) suggested that it is the interaction of the Dynein–Dynactin protein subunits with various cytoskeletal components, including F-actin, which maintains spectrin cytoskeleton assembly and supports continued growth of elongating spermatids within the *Drosophila* testis. Moreover, the spectrin–MT (F-actin) interaction itself is facilitated by the Dynein–Dynactin complex. Altogether, these interactions likely mediate the trafficking of vesicles within the cytoplasm of the distal tail-end region, including axoneme-specific cargo that contribute to axonemal sheath development.

In light of this, it could be possible that Imp is one of many key biological players within this wider protein interactome that regulates spermatid tail growth, aiding the active transport of mRNAs to a large multi-protein-cytoskeleton-interacting complex at the tail-ends, which provides an anchoring point for localisation.

Presence of Combover (Cmb) in our Imp-enriched precipitates further supports this argument since it is vital for actin-based dynamics in sperm development, including in the process of spermatid individualisation. However, Cmb does not bind directly with actin in the male germline. Instead, Cmb interacts with axonemal components, such as Radial spoke protein 3 (Rsp3), suggesting evidence of a wider complex of actin-based, axoneme-associated protein interactors in the spermatids (Steinhauer et al. 2019). While published evidence only so far suggests that these interactions coordinate individualisation complex stability and migration via its association to the axoneme (Steinhauer et al. 2019), it could also be possible that a similar structure is already present at the spermatid tail-ends prior to this, mediating spermatid growth via the localisation of axoneme and growth-related cargo, including post-meiotic mRNA transcripts.

Under this hypothesis, proteins already known to be involved in spermatid individualisation, including Cmb, may also contribute to spermatid elongation. These protein interactors, along with Imp, could therefore be common to both processes of spermatid elongation and individualisation due to regulating the transition between two.

6.6. There is extensive evidence in the published literature that supports Imp's role in actin and microtubule regulation

6.6.1. Imp's homologues are implicated in cancer development and metastasis

In the literature, members of the wider Imp protein family have been repeatedly implicated in cancer malignancy and metastasis – and this oncogenic activity has been consistently linked to cytoskeletal regulatory mechanisms, including the localisation of actin and microtubule components (Shestakova et al. 1999; Ioannidis et al. 2001; Hamilton et al. 2013). The fact that multiple actin types and actin-associated regulators came up at both a protein and RNA level here reinforces a clear link with Imp.

As mentioned previously, ZBP1/Imp has long been evidenced in the regulated localisation of *β-actin* mRNA transcripts to the leading edge of migratory cells (Kislauskis et al. 1997; Ross et al. 1997; Eom et al. 2003). In rat adenocarcinoma cell lines, the ability to localise *β-actin* mRNAs was also correlated with the efficiency of motility and this, in turn, correlated with metastatic potential (Shestakova et al. 1999). Overall *β-actin* mRNA localisation patterns were linked to the polarity and plasticity of cell motility, and proper *β-actin* localisation was suggested to be the regulatory switch between directed cell locomotion and invasiveness (Shestakova et al. 1999). This confirmed that specific targeting of mRNA transcripts by RBPs such as Imp, including those mRNAs that encode the actin types, is therefore crucial to achieving cell-level functionality.

Not only is the Imp family involved in determining the metastatic potential of a cell, but Imp proteins may also contribute to growth potential (Ioannidis et al. 2001). The human homologue, IMP-1, was found to be expressed in a wide range of mesenchymal tumours and has been suggested to play a role in abnormal cell proliferation because of this. Although expression was not limited to malignant cell lines alone, IMP-1 expression correlated with the development of a transformed phenotype and was found to be an early event in malignant transformation – indeed suggesting that IMP-1 is not caused by malignancy but instead contributes to the establishment of these oncogenic and proliferative abnormalities (Ioannidis et al. 2001).

6.6.2. Previous work has reinforced the involvement of *Drosophila* Imp RNP complexes in the modulation of F-actin formation and polymerisation

The most definitive support for our actin-enriched Imp interactome comes from Hansen et al. (2015). They carried out an individual nucleotide resolution cross-linking and immunoprecipitation (iCLIP) on Imp protein isolated from *Drosophila* S2 cell lysates. Similar to the CI-AP experimentation performed here, iCLIP preserves *in vivo* mRNA:RBP interactions, which permitted them to study cytoplasmic RNP complexes containing Imp. They found extensive binding of Imp to the 3' UTRs of transcripts implicated in F-actin formation and cytoskeletal remodelling. When Imp was knocked down via RNAi in single *Drosophila* S2 cells, decreased Imp levels resulted in diminished F-actin formation, while whole fly analysis showed Imp depletion led to severe neuronal patterning defects in embryos and reduced pharate adult viability. As a reduction in Imp corresponded to defective actin cytoskeletal dynamics, both in single cells and in whole intact flies, this suggested a role for Imp in the coordination of F-actin assembly. They concluded that Imp RNPs likely function as a cytoplasmic source of mRNAs, which in turn encode protein products that contribute to actin cytoskeletal remodelling (Hansen et al. 2015).

In addition, they identified both the *PABP* and *yps* transcripts in their top 200 most highly enriched hits, which is interesting considering we found both of their protein products as enriched in our Imp-bound proteome. Transcripts for *14-3-3ε* were also detected in their top 200 hits, which we found in both our Imp-enriched proteomics and RNA-Seq datasets. Other transcripts in common between the Imp-enriched RNA-Seq datasets included *eff*, *Act42a* and *Rho1*. They also evidenced a direct *in vitro* association of Imp with the 3' UTR of the *pabp* mRNA. Overall, this study supports some of our main theories on Imp functionality in the testis.

6.7. Wider Imp RNP translation-related protein interactors may also associate with this actin structure

As the canonical ribosome contains eighty ribosomal proteins in total, including thirteen paralogue pairs in *Drosophila*, it may be unsurprising that more than 20% of our Imp-enriched protein interactors were ribosomal subunit proteins of some sort (Garlovsky et al. 2022). In fact, paralogue switching and ribosome heterogeneity is a well-known phenomenon that occurs during the course of sperm development to regulate specialised translational activities (Hopes et al. 2022).

In the current update of the *Drosophila melanogaster* sperm proteome (DmSP3), over 3000 proteins were identified as being enriched within sperm (Garlovsky et al. 2022). Of these, almost one-half of all known *Drosophila* ribosomal proteins were detected, which was intriguing given that sperm are believed to be translationally quiescent. Interestingly, RpL22 was highly abundant in the DmSP3 dataset, supporting its expression within mature sperm cells, as well as in the wider testis. This supports the enrichment of RpL22 we found in our Imp-bound CI-AP sample and confirms that it is a ribosomal subunit protein that likely predominates and functions within the late stages of sperm development.

The subset of ribosomal proteins we have identified here may therefore reflect spermiogenesis-specific translation, some of which may be regulated by action of Imp. We therefore speculate that these could be the components that contribute to the final stages of Imp-driven mRNA localisation – once the actin anchor site has been reached at the extreme tail-ends of the spermatids. As such, these ribosomal proteins are recruited to the wider Imp RNP complex, as part of the large F-actin enriched structure, by PABP and the cascade of translation initiation machinery that have already bound to the incoming complex – thereby driving the timely activation of local translation. We provide details of this hypothesised model in the next section.

6.8. Our Imp proteomics and RNA-Seq data can be summarised speculatively by a hypothetical model of localising multi-protein Imp:mRNA RNP complexes

We know from the literature that Imp can oligomerise and form higher-order RNP complexes, many of which are associated with functions in F-actin coordination and polymerisation (Hansen et al. 2015). We have therefore developed a hypothetical model of Imp RNP transport in the spermatids, as well as in the F-actin based structure we have speculated to be at the tail-ends of the spermatids – which likely corresponds to the “elongation complex”, as its referred to in some papers (Ghosh-Roy et al. 2004; Steinhauer et al. 2019). This hypothesis is based purely on our data shown here, alongside support from the wider literature (Fig. 41.).

We propose that Imp associates with its target mRNA, either directly or indirectly via adaptor or scaffolding protein of some sorts, potentially via 14-3-3ε (Courchet et al. 2008). In doing so, Imp forms an mRNA:RNP complex alongside other key *trans*-acting factors, for example the fellow RBPs, Lost, Exu and YPS.

Imp is known to be transported by microtubules in the *Drosophila* oocytes and neurones, so by analogy Imp-associated RNP complexes are likely localised in the same manner (Boylan et al. 2008). It is likely that this transport is mediated via an interaction with an MT-associated adaptor protein such as CLIP-190, as it is associated with molecular trafficking to the fast-growing plus-end of microtubules (Dzhindzhev et al. 2005). In association with a molecular motor, Imp can modulate the localisation of complexed mRNA transcripts, such as those that encode the comet and cup mRNAs or *actin* transcripts (Barreau et al. 2008a; Barreau et al. 2008b; Hansen et al. 2015). Although, it must be noted that none of the common molecular motor proteins that are associated with active transport via actin filaments and microtubules, including kinesin, myosin or those of the BicD-Egl-Dynein motor complex, were identified as Imp-enriched or in the wider dataset. This may be due to the efficient yet intermittent nature of interacting motor proteins; which undergo dynamic and transient recruitment to target RNP complexes as and when they are needed.

Once the Imp RNP complex reaches the final site of localisation at the tail-ends of the spermatids, Imp may contribute to the anchoring of the complex to the large F-actin

structure. At this point, proteins linked to translational activation may bind; first PABP and then eIF4G2, which sets off a cascade of translational machinery recruitment (Mendez and Richter 2001; Richter and Sonenberg 2005; Sonenberg and Hinnebusch 2009).

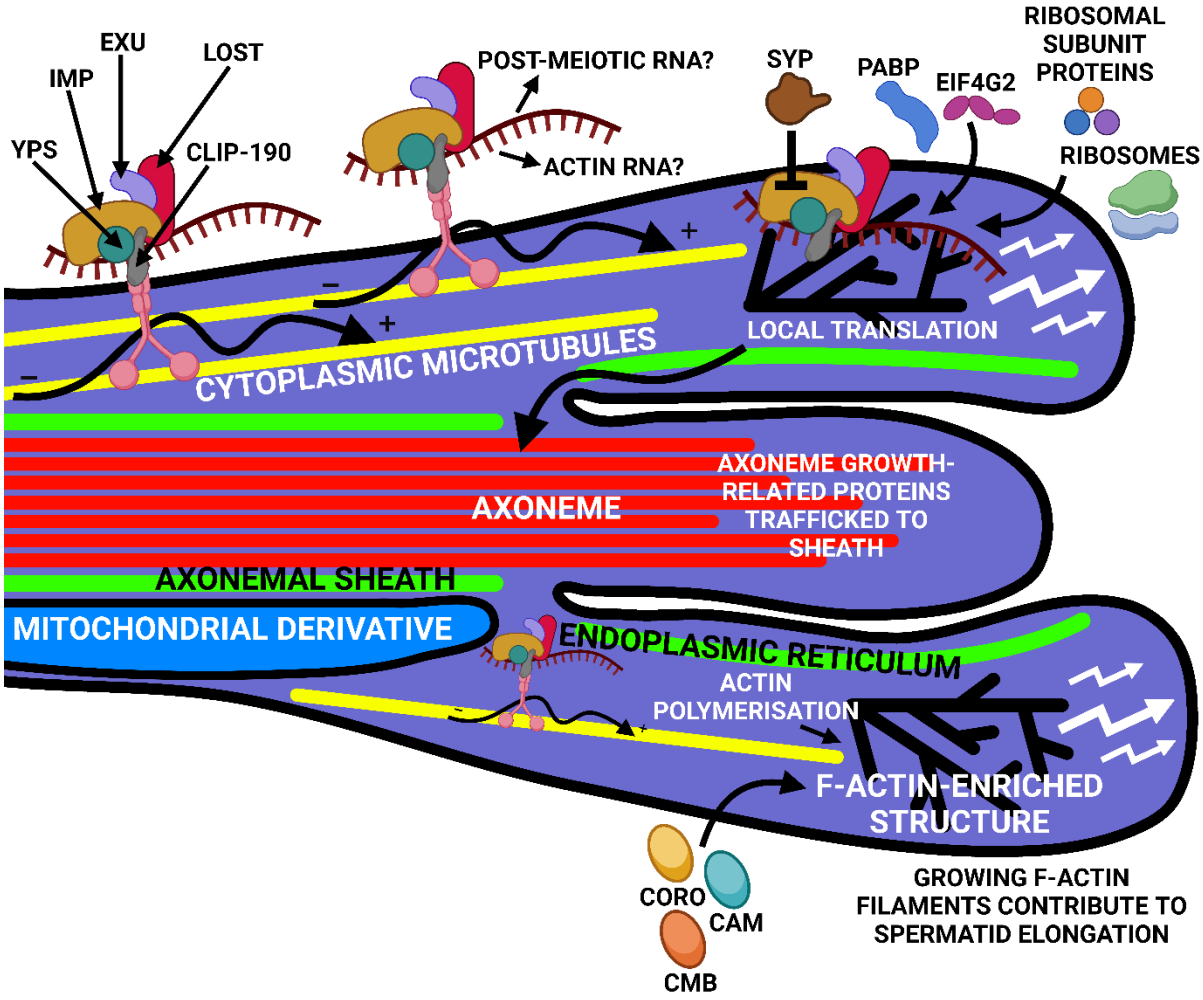

Figure 41. Hypothetical model of the Imp RNP complex life cycle, including the Imp-facilitated, F-actin-dependent elongation of spermatid tail-ends in the *Drosophila* testis. Schematic representation of the extreme, distal tail end of a single spermatid is shown, not drawn to scale. See main text in the Discussion (Section 6.8.) for a detailed written description of the speculated mechanism of action. Spermatid tail-end ultrastructure modified from Tokuyasu (1975) and H. White-Cooper (Personal Communication). **Created using BioRender.com.**

Proteins involved in ribosome synthesis associate, including the 40S and 60S ribosomal subunits and other ribosomal subunit proteins that dictate testis-specific translational activities. Local translation of post-meiotic proteins, actins and other sperm components takes place, with some of these products perhaps shuttled to the axonemal sheath to drive axoneme assembly and growth in the elongating spermatids (Ghosh-Roy et al. 2004).

Newly synthesised actin proteins may undergo polymerisation to promote further assembly of an F-actin-rich structure at the spermatid tail-ends; forming a filamentous network at the “leading edge” of the tail (i.e., the elongation complex) that may provide a contributing driving force for spermatid elongation by pushing the membrane at the tail-end forward, similar to actin-based mechanisms seen in dendrites and fibroblasts (Lawrence and Singer 1986; Kislauskis et al. 1994; Miller 2002). This hypothesis of an Imp-facilitated, F-actin-dependent elongation mechanism in spermatids has also been, albeit briefly, speculated by Hansen et al. (2015). As Imp RNP complexes provide a pool of actin cytoskeleton re-modellers, proteins such as Calmodulin and Coronin may also bind at this point to regulate actin dynamics accordingly (Hansen et al. 2015).

Speculatively, Syp’s association with the Imp RNP complex may dictate an antagonistic role, similar to those in the *Drosophila* nervous system (Liu et al. 2015; Yang et al. 2017). Syp may bind early on to suppress the translational activity of Imp and prevent ectopic translation of associated mRNAs, or it could bind once this large, tail-end-enriched F-actin filament network has been reached to promote Imp dissociation or negatively regulate local protein expression.

We must now continue to build and expand upon this hypothetical model by validating what we have theorised here with further experimental evidence. This will include verifying the various interacting components of the F-actin associated Imp RNP complex, alongside its mechanism of assembly and mechanism of regulating localised mRNAs *in vivo*. This will ultimately require an extensive, multi-step approach to encompass every stage in the process of: RNA transport, stabilisation, protection, anchoring and translational activation.

Another point to consider is the potential autoregulatory function that Imp may play in terms of its own *imp* transcripts. *Imp* mRNAs were identified as a potential interactor

in the wider RNA-Seq dataset when the bound Cl-AP extract was analysed; however, we are yet to determine how this feeds into the above model we have theorised. It would be interesting to use HCR-FISH to probe for *imp* RNA expression profiles in the spermatid cyst bundles of Imp-GFP testes. In doing so, we could use LSFM to visualise the co-localisation of both the *imp* mRNA transcripts and its protein product, and even optimise our multiplexing approach to determine their spatial expression profiles in relation to F-actin and other potential Imp RNP components in the spermatid tail-ends.

6.9. Developing a Bam-Gal4:VP16//Rbp4-Gal4 recombinant driver fly line is the next logical step in our analysis

While studies into the post-meiotic stages of sperm development are of the utmost importance, the Gal4 driver lines we have had at our disposal to investigate these have been somewhat lacking. Very few are effective for the user-defined control of gene expression after the transit-amplifying mitotic divisions and, as such, leave us without the capacity to observe true, penetrant RNAi effects in late spermatocytes and spermatids (White-Cooper 2012; Demarco et al. 2014). Establishment of gene functionality in spermiogenesis is therefore a challenge, particularly if this corresponds to key roles in sperm differentiation, elongation and/or individualisation. We ultimately chose the Bam-Gal4:VP16 driver because it was the most likely to achieve a modest level of phenotypic effects post-meiotically.

Our “doubling-up” strategy of expressing two copies of the UAS-RNAi construct instead of one improved this efficiency to some degree, but a proportion of WT phenotypes persisted. This could indeed be due to redundancy, as previously discussed, or this may indeed relate to inherent Gal4-UAS-driven RNAi limitations.

There are many approaches that can be taken when attempting to improve the effectiveness and efficiency of the *Drosophila* Gal4-UAS RNAi system, the majority of which require further genetic manipulation. This includes: (i) increasing the number of Gal4 drivers and/or UAS-RNAi transgene constructs expressed within the system, (ii) increasing the total number of UAS sites in the UAS-RNAi effector transgene, (iii)

modifying the combination of Gal4 driver and UAS-RNAi transgenes that constitute the Gal4-UAS binary expression system, and/or (iii) introducing a double-stranded RNA cleavage/processing component such as Dicer-2 (Dietzl et al. 2007; Ni et al. 2008; Di Cara et al. 2010; Doggett et al. 2011). However, not all of these are equally as powerful on their own, and combining any number of these into one or more fly lines is not an easy task. Even when compared to the co-expression of Dicer-2 to increase processing of longer-length RNAi hairpins, doubling the amount of Gal4 has been found to be the most effective at enhancing RNAi potency and hence the severity of the overall phenotype (Dietzl et al. 2007; Ni et al. 2008).

However, a new addition to the repertoire of male germline Gal4 drivers may now address this research gap. Butsch et al. (2023) have recently developed the germline-specific Rbp4-Gal4 driver line, which activates transgene expression from the early spermatocyte stage onwards. The transgenic *pRbp4-Gal4* driver construct itself (pDESTsvaw-*pRbp4-Gal4*) comprises a 2.3 kb promoter/regulatory region, which corresponds to the genomic DNA directly upstream of the native coding gene sequence for *Rbp4*, cloned upstream of the Gal4 coding sequence from the pENTR L5-GAL4-L2 (Addgene Plasmid #32304) and alongside a *mini-white* gene rescue marker (Petersen and Stowers 2011; Butsch et al. 2023). The Rbp4-Gal4 fly line was generated using ΦC31 integration, with the Rbp4-Gal4 driver transgene arrangement inserted on chromosome III at the docking site VK27 and balanced over the third chromosome balancer, TM6B (Butsch et al. 2023).

The group have already published a proof-of-principle paper, in which they successfully used the Rbp4-Gal4-UAS system to perform a functional analysis of the AAA+ ATPase, VCP, after meiosis had taken place. Rbp4-Gal4 was found to reliably and efficiently knockdown *VCP* gene expression via RNAi in both spermatocytes and spermatids. Using a Gal4 driver that activated developmentally later than Bam-Gal4:VP16 ultimately allowed the post-meiotic, pleiotropic activities of VCP to be investigated fully, without risk of obscuring downstream effects due to early interference in pre-meiotic sperm development (Butsch et al. 2023).

We were kindly gifted the Rbp4-Gal4 fly line from the Bohnert and Johnson labs (Louisiana State University, USA). However, this was unfortunately quite far into the progression of this PhD project and left us with no time to re-test our Imp-UAS-RNAi

hairpin knockdowns under the control of the Rbp4-Gal4 transgene. We did, nonetheless, endeavour to recombine the Rbp4-Gal4 driver with the Bam-Gal4:VP16 driver on the third chromosome – with the aim of having a single fly line that expresses both Gal4 drivers.

We know that there has been variable success with the penetration and efficiency of Bam-Gal4:VP16-induced RNAi knockdowns in the fly testis when used on its own, but we were curious to find out how this would fare when in combination with the novel Rbp4-Gal4 driver (Di Cara et al. 2010; Doggett et al. 2011; Butsch et al. 2023). Gal4 dosage is a limiting factor in the efficiency of the Gal4-UAS binary expression system, and research suggests that doubling the amount of Gal4 tends to result in a more profound effect than doubling the number of UAS hairpins in the system (Ni et al. 2008; Di Cara et al. 2010; Doggett et al. 2011). Although, caution must be taken to ensure that the high concentrations of Gal4 products do not have an adverse quenching effect on the UAS-RNAi hairpin constructs (Di Cara et al. 2010).

As we had already tried to increase the number of USA-RNAi hairpins being expressed to silence *imp*, our next logical test was to increase the source of Gal4 protein by increasing the number of Gal4 drivers. By recombining Bam-Gal4:VP16 with Rbp4-Gal4, we could achieve not only this but drive the activation of Imp-UAS-RNAi hairpin expression far into the post-spermatogonia and spermatocyte stages of sperm development.

In the final stretch of this PhD project, we successfully generated seven independent recombinant lines, expressing a Bam-Gal4:VP16//Rbp4-Gal4 recombination balanced on the third chromosome with either the TM6B or TM3,Sb balancer chromosome. All of these have now been PCR-validated to confirm the presence of both the Bam-Gal4 and Rbp4-Gal4 transgenes, respectively.

If we had more time, we would perform our RNAi screening again using both the single Rbp4-Gal4 driver line and recombinant Bam-Gal4:VP16//Rbp4-Gal4 lines to determine whether any of these made an obvious difference or improvement to the Imp-UAS-RNAi knockdown phenotypes we have already characterised. Having these additions to our genetic toolkit earlier would have almost certainly helped us to gain a clearer picture of Imp's functional role in the male germline; particularly if these had boosted Imp-RNAi hairpin expression in the post-meiotic spermatids.

However, now that we have two germline Gal4 fly lines to hand, this offers a solid foundation that can be revisited again in the future. These drivers are not restricted to the investigation of Imp alone and can therefore be utilised to knockdown any other gene that is predicted to have regulatory roles in spermatid differentiation, elongation and individualisation. The only limitation we now face is the availability of gene-specific UAS-RNAi lines from stock centres. However, there are many such reagents that exist already, and it is moderately straightforward to generate new lines, if needed.

6.10. Future directions

We have conducted an extensive degree of optimisation for every technique we have employed here for our functional analysis of Imp. However, now that we have these methodologies finalised, this will make our next gene analysis a much easier endeavour in the long run.

As with any piece of scientific research, more questions may have been raised here than answered.

For example:

1. Does Imp bind some comet and cup mRNA transcripts directly and others indirectly? If so, what mediates the preference between the two? Is it purely due to differences in binding sequence motifs?

2. Do the Imp-enriched RNAs we have elucidated here contain putative IBEs, indicative of Imp recognition and binding?

3. If Imp is indeed functionally redundant in certain regulatory contexts, which *trans*-acting factors in the Imp RNP complex act to replace Imp activity and/or exhibit shared combinatorial binding profiles?

4. Do fertility assays for the double Imp-RNAi knockouts show a negative effect on fertility and fecundity? Are F1 males sterile or are they still capable of producing progeny despite evident defects in sperm development?

5. Can we indeed validate this F-actin enriched structural assembly/anchor in the elongating spermatid cyst bundles once co-localisation and co-immunostaining protocols have been optimised? And if so, which proteins and RNAs are associated with this structure?

Although these questions are now outside the remit of what is possible in this project, these offer a good starting point for all future work. As such, there are several experimental approaches that could be considered in order to address these questions. This includes, but is not limited to:

1. EMSAs of purified mRNAs components with Imp – including fragments that correspond to the different regions of the respective transcript – to determine which binding sites are preferentially recognised and bound by Imp, as well as sequence specificity.

2. Computational prediction of putative Imp binding sites using known databases and automated bioinformatic tools similar to SITEHOUND (Ghersi and Sanchez 2009; Hernandez et al. 2009).

3. An integrated combination of binding competition assays, again using EMSAs, as described in Results Chapter 3 (Section 5.10.2.1).

4. Fertility assays to compare the number of progeny generated from all double Imp-UAS-RNAi crosses in direct comparison to the WT control cross (n=10). After ~3 days of isolation, each cross would be set-up with at least three females and one male. Following mating for five days at 25°C, parental flies would be discarded and resultant progeny counted as they eclose daily, for up to 20 consecutive days. Any differences between fertility outputs could then be statistically analysed relative to the WT.

5. A large-scale tagging project to explore the expanding repertoire of post-meiotically transcribed genes, and hence where they are spatially distributed in relation to Imp in the *Drosophila* testis.

6. Optimisation of a combined immunostaining and HCR-FISH methodology to enable multiplexing for simultaneous co-localisation analysis of Imp with suspected protein and mRNA interactors. Split-initiator probe pairs would need to be designed for each transcript in question and the HCR-FISH protocol would require some troubleshooting for testes to ensure compatibility with antibody incubations.

Several of the ever-expanding list of post-meiotic genes have yet to be characterised functionally (Barreau et al. 2008a; Barreau et al. 2008b; Li et al. 2022; Raz et al. 2023). However, we do know that, apart from some key exceptions, the majority are not found in the sperm proteome and are therefore not components of the mature sperm (Barreau et al. 2008a). A recent update to the sperm proteome did identify Davis cup in the sperm and detected comets such as Boly, Cola, Hubl, Sowi, Swif and Pglym 87, to name just a few of the original classification (Garlovsky et al. 2022).

Both *boly* and *sowi* were detected in our wider Imp-enriched RNA-Seq dataset, which may suggest a structural role at the spermatid tail-ends. Nevertheless, the roles of many of these post-meiotic genes appear to be exclusively in the proper progression of sperm development; likely mediating spermiogenesis and other activities allied to spermatid differentiation due to their localisation patterns in mid-to-late elongating spermatids.

Based on our model, it could be that some of these genes have a growth-related role, such as contributing to spermatid morphogenesis and elongation stages by aiding axonemal-cargo trafficking. Once the sperm has reached its desired length, this is activity is no longer required – resulting in a downregulation and degradation of post-meiotic products in the fully mature sperm. While this is consistent with the tagged protein reporter lines we looked at, it is again speculative, and a large-scale functional screen of these genes is required to substantiate these suggestions. It would also be of value to generate mutants for some of these post-meiotically transcribed genes, potentially by a CRISPR-Cas9 approach.

For all forthcoming Western Blot applications, we will also take care to include the input fraction and use an appropriate loading control to permit a more robust means of protein signal quantification – particularly when analysing RNA-affinity pull-down outputs and immunoprecipitation data. Perhaps a good loading control for Western

Blot normalisation in our case would be a total protein stain corresponding to our various input fractions.

For all future experiments requiring fluorescence microscopy of key GFP-labelled fusion proteins, including that of the Imp-GFP G80 protein trap (G00080 exon-trap line; Quiñones-Coello et al. 2007), we will also consider using an updated method of visualisation. This would involve testes being dissected, fixed as standard using 4% PFA fixative solution and then treated using a preparation of GFP-Booster nanobody in accordance with the manufacturer's instructions. Treatment with a 1:500–1:1000 dilution of GFP-Booster Alexa Fluor® 488 (ChromoTek, Cat. No. gb2AF488) or 1:200 dilution of GFP-Booster ATTO488 (ChromoTek, Cat. No. gba488) would suffice in this instance. Such ChromoTek GFP-Booster products act to stabilise, enhance and reactivate the GFP signal after tissue fixation with 4% PFA. These small, single domain nanobodies can penetrate the *Drosophila* testis with high efficiency; improving the overall resolution of signals when imaging GFP-tagged components. This would broaden multiplexing possibilities for the analysis of co-localisation *in vivo* – particularly when investigating other potential protein and mRNA interactors of the F-actin associated Imp RNP complex at the ends of the elongating spermatid cyst bundles.

6.11. Concluding points

Taken together, we have conducted an all-round analysis of the highly-conserved *Drosophila* IGF-II mRNA-binding protein (Imp), including characterisation of its binding relationships with post-meiotic comet and cup mRNAs, an investigation into its wider protein and transcript interactome, and an elucidation of potential pleiotropic gene roles within sperm development. We have hypothesised a putative model of localised transport, anchoring and translation, regulated by multi-protein Imp:mRNA RNP complexes in the growing *Drosophila* spermatid cyst bundles. We speculate that there may be an F-actin rich structure at the spermatid tail-ends which contributes to these activities, and functions to promote growth and elongation of the spermatids.

7. BIBLIOGRAPHY

Acevedo, S. F., Tsigkari, K. K., Grammenoudi, S. and Skoulakis, E. M. C. 2007. *In Vivo* Functional Specificity and Homeostasis of *Drosophila* 14-3-3 Proteins. *Genetics* 177(1), pp. 239-253. doi: 10.1534/genetics.107.072280

Adams, M. D. et al. 2000. The Genome Sequence of *Drosophila melanogaster*. *Science* 287(5461), pp. 2185-2195. doi: 10.1126/science.287.5461.2185

Agianian, B., Tucker, P. A., Schouten, A., Leonard, K., Bullard, B. and Gros, P. 2003. Structure of a *Drosophila* Sigma Class Glutathione S-transferase Reveals a Novel Active Site Topography Suited for Lipid Peroxidation Products. *Journal of Molecular Biology* 326(1), pp. 151-165. doi: https://doi.org/10.1016/S0022-2836(02)01327-X

Aizer, A. et al. 2014. Quantifying mRNA targeting to P-bodies in living human cells reveals their dual role in mRNA decay and storage. *Journal of Cell Science* 127(20), pp. 4443-4456. doi: 10.1242/jcs.152975

Alami, Nael H. et al. 2014. Axonal Transport of TDP-43 mRNA Granules Is Impaired by ALS-Causing Mutations. *Neuron* 81(3), pp. 536-543. doi: 10.1016/j.neuron.2013.12.018

Almoalem, A. 2023. *Novel insights into the non-neuronal expression & function of the RNA-binding protein Alan Shepard (Shep) during D. melanogaster Oogenesis.* Cardiff University.

Alpern, J. H. M., Asselin, M. M. and Moehring, A. J. 2019. Identification of a novel sperm class and its role in fertilization in *Drosophila*. *Journal of Evolutionary Biology* 32(3), pp. 259-266. doi: 10.1111/jeb.13409

Altschul, S. F., Gish, W., Miller, W., Myers, E. W. and Lipman, D. J. 1990. Basic local alignment search tool. *Journal of Molecular Biology* 215(3), pp. 403-410. doi: https://doi.org/10.1016/S0022-2836(05)80360-2

Ameku, T. and Niwa, R. 2016. Mating-Induced Increase in Germline Stem Cells via the Neuroendocrine System in Female *Drosophila*. *PLOS Genetics* 12(6), p. e1006123. doi: 10.1371/journal.pgen.1006123

Ameku, T., Yoshinari, Y., Fukuda, R. and Niwa, R. 2017. Ovarian ecdysteroid biosynthesis and female germline stem cells. *Fly* 11(3), pp. 185-193. doi: 10.1080/19336934.2017.1291472

Amero, S. A., Elgin, S. C. and Beyer, A. L. 1991. A unique zinc finger protein is associated preferentially with active ecdysone-responsive loci in *Drosophila*. *Genes & Development* 5(2), pp. 188-200.

Amero, S. A., Matunis, M. J., Matunis, E. L., Hockensmith, J. W., Raychaudhuri, G. and Beyer, A. L. 1993. A Unique Ribonucleoprotein Complex Assembles Preferentially on Ecdysone-Responsive Sites in *Drosophila melanogaster*. *Molecular and cellular biology* 13(9), pp. 5323-5330. doi: 10.1128/mcb.13.9.5323-5330.1993

Amrute-Nayak, M. and Bullock, S. L. 2012. Single-molecule assays reveal that RNA localization signals regulate dynein–dynactin copy number on individual transcript cargoes. *Nature Cell Biology* 14(4), pp. 416-423. doi: 10.1038/ncb2446

Anderson, J. T., Henikoff, S. and Ahmad, K. 2023. Chromosome-specific maturation of the epigenome in the *Drosophila* male germline. *eLife* 12, p. RP89373. doi: 10.7554/eLife.89373

Andreassi, C. and Riccio, A. 2009. To localize or not to localize: mRNA fate is in 3'UTR ends. *Trends in Cell Biology* 19(9), pp. 465-474. doi: 10.1016/j.tcb.2009.06.001

Andrews, J., Bouffard, G. G., Cheadle, C., Lü, J., Becker, K. G. and Oliver, B. 2000. Gene Discovery Using Computational and Microarray Analysis of Transcription in the *Drosophila melanogaster* Testis. *Genome Research* 10(12), pp. 2030-2043.

Andrews, S. 2010. *FastQC - Function: A quality control tool for high throughput sequence data.* Babraham Bioinformatics. Available at: http://www.bioinformatics.babraham.ac.uk/projects/fastqc/ [Accessed: June 2024].

Aram, L., Braun, T., Braverman, C., Kaplan, Y., Ravid, L., Levin-Zaidman, S. and Arama, E. 2016. A Krebs Cycle Component Limits Caspase Activation Rate through Mitochondrial Surface Restriction of CRL Activation. *Developmental Cell* 37(1), pp. 15-33. doi: 10.1016/j.devcel.2016.02.025

Armstrong, J. D., Texada, M. J., Munjaal, R., Baker, D. A. and Beckingham, K. M. 2006. Gravitaxis in *Drosophila melanogaster*: a forward genetic screen. *Genes, Brain and Behavior* 5(3), pp. 222-239. doi: https://doi.org/10.1111/j.1601-183X.2005.00154.x

Babu, K., Cai, Y., Bahri, S., Yang, X. and Chia, W. 2004. Roles of Bifocal, Homer, and F-actin in anchoring Oskar to the posterior cortex of *Drosophila* oocytes. *Genes & Development* 18(2), pp. 138-143. doi: 10.1101/gad.282604

Baj, G., Leone, E., Chao, M. V. and Tongiorgi, E. 2011. Spatial segregation of BDNF transcripts enables BDNF to differentially shape distinct dendritic compartments. *Proceedings of the National Academy of Sciences* 108(40), p. 16813. doi: 10.1073/pnas.1014168108

Baker, C. C. and Fuller, M. T. 2007. Translational control of meiotic cell cycle progression and spermatid differentiation in male germ cells by a novel eIF4G homolog. *Development* 134(15), pp. 2863-2869. doi: 10.1242/dev.003764

Baker, C. C. et al. 2023. Cell-type-specific interacting proteins collaborate to regulate the timing of Cyclin B protein expression in male meiotic prophase. *Development* 150(22), p. dev201709. doi: 10.1242/dev.201709

Baker, C. C., Gim, B. S. and Fuller, M. T. 2015. Cell type-specific translational repression of Cyclin B during meiosis in males. *Development* 142(19), pp. 3394-3402. doi: 10.1242/dev.122341

Baker, N. E. 1987. Molecular cloning of sequences from *wingless*, a segment polarity gene in *Drosophila*: the spatial distribution of a transcript in embryos. *The EMBO Journal* 6(6), pp. 1765-1773.

Balzer, E., Heine, C., Jiang, Q., Lee, V. M. and Moss, E. G. 2010. LIN28 alters cell fate succession and acts independently of the let-7 microRNA during neurogliogenesis in vitro. *Development* 137(6), pp. 891-900. doi: 10.1242/dev.042895

Banani, S. F., Lee, H. O., Hyman, A. A. and Rosen, M. K. 2017. Biomolecular condensates: organizers of cellular biochemistry. *Nature Reviews Molecular Cell Biology* 18(5), pp. 285-298. doi: 10.1038/nrm.2017.7

Bangi, E. et al. 2021. A *Drosophila* platform identifies a novel, personalized therapy for a patient with adenoid cystic carcinoma. *iScience* 24(3), doi: 10.1016/j.isci.2021.102212

Barreau, C., Benson, E., Gudmannsdottir, E., Newton, F. and White-Cooper, H. 2008a. Post-meiotic transcription in *Drosophila* testes. *Development* 135(11), p. 1897. doi: 10.1242/dev.021949

Barreau, C., Benson, E. and White-Cooper, H. 2008b. Comet and cup genes in *Drosophila* spermatogenesis: the first demonstration of post-meiotic transcription. *Biochemical Society Transactions* 36(3), pp. 540-542. doi: 10.1042/bst0360540

Barreau, C., Paillard, L., Méreau, A. and Osborne, H. B. 2006. Mammalian CELF/Bruno-like RNA-binding proteins: molecular characteristics and biological functions. *Biochimie* 88(5), pp. 515-525. doi: https://doi.org/10.1016/j.biochi.2005.10.011

Bassett, Andrew R., Tibbit, C., Ponting, Chris P. and Liu, J.-L. 2013. Highly Efficient Targeted Mutagenesis of *Drosophila* with the CRISPR/Cas9 System. *Cell Reports* 4(1), pp. 220-228. doi: 10.1016/j.celrep.2013.06.020

Bateman, J. R., Lee, A. M. and Wu, C. t. 2006. Site-Specific Transformation of *Drosophila* via ϕC31 Integrase-Mediated Cassette Exchange. *Genetics* 173(2), pp. 769-777. doi: 10.1534/genetics.106.056945

Baumgartner, M. E., Mastrogiannopoulos, A., Kucinski, I., Langton, P. F. and Piddini, E. 2022. The Gr64 cluster of gustatory receptors promotes survival and proteostasis of epithelial cells in *Drosophila*. *PLOS Biology* 20(7), p. e3001710. doi: 10.1371/journal.pbio.3001710

Bazylev, S. S., Adashev, V. E., Shatskikh, A. S., Olenina, L. V. and Kotov, A. A. 2021. Somatic Cyst Cells as a Microenvironment for the Maintenance and Differentiation of Germline Cells in *Drosophila* Spermatogenesis. *Russian Journal of Developmental Biology* 52(1), pp. 16-32. doi: 10.1134/S1062360421010021

Beall, C., Fyrberg, C., Song, S. and Fyrberg, E. 1992. Isolation of a *Drosophila* gene encoding glutathioneS-transferase. *Biochemical Genetics* 30(9), pp. 515-527. doi: 10.1007/BF01037590

Beaven, R. et al. 2017. 14-3-3 regulation of Ncd reveals a new mechanism for targeting proteins to the spindle in oocytes. *Journal of Cell Biology* 216(10), pp. 3029-3039. doi: 10.1083/jcb.201704120

Beaven, R., Dzhindzhev, N. S., Qu, Y., Hahn, I., Dajas-Bailador, F., Ohkura, H. and Prokop, A. 2015. *Drosophila* CLIP-190 and mammalian CLIP-170 display reduced microtubule plus end association in the nervous system. *Molecular biology of the cell* 26(8), pp. 1491-1508. doi: 10.1091/mbc.E14-06-1083

Begun, D. J. et al. 2007. Population Genomics: Whole-Genome Analysis of Polymorphism and Divergence in *Drosophila simulans*. *PLOS Biology* 5(11), p. e310. doi: 10.1371/journal.pbio.0050310

Bendena, W. G., Ayme-Southgate, A., Garbe, J. C. and Pardue, M. L. 1991. Expression of heat-shock locus hsr-omega in nonstressed cells during development in *Drosophila melanogaster*. *Developmental Biology* 144(1), pp. 65-77. doi: https://doi.org/10.1016/0012-1606(91)90479-M

Benoit, B. et al. 2005. An Essential Cytoplasmic Function for the Nuclear Poly(A) Binding Protein, PABP2, in Poly(A) Tail Length Control and Early Development in *Drosophila*. *Developmental Cell* 9(4), pp. 511-522. doi: 10.1016/j.devcel.2005.09.002

Benoit Bouvrette, L. P. et al. 2018. CeFra-seq reveals broad asymmetric mRNA and noncoding RNA distribution profiles in *Drosophila* and human cells. *RNA* 24(1), pp. 98-113.

Bergsten, S. E. and Gavis, E. R. 1999. Role for mRNA localization in translational activation but not spatial restriction of *nanos* RNA. *Development* 126(4), pp. 659-669. doi: 10.1242/dev.126.4.659

Berleth, T., Burri, M., Thoma, G., Bopp, D., Richstein, S., Frigerio, G. and Noll, M. 1988. The role of localization of *bicoid* RNA in organizing the anterior pattern of the *Drosophila* embryo. *The EMBO Journal* 7(6), pp. 1749-1756.

Besse, F. and Ephrussi, A. 2008. Translational control of localized mRNAs: restricting protein synthesis in space and time. *Nature Reviews Molecular Cell Biology* 9(12), pp. 971-980. doi: 10.1038/nrm2548

Besse, F., López de Quinto, S., Marchand, V., Trucco, A. and Ephrussi, A. 2009. *Drosophila* PTB promotes formation of high-order RNP particles and represses oskar translation. *Genes & Development* 23(2), pp. 195-207.

Betrán, E., Thornton, K. and Long, M. 2002. Retroposed New Genes Out of the X in *Drosophila*. *Genome Research* 12(12), pp. 1854-1859.

Beumer, K. J. and Carroll, D. 2014. Targeted genome engineering techniques in *Drosophila*. *Methods* 68(1), pp. 29-37. doi: https://doi.org/10.1016/j.ymeth.2013.12.002

Bevilacqua, P. C., Williams, A. M., Chou, H.-L. and Assmann, S. M. 2022. RNA multimerization as an organizing force for liquid–liquid phase separation. *RNA* 28(1), pp. 16-26. doi: 10.1261/rna.078999.121

Bharathi, V., Pallavi, S. K., Bajpai, R., Emerald, B. S. and Shashidhara, L. S. 2004. Genetic characterization of the *Drosophila* homologue of coronin. *Journal of Cell Science* 117(10), pp. 1911-1922. doi: 10.1242/jcs.01034

Bier, E. 2005. *Drosophila*, the golden bug, emerges as a tool for human genetics. *Nature Reviews Genetics* 6(1), pp. 9-23. doi: 10.1038/nrg1503

Birmingham, A. et al. 2009. Statistical methods for analysis of high-throughput RNA interference screens. *Nature Methods* 6(8), pp. 569-575. doi: 10.1038/nmeth.1351

Birner-Gruenberger, R. et al. 2012. Functional fat body proteomics and gene targeting reveal *in vivo* functions of *Drosophila melanogaster α-Esterase-7*. *Insect Biochemistry and Molecular Biology* 42(3), pp. 220-229. doi: https://doi.org/10.1016/j.ibmb.2011.12.004

Bischof, J., Björklund, M., Furger, E., Schertel, C., Taipale, J. and Basler, K. 2013. A versatile platform for creating a comprehensive UAS-ORFeome library in *Drosophila*. *Development* 140(11), pp. 2434-2442. doi: 10.1242/dev.088757

Bischof, J., Maeda, R. K., Hediger, M., Karch, F. and Basler, K. 2007. An optimized transgenesis system for *Drosophila* using germ-line-specific φC31 integrases. *Proceedings of the National Academy of Sciences* 104(9), pp. 3312-3317.

Blagden, S. P. et al. 2009. *Drosophila* Larp associates with poly(A)-binding protein and is required for male fertility and syncytial embryo development. *Developmental Biology* 334(1), pp. 186-197. doi: https://doi.org/10.1016/j.ydbio.2009.07.016

Blanchette, M., Green, R. E., MacArthur, S., Brooks, A. N., Brenner, S. E., Eisen, M. B. and Rio, D. C. 2009. Genome-wide Analysis of Alternative Pre-mRNA Splicing and

RNA-Binding Specificities of the *Drosophila* hnRNP A/B Family Members. *Molecular Cell* 33(4), pp. 438-449. doi: 10.1016/j.molcel.2009.01.022

Blunk, A. D. et al. 2014. Postsynaptic actin regulates active zone spacing and glutamate receptor apposition at the *Drosophila* neuromuscular junction. *Molecular and Cellular Neuroscience* 61, pp. 241-254. doi: https://doi.org/10.1016/j.mcn.2014.07.005

Bodanszky, A. and Bodanszky, M. 1970. Sepharose-avidin column for the binding of biotin or biotin-containing peptides. *Experientia* 26(3), pp. 327-327. doi: 10.1007/BF01900128

Bolstad, B. M., Irizarry, R. A., Åstrand, M. and Speed, T. P. 2003. A comparison of normalization methods for high density oligonucleotide array data based on variance and bias. *Bioinformatics* 19(2), pp. 185-193. doi: 10.1093/bioinformatics/19.2.185

Bolus, H., Crocker, K., Boekhoff-Falk, G. and Chtarbanova, S. 2020. Modeling Neurodegenerative Disorders in *Drosophila melanogaster*. *International Journal of Molecular Sciences* 21 (9). doi: 10.3390/ijms21093055

Bonaccorsi, S., Pisano, C., Puoti, F. and Gatti, M. 1988. Y chromosome loops in *Drosophila melanogaster*. *Genetics* 120(4), pp. 1015-1034. doi: 10.1093/genetics/120.4.1015

Boquet, I., Boujemaa, R., Carlier, M.-F. and Préat, T. 2000a. Ciboulot Regulates Actin Assembly during *Drosophila* Brain Metamorphosis. *Cell* 102(6), pp. 797-808. doi: https://doi.org/10.1016/S0092-8674(00)00068-4

Boquet, I., Hitier, R., Dumas, M., Chaminade, M. and Préat, T. 2000b. Central brain postembryonic development in *Drosophila*: implication of genes expressed at the interhemispheric junction. *Journal of neurobiology* 42(1), pp. 33-48.

Bose, M., Lampe, M., Mahamid, J. and Ephrussi, A. 2022. Liquid-to-solid phase transition of *oskar* ribonucleoprotein granules is essential for their function in *Drosophila* embryonic development. *Cell* 185(8), pp. 1308-1324.e1323. doi: 10.1016/j.cell.2022.02.022

Bouska, M. J. and Bai, H. 2021. Long noncoding RNA regulation of spermatogenesis via the spectrin cytoskeleton in *Drosophila*. *G3 Genes*|*Genomes*|*Genetics* 11(5), p. jkab080. doi: 10.1093/g3journal/jkab080

Boyerinas, B. et al. 2008. Identification of Let-7–Regulated Oncofetal Genes. *Cancer Research* 68(8), pp. 2587-2591. doi: 10.1158/0008-5472.CAN-08-0264

Boylan, K. L. M., Mische, S., Li, M., Marqués, G., Morin, X., Chia, W. and Hays, T. S. 2008. Motility Screen Identifies *Drosophila* IGF-II mRNA-Binding Protein—Zipcode-Binding Protein Acting in Oogenesis and Synaptogenesis. *PLOS Genetics* 4(2), p. e36. doi: 10.1371/journal.pgen.0040036

Boyle, M., Wong, C., Rocha, M. and Jones, D. L. 2007. Decline in Self-Renewal Factors Contributes to Aging of the Stem Cell Niche in the *Drosophila* Testis. *Cell Stem Cell* 1(4), pp. 470-478. doi: https://doi.org/10.1016/j.stem.2007.08.002

Brand, A. H. and Perrimon, N. 1993. Targeted gene expression as a means of altering cell fates and generating dominant phenotypes. *Development* 118(2), pp. 401-415. doi: 10.1242/dev.118.2.401

Brangwynne, C. P. et al. 2009. Germline P Granules Are Liquid Droplets That Localize by Controlled Dissolution/Condensation. *Science* 324(5935), pp. 1729-1732. doi: 10.1126/science.1172046

Brendza, R. P., Serbus, L. R., Duffy, J. B. and Saxton, W. M. 2000. A Function for Kinesin I in the Posterior Transport of oskar mRNA and Staufen Protein. *Science* 289(5487), pp. 2120-2122. doi: 10.1126/science.289.5487.2120

Brendza, R. P., Serbus, L. R., Saxton, W. M. and Duffy, J. B. 2002. Posterior Localization of Dynein and Dorsal-Ventral Axis Formation Depend on Kinesin in *Drosophila* Oocytes. *Current Biology* 12(17), pp. 1541-1545. doi: 10.1016/S0960-9822(02)01108-9

Broadus, J., Fuerstenberg, S. and Doe, C. Q. 1998. Staufen-dependent localization of prospero mRNA contributes to neuroblast daughter-cell fate. *Nature* 391(6669), pp. 792-795. doi: 10.1038/35861

Brogna, S., Sato, T.-A. and Rosbash, M. 2002. Ribosome Components Are Associated with Sites of Transcription. *Molecular Cell* 10(1), pp. 93-104. doi: https://doi.org/10.1016/S1097-2765(02)00565-8

Brooks, D. S., Vishal, K., Bawa, S., Alder, A. and Geisbrecht, E. R. 2021. Integration of proteomic and genetic approaches to assess developmental muscle atrophy. *Journal of Experimental Biology* 224(21), p. jeb242698. doi: 10.1242/jeb.242698

Brown, J. B. et al. 2014. Diversity and dynamics of the *Drosophila* transcriptome. *Nature* 512(7515), pp. 393-399. doi: 10.1038/nature12962

Bullock, S. L. and Ish-Horowicz, D. 2001. Conserved signals and machinery for RNA transport in *Drosophila* oogenesis and embryogenesis. *Nature* 414(6864), pp. 611-616. doi: 10.1038/414611a

Bullock, S. L., Nicol, A., Gross, S. P. and Zicha, D. 2006. Guidance of Bidirectional Motor Complexes by mRNA Cargoes through Control of Dynein Number and Activity. *Current Biology* 16(14), pp. 1447-1452. doi: 10.1016/j.cub.2006.05.055

Bullock, S. L., Zicha, D. and Ish-Horowicz, D. 2003. The *Drosophila hairy* RNA localization signal modulates the kinetics of cytoplasmic mRNA transport. *The EMBO Journal* 22(10), pp. 2484-2494.

Butsch, T. J., Johnson, A. E. and Bohnert, K. A. 2023. Rbp4-Gal4, a germline driver that activates in meiosis, reveals functions for VCP in spermatid development. *Fly* 17(1), p. 2234795. doi: 10.1080/19336934.2023.2234795

Buxbaum, A. R., Haimovich, G. and Singer, R. H. 2015. In the right place at the right time: visualizing and understanding mRNA localization. *Nature Reviews Molecular Cell Biology* 16(2), pp. 95-109. doi: 10.1038/nrm3918

Cabili, M. N. et al. 2015. Localization and abundance analysis of human lncRNAs at single-cell and single-molecule resolution. *Genome biology* 16(1), p. 20. doi: 10.1186/s13059-015-0586-4

Cáceres, L. and Nilson, L. A. 2009. Translational repression of *gurken* mRNA in the *Drosophila* oocyte requires the hnRNP Squid in the nurse cells. *Developmental Biology* 326(2), pp. 327-334. doi: https://doi.org/10.1016/j.ydbio.2008.11.030

Cáceres, L. a. and Nilson, L. A. 2005. Production of *gurken* in the nurse cells is sufficient for axis determination in the *Drosophila* oocyte. *Development* 132(10), pp. 2345-2353. doi: 10.1242/dev.01820

Camilleri-Robles, C., Amador, R., Klein, C. C., Guigó, R., Corominas, M. and Ruiz-Romero, M. 2022. Genomic and functional conservation of lncRNAs: lessons from flies. *Mammalian Genome* 33(2), pp. 328-342. doi: 10.1007/s00335-021-09939-4

Canal Domenech, B. and Fricke, C. 2023. Developmental heat stress interrupts spermatogenesis inducing early male sterility in *Drosophila melanogaster*. *Journal of Thermal Biology* 114, p. 103589. doi: https://doi.org/10.1016/j.jtherbio.2023.103589

Carlevaro-Fita, J. and Johnson, R. 2019. Global Positioning System: Understanding Long Noncoding RNAs through Subcellular Localization. *Molecular Cell* 73(5), pp. 869-883. doi: 10.1016/j.molcel.2019.02.008

Carlevaro-Fita, J., Rahim, A., Guigó, R., Vardy, L. A. and Johnson, R. 2016. Cytoplasmic long noncoding RNAs are frequently bound to and degraded at ribosomes in human cells. *RNA* 22(6), pp. 867-882.

Carvalho, A. B., Vicoso, B., Russo, C. A. M., Swenor, B. and Clark, A. G. 2015. Birth of a new gene on the Y chromosome of *Drosophila melanogaster*. *Proceedings of the National Academy of Sciences* 112(40), p. 12450. doi: 10.1073/pnas.1516543112

Castagnetti, S., Hentze, M. W., Ephrussi, A. and Gebauer, F. 2000. Control of oskar mRNA translation by Bruno in a novel cell-free system from *Drosophila* ovaries. *Development* 127(5), pp. 1063-1068. doi: 10.1242/dev.127.5.1063

Castello, A. et al. 2012. Insights into RNA Biology from an Atlas of Mammalian mRNA-Binding Proteins. *Cell* 149(6), pp. 1393-1406. doi: 10.1016/j.cell.2012.04.031

Castello, A. et al. 2013. System-wide identification of RNA-binding proteins by interactome capture. *Nature Protocols* 8(3), pp. 491-500. doi: 10.1038/nprot.2013.020

Castrillon, D. H. et al. 1993. Toward a molecular genetic analysis of spermatogenesis in *Drosophila melanogaster*: characterization of male-sterile mutants generated by single P element mutagenesis. *Genetics* 135(2), p. 489.

Caudy, A. A. et al. 2003. A micrococcal nuclease homologue in RNAi effector complexes. *Nature* 425(6956), pp. 411-414. doi: 10.1038/nature01956

Caudy, A. A., Myers, M., Hannon, G. J. and Hammond, S. M. 2002. Fragile X-related protein and VIG associate with the RNA interference machinery. *Genes & Development* 16(19), pp. 2491-2496.

Cenci, G. et al. 1997. UbcD1, a *Drosophila* ubiquitin-conjugating enzyme required for proper telomere behavior. *Genes & Development* 11(7), pp. 863-875.

Cermakova, K. and Hodges, H. C. 2018. Next-Generation Drugs and Probes for Chromatin Biology: From Targeted Protein Degradation to Phase Separation. *Molecules* 23(8), doi: 10.3390/molecules23081958

Cermelli, S., Guo, Y., Gross, S. P. and Welte, M. A. 2006. The Lipid-Droplet Proteome Reveals that Droplets Are a Protein-Storage Depot. *Current Biology* 16(18), pp. 1783-1795. doi: https://doi.org/10.1016/j.cub.2006.07.062

Cesana, M. et al. 2011. A Long Noncoding RNA Controls Muscle Differentiation by Functioning as a Competing Endogenous RNA. *Cell* 147(2), pp. 358-369. doi: https://doi.org/10.1016/j.cell.2011.09.028

Cha, B.-J., Koppetsch, B. S. and Theurkauf, W. E. 2001. In Vivo Analysis of *Drosophila bicoid* mRNA Localization Reveals a Novel Microtubule-Dependent Axis Specification Pathway. *Cell* 106(1), pp. 35-46. doi: 10.1016/S0092-8674(01)00419-6

Chang, H. C. and Rubin, G. M. 1997. 14-3-3 epsilon positively regulates Ras-mediated signaling in *Drosophila*. *Genes & Development* 11(9), pp. 1132-1139.

Chekulaeva, M., Hentze, M. W. and Ephrussi, A. 2006. Bruno Acts as a Dual Repressor of oskar Translation, Promoting mRNA Oligomerization and Formation of Silencing Particles. *Cell* 124(3), pp. 521-533. doi: https://doi.org/10.1016/j.cell.2006.01.031

Chen, B.-C. et al. 2014a. Lattice light-sheet microscopy: Imaging molecules to embryos at high spatiotemporal resolution. *Science* 346(6208), p. 1257998. doi: 10.1126/science.1257998

Chen, B., Zhang, Y., Zhang, X., Jia, S., Chen, S. and Kang, L. 2016. Genome-wide identification and developmental expression profiling of long noncoding RNAs during *Drosophila* metamorphosis. *Scientific Reports* 6(1), p. 23330. doi: 10.1038/srep23330

Chen, D., Brovkina, M., Matzat, L. H. and Lei, E. P. 2019. Shep RNA-Binding Capacity Is Required for Antagonism of *gypsy* Chromatin Insulator Activity. *G3: Genes|Genomes|Genetics* 9(3), p. 749. doi: 10.1534/g3.118.200923

Chen, D., Dale, R. K. and Lei, E. P. 2018. Shep regulates *Drosophila* neuronal remodeling by controlling transcription of its chromatin targets. *Development* 145(1), doi: 10.1242/dev.154047

Chen, D., Gu, T., Pham, T. N., Zachary, M. J. and Hewes, R. S. 2017. Regulatory Mechanisms of Metamorphic Neuronal Remodeling Revealed Through a Genome-Wide Modifier Screen in *Drosophila melanogaster*. *Genetics* 206(3), pp. 1429-1443. doi: 10.1534/genetics.117.200378

Chen, D. and McKearin, D. 2003a. Dpp Signaling Silences bam Transcription Directly to Establish Asymmetric Divisions of Germline Stem Cells. *Current Biology* 13(20), pp. 1786-1791. doi: https://doi.org/10.1016/j.cub.2003.09.033

Chen, D. and McKearin, D. M. 2003b. A discrete transcriptional silencer in the bam gene determines asymmetric division of the *Drosophila* germline stem cell. *Development* 130(6), pp. 1159-1170. doi: 10.1242/dev.00325

Chen, D., McManus, C. E., Radmanesh, B., Matzat, L. H. and Lei, E. P. 2021. Temporal inhibition of chromatin looping and enhancer accessibility during neuronal remodeling. *Nature Communications* 12(1), p. 6366. doi: 10.1038/s41467-021-26628-7

Chen, D., Qu, C., Bjorum, S. M., Beckingham, K. M. and Hewes, R. S. 2014b. Neuronal Remodeling During Metamorphosis Is Regulated by the alan shepard (shep) Gene in *Drosophila melanogaster*. *Genetics* 197(4), pp. 1267-1283. doi: 10.1534/genetics.114.166181

Chen, D. et al. 2009. Effete-mediated degradation of Cyclin A is essential for the maintenance of germline stem cells in *Drosophila*. *Development* 136(24), pp. 4133-4142. doi: 10.1242/dev.039032

Chen, D. et al. 2014c. Three RNA Binding Proteins Form a Complex to Promote Differentiation of Germline Stem Cell Lineage in *Drosophila*. *PLOS Genetics* 10(11), p. e1004797. doi: 10.1371/journal.pgen.1004797

Chen, H.-L., Kasuya, J., Lansdon, P., Kaas, G., Tang, H., Sodders, M. and Kitamoto, T. 2020. Reduced Function of the Glutathione S-Transferase S1 Suppresses Behavioral Hyperexcitability in *Drosophila* Expressing Mutant Voltage-Gated Sodium Channels. *G3 Genes|Genomes|Genetics* 10(4), pp. 1327-1340. doi: 10.1534/g3.119.401025

Chen, L.-L. 2016. Linking Long Noncoding RNA Localization and Function. *Trends in Biochemical Sciences* 41(9), pp. 761-772. doi: https://doi.org/10.1016/j.tibs.2016.07.003

Chen, X. et al. 2024. Single-cell transcriptome characteristics of testicular terminal epithelium lineages during aging in the *Drosophila*. *Aging Cell* 23(3), p. e14057.

Cheng, J., Tiyaboonchai, A., Yamashita, Y. M. and Hunt, A. J. 2011. Asymmetric division of cyst stem cells in *Drosophila* testis is ensured by anaphase spindle repositioning. *Development* 138(5), pp. 831-837. doi: 10.1242/dev.057901

Chin, A. and Lécuyer, E. 2017. RNA localization: Making its way to the center stage. *Biochimica et Biophysica Acta (BBA) - General Subjects* 1861(11, Part B), pp. 2956-2970. doi: https://doi.org/10.1016/j.bbagen.2017.06.011

Chintapalli, V. R., Wang, J. and Dow, J. A. T. 2007. Using FlyAtlas to identify better *Drosophila melanogaster* models of human disease. *Nature Genetics* 39(6), pp. 715-720. doi: 10.1038/ng2049

Cho, A., Kato, M., Whitwam, T., Kim, Ji H. and Montell, Denise J. 2016. An Atypical Tropomyosin in *Drosophila* with Intermediate Filament-like Properties. *Cell Reports* 16(4), pp. 928-938. doi: https://doi.org/10.1016/j.celrep.2016.06.054

Choi, H. M. T., Beck, V. A. and Pierce, N. A. 2014. Next-Generation in Situ Hybridization Chain Reaction: Higher Gain, Lower Cost, Greater Durability. *ACS Nano* 8(5), pp. 4284-4294. doi: 10.1021/nn405717p

Choi, H. M. T. et al. 2016. Mapping a multiplexed zoo of mRNA expression. *Development* 143(19), pp. 3632-3637. doi: 10.1242/dev.140137

Choi, H. M. T., Chang, J. Y., Trinh, L. A., Padilla, J. E., Fraser, S. E. and Pierce, N. A. 2010. Programmable in situ amplification for multiplexed imaging of mRNA expression. *Nature Biotechnology* 28(11), pp. 1208-1212. doi: 10.1038/nbt.1692

Choi, H. M. T. et al. 2018. Third-generation in situ hybridization chain reaction: multiplexed, quantitative, sensitive, versatile, robust. *Development* 145(12), doi: 10.1242/dev.165753

Christian, J. L. 2012. Morphogen gradients in development: from form to function. *WIREs Developmental Biology* 1(1), pp. 3-15. doi: https://doi.org/10.1002/wdev.2

Christiansen, J., Kolte, A. M., Hansen, T. v. O. and Nielsen, F. C. 2009. IGF2 mRNA-binding protein 2: biological function and putative role in type 2 diabetes. *Journal of Molecular Endocrinology* 43(5), pp. 187-195. doi: 10.1677/JME-09-0016

Cinnamon, E. et al. 2016. *Drosophila* Spidey/Kar Regulates Oenocyte Growth via PI3-Kinase Signaling. *PLOS Genetics* 12(8), p. e1006154. doi: 10.1371/journal.pgen.1006154

Civetta, A. and Singh, R. S. 1995. High divergence of reproductive tract proteins and their association with postzygotic reproductive isolation in *Drosophila melanogaster* and *Drosophila* virilis group species. *Journal of Molecular Evolution* 41(6), pp. 1085-1095. doi: 10.1007/BF00173190

Clancy, D. J., Hime, G. R. and Shirras, A. D. 2011. Cytoplasmic male sterility in *Drosophila melanogaster* associated with a mitochondrial CYTB variant. *Heredity* 107(4), pp. 374-376. doi: 10.1038/hdy.2011.12

Clark, A., Meignin, C. and Davis, I. 2007. A Dynein-dependent shortcut rapidly delivers axis determination transcripts into the *Drosophila* oocyte. *Development* 134(10), pp. 1955-1965. doi: 10.1242/dev.02832

Clark, I., Giniger, E., Ruohola-Baker, H., Jan, L. Y. and Jan, Y. N. 1994. Transient posterior localization of a kinesin fusion protein reflects anteroposterior polarity of the *Drosophila* oocyte. *Current Biology* 4(4), pp. 289-300. doi: 10.1016/S0960-9822(00)00068-3

Clouse, K. N., Ferguson, S. B. and Schüpbach, T. 2008. Squid, Cup, and PABP55B function together to regulate *gurken* translation in *Drosophila*. *Developmental Biology* 313(2), pp. 713-724. doi: https://doi.org/10.1016/j.ydbio.2007.11.008

Clyne, P. J., Brotman, J. S., Sweeney, S. T. and Davis, G. 2003. Green Fluorescent Protein Tagging *Drosophila* Proteins at Their Native Genomic Loci With Small P Elements. *Genetics* 165(3), pp. 1433-1441. doi: 10.1093/genetics/165.3.1433

Cohen, R. J. and Benedek, G. B. 1982. Equilibrium and kinetic theory of polymerization and the sol-gel transition. *The Journal of Physical Chemistry* 86(19), pp. 3696-3714.

Condeelis, J. and Singer, R. H. 2005. How and why does β-actin mRNA target? *Biology of the Cell* 97(1), pp. 97-110. doi: https://doi.org/10.1042/BC20040063

Conway, Anne E. et al. 2016. Enhanced CLIP Uncovers IMP Protein-RNA Targets in Human Pluripotent Stem Cells Important for Cell Adhesion and Survival. *Cell Reports* 15(3), pp. 666-679. doi: https://doi.org/10.1016/j.celrep.2016.03.052

Corrales, M. et al. 2022. A single-cell transcriptomic atlas of complete insect nervous systems across multiple life stages. *Neural Development* 17(1), p. 8. doi: 10.1186/s13064-022-00164-6

Cotten, M. L., Starich, M. R., He, Y., Yin, J., Yuan, Q. and Tjandra, N. 2024. NMR chemical shift assignment of *Drosophila* odorant binding protein 44a in complex with 8(Z)-eicosenoic acid. *Biomolecular NMR Assignments*, doi: 10.1007/s12104-024-10178-2

Courchet, J., Buchet-Poyau, K., Potemski, A., Brès, A., Jariel-Encontre, I. and Billaud, M. 2008. Interaction with 14-3-3 Adaptors Regulates the Sorting of hMex-3B RNA-binding Protein to Distinct Classes of RNA Granules*. *Journal of Biological Chemistry* 283(46), pp. 32131-32142. doi: https://doi.org/10.1074/jbc.M802927200

Crofts, A. J., Washida, H., Okita, T. W., Satoh, M., Ogawa, M., Kumamaru, T. and Satoh, H. 2005. The role of mRNA and protein sorting in seed storage protein synthesis, transport, and deposition. *Biochemistry and Cell Biology* 83(6), pp. 728-737. doi: 10.1139/o05-156 %M 16333324

Cross, D. P. and Shellenbarge, D. L. 1979. The dynamics of *Drosophila melanogaster* spermatogenesis in *in vitro* cultures. *Development* 53(1), pp. 345-351. doi: 10.1242/dev.53.1.345

Cuatrecasas, P. and Wilchek, M. 1968. Single-step purification of avidin from egg white by affinity chromatography on biocytin-Sepharose columns. *Biochemical and Biophysical Research Communications* 33(2), pp. 235-239. doi: https://doi.org/10.1016/0006-291X(68)90774-2

Dahanukar, A., Walker, J. A. and Wharton, R. P. 1999. Smaug, a Novel RNA-Binding Protein that Operates a Translational Switch in *Drosophila*. *Molecular Cell* 4(2), pp. 209-218. doi: 10.1016/S1097-2765(00)80368-8

Dale, R. K., Matzat, L. H. and Lei, E. P. 2014. metaseq: a Python package for integrative genome-wide analysis reveals relationships between chromatin insulators and associated nuclear mRNA. *Nucleic Acids Research* 42(14), pp. 9158-9170. doi: 10.1093/nar/gku644

Davie, K. et al. 2018. A Single-Cell Transcriptome Atlas of the Aging *Drosophila* Brain. *Cell* 174(4), pp. 982-998.e920. doi: https://doi.org/10.1016/j.cell.2018.05.057

Davis, M. B., Sun, W. and Standiford, D. M. 2002. Lineage-specific expression of polypyrimidine tract binding protein (PTB) in *Drosophila* embryos. *Mechanisms of Development* 111(1), pp. 143-147. doi: https://doi.org/10.1016/S0925-4773(01)00595-0

De Meyer, T., Muyldermans, S. and Depicker, A. 2014. Nanobody-based products as research and diagnostic tools. *Trends in Biotechnology* 32(5), pp. 263-270. doi: https://doi.org/10.1016/j.tibtech.2014.03.001

DeCaprio, J. and Kohl, T. O. 2017. Detergent Lysis of Tissue Culture Cells for Immunoprecipitation. *Cold Spring Harbor Protocols* 2017(12), p. pdb.prot098558.

DeCaprio, J. and Kohl, T. O. 2019. Using Dounce Homogenization to Lyse Cells for Immunoprecipitation. *Cold Spring Harbor Protocols* 2019(7), p. pdb.prot098574.

Degrauwe, N., Suvà, M. L., Janiszewska, M., Riggi, N. and Stamenkovic, I. 2016. IMPs: an RNA-binding protein family that provides a link between stem cell maintenance in normal development and cancer. (1549-5477 (Electronic)),

del Valle Rodríguez, A., Didiano, D. and Desplan, C. 2012. Power tools for gene expression and clonal analysis in *Drosophila*. *Nature Methods* 9(1), pp. 47-55. doi: 10.1038/nmeth.1800

Delanoue, R. and Davis, I. 2005. Dynein Anchors Its mRNA Cargo after Apical Transport in the *Drosophila* Blastoderm Embryo. *Cell* 122(1), pp. 97-106. doi: 10.1016/j.cell.2005.04.033

Delanoue, R., Herpers, B., Soetaert, J., Davis, I. and Rabouille, C. 2007. *Drosophila* Squid/hnRNP Helps Dynein Switch from a *gurken* mRNA Transport Motor to an Ultrastructural Static Anchor in Sponge Bodies. *Developmental Cell* 13(4), pp. 523-538. doi: 10.1016/j.devcel.2007.08.022

Della-Penna, D., Christoffersen, R. E. and Bennett, A. B. 1986. Biotinylated proteins as molecular weight standards on Western blots. *Analytical Biochemistry* 152(2), pp. 329-332. doi: https://doi.org/10.1016/0003-2697(86)90417-3

Demarco, R. S., Eikenes, Å. H., Haglund, K. and Jones, D. L. 2014. Investigating spermatogenesis in *Drosophila melanogaster*. *Methods* 68(1), pp. 218-227. doi: https://doi.org/10.1016/j.ymeth.2014.04.020

Derrien, T. et al. 2012. The GENCODE v7 catalog of human long noncoding RNAs: Analysis of their gene structure, evolution, and expression. *Genome Research* 22(9), pp. 1775-1789.

Desai, B. S., Shirolikar, S. and Ray, K. 2009. F-actin-based extensions of the head cyst cell adhere to the maturing spermatids to maintain them in a tight bundle and prevent their premature release in *Drosophila* testis. *BMC Biology* 7(1), p. 19. doi: 10.1186/1741-7007-7-19

Di Cara, F., Cavaliere, D., Galliero, V., Polito, L. and Digilio, F. 2010. Expressional and functional analysis of the male-specific cluster mst36F during *Drosophila* spermatogenesis. *Insect molecular biology* 19(6), pp. 807-813.

Dietzl, G. et al. 2007. A genome-wide transgenic RNAi library for conditional gene inactivation in *Drosophila*. *Nature* 448(7150), pp. 151-156. doi: 10.1038/nature05954

Dimitriadis, E. et al. 2007. Expression of oncofetal RNA-binding protein CRD-BP/IMP1 predicts clinical outcome in colon cancer. *International journal of cancer.* 121(3), pp. 486-494. doi: 10.1002/ijc.22716

Dimitrova-Paternoga, L. et al. 2021. Molecular basis of mRNA transport by a kinesin-1–atypical tropomyosin complex. *Genes & Development* 35(13-14), pp. 976-991.

Dirks, R. M. and Pierce, N. A. 2004. Triggered amplification by hybridization chain reaction. *Proceedings of the National Academy of Sciences* 101(43), pp. 15275-15278. doi: 10.1073/pnas.0407024101

Dobin, A. et al. 2013. STAR: ultrafast universal RNA-seq aligner. *Bioinformatics* 29(1), pp. 15-21. doi: 10.1093/bioinformatics/bts635

Doe, C. Q., Chu-LaGraff, Q., Wright, D. M. and Scott, M. P. 1991. The prospero gene specifies cell fates in the *drosophila* central nervous system. *Cell* 65(3), pp. 451-464. doi: https://doi.org/10.1016/0092-8674(91)90463-9

Doetsch, M., Schroeder, R. and Fürtig, B. 2011. Transient RNA–protein interactions in RNA folding. *The FEBS journal* 278(10), pp. 1634-1642.

Doggett, K., Jiang, J., Aleti, G. and White-Cooper, H. 2011. Wake-up-call, a *lin-52* paralogue, and Always early, a *lin-9* homologue physically interact, but have opposing functions in regulating testis-specific gene expression. *Developmental Biology* 355(2), pp. 381-393. doi: https://doi.org/10.1016/j.ydbio.2011.04.030

Dong, Y., Avva, S. V. S. P., Maharjan, M., Jacobi, J. and Hart, C. M. 2020. Promoter-Proximal Chromatin Domain Insulator Protein BEAF Mediates Local and Long-Range Communication with a Transcription Factor and Directly Activates a Housekeeping Promoter in *Drosophila*. *Genetics* 215(1), pp. 89-101. doi: 10.1534/genetics.120.303144

Doren, M. V., Williamson, A. L. and Lehmann, R. 1998. Regulation of zygotic gene expression in *Drosophila* primordial germ cells. *Current Biology* 8(4), pp. 243-246. doi: 10.1016/S0960-9822(98)70091-0

Dreyfuss, G., Kim, V. N. and Kataoka, N. 2002. Messenger-RNA-binding proteins and the messages they carry. *Nature Reviews Molecular Cell Biology* 3(3), pp. 195-205. doi: 10.1038/nrm760

Driever, W. and Nüsslein-Volhard, C. 1988a. The bicoid protein determines position in the *Drosophila* embryo in a concentration-dependent manner. *Cell* 54(1), pp. 95-104. doi: https://doi.org/10.1016/0092-8674(88)90183-3

Driever, W. and Nüsslein-Volhard, C. 1988b. A gradient of bicoid protein in *Drosophila* embryos. *Cell* 54(1), pp. 83-93. doi: https://doi.org/10.1016/0092-8674(88)90182-1

Du, T.-G., Schmid, M. and Jansen, R.-P. 2007. Why cells move messages: The biological functions of mRNA localization. *Seminars in Cell & Developmental Biology* 18(2), pp. 171-177. doi: https://doi.org/10.1016/j.semcdb.2007.01.010

Duffy, J. B. 2002. GAL4 system in *Drosophila*: a fly geneticist's Swiss army knife. *genesis* 34(1-2), pp. 1-15.

Duncan, J. E. and Warrior, R. 2002. The Cytoplasmic Dynein and Kinesin Motors Have Interdependent Roles in Patterning the *Drosophila* Oocyte. *Current Biology* 12(23), pp. 1982-1991. doi: 10.1016/S0960-9822(02)01303-9

Dzhindzhev, N. S., Rogers, S. L., Vale, R. D. and Ohkura, H. 2005. Distinct mechanisms govern the localisation of *Drosophila* CLIP-190 to unattached kinetochores and microtubule plus-ends. *Journal of Cell Science* 118(16), pp. 3781-3790. doi: 10.1242/jcs.02504

Eggert, U. S., Kiger, A. A., Richter, C., Perlman, Z. E., Perrimon, N., Mitchison, T. J. and Field, C. M. 2004. Parallel Chemical Genetic and Genome-Wide RNAi Screens

Identify Cytokinesis Inhibitors and Targets. *PLOS Biology* 2(12), p. e379. doi: 10.1371/journal.pbio.0020379

Elbaum-Garfinkle, S., Kim, Y., Szczepaniak, K., Chen, C. C.-H., Eckmann, C. R., Myong, S. and Brangwynne, C. P. 2015. The disordered P granule protein LAF-1 drives phase separation into droplets with tunable viscosity and dynamics. *Proceedings of the National Academy of Sciences* 112(23), pp. 7189-7194.

Elgar, S. J., Han, J. and Taylor, M. V. 2008. mef2 activity levels differentially affect gene expression during *Drosophila* muscle development. *Proceedings of the National Academy of Sciences* 105(3), pp. 918-923. doi: 10.1073/pnas.0711255105

Elisha, Z., Havin, L., Ringel, I. and Yisraeli, J. 1995. Vg1 RNA binding protein mediates the association of Vg1 RNA with microtubules in *Xenopus* oocytes. *The EMBO Journal* 14(20), pp. 5109-5114.

Elvira, G. et al. 2006. Characterization of an RNA Granule from Developing Brain *. *Molecular & Cellular Proteomics* 5(4), pp. 635-651. doi: 10.1074/mcp.M500255-MCP200

Eom, T., Antar, L. N., Singer, R. H. and Bassell, G. J. 2003. Localization of a β-Actin Messenger Ribonucleoprotein Complex with Zipcode-Binding Protein Modulates the Density of Dendritic Filopodia and Filopodial Synapses. *The Journal of Neuroscience* 23(32), p. 10433. doi: 10.1523/JNEUROSCI.23-32-10433.2003

Erdélyi, M., Michon, A.-M., Guichet, A., Glotzer, J. B. and Ephrussi, A. 1995. Requirement for *Drosophila* cytoplasmic tropomyosin in oskar mRNA localization. *Nature* 377(6549), pp. 524-527. doi: 10.1038/377524a0

Espinoza, C. Y. and Berg, C. A. 2020. Detecting New Allies: Modifier Screen Identifies a Genetic Interaction Between *Imaginal disc growth factor 3* and *combover*, a Rho-kinase Substrate, During Dorsal Appendage Tube Formation in *Drosophila*. *G3 Genes|Genomes|Genetics* 10(10), pp. 3585-3599. doi: 10.1534/g3.120.401476

Fabian, L. and Brill, J. A. 2012. *Drosophila* spermiogenesis. *Spermatogenesis* 2(3), pp. 197-212. doi: 10.4161/spmg.21798

Fabrizio, J., Hickey, C. A., Stabrawa, C., Meytes, V., Hunter, J. A., Talbert, C. and Regis, N. 2008. Imp (IGF-II mRNA-Binding Protein) Is Expressed During Spermatogenesis in *Drosophila melanogaster*. *Fly* 2(1), pp. 47-52. doi: 10.4161/fly.5659

Fabrizio, J. J., Hime, G., Lemmon, S. K. and Bazinet, C. 1998. Genetic dissection of sperm individualization in *Drosophila melanogaster*. *Development* 125(10), pp. 1833-1843. doi: 10.1242/dev.125.10.1833

Fagan, J. K. et al. 2014. Combover/CG10732, a Novel PCP Effector for *Drosophila* Wing Hair Formation. *PloS one* 9(9), p. e107311. doi: 10.1371/journal.pone.0107311

Fairchild, M. J., Islam, F. and Tanentzapf, G. 2017. Identification of genetic networks that act in the somatic cells of the testis to mediate the developmental program of spermatogenesis. *PLOS Genetics* 13(9), p. e1007026. doi: 10.1371/journal.pgen.1007026

Fanara, J. J., Beti, M. I. L., Gandini, L. and Hasson, E. 2023. Oviposition behaviour in *Drosophila melanogaster*: Genetic and behavioural decoupling between oviposition acceptance and preference for natural fruits. *Journal of Evolutionary Biology* 36(1), pp. 251-263. doi: 10.1111/jeb.14109

Fang, C.-T., Kuo, H.-H., Amartuvshin, O., Hsu, H.-J., Liu, S.-L., Yao, J.-S. and Yih, L.-H. 2023. Inhibition of acetyl-CoA carboxylase impaired tubulin palmitoylation and induced spindle abnormalities. *Cell Death Discovery* 9(1), p. 4. doi: 10.1038/s41420-023-01301-8

Fang, Y. et al. 2024. RpL38 modulates germ cell differentiation by controlling Bam expression in *Drosophila* testis. *Science China Life Sciences* 67(11), pp. 2411-2425. doi: 10.1007/s11427-024-2646-3

Fasulo, B., Meccariello, A., Morgan, M., Borufka, C., Papathanos, P. A. and Windbichler, N. 2020. A fly model establishes distinct mechanisms for synthetic CRISPR/Cas9 sex distorters. *PLOS Genetics* 16(3), p. e1008647. doi: 10.1371/journal.pgen.1008647

Fernández-Moreno, M. A., Farr, C. L., Kaguni, L. S. and Garesse, R. 2007. *Drosophila melanogaster* as a Model System to Study Mitochondrial Biology. In: Leister, D. and Herrmann, J.M. eds. *Mitochondria: Practical Protocols*. Totowa, NJ: Humana Press, pp. 33-49.

Ferrandon, D., Koch, I., Westhof, E. and Nüsslein–Volhard, C. 1997. RNA–RNA interaction is required for the formation of specific *bicoid* mRNA 3′ UTR–STAUFEN ribonucleoprotein particles. *The EMBO Journal*,

Filardo, P. and Ephrussi, A. 2003. Bruno regulates gurken during *Drosophila* oogenesis. *Mechanisms of Development* 120(3), pp. 289-297. doi: https://doi.org/10.1016/S0925-4773(02)00454-9

Findlay, G. D., Yi, X., MacCoss, M. J. and Swanson, W. J. 2008. Proteomics Reveals Novel *Drosophila* Seminal Fluid Proteins Transferred at Mating. *PLOS Biology* 6(7), p. e178. doi: 10.1371/journal.pbio.0060178

Fingerhut, J. M., Moran, J. V. and Yamashita, Y. M. 2019. Satellite DNA-containing gigantic introns in a unique gene expression program during *Drosophila* spermatogenesis. *PLOS Genetics* 15(5), p. e1008028. doi: 10.1371/journal.pgen.1008028

Fingerhut, J. M. and Yamashita, Y. M. 2020. mRNA localization mediates maturation of cytoplasmic cilia in *Drosophila* spermatogenesis. *Journal of Cell Biology* 219(9), p. e202003084. doi: 10.1083/jcb.202003084

Fischer, J. A., Giniger, E., Maniatis, T. and Ptashne, M. 1988. GAL4 activates transcription in *Drosophila*. *Nature* 332(6167), pp. 853-856. doi: 10.1038/332853a0

Flory, P. J. 1942. Thermodynamics of High Polymer Solutions. *The Journal of Chemical Physics* 10(1), pp. 51-61. doi: 10.1063/1.1723621

Forrest, K. M. and Gavis, E. R. 2003. Live Imaging of Endogenous RNA Reveals a Diffusion and Entrapment Mechanism for nanos mRNA Localization in *Drosophila*. *Current Biology* 13(14), pp. 1159-1168. doi: https://doi.org/10.1016/S0960-9822(03)00451-2

Fortini, M. E., Skupski, M. P., Boguski, M. S. and Hariharan, I. K. 2000. A Survey of Human Disease Gene Counterparts in the *Drosophila* Genome. *Journal of Cell Biology* 150(2), pp. F23-F30. doi: 10.1083/jcb.150.2.F23

François, C. M., Pihl, T., Dunoyer de Segonzac, M., Hérault, C. and Hudry, B. 2023. Metabolic regulation of proteome stability via N-terminal acetylation controls male germline stem cell differentiation and reproduction. *Nature Communications* 14(1), p. 6737. doi: 10.1038/s41467-023-42496-9

Franklin-Dumont, T. M., Chatterjee, C., Wasserman, S. A. and DiNardo, S. 2007. A novel eIF4G homolog, Off-schedule, couples translational control to meiosis and differentiation in *Drosophila* spermatocytes. *Development* 134(15), pp. 2851-2861. doi: 10.1242/dev.003517

Frappaolo, A., Piergentili, R. and Giansanti, M. G. 2022. Microtubule and Actin Cytoskeletal Dynamics in Male Meiotic Cells of *Drosophila melanogaster*. *Cells* 11 (4). doi: 10.3390/cells11040695

Fridy, P. C., Thompson, M. K., Ketaren, N. E. and Rout, M. P. 2015. Engineered high-affinity nanobodies recognizing staphylococcal Protein A and suitable for native isolation of protein complexes. *Analytical Biochemistry* 477, pp. 92-94. doi: https://doi.org/10.1016/j.ab.2015.02.013

Fritzsche, R. et al. 2013. Interactome of Two Diverse RNA Granules Links mRNA Localization to Translational Repression in Neurons. *Cell Reports* 5(6), pp. 1749-1762. doi: 10.1016/j.celrep.2013.11.023

Fuller, M. 1993. Spermatogenesis. In: Bate, M.a.M.A., A. ed. *The Development of Drosophila melanogaster*. Vol. 1. Cold Spring Harbor Laboratory Press, pp. 71-147.

Fuller, M. T. 1998. Genetic control of cell proliferation and differentiation in*Drosophila*spermatogenesis. *Seminars in Cell & Developmental Biology* 9(4), pp. 433-444. doi: https://doi.org/10.1006/scdb.1998.0227

Gallagher, C. and Ramos, A. 2018. Joining the dots – protein-RNA interactions mediating local mRNA translation in neurons. *FEBS Letters* 592(17), pp. 2932-2947. doi: https://doi.org/10.1002/1873-3468.13121

Galletta, B. J. et al. 2014. *Drosophila* pericentrin requires interaction with calmodulin for its function at centrosomes and neuronal basal bodies but not at sperm basal bodies. *Molecular biology of the cell* 25(18), pp. 2682-2694. doi: 10.1091/mbc.e13-10-0617

García-Blanco, M. A., Jamison, S. F. and Sharp, P. A. 1989. Identification and purification of a 62,000-dalton protein that binds specifically to the polypyrimidine tract of introns. *Genes & Development* 3(12a), pp. 1874-1886. doi: 10.1101/gad.3.12a.1874

Garcia-Jove Navarro, M., Kashida, S., Chouaib, R., Souquere, S., Pierron, G., Weil, D. and Gueroui, Z. 2019. RNA is a critical element for the sizing and the composition of phase-separated RNA–protein condensates. *Nature Communications* 10(1), p. 3230. doi: 10.1038/s41467-019-11241-6

Garlovsky, M. D., Sandler, J. A. and Karr, T. L. 2022. Functional Diversity and Evolution of the *Drosophila* Sperm Proteome. *Molecular & Cellular Proteomics* 21(10), doi: 10.1016/j.mcpro.2022.100281

Garrido, D., Rubin, T., Poidevin, M., Maroni, B., Le Rouzic, A., Parvy, J.-P. and Montagne, J. 2015. Fatty Acid Synthase Cooperates with Glyoxalase 1 to Protect against Sugar Toxicity. *PLOS Genetics* 11(2), p. e1004995. doi: 10.1371/journal.pgen.1004995

Gärtner, S. M. K. et al. 2019. Stage-specific testes proteomics of *Drosophila melanogaster* identifies essential proteins for male fertility. *European Journal of Cell Biology* 98(2), pp. 103-115. doi: https://doi.org/10.1016/j.ejcb.2019.01.001

Gáspár, I., Sysoev, V., Komissarov, A. and Ephrussi, A. 2017. An RNA-binding atypical tropomyosin recruits kinesin-1 dynamically to *oskar* mRNPs. *The EMBO Journal* 36(3), pp. 319-333-333. doi: https://doi.org/10.15252/embj.201696038

Gavis, E. R. and Lehmann, R. 1992. Localization of nanos RNA controls embryonic polarity. *Cell* 71(2), pp. 301-313. doi: https://doi.org/10.1016/0092-8674(92)90358-J

Gavis, E. R. and Lehmann, R. 1994. Translational regulation of *nanos* by RNA localization. *Nature* 369(6478), pp. 315-318. doi: 10.1038/369315a0

Gavis, E. R., Lunsford, L., Bergsten, S. E. and Lehmann, R. 1996. A conserved 90 nucleotide element mediates translational repression of *nanos* RNA. *Development* 122(9), pp. 2791-2800. doi: 10.1242/dev.122.9.2791

Gemmill, D., D'souza, S., Meier-Stephenson, V. and Patel, T. R. 2019. Current approaches for RNA-labelling to identify RNA-binding proteins. *Biochemistry and Cell Biology* 98(1), pp. 31-41. doi: 10.1139/bcb-2019-0041

Geng, C. and Macdonald, P. M. 2006. Imp Associates with Squid and Hrp48 and Contributes to Localized Expression of gurken in the Oocyte. *Molecular and cellular biology* 26(24), pp. 9508-9516. doi: 10.1128/MCB.01136-06

Gershman, B. W., Pritchard, C. E., Chaney, K. P. and Ware, V. C. 2020. Tissue-specific expression of ribosomal protein Paralogue eRpL22-like in *Drosophila melanogaster* eye development. *Developmental Dynamics* 249(9), pp. 1147-1165.

Ghersi, D. and Sanchez, R. 2009. EasyMIFs and SiteHound: a toolkit for the identification of ligand-binding sites in protein structures. *Bioinformatics* 25(23), pp. 3185-3186. doi: 10.1093/bioinformatics/btp562

Ghosh-Roy, A., Kulkarni, M., Kumar, V., Shirolikar, S. and Ray, K. 2004. Cytoplasmic Dynein–Dynactin Complex Is Required for Spermatid Growth but Not Axoneme Assembly in *Drosophila*. *Molecular biology of the cell* 15(5), pp. 2470-2483. doi: 10.1091/mbc.e03-11-0848

Ghosh, S. and Lasko, P. 2015. Loss-of-Function Analysis Reveals Distinct Requirements of the Translation Initiation Factors eIF4E, eIF4E-3, eIF4G and eIF4G2 in *Drosophila* Spermatogenesis. *PloS one* 10(4), p. e0122519. doi: 10.1371/journal.pone.0122519

Gilmutdinov, R. et al. 2021. The 3′UTR of the *Drosophila* CPEB translation factor gene orb2 plays a crucial role in spermatogenesis. *Development* 148(17), doi: 10.1242/dev.198788

Giordano, E., Peluso, I., Rendina, R., Digilio, A. and Furia, M. 2003. The *clot* gene of *Drosophila melanogaster* encodes a conserved member of the Thioredoxin-like protein superfamily. *Molecular Genetics and Genomics* 268(5), pp. 692-697. doi: 10.1007/s00438-002-0792-0

Giorgi, C. and Moore, M. J. 2007. The nuclear nurture and cytoplasmic nature of localized mRNPs. *Seminars in Cell & Developmental Biology* 18(2), pp. 186-193. doi: https://doi.org/10.1016/j.semcdb.2007.01.002

Gönczy, P. and DiNardo, S. 1996. The germ line regulates somatic cyst cell proliferation and fate during *Drosophila* spermatogenesis. *Development* 122(8), pp. 2437-2447. doi: 10.1242/dev.122.8.2437

Gonsalvez, G. B., Urbinati, C. R. and Long, R. M. 2005. RNA localization in yeast: moving towards a mechanism. *Biology of the Cell* 97(1), pp. 75-86. doi: https://doi.org/10.1042/BC20040066

González, C., Casal, J. and Ripoll, P. 1989. Relationship between chromosome content and nuclear diameter in early spermatids of *Drosophila melanogaster*. *Genetical Research* 54(3), pp. 205-212. doi: 10.1017/S0016672300028664

González Morales, N. et al. 2023. The oxoglutarate dehydrogenase complex is involved in myofibril growth and Z-disc assembly in *Drosophila*. *Journal of Cell Science* 136(13), p. jcs260717. doi: 10.1242/jcs.260717

Good, P. J., Chen, Q., Warner, S. J. and Herring, D. C. 2000. A Family of Human RNA-binding Proteins Related to the *Drosophila* Bruno Translational Regulator*. *Journal of Biological Chemistry* 275(37), pp. 28583-28592. doi: https://doi.org/10.1074/jbc.M003083200

Goodrich, J. S., Clouse, K. N. and Schüpbach, T. 2004. Hrb27C, Sqd and Otu cooperatively regulate *gurken* RNA localization and mediate nurse cell chromosome dispersion in *Drosophila* oogenesis. *Development* 131(9), pp. 1949-1958. doi: 10.1242/dev.01078

Goshima, G., Wollman, R., Goodwin, S. S., Zhang, N., Scholey, J. M., Vale, R. D. and Stuurman, N. 2007. Genes Required for Mitotic Spindle Assembly in *Drosophila* S2 Cells. *Science* 316(5823), pp. 417-421. doi: 10.1126/science.1141314

Gould-Somero, M. and Holland, L. 1974. The timing of RNA synthesis for spermiogenesis in organ cultures of *Drosophila melanogaster* testes. *Wilhelm Roux' Archiv für Entwicklungsmechanik der Organismen* 174(2), pp. 133-148. doi: 10.1007/BF00573626

Gracheva, E., Dus, M. and Elgin, S. C. R. 2009. *Drosophila* RISC Component VIG and Its Homolog Vig2 Impact Heterochromatin Formation. *PloS one* 4(7), p. e6182. doi: 10.1371/journal.pone.0006182

Gratz, S. J. et al. 2013. Genome Engineering of *Drosophila* with the CRISPR RNA-Guided Cas9 Nuclease. *Genetics* 194(4), pp. 1029-1035. doi: 10.1534/genetics.113.152710

Greger, K., Swoger, J. and Stelzer, E. H. K. 2007. Basic building units and properties of a fluorescence single plane illumination microscope. *Review of Scientific Instruments* 78(2), p. 023705. doi: 10.1063/1.2428277

Groth, A. C., Fish, M., Nusse, R. and Calos, M. P. 2004. Construction of Transgenic *Drosophila* by Using the Site-Specific Integrase From Phage φC31. *Genetics* 166(4), pp. 1775-1782. doi: 10.1093/genetics/166.4.1775

Gu, W. et al. 2012. Regulation of local expression of cell adhesion and motility-related mRNAs in breast cancer cells by IMP1/ZBP1. *Journal of Cell Science* 125(1), pp. 81-91. doi: 10.1242/jcs.086132

Gunkel, N., Yano, T., Markussen, F.-H., Olsen, L. C. and Ephrussi, A. 1998. Localization-dependent translation requires a functional interaction between the 5′ and 3′ ends ofoskar mRNA. *Genes & Development* 12(11), pp. 1652-1664.

Guo, M. et al. 2022. Uncoupling transcription and translation through miRNA-dependent poly(A) length control in haploid male germ cells. *Development* 149(12), p. dev199573. doi: 10.1242/dev.199573

Hachet, O. and Ephrussi, A. 2004. Splicing of *oskar* RNA in the nucleus is coupled to its cytoplasmic localization. *Nature* 428(6986), pp. 959-963. doi: 10.1038/nature02521

Hackstein, J. H. P., Hochstenbach, R. and Pearson, P. L. 2000. Towards an understanding of the genetics of human male infertility: lessons from flies. *Trends in Genetics* 16(12), pp. 565-572. doi: https://doi.org/10.1016/S0168-9525(00)02140-5

Hamann, S. and Strätling, W. H. 1998. Specific binding of *Drosophila* nuclear protein PEP (protein on ecdysone puffs) to hsp70 DNA and RNA. *Nucleic Acids Research* 26(18), pp. 4108-4115. doi: 10.1093/nar/26.18.4108

Hamilton, K. E. et al. 2013. IMP1 promotes tumor growth, dissemination and a tumor-initiating cell phenotype in colorectal cancer cell xenografts. *Carcinogenesis* 34(11), pp. 2647-2654. doi: 10.1093/carcin/bgt217

Hammer, N. A. et al. 2005. Expression of IGF-II mRNA-binding proteins (IMPs) in gonads and testicular cancer. *Reproduction : the official journal of the Society for the Study of Fertility.* 130(2), pp. 203-212. doi: 10.1530/rep.1.00664

Hansen, H. T. et al. 2015. *Drosophila* Imp iCLIP identifies an RNA assemblage coordinating F-actin formation. *Genome biology* 16(1), p. 123. doi: 10.1186/s13059-015-0687-0

Hansen, T. V. O. et al. 2004. Dwarfism and Impaired Gut Development in Insulin-Like Growth Factor II mRNA-Binding Protein 1-Deficient Mice. *Molecular and cellular biology* 24(10), pp. 4448-4464. doi: 10.1128/MCB.24.10.4448-4464.2004

Hansji, H., Leung, E. Y., Baguley, B. C., Finlay, G. J., Cameron-Smith, D., Figueiredo, V. C. and Askarian-Amiri, M. E. 2016. ZFAS1: a long noncoding RNA associated with ribosomes in breast cancer cells. *Biology Direct* 11(1), p. 62. doi: 10.1186/s13062-016-0165-y

Hardy, R. W., Tokuyasu, K. T. and Lindsley, D. L. 1981. Analysis of spermatogenesis in *Drosophila melanogaster* bearing deletions for Y-chromosome fertility genes. *Chromosoma* 83(5), pp. 593-617. doi: 10.1007/BF00328522

Hardy, R. W., Tokuyasu, K. T., Lindsley, D. L. and Garavito, M. 1979. The germinal proliferation center in the testis of *Drosophila melanogaster*. *Journal of Ultrastructure Research* 69(2), pp. 180-190. doi: https://doi.org/10.1016/S0022-5320(79)90108-4

Hartmann, B. et al. 2011. Distinct regulatory programs establish widespread sex-specific alternative splicing in *Drosophila melanogaster*. *RNA* 17(3), pp. 453-468. doi: 10.1261/rna.2460411

Havin, L. et al. 1998. RNA-binding protein conserved in both microtubule- and microfilament-based RNA localization. *Genes & Development* 12(11), pp. 1593-1598. doi: 10.1101/gad.12.11.1593

Hayashi, S. et al. 2002. GETDB, a database compiling expression patterns and molecular locations of a collection of Gal4 enhancer traps. *genesis* 34(1-2), pp. 58-61.

Hazelrigg, T., Watkins, W. S., Marcey, D., Tu, C., Karow, M. and Lin, X. R. 1990. The exuperantia gene is required for *Drosophila* spermatogenesis as well as anteroposterior polarity of the developing oocyte, and encodes overlapping sex-specific transcripts. *Genetics* 126(3), pp. 607-617. doi: 10.1093/genetics/126.3.607

He, Y., Cotten, M. L., Yin, J., Yuan, Q. and Tjandra, N. 2023. Expression and purification of *Drosophila* OBP44a with the aids of LC-MS and NMR. *Protein Expression and Purification* 212, p. 106354. doi: https://doi.org/10.1016/j.pep.2023.106354

Heigwer, F., Port, F. and Boutros, M. 2018. RNA Interference (RNAi) Screening in *Drosophila*. *Genetics* 208(3), pp. 853-874. doi: 10.1534/genetics.117.300077

Herman-Bachinsky, Y., Ryoo, H. D., Ciechanover, A. and Gonen, H. 2007. Regulation of the *Drosophila* ubiquitin ligase DIAP1 is mediated via several distinct ubiquitin system pathways. *Cell Death & Differentiation* 14(4), pp. 861-871. doi: 10.1038/sj.cdd.4402079

Hermanson, G. T. 2013. Chapter 11 - (Strept)avidin–Biotin Systems. In: Hermanson, G.T. ed. *Bioconjugate Techniques (Third Edition)*. Boston: Academic Press, pp. 465-505.

Hernández, G., del Mar Castellano, M., Agudo, M. and Sierra, J. M. 1998. Isolation and characterization of the cDNA and the gene for eukaryotic translation initiation factor 4G from *Drosophila melanogaster*. *European journal of biochemistry* 253(1), pp. 27-35.

Hernández, G. et al. 2012. Eukaryotic initiation factor 4E-3 is essential for meiotic chromosome segregation, cytokinesis and male fertility in *Drosophila*. *Development* 139(17), pp. 3211-3220. doi: 10.1242/dev.073122

Hernandez, M., Ghersi, D. and Sanchez, R. 2009. SITEHOUND-web: a server for ligand binding site identification in protein structures. *Nucleic Acids Research* 37(suppl_2), pp. W413-W416. doi: 10.1093/nar/gkp281

Hilgers, V., Perry, M. W., Hendrix, D., Stark, A., Levine, M. and Haley, B. 2011. Neural-specific elongation of 3′ UTRs during *Drosophila* development. *Proceedings of the National Academy of Sciences* 108(38), pp. 15864-15869. doi: 10.1073/pnas.1112672108

Hirata, J., Nakagoshi, H., Nabeshima, Y.-i. and Matsuzaki, F. 1995. Asymmetric segregation of the homeodomain protein Prospero during *Drosophila* development. *Nature* 377(6550), pp. 627-630. doi: 10.1038/377627a0

Hogan, C. C. and Bettencourt, B. R. 2009. Duplicate Gene Evolution Toward Multiple Fates at the *Drosophila melanogaster HIP/HIP-Replacement* Locus. *Journal of Molecular Evolution* 68(4), pp. 337-350. doi: 10.1007/s00239-009-9213-x

Hogan, D. J., Riordan, D. P., Gerber, A. P., Herschlag, D. and Brown, P. O. 2008. Diverse RNA-Binding Proteins Interact with Functionally Related Sets of RNAs, Suggesting an Extensive Regulatory System. *PLOS Biology* 6(10), p. e255. doi: 10.1371/journal.pbio.0060255

Holt, Christine E. and Schuman, Erin M. 2013. The Central Dogma Decentralized: New Perspectives on RNA Function and Local Translation in Neurons. *Neuron* 80(3), pp. 648-657. doi: https://doi.org/10.1016/j.neuron.2013.10.036

Hopes, T. et al. 2022. Ribosome heterogeneity in *Drosophila melanogaster* gonads through paralog-switching. *Nucleic Acids Research* 50(4), pp. 2240-2257. doi: 10.1093/nar/gkab606

Hu, Y. et al. 2021. FlyRNAi.org—the database of the *Drosophila* RNAi screening center and transgenic RNAi project: 2021 update. *Nucleic Acids Research* 49(D1), pp. D908-D915. doi: 10.1093/nar/gkaa936

Hu, Z. et al. 2014. Association analysis identifies new risk loci for non-obstructive azoospermia in Chinese men. *Nature Communications* 5(1), p. 3857. doi: 10.1038/ncomms4857

Huang, J., Zhou, W., Dong, W., Watson, A. M. and Hong, Y. 2009. Directed, efficient, and versatile modifications of the *Drosophila* genome by genomic engineering. *Proceedings of the National Academy of Sciences* 106(20), pp. 8284-8289. doi: 10.1073/pnas.0900641106

Huang, Y. S., Ku, H. Y., Tsai, Y. C., Chang, C. H., Pao, S. H., Sun, Y. H. and Chiou, A. 2017. 5D imaging via light sheet microscopy reveals cell dynamics during the eye-antenna disc primordium formation in *Drosophila*. *Scientific Reports* 7(1), p. 44945. doi: 10.1038/srep44945

Hubstenberger, A. et al. 2017. P-Body Purification Reveals the Condensation of Repressed mRNA Regulons. *Molecular Cell* 68(1), pp. 144-157.e145. doi: 10.1016/j.molcel.2017.09.003

Hubstenberger, A., Noble, Scott L., Cameron, C. and Evans, Thomas C. 2013. Translation Repressors, an RNA Helicase, and Developmental Cues Control RNP Phase Transitions during Early Development. *Developmental Cell* 27(2), pp. 161-173. doi: 10.1016/j.devcel.2013.09.024

Hughes, J. R., Bullock, S. L. and Ish-Horowicz, D. 2004. inscuteable mRNA Localization Is Dynein-Dependent and Regulates Apicobasal Polarity and Spindle

Length in *Drosophila* Neuroblasts. *Current Biology* 14(21), pp. 1950-1956. doi: https://doi.org/10.1016/j.cub.2004.10.022

Huh, J. R., Vernooy, S. Y., Yu, H., Yan, N., Shi, Y., Guo, M. and Hay, B. A. 2003. Multiple Apoptotic Caspase Cascades Are Required in Nonapoptotic Roles for *Drosophila* Spermatid Individualization. *PLOS Biology* 2(1), p. e15. doi: 10.1371/journal.pbio.0020015

Huisken, J., Swoger, J., Del Bene, F., Wittbrodt, J. and Ernst, H. K. S. 2004. Optical Sectioning Deep inside Live Embryos by Selective Plane Illumination Microscopy. *Science* 305(5686), pp. 1007-1009.

Hüttelmaier, S. et al. 2005. Spatial regulation of β-actin translation by Src-dependent phosphorylation of ZBP1. *Nature* 438(7067), pp. 512-515. doi: 10.1038/nature04115

Huylmans, A. K. and Parsch, J. 2014. Population- and Sex-Biased Gene Expression in the Excretion Organs of *Drosophila melanogaster*. *G3 Genes|Genomes|Genetics* 4(12), pp. 2307-2315. doi: 10.1534/g3.114.013417

Ikawa, K., Hiro, S., Kondo, S., Ohsawa, S. and Sugimura, K. 2023. Coronin-1 promotes directional cell rearrangement in *Drosophila* wing epithelium. *Cell Structure and Function* 48(2), pp. 251-257. doi: 10.1247/csf.23049

Inagaki, S., Numata, K., Kondo, T., Tomita, M., Yasuda, K., Kanai, A. and Kageyama, Y. 2005. Identification and expression analysis of putative mRNA-like non-coding RNA in *Drosophila*. *Genes to cells* 10(12), pp. 1163-1173.

Insco, Megan L., Bailey, Alexis S., Kim, J., Olivares, Gonzalo H., Wapinski, Orly L., Tam, Cheuk H. and Fuller, Margaret T. 2012. A Self-Limiting Switch Based on

Translational Control Regulates the Transition from Proliferation to Differentiation in an Adult Stem Cell Lineage. *Cell Stem Cell* 11(5), pp. 689-700. doi: 10.1016/j.stem.2012.08.012

Ioannidis, P. et al. 2001. *C-MYC* and IGF-II mRNA-binding protein (CRD-BP/IMP-1) in benign and malignant mesenchymal tumors. *International journal of cancer* 94(4), pp. 480-484.

Ivanov, K. I., Tselykh, T. V., Heino, T. I. and Mäkinen, K. 2005. The RISC component VIG is a target for dsRNA-independent protein kinase activity in *Drosophila* S2 cells. *Journal of Rnai and Gene Silencing: an International Journal of RNA and Gene Targeting Research* 1(1), p. 12.

Jankovics, F., Sinka, R., Lukácsovich, T. and Erdélyi, M. 2002. MOESIN Crosslinks Actin and Cell Membrane in *Drosophila* Oocytes and Is Required for OSKAR Anchoring. *Current Biology* 12(23), pp. 2060-2065. doi: 10.1016/S0960-9822(02)01256-3

Jansen, R.-P. 2001. mRNA localization: message on the move. *Nature Reviews Molecular Cell Biology* 2(4), pp. 247-256. doi: 10.1038/35067016

Januschke, J. et al. 2002. Polar Transport in the *Drosophila* Oocyte Requires Dynein and Kinesin I Cooperation. *Current Biology* 12(23), pp. 1971-1981. doi: 10.1016/S0960-9822(02)01302-7

Jayaramaiah Raja, S. and Renkawitz-Pohl, R. 2005. Replacement by *Drosophila melanogaster* Protamines and Mst77F of Histones during Chromatin Condensation in Late Spermatids and Role of Sesame in the Removal of These Proteins from the Male Pronucleus. *Molecular and cellular biology* 25(14), pp. 6165-6177. doi: 10.1128/MCB.25.14.6165-6177.2005

Jenett, A. et al. 2012. A GAL4-Driver Line Resource for *Drosophila* Neurobiology. *Cell Reports* 2(4), pp. 991-1001. doi: 10.1016/j.celrep.2012.09.011

Jiang, J., Benson, E., Bausek, N., Doggett, K. and White-Cooper, H. 2007. Tombola, a tesmin/TSO1-family protein, regulates transcriptional activation in the *Drosophila* male germline and physically interacts with Always early. *Development* 134(8), pp. 1549-1559. doi: 10.1242/dev.000521

Jin, L. H., Shim, J., Yoon, J. S., Kim, B., Kim, J., Kim-Ha, J. and Kim, Y.-J. 2008. Identification and Functional Analysis of Antifungal Immune Response Genes in *Drosophila*. *PLOS Pathogens* 4(10), p. e1000168. doi: 10.1371/journal.ppat.1000168

Jodoin, Jeanne N. et al. 2015. Stable Force Balance between Epithelial Cells Arises from F-Actin Turnover. *Developmental Cell* 35(6), pp. 685-697. doi: https://doi.org/10.1016/j.devcel.2015.11.018

Johnston, D. S., Driever, W., Berleth, T., Richstein, S. and Nüsslein-Volhard, C. 1989. Multiple steps in the localization of *bicoid* RNA to the anterior pole of the *Drosophila* oocyte. *Development* 107(Supplement), pp. 13-19. doi: 10.1242/dev.107.Supplement.13

Johnston, S. A., Bramble, J. P., Yeung, C. L., Mendes, P. M. and Machesky, L. M. 2008. Arp2/3 complex activity in filopodia of spreading cells. *BMC Cell Biology* 9(1), p. 65. doi: 10.1186/1471-2121-9-65

Johnstone, O. and Lasko, P. 2001. Translational Regulation and RNA Localization in *Drosophila* Oocytes and Embryos. *Annual Review of Genetics* 35(1), pp. 365-406. doi: 10.1146/annurev.genet.35.102401.090756

Joly, D., Bressac, C. and Lachaise, D. 1995. Disentangling giant sperm. *Nature* 377(6546), pp. 202-202. doi: 10.1038/377202a0

Joly, D., Cariou, M. L., Lachaise, D. and David, J. R. 1989. Variation of sperm length and heteromorphism in drosophilid species. *Genetics Selection Evolution* 21(3), p. 283. doi: 10.1186/1297-9686-21-3-283

Joly, D. and Lachaise, D. 1994. Polymorphism in the sperm heteromorphic species of the *Drosophila obscura* group. *Journal of Insect Physiology* 40(11), pp. 933-938. doi: https://doi.org/10.1016/0022-1910(94)90131-7

Jones, W. D. 2009. The expanding reach of the GAL4/UAS system into the behavioral neurobiology of *Drosophila*. *BMB reports* 42(11), pp. 705-712.

Jongens, T. A., Ackerman, L. D., Swedlow, J. R., Jan, L. Y. and Jan, Y. N. 1994. *Germ cell-less* encodes a cell type-specific nuclear pore-associated protein and functions early in the germ-cell specification pathway of *Drosophila*. *Genes & Development* 8(18), pp. 2123-2136.

Jongens, T. A., Hay, B., Jan, L. Y. and Jan, Y. N. 1992. The *germ cell-less* gene product: a posteriorly localized component necessary for germ cell development in *Drosophila*. *Cell* 70(4), pp. 569-584.

Jouandin, P. et al. 2022. Lysosomal cystine mobilization shapes the response of TORC1 and tissue growth to fasting. *Science* 375(6582), p. eabc4203. doi: 10.1126/science.abc4203

Jung, H., Gkogkas, Christos G., Sonenberg, N. and Holt, Christine E. 2014. Remote Control of Gene Function by Local Translation. *Cell* 157(1), pp. 26-40. doi: https://doi.org/10.1016/j.cell.2014.03.005

Kaessmann, H. 2010. Origins, evolution, and phenotypic impact of new genes. *Genome Research* 20(10), pp. 1313-1326.

Kafasla, P. et al. 2012. Defining the roles and interactions of PTB. *Biochemical Society Transactions* 40(4), pp. 815-820. doi: 10.1042/BST20120044

Kanai, Y., Dohmae, N. and Hirokawa, N. 2004. Kinesin Transports RNA: Isolation and Characterization of an RNA-Transporting Granule. *Neuron* 43(4), pp. 513-525. doi: 10.1016/j.neuron.2004.07.022

Kaplan, Y., Gibbs-Bar, L., Kalifa, Y., Feinstein-Rotkopf, Y. and Arama, E. 2010. Gradients of a Ubiquitin E3 Ligase Inhibitor and a Caspase Inhibitor Determine Differentiation or Death in Spermatids. *Developmental Cell* 19(1), pp. 160-173. doi: 10.1016/j.devcel.2010.06.009

Karam, C. S., Kellner, W. A., Takenaka, N., Clemmons, A. W. and Corces, V. G. 2010. 14-3-3 Mediates Histone Cross-Talk during Transcription Elongation in *Drosophila*. *PLOS Genetics* 6(6), p. e1000975. doi: 10.1371/journal.pgen.1000975

Karpiński, A. A. et al. 2022. Study on Tissue Homogenization Buffer Composition for Brain Mass Spectrometry-Based Proteomics. *Biomedicines* 10 (10). doi: 10.3390/biomedicines10102466

Karpova, N., Bobinnec, Y., Fouix, S., Huitorel, P. and Debec, A. 2006. Jupiter, a new *Drosophila* protein associated with microtubules. *Cell motility and the cytoskeleton* 63(5), pp. 301-312.

Katewa, Subhash D. et al. 2012. Intramyocellular Fatty-Acid Metabolism Plays a Critical Role in Mediating Responses to Dietary Restriction in *Drosophila melanogaster*. *Cell Metabolism* 16(1), pp. 97-103. doi: 10.1016/j.cmet.2012.06.005

Kavi, H., Lu, X., Xu, N., Bartholdy, B. A., Vershilova, E., Skoultchi, A. I. and Fyodorov, D. V. 2015. A Genetic Screen and Transcript Profiling Reveal a Shared Regulatory Program for *Drosophila* Linker Histone H1 and Chromatin Remodeler CHD1. *G3 Genes|Genomes|Genetics* 5(4), pp. 677-687. doi: 10.1534/g3.115.016709

Kawamoto, T., Kawai, K., Kodama, T., Yokokura, T. and Niki, Y. 2008. Autonomous differentiation of *Drosophila* spermatogonia in vitro. *Development, Growth & Differentiation* 50(7), pp. 623-632. doi: https://doi.org/10.1111/j.1440-169X.2008.01060.x

Kearse, M. G., Chen, A. S. and Ware, V. C. 2011. Expression of ribosomal protein L22e family members in *Drosophila melanogaster*: *rpL22-like* is differentially expressed and alternatively spliced. *Nucleic Acids Research* 39(7), pp. 2701-2716. doi: 10.1093/nar/gkq1218

Kearse, M. G., Ireland, J. A., Prem, S. M., Chen, A. S. and Ware, V. C. 2013. RpL22e, but not RpL22e-like-PA, is SUMOylated and localizes to the nucleoplasm of *Drosophila* meiotic spermatocytes. *Nucleus* 4(3), pp. 241-258. doi: 10.4161/nucl.25261

Kedersha, N. et al. 2000. Dynamic Shuttling of Tia-1 Accompanies the Recruitment of mRNA to Mammalian Stress Granules. *Journal of Cell Biology* 151(6), pp. 1257-1268. doi: 10.1083/jcb.151.6.1257

Kedersha, N. L., Gupta, M., Li, W., Miller, I. and Anderson, P. 1999. RNA-Binding Proteins Tia-1 and Tiar Link the Phosphorylation of Eif-2α to the Assembly of Mammalian Stress Granules. *Journal of Cell Biology* 147(7), pp. 1431-1442. doi: 10.1083/jcb.147.7.1431

Keiler, K. C. 2011. RNA localization in bacteria. *Current Opinion in Microbiology* 14(2), pp. 155-159. doi: https://doi.org/10.1016/j.mib.2011.01.009

Keller, P. J. 2013. Imaging Morphogenesis: Technological Advances and Biological Insights. *Science* 340(6137), p. 1234168. doi: 10.1126/science.1234168

Kelley, R. L. 1993. Initial organization of the *Drosophila* dorsoventral axis depends on an RNA-binding protein encoded by the squid gene. *Genes & Development* 7(6), pp. 948-960. doi: 10.1101/gad.7.6.948

Kelly, K. K., Meadows, S. M. and Cripps, R. M. 2002. *Drosophila* MEF2 is a direct regulator of Actin57B transcription in cardiac, skeletal, and visceral muscle lineages. *Mechanisms of Development* 110(1), pp. 39-50. doi: https://doi.org/10.1016/S0925-4773(01)00586-X

Khairy, K. and Keller, P. J. 2011. Reconstructing embryonic development. *genesis* 49(7), pp. 488-513. doi: https://doi.org/10.1002/dvg.20698

Khokhar, A. et al. 2008. Conditional Switches for Extracellular Matrix Patterning in *Drosophila melanogaster*. *Genetics* 178(3), pp. 1283-1293. doi: 10.1534/genetics.106.065912

Kiger, A. A., White-Cooper, H. and Fuller, M. T. 2000. Somatic support cells restrict germline stem cell self-renewal and promote differentiation. *Nature* 407(6805), pp. 750-754. doi: 10.1038/35037606

Kim-Ha, J., Kerr, K. and Macdonald, P. M. 1995. Translational regulation of oskar mRNA by Bruno, an ovarian RNA-binding protein, is essential. *Cell* 81(3), pp. 403-412. doi: https://doi.org/10.1016/0092-8674(95)90393-3

Kim, G., Pai, C.-I., Sato, K., Person, M. D., Nakamura, A. and Macdonald, P. M. 2015. Region-Specific Activation of oskar mRNA Translation by Inhibition of Bruno-Mediated Repression. *PLOS Genetics* 11(2), p. e1004992. doi: 10.1371/journal.pgen.1004992

Kim, K. 2018. Structure-based analysis of clot as a thioredoxin-related protein of 14 kDa in *Drosophila* via experimental and computational approaches. *Biotechnology and Applied Biochemistry* 65(3), pp. 338-345.

King, S. J., Brown, C. L., Maier, K. C., Quintyne, N. J. and Schroer, T. A. 2003. Analysis of the Dynein-Dynactin Interaction In Vitro and In Vivo. *Molecular biology of the cell* 14(12), pp. 5089-5097. doi: 10.1091/mbc.e03-01-0025

King, S. J. and Schroer, T. A. 2000. Dynactin increases the processivity of the cytoplasmic dynein motor. *Nature Cell Biology* 2(1), pp. 20-24. doi: 10.1038/71338

Kingsley, E. P., Chan, X. Y., Duan, Y. and Lambert, J. D. 2007. Widespread RNA segregation in a spiralian embryo. *Evolution & Development* 9(6), pp. 527-539. doi: https://doi.org/10.1111/j.1525-142X.2007.00194.x

Kislauskis, E. H., Li, Z., Singer, R. H. and Taneja, K. L. 1993. Isoform-specific 3'-untranslated sequences sort alpha-cardiac and beta-cytoplasmic actin messenger RNAs to different cytoplasmic compartments. *Journal of Cell Biology* 123(1), pp. 165-172. doi: 10.1083/jcb.123.1.165

Kislauskis, E. H. and Singer, R. H. 1992. Determinants of mRNA localization. *Current Opinion in Cell Biology* 4(6), pp. 975-978. doi: https://doi.org/10.1016/0955-0674(92)90128-Y

Kislauskis, E. H., Zhu, X.-c. and Singer, R. H. 1997. β-Actin Messenger RNA Localization and Protein Synthesis Augment Cell Motility. *Journal of Cell Biology* 136(6), pp. 1263-1270. doi: 10.1083/jcb.136.6.1263

Kislauskis, E. H., Zhu, X. and Singer, R. H. 1994. Sequences responsible for intracellular localization of beta-actin messenger RNA also affect cell phenotype. *Journal of Cell Biology* 127(2), pp. 441-451. doi: 10.1083/jcb.127.2.441

Kitaoka, M. and Yamashita, Y. M. 2024. Running the gauntlet: challenges to genome integrity in spermiogenesis. *Nucleus* 15(1), p. 2339220. doi: 10.1080/19491034.2024.2339220

Knoblich, J. A., Jan and Nung Jan, Y. 1995. Asymmetric segregation of Numb and Prospero during cell division. *Nature* 377(6550), pp. 624-627. doi: 10.1038/377624a0

Knoblich, J. A., Jan, L. Y. and Jan, Y. N. 1999. Deletion analysis of the *Drosophila* Inscuteable protein reveals domains for cortical localization and asymmetric localization. *Current Biology* 9(3), pp. 155-158. doi: 10.1016/S0960-9822(99)80070-0

Knoch, K.-P., Bergert, H., Borgonovo, B., Saeger, H.-D., Altkrüger, A., Verkade, P. and Solimena, M. 2004. Polypyrimidine tract-binding protein promotes insulin secretory granule biogenesis. *Nature Cell Biology* 6(3), pp. 207-214. doi: 10.1038/ncb1099

Kohata, K. and Miyoshi, D. 2020. RNA phase separation–mediated direction of molecular trafficking under conditions of molecular crowding. *Biophysical Reviews* 12(3), pp. 669-676. doi: 10.1007/s12551-020-00696-3

Kolberg, L., Raudvere, U., Kuzmin, I., Adler, P., Vilo, J. and Peterson, H. 2023. g:Profiler—interoperable web service for functional enrichment analysis and gene identifier mapping (2023 update). *Nucleic Acids Research* 51(W1), pp. W207-W212. doi: 10.1093/nar/gkad347

Kondylis, V. and Rabouille, C. 2009. The Golgi apparatus: Lessons from *Drosophila*. *FEBS Letters* 583(23), pp. 3827-3838. doi: https://doi.org/10.1016/j.febslet.2009.09.048

Kovalick, G. E. and Griffin, D. L. 2005. Characterization of the SCP/TAPS gene family in *Drosophila melanogaster*. *Insect Biochemistry and Molecular Biology* 35(8), pp. 825-835. doi: https://doi.org/10.1016/j.ibmb.2005.03.003

Koyama, Y., Katagiri, S., Hanai, S., Uchida, K. and Miwa, M. 1999. Poly(ADP-ribose) polymerase interacts with novel *Drosophila* ribosomal proteins, L22 and L23a, with unique histone-like amino-terminal extensions. *Gene* 226(2), pp. 339-345. doi: https://doi.org/10.1016/S0378-1119(98)00529-0

Krause, S. A., Overend, G., Dow, J. A. T. and Leader, D. P. 2022. FlyAtlas 2 in 2022: enhancements to the *Drosophila melanogaster* expression atlas. *Nucleic Acids Research* 50(D1), pp. D1010-D1015. doi: 10.1093/nar/gkab971

Kraut, R. and Campos-Ortega, J. A. 1996. *inscuteable*, A Neural Precursor Gene of *Drosophila*, Encodes a Candidate for a Cytoskeleton Adaptor Protein. *Developmental Biology* 174(1), pp. 65-81. doi: https://doi.org/10.1006/dbio.1996.0052

Kraut, R., Chia, W., Jan, L. Y., Jan, Y. N. and Knoblich, J. A. 1996. Role of inscuteable in orienting asymmetric cell divisions in *Drosophila*. *Nature* 383(6595), pp. 50-55. doi: 10.1038/383050a0

Krichevsky, A. M. and Kosik, K. S. 2001. Neuronal RNA Granules: A Link between RNA Localization and Stimulation-Dependent Translation. *Neuron* 32(4), pp. 683-696. doi: 10.1016/S0896-6273(01)00508-6

Kroschwald, S. et al. 2015. Promiscuous interactions and protein disaggregases determine the material state of stress-inducible RNP granules. *eLife* 4, p. e06807. doi: 10.7554/eLife.06807

Kroschwald, S., Maharana, S. and Simon, A. 2017. Hexanediol: a chemical probe to investigate the material properties of membrane-less compartments. *Matters* 3(5), pp. 1-6. doi: 10.19185/matters.201702000010

Krueger, F. 2012. *Trim Galore - Function: A wrapper tool around Cutadapt and FastQC to consistently apply quality and adapter trimming to FastQ files, with some extra functionality for MspI-digested RRBS-type (Reduced Representation Bisufite-Seq) libraries.* Babraham Bioinformatics. Available at:

https://www.bioinformatics.babraham.ac.uk/projects/trim_galore/ [Accessed: June 2024].

Krzic, U., Gunther, S., Saunders, T. E., Streichan, S. J. and Hufnagel, L. 2012. Multiview light-sheet microscope for rapid in toto imaging. *Nature Methods* 9(7), pp. 730-733. doi: 10.1038/nmeth.2064

Kubrak, O. I., Kučerová, L., Theopold, U., Nylin, S. and Nässel, D. R. 2016. Characterization of Reproductive Dormancy in Male *Drosophila melanogaster*. *Frontiers in Physiology* 7, doi: 10.3389/fphys.2016.00572

Kuhn, R., Kuhn, C., Börsch, D., Glätzer, K. H., Schäfer, U. and Schäfer, M. 1991. A cluster of four genes selectively expressed in the male germ line of *Drosophila melanogaster*. *Mechanisms of Development* 35(2), pp. 143-151. doi: https://doi.org/10.1016/0925-4773(91)90064-D

Kuhn, R., Schäfer, U. and Schäfer, M. 1988. Cis-acting regions sufficient for spermatocyte-specific transcriptional and spermatid-specific translational control of the *Drosophila melanogaster* gene *mst(3)gl-9*. *The EMBO Journal* 7(2), pp. 447-454-454. doi: https://doi.org/10.1002/j.1460-2075.1988.tb02832.x

Kulkarni, M. M., Booker, M., Silver, S. J., Friedman, A., Hong, P., Perrimon, N. and Mathey-Prevot, B. 2006. Evidence of off-target effects associated with long dsRNAs in *Drosophila melanogaster* cell-based assays. *Nature Methods* 3(10), pp. 833-838. doi: 10.1038/nmeth935

Kuo, C. T., Zhu, S., Younger, S., Jan, L. Y. and Jan, Y. N. 2006. Identification of E2/E3 Ubiquitinating Enzymes and Caspase Activity Regulating *Drosophila* Sensory Neuron Dendrite Pruning. *Neuron* 51(3), pp. 283-290. doi: 10.1016/j.neuron.2006.07.014

Kvon, E. Z. et al. 2014. Genome-scale functional characterization of *Drosophila* developmental enhancers in vivo. *Nature* 512(7512), pp. 91-95. doi: 10.1038/nature13395

Lambert, J. D. and Nagy, L. M. 2002. Asymmetric inheritance of centrosomally localized mRNAs during embryonic cleavages. *Nature* 420(6916), pp. 682-686. doi: 10.1038/nature01241

Langdon Erin, M. et al. 2018. mRNA structure determines specificity of a polyQ-driven phase separation. *Science* 360(6391), pp. 922-927. doi: 10.1126/science.aar7432

Lange, S., Katayama, Y., Schmid, M., Burkacky, O., Bräuchle, C., Lamb, D. C. and Jansen, R. P. 2008. Simultaneous transport of different localized mRNA species revealed by live-cell imaging. *Traffic* 9(8), pp. 1256-1267.

Langevin, S. M., Kuhnell, D., Orr-Asman, M. A., Biesiada, J., Zhang, X., Medvedovic, M. and Thomas, H. E. 2019. Balancing yield, purity and practicality: a modified differential ultracentrifugation protocol for efficient isolation of small extracellular vesicles from human serum. *RNA Biology* 16(1), pp. 5-12. doi: 10.1080/15476286.2018.1564465

Langille, M. G. I. and Clark, D. V. 2007. Parent genes of retrotransposition-generated gene duplicates in *Drosophila melanogaster* have distinct expression profiles. *Genomics* 90(3), pp. 334-343. doi: https://doi.org/10.1016/j.ygeno.2007.06.001

Lantz, V. A. and Miller, K. G. 1998. A Class VI Unconventional Myosin Is Associated with a Homologue of a Microtubule-binding Protein, Cytoplasmic Linker Protein–170, in Neurons and at the Posterior Pole of *Drosophila* Embryos. *Journal of Cell Biology* 140(4), pp. 897-910. doi: 10.1083/jcb.140.4.897

Laver, J. D., Li, X., Ancevicius, K., Westwood, J. T., Smibert, C. A., Morris, Q. D. and Lipshitz, H. D. 2013. Genome-wide analysis of Staufen-associated mRNAs identifies secondary structures that confer target specificity. *Nucleic Acids Research* 41(20), pp. 9438-9460. doi: 10.1093/nar/gkt702

Lawniczak, M. K. and Begun, D. J. 2004. A genome-wide analysis of courting and mating responses in *Drosophila melanogaster* females. *Genome* 47(5), pp. 900-910.

Lawrence, J. B. and Singer, R. H. 1986. Intracellular localization of messenger RNAs for cytoskeletal proteins. *Cell* 45(3), pp. 407-415. doi: https://doi.org/10.1016/0092-8674(86)90326-0

Lazzaretti, D., Veith, K., Kramer, K., Basquin, C., Urlaub, H., Irion, U. and Bono, F. 2016. The bicoid mRNA localization factor Exuperantia is an RNA-binding pseudonuclease. *Nature Structural & Molecular Biology* 23(8), pp. 705-713. doi: 10.1038/nsmb.3254

Leader, D. P., Krause, S. A., Pandit, A., Davies, S. A. and Dow, J. A. T. 2018. FlyAtlas 2: a new version of the *Drosophila melanogaster* expression atlas with RNA-Seq, miRNA-Seq and sex-specific data. *Nucleic Acids Research* 46(D1), pp. D809-D815. doi: 10.1093/nar/gkx976

Lécuyer, E. et al. 2007. Global Analysis of mRNA Localization Reveals a Prominent Role in Organizing Cellular Architecture and Function. *Cell* 131(1), pp. 174-187. doi: https://doi.org/10.1016/j.cell.2007.08.003

Lederer, M., Bley, N., Schleifer, C. and Hüttelmaier, S. 2014. The role of the oncofetal IGF2 mRNA-binding protein 3 (IGF2BP3) in cancer. *Seminars in Cancer Biology* 29, pp. 3-12. doi: https://doi.org/10.1016/j.semcancer.2014.07.006

Lee, H., Zhang, Z. and Krause, H. M. 2019. Long Noncoding RNAs and Repetitive Elements: Junk or Intimate Evolutionary Partners? *Trends in Genetics* 35(12), pp. 892-902. doi: 10.1016/j.tig.2019.09.006

Lee, J., Yoo, E., Lee, H., Park, K., Hur, J.-H. and Lim, C. 2017. LSM12 and ME31B/DDX6 Define Distinct Modes of Posttranscriptional Regulation by ATAXIN-2 Protein Complex in *Drosophila* Circadian Pacemaker Neurons. *Molecular Cell* 66(1), pp. 129-140.e127. doi: https://doi.org/10.1016/j.molcel.2017.03.004

Lee, K.-A. et al. 2018. Inflammation-Modulated Metabolic Reprogramming Is Required for DUOX-Dependent Gut Immunity in *Drosophila*. *Cell Host & Microbe* 23(3), pp. 338-352.e335. doi: https://doi.org/10.1016/j.chom.2018.01.011

Lefrère, V., Vincent, A. and Amalric, F. 1990. *Drosophila melanogaster* poly(A)-binding protein: cDNA cloning reveals an usually long 3′-untranslated region of the mRNA, also present in other eukaryotic species. *Gene* 96(2), pp. 219-225. doi: https://doi.org/10.1016/0378-1119(90)90256-Q

Lemon, W. C., Pulver, S. R., Höckendorf, B., McDole, K., Branson, K., Freeman, J. and Keller, P. J. 2015. Whole-central nervous system functional imaging in larval *Drosophila*. *Nature Communications* 6(1), p. 7924. doi: 10.1038/ncomms8924

Lerit, D. A., Shebelut, C. W., Lawlor, K. J., Rusan, N. M., Gavis, E. R., Schedl, P. and Deshpande, G. 2017. Germ Cell-less Promotes Centrosome Segregation to Induce Germ Cell Formation. *Cell Reports* 18(4), pp. 831-839. doi: 10.1016/j.celrep.2016.12.074

Levine, M. T., Jones, C. D., Kern, A. D., Lindfors, H. A. and Begun, D. J. 2006. Novel genes derived from noncoding DNA in *Drosophila melanogaster* are frequently X-

linked and exhibit testis-biased expression. *Proceedings of the National Academy of Sciences* 103(26), pp. 9935-9939. doi: 10.1073/pnas.0509809103

Li, C., Ren, Y., Chen, M.-Y., Wang, Q., He, Z. and Wang, Y.-F. 2024. CG9920 is necessary for mitochondrial morphogenesis and individualization during spermatogenesis in *Drosophila melanogaster*. *Developmental Biology* 512, pp. 13-25. doi: https://doi.org/10.1016/j.ydbio.2024.04.008

Li, H.-H., Kroll, Jason R., Lennox, Sara M., Ogundeyi, O., Jeter, J., Depasquale, G. and Truman, James W. 2014a. A GAL4 Driver Resource for Developmental and Behavioral Studies on the Larval CNS of *Drosophila*. *Cell Reports* 8(3), pp. 897-908. doi: https://doi.org/10.1016/j.celrep.2014.06.065

Li, H. et al. 2009a. The Sequence Alignment/Map format and SAMtools. *Bioinformatics* 25(16), pp. 2078-2079. doi: 10.1093/bioinformatics/btp352

Li, H. et al. 2022. Fly Cell Atlas: A single-nucleus transcriptomic atlas of the adult fruit fly. *Science* 375(6584), p. eabk2432. doi: doi:10.1126/science.abk2432

Li, P. et al. 2012. Phase transitions in the assembly of multivalent signalling proteins. *Nature* 483(7389), pp. 336-340. doi: 10.1038/nature10879

Li, P., Yang, X., Wasser, M., Cai, Y. and Chia, W. 1997. Inscuteable and Staufen Mediate Asymmetric Localization and Segregation of *prospero*RNA during *Drosophila* Neuroblast Cell Divisions. *Cell* 90(3), pp. 437-447. doi: 10.1016/S0092-8674(00)80504-8

Li, W., Klovstad, M. and Schüpbach, T. 2014b. Repression of Gurken translation by a meiotic checkpoint in *Drosophila* oogenesis is suppressed by a reduction in the dose of *eIF1A*. *Development* 141(20), pp. 3910-3921. doi: 10.1242/dev.109306

Li, Z. et al. 2009b. Detection of intergenic non-coding RNAs expressed in the main developmental stages in *Drosophila melanogaster*. *Nucleic Acids Research* 37(13), pp. 4308-4314. doi: 10.1093/nar/gkp334

Liao, G., Simone, B. and Liu, G. 2011. Mis-localization of Arp2 mRNA impairs persistence of directional cell migration. *Experimental Cell Research* 317(6), pp. 812-822. doi: https://doi.org/10.1016/j.yexcr.2010.12.002

Liao, Y., Smyth, G. K. and Shi, W. 2014. featureCounts: an efficient general purpose program for assigning sequence reads to genomic features. *Bioinformatics* 30(7), pp. 923-930. doi: 10.1093/bioinformatics/btt656

Lie, Y. S. and Macdonald, P. M. 1999. Apontic binds the translational repressor Bruno and is implicated in regulation of oskar mRNA translation. *Development* 126(6), pp. 1129-1138. doi: 10.1242/dev.126.6.1129

Lilleväli, K., Kulla, A. and Örd, T. 2001. Comparative expression analysis of the genes encoding polypyrimidine tract binding protein (PTB) and its neural homologue (brPTB) in prenatal and postnatal mouse brain. *Mechanisms of Development* 101(1), pp. 217-220. doi: https://doi.org/10.1016/S0925-4773(00)00566-9

Lim, C., Tarayrah, L. and Chen, X. 2012. Transcriptional regulation during *Drosophila* spermatogenesis. *Spermatogenesis* 2(3), pp. 158-166. doi: 10.4161/spmg.21775

Lim, J. G. Y. and Fuller, M. T. 2012. Somatic cell lineage is required for differentiation and not maintenance of germline stem cells in *Drosophila* testes. *Proceedings of the National Academy of Sciences* 109(45), pp. 18477-18481. doi: 10.1073/pnas.1215516109

Lim, S. Y. et al. 2021. Identification and characterization of GAL4 drivers that mark distinct cell types and regions in the *Drosophila* adult gut. *Journal of Neurogenetics* 35(1), pp. 33-44. doi: 10.1080/01677063.2020.1853722

Lin, C.-H. et al. 2020. Mitochondrial UQCRC1 mutations cause autosomal dominant parkinsonism with polyneuropathy. *Brain* 143(11), pp. 3352-3373. doi: 10.1093/brain/awaa279

Lin, J. I. et al. 2011. *Drosophila* Ribosomal Protein Mutants Control Tissue Growth Non-Autonomously via Effects on the Prothoracic Gland and Ecdysone. *PLOS Genetics* 7(12), p. e1002408. doi: 10.1371/journal.pgen.1002408

Lin, M. H., Nguyen, H. T., Dybala, C. and Storti, R. V. 1996. Myocyte-specific enhancer factor 2 acts cooperatively with a muscle activator region to regulate *Drosophila* tropomyosin gene muscle expression. *Proceedings of the National Academy of Sciences* 93(10), pp. 4623-4628. doi: 10.1073/pnas.93.10.4623

Lindsley, D. L. a. T., K.T. 1980. Spermatogenesis. In: Ashburner, M.a.W., T.R.F. ed. *The Genetics and Biology of Drosophila*. Vol. 2d. London: Academic Press, pp. 225-294.

Lipshitz, H. D. and Smibert, C. A. 2000. Mechanisms of RNA localization and translational regulation. *Current Opinion in Genetics & Development* 10(5), pp. 476-488. doi: https://doi.org/10.1016/S0959-437X(00)00116-7

Liu, X., Jiang, S., Ma, L., Qu, J., Zhao, L., Zhu, X. and Ding, J. 2021. Time-dependent effect of 1,6-hexanediol on biomolecular condensates and 3D chromatin organization. *Genome biology* 22(1), p. 230. doi: 10.1186/s13059-021-02455-3

Liu, Z. et al. 2015. Opposing intrinsic temporal gradients guide neural stem cell production of varied neuronal fates. *Science* 350(6258), pp. 317-320. doi: 10.1126/science.aad1886

Long, R. M., Singer, R. H., Meng, X., Gonzalez, I., Nasmyth, K. and Jansen, R.-P. 1997. Mating Type Switching in Yeast Controlled by Asymmetric Localization of ASH1 mRNA. *Science* 277(5324), pp. 383-387.

Lowe, N. et al. 2014. Analysis of the expression patterns, subcellular localisations and interaction partners of *Drosophila* proteins using a pigP protein trap library. *Development* 141(20), pp. 3994-4005. doi: 10.1242/dev.111054

Lunde, B. M., Moore, C. and Varani, G. 2007. RNA-binding proteins: modular design for efficient function. *Nature Reviews Molecular Cell Biology* 8(6), pp. 479-490. doi: 10.1038/nrm2178

Macdonald, P. M., Kanke, M. and Kenny, A. 2016. Community effects in regulation of translation. *eLife* 5, p. e10965. doi: 10.7554/eLife.10965

Macdonald, P. M., Luk, S. K. and Kilpatrick, M. 1991. Protein encoded by the *exuperantia* gene is concentrated at sites of *bicoid* mRNA accumulation in *Drosophila* nurse cells but not in oocytes or embryos. *Genes & Development* 5(12b), pp. 2455-2466.

MacDougall, N., Clark, A., MacDougall, E. and Davis, I. 2003. *Drosophila gurken* (TGFalpha) mRNA Localizes as Particles that Move within the Oocyte in Two Dynein-Dependent Steps. *Developmental Cell* 4(3), pp. 307-319. doi: 10.1016/S1534-5807(03)00058-3

Machesky, M. L. et al. 1997. Mammalian actin-related protein 2/3 complex localizes to regions of lamellipodial protrusion and is composed of evolutionarily conserved proteins. *Biochemical Journal* 328(1), pp. 105-112. doi: 10.1042/bj3280105

Mageeney, C. M., Kearse, M. G., Gershman, B. W., Pritchard, C. E., Colquhoun, J. M. and Ware, V. C. 2018. Functional interplay between ribosomal protein paralogues in the *eRpL22* family in *Drosophila melanogaster*. *Fly* 12(3-4), pp. 143-163.

Mageeney, C. M. and Ware, V. C. 2019. Specialized eRpL22 paralogue-specific ribosomes regulate specific mRNA translation in spermatogenesis in *Drosophila melanogaster*. *Molecular biology of the cell* 30(17), pp. 2240-2253. doi: 10.1091/mbc.E19-02-0086

Maharana, S. et al. 2018. RNA buffers the phase separation behavior of prion-like RNA binding proteins. *Science* 360(6391), pp. 918-921. doi: 10.1126/science.aar7366

Mansfield, J. H., Wilhelm, J. E. and Hazelrigg, T. 2002. Ypsilon Schachtel, a *Drosophila* Y-box protein, acts antagonistically to Orb in the *oskar* mRNA localization and translation pathway. *Development* 129(1), pp. 197-209. doi: 10.1242/dev.129.1.197

Markstein, M., Pitsouli, C., Villalta, C., Celniker, S. E. and Perrimon, N. 2008. Exploiting position effects and the gypsy retrovirus insulator to engineer precisely expressed transgenes. *Nature Genetics* 40(4), pp. 476-483. doi: 10.1038/ng.101

Marrone, A. K., Kucherenko, M. M., Rishko, V. M. and Shcherbata, H. R. 2011. New Dystrophin/Dystroglycan interactors control neuron behavior in *Drosophila* eye. *BMC Neuroscience* 12(1), p. 93. doi: 10.1186/1471-2202-12-93

Martin, I. et al. 2014. Ribosomal Protein s15 Phosphorylation Mediates LRRK2 Neurodegeneration in Parkinson's Disease. *Cell* 157(2), pp. 472-485. doi: https://doi.org/10.1016/j.cell.2014.01.064

Martin, K. C. and Ephrussi, A. 2009. mRNA Localization: Gene Expression in the Spatial Dimension. *Cell* 136(4), pp. 719-730. doi: 10.1016/j.cell.2009.01.044

Martin, S. G., Leclerc, V., Smith-Litière, K. and Johnston, D. S. 2003. The identification of novel genes required for *Drosophila* anteroposterior axis formation in a germline clone screen using GFP-Staufen. *Development* 130(17), pp. 4201-4215. doi: 10.1242/dev.00630

Martinez, D. et al. 2021. Mask, the *Drosophila* ankyrin repeat and KH domain-containing protein, affects microtubule stability. *Journal of Cell Science* 134(20), p. jcs258512. doi: 10.1242/jcs.258512

Marygold, S. J. et al. 2007. The ribosomal protein genes and *Minute* loci of *Drosophila melanogaster*. *Genome biology* 8(10), p. R216. doi: 10.1186/gb-2007-8-10-r216

Marzano, M. et al. 2021. AMPK adapts metabolism to developmental energy requirement during dendrite pruning in *Drosophila*. *Cell Reports* 37(7), p. 110024. doi: https://doi.org/10.1016/j.celrep.2021.110024

Matunis, E. L., Kelley, R. and Dreyfuss, G. 1994. Essential role for a heterogeneous nuclear ribonucleoprotein (hnRNP) in oogenesis: hrp40 is absent from the germ line

in the dorsoventral mutant squid. *Proceedings of the National Academy of Sciences* 91(7), pp. 2781-2784.

Matunis, E. L., Matunis, M. J. and Dreyfuss, G. 1992a. Characterization of the major hnRNP proteins from *Drosophila melanogaster*. *Journal of Cell Biology* 116(2), pp. 257-269. doi: 10.1083/jcb.116.2.257

Matunis, E. L., Stine, R. R. and de Cuevas, M. 2012. Recent advances in *Drosophila* male germline stem cell biology. *Spermatogenesis* 2(3), pp. 137-144. doi: 10.4161/spmg.21763

Matunis, M. J., Matunis, E. L. and Dreyfuss, G. 1992b. Isolation of hnRNP complexes from *Drosophila melanogaster*. *Journal of Cell Biology* 116(2), pp. 245-255. doi: 10.1083/jcb.116.2.245

Matzat, L. H., Dale, R. K., Moshkovich, N. and Lei, E. P. 2012. Tissue-Specific Regulation of Chromatin Insulator Function. *PLOS Genetics* 8(11), p. e1003069. doi: 10.1371/journal.pgen.1003069

McCarthy, D. J., Chen, Y. and Smyth, G. K. 2012. Differential expression analysis of multifactor RNA-Seq experiments with respect to biological variation. *Nucleic Acids Research* 40(10), pp. 4288-4297. doi: 10.1093/nar/gks042

McDermott, S. M. and Davis, I. 2013. *Drosophila* Hephaestus/Polypyrimidine Tract Binding Protein Is Required for Dorso-Ventral Patterning and Regulation of Signalling between the Germline and Soma. *PloS one* 8(7), p. e69978. doi: 10.1371/journal.pone.0069978

McDermott, S. M., Meignin, C., Rappsilber, J. and Davis, I. 2012. *Drosophila* Syncrip binds the *gurken* mRNA localisation signal and regulates localised transcripts during axis specification. *Biology Open* 1(5), pp. 488-497. doi: 10.1242/bio.2012885

McDermott, S. M., Yang, L., Halstead, J. M., Hamilton, R. S., Meignin, C. and Davis, I. 2014. *Drosophila* Syncrip modulates the expression of mRNAs encoding key synaptic proteins required for morphology at the neuromuscular junction. *RNA* 20(10), pp. 1593-1606.

McGuire, S. E., Le, P. T., Osborn, A. J., Matsumoto, K. and Davis, R. L. 2003. Spatiotemporal Rescue of Memory Dysfunction in *Drosophila*. *Science* 302(5651), pp. 1765-1768. doi: 10.1126/science.1089035

McGuire, S. E., Roman, G. and Davis, R. L. 2004. Gene expression systems in *Drosophila*: a synthesis of time and space. *Trends in Genetics* 20(8), pp. 384-391. doi: 10.1016/j.tig.2004.06.012

McKearin, D. 1997. The *Drosophila* fusome, organelle biogenesis and germ cell differentiation: if you build it... *BioEssays* 19(2), pp. 147-152. doi: doi: 10.1002/bies.950190209

McKenney, R. J., Huynh, W., Tanenbaum, M. E., Bhabha, G. and Vale, R. D. 2014. Activation of cytoplasmic dynein motility by dynactin-cargo adapter complexes. *Science* 345(6194), pp. 337-341. doi: doi:10.1126/science.1254198

Medioni, C., Mowry, K. and Besse, F. 2012. Principles and roles of mRNA localization in animal development. *Development* 139(18), p. 3263. doi: 10.1242/dev.078626

Medioni, C., Ramialison, M., Ephrussi, A. and Besse, F. 2014. Imp Promotes Axonal Remodeling by Regulating profilin mRNA during Brain Development. *Current Biology* 24(7), pp. 793-800. doi: https://doi.org/10.1016/j.cub.2014.02.038

Meiklejohn, C. D., Parsch, J., Ranz, J. M. and Hartl, D. L. 2003. Rapid evolution of male-biased gene expression in *Drosophila*. *Proceedings of the National Academy of Sciences* 100(17), pp. 9894-9899. doi: 10.1073/pnas.1630690100

Mendez, R. and Richter, J. D. 2001. Translational control by CPEB: a means to the end. *Nature Reviews Molecular Cell Biology* 2(7), pp. 521-529. doi: 10.1038/35080081

Merz, C., Urlaub, H., Will, C. L. and Lührmann, R. 2007. Protein composition of human mRNPs spliced in vitro and differential requirements for mRNP protein recruitment. *RNA* 13(1), pp. 116-128.

Messer, F. R. 2022. *Developmental and molecular analysis of sperm in Drosophila pseudoobscura.* Cardiff University.

Miquel, J., Lundgren, P. R., Bensch, K. G. and Atlan, H. 1976. Effects of temperature on the life span, vitality and fine structure of *Drosophila melanogaster*. *Mechanisms of Ageing and Development* 5, pp. 347-370. doi: https://doi.org/10.1016/0047-6374(76)90034-8

Mhlanga, M. M., Bratu, D. P., Genovesio, A., Rybarska, A., Chenouard, N., Nehrbass, U. and Olivo-Marin, J.-C. 2009. *In Vivo* Colocalisation of *oskar* mRNA and *Trans*-Acting Proteins Revealed by Quantitative Imaging of the *Drosophila* Oocyte. *PloS one* 4(7), p. e6241. doi: 10.1371/journal.pone.0006241

Miller, K. G. 2002. Extending the Arp2/3 complex and its regulation beyond the leading edge. *Journal of Cell Biology* 156(4), pp. 591-593. doi: 10.1083/jcb.200201107

Minervini, C. F., Berloco, M. F., Marsano, R. M. and Viggiano, L. 2022. The Ribosomal Protein RpL22 Interacts In Vitro with 5′-UTR Sequences Found in Some *Drosophila melanogaster* Transposons. *Genes* 13 (2). doi: 10.3390/genes13020305

Ming, Y. et al. 2019. Targeting liquid-liquid phase separation in pancreatic cancer. *Translational Cancer Research* 8(1), pp. 96-103.

Mingle, L. A., Okuhama, N. N., Shi, J., Singer, R. H., Condeelis, J. and Liu, G. 2005. Localization of all seven messenger RNAs for the actin-polymerization nucleator Arp2/3 complex in the protrusions of fibroblasts. *Journal of Cell Science* 118(11), pp. 2425-2433. doi: 10.1242/jcs.02371

Misra, S. et al. 2002. Annotation of the *Drosophila melanogaster* euchromatic genome: a systematic review. *Genome biology* 3(12), p. research0083.0081. doi: 10.1186/gb-2002-3-12-research0083

Mohr, S. E. 2014. RNAi screening in *Drosophila* cells and *in vivo*. *Methods* 68(1), pp. 82-88. doi: https://doi.org/10.1016/j.ymeth.2014.02.018

Mołoń, M. et al. 2020. Effects of Temperature on Lifespan of *Drosophila melanogaster* from Different Genetic Backgrounds: Links between Metabolic Rate and Longevity. *Insects* 11 (8). doi: 10.3390/insects11080470

Mongroo, P. S. et al. 2011. IMP-1 Displays Cross-Talk with K-Ras and Modulates Colon Cancer Cell Survival through the Novel Proapoptotic Protein CYFIP2. *Cancer Research* 71(6), pp. 2172-2182. doi: 10.1158/0008-5472.CAN-10-3295

Moore, J., Han, H. and Lasko, P. 2009. Bruno negatively regulates germ cell-less expression in a BRE-independent manner. *Mechanisms of Development* 126(7), pp. 503-516. doi: https://doi.org/10.1016/j.mod.2009.04.002

Moore, M. J. 2005. From Birth to Death: The Complex Lives of Eukaryotic mRNAs. *Science* 309(5740), pp. 1514-1518. doi: 10.1126/science.1111443

Morgan, T. H. 1910. Sex Limited Inheritance in *Drosophila*. *Science* 32(812), pp. 120-122. doi: 10.1126/science.32.812.120

Morin, X., Daneman, R., Zavortink, M. and Chia, W. 2001. A protein trap strategy to detect GFP-tagged proteins expressed from their endogenous loci in *Drosophila*. *Proceedings of the National Academy of Sciences of the United States of America* 98(26), pp. 15050-15055. doi: 10.1073/pnas.261408198

Morris, C. A., Benson, E. and White-Cooper, H. 2009. Determination of gene expression patterns using in situ hybridization to *Drosophila* testes. *Nature Protocols* 4(12), pp. 1807-1819. doi: 10.1038/nprot.2009.192

Müller-McNicoll, M., Rossbach, O., Hui, J. and Medenbach, J. 2019. Auto-regulatory feedback by RNA-binding proteins. *Journal of Molecular Cell Biology* 11(10), pp. 930-939. doi: 10.1093/jmcb/mjz043

Muller, H. J. 1918. GENETIC VARIABILITY, TWIN HYBRIDS AND CONSTANT HYBRIDS, IN A CASE OF BALANCED LETHAL FACTORS. *Genetics* 3(5), pp. 422-499. doi: 10.1093/genetics/3.5.422

Müller, J. M., Moos, K., Baar, T., Maier, K. C., Zumer, K. and Tresch, A. 2024. Nuclear export is a limiting factor in eukaryotic mRNA metabolism. *PLOS Computational Biology* 20(5), p. e1012059. doi: 10.1371/journal.pcbi.1012059

Mullins, R. D., Heuser, J. A. and Pollard, T. D. 1998. The interaction of Arp2/3 complex with actin: Nucleation, high affinity pointed end capping, and formation of branching networks of filaments. *Proceedings of the National Academy of Sciences* 95(11), pp. 6181-6186. doi: 10.1073/pnas.95.11.6181

Mummery-Widmer, J. L. et al. 2009. Genome-wide analysis of Notch signalling in *Drosophila* by transgenic RNAi. *Nature* 458(7241), pp. 987-992. doi: 10.1038/nature07936

Munro , T. P., Kwon , S., Schnapp , B. J. and St Johnston , D. 2006. A repeated IMP-binding motif controls oskar mRNA translation and anchoring independently of *Drosophila melanogaster* IMP. *Journal of Cell Biology* 172(4), pp. 577-588. doi: 10.1083/jcb.200510044

Nakahara, K., Kim, K., Sciulli, C., Dowd, S. R., Minden, J. S. and Carthew, R. W. 2005. Targets of microRNA regulation in the *Drosophila* oocyte proteome. *Proceedings of the National Academy of Sciences* 102(34), pp. 12023-12028.

Nakamura, A., Amikura, R., Hanyu, K. and Kobayashi, S. 2001. Me31B silences translation of oocyte-localizing RNAs through the formation of cytoplasmic RNP complex during *Drosophila* oogenesis. *Development* 128(17), pp. 3233-3242. doi: 10.1242/dev.128.17.3233

Nakamura, A., Sato, K. and Hanyu-Nakamura, K. 2004. *Drosophila* Cup Is an eIF4E Binding Protein that Associates with Bruno and Regulates *oskar* mRNA Translation in

Oogenesis. *Developmental Cell* 6(1), pp. 69-78. doi: 10.1016/S1534-5807(03)00400-3

Nam, S., Le, T. P., Chung, S. and Choi, K.-W. 2022. Tctp regulates the level and localization of Foxo for cell growth in *Drosophila*. *Cell Death Discovery* 8(1), p. 146. doi: 10.1038/s41420-022-00937-2

Nelson, C., Ambros, V. and Baehrecke, Eric H. 2014. *miR-14* Regulates Autophagy during Developmental Cell Death by Targeting *ip3-kinase 2*. *Molecular Cell* 56(3), pp. 376-388. doi: 10.1016/j.molcel.2014.09.011

Nelson, M. R., Leidal, A. M. and Smibert, C. A. 2004. *Drosophila* Cup is an eIF4E-binding protein that functions in Smaug-mediated translational repression. *The EMBO Journal* 23(1), pp. 150-159.

Neophytou, C. and Pitsouli, C. 2022. Biotin controls intestinal stem cell mitosis and host-microbiome interactions. *Cell Reports* 38(10), doi: 10.1016/j.celrep.2022.110505

Nerusheva, O., Dorogova, N. and Omelyanchuk, L. 2009. GFP markers for studying *D. melanogaster* spermatogenesis. 4(4), pp. 452-460. doi: doi:10.2478/s11535-009-0052-y

Neufeld, T. P., Tang, A. H. and Rubin, G. M. 1998. A Genetic Screen to Identify Components of the sina Signaling Pathway in *Drosophila* Eye Development. *Genetics* 148(1), pp. 277-286. doi: 10.1093/genetics/148.1.277

Neumüller, R. A. et al. 2008. Mei-P26 regulates microRNAs and cell growth in the *Drosophila* ovarian stem cell lineage. *Nature* 454(7201), pp. 241-245. doi: 10.1038/nature07014

Ng, A. Y. E., Chan, S. N. and Pek, J. W. 2024. Genetic compensation between ribosomal protein paralogs mediated by a cognate circular RNA. *Cell Reports* 43(5), p. 114228. doi: https://doi.org/10.1016/j.celrep.2024.114228

Ni, J.-Q. et al. 2009. A *Drosophila* Resource of Transgenic RNAi Lines for Neurogenetics. *Genetics* 182(4), pp. 1089-1100. doi: 10.1534/genetics.109.103630

Ni, J.-Q. et al. 2008. Vector and parameters for targeted transgenic RNA interference in *Drosophila melanogaster*. *Nature Methods* 5(1), pp. 49-51. doi: 10.1038/nmeth1146

Ni, J.-Q. et al. 2011. A genome-scale shRNA resource for transgenic RNAi in *Drosophila*. *Nature Methods* 8(5), pp. 405-407. doi: 10.1038/nmeth.1592

Nielsen, F. C., Nielsen, J., Kristensen, M. A., Koch, G. and Christiansen, J. 2002. Cytoplasmic trafficking of IGF-II mRNA-binding protein by conserved KH domains. *Journal of Cell Science* 115(10), pp. 2087-2097. doi: 10.1242/jcs.115.10.2087

Nielsen, J., Adolph, S. K., Rajpert-De Meyts, E., Lykke-Andersen, J., Koch, G., Christiansen, J. and Nielsen, F. C. 2003. Nuclear transit of human zipcode-binding protein IMP1. *Biochemical Journal* 376(2), pp. 383-391. doi: 10.1042/bj20030943

Nielsen, J., Christiansen, J., Lykke-Andersen, J., Johnsen Anders, H., Wewer Ulla, M. and Nielsen Finn, C. 1999. A Family of Insulin-Like Growth Factor II mRNA-Binding Proteins Represses Translation in Late Development. *Molecular and cellular biology* 19(2), pp. 1262-1270. doi: 10.1128/MCB.19.2.1262

Nielsen, J., Cilius Nielsen, F., Kragh Jakobsen, R. and Christiansen, J. 2000. The biphasic expression of IMP/Vg1-RBP is conserved between vertebrates and

Drosophila. *Mechanisms of Development* 96(1), pp. 129-132. doi: https://doi.org/10.1016/S0925-4773(00)00383-X

Nielsen, J., Kristensen, M. A., Willemoës, M., Nielsen, F. C. and Christiansen, J. 2004. Sequential dimerization of human zipcode-binding protein IMP1 on RNA: a cooperative mechanism providing RNP stability. *Nucleic Acids Research* 32(14), pp. 4368-4376. doi: 10.1093/nar/gkh754

Noguchi, T., Koizumi, M. and Hayashi, S. 2011. Sustained Elongation of Sperm Tail Promoted by Local Remodeling of Giant Mitochondria in *Drosophila*. *Current Biology* 21(10), pp. 805-814. doi: https://doi.org/10.1016/j.cub.2011.04.016

Noguchi, T. and Miller, K. G. 2003. A role for actin dynamics in individualization during spermatogenesis in *Drosophila melanogaster*. *Development* 130(9), pp. 1805-1816. doi: 10.1242/dev.00406

Norvell, A., Debec, A., Finch, D., Gibson, L. and Thoma, B. 2005. Squid is required for efficient posterior localization of *oskar* mRNA during *Drosophila* oogenesis. *Development Genes and Evolution* 215(7), pp. 340-349. doi: 10.1007/s00427-005-0480-2

Norvell, A., Kelley, R. L., Wehr, K. and Schüpbach, T. 1999. Specific isoforms of Squid, a *Drosophila* hnRNP, perform distinct roles in Gurken localization during oogenesis. *Genes & Development* 13(7), pp. 864-876.

Oberstrass, F. C. et al. 2005. Structure of PTB Bound to RNA: Specific Binding and Implications for Splicing Regulation. *Science* 309(5743), p. 2054. doi: 10.1126/science.1114066

O'Day, E. et al. 2015. An RNA-binding Protein, Lin28, Recognizes and Remodels G-quartets in the MicroRNAs (miRNAs) and mRNAs It Regulates*. *Journal of Biological Chemistry* 290(29), pp. 17909-17922. doi: https://doi.org/10.1074/jbc.M115.665521

Oeffinger, M., Wei, K. E., Rogers, R., DeGrasse, J. A., Chait, B. T., Aitchison, J. D. and Rout, M. P. 2007. Comprehensive analysis of diverse ribonucleoprotein complexes. *Nature Methods* 4(11), pp. 951-956. doi: 10.1038/nmeth1101

Ohlendieck, K. and Harding, S. E. 2018. Centrifugation and Ultracentrifugation. In: Hofmann, A. and Clokie, S. eds. *Wilson and Walker's Principles and Techniques of Biochemistry and Molecular Biology*. 8 ed. Cambridge: Cambridge University Press, pp. 424-453.

Olesnicky, E. C. et al. 2018. Shep interacts with posttranscriptional regulators to control dendrite morphogenesis in sensory neurons. *Developmental Biology* 444(2), pp. 116-128. doi: https://doi.org/10.1016/j.ydbio.2018.09.022

Olesnicky, E. C., Killian, D. J., Garcia, E., Morton, M. C., Rathjen, A. R., Sola, I. E. and Gavis, E. R. 2014. Extensive Use of RNA-Binding Proteins in *Drosophila* Sensory Neuron Dendrite Morphogenesis. *G3 Genes|Genomes|Genetics* 4(2), pp. 297-306. doi: 10.1534/g3.113.009795

Oleynikov, Y. and Singer, R. H. 2003. Real-Time Visualization of ZBP1 Association with β-Actin mRNA during Transcription and Localization. *Current Biology* 13(3), pp. 199-207. doi: https://doi.org/10.1016/S0960-9822(03)00044-7

Olivieri, G. and Olivieri, A. 1965. Autoradiographic study of nucleic acid synthesis during spermatogenesis in *Drosophila melanogaster*. *Mutation Research/Fundamental and Molecular Mechanisms of Mutagenesis* 2(4), pp. 366-380. doi: https://doi.org/10.1016/0027-5107(65)90072-2

Ong, C., Yung, L.-Y. L., Cai, Y., Bay, B.-H. and Baeg, G.-H. 2015. *Drosophila melanogaster* as a model organism to study nanotoxicity. *Nanotoxicology* 9(3), pp. 396-403. doi: 10.3109/17435390.2014.940405

Otero, L. J., Devaux, A. and Standart, N. 2001. A 250-nucleotide UA-rich element in the 3′ untranslated region of Xenopus laevis Vg1 mRNA represses translation both in vivo and in vitro. *RNA* 7(12), pp. 1753-1767. doi: undefined

Owusu-Ansah, E., Song, W. and Perrimon, N. 2013. Muscle Mitohormesis Promotes Longevity via Systemic Repression of Insulin Signaling. *Cell* 155(3), pp. 699-712. doi: https://doi.org/10.1016/j.cell.2013.09.021

Öztürk-Çolak, A. et al. 2024. FlyBase: updates to the *Drosophila* genes and genomes database. *Genetics* 227(1), p. iyad211. doi: 10.1093/genetics/iyad211

Page, S. L., McKim, K. S., Deneen, B., Van Hook, T. L. and Hawley, R. S. 2000. Genetic Studies of mei-P26 Reveal a Link Between the Processes That Control Germ Cell Proliferation in Both Sexes and Those That Control Meiotic Exchange in *Drosophila*. *Genetics* 155(4), pp. 1757-1772. doi: 10.1093/genetics/155.4.1757

Pahl, M. C., Doyle, S. E. and Siegrist, S. E. 2019. E93 Integrates Neuroblast Intrinsic State with Developmental Time to Terminate MB Neurogenesis via Autophagy. *Current Biology* 29(5), pp. 750-762.e753. doi: 10.1016/j.cub.2019.01.039

Palacios, I. M. and Johnston, D. S. 2001. Getting the Message Across: The Intracellular Localization of mRNAs in Higher Eukaryotes. *Annual Review of Cell and Developmental Biology* 17(1), pp. 569-614. doi: 10.1146/annurev.cellbio.17.1.569

Palacios, I. M. and Johnston, D. S. 2002. Kinesin light chain-independent function of the Kinesin heavy chain in cytoplasmic streaming and posterior localisation in the *Drosophila* oocyte. *Development* 129(23), pp. 5473-5485. doi: 10.1242/dev.00119

Pallavi, S. K. and Shashidhara, L. S. 2003. Egfr/Ras pathway mediates interactions between peripodial and disc proper cells in *Drosophila* wing discs. *Development* 130(20), pp. 4931-4941. doi: 10.1242/dev.00719

Palumbo, V. et al. 2015. Misato Controls Mitotic Microtubule Generation by Stabilizing the TCP-1 Tubulin Chaperone Complex. *Current Biology* 25(13), pp. 1777-1783. doi: 10.1016/j.cub.2015.05.033

Pan, C. et al. 2017. UbcD1 regulates Hedgehog signaling by directly modulating Ci ubiquitination and processing. *EMBO reports* 18(11), pp. 1922-1934.

Pan, D. A. and Hardie, D. G. 2002. A homologue of AMP-activated protein kinase in *Drosophila melanogaster* is sensitive to AMP and is activated by ATP depletion. *Biochemical Journal* 367(1), pp. 179-186. doi: 10.1042/bj20020703

Panda, A. C., Martindale, J. L. and Gorospe, M. 2016. Affinity Pulldown of Biotinylated RNA for Detection of Protein-RNA Complexes. *Bio-protocol* 6(24), p. e2062. doi: 10.21769/BioProtoc.2062

Park, K. et al. 2024. Molecular and cellular organization of odorant binding protein genes in *Drosophila*. *Heliyon* 10(9), p. e29358. doi: https://doi.org/10.1016/j.heliyon.2024.e29358

Parton, R. M., Davidson, A., Davis, I. and Weil, T. T. 2014a. Subcellular mRNA localisation at a glance. *Journal of Cell Science* 127(10), p. 2127. doi: 10.1242/jcs.114272

Parton, R. M., Davidson, A., Davis, I. and Weil, T. T. 2014b. Subcellular mRNA localisation at a glance. *Journal of Cell Science* 127(10), pp. 2127-2133. doi: 10.1242/jcs.114272

Parvy, J.-P., Napal, L., Rubin, T., Poidevin, M., Perrin, L., Wicker-Thomas, C. and Montagne, J. 2012. *Drosophila melanogaster* Acetyl-CoA-Carboxylase Sustains a Fatty Acid–Dependent Remote Signal to Waterproof the Respiratory System. *PLOS Genetics* 8(8), p. e1002925. doi: 10.1371/journal.pgen.1002925

Patel, M. R. et al. 2016. A mitochondrial DNA hypomorph of cytochrome oxidase specifically impairs male fertility in *Drosophila melanogaster*. *eLife* 5, p. e16923. doi: 10.7554/eLife.16923

Patel, V. L. et al. 2012. Spatial arrangement of an RNA zipcode identifies mRNAs under post-transcriptional control. *Genes & Development* 26(1), pp. 43-53. doi: 10.1101/gad.177428.111

Pchelintsev, N. A., Adams, P. D. and Nelson, D. M. 2016. Critical Parameters for Efficient Sonication and Improved Chromatin Immunoprecipitation of High Molecular Weight Proteins. *PloS one* 11(1), p. e0148023. doi: 10.1371/journal.pone.0148023

Pérez, I., Lin, C. H., McAfee, J. G. and Patton, J. G. 1997. Mutation of PTB binding sites causes misregulation of alternative 3' splice site selection in vivo. *RNA* 3(7), pp. 764-778.

Perkins, L. A. et al. 2015. The Transgenic RNAi Project at Harvard Medical School: Resources and Validation. *Genetics* 201(3), pp. 843-852. doi: 10.1534/genetics.115.180208

Perrimon, N. and Mathey-Prevot, B. 2007. Applications of High-Throughput RNA Interference Screens to Problems in Cell and Developmental Biology. *Genetics* 175(1), pp. 7-16. doi: 10.1534/genetics.106.069963

Pertceva, J. A., Dorogova, N. V., Bolobolova, E. U., Nerusheva, O. O., Fedorova, S. A. and Omelyanchuk, L. V. 2010. The role of *Drosophila hyperplastic discs* gene in spermatogenesis. *Cell Biology International* 34(10), pp. 991-996. doi: https://doi.org/10.1042/CBI20100105

Petersen, L. K. and Stowers, R. S. 2011. A Gateway MultiSite Recombination Cloning Toolkit. *PloS one* 6(9), p. e24531. doi: 10.1371/journal.pone.0024531

Petit, C. et al. 2024. The evolutionarily conserved PhLP3 is essential for sperm development in *Drosophila melanogaster*. *PloS one* 19(10), p. e0306676. doi: 10.1371/journal.pone.0306676

Pfeiffer, B. D. et al. 2008. Tools for neuroanatomy and neurogenetics in *Drosophila*. *Proceedings of the National Academy of Sciences* 105(28), pp. 9715-9720. doi: 10.1073/pnas.0803697105

Pfeiffer, B. D., Ngo, T.-T. B., Hibbard, K. L., Murphy, C., Jenett, A., Truman, J. W. and Rubin, G. M. 2010. Refinement of Tools for Targeted Gene Expression in *Drosophila*. *Genetics* 186(2), pp. 735-755. doi: 10.1534/genetics.110.119917

Piergentili, R. 2007. Evolutionary conservation of lampbrush-like loops in drosophilids. *BMC Cell Biology* 8(1), p. 35. doi: 10.1186/1471-2121-8-35

Pinkert-Leetsch, D., Rost, J. U., Schmiedeknecht, M. U. H., Stadelmann, C., Alves, F. and Missbach-Guentner, J. 2022. The murine male reproductive organ at a glance: Three-dimensional insights and virtual histology using label-free light sheet microcopy. *Andrology* 10(8), pp. 1660-1672. doi: https://doi.org/10.1111/andr.13292

Pinnola, A., Naumova, N., Shah, M. and Tulin, A. V. 2007. Nucleosomal Core Histones Mediate Dynamic Regulation of Poly(ADP-ribose) Polymerase 1 Protein Binding to Chromatin and Induction of Its Enzymatic Activity*. *Journal of Biological Chemistry* 282(44), pp. 32511-32519. doi: https://doi.org/10.1074/jbc.M705989200

Pitnick, S. 1993. Operational sex ratios and sperm limitation in populations of *Drosophila pachea*. *Behavioral Ecology and Sociobiology* 33(6), pp. 383-391. doi: 10.1007/BF00170253

Pitnick, S. and Markow, T. A. 1994. Large-male advantages associated with costs of sperm production in *Drosophila hydei*, a species with giant sperm. *Proceedings of the National Academy of Sciences* 91(20), pp. 9277-9281. doi: doi:10.1073/pnas.91.20.9277

Pitnick, S., Markow, T. A. and Spicer, G. S. 1995. Delayed male maturity is a cost of producing large sperm in *Drosophila*. *Proceedings of the National Academy of Sciences* 92(23), pp. 10614-10618. doi: 10.1073/pnas.92.23.10614

Pitnick, S., Spicer, G. S. and Markow, T. A. 1995. How long is a giant sperm? *Nature* 375(6527), pp. 109-109. doi: 10.1038/375109a0

Pokrywka, N. J. and Stephenson, E. C. 1991. Microtubules mediate the localization of *bicoid* RNA during *Drosophila* oogenesis. *Development* 113(1), pp. 55-66. doi: 10.1242/dev.113.1.55

Port, F., Chen, H.-M., Lee, T. and Bullock, S. L. 2014. Optimized CRISPR/Cas tools for efficient germline and somatic genome engineering in *Drosophila*. *Proceedings of the National Academy of Sciences* 111(29), pp. E2967-E2976. doi: 10.1073/pnas.1405500111

Prévôt, D., Darlix, J.-L. and Ohlmann, T. 2003. Conducting the initiation of protein synthesis: the role of eIF4G. *Biology of the Cell* 95(3-4), pp. 141-156. doi: https://doi.org/10.1016/S0248-4900(03)00031-5

Prokupek, A. M., Kachman, S. D., Ladunga, I. and Harshman, L. G. 2009. Transcriptional profiling of the sperm storage organs of *Drosophila melanogaster*. *Insect molecular biology* 18(4), pp. 465-475. doi: https://doi.org/10.1111/j.1365-2583.2009.00887.x

Qiu, S., Adema, C. M. and Lane, T. 2005. A computational study of off-target effects of RNA interference. *Nucleic Acids Research* 33(6), pp. 1834-1847. doi: 10.1093/nar/gki324

Quiñones-Coello, A. T. et al. 2007. Exploring Strategies for Protein Trapping in *Drosophila*. *Genetics* 175(3), pp. 1089-1104. doi: 10.1534/genetics.106.065995

R Core Team 2024. *R: A Language and Environment for Statistical Computing.* Vienna, Austria: R Foundation for Statistical Computing. Available at: https://www.R-project.org/ [Accessed: July 2024].

Rathke, C., Baarends, W. M., Jayaramaiah-Raja, S., Bartkuhn, M., Renkawitz, R. and Renkawitz-Pohl, R. 2007. Transition from a nucleosome-based to a protamine-based chromatin configuration during spermiogenesis in *Drosophila. Journal of Cell Science* 120(9), p. 1689. doi: 10.1242/jcs.004663

Rauzi, M., Krzic, U., Saunders, T. E., Krajnc, M., Ziherl, P., Hufnagel, L. and Leptin, M. 2015. Embryo-scale tissue mechanics during *Drosophila* gastrulation movements. *Nature Communications* 6(1), p. 8677. doi: 10.1038/ncomms9677

Raz, A. A. et al. 2023. Emergent dynamics of adult stem cell lineages from single nucleus and single cell RNA-Seq of *Drosophila* testes. *eLife* 12, p. e82201. doi: 10.7554/eLife.82201

Recasens-Alvarez, C., Alexandre, C., Kirkpatrick, J., Nojima, H., Huels, D. J., Snijders, A. P. and Vincent, J.-P. 2021. Ribosomopathy-associated mutations cause proteotoxic stress that is alleviated by TOR inhibition. *Nature Cell Biology* 23(2), pp. 127-135. doi: 10.1038/s41556-020-00626-1

Reiter, L. T., Potocki, L., Chien, S., Gribskov, M. and Bier, E. 2001. A Systematic Analysis of Human Disease-Associated Gene Sequences In *Drosophila melanogaster*. *Genome Research* 11(6), pp. 1114-1125.

Ren, F., Zhang, L. and Jiang, J. 2010. Hippo signaling regulates Yorkie nuclear localization and activity through 14-3-3 dependent and independent mechanisms. *Developmental Biology* 337(2), pp. 303-312. doi: https://doi.org/10.1016/j.ydbio.2009.10.046

Ren, Q. et al. 2017. Stem Cell-Intrinsic, Seven-up-Triggered Temporal Factor Gradients Diversify Intermediate Neural Progenitors. *Current Biology* 27(9), pp. 1303-1313. doi: 10.1016/j.cub.2017.03.047

Reveal, B., Garcia, C., Ellington, A. and Macdonald, P. 2011. Multiple RNA binding domains of Bruno confer recognition of diverse binding sites for translational repression. *RNA Biology* 8(6), pp. 1047-1060. doi: 10.4161/rna.8.6.17542

Reveal, B., Yan, N., Snee, M. J., Pai, C.-I., Gim, Y. and Macdonald, P. M. 2010. BREs Mediate Both Repression and Activation of oskar mRNA Translation and Act In trans. *Developmental Cell* 18(3), pp. 496-502. doi: https://doi.org/10.1016/j.devcel.2009.12.021

Reynaud, E. G., Kržič, U., Greger, K. and Stelzer, E. H. K. 2008. Light sheet-based fluorescence microscopy: More dimensions, more photons, and less photodamage. *HFSP Journal* 2(5), pp. 266-275. doi: 10.2976/1.2974980

Richards, S. et al. 2005. Comparative genome sequencing of *Drosophila pseudoobscura*: Chromosomal, gene, and cis-element evolution. *Genome Research* 15(1), pp. 1-18.

Richter, J. D. and Sonenberg, N. 2005. Regulation of cap-dependent translation by eIF4E inhibitory proteins. *Nature* 433(7025), pp. 477-480. doi: 10.1038/nature03205

Roach, T. V. and Lenhart, K. F. 2024. Mating-induced Ecdysone in the testis disrupts soma-germline contacts and stem cell cytokinesis. *Development* 151(11), p. dev202542. doi: 10.1242/dev.202542

Robertson, S. E., Dockendorff, T. C., Leatherman, J. L., Faulkner, D. L. and Jongens, T. A. 1999. *germ cell-less* Is Required Only during the Establishment of the Germ Cell Lineage of *Drosophila* and Has Activities Which Are Dependent and Independent of Its Localization to the Nuclear Envelope. *Developmental Biology* 215(2), pp. 288-297. doi: https://doi.org/10.1006/dbio.1999.9453

Robida, M., Sridharan, V., Morgan, S., Rao, T. and Singh, R. 2010. *Drosophila* polypyrimidine tract-binding protein is necessary for spermatid individualization. *Proceedings of the National Academy of Sciences* 107(28), p. 12570. doi: 10.1073/pnas.1007935107

Robida, M. D. and Singh, R. 2003. *Drosophila* polypyrimidine-tract binding protein (PTB) functions specifically in the male germline. *The EMBO Journal* 22(12), pp. 2924-2933. doi: https://doi.org/10.1093/emboj/cdg301

Robinson, M. D., McCarthy, D. J. and Smyth, G. K. 2010. edgeR: a Bioconductor package for differential expression analysis of digital gene expression data. *Bioinformatics* 26(1), pp. 139-140. doi: 10.1093/bioinformatics/btp616

Robinson, M. D. and Oshlack, A. 2010. A scaling normalization method for differential expression analysis of RNA-seq data. *Genome biology* 11(3), p. R25. doi: 10.1186/gb-2010-11-3-r25

Rodriguez, A. J., Shenoy, S. M., Singer, R. H. and Condeelis, J. 2006. Visualization of mRNA translation in living cells. *Journal of Cell Biology* 175(1), pp. 67-76. doi: 10.1083/jcb.200512137

Rogoyski, O. M., Pueyo, J. I., Couso, J. P. and Newbury, S. F. 2017. Functions of long non-coding RNAs in human disease and their conservation in *Drosophila* development. *Biochemical Society Transactions* 45(4), pp. 895-904. doi: 10.1042/BST20160428

Ross, A. F., Oleynikov, Y., Kislauskis, E. H., Taneja, K. L. and Singer, R. H. 1997. Characterization of a β-Actin mRNA Zipcode-Binding Protein. *Molecular and cellular biology* 17(4), pp. 2158-2165. doi: 10.1128/MCB.17.4.2158

Ross, C. L. N., Patel, R. R., Mendelson, T. C. and Ware, V. C. 2007. Functional conservation between structurally diverse ribosomal proteins from *Drosophila melanogaster* and *Saccharomyces cerevisiae*: fly L23a can substitute for yeast L25 in ribosome assembly and function. *Nucleic Acids Research* 35(13), pp. 4503-4514. doi: 10.1093/nar/gkm428

Roy, G., Miron, M., Khaleghpour, K., Lasko, P. and Sonenberg, N. 2004. The *Drosophila* Poly(A) Binding Protein-Interacting Protein, dPaip2, Is a Novel Effector of Cell Growth. *Molecular and cellular biology* 24(3), pp. 1143-1154. doi: 10.1128/MCB.24.3.1143-1154.2004

Rubin, G. M. and Spradling, A. C. 1982. Genetic Transformation of *Drosophila* with Transposable Element Vectors. *Science* 218(4570), pp. 348-353. doi: doi:10.1126/science.6289436

Rubin, G. M. et al. 2000. Comparative Genomics of the Eukaryotes. *Science* 287(5461), pp. 2204-2215. doi: 10.1126/science.287.5461.2204

Rugjee, K. N., Roy Chaudhury, S., Al-Jubran, K., Ramanathan, P., Matina, T., Wen, J. and Brogna, S. 2013. Fluorescent protein tagging confirms the presence of ribosomal proteins at *Drosophila* polytene chromosomes. *PeerJ* 1, p. e15. doi: 10.7717/peerj.15

Runge, S., Nielsen, F. C., Nielsen, J., Lykke-Andersen, J., Wewer, U. M. and Christiansen, J. 2000. H19 RNA Binds Four Molecules of Insulin-like Growth Factor II mRNA-binding Protein*. *Journal of Biological Chemistry* 275(38), pp. 29562-29569. doi: https://doi.org/10.1074/jbc.M001156200

Rybakin, V. and Clemen, C. S. 2005. Coronin proteins as multifunctional regulators of the cytoskeleton and membrane trafficking. *BioEssays* 27(6), pp. 625-632. doi: https://doi.org/10.1002/bies.20235

Ryoo, H. D., Bergmann, A., Gonen, H., Ciechanover, A. and Steller, H. 2002. Regulation of *Drosophila* IAP1 degradation and apoptosis by *reaper* and *ubcD1*. *Nature Cell Biology* 4(6), pp. 432-438. doi: 10.1038/ncb795

Sabari Benjamin, R. et al. 2018. Coactivator condensation at super-enhancers links phase separation and gene control. *Science* 361(6400), p. eaar3958. doi: 10.1126/science.aar3958

Sadowski, I., Ma, J., Triezenberg, S. and Ptashne, M. 1988. GAL4-VP16 is an unusually potent transcriptional activator. *Nature* 335(6190), pp. 563-564. doi: 10.1038/335563a0

Saisawang, C., Wongsantichon, J. and Ketterman, Albert J. 2012. A preliminary characterization of the cytosolic glutathione transferase proteome from *Drosophila melanogaster*. *Biochemical Journal* 442(1), pp. 181-190. doi: 10.1042/BJ20111747

Salminen, T. S., Cannino, G., Oliveira, M. T., Lillsunde, P., Jacobs, H. T. and Kaguni, L. S. 2019. Lethal Interaction of Nuclear and Mitochondrial Genotypes in *Drosophila melanogaster*. *G3 Genes|Genomes|Genetics* 9(7), pp. 2225-2234. doi: 10.1534/g3.119.400315

Sanghavi, P., Lu, S. and Gonsalvez, G. B. 2012. A functional link between localized Oskar, dynamic microtubules, and endocytosis. *Developmental Biology* 367(1), pp. 66-77. doi: https://doi.org/10.1016/j.ydbio.2012.04.024

Sardet, C., Nishida, H., Prodon, F. and Sawada, K. 2003. Maternal mRNAs of *PEM* and macho 1, the ascidian muscle determinant, associate and move with a rough endoplasmic reticulum network in the egg cortex. *Development* 130(23), p. 5839. doi: 10.1242/dev.00805

Sasamura, T., Matsuno, K. and Fortini, M. E. 2013. Disruption of *Drosophila melanogaster* Lipid Metabolism Genes Causes Tissue Overgrowth Associated with Altered Developmental Signaling. *PLOS Genetics* 9(11), p. e1003917. doi: 10.1371/journal.pgen.1003917

Satterfield, T. F. and Pallanck, L. J. 2006. Ataxin-2 and its *Drosophila* homolog, ATX2, physically assemble with polyribosomes. *Human Molecular Genetics* 15(16), pp. 2523-2532. doi: 10.1093/hmg/ddl173

Sawicka, K., Bushell, M., Spriggs, Keith A. and Willis, Anne E. 2008. Polypyrimidine-tract-binding protein: a multifunctional RNA-binding protein. *Biochemical Society Transactions* 36(4), pp. 641-647. doi: 10.1042/BST0360641

Schachtner, L. T. et al. 2015. *Drosophila* Shep and C. elegans SUP-26 are RNA-binding proteins that play diverse roles in nervous system development. *Development Genes and Evolution* 225(6), pp. 319-330. doi: 10.1007/s00427-015-0514-3

Schäfer, U. 1986. The regulation of male-specific transcripts by sex determining genes in *Drosophila melanogaster*. *The EMBO Journal* 5(13), pp. 3579-3582-3582. doi: https://doi.org/10.1002/j.1460-2075.1986.tb04685.x

Schäfer, M., Börsch, D., Hülster, A. and Schäfer, U. 1993. Expression of a Gene Duplication Encoding Conserved Sperm Tail Proteins Is Translationally Regulated in *Drosophila melanogaster*. *Molecular and cellular biology* 13(3), pp. 1708-1718. doi: 10.1128/mcb.13.3.1708-1718.1993

Schäfer, M., Kuhn, R., Bosse, F. and Schäfer, U. 1990. A conserved element in the leader mediates post-meiotic translation as well as cytoplasmic polyadenylation of a *Drosophila* spermatocyte mRNA. *The EMBO Journal* 9(13), pp. 4519-4525-4525. doi: https://doi.org/10.1002/j.1460-2075.1990.tb07903.x

Schäfer, M., Nayernia, K., Engel, W. and Schäfer, U. 1995. Translational Control in Spermatogenesis. *Developmental Biology* 172(2), pp. 344-352. doi: https://doi.org/10.1006/dbio.1995.8049

Schertel, C. et al. 2013. Systematic Screening of a *Drosophila* ORF Library In Vivo Uncovers Wnt/Wg Pathway Components. *Developmental Cell* 25(2), pp. 207-219. doi: https://doi.org/10.1016/j.devcel.2013.02.019

Schlager, M. A., Hoang, H. T., Urnavicius, L., Bullock, S. L. and Carter, A. P. 2014. *In vitro* reconstitution of a highly processive recombinant human dynein complex. *The EMBO Journal* 33(17), pp. 1855-1868.

Schmied, C. and Tomancak, P. 2016. Sample Preparation and Mounting of *Drosophila* Embryos for Multiview Light Sheet Microscopy. In: Dahmann, C. ed. *Drosophila: Methods and Protocols*. New York, NY: Springer New York, pp. 189-202.

Schneider, C. A., Rasband, W. S. and Eliceiri, K. W. 2012. NIH Image to ImageJ: 25 years of image analysis. *Nature Methods* 9(7), pp. 671-675. doi: 10.1038/nmeth.2089

Schnorrer, F., Bohmann, K. and Nüsslein-Volhard, C. 2000. The molecular motor dynein is involved in targeting Swallow and *bicoid* RNA to the anterior pole of *Drosophila* oocytes. *Nature Cell Biology* 2(4), pp. 185-190. doi: 10.1038/35008601

Schnorrer, F. et al. 2010. Systematic genetic analysis of muscle morphogenesis and function in *Drosophila*. *Nature* 464(7286), pp. 287-291. doi: 10.1038/nature08799

Schoborg, T., Zajac, A. L., Fagerstrom, C. J., Guillen, R. X. and Rusan, N. M. 2015. An Asp–CaM complex is required for centrosome–pole cohesion and centrosome inheritance in neural stem cells. *Journal of Cell Biology* 211(5), pp. 987-998. doi: 10.1083/jcb.201509054

Schor, I. E., Bussotti, G., Maleš, M., Forneris, M., Viales, R. R., Enright, A. J. and Furlong, E. E. M. 2018. Non-coding RNA Expression, Function, and Variation during *Drosophila* Embryogenesis. *Current Biology* 28(22), pp. 3547-3561.e3549. doi: 10.1016/j.cub.2018.09.026

Schupbach, T. and Wieschaus, E. 1986. Germline autonomy of maternal-effect mutations altering the embryonic body pattern of *Drosophila*. *Developmental Biology* 113(2), pp. 443-448. doi: https://doi.org/10.1016/0012-1606(86)90179-X

Schüpbach, T. and Wieschaus, E. 1991. Female sterile mutations on the second chromosome of *Drosophila melanogaster*. II. Mutations blocking oogenesis or altering egg morphology. *Genetics* 129(4), pp. 1119-1136. doi: 10.1093/genetics/129.4.1119

Schwartz, S. P., Aisenthal, L., Elisha, Z., Oberman, F. and Yisraeli, J. K. 1992. A 69-kDa RNA-binding protein from *Xenopus* oocytes recognizes a common motif in two vegetally localized maternal mRNAs. *Proceedings of the National Academy of Sciences* 89(24), pp. 11895-11899.

Scott, K., Sun, Y., Beckingham, K. and Zuker, C. S. 1997. Calmodulin Regulation of *Drosophila* Light-Activated Channels and Receptor Function Mediates Termination of the Light Response In Vivo. *Cell* 91(3), pp. 375-383. doi: 10.1016/S0092-8674(00)80421-3

Sebo, Z. L., Lee, H. B., Peng, Y. and Guo, Y. 2014. A simplified and efficient germline-specific CRISPR/Cas9 system for *Drosophila* genomic engineering. *Fly* 8(1), pp. 52-57. doi: 10.4161/fly.26828

Sechi, S. et al. 2019. *Drosophila* Doublefault protein coordinates multiple events during male meiosis by controlling mRNA translation. *Development* 146(22), p. dev183053. doi: 10.1242/dev.183053

Seddigh, S. and Darabi, M. 2018. Functional, structural, and phylogenetic analysis of mitochondrial cytochrome b (cytb) in insects. *Mitochondrial DNA Part A* 29(2), pp. 236-249. doi: 10.1080/24701394.2016.1275596

Shah, A. P. et al. 2011. Cardiac remodeling in *Drosophila* arises from changes in actin gene expression and from a contribution of lymph gland-like cells to the heart musculature. *Mechanisms of Development* 128(3), pp. 222-233. doi: https://doi.org/10.1016/j.mod.2011.01.001

Shah, S. et al. 2016. Single-molecule RNA detection at depth by hybridization chain reaction and tissue hydrogel embedding and clearing. *Development* 143(15), pp. 2862-2867. doi: 10.1242/dev.138560

Shahbabian, K. and Chartrand, P. 2012. Control of cytoplasmic mRNA localization. *Cellular and Molecular Life Sciences* 69(4), pp. 535-552. doi: 10.1007/s00018-011-0814-3

Shao, L. et al. 2023. Eukaryotic translation initiation factor eIF4E-5 is required for spermiogenesis in *Drosophila melanogaster*. *Development* 150(4), p. dev200477. doi: 10.1242/dev.200477

Shao, Z. et al. 2024. Spatially revealed roles for lncRNAs in *Drosophila* spermatogenesis, Y chromosome function and evolution. *Nature Communications* 15(1), p. 3806. doi: 10.1038/s41467-024-47346-w

Shestakova, E. A., Singer, R. H. and Condeelis, J. 2001. The physiological significance of β-actin mRNA localization in determining cell polarity and directional motility. *Proceedings of the National Academy of Sciences* 98(13), pp. 7045-7050. doi: 10.1073/pnas.121146098

Shestakova, E. A., Wyckoff, J., Jones, J., Singer, R. H. and Condeelis, J. 1999. Correlation of β-Actin Messenger RNA Localization with Metastatic Potential in Rat Adenocarcinoma Cell Lines1. *Cancer Research* 59(6), pp. 1202-1205.

Shevchenko, G., Musunuri, S., Wetterhall, M. and Bergquist, J. 2012. Comparison of Extraction Methods for the Comprehensive Analysis of Mouse Brain Proteome using Shotgun-based Mass Spectrometry. *Journal of Proteome Research* 11(4), pp. 2441-2451. doi: 10.1021/pr201169q

Simmonds, A. J., dosSantos, G., Livne-Bar, I. and Krause, H. M. 2001. Apical Localization of wingless Transcripts Is Required for Wingless Signaling. *Cell* 105(2), pp. 197-207. doi: https://doi.org/10.1016/S0092-8674(01)00311-7

Singh, R., Valcarcel, J. and Green, M. R. 1995. Distinct binding specificities and functions of higher eukaryotic polypyrimidine tract-binding proteins. *Science* 268(5214), p. 1173. doi: 10.1126/science.7761834

Singh, S. P., Coronella, J. A., Beneš, H., Cochrane, B. J. and Zimniak, P. 2001. Catalytic function of *Drosophila melanogaster* glutathione S-transferase DmGSTS1-1

(GST-2) in conjugation of lipid peroxidation end products. *European journal of biochemistry* 268(10), pp. 2912-2923.

Singh, S. R. et al. 2006. The *Drosophila* homolog of the human tumor suppressor gene BHD interacts with the JAK-STAT and Dpp signaling pathways in regulating male germline stem cell maintenance. *Oncogene* 25(44), pp. 5933-5941. doi: 10.1038/sj.onc.1209593

Sinsimer, K. S., Jain, R. A., Chatterjee, S. and Gavis, E. R. 2011. A late phase of germ plasm accumulation during *Drosophila* oogenesis requires Lost and Rumpelstiltskin. *Development* 138(16), pp. 3431-3440. doi: 10.1242/dev.065029

Sirot, L. K., Findlay, G. D., Sitnik, J. L., Frasheri, D., Avila, F. W. and Wolfner, M. F. 2014. Molecular Characterization and Evolution of a Gene Family Encoding Both Female- and Male-Specific Reproductive Proteins in *Drosophila*. *Molecular Biology and Evolution* 31(6), pp. 1554-1567. doi: 10.1093/molbev/msu114

Sisson, J. C., Field, C., Ventura, R., Royou, A. and Sullivan, W. 2000. Lava Lamp, a Novel Peripheral Golgi Protein, Is Required for *Drosophila melanogaster* Cellularization. *Journal of Cell Biology* 151(4), pp. 905-918. doi: 10.1083/jcb.151.4.905

Smibert, C. A., Lie, Y. S., Shillinglaw, W., Henzel, W. J. and Macdonald, P. M. 1999. Smaug, a novel and conserved protein, contributes to repression of nanos mRNA translation in vitro. *RNA* 5(12), pp. 1535-1547. doi: 10.1017/S1355838299991392

Smith, G. A. et al. 2019. Glutathione S-Transferase Regulates Mitochondrial Populations in Axons through Increased Glutathione Oxidation. *Neuron* 103(1), pp. 52-65.e56. doi: 10.1016/j.neuron.2019.04.017

Snee, M., Benz, D., Jen, J. and Macdonald, P. M. 2008. Two distinct domains of Bruno bind specifically to the oskar mRNA. *RNA Biology* 5(1), pp. 49-57. doi: 10.4161/rna.5.1.5735

Snee, M. J. and Macdonald, P. M. 2009. Dynamic organization and plasticity of sponge bodies. *Developmental Dynamics* 238(4), pp. 918-930.

Snook, R. R. 1997. Is the production of multiple sperm types adaptive? *Evolution* 51(3), pp. 797-808.

Sohal, R. S., Toroser, D., Brégère, C., Mockett, R. J. and Orr, W. C. 2008. Age-related decrease in expression of mitochondrial DNA encoded subunits of cytochrome c oxidase in *Drosophila melanogaster*. *Mechanisms of Ageing and Development* 129(9), pp. 558-561. doi: https://doi.org/10.1016/j.mad.2008.04.006

Sonenberg, N. and Hinnebusch, A. G. 2009. Regulation of Translation Initiation in Eukaryotes: Mechanisms and Biological Targets. *Cell* 136(4), pp. 731-745. doi: https://doi.org/10.1016/j.cell.2009.01.042

Sonnenblick, B. P. 1941. Germ Cell Movements and Sex Differentiation of the Gonads in the *Drosophila* Embryo. *Proceedings of the National Academy of Sciences* 27(10), pp. 484-489. doi: 10.1073/pnas.27.10.484

Spana, E. P. and Doe, C. Q. 1995. The prospero transcription factor is asymmetrically localized to the cell cortex during neuroblast mitosis in *Drosophila*. *Development* 121(10), pp. 3187-3195. doi: 10.1242/dev.121.10.3187

Speel, E. J. M. 1999. Detection and amplification systems for sensitive, multiple-target DNA and RNA in situ hybridization: looking inside cells with a spectrum of colors. *Histochemistry and Cell Biology* 112(2), pp. 89-113. doi: 10.1007/s004180050396

Spirov, A., Fahmy, K., Schneider, M., Frei, E., Noll, M. and Baumgartner, S. 2009. Formation of the *bicoid* morphogen gradient: an mRNA gradient dictates the protein gradient. *Development* 136(4), p. 605. doi: 10.1242/dev.031195

Spletter, M. L. et al. 2015. The RNA-binding protein Arrest (Bruno) regulates alternative splicing to enable myofibril maturation in *Drosophila* flight muscle. *EMBO reports* 16(2), pp. 178-191. doi: https://doi.org/10.15252/embr.201439791

Spradling, A. C. and Rubin, G. M. 1982. Transposition of Cloned P Elements into *Drosophila* Germ Line Chromosomes. *Science* 218(4570), pp. 341-347. doi: 10.1126/science.6289435

Spradling, A. C. et al. 1999. The Berkeley *Drosophila* Genome Project Gene Disruption Project: Single P-Element Insertions Mutating 25% of Vital *Drosophila* Genes. *Genetics* 153(1), pp. 135-177. doi: 10.1093/genetics/153.1.135

Sreejith, P., Jang, W., To, V., Hun Jo, Y., Biteau, B. and Kim, C. 2019. Lin28 is a critical factor in the function and aging of *Drosophila* testis stem cell niche. *Aging* 11, pp. 855-873. doi: https://doi.org/10.18632/aging.101765

Sreejith, P., Malik, S., Kim, C. and Biteau, B. 2022. Imp interacts with Lin28 to regulate adult stem cell proliferation in the *Drosophila* intestine. *PLOS Genetics* 18(9), p. e1010385. doi: 10.1371/journal.pgen.1010385

Sridharan, V., Heimiller, J., Robida, M. D. and Singh, R. 2016. High Throughput Sequencing Identifies Misregulated Genes in the *Drosophila* Polypyrimidine Tract-Binding Protein (hephaestus) Mutant Defective in Spermatogenesis. *PloS one* 11(3), p. e0150768. doi: 10.1371/journal.pone.0150768

Statistics Kingdom. (2017). *Shapiro-Wilk Test Calculator*. [Web Application]. https://www.statskingdom.com/shapiro-wilk-test-calculator.html [Accessed: April 2025]

St Johnston, D. 2005. Moving messages: the intracellular localization of mRNAs. *Nature Reviews Molecular Cell Biology* 6(5), pp. 363-375. doi: 10.1038/nrm1643

St Johnston, D. 2013. Using mutants, knockdowns, and transgenesis to investigate gene function in *Drosophila*. *WIREs Developmental Biology* 2(5), pp. 587-613. doi: https://doi.org/10.1002/wdev.101

Steinhauer, J. et al. 2019. Combover interacts with the axonemal component Rsp3 and is required for *Drosophila* sperm individualization. *Development* 146(17), p. dev179275. doi: 10.1242/dev.179275

Stern, C. and Hadorn, E. 1939. The Relation between the Color of Testes and Vasa Efferentia in *Drosophila*. (0016-6731 (Print)),

Stewart, M. J. and Denell, R. 1993. Mutations in the *Drosophila* Gene Encoding Ribosomal Protein S6 Cause Tissue Overgrowth. *Molecular and cellular biology* 13(4), pp. 2524-2535. doi: 10.1128/mcb.13.4.2524-2535.1993

Subach, O. M. et al. 2008. Conversion of Red Fluorescent Protein into a Bright Blue Probe. *Chemistry & Biology* 15(10), pp. 1116-1124. doi: https://doi.org/10.1016/j.chembiol.2008.08.006

Sugimura, I. and Lilly, M. A. 2006. Bruno Inhibits the Expression of Mitotic Cyclins during the Prophase I Meiotic Arrest of *Drosophila* Oocytes. *Developmental Cell* 10(1), pp. 127-135. doi: 10.1016/j.devcel.2005.10.018

Sutherland, J. M., Siddall, N. A., Hime, G. R. and McLaughlin, E. A. 2015. RNA binding proteins in spermatogenesis: an in depth focus on the Musashi family. *Asian journal of andrology* 17(4), pp. 529-536. doi: 10.4103/1008-682X.151397

Takatori, N., Kumano, G., Saiga, H. and Nishida, H. 2010. Segregation of Germ Layer Fates by Nuclear Migration-Dependent Localization of Not mRNA. *Developmental Cell* 19(4), pp. 589-598. doi: https://doi.org/10.1016/j.devcel.2010.09.003

Talross, G. J. S. and Carlson, J. R. 2023. The rich non-coding RNA landscape of the *Drosophila* antenna. *Cell Reports* 42(5), doi: 10.1016/j.celrep.2023.112482

Tansey, T., Schultz, J. R., Miller, R. C. and Storti, R. V. 1991. NOTES: Small Differences in *Drosophila* Tropomyosin Expression Have Significant Effects on Muscle Function. *Molecular and cellular biology* 11(12), pp. 6337-6342. doi: 10.1128/mcb.11.12.6337-6342.1991

Tariq, A., Green, L., Jeynes, J. C. G., Soeller, C. and Wakefield, J. G. 2020a. In vitro reconstitution of branching microtubule nucleation. *eLife* 9, p. e49769. doi: 10.7554/eLife.49769

Tariq, A., Green, L., Soeller, C. and Wakefield, J. 2020b. Cleavable Affinity Purification (Cl-AP): A One-step Procedure to Affinity Purify Protein Complexes. *Bio-protocol* 10(22), p. e3821. doi: 10.21769/BioProtoc.3821

Teets, N. M. and Hahn, D. A. 2018. Genetic variation in the shape of cold-survival curves in a single fly population suggests potential for selection from climate variability. *Journal of Evolutionary Biology* 31(4), pp. 543-555. doi: 10.1111/jeb.13244

Tessier, C. R., Doyle, G. A., Clark, B. A., Pitot, H. C. and Ross, J. 2004. Mammary Tumor Induction in Transgenic Mice Expressing an RNA-Binding Protein. *Cancer Research* 64(1), pp. 209-214. doi: 10.1158/0008-5472.CAN-03-2927

Texada, M. J., Simonette, R. A., Deery, W. J. and Beckingham, K. M. 2011. Tropomyosin is an interaction partner of the *Drosophila* coiled coil protein Yuri Gagarin. *Experimental Cell Research* 317(4), pp. 474-487. doi: https://doi.org/10.1016/j.yexcr.2010.11.012

The jamovi project (2025). *jamovi (Version 2.6.44)* [Computer Software]. Retrieved from: https://www.jamovi.org [Accessed: April 2025]

Thornton, J. E. and Gregory, R. I. 2012. How does Lin28 let-7 control development and disease? *Trends in Cell Biology* 22(9), pp. 474-482. doi: https://doi.org/10.1016/j.tcb.2012.06.001

Tirian, L. and Dickson, B. J. 2017. The VT GAL4, LexA, and split-GAL4 driver line collections for targeted expression in the *Drosophila* nervous system. *bioRxiv*, p. 198648. doi: 10.1101/198648

Titlow, J., Robertson, F., Järvelin, A., Ish-Horowicz, D., Smith, C., Gratton, E. and Davis, I. 2020. Syncrip/hnRNP Q is required for activity-induced Msp300/Nesprin-1 expression and new synapse formation. *Journal of Cell Biology* 219(3), p. e201903135. doi: 10.1083/jcb.201903135

Tokuyasu, K. T. 1974a. Dynamics of spermiogenesis in *Drosophila melanogaster*: III. Relation between axoneme and mitochondrial derivatives. *Experimental Cell Research* 84(1), pp. 239-250. doi: https://doi.org/10.1016/0014-4827(74)90402-9

Tokuyasu, K. T. 1974b. Dynamics of spermiogenesis in *Drosophila melanogaster*: IV. Nuclear transformation. *Journal of Ultrastructure Research* 48(2), pp. 284-303. doi: https://doi.org/10.1016/S0022-5320(74)80083-3

Tokuyasu, K. T. 1975. Dynamics of spermiogenesis in *Drosophila melanogaster*. VI. Significance of “onion” nebenkern formation. *Journal of Ultrastructure Research* 53(1), pp. 93-112. doi: https://doi.org/10.1016/S0022-5320(75)80089-X

Tokuyasu, K. T., Peacock, W. J. and Hardy, R. W. 1972. Dynamics of spermiogenesis in *Drosophila melanogaster*: I. Individualization process. *Zeitschrift für Zellforschung und Mikroskopische Anatomie* 124(4), pp. 479-506. doi: 10.1007/BF00335253

Toledano, H., D’Alterio, C., Czech, B., Levine, E. and Jones, D. L. 2012. The let-7–Imp axis regulates ageing of the *Drosophila* testis stem-cell niche. *Nature* 485(7400), pp. 605-610. doi: 10.1038/nature11061

Tomer, R., Khairy, K., Amat, F. and Keller, P. J. 2012. Quantitative high-speed imaging of entire developing embryos with simultaneous multiview light-sheet microscopy. *Nature Methods* 9(7), pp. 755-763. doi: 10.1038/nmeth.2062

Torgerson, D. G. and Singh, R. S. 2004. Rapid Evolution Through Gene Duplication and Subfunctionalization of the Testes-Specific α4 Proteasome Subunits in *Drosophila* Sequence data from this article have been deposited with the EMBL/GenBank Data Libraries under accession nos. AY542377, AY542378, AY542379, AY542380, AY542381, AY542382, AY542383, AY542384, AY542385, AY542386, AY542387, AY542388, AY542389, AY542390, AY542391, AY542392, AY542393, AY542394,

AY542395, AY542396, AY542397, AY542398, AY542399, AY542400, AY542401, AY542402, AY542403, AY542404, AY542405, AY542406, AY542407, AY542408, AY542409, AY542410, AY542411, AY542412, AY542413, AY542414, AY542415, AY542416, AY542417, AY542418, AY542419, AY542420, AY542421, AY542422, AY542423, AY542424, AY542425, AY542426, AY542427, AY542428, AY542429, AY542430, AY542431, AY542432. *Genetics* 168(3), pp. 1421-1432. doi: 10.1534/genetics.104.027631

Tracey, W. D., Jr., Ning, X., Klingler, M., Kramer, S. G. and Gergen, J. P. 2000. Quantitative Analysis of Gene Function in the *Drosophila* Embryo. *Genetics* 154(1), pp. 273-284. doi: 10.1093/genetics/154.1.273

Tran, J., Brenner, T. J. and DiNardo, S. 2000. Somatic control over the germline stem cell lineage during *Drosophila* spermatogenesis. *Nature* 407(6805), pp. 754-757. doi: 10.1038/35037613

Treier, M., Seufert, W. and Jentsch, S. 1992. *Drosophila* UbcD1 encodes a highly conserved ubiquitin-conjugating enzyme involved in selective protein degradation. *The EMBO Journal* 11(1), pp. 367-372.

Trivedi, V., Choi, H. M. T., Fraser, S. E. and Pierce, N. A. 2018. Multidimensional quantitative analysis of mRNA expression within intact vertebrate embryos. *Development* 145(1), p. dev156869. doi: 10.1242/dev.156869

Tsigkari, K. K., Acevedo, S. F. and Skoulakis, E. M. C. 2012. 14-3-3ε Is Required for Germ Cell Migration in *Drosophila*. *PloS one* 7(5), p. e36702. doi: 10.1371/journal.pone.0036702

Tunstall, N. E., Herr, A., de Bruyne, M. and Warr, C. G. 2012. A Screen for Genes Expressed in the Olfactory Organs of *Drosophila melanogaster* Identifies Genes

Involved in Olfactory Behaviour. *PloS one* 7(4), p. e35641. doi: 10.1371/journal.pone.0035641

Uda, K., Fujimoto, N., Akiyama, Y., Mizuta, K., Tanaka, K., Ellington, W. R. and Suzuki, T. 2006. Evolution of the arginine kinase gene family. *Comparative Biochemistry and Physiology Part D: Genomics and Proteomics* 1(2), pp. 209-218. doi: https://doi.org/10.1016/j.cbd.2005.10.007

Uebel, C. J. and Phillips, C. M. 2019. Phase-separated protein dynamics are affected by fluorescent tag choice. *microPublication biology.* doi: 10.17912/micropub.biology.000143.

Ugur, B., Chen, K. and Bellen, H. J. 2016. *Drosophila* tools and assays for the study of human diseases. *Disease Models & Mechanisms* 9(3), pp. 235-244. doi: 10.1242/dmm.023762

Updike, D. L., Hachey, S. J., Kreher, J. and Strome, S. 2011. P granules extend the nuclear pore complex environment in the *C. elegans* germ line. *Journal of Cell Biology* 192(6), pp. 939-948. doi: 10.1083/jcb.201010104

van Heesch, S. et al. 2014. Extensive localization of long noncoding RNAs to the cytosol and mono- and polyribosomal complexes. *Genome biology* 15(1), p. R6. doi: 10.1186/gb-2014-15-1-r6

VanBerkum, M. F. A. and Goodman, C. S. 1995. Targeted disruption of Ca2+-calmodulin signaling in *Drosophila* growth cones leads to stalls in axon extension and errors in axon guidance. *Neuron* 14(1), pp. 43-56. doi: https://doi.org/10.1016/0896-6273(95)90239-2

Vazquez-Pianzola, P., Urlaub, H. and Suter, B. 2011. Pabp binds to the *osk* 3′UTR and specifically contributes to *osk* mRNA stability and oocyte accumulation. *Developmental Biology* 357(2), pp. 404-418. doi: https://doi.org/10.1016/j.ydbio.2011.07.009

Veeranan-Karmegam, R., Boggupalli, D. P., Liu, G. and Gonsalvez, G. B. 2016. A new isoform of *Drosophila* non-muscle Tropomyosin 1 interacts with Kinesin-1 and functions in oskar mRNA localization. *Journal of Cell Science* 129(22), pp. 4252-4264. doi: 10.1242/jcs.194332

Venables, J. P. and Eperon, I. C. 1999. The roles of RNA-binding proteins in spermatogenesis and male Infertility. *Current Opinion in Genetics & Development* 9(3), pp. 346-354. doi: https://doi.org/10.1016/S0959-437X(99)80052-5

Venken, K. J. T. and Bellen, H. J. 2014. Chemical mutagens, transposons, and transgenes to interrogate gene function in *Drosophila melanogaster*. *Methods* 68(1), pp. 15-28. doi: https://doi.org/10.1016/j.ymeth.2014.02.025

Verheyen, E. M. 2022. The power of *Drosophila* in modeling human disease mechanisms. *Disease Models & Mechanisms* 15(3), p. dmm049549. doi: 10.1242/dmm.049549

Vibranovski, M. D., Chalopin, D. S., Lopes, H. F., Long, M. and Karr, T. L. 2010. Direct Evidence for Postmeiotic Transcription During *Drosophila melanogaster* Spermatogenesis. *Genetics* 186(1), p. 431. doi: 10.1534/genetics.110.118919

Vibranovski, M. D., Lopes, H. F., Karr, T. L. and Long, M. 2009. Stage-Specific Expression Profiling of *Drosophila* Spermatogenesis Suggests that Meiotic Sex Chromosome Inactivation Drives Genomic Relocation of Testis-Expressed Genes. *PLOS Genetics* 5(11), p. e1000731. doi: 10.1371/journal.pgen.1000731

Vieira, F. G. and Rozas, J. 2011. Comparative Genomics of the Odorant-Binding and Chemosensory Protein Gene Families across the Arthropoda: Origin and Evolutionary History of the Chemosensory System. *Genome Biology and Evolution* 3, pp. 476-490. doi: 10.1093/gbe/evr033

Wächter, K., Köhn, M., Stöhr, N. and Hüttelmaier, S. 2013. Subcellular localization and RNP formation of IGF2BPs (IGF2 mRNA-binding proteins) is modulated by distinct RNA-binding domains. 394(8), pp. 1077-1090. doi: doi:10.1515/hsz-2013-0111

Wagner, M., Kunsch, S., Duerschmied, D., Beil, M., Adler, G., Mueller, F. and Gress, T. M. 2003. Transgenic overexpression of the oncofetal RNA binding protein KOC leads to remodeling of the exocrine pancreas. *Gastroenterology* 124(7), pp. 1901-1914. doi: https://doi.org/10.1016/S0016-5085(03)00402-5

Wakimoto, B. T., Lindsley, D. L. and Herrera, C. 2004. Toward a Comprehensive Genetic Analysis of Male Fertility in *Drosophila melanogaster*. *Genetics* 167(1), pp. 207-216. doi: 10.1534/genetics.167.1.207

Wang, A. M. et al. 2013. Activation of Hsp70 reduces neurotoxicity by promoting polyglutamine protein degradation. *Nature Chemical Biology* 9(2), pp. 112-118. doi: 10.1038/nchembio.1140

Wang, B., Sullivan, K. M. C. and Beckingham, K. 2003a. *Drosophila* Calmodulin Mutants With Specific Defects in the Musculature or in the Nervous System. *Genetics* 165(3), pp. 1255-1268. doi: 10.1093/genetics/165.3.1255

Wang, C., Schmich, F., Srivatsa, S., Weidner, J., Beerenwinkel, N. and Spang, A. 2018. Context-dependent deposition and regulation of mRNAs in P-bodies. *eLife* 7, p. e29815.

Wang, K. et al. 2014. Rapid adaptive optical recovery of optimal resolution over large volumes. *Nature Methods* 11(6), pp. 625-628. doi: 10.1038/nmeth.2925

Wang, M., Ly, M., Lugowski, A., Laver, J. D., Lipshitz, H. D., Smibert, C. A. and Rissland, O. S. 2017. ME31B globally represses maternal mRNAs by two distinct mechanisms during the *Drosophila* maternal-to-zygotic transition. *eLife* 6, p. e27891. doi: 10.7554/eLife.27891

Wang, T. et al. 2003b. L523S, an RNA-binding protein as a potential therapeutic target for lung cancer. *British Journal of Cancer* 88(6), pp. 887-894. doi: 10.1038/sj.bjc.6600806

Wang, Z. and Lin, H. 2007. Sex-lethal is a target of Bruno-mediated translational repression in promoting the differentiation of stem cell progeny during *Drosophila* oogenesis. *Developmental Biology* 302(1), pp. 160-168. doi: https://doi.org/10.1016/j.ydbio.2006.09.016

Watson, K. L., Konrad, K. D., Woods, D. F. and Bryant, P. J. 1992. *Drosophila* homolog of the human S6 ribosomal protein is required for tumor suppression in the hematopoietic system. *Proceedings of the National Academy of Sciences* 89(23), pp. 11302-11306.

Weatheritt, R. J., Gibson, T. J. and Babu, M. M. 2014. Asymmetric mRNA localization contributes to fidelity and sensitivity of spatially localized systems. *Nature Structural & Molecular Biology* 21(9), pp. 833-839. doi: 10.1038/nsmb.2876

Weber, Stephanie C. and Brangwynne, Clifford P. 2012. Getting RNA and Protein in Phase. *Cell* 149(6), pp. 1188-1191. doi: https://doi.org/10.1016/j.cell.2012.05.022

Webster, P. J., Liang, L., Berg, C. A., Lasko, P. and Macdonald, P. M. 1997a. Translational repressor bruno plays multiple roles in development and is widely conserved. *Genes & Development* 11(19), pp. 2510-2521.

Webster, P. J., Liang, L., Berg, C. A., Lasko, P. and Macdonald, P. M. 1997b. Translational repressorbruno plays multiple roles in development and is widely conserved. *Genes & Development* 11(19), pp. 2510-2521.

Weil, T. T. 2014. mRNA localization in the *Drosophila* germline. *RNA Biology* 11(8), pp. 1010-1018. doi: 10.4161/rna.36097

Weil, T. T., Forrest, K. M. and Gavis, E. R. 2006. Localization of bicoid mRNA in Late Oocytes Is Maintained by Continual Active Transport. *Developmental Cell* 11(2), pp. 251-262. doi: https://doi.org/10.1016/j.devcel.2006.06.006

Welch, M. D., DePace, A. H., Verma, S., Iwamatsu, A. and Mitchison, T. J. 1997. The Human Arp2/3 Complex Is Composed of Evolutionarily Conserved Subunits and Is Localized to Cellular Regions of Dynamic Actin Filament Assembly. *Journal of Cell Biology* 138(2), pp. 375-384. doi: 10.1083/jcb.138.2.375

Wen, K. et al. 2016. Critical roles of long noncoding RNAs in *Drosophila* spermatogenesis. *Genome Research* 26(9), pp. 1233-1244. doi: 10.1101/gr.199547.115

Westfall, S., Lomis, N. and Prakash, S. 2018. Longevity extension in *Drosophila* through gut-brain communication. *Scientific Reports* 8(1), p. 8362. doi: 10.1038/s41598-018-25382-z

Wharton, R. P. and Struhl, G. 1991. RNA regulatory elements mediate control of *Drosophila* body pattern by the posterior morphogen nanos. *Cell* 67(5), pp. 955-967. doi: https://doi.org/10.1016/0092-8674(91)90368-9

White-Cooper, H. 2004. Spermatogenesis. In: Henderson, D.S. ed. *Drosophila Cytogenetics Protocols*. Totowa, NJ: Humana Press, pp. 45-75.

White-Cooper, H. 2009. Studying how flies make sperm—Investigating gene function in *Drosophila* testes. *Molecular and Cellular Endocrinology* 306(1), pp. 66-74. doi: https://doi.org/10.1016/j.mce.2008.11.026

White-Cooper, H. 2010. Molecular mechanisms of gene regulation during *Drosophila* spermatogenesis. *REPRODUCTION* 139(1), pp. 11-21. doi: 10.1530/REP-09-0083

White-Cooper, H. 2012. Tissue, cell type and stage-specific ectopic gene expression and RNAi induction in the *Drosophila* testis. *Spermatogenesis* 2(1), pp. 11-22. doi: 10.4161/spmg.19088

White-Cooper, H. and Bausek, N. 2010. Evolution and spermatogenesis. *Philosophical Transactions of the Royal Society B: Biological Sciences* 365(1546), pp. 1465-1480. doi: 10.1098/rstb.2009.0323

Whitworth, A. J., Theodore, D. A., Greene, J. C., Beneš, H., Wes, P. D. and Pallanck, L. J. 2005. Increased glutathione S-transferase activity rescues dopaminergic neuron loss in a *Drosophila* model of Parkinson's disease. *Proceedings of the National Academy of Sciences* 102(22), pp. 8024-8029.

Wiederrecht, G. J. and Brown, G. M. 1984. Purification and properties of the enzymes from *Drosophila melanogaster* that catalyze the conversion of dihydroneopterin

triphosphate to the pyrimidodiazepine precursor of the drosopterins. *Journal of Biological Chemistry* 259(22), pp. 14121-14127. doi: https://doi.org/10.1016/S0021-9258(18)89865-9

Wilhelm, J. E., Buszczak, M. and Sayles, S. 2005. Efficient Protein Trafficking Requires Trailer Hitch, a Component of a Ribonucleoprotein Complex Localized to the ER in *Drosophila*. *Developmental Cell* 9(5), pp. 675-685. doi: https://doi.org/10.1016/j.devcel.2005.09.015

Wilhelm, J. E., Mansfield, J., Hom-Booher, N., Wang, S., Turck, C. W., Hazelrigg, T. and Vale, R. D. 2000. Isolation of a Ribonucleoprotein Complex Involved in mRNA Localization in *Drosophila* Oocytes. *Journal of Cell Biology* 148(3), pp. 427-440. doi: 10.1083/jcb.148.3.427

Wilk, R., Hu, J., Blotsky, D. and Krause, H. M. 2016. Diverse and pervasive subcellular distributions for both coding and long noncoding RNAs. *Genes & Development* 30(5), pp. 594-609.

Wilkie, G. S. and Davis, I. 2001. *Drosophila* wingless and Pair-Rule Transcripts Localize Apically by Dynein-Mediated Transport of RNA Particles. *Cell* 105(2), pp. 209-219. doi: https://doi.org/10.1016/S0092-8674(01)00312-9

Wilkie, G. S., Dickson, K. S. and Gray, N. K. 2003. Regulation of mRNA translation by 5'- and 3'-UTR-binding factors. *Trends in Biochemical Sciences* 28(4), pp. 182-188. doi: 10.1016/S0968-0004(03)00051-3

Willett, M., Brocard, M., Pollard, Hilary J. and Morley, Simon J. 2013. mRNA encoding WAVE–Arp2/3-associated proteins is co-localized with foci of active protein synthesis at the leading edge of MRC5 fibroblasts during cell migration. *Biochemical Journal* 452(1), pp. 45-55. doi: 10.1042/BJ20121803

Williams, J., Boin, N. G., Valera, J. M. and Johnson, A. N. 2015. Noncanonical roles for Tropomyosin during myogenesis. *Development* 142(19), pp. 3440-3452. doi: 10.1242/dev.117051

Wilsch-Bräuninger, M., Schwarz, H. and Nüsslein-Volhard, C. 1997. A Sponge-like Structure Involved in the Association and Transport of Maternal Products during *Drosophila* Oogenesis. *Journal of Cell Biology* 139(3), pp. 817-829. doi: 10.1083/jcb.139.3.817

Witt, E., Benjamin, S., Svetec, N. and Zhao, L. 2019. Testis single-cell RNA-seq reveals the dynamics of de novo gene transcription and germline mutational bias in *Drosophila*. *eLife* 8, p. e47138. doi: 10.7554/eLife.47138

Wolf, M. J., Amrein, H., Izatt, J. A., Choma, M. A., Reedy, M. C. and Rockman, H. A. 2006. *Drosophila* as a model for the identification of genes causing adult human heart disease. *Proceedings of the National Academy of Sciences* 103(5), pp. 1394-1399. doi: 10.1073/pnas.0507359103

Wormser, O. et al. 2021. Absence of SCAPER causes male infertility in humans and *Drosophila* by modulating microtubule dynamics during meiosis. *Journal of Medical Genetics* 58(4), p. 254. doi: 10.1136/jmedgenet-2020-106946

Wu, C. et al. 2012. Arp2/3 Is Critical for Lamellipodia and Response to Extracellular Matrix Cues but Is Dispensable for Chemotaxis. *Cell* 148(5), pp. 973-987. doi: 10.1016/j.cell.2011.12.034

Wu, H. et al. 2016. Major spliceosome defects cause male infertility and are associated with nonobstructive azoospermia in humans. *Proceedings of the National Academy of Sciences* 113(15), pp. 4134-4139. doi: 10.1073/pnas.1513682113

Wu, J. S. and Luo, L. 2006. A protocol for mosaic analysis with a repressible cell marker (MARCM) in *Drosophila*. *Nature Protocols* 1(6), pp. 2583-2589. doi: 10.1038/nprot.2006.320

Xia, N.-S. et al. 2002. Bioluminescence of Aequorea macrodactyla, a Common Jellyfish Species in the East China Sea. *Marine Biotechnology* 4(2), pp. 155-162. doi: 10.1007/s10126-001-0081-7

Xiao, H. et al. 2015. The Pallbearer E3 Ligase Promotes Actin Remodeling via RAC in Efferocytosis by Degrading the Ribosomal Protein S6. *Developmental Cell* 32(1), pp. 19-30. doi: https://doi.org/10.1016/j.devcel.2014.11.015

Xie, Y., Budhathoki, R. and Blankenship, J. T. 2021. Combinatorial deployment of F-actin regulators to build complex 3D actin structures in vivo. *eLife* 10, p. e63046. doi: 10.7554/eLife.63046

Xu, D., Pan, J., Fang, Y., Zhao, L. and Su, Y. 2024. RpS25 is required for sperm elongation and individualization during *Drosophila* spermatogenesis. *Biochemical and Biophysical Research Communications* 702, p. 149633. doi: https://doi.org/10.1016/j.bbrc.2024.149633

Xu, E. Y., Lee, D. F., Klebes, A., Turek, P. J., Kornberg, T. B. and Reijo Pera, R. A. 2003. Human BOULE gene rescues meiotic defects in infertile flies. *Human Molecular Genetics* 12(2), pp. 169-175. doi: 10.1093/hmg/ddg017

Xu, S., Hafer, N., Agunwamba, B. and Schedl, P. 2012. The CPEB Protein Orb2 Has Multiple Functions during Spermatogenesis in *Drosophila melanogaster*. *PLOS Genetics* 8(11), p. e1003079. doi: 10.1371/journal.pgen.1003079

Xu, S., Tyagi, S. and Schedl, P. 2014. Spermatid Cyst Polarization in *Drosophila* Depends upon apkc and the CPEB Family Translational Regulator orb2. *PLOS Genetics* 10(5), p. e1004380. doi: 10.1371/journal.pgen.1004380

Xu, X.-Z. S. et al. 1998. Retinal Targets for Calmodulin Include Proteins Implicated in Synaptic Transmission *. *Journal of Biological Chemistry* 273(47), pp. 31297-31307. doi: 10.1074/jbc.273.47.31297

Yamazaki, D. et al. 2014. Glial Dysfunction Causes Age-Related Memory Impairment in *Drosophila*. *Neuron* 84(4), pp. 753-763. doi: https://doi.org/10.1016/j.neuron.2014.09.039

Yan, N. and Macdonald, P. M. 2004. Genetic Interactions of *Drosophila melanogaster* arrest Reveal Roles for Translational Repressor Bruno in Accumulation of Gurken and Activity of Delta. *Genetics* 168(3), pp. 1433-1442. doi: 10.1534/genetics.104.033985

Yang, C.-P., Samuels, T. J., Huang, Y., Yang, L., Ish-Horowicz, D., Davis, I. and Lee, T. 2017. Imp and Syp RNA-binding proteins govern decommissioning of *Drosophila* neural stem cells. *Development* 144(19), pp. 3454-3464. doi: 10.1242/dev.149500

Yang, T. and Terman, Jonathan R. 2012. 14-3-3ε Couples Protein Kinase A to Semaphorin Signaling and Silences Plexin RasGAP-Mediated Axonal Repulsion. *Neuron* 74(1), pp. 108-121. doi: https://doi.org/10.1016/j.neuron.2011.12.034

Yaniv, K. and Yisraeli, J. K. 2002. The involvement of a conserved family of RNA binding proteins in embryonic development and carcinogenesis. *Gene* 287(1), pp. 49-54. doi: https://doi.org/10.1016/S0378-1119(01)00866-6

Ye, X., Prieto, D. A., Chan, K. C., Wei, B.-R. and Blonder, J. 2013. Chapter 3 - Tissue Sample Preparation for Proteomic Analysis. In: Issaq, H.J. and Veenstra, T.D. eds. *Proteomic and Metabolomic Approaches to Biomarker Discovery*. Boston: Academic Press, pp. 39-50.

Yin, J. et al. 2024. Glia-derived secretory fatty acid binding protein Obp44a regulates lipid storage and efflux in the developing *Drosophila* brain. *bioRxiv*, p. 2024.2004.2010.588417. doi: 10.1101/2024.04.10.588417

Ying, M., Huang, X., Zhao, H., Wu, Y., Wan, F., Huang, C. and Jie, K. 2011. Comprehensively Surveying Structure and Function of RING Domains from *Drosophila melanogaster*. *PloS one* 6(9), p. e23863. doi: 10.1371/journal.pone.0023863

Yisraeli, J. K. 2005. VICKZ proteins: a multi-talented family of regulatory RNA-binding proteins. *Biology of the Cell* 97(1), pp. 87-96. doi: https://doi.org/10.1042/BC20040151

Yoshiyama-Yanagawa, T. et al. 2011. The Conserved Rieske Oxygenase DAF-36/Neverland Is a Novel Cholesterol-metabolizing Enzyme *. *Journal of Biological Chemistry* 286(29), pp. 25756-25762. doi: 10.1074/jbc.M111.244384

Yoshiyama, T., Namiki, T., Mita, K., Kataoka, H. and Niwa, R. 2006. Neverland is an evolutionally conserved Rieske-domain protein that is essential for ecdysone synthesis and insect growth. *Development* 133(13), pp. 2565-2574. doi: 10.1242/dev.02428

Young, R. S., Marques, A. C., Tibbit, C., Haerty, W., Bassett, A. R., Liu, J.-L. and Ponting, C. P. 2012. Identification and Properties of 1,119 Candidate LincRNA Loci in the *Drosophila melanogaster* Genome. *Genome Biology and Evolution* 4(4), pp. 427-442. doi: 10.1093/gbe/evs020

Yu, J. et al. 2019a. ATP synthase is required for male fertility and germ cell maturation in *Drosophila* testes. *Molecular Medicine Reports* 19(3), pp. 1561-1570.

Yu, J. et al. 2023. Single-cell RNA sequencing reveals cell landscape following antimony exposure during spermatogenesis in *Drosophila* testes. *Cell Death Discovery* 9(1), p. 86. doi: 10.1038/s41420-023-01391-4

Yu, J. et al. 2016. CHES-1-like , the ortholog of a non-obstructive azoospermia-associated gene, blocks germline stem cell differentiation by upregulating Dpp expression in *Drosophila* testis. *Oncotarget* 7(27),

Yu, J. et al. 2014. Identification of seven genes essential for male fertility through a genome-wide association study of non-obstructive azoospermia and RNA interference-mediated large-scale functional screening in *Drosophila*. *Human Molecular Genetics* 24(5), pp. 1493-1503. doi: 10.1093/hmg/ddu557

Yu, J. et al. 2019b. Srlp is crucial for the self-renewal and differentiation of germline stem cells via RpL6 signals in *Drosophila* testes. *Cell Death & Disease* 10(4), p. 294. doi: 10.1038/s41419-019-1527-z

Yu, Z., Ren, M., Wang, Z., Zhang, B., Rong, Y. S., Jiao, R. and Gao, G. 2013. Highly Efficient Genome Modifications Mediated by CRISPR/Cas9 in *Drosophila*. *Genetics* 195(1), pp. 289-291. doi: 10.1534/genetics.113.153825

Yuan, X. et al. 2019. *Drosophila* Pif1A is essential for spermatogenesis and is the homolog of human CCDC157, a gene associated with idiopathic NOA. *Cell Death & Disease* 10(2), p. 125. doi: 10.1038/s41419-019-1398-3

Zaessinger, S., Busseau, I. and Simonelig, M. 2006. Oskar allows *nanos* mRNA translation in *Drosophila* embryos by preventing its deadenylation by Smaug/CCR4. *Development* 133(22), pp. 4573-4583. doi: 10.1242/dev.02649

Zappavigna, V., Piccioni, F., Villaescusa, J. C. and Verrotti, A. C. 2004. Cup is a nucleocytoplasmic shuttling protein that interacts with the eukaryotic translation initiation factor 4E to modulate *Drosophila* ovary development. *Proceedings of the National Academy of Sciences* 101(41), pp. 14800-14805.

Zeng, C., Fukunaga, T. and Hamada, M. 2018. Identification and analysis of ribosome-associated lncRNAs using ribosome profiling data. *BMC Genomics* 19(1), p. 414. doi: 10.1186/s12864-018-4765-z

Zeng, X. et al. 2015. Genome-wide RNAi Screen Identifies Networks Involved in Intestinal Stem Cell Regulation in *Drosophila*. *Cell Reports* 10(7), pp. 1226-1238. doi: https://doi.org/10.1016/j.celrep.2015.01.051

Zeringer, E. et al. 2013. Methods for the extraction and RNA profiling of exosomes. *World journal of methodology* 3(1), p. 11.

Zhang, H. et al. 2015. RNA Controls PolyQ Protein Phase Transitions. *Molecular Cell* 60(2), pp. 220-230. doi: https://doi.org/10.1016/j.molcel.2015.09.017

Zhang, J., Yu, Z., Shen, J., Vandenberg, L. N. and Yin, D. 2021. Influences of sex, rhythm and generation on the obesogenic potential of erythromycin to *Drosophila melanogaster*. *Science of The Total Environment* 771, p. 145315. doi: https://doi.org/10.1016/j.scitotenv.2021.145315

Zhang, Y., Rai, M., Wang, C., Gonzalez, C. and Wang, H. 2016. Prefoldin and Pins synergistically regulate asymmetric division and suppress dedifferentiation. *Scientific Reports* 6(1), p. 23735. doi: 10.1038/srep23735

Zhang, Z., Hambuch, T. M. and Parsch, J. 2004. Molecular Evolution of Sex-Biased Genes in *Drosophila*. *Molecular Biology and Evolution* 21(11), pp. 2130-2139. doi: 10.1093/molbev/msh223

Zhao, S., Chen, D., Geng, Q. and Wang, Z. 2013. The highly conserved LAMMER/CLK2 protein kinases prevent germ cell overproliferation in *Drosophila*. *Developmental Biology* 376(2), pp. 163-170. doi: https://doi.org/10.1016/j.ydbio.2013.01.023

Zhu, S., Lin, S., Kao, C.-F., Awasaki, T., Chiang, A.-S. and Lee, T. 2006. Gradients of the *Drosophila* Chinmo BTB-Zinc Finger Protein Govern Neuronal Temporal Identity. *Cell* 127(2), pp. 409-422. doi: 10.1016/j.cell.2006.08.045

Zimyanin, V. L., Belaya, K., Pecreaux, J., Gilchrist, M. J., Clark, A., Davis, I. and St Johnston, D. 2008. In Vivo Imaging of *oskar* mRNA Transport Reveals the Mechanism of Posterior Localization. *Cell* 134(5), pp. 843-853. doi: 10.1016/j.cell.2008.06.053

Zirin, J. et al. 2020. Large-Scale Transgenic *Drosophila* Resource Collections for Loss- and Gain-of-Function Studies. *Genetics* 214(4), pp. 755-767. doi: 10.1534/genetics.119.302964

Zou, F. et al. 2020. *Drosophila* YBX1 homolog YPS promotes ovarian germ line stem cell development by preferentially recognizing 5-methylcytosine RNAs. *Proceedings of the National Academy of Sciences* 117(7), pp. 3603-3609.